STRATEGIES PLAYED BY IMMUNE CELLS AND MYCOBACTERIA IN THE BATTLE BETWEEN ANTIMICROBIAL ACTIVITY AND BACTERIAL SURVIVAL

EDITED BY: Veronica Schmitz, Maria Teresa Ochoa, Rosane M. B. Teles and Eun-Kyeong Jo

PUBLISHED IN: Frontiers in Immunology

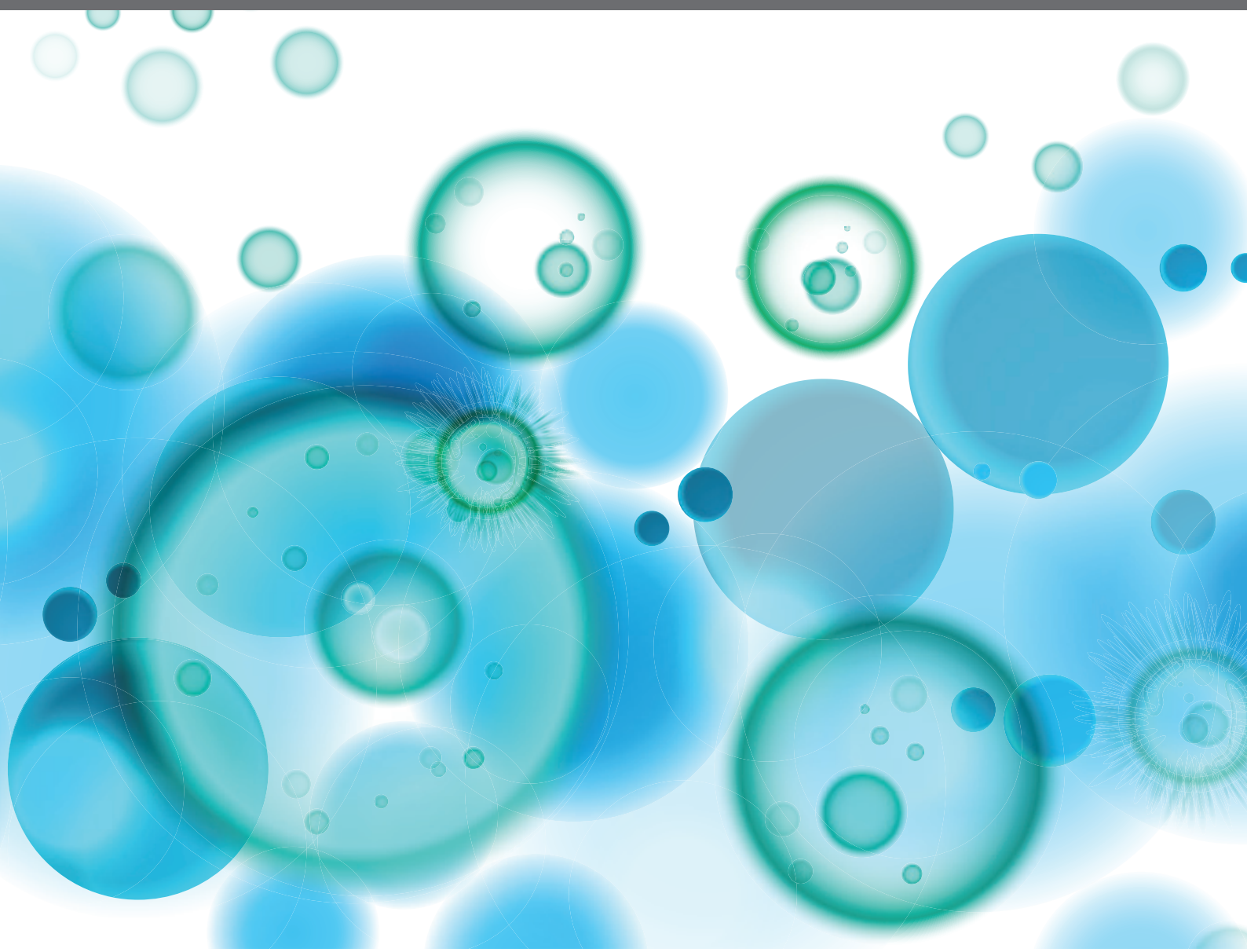

frontiers Research Topics

frontiers

ISSN 1664-8714
ISBN 978-2-88974-742-9
DOI 10.3389/978-2-88974-742-9

About Frontiers

Frontiers is more than just an open-access publisher of scholarly articles: it is a pioneering approach to the world of academia, radically improving the way scholarly research is managed. The grand vision of Frontiers is a world where all people have an equal opportunity to seek, share and generate knowledge. Frontiers provides immediate and permanent online open access to all its publications, but this alone is not enough to realize our grand goals.

Frontiers Journal Series

The Frontiers Journal Series is a multi-tier and interdisciplinary set of open-access, online journals, promising a paradigm shift from the current review, selection and dissemination processes in academic publishing. All Frontiers journals are driven by researchers for researchers; therefore, they constitute a service to the scholarly community. At the same time, the Frontiers Journal Series operates on a revolutionary invention, the tiered publishing system, initially addressing specific communities of scholars, and gradually climbing up to broader public understanding, thus serving the interests of the lay society, too.

Dedication to Quality

Each Frontiers article is a landmark of the highest quality, thanks to genuinely collaborative interactions between authors and review editors, who include some of the world's best academicians. Research must be certified by peers before entering a stream of knowledge that may eventually reach the public - and shape society; therefore, Frontiers only applies the most rigorous and unbiased reviews.
Frontiers revolutionizes research publishing by freely delivering the most outstanding research, evaluated with no bias from both the academic and social point of view. By applying the most advanced information technologies, Frontiers is catapulting scholarly publishing into a new generation.

What are Frontiers Research Topics?

Frontiers Research Topics are very popular trademarks of the Frontiers Journals Series: they are collections of at least ten articles, all centered on a particular subject. With their unique mix of varied contributions from Original Research to Review Articles, Frontiers Research Topics unify the most influential researchers, the latest key findings and historical advances in a hot research area! Find out more on how to host your own Frontiers Research Topic or contribute to one as an author by contacting the Frontiers Editorial Office: frontiersin.org/about/contact

STRATEGIES PLAYED BY IMMUNE CELLS AND MYCOBACTERIA IN THE BATTLE BETWEEN ANTIMICROBIAL ACTIVITY AND BACTERIAL SURVIVAL

Topic Editors:
Veronica Schmitz, Oswaldo Cruz Foundation (Fiocruz), Brazil
Maria Teresa Ochoa, University of Southern California, United States
Rosane M. B. Teles, University of California, United States
Eun-Kyeong Jo, Chungnam National University, South Korea

Citation: Schmitz, V., Ochoa, M. T., Teles, R. M. B., Jo, E.-K., eds. (2022). Strategies Played by Immune Cells and Mycobacteria in the Battle Between Antimicrobial Activity and Bacterial Survival. Lausanne: Frontiers Media SA. doi: 10.3389/978-2-88974-742-9

Table of Contents

frontiers in Immunology

EDITORIAL
published: 02 March 2022
doi: 10.3389/fimmu.2022.869692

Editorial: Strategies Played by Immune Cells and Mycobacteria in the Battle Between Antimicrobial Activity and Bacterial Survival

Veronica Schmitz[1], *Eun-Kyeong Jo*[2], *Maria Teresa Ochoa*[3] *and Rosane M. B. Teles*[4]*

[1] Leprosy Laboratory, Oswaldo Cruz Institute, Oswaldo Cruz Foundation (FIOCRUZ), Rio de Janeiro, Brazil, [2] Department of Microbiology, and Infection Control Convergence Research Center, College of Medicine, Chungnam National University, Daejeon, South Korea, [3] Keck School of Medicine, University of Southern California, Los Angeles, CA, United States, [4] Division of Dermatology, Department of Medicine, University of California, Los Angeles, Los Angeles, CA, United States

Keywords: leprosy, mycobacterial diseases, cell death, cellular targets, immune evasion, autophagy, mycobacteria-host cell interactions

Editorial on the Research Topic

Strategies Played by Immune Cells and Mycobacteria in the Battle Between Antimicrobial Activity and Bacterial Survival

OPEN ACCESS

Edited and reviewed by:
Imtiaz Ahmed Khan, George Washington University, United States

***Correspondence:**
Rosane M. B. Teles
rteles@mednet.ucla.edu

Specialty section:
This article was submitted to Microbial Immunology, a section of the journal Frontiers in Immunology

Received: *04 February 2022*
Accepted: *10 February 2022*
Published: *02 March 2022*

Citation:
Schmitz V, Jo E-K, Ochoa MT and Teles RMB (2022) Editorial: Strategies Played by Immune Cells and Mycobacteria in the Battle Between Antimicrobial Activity and Bacterial Survival. Front. Immunol. 13:869692. doi: 10.3389/fimmu.2022.869692

The interaction between host immunity and mycobacterial scape mechanisms determines the balance between antimicrobial activity and/or mycobacterial survival. This Research Topic, presented as original research and review articles, focused on mycobacteria-host cell interaction studies, including cellular and molecular targets of mycobacterial diseases, mycobacteria-mediated cell death mechanisms, host cell factors/pathways that act on mycobacteria to contain the infection, and immune evasion mechanisms utilized by mycobacteria (1–3).

The immune cells' polarization and plasticity in response to mycobacteria are essential for an efficient innate and adaptative immunity. Ge et al. review the importance of macrophage diversity and polarization for the granuloma formation in mycobacterial diseases. Specifically, they focus on the importance of less studied types of macrophages such as multinucleated giant cells, epithelioid cells, and foamy macrophages. Nogueira et al. focused on the B cell diversity in response to mycobacterial infection analyzing the B cells subpopulations in the peripheral blood of patients across the leprosy spectrum. They found that patients with a high bacillary load have an alteration in the frequency and function of mature and memory B cells. A better understanding of the immune cell's polarization and plasticity in response to mycobacterial infection is essential to preventing and treating mycobacterial diseases.

The activation of intracellular mechanisms by mycobacteria contributes to an efficient antimicrobial response, antigen presentation, and metabolic homeostasis. Kundu and Basu's review article focused on the role of non-coding RNAs (miRNAs and lncRNAs) as immune regulators in host immune response to mycobacterial infection, acting in important pathways such as inflammation, autophagy, apoptosis, the polarization of macrophages, and mycobacterial survival. The presence of different non-code RNAs in the fluids of latent and active tuberculosis (TB) patients opens an important window for using non-coding RNAs as a therapeutic tool and as biomarkers of active and latent tuberculosis. In addition, Park et al. review the influence of host

immune-mediated stresses, such as lysosomal activation, metabolic changes, oxidative stress, mitochondrial damage, and immune mediators, on the activities of the currently anti-TB drugs. Indeed, they also discussed how TB treatment facilitates the generation of *Mycobacterium tuberculosis* (Mtb) populations that are resistant to host immune response or disrupt host immunity. The long-term treatment may increase the risk of multidrug-resistant (MDR)- and extensively drug-resistant (XDR)-Mtb emergence.

Moreover, the ability of mycobacteria to inhibit phagolysosomal fusion also represents a key step in the determination of latent and active disease and can weaken the ability of the host immunity to fight against MDR- and XDR-Mtb. Saha et al. provide a new mechanism for mycobacteria evasion mediated by the macrophage at protein Coronin1 by the increase of intracellular cAMP levels upon mycobacterial infection. The increase of cAMP enhances cytoskeletal protein Cofilin1 to depolymerize F-actin around the mycobacteria-containing phagosome leading to the retarded phagosome maturation and acidification processes, providing mycobacterial survival. In their contribution, Zhou et al. showed that Mtb infection down-regulated GSK-3α/β activity and induced matrix metalloproteinase-1 (MMP-1) and -9 expressions in THP-1 derived-macrophages. MMP-9 protein expression was increased in the lungs of pulmonary tuberculosis and lymph nodes lymphatic tuberculosis patients, compared with that in patients of chronic inflammation. Their study has detected autophagy, pro-inflammatory and anti-inflammatory cytokines including IFNs and IFN stimulated genes (ISGs) upon Mtb infection with the treatment of SB216763, a GSK-3α/β inhibitor, in THP-1-macrophages. A better understanding of how mycobacteria interact with macrophage to block phagolysosome fusion and manipulate inflammation is important for the development of better therapeutic strategies.

An efficient antimicrobial response is critical for the clearance of mycobacteria inside of macrophages, metabolic response to hypoxia can regulate the expression and release of antimicrobial peptides. Zenk et al. showed the effects of one of the prolylhydroxylases inhibitors, Molidustat, which interferes with the interplay between Mtb and macrophages by interfering with the MAPK pathway *via* inhibition of p38 phosphorylation and stabilizes Mtb antigen mediated induction of hypoxia-inducible factor (HIF)-1α *via* TLR-signaling. These events lead to HIF-1α translocation into the nucleus and induction of the vitamin D antimicrobial pathway expression, resulting in the reduction of the proliferation of virulent Mtb in human macrophages. The study of how hypoxia can help to control intracellular pathogens including mycobacteria can be used as a new therapeutical strategy against mycobacterial diseases. Rasi et al. demonstrated that the enzymatic activity of Granzyme A (GzmA) is dispensable to mediate mycobacterial growth inhibition in primary monocytes infected by BCG. Global proteomic analysis of BCG-infected primary monocytes demonstrated that the ER stress response and ATP producing proteins were upregulated after GzmA treatment. These data raise the possibility for new targets for host-directed therapies to better control mycobacteria infections. According to the authors, future experiments are required to discern whether primary alveolar macrophages infected with Mtb recapitulate their findings.

The old antimycobacterial function of nitric oxide (NO) was revisited in this Research Topic. Zhang et al. highlight that sirtuin (SIRT) 7 contributes to limiting intracellular Mtb growth in RAW264.7 macrophages. SIRT7-mediated antimicrobial responses are partly due to NO production and apoptosis induction during Mtb infection. In addition, Ahn et al. presented the antimicrobial effects of recombinant interferon (IFN)-β for intracellular growth of *M. abscessus* infection. The pretreatment of recombinant type I IFN led to an increased NO production in the mouse lungs during *M. abscessus* infection, highlighting the function of the type I IFN-NO axis in the host defense against *M. abscessus*. Because cytotoxic NO action appears to be controversial in human monocytes/macrophages, future studies are warranted to clarify the function of SIRT7 and type I IFN in the context of NO regulation during the human antimycobacterial defense. In this Research Topic, Silwal et al. review the emerging position of autophagy in host defense against nontuberculous mycobacteria (NTM) infections. Although it is still in its infancy to understand the role of autophagy in various NTM diseases, compelling evidence suggests that autophagy-modulating strategies promote antimicrobial host defense and ameliorate pathological inflammation during several NTM infections. Together, these studies suggest that NO-inducing and autophagy-activating strategies may be curative therapeutic weapons to fight against TB and NTM infections.

This special Research Topic highlighted the innovative and review studies focusing on a complex interplay at the interface of mycobacteria and host factors, thereby counteracting mycobacterial pathogenesis and enhancing of protective host defense system. A deeper understanding of complex host-pathogen relationships will facilitate future investigations on this area for the development of potential candidates and the improved therapy against mycobacterial diseases.

AUTHOR CONTRIBUTIONS

The four authors reviewed and edited the manuscript. All authors contributed to the article and approved the submitted version.

ACKNOWLEDGMENTS

The editors thank all the authors for the amazing work grouped in this Research Topic and all the scientists that achieved the reviewing of these manuscripts.

REFERENCES

1. Koul A, Herget T, Klebl B, Ullrich A. Interplay Between Mycobacteria and Host Signaling Pathways. *Nat Rev Microbiol* (2004) 2:189–202. doi: 10.1038/nrmicro840
2. Nguyen L, Pieters J. The Trojan Horse: Survival Tactics of Pathogenic Mycobacteria in Macrophages. *Trends Cell Biol* (2005) 15:269–76. doi: 10.1016/j.tcb.2005.03.009
3. Houben EN, Nguyen L, Pieters J. Interaction of Pathogenic Mycobacteria With the Host Immune System. *Curr Opin Microbiol* (2006) 9:76–85. doi: 10.1016/j.mib.2005.12.014

Conflict of Interest: The authors declare that the research was conducted in the absence of any commercial or financial relationships that could be construed as a potential conflict of interest.

Publisher's Note: All claims expressed in this article are solely those of the authors and do not necessarily represent those of their affiliated organizations, or those of the publisher, the editors and the reviewers. Any product that may be evaluated in this article, or claim that may be made by its manufacturer, is not guaranteed or endorsed by the publisher.

frontiers in Immunology

ORIGINAL RESEARCH
published: 15 February 2021
doi: 10.3389/fimmu.2021.619362

Novel Secreted Protein of *Mycoplasma bovis* MbovP280 Induces Macrophage Apoptosis Through CRYAB

Gang Zhao[1,2], *Xifang Zhu*[1,2], *Hui Zhang*[1,2], *Yingyu Chen*[1,2,3,4,5,6], *Elise Schieck*[7], *Changmin Hu*[1], *Huanchun Chen*[1,2,3,4,5,6] *and Aizhen Guo*[1,2,3,4,5,6]*

[1] State Key Laboratory of Agricultural Microbiology, Huazhong Agricultural University, Wuhan, China, [2] College of Veterinary Medicine, Huazhong Agricultural University, Wuhan, China, [3] Key Laboratory of Development of Veterinary Diagnostic Products, Ministry of Agriculture, Huazhong Agricultural University, Wuhan, China, [4] Hubei International Scientific and Technological Cooperation Base of Veterinary Epidemiology, Huazhong Agricultural University, Wuhan, China, [5] Key Laboratory of Ruminant Bio-Products of Ministry of Agriculture and Rural Affairs, Huazhong Agriculture University, Wuhan, China, [6] International Research Center for Animal Disease, Ministry of Science and Technology, Huazhong Agricultural University, Wuhan, China, [7] International Livestock Research Institute, Nairobi, Kenya

Mycoplasma bovis causes important diseases and great losses on feedlots and dairy farms. However, there are only a few measures to control *M. bovis*-related diseases. As in other mycoplasma species, this is predominantly because the virulence related factors of this pathogen are largely unknown. Therefore, in this study, we aimed to identify novel virulence-related factors among the secreted proteins of *M. bovis*. Using bioinformatic tools to analyze its secreted proteins, we preliminarily predicted 39 secreted lipoproteins, and then selected 11 of them for confirmation based on SignalP scores >0.6 or SceP scores >0.8 and conserved domains. These 11 genes were cloned after gene modification based on the codon bias of *Escherichia coli* and expressed. Mouse antiserum to each recombinant protein was developed. A western blotting assay with these antisera confirmed that MbovP280 and MbovP475 are strongly expressed and secreted proteins, but only MbovP280 significantly reduced the viability of bovine macrophages (BoMac). In further experiments, MbovP280 induced the apoptosis of BoMac treated with both live *M. bovis* and MbovP280 protein. The conserved coiled-coil domain of MbovP280 at amino acids 210–269 is essential for its induction of apoptosis. Further, immunoprecipitation, mass spectrometry, and coimmunoprecipitation assays identified the anti-apoptosis regulator αB-crystallin (CRYAB) as an MbovP280-binding ligand. An αβ-crystallin knockout cell line BoMac-cryab^{-}, Mbov0280-knockout *M. bovis* strain T9.297, and its complemented *M. bovis* strain CT9.297 were constructed and the apoptosis of BoMac-cryab^{-} induced by these strains was compared. The results confirmed that CRYAB is critical for MbovP280 function as an apoptosis inducer in BoMac. In conclusion, in this study, we identified MbovP280 as a novel secreted protein of *M. bovis* that induces the apoptosis of BoMac via its coiled-coil domain and cellular ligand CRYAB. These findings extend our understanding of the virulence mechanism of mycoplasmal species.

Keywords: ***Mycoplasma bovis*, MbovP280, secreted protein, apoptosis, CRYAB, macrophage**

OPEN ACCESS

Edited by:
Maria Teresa Ochoa, University of Southern California, United States

Reviewed by:
José Ángel Gutiérrez-Pabello, National Autonomous University of Mexico, Mexico
Hedwich Fardau Kuipers, University of Calgary, Canada

***Correspondence:**
Aizhen Guo
aizhen@mail.hzau.edu.cn

Specialty section:
This article was submitted to Microbial Immunology, a section of the journal Frontiers in Immunology

Received: *20 October 2020*
Accepted: *25 January 2021*
Published: *15 February 2021*

Citation:
Zhao G, Zhu X, Zhang H, Chen Y, Schieck E, Hu C, Chen H and Guo A (2021) Novel Secreted Protein of Mycoplasma bovis MbovP280 Induces Macrophage Apoptosis Through CRYAB. Front. Immunol. 12:619362. doi: 10.3389/fimmu.2021.619362

INTRODUCTION

Mycoplasma bovis is a member of the class *Mollicutes*, a group of the smallest self-replicating wall-less prokaryotes. It causes several important diseases, including pneumonia, mastitis, and arthritis, in cattle throughout the world (1–3). In addition, it usually co-infects cattle together with other pathogens, such as *Pasteurella multocida*, *Mannheimia haemolytica*, bovine viral diarrhea virus (BVDV), bovine respiratory syncytial virus (BRSV), *Bovine herpes virus 1* (BHV-1), etc to cause bovine respiratory disease complex (BRD) (4). Despite its minimal genome, *M. bovis* is a successful pathogen capable of developing both persistent infections and clinical diseases in cattle. As is well-known, *M. bovis,* like other mycoplasma species, lacks conventional toxins and its virulence mechanism is still poorly understood.

Although many previous studies have focused on the membrane and membrane-associated proteins of mycoplasmal species that are involved in virulence-related processes, such as adhesion (5), invasion (6, 7), and the inflammatory response (8), secreted proteins haven't yet attracted considerable attention until only recent years. However, secreted proteins often function as virulence-related factors or important antigens in pathogenic bacteria. Several studies have shown that the culture supernatant of *M. bovis* (9) induces the expression of several cytokines in different types of host cells and that live *M. bovis* behaves differently from the killed bacterium in inducing cytokine expression (10). Furthermore, several proteins of *Mycoplasma* species, including P80 of *M. hominis* (11), P102 of *M. hyopneumoniae* (12), Mpn491 of *M. pneumoniae* (13), CARDS toxin of *M. pneumoniae* (14), and a nuclease encoded by MBOV_RS02825 of *M. bovis* (15), have been shown to be secreted proteins. More recently, the secretomes and extracellular vesicles of several mycoplasmas species have been investigated with proteomic approaches, such as two-dimensional electrophoresis and liquid chromatography–tandem mass spectrometry (LC–MS/MS), isobaric tags for relative and absolute quantitation (iTRACK), and label-free proteomic analyses (16–18). However, the progress is relatively slow because it is usually difficult to confirm the secretomes and secreted proteins of mycoplasma species based on following reasons: (1) Mycoplasma species grow slowly and it is difficult to get sufficient proteins in short time; (2) Mycoplasma species growth requires rich medium supplemented with high concentrations of serum and yeast extract and it is difficult to exclude the contamination of abundant foreign proteins from the secretome in the culture supernatant; (3) There is no efficient genetic tools to manipulate gene expression of mycoplasma species by knock-out and knock-in to verify the predicted secreted proteins; (4) Most of the genes in mycoplasmal genomes are functionally unknown. One way dealing with this awkward situation tactfully is to combine the prediction of secreted proteins with bioinformatic tools, such as SignalP, SecretomeP, PSORT-B, and PrediSi (17–19) and identification of the secreted proteins with proteomic methods.

Therefore, in this study, we aimed to determine the novel secreted proteins of *M. bovis* and examine their association with *M. bovis* virulence. The secreted lipoproteins were first predicted with online softwares, and then the predicted secreted proteins were expressed and verified. Among the 11 predicted proteins, MbovP280 was identified as a secreted protein that induces apoptosis in a bovine macrophage cell line (BoMac) via the anti-apoptosis regulator αB-crystallin (CRYAB).

MATERIALS AND METHODS

Ethics Statement

The protocols for the mouse experiments in this study were approved by the Experimental Animal Ethics Committee of Huazhong Agricultural University (Wuhan, China) (Permit number: HZAUMO-2018-027) and were performed in accordance with the Hubei Regulations for the Administration of Affairs Concerning Experimental Animals.

Growth of Bacterial Strains and Cells

Mycoplasma bovis strain HB0801 (GenBank accession no. NC_018077.1) was isolated from the lesioned lung of an infected beef cattle from Yingcheng city in Hubei province, China and characterized by this laboratory (20). The strain was grown in pleuropneumonia-like organism (PPLO) medium (BD Company, Sparks, MD, USA), as previously described (20). *Mycoplasma bovis* mutants were grown in the same PPLO medium but supplemented with 100 μg/mL gentamycin or 10 μg/mL puromycin, depending upon the resistance genes the mutants carried. Recombinant *Escherichia coli* strains DH5α and BL21 (TransGen, Beijing, China) were grown in Luria–Bertani (LB) medium with antibiotics as necessary.

The BoMac cell line was kindly provided by Prof. Judith R. Stabel from the Johne's Disease Research Project at the United States Department of Agriculture in Ames, Iowa, and grown in RPIM 1640 medium (HyClone, UT, USA) supplemented with 10% heat-inactivated fetal bovine serum (FBS) (Gibco, Sydney, Australia) as described previously (21). The HEK293T cell line was purchased from the China Center for Type Culture Collection and cultured in high-glucose Dulbecco's modified Eagle's medium (HyClone) supplemented with 10% heat-inactivated FBS (Gibco).

Prediction of Secreted Proteins Based on *M. bovis* HB0801 Genome

Classical secreted proteins were predicted with SignalP 4.1 (http://www.cbs.dtu.dk/services/SignalP/), while non-classical secreted proteins with SecretomeP 2.0 (http://www.cbs.dtu.dk/services/SecretomeP/) as described previously (19). The conserved domains in the predicted proteins were analyzed online with the National Center for Biotechnology Information (NCBI) Conserved Domain Database (http://www.ncbi.nlm.nih.gov/Structure/cdd/wrpsb.cgi). Proteins homologous to MbovP280 were identified with MolliGen 3.0 (http://services.cbib.u-bordeaux.fr/molligen/). The coiled-coil domain of MbovP280 was predicted with COILS (https://embnet.vital-it.ch/software/COILS_form.html). The homology models of CRYAB, caspase 3, and MbovP280 were generated with SWISS-MODEL (https://swissmodel.expasy.org/), and the interactions

between CRYAB, caspase 3, and MbovP280 were analyzed with ClusPro 2.0 (https://cluspro.bu.edu/login.php).

Gene Cloning and Expression of the Recombinant Proteins, and Polyclonal Antibody Production

The putative secreted lipoproteins with the highest prediction values and carrying conserved domains were selected for further analysis. First, the sequences of the selected genes were site-directedly edited by replacing the TGA codon with TGG to ensure that *M. bovis* tryptophan was correctly translated in *E. coli*. The sequences were synthesized by Beijing Tianyi Huiyuan Bioscience & Technology Inc. (Wuhan, China) and ligated into the pET-30a vector (Novagen, Darmstadt, Germany) (**Supplementary Table 1**). The modified genes were individually cloned into the pET-30a vector after digestion with restriction endonucleases *Bam*HI and *Xho*I. The MbovP280 mutant in which amino acids 210–269 (predicted to form a coiled-coil domain by the COILS software) were deleted was similarly cloned into pET-30a to generate pET-30a-Mbov_0280$^{\Delta 210-269}$. *Escherichia coli* strain BL21 (TransGen, Beijing, China) was then transformed with each of the constructed plasmids individually, and the recombinant proteins were expressed after the cells were treated with isopropyl β-D-1-thiogalactopyranoside (IPTG) (0.8 mM). The proteins were purified with nickel affinity chromatography (GE Healthcare, NJ, USA), as described previously (7).

Mouse antisera against eight recombinant secreted proteins (rMbovP280, rMbovP290, rMbovP475, rMbovP458, rMbovP468, rMbovP537, rMbovP682, and rMbovP838) were produced in this study with a previously described method (7). Briefly, 4-week-old female BALB/c mice were purchased from China Hubei Provincial Center for Disease Control and Prevention (Wuhan, China) and raised in the Animal Facility of Huazhong Agriculture University. For each protein, five mice were immunized with 100 μg of each purified protein emulsified in an equal volume of Freund's complete adjuvant (Sigma, USA) for the priming immunization or with Freund's incomplete adjuvant for the subsequent immunization. Immunizations were performed by subcutaneous injection at an interval of 2 weeks. When the antiserum titers peaked, the mice were euthanized and bled. The antisera were collected and stored at −20°C for further use, and the preimmunization sera were stored for use as the negative controls.

Antibodies directed against the predicted secreted proteins rMbovP116, rMbovP275, and rMbovP739, which were previously developed by this laboratory (22), were also used in this study.

Verification of the Secretion of Selected Proteins

The secretomes and whole-cell proteins of *M. bovis* were extracted to confirm the secreted nature of the predicted proteins with western blotting assays. The secretome of *M. bovis* was extracted with a previously described method (18). Briefly, *M. bovis* was cultured for 36 h to late log phase and harvested by centrifugation at 140,000 × g for 20 min. The bacterial debris in the supernatant was removed with a 0.22 μm filter. The filtered solution was then precipitated with 10% trichloroacetic acid (TCA), stored at 4°C overnight, and pelleted by centrifugation at 16,000 × g for 20 min at 4°C. The pellet was washed three times with cold acetone (−20°C) and resuspended in lysis buffer [8 M urea, 4% CHAPS, 2 M thiourea, 60 mM dithiothreitol, 2% amidosulfobetaine-14, 40 mM Tris-HCl (pH 8.8)]. The whole-cell proteins of *M. bovis* were prepared by sonicating the cells (200 W) on ice for 5 min. The protein concentrations of the secretome and whole-cell proteins were determined with the 2D Quant Kit (GE Healthcare, Sweden) and the BCA Protein Assay Kit (Cellchip Biotechnology Company, Beijing, China), respectively.

The western blotting assay was performed as follows. The secretome and whole-cell proteins were resolved with SDS-PAGE and then transferred onto polyvinylidene difluoride (PVDF) membranes (Millipore, Darmstadt, Germany). The mouse antisera directed against the 11 proteins and negative control sera were prediluted to 1:500 and separately overlaid onto the blotted PVDF strips. The proteins that specifically interacted with the antisera were visualized with WesternBright™ ECL (Advansta, CA, USA).

To detect the secretion process of MbovP280 and MbovP475 *in vitro*, the cultural supernatant of *M. bovis* HB0801 at 6, 12, 24, and 36 h was collected by centrifugation (15,400 g, 20 min, 4°C). Then, the supernatant (10 mL) was concentrated to 1 mL in an Amicon Ultra-4 Centrifugal Filter Unit (15 mL, 10 kDa) (Millipore). The equal volume of PPLO medium was concentrated as the negative control. The equal volume of supernatant (10 uL) from culture at each time point was resolved with SDS-PAGE and then transferred onto PVDF membranes (Millipore). The whole-cell proteins served as positive control and the membrane-associated protein NOX (7) of *M. bovis* was used as negative control. The bands were visualized by western blotting assay using the method described above.

Observation of MbovP280 Binding With Confocal Microscopy

BoMac cells (1×10^5) were propagated overnight on a microscope coverslip in each well of a 12-well-plate. To observe the binding of MbovP280 to BoMac, 0.5 μM MbovP280 was added to each well and incubated for 1 h at 37 °C. Phosphate-buffered saline (PBS) was used as the negative control. After the medium was removed, all the cells on the coverslips were washed three times with PBS, fixed with 4% paraformaldehyde in PBS for 10 min, and permeabilized with 0.5% Triton X-100 for 5 min at room temperature. All the cells were then blocked with 1% (w/v) bovine serum albumin (BSA) in PBS for 2 h. The cells were immunolabeled with mouse antiserum directed against rMbovP280 (1:500), and an Alexa-Fluor-488-conjugated goat anti-mouse IgG (H+L) secondary antibody (1:1,000) (Southern Biotech, MI, USA). Finally, the nuclei were counterstained with 4′,6-diamidino-2-phenylindole (DAPI) 5 mg/ml (Beyotime, Shanghai, China), and the polymerized form of actin was labeled with rhodamine phalloidin (100 nM) (Cytoskeleton, CO, USA).

Finally, the slides were cover-slipped and observed with a confocal laser fluorescence microscope (Olympus FV1000 and IX81, Tokyo, Japan).

Effect of MbovP280 on Cell Viability

The relative viability of BoMac and RAW264.7 cells after treatment with either recombinant MbovP280 (rMbovP280) or rMbovP475 was determined with a Cell Counting Kit-8 (CCK-8) (Dojindo Laboratories, Kumamoto, Japan). The cells were seeded at a density of 5,000 cells/well in 96-well-plates and incubated overnight at 37°C. They were then treated in triplicate with either rMbovP280 or rMboP475 at a concentration of 1 μM for 24 h. Cells treated with PBS were used as the negative control. CCK-8 (10 μl) was then added to each well, and the samples incubated for 2 h. The optical density at a wavelength of 450 nm (OD_{450}) was measured and the relative cell viability was calculated as:

$$\text{Relative cell viability (\%)} = (OD_{sample} - OD_{blank})/(OD_{NC} - OD_{blank}) \times 100\%$$

The cells were then treated with either rMbovP280 or its mutant rMbovP280$^{\Delta 210-269}$ at a concentration of 0.25, 0.5, or 1 μM for 24 h and the relative cell viability of BoMac was determined with the CCK-8 assay, as described above. Each treatment was carried out in five repeat and all experiments were performed independently three times.

Screening for MbovP280-Binding Ligands With Immunoprecipitation (IP)–MS

An IP–MS method was used to screen for MbovP280-binding proteins. Briefly, BoMac cells were cultured, harvested, and lysed in RIPA buffer supplemented with cOmplete™ Protease Inhibitor Cocktail (Roche, Mannheim, Germany). The whole-cell lysates (400 μg) were incubated with 10 μg of either rMbovP280 or rMbovP280$^{\Delta 210-269}$ for 1 h at 4°C. Mouse antiserum (5 μg) directed against MbovP280 was added to the lysates for 12 h at 4°C, and then 50 μl of Protein A/G Agarose Beads (Beyotime) were added and incubated for an additional 1 h. The immunoprecipitates were extensively washed with NP-40 buffer and eluted with SDS loading buffer by boiling them for 5 min. The cellular proteins co-precipitated with rMbovP280 or rMbovP280$^{\Delta 210-269}$ were resolved with SDS-PAGE and stained with silver staining. The specific bands that bound only rMbovP280 were commercially sequenced and analyzed with MS by Applied Protein Technology (Shanghai, China).

Verification of MbovP280-Binding Ligand CRYAB With Coimmunoprecipitation (Co-IP)

To confirm the interaction between MbovP280 and α-crystallin (CRYAB) in BoMac cells, the *CRYAB* gene (GenBank accession no. AF029793.2) was commercially synthesized at Beijing Tianyi Huiyuan Bioscience & Technology Inc. and cloned into pCAGGS-Flag, kindly provided by Prof. Xiao Shaobo (23). The Mbov_0280 gene (GenBank accession no. AFM51648.1) of *M. bovis* was synthesized and cloned into pCAGGS-HA, kindly provided by Prof. Xiao Shaobo at Huazhong Agricultural University, Wuhan, China (23). *Escherichia coli* strain DH5α (TransGen Biotech, Beijing, China) was transformed with the individual constructed plasmids, pCAGGS-Flag–CRYAB or pCAGGS-HA–Mbov_0280. The endotoxin-free plasmids were prepared with the E.Z.N.A.® Endo-Free Plasmid Mini Kit II (Omega Bio-tek, GA, USA) and then stored at −20°C until use. For the Co-IP assay, HEK-293T cells were cotransfected with both pCAGGS-Flag–CRYAB (8 μg) and pCAGGS-HA–Mbov_0280 (8 μg) using Lipofectamine 2000 (Invitrogen, Carlsbad, CA, USA) in a 10 cm dish. After 32 h, the cells were harvested and lysed in 1.5 ml of NP-40 buffer supplemented with cOmplete™ Protease Inhibitor Cocktail (Roche). The cell lysates (600 μl) were immunoprecipitated with 2 μg of commercial antibody directed against one of the recombinant tags [either Flag or hemagglutinin (HA)] for 12 h at 4°C. After the addition of Protein A/G Agarose Beads for 1 h, the immunoprecipitates were washed extensively with NP-40 buffer and eluted with SDS loading buffer by boiling for 5 min. A western blotting assay was then performed. The samples were resolved with SDS-PAGE and transferred to PVDF membranes (Millipore). The proteins were immunodetected with antibodies directed against either Flag (MBL, Nagoya, Japan) or HA (MBL, Nagoya, Japan). MbovP280 and CRYAB reacted with the antibodies directed against the corresponding tags on the PVDF membrane and were visualized with WesternBright™ ECL (Advansta).

Construction of Strain Complementing the Mbov_0280 Mutant

The Mbov_0280-knockout mutant T9.297 was identified from a transposon-mediated *M. bovis* mutant library previously constructed in this laboratory (24). The mutated site was at nucleotide (nt) 418 of the Mbov_0280 coding sequence (CDS) or nt 323, 346 of the *M. bovis* HB0801 genome.

To construct a strain to complement the mutant T9.297, the sequence of the *M. agalactiae P40* promoter followed by the intact Mbov_0280 CDS was synthesized at Beijing Tianyi Huiyuan Bioscience & Technology Inc. and ligated into the pOH/P plasmid after digestion with restriction enzyme *Not*I, generating the recombinant plasmid pOH/P–Mbov_0280. T9.297 cells were transfected with pOH/P–Mbov_0280 to generate the complementing strain CT9.297, with a previously described method (25). Single colonies were selected with puromycin (10 μg/ml) in the medium and then confirmed with DNA sequencing. The T9.297 and CT9.297 strains were cultured in s medium containing 100 μg/ml gentamycin and 10 μg/ml puromycin, respectively, and their growth curves were determined with a colony counting method.

MbovP280 expression in mutant strain T9.297 and complementary strain CT9.297 was tested with western blotting assay. First, both strains were cultured in 20 ml of PPLO medium with the necessary antibiotics for 36 h and precipitated by centrifugation. The pellet of each strain was then suspended in 1 ml of PBS and lysed by sonication (200 W) on ice for 5 min. The proteins in the lysate were then separated with SDS-PAGE (10%) and transferred onto PVDF membrane (Millipore). The membrane was incubated with mouse antiserum (1:500) directed

TABLE 1 | Oligonucleotide primers used for PCR in this study.

Names	Primer sequences (5′ →3′)
CRYABsgRNAoligo1	caccgTTCGGCCGCCCTCATTTCTG
CRYABsgRNAoligo2	aaacCAGAAATGAGGGCGGCCGAAc
U6-F	GAGGGCCTATTTCCCATGATTCC
CRYAB-C-F	AGCTCAGTGAGTACTGGGTAT
CRYAB-C-R	TGTAAGACAAAGGCCCCTTCT

against rMbovP280 or rMbovP579 at room temperature for 1 h. After the membrane was washed, it was reacted with horseradish peroxidase (HRP)-conjugated goat anti-mouse IgG antibody (1:5,000; Southern Biotech) for 1 h at room temperature. The bands on the membrane were visualized with WesternBright™ ECL (Advansta).

Construction of BoMac cryab⁻ Cell Line and Its Confirmation

CRISPR/cas9 gene editing was used to mutate the *CRYAB* gene in the BoMac cell line as described below. Single guide RNA (sgRNA) oligonucleotides to the *CRYAB* gene were designed with CCTop (https://cctop.cos.uni-heidelberg.de/) (**Table 1**). Ten microliter mixture of 100 μM *CRYAB* sgRNA oligonucleotides 1 (CRYABsgRNAoligo1) and 2 (CRYABsgRNAoligo2) (each 1 μl) (**Table 1**), NEB buffer 2 (1 μl), and ddH_2O (7 μl) were prepared, and then annealed at 37°C for 30 min, heated at 95°C for 5 min, and cooled to 25°C. The lentiCRISPRv2 plasmid (Addgene plasmid #52961; http://n2t.net/addgene:52961; RRID: Addgene_52961) (26) was cut with *Bsm*BI and purified with the EasyPure® PCR Purification Kit (TransGen Biotech). Then 1 μl of the diluted (1:50) and annealed oligonucleotides was cloned into lentiCRISPRv2 with T4 ligase (New England Biolabs, Beijing, China) at 16°C for 12 h. Competent *E. coli* DH5α cells were transformed with the constructed plasmid plentiCRISPRv2-CRYABsgRNA and the construct was verified by sequencing with the primer U6-F (**Table 1**).

The constructed plasmid plentiCRISPRv2-CRYABsgRNA and packaging plasmids pMD2.G (Addgene plasmids #12259; http://n2t.net/addgene:12259; RRID: Addgene_12259) and psPAX2 (Addgene plasmids #12260; http://n2t.net/addgene:12260; RRID: Addgene_12260) were amplified and purified with an Endo-free Plasmid Mini Kit II (Omega Bio-tek). The lentivirus was rescued as described previously (26) with some modification as follows. HEK293T cells were transfected with 12 μg of plentiCRISPRv2-CRYABsgRNA, 8 μg of psPAX2, and 4 μg of pMD2.G in 500 μl of jetPRIME® buffer (PolyPlus, Ilkirch, France) containing 48 μl of jetPRIME® reagent (PolyPlus). After 6 h, the medium was changed to DMEM containing 10% FBS and the cells were further cultured for 48 h. The lentivirus was harvested by centrifugation at 3,000 × g at 4°C for 10 min and then filtered through a 0.45 μm membrane (Millipore), concentrated 10-folds with Lenti-Pac™ Lentivirus Concentration Solution (GeneCopoeia, MD, USA), purified as described in the manual, and resuspended in 1 ml of PBS.

The BoMac cells with 50% confluency in each well of a 24-well-plate were infected with 100 μl of the purified lentivirus for 12 h. The medium was then changed to RPMI 1640 containing 10% FBS and 1% penicillin–streptomycin, and the cells were incubated for 36 h more. The media in the infected and uninfected wells were changed to fresh RPMI 1640, as described above, but with the addition of 2 μg/ml puromycin. After 3 days, the adherent cells were propagated in one well of a six-well-plate and cultured in RPMI 1640 (10% FBS, 1% penicillin–streptomycin) with 2 μg/ml puromycin for 3 days. The cells in the wells of the six-well-plate were then counted and 10-fold serially diluted in RPMI 1640 to a final concentration of 1 cell per 100 μl. The diluted cells (100 μl) were seeded to the wells of two 96-well-plates. The clonal cell lines were isolated from the 96-well-plates after 7 days, and expanded for 14 days.

The genome of the selected mutated cell line in each well was isolated with the TIANamp Genomic DNA Kit (Tiangen, Beijing, China). Q5 High-Fidelity 2× Master Mix (NEB, Beijing, China) and the primers CRYAB-C-F and CRYAB-C-R (**Table 1**) were then used to amplify the sequences edited by CRISPR/cas9. The whole-cell proteins of each mutated cell line and those of the wild type (WT) were prepared in RIPA lysis buffer (Beyotime) and then resolved with SDS-PAGE, transferred onto PVDF membrane (Millipore), and incubated with a mouse monoclonal antibody directed against CRYAB (1:1,000) (Abcam, ON, Canada) at room temperature for 1 h. The membranes were then incubated with a HRP-conjugated goat anti-mouse IgG antibody (1:5,000) (Southern Biotech) for 1 h at room temperature. The bands on the membrane were visualized with Western Bright™ ECL (Advansta).

Apoptosis of BoMac Specifically Induced by MbovP280

To examine the specific effect of rMbovP280 on the induction of BoMac apoptosis, the WT BoMac and mutant BoMac cryab⁻ cells were seeded at a density of 5×10^5 cells per well in six-well-plates and incubated overnight at 37°C. They were then treated with rMbovP280 or its mutant rMbovP280$^{\Delta 210-269}$ at three concentrations (0.25, 0.5, or 1 μM) for 24 h.

To observe the effect of MbovP280 expression in *M. bovis* strains on cell apoptosis, 5×10^5 BoMac cells were seeded into each well of a six-well-plate and incubated overnight. The cells were then infected with WT *M. bovis* HB0801, the mutant T9.297, or complementary strain CT9.297, respectively, at an MOI of 1,000 for 24 h. The cells were harvested and stained with the Annexin V-FITC Apoptosis Detection Kit (Vazyme, Nanjing, China) according to the manufacturer's instructions (15). An Apoptosis Inducer Kit (Beyotime) was used as the positive control. Flow cytometry (BD Company, NJ, USA) was used to detect the apoptotic cells, and the data were analyzed with the FlowJo VX software. The experiments were performed independently three times.

To confirm the apoptosis determined by Annexin V-FITC Apoptosis Detection Kit, the levels of cleaved caspase-3 in BoMac cells infected with *M. bovis* or treated with rMbvoP280 and rMbovP280$^{\Delta 210-269}$ as described above were detected

TABLE 2 | Information on 11 predicted secreted proteins.

Genes	Protein	SignalP Score	SecP Score	Domain
Mbov_0739	Lipoprotein	<0.6	0.83	N
Mbov_0537	Lipoprotein	<0.6	0.81	Aromatic cluster surface protein
Mbov_0275	Lipoprotein	<0.6	0.90	N
Mbov_0475	Lipoprotein	<0.6	0.83	DUF285
Mbov_0280	Lipoprotein	0.60	<0.8	N
Mbov_0116	Lipoprotein	0.61	0.86	N
Mbov_0458	Lipoprotein	0.61	0.93	PAP1 super family
Mbov_0468	Lipoprotein	0.61	0.90	DUF31
Mbov_0290	Lipoprotein	0.61	<0.8	Leucine-rich repeat 5
Mbov_0838	Lipoprotein	0.69	0.91	DUF285
Mbov_0682	Lipoprotein	0.72	0.90	PRK08581

SignalP score and SecP score were determined with SignalP 4.1 (http://www.cbs.dtu.dk/services/SignalP/) and SecretomeP 2.0 (http://www.cbs.dtu.dk/services/SecretomeP/), respectively. "N" indicates none predicted. "DUF" indicates domain of unknown function.

by western blotting assay. The cells were washed with cold PBS, resuspended with RIPA buffer containing proteinase and phosphatase inhibitors, and lysed at 4°C for 1 h. The proteins in the lysates were then separated with SDS-PAGE (10%) and transferred onto PVDF membrane (Millipore). The membrane was incubated with cleaved caspase-3 (Asp175) antibody (Cell Signaling Technology, DANVERS, MA, USA) (1:1,000) at 4°C overnight after blocking with 5% skimmed milk. After the membrane was washed, it reacted with HRP-conjugated goat anti-mouse IgG antibody (1:5,000) (Southern Biotech) for 1 h at room temperature. The bands on the membrane were visualized with WesternBright^{TM} ECL (Advansta).

Statistical Analysis

Data were expressed as means ± standard error of mean (SEM). Student's *t*-test was used for single comparison and one-way ANOVA for multiple comparisons with the GraphPad Prism version 5 software (GraphPad Software, La Jolla, CA, USA).

RESULTS

Prediction of Secreted Proteins Based on the Genome of *M. bovis* HB0801

A total of 39 secreted lipoproteins were predicted with a genome-wide analysis of *M. bovis* based on the SignalP-TM score and the SecP score (**Supplementary Table 1**). Among these lipoproteins, 19 were non-classical secreted proteins, four were classical secreted proteins, and 16 were non-classical/classical secreted proteins. Using the criteria of a SignalP score >0.6 or SceP score >0.8 and the prediction of conserved domains, 11 of the predicted secreted lipoproteins were selected for further investigation, including two classical, four non-classical, and five non-classical/classical secreted proteins, and seven of which contained conserved domains. For example, MbovP537 contains the aromatic cluster surface protein domain, which suggests its surface expression; MbovP458 contains the PAP1 superfamily domain, which may regulate the transcription of antioxidant genes in response to H_2O_2; and MbovP682 contains the PRK08581 domain, which may function as an N-acetylmuramoyl-L-alanine amidase (**Table 2**).

Confirmation of the Expression and Secretion of Selected Proteins

The 11 selected genes of *M. bovis* were modified appropriately and cloned into *E. coli*. The recombinant proteins were shown to be correctly expressed, with the expected molecular masses, with SDS-PAGE (**Figure 1A**). The antiserum against each recombinant protein was used to detect the presence of each protein in the secretome and whole-cell proteins of *M. bovis* HB0801 with western blotting assays. The results indicated that all the proteins were present in large amounts in the whole-cell proteins, but only MbovP280 and MbovP475 were abundant in the secretome, whereas the other proteins were represented by only variously weak bands in the secretome (**Figure 1B**, **Supplementary Figure 1**). In order to detect the secretion process of MbovP280 and MbovP475 *in vitro*, the presence of MbovP280 and MbovP475 in the culture supernatant of *M. bovis* was kinetically examined, while the membrane-associated protein NOX served as the negative control. The results indicated the MbovP475 was detected in the supernatant after *M. bovis* was cultured for 24 h. But MbovP280 wasn't detected in the supernatant until *M. bovis* was cultured for 36 h. The membrane-associated protein NOX of *M. bovis* wasn't detected in the culture supernatant as expected (**Figure 1C**, **Supplementary Figure 2**).

The rMbovP280 Reduces Cell Viability

The effects of rMbovP280 and rMboP475, at concentrations of 1 μM, on the viability of BoMac and RAW264.7 cells were determined with a CCK-8 kit after the cells were treated for 24 h. The viability of mock-treated cells as the negative control was taken as 100%. As a result, the rMbovP280 significantly reduced cell viability in a cell-type-dependent way. The rMbovP280 caused the viability a reduction of ∼77.3% in BoMac cells ($p < 0.001$), but a reduction of only about 12.9% in RAW264.7 cells ($p < 0.05$). This is in agreement with our expectation that

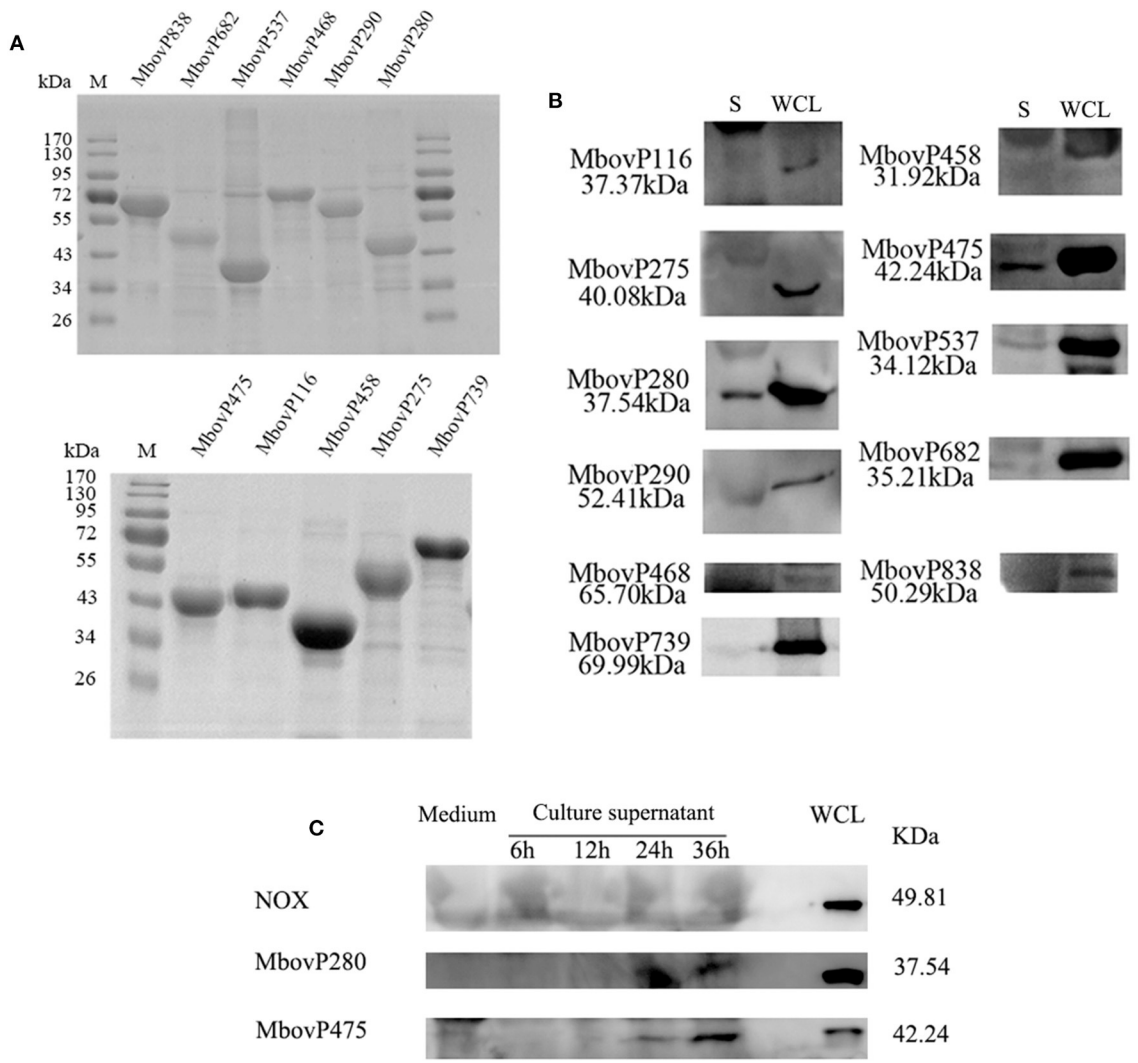

FIGURE 1 | Secretion of MbovP280. **(A)** Purification of 11 predicted secreted proteins. The proteins were purified with nickel affinity chromatography and resolved with SDS-PAGE. **(B)** Confirmation of the predicted secreted proteins with western blotting assays. Secretome (S) and whole-cell lysate (WCL) of *M. bovis* were resolved with SDS-PAGE and transferred onto polyvinylidene difluoride membranes. Polyclonal antibodies directed against rMbovP280, rMbovP290, rMbovP475, rMbovP468, rMbovP838, rMbovP537, rMbovP458, rMbovP682, rMbovP116, rMbovP275, and rMbovP739 were used to detect the proteins in the secretome. **(C)** Visualization of the secreted MbvoP280 in culture supernatant. *M. bovis* HB0801 was cultured in PPLO medium. The culture supernatant was collected and concentrated at 6, 12, 24, and 36 h after incubation. The antiserum against rMbovP280 and rMbovP475 were used to detect the proteins in the supernatant, while *M. bovis* NOX known as the membrane-associated protein served as the negative control (NC).

the macrophages of bovine origin is more sensitive to MbovP280 of *M. bovis*, the bovine pathogen, than the cells of mouse origin. However, rMbovP475 had no significant effect on the viability of either BoMac or RAW cells (**Figures 2A,B**).

A BLAST analysis with MolliGen 3.0 revealed that MbovP280 only shares some homology with genes in *M. agalactiae* strain PG2, including MAG2400 (GenBank accession no. CAL58938.1, similarity = 62%), MAG2410 (GenBank accession no. CAL58939.1, similarity = 36%), and MAG7060 (GenBank accession no. CAL59406.1, similarity = 31%). MbovP280 was also predicted to contain a conserved coiled-coil domain in the fragment defined by amino acids 210–269, which was predicted with COILS. This domain is potentially involved in protein–protein interactions (**Figure 2C**). To verify the role of the coiled-coil domain in reducing cell viability, the Mbov_0280 gene was mutated by deleting the coiled-coil domain, and the resultant recombinant protein MbovP280$^{\Delta 210-269}$ was expressed. The relative viability of BoMac treated with different concentrations of rMbovP280 and rMbovP280$^{\Delta 210-269}$ was determined in parallel, with a CCK-8 kit, and decreased significantly as the rMbovP280 concentration increased from 0.25 μM to 1 μM ($p < 0.001$). However, treatment with rMbovP280$^{\Delta 210-269}$ at any concentration (0.25, 0.50, or 1 μM) had no effect on BoMac viability (**Figure 2D**).

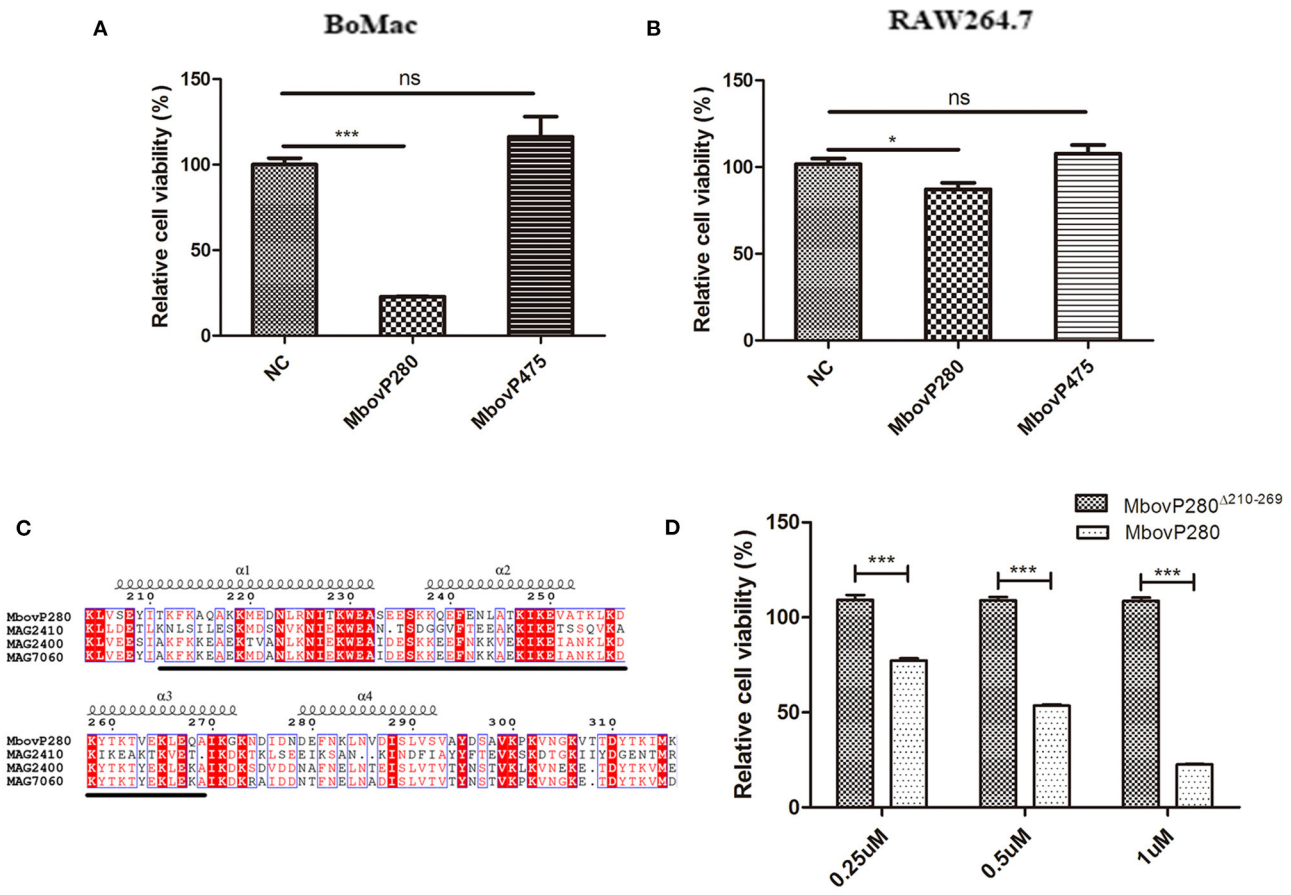

FIGURE 2 | Viability change of macrophages stimulated with the recombinant proteins of *M.bovis*. **(A)** BoMac cells (5×10^3 per well) or **(B)** RAW264.7 cells (1×10^4) were treated with either 1 μM MbovP280 or 1 μM MbovP475 for 24 h, and then CCK-8 was added to each well to determine cell viability. Wells treated with PBS were used as the negative control (NC). **(C)** Proteins homologous to MbovP280 in *Mycoplasma agalactiae* were identified with MolliGen 3.0 (http://services.cbib.u-bordeaux.fr/molligen/). Amino acids 210–269 (black underline) were predicted to form a coiled-coil domain. A protein alignment was constructed with the ClustalW multiple sequence alignment programs (https://www.ebi.ac.uk/Tools/msa/clustalw2/) combined with ESPript 3.0 (http://espript.ibcp.fr/ESPript/ESPript/). **(D)** Relative cell viability of BoMac (5×10^3 cells per well) treated with MbovP280 or MbovP280$^{\Delta 210-269}$ at concentrations of 0.25, 0.5, or 1 μM for 24 h was tested with a CCK-8 assay. $^*p < 0.05$, $^{***}p < 0.001$ indicate statistically significant differences; while ns indicates no difference.

Induction of BoMac Apoptosis by MbovP280 Is Associated With Expression of Cellular CRYAB

To investigate the mechanism underlying the reduction in cell viability induced by MbovP280, the ability of rMbovP280 to reduce cell viability of BoMac was assayed with CCK-8. This assay demonstrated that rMbovP280 significantly reduced the cell viability of BoMac in a dose-dependent way (between 0.25 and 1.00 μM) (**Figure 3A**). In contrast, the mutant MbovP280$^{\Delta 210-269}$ at 0.25 and 0.50 μM did not apparently reduce the cell viability of BoMac presenting the levels of cell viability similar to those in the negative control. However, 1.00 μM MbovP280$^{\Delta 210-269}$ reduced cell viability, but the level was much lower than that in the rMbovP280-treated group (**Figure 3B**).

Further, the Mbov_0280 knockout mutant T9.297 and its complementary strain CT9.297 in which the fragment of the whole gene Mbov_0280 was inserted into the mutant T9.297, were constructed and confirmed with DNA sequencing. Although the growth curves of the three strains (HB0801, CT9.297, and T9.297) did not differ significantly (**Figure 3C**), the western blotting assay demonstrated that MbovP280 was expressed in both *M.bovis* HB0801 and CT9.297 strains, but not in the mutant T9.297 strain (**Figure 3D**).

In order to further verify the apoptosis of BoMac specifically induced by MbovP280, the levels of cleaved caspase-3 in BoMac cells either infected with *M. bovis* strains or treated with rMbovP280 or its mutant were detected by western blot assays. As a result, the rMbovP280 increased the amount of cleaved caspase-3, while the rMbovP280$^{\Delta 210-269}$ did not (**Figure 3E**, **Supplementary Figure 3**). For the infection with *M. bovis* strains, the wild type strain HB0801 and complementary strain CT9.297 increased the levels of cleaved caspase-3 in BoMac, however the Mbov_0280 knock-out mutant T9.297 didn't (**Figure 3F**, **Supplementary Figure 3**).

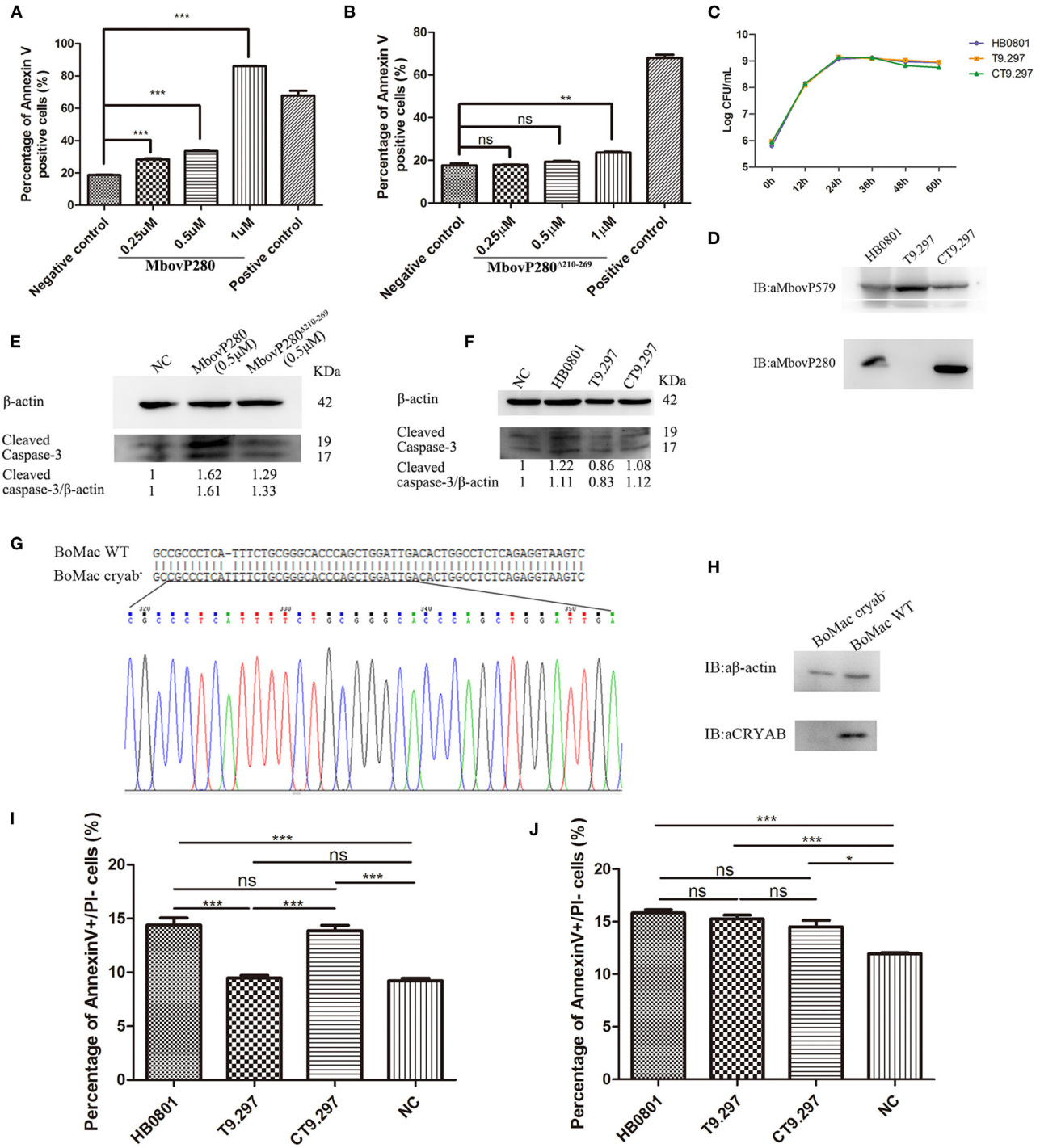

FIGURE 3 | Apoptosis of BoMac cells induced by MbovP280 in mycoplasmas cells or as the recombinant protein. Cells (5×10^5 per well) were treated with MbovP280 **(A)** or MbovP280$^{\Delta 210-269}$ **(B)** at concentrations of 0.25, 0.5, or 1 μM for 24 h. The cells were then stained with annexin V and propidium iodide (PI) and detected with flow cytometry. **(C)** Growth curves of strains HB0801, the Mbov_0280 mutant T9.297, and its complement CT9.297. Growth of *M. bovis* at each time point was determined with a plating assay. **(D)** Visualization of MbovP280 expression in T9.297 and CT9.297 strains with a western blotting assay. Wild-type strain HB0801 was used as the positive control. **(E)** The cleaved caspase-3 of BoMac cells treated with rMbovP280. The cell lysates of BoMac treated with 0.5 μM rMbovP280 or rMbovP280$^{\Delta 210-269}$ were resolved with SDS-PAGE, transferred onto membrane, and then immunodetected with an antibody directed against cleaved caspase-3. β-actin was used as the internal control. The ratio of the amount of cleaved caspase-3 to the amount of β-actin was calculated and normalized to the NC. **(F)** The cleaved caspase-3 of BoMac cells infected with *M. bovis*. The cell lysates of BoMac infected with HB0801, T9.297, or CT9.297 (MOI = 1,000) were resolved

(Continued)

FIGURE 3 | with SDS-PAGE, transferred onto PVDF membrane, and then immunodetected with the antibody directed against cleaved caspase-3. β-actin was used as the internal control. The ratio of the amount of cleaved caspase-3 to the amount of β-actin was calculated and normalized to the NC. **(G)** Single peak around the protospacer adjacent motif (PAM) in the sequence of BoMac cryab$^-$ clonal cell line. BLAST analysis of sequences around the PAM sequence of WT BoMac (BoMac WT) and BoMac cryab$^-$ cell lines. **(H)** Expression of CRYAB in BoMac WT and BoMac cryab$^-$ cells. Whole-cell lysates of BoMac WT and BoMac cryab$^-$ cells were resolved with SDS-PAGE, transferred onto membrane, and then immunodetected with the antibody directed against CRYAB. β-actin was used as the internal control. **(I)** Early apoptosis of BoMac induced by HB0801, T9.297, or CT9.297 was compared. BoMac (5×10^5 cells per well) were treated with 5×10^8 CFU of HB0801, T9.297, or CT9.297, or with PBS for 24 h. The cells only stained with annexin V are defined as undergoing early apoptosis. **(J)** Early apoptosis of BoMac-cryab$^-$ cell line induced by *M. bovis*. BoMac (5×10^5 cells per well) were infected with HB0801 (5×10^8 CFU), T9.297 (5×10^8 CFU), or CT9.297 (5×10^8 CFU), or treated with PBS (NC) for 24 h. $^*p < 0.05$, $^{**}p < 0.01$, $^{***}p < 0.001$ indicate statistically significant differences; ns indicates no difference.

The *CRYAB* gene of BoMac was knocked out with the CRISPR-Cas9 lentiviral system. Then the genome of the *CRYAB*-knockout cell line (BoMac-cryab$^-$) was isolated and used as the template to amplify the edited sequence. The sequencing results indicated that the *CRYAB* gene was correctly mutated by the insertion of an additional T at nt 159 in the CDS of the *CRYAB* gene (**Figure 3G**). The deficiency of CRYAB expression in the clonal cell line (BoMac-cryab$^-$) was confirmed with a western blotting assay (**Figure 3H**).

Further, the flow cytometry was used to test the apoptosis of BoMac-cryab$^-$ cell line and its WT BoMac induced by the three strains of *M. bovis*: HB0801, the Mbov_0280 knock-out mutant T9.297, and its complementary strain CT9.297 after stained with annexin V and PI. As a result, the proportions of the cells at the early stage of apoptosis stained only by annexin V were apparently associated with MbovP280 stimulation. In WT BoMac, the apoptosis levels induced by HB0801, T9.297, CT9.297, and PBS were 14.40, 9.48, 13.87, and 9.21%, respectively. There is no difference in the apoptosis levels between HB0801/CT9.297; and T9.297/NC (PBS) groups ($p > 0.05$); However, there is a significant difference between HB0801/T9.297, CT9.297/T9.297, HB0801/NC, and CT9.297/NC ($p < 0.001$) (**Figure 3I**). In contrast, in BoMac-cryab$^-$ cells, the levels of apoptosis induced by HB0801 (15.83%), T9.297 (15.27%), and CT9.297 (14.5%) did not change significantly ($p > 0.05$), although all three strains indeed generated some degree of cellular apoptosis compared to NC ($p < 0.05$) suggesting there is some other mechanism in *M. bovis* to induce BoMac apoptosis independent of MbovP280/CRYAB (**Figure 3J**). Taken altogether, these results revealed that the induction of apoptosis by MbovP280 depends on the expression of CRYAB and the amino acids 210–269 in MbovP280 constitute an essential domain for this function.

CRYAB Is a Ligand of MbovP280

Confocal laser microscopy was used to observe the binding of MbovP280 to BoMac. As shown in **Figure 4A**, rMbovP280 bound strongly to BoMac cells after it was incubated with the cells for 1 h at 37°C, demonstrated by the co-localization (merged yellow signal) of rMbovP280 (green) and F-actin (red).

Further the IP–MS method was to screen for MbovP280-binding proteins by using the antisera against rMbovP280 and rMbovP280$^{\Delta 210-269}$ to catch the interactive components from lysates of the BoMac cells, separated by Protein A/G Agarose Beads and resolved by SDS-PAGE and specific bands were analyzed with mass spectrometry (MS). As a result, two specific bands (arrows) from BoMac were precipitated by rMbovP280, but not by rMbovP280$^{\Delta 210-269}$. And the asterisks represent MbovP280 or MbovP280$^{\Delta 210-269}$ (**Figure 4B**). Then the bands were subject to be assayed with MS and the resultant proteomics data have been deposited to the ProteomeXchange Consortium via the PRIDE partner repository with the dataset identifier PXD022080. From the MS data, CRYAB, endothelin 2, lipocalin 2, THO complex subunit 4, and DCN1-like protein were preliminarily identified. Among these, CRYAB had the highest percentage coverage (12.57%) (**Table 3**). CRYAB is a known anti-apoptosis protein, which is consistent with our previous finding that MbovP280 induced the apoptosis of its host cells. Therefore, further experiments were performed to verify the interaction between CRYAB and MbovP280.

HEK293T cells were cotransfected with plasmids expressing Flag–CRYAB and HA–MbovP280, and a Co-IP assay was performed. The total cellular proteins were prepared and the components immunoprecipitated with either the anti-Flag or anti-HA antibodies. The precipitates were resolved with SDS-PAGE and analyzed with either the anti-HA or anti-Flag antibody by western blotting assays. As shown in **Figure 4C**, **Supplementary Figure 4**, the coprecipitated MbovP280 was detected in the compounds precipitated with anti-Flag antibody, and the coprecipitated CRYAB was detected in the compounds precipitated with anti-HA antibody. These results confirmed that MbovP280 specifically interacted with CRYAB.

DISCUSSION

A number of software are usually used to predict the secreted proteins of *Mycoplasma* species *in silico*. The SignalP4.1 server is used to identify the classically secreted proteins, such as P80 of *M. hominis* (11), which are secreted after the cleavage of the signal peptide, and the SecretomeP 2.0 server is used to predict the non-classical secreted proteins, which may be secreted independently of any signal peptide (27), for example via the extracellular vesicles recently identified in *M. mycoides* subsp. *mycoides* (16) and *Acholeplasma laidlawii* PG8 (28). However, these predictions should be confirmed with other methods, such as western blotting assays. During this study, only two of 11 predicted secreted proteins (MbovP280 and MbovP475) were confirmed as both highly expressed and immunogenic (**Figure 1B**) suggesting the difficulties in identifying the secreted proteins of mycoplasmal species. Several factors might affect this process, including the reliability of prediction, the relative times and levels of expression and the immunogenicity of the

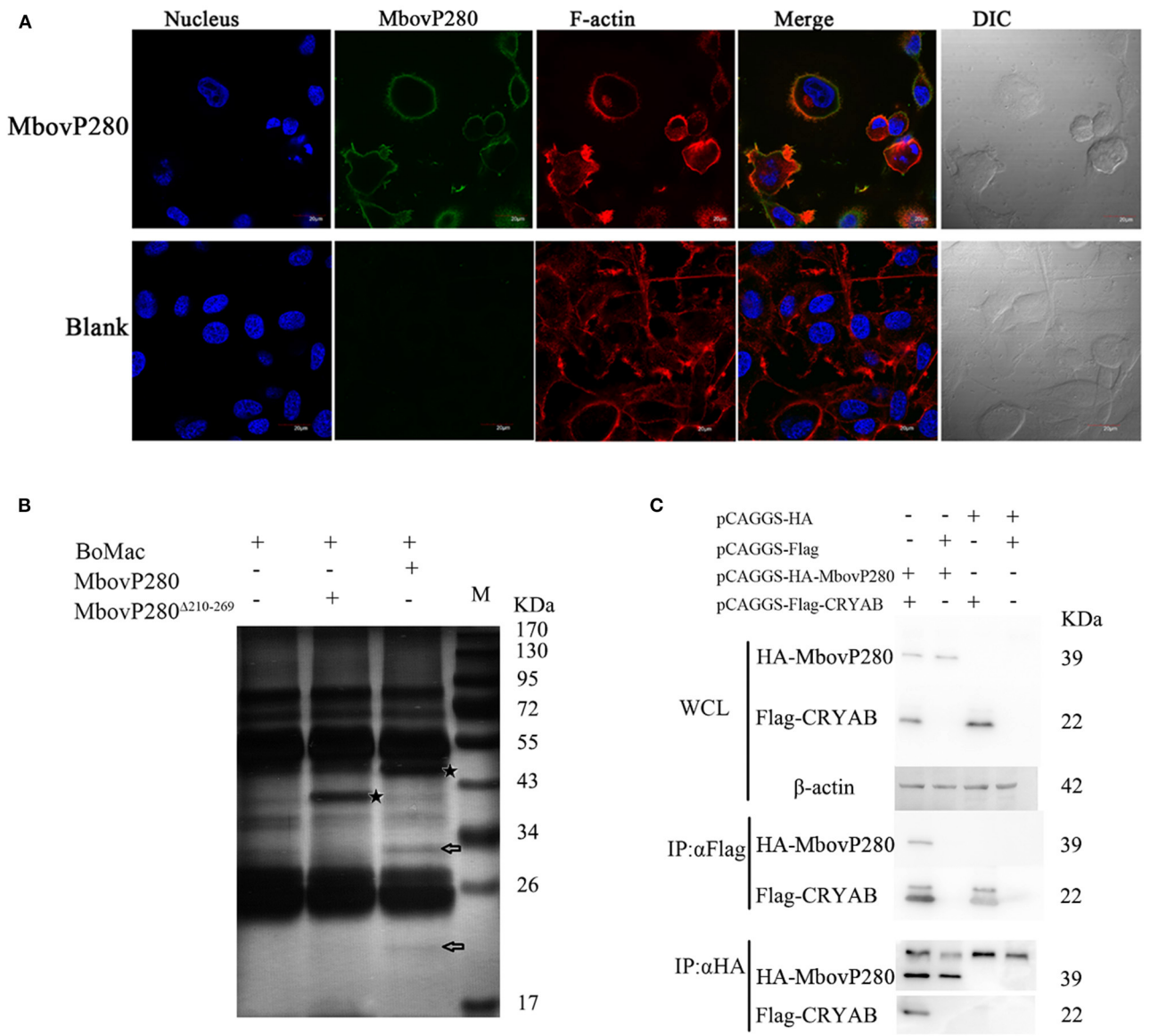

FIGURE 4 | Interaction between MbovP280 and BoMac. **(A)** Binding assay of MbovP280 to BoMac cells. BoMac cells (1×10^5) were incubated with 0.5 μM MbovP280 for 1 h at 37°C. MbovP280 was probed with polyclonal antibody directed against MbovP280 (1:500) and Alexa-Fluor-488-conjugated anti-IgG antibody (1:1,000) (green). Nuclei were stained with DAPI (5 μg/ml) and actin filaments with rhodamine phalloidin (100 nM). **(B)** Identification of MbovP280-binding ligands with mass spectrometry. BoMac cell lysates were incubated with MbovP280 (10 μg), MbovP280$^{\Delta 210-269}$ (10 μg), or PBS, and immunoprecipitated (IP) with a polyclonal antibody directed against MbovP280 (5 μg) and agarose bead (50 μl) labeled with Protein A/G. Arrows indicate specific MbovP280-binding ligands resolved with SDS-PAGE. And the asterisks represent either MbovP280 or MbovP280$^{\Delta 210-269}$. **(C)** Interaction between MbovP280 and CRYAB. At 32 h post transfection with plasmids encoding HA, HA–MbovP280, Flag, or Flag–CRYAB, HEK293T cells were harvested and the whole-cell lysates were immunoprecipitated with commercial antibodies directed against either the HA or Flag tag, and Protein A/G agarose beads. MbovP280 and CRYAB were then detected with western blotting assays using the antibodies against either the HA or Flag tags.

secreted proteins, the complex background of proteins in the media (derived from serum and yeast extracts), and the strong contamination of the secretomes with cytoplasmic proteins during the extraction process (29). Because the lipoproteins of mycoplasmas usually function as virulence factors, such as OppA, a lipoprotein of both *M. agalactiae* and *M. fermentans* that induces apoptosis (16, 30), the secreted lipoproteins MbovP280 and MbovP475 could play critical roles in the pathogenesis of *M. bovis*.

It has previously been reported that *M. bovis* functions as an inducer or inhibitor of the apoptosis of infected cells, probably dependent on the strain or cell type infected

(31, 32). For example, *M. bovis* induced the apoptosis of bovine peripheral blood mononuclear cells (PBMCs) (31) and macrophages (33), but is also reported to inhibit the apoptosis of PBMCs, monocytes, primary bovine macrophages, and bovine macrophages (32, 34–36). However, few studies have determined the specific mechanism responsible for this effect.

In this study, we first demonstrated that MbovP280 significantly reduced cell viability and then confirmed it induced the apoptosis of BoMac when applied as either mycoplasmal cells or the purified recombinant protein. However, there is a large discrepancy in proportions of apoptotic cells between induction of purified rMbovP280 (25–80%) and *M. bovis* infection (about 15%). We think this discrepancy might be caused by following reasons. Firstly, the amount of purified rMbovP280 used to treat BoMac is larger than the amount of MbovP280 naturally expressed by the HB0801 strains. Secondly, in *M. bovis* strains, there may be other proteins except MbovP280 function as either inducers or inhibitors of the apoptosis. Therefore, the overall effect of MbovP280 in the strain on apoptosis might be partially contradicted. Since the secreted proteins in the cultural supernatant is very low, the further study should verify whether the concentration of secreted MbovP280 of *M. bovis* increases or not under natural infection and the increase concentration of MbovP280 is necessary to induce apoptosis.

TABLE 3 | MbovP280-binding ligands in BoMac screened with IP-MS.

Protein	UniProt ID	Unique Peptide Count	Percentage coverage	MW (kDa)	PI
α-Crystallin B chain	V6F832	2	12.57%	20.1	6.76
Endothelin 2	Q867A9	1	2.82%	19.7	10.46
Lipocalin 2	E1B6Z6	1	3.50%	22.9	9.35
THO complex subunit 4	Q3T0I4	2	7.00%	26.9	11.15
DCN1-like protein	F1MRG9	1	1.93%	29.6	6.21

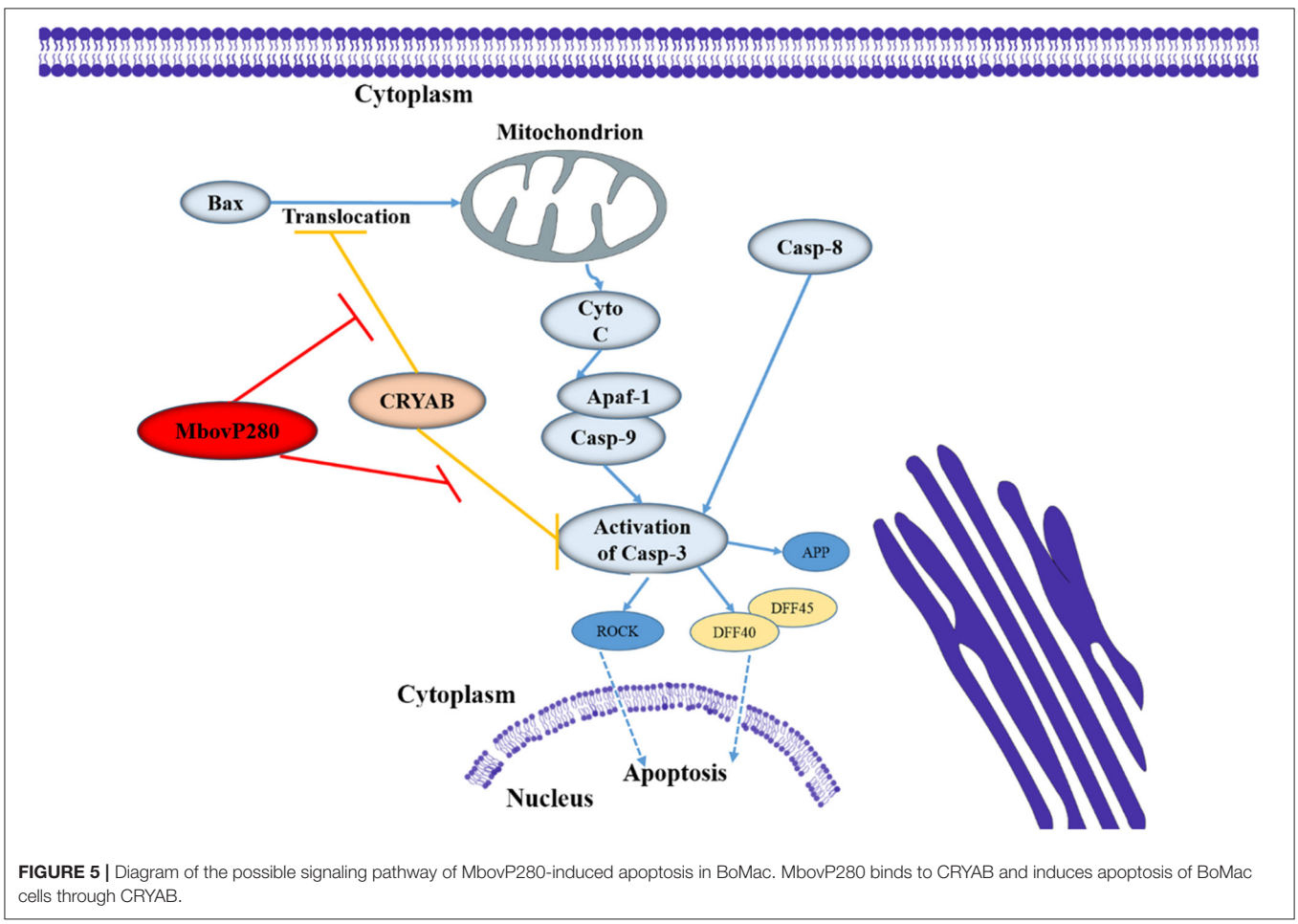

FIGURE 5 | Diagram of the possible signaling pathway of MbovP280-induced apoptosis in BoMac. MbovP280 binds to CRYAB and induces apoptosis of BoMac cells through CRYAB.

CRYAB is a molecular chaperone that is induced by stress and suppresses the aggregation of denatured proteins (37). It belongs to the conserved small heat shock protein family and is highly constitutively expressed in human cancers. Recent studies have shown that CRYAB inhibits apoptosis during myogenic differentiation (38) or differentiation induced by a wide range of stimuli, such as staurosporine, tumor necrosis factor α (TNF-α), UVA irradiation, okadaic acid, hydrogen peroxide, and TNF-related apoptosis-inducing ligand (TRAIL) (39–44). Several studies have demonstrated that CRYAB inhibits apoptosis by suppressing the activation of caspase 3 by interacting with its precursor (38, 45), and by interacting with Bcl-XS and Bax to suppress their translocation (41, 46). In the present study, IP-MS, and Co-IP methods were used to identify the interaction between MbovP280 and CRYAB in BoMac, and confirmed that CRYAB is a specific ligand of MbovP280. A homology model of CRYAB, MbovP280, and caspase 3 was established with SWISS-MODEL, and protein–protein docking was examined with ClusPro 2.0. The results suggested that MbovP280 and the caspase 3 precursor competitively bind to the surface pocket of the CRYAB protein (**Supplementary Figure 5**) to suppress the anti-apoptosis effect of CRYAB (**Figure 5**).

In conclusion, in this study, we have demonstrated that MbovP280 is a highly expressed and immunogenic secreted protein that induces the apoptosis of BoMac through its ligand CRYAB and the functional domain is located at amino acids 210–269 which form a coiled-coil domain.

DATA AVAILABILITY STATEMENT

The datasets presented in this study can be found in online repositories. The names of the repository/repositories and accession number(s) can be found in the article/**Supplementary Material**.

ETHICS STATEMENT

The animal study was reviewed and approved by Experimental Animal Ethics Committee of Huazhong Agricultural University.

AUTHOR CONTRIBUTIONS

GZ, HZ, and AG: study design. GZ and XZ: study conduct. YC, CH, and HC: data analysis and interpretation. GZ, AG, and ES: wrote the manuscript with all authors providing feedback.

FUNDING

This work was supported by National Natural Science Foundation of International (Regional) Cooperation Projects (#31661143015), Special Fund for Chinese Agricultural Research System (Beef/yaks) (#CARS-37), the Special Fund for National Distinguished Scholars in Agricultural Research and Technical Innovative Team and the Fundamental Research Funds for the Central Universities (2013QC001).

SUPPLEMENTARY MATERIAL

The Supplementary Material for this article can be found online at: https://www.frontiersin.org/articles/10.3389/fimmu.2021.619362/full#supplementary-material

Supplementary Figure 1 | Secretion of predicted secreted proteins was detected with western blotting assays. Secretome (S) and whole-cell lysate (WCL) of *M. bovis* were resolved with SDS-PAGE, transferred onto the polyvinylidene difluoride membranes, and immunodetected with polyclonal antibodies in the antisera directed against each predicted protein.

Supplementary Figure 2 | Verification of secreted MbovP280 and MbovP475 in culture supernatant with western blotting assays. *M. bovis* HB0801 was cultured in PPLO medium and culture supernatant was collected and concentrated at 6, 12, 24, and 36 h. Polyclonal antibodies in the antisera against rMbovP280 and rMbovP475 were used to detect the proteins in the supernatant, while the known *M. bovis* membrane-associated protein NOX served as negative control.

Supplementary Figure 3 | MbovP280 increased the levels of cleaved caspase-3. The cell lysates of BoMac cells treated with 0.5 μM rMbovP280 or rMbovP280$^{\Delta 210-269}$ or infected with *M. bovis* strains (MOI = 1,000) were resolved with SDS-PAGE, transferred onto the polyvinylidene difluoride membrane, and then immunodetected with the antibody directed against cleaved caspase-3. β-actin was used as the internal control.

Supplementary Figure 4 | Interaction between MbovP280 and CRYAB. **(A)** Expression of MbovP280 and CRYAB in HEK293T cells at 32 h after transfection with the plasmids encoding HA or HA–MbovP280 together with the plasmids encoding Flag or Flag–CRYAB. **(B)** Interaction between MbovP280 and CRYAB was detected with a western blotting assay.The cell lysates were immunoprecipitated with the antibody against the Flag tag and immunoblotted with the antibody against the HA tag. **(C)** Interaction between MbovP280 and CRYAB was detected with a western blotting assay. The cell lysates were immunoprecipitated with the antibody against the HA tag and immunoblotted with the antibody against the Flag tag.

Supplementary Figure 5 | Images of protein–protein docking. **(A)** Homology model of CRYAB and the MbovP280 functional domain (amino acids 206–294) was generated with SWISS-MODEL. Protein–protein docking between CRYAB and MbovP280 (amino acids 206–294) was established with ClusPro 2.0. **(B)** Homology model of CRYAB and caspase 3 was generated with SWISS-MODEL. Protein–protein docking between CRYAB and caspase 3 was established with ClusPro 2.0.

Supplementary Table 1 | The predicted secreted lipoproteins of *Mycoplasma bovis*.

REFERENCES

1. Caswell JL, Bateman KG, Cai HY, Castillo-Alcala F. *Mycoplasma bovis* in respiratory disease of feedlot cattle. *Vet Clin North Am Food Anim Pract.* (2010) 26:365–79. doi: 10.1016/j.cvfa.2010.03.003
2. Nicholas RA. Bovine mycoplasmosis: silent and deadly. *Vet Rec.* (2011) 168:459–62. doi: 10.1136/vr.d2468
3. Zhang R, Han X, Chen Y, Mustafa R, Qi J, Chen X, et al. Attenuated *Mycoplasma bovis* strains provide protection against virulent infection in calves. *Vaccine.* (2014) 32:3107–14. doi: 10.1016/j.vaccine.2013.12.004
4. Arcangioli MA, Duet A, Meyer G, Dernburg A, Bezille P, Poumarat F, et al. The role of *Mycoplasma bovis* in bovine respiratory disease outbreaks in veal calf feedlots. *Vet J.* (2008) 177:89–93. doi: 10.1016/j.tvjl.2007.03.008
5. Sachse K, Helbig JH, Lysnyansky I, Grajetzki C, Muller W, Jacobs E, et al. Epitope mapping of immunogenic and adhesive structures in repetitive domains of *Mycoplasma bovis* variable surface lipoproteins. *Infect Immun.* (2000) 68:680–7. doi: 10.1128/IAI.68.2.680-687.2000

6. Guo Y, Zhu H, Wang J, Huang J, Khan FA, Zhang J, et al. TrmFO, a fibronectin-binding adhesin of *Mycoplasma bovis*. *Int J Mol Sci.* (2017) 18:1732. doi: 10.3390/ijms18081732
7. Zhao G, Zhang H, Chen X, Zhu X, Guo Y, He C, et al. *Mycoplasma bovis* NADH oxidase functions as both a NADH oxidizing and O_2 reducing enzyme and an adhesin. *Sci Rep.* (2017) 7:44. doi: 10.1038/s41598-017-00121-y
8. Wang Y, Liu S, Li Y, Wang Q, Shao J, Chen Y, et al. *Mycoplasma bovis*-derived lipid-associated membrane proteins activate IL-1beta production through the NF-kappaB pathway via toll-like receptor 2 and MyD88. *Dev Comp Immunol.* (2016) 55:111–8. doi: 10.1016/j.dci.2015.10.017
9. Gondaira S, Higuchi H, Iwano H, Nakajima K, Kawai K, Hashiguchi S, et al. Cytokine mRNA profiling and the proliferative response of bovine peripheral blood mononuclear cells to *Mycoplasma bovis*. *Vet Immunol Immunopathol.* (2015) 165:45–53. doi: 10.1016/j.vetimm.2015.03.002
10. Zbinden C, Pilo P, Frey J, Bruckmaier RM, Wellnitz O. The immune response of bovine mammary epithelial cells to live or heat-inactivated *Mycoplasma bovis*. *Vet Microbiol.* (2015) 179:336–40. doi: 10.1016/j.vetmic.2015.07.007
11. Hopfe M, Hoffmann R, Henrich B. P80, the HinT interacting membrane protein, is a secreted antigen of *Mycoplasma hominis*. *BMC Microbiol.* (2004) 4:46. doi: 10.1186/1471-2180-4-46
12. Djordjevic SP, Cordwell SJ, Djordjevic MA, Wilton J, Minion FC. Proteolytic processing of the *Mycoplasma hyopneumoniae* cilium adhesin. *Infect Immun.* (2004) 72:2791–802. doi: 10.1128/IAI.72.5.2791-2802.2004
13. Yamamoto T, Kida Y, Sakamoto Y, Kuwano K. Mpn491, a secreted nuclease of *Mycoplasma pneumoniae*, plays a critical role in evading killing by neutrophil extracellular traps. *Cell Microbiol.* (2017) 19:e12666. doi: 10.1111/cmi.12666
14. Kannan TR, Krishnan M, Ramasamy K, Becker A, Pakhomova ON, Hart PJ, et al. Functional mapping of community-acquired respiratory distress syndrome (CARDS) toxin of *Mycoplasma pneumoniae* defines regions with ADP-ribosyltransferase, vacuolating and receptor-binding activities. *Mol Microbiol.* (2014) 93:568–81. doi: 10.1111/mmi.12680
15. Zhang H, Zhao G, Guo Y, Menghwar H, Chen Y, Chen H, et al. *Mycoplasma bovis* MBOV_RS02825 encodes a secretory nuclease associated with cytotoxicity. *Int J Mol Sci.* (2016) 17:628. doi: 10.3390/ijms17050628
16. Gaurivaud P, Ganter S, Villard A, Manso-Silvan L, Chevret D, Boule C, et al. Mycoplasmas are no exception to extracellular vesicles release: revisiting old concepts. *PLoS ONE.* (2018) 13:e0208160. doi: 10.1371/journal.pone.0208160
17. Paes JA, Lorenzatto KR, de Moraes SN, Moura H, Barr JR, Ferreira HB. Secretomes of *Mycoplasma hyopneumoniae* and *Mycoplasma flocculare* reveal differences associated to pathogenesis. *J Proteomics.* (2017) 154:69–77. doi: 10.1016/j.jprot.2016.12.002
18. Rebollo Couto MS, Klein CS, Voss-Rech D, Terenzi H. Extracellular proteins of *Mycoplasma synoviae*. *ISRN Vet Sci.* (2012) 2012:802308. doi: 10.5402/2012/802308
19. Rasheed MA, Qi J, Zhu X, Chenfei H, Menghwar H, Khan FA, et al. Comparative genomics of *Mycoplasma bovis* strains reveals that decreased virulence with increasing passages might correlate with potential virulence-related factors. *Front Cell Infect Microbiol.* (2017) 7:177. doi: 10.3389/fcimb.2017.00177
20. Qi J, Guo A, Cui P, Chen Y, Mustafa R, Ba X, et al. Comparative geno-plasticity analysis of *Mycoplasma bovis* HB0801 (Chinese Isolate). *PLoS ONE.* (2012) 7:e38239. doi: 10.1371/journal.pone.0038239
21. Stabel JR, Stabel TJ. Immortalization and characterization of bovine peritoneal macrophages transfected with SV40 plasmid DNA. *Vet Immunol Immunopathol.* (1995) 45:211–20. doi: 10.1016/0165-2427(94)05348-V
22. Khan F, Chao J, Liu K, Chen X, Zhao G, Menghwar H, et al. Immunoproteomic identification of MbovP579, a promising diagnostic biomarker for serological detection of *Mycoplasma bovis* infection. *Oncotarget.* (2016) 7:39376–95. doi: 10.18632/oncotarget.9799
23. Wang D, Chen J, Yu C, Zhu X, Xu S, Fang L, et al. 2019. Porcine reproductive and respiratory syndrome virus nsp11 antagonizes type I interferon signaling by targeting IRF9. *J Virol.* (2019) 93:e00623-19. doi: 10.1128/JVI.00623-19
24. Zhu X, Baranowski E, Dong Y, Li X, Hao Z, Zhao G, et al. An emerging role for cyclic dinucleotide phosphodiesterase and nanoRNase activities in *Mycoplasma bovis*: securing survival in cell culture. *PLoS Pathog.* (2020) 16:e1008661. doi: 10.1371/journal.ppat.1008661
25. Baranowski E, Guiral S, Sagne E, Skapski A, Citti C. Critical role of dispensable genes in *Mycoplasma agalactiae* interaction with mammalian cells. *Infect Immun.* (2010) 78:1542–51. doi: 10.1128/IAI.01195-09
26. Sanjana NE, Shalem O, Zhang F. Improved vectors and genome-wide libraries for CRISPR screening. *Nat Methods.* (2014) 11:783–4. doi: 10.1038/nmeth.3047
27. Bendtsen JD, Kiemer L, Fausboll A, Brunak S. Non-classical protein secretion in bacteria. *BMC Microbiol.* (2005) 5:58. doi: 10.1186/1471-2180-5-58
28. Chernov VM, Mouzykantov AA, Baranova NB, Medvedeva ES, Grygorieva TY, Trushin MV, et al. Extracellular membrane vesicles secreted by mycoplasma Acholeplasma laidlawii PG8 are enriched in virulence proteins. *J Proteomics.* (2014) 110:117–28. doi: 10.1016/j.jprot.2014.07.020
29. Weng Y, Sui Z, Shan Y, Jiang H, Zhou Y, Zhu X, et al. In-depth proteomic quantification of cell secretome in serum-containing conditioned medium. *Anal Chem.* (2016) 88:4971–8. doi: 10.1021/acs.analchem.6b00910
30. Hopfe M, Henrich B. OppA, the ecto-ATPase of *Mycoplasma hominis* induces ATP release and cell death in HeLa cells. *BMC Microbiol.* (2008) 8:55. doi: 10.1186/1471-2180-8-55
31. Vanden Bush TJ, Rosenbusch RF. *Mycoplasma bovis* induces apoptosis of bovine lymphocytes. *FEMS Immunol Med Microbiol.* (2002) 32:97–103. doi: 10.1111/j.1574-695X.2002.tb00540.x
32. Maina T, Prysliak T, Perez-Casal J. *Mycoplasma bovis* delay in apoptosis of macrophages is accompanied by increased expression of anti-apoptotic genes, reduced cytochrome C translocation and inhibition of DNA fragmentation. *Vet Immunol Immunopathol.* (2019) 208:16–24. doi: 10.1016/j.vetimm.2018.12.004
33. Burgi N, Josi C, Burki S, Schweizer M, Pilo P. *Mycoplasma bovis* co-infection with bovine viral diarrhea virus in bovine macrophages. *Vet Res.* (2018) 49:2. doi: 10.1186/s13567-017-0499-1
34. van der Merwe J, Prysliak T, Perez-Casal J. Invasion of bovine peripheral blood mononuclear cells and erythrocytes by *Mycoplasma bovis*. *Infect Immun.* (2010) 78:4570–8. doi: 10.1128/IAI.00707-10
35. Mulongo M, Prysliak T, Scruten E, Napper S, Perez-Casal J. *In vitro* infection of bovine monocytes with *Mycoplasma bovis* delays apoptosis and suppresses production of gamma interferon and tumor necrosis factor alpha but not interleukin-10. *Infect Immun.* (2014) 82:62–71. doi: 10.1128/IAI.00961-13
36. Suleman M, Prysliak T, Clarke K, Burrage P, Windeyer C, Perez-Casal J. *Mycoplasma bovis* isolates recovered from cattle and bison (Bison bison) show differential *in vitro* effects on PBMC proliferation, alveolar macrophage apoptosis and invasion of epithelial and immune cells. *Vet Microbiol.* (2016) 186:28–36. doi: 10.1016/j.vetmic.2016.02.016
37. Horwitz J. Alpha-crystallin can function as a molecular chaperone. *Proc Natl Acad Sci USA.* (1992) 89:10449–53. doi: 10.1073/pnas.89.21.10449
38. Kamradt MC, Chen F, Sam S, Cryns VL. The small heat shock protein αB-crystallin negatively regulates apoptosis during myogenic differentiation by inhibiting caspase-3 activation. *J Biol Chem.* (2002) 277:38731–36. doi: 10.1074/jbc.M201770200
39. Mao YW, Xiang H, Wang J, Korsmeyer S, Reddan J, Li DW. Human bcl-2 gene attenuates the ability of rabbit lens epithelial cells against H_2O_2-induced apoptosis through down-regulation of the alpha B-crystallin gene. *J Biol Chem.* (2001) 276:43435–45. doi: 10.1074/jbc.M102195200
40. Li DW, Xiang H, Mao YW, Wang J, Fass U, Zhang XY, et al. Caspase-3 is actively involved in okadaic acid-induced lens epithelial cell apoptosis. *Exp Cell Res.* (2001) 266:279–91. doi: 10.1006/excr.2001.5223
41. Mao YW, Liu JP, Xiang H, Li DW. Human alphaA- and alphaB-crystallins bind to Bax and Bcl-X(S) to sequester their translocation during staurosporine-induced apoptosis. *Cell Death Differ.* (2004) 11:512–26. doi: 10.1038/sj.cdd.4401384
42. Kamradt MC, Lu M, Werner ME, Kwan T, Chen F, Strohecker A, et al. The small heat shock protein alpha B-crystallin is a novel inhibitor of TRAIL-induced apoptosis that suppresses the activation of caspase-3. *J Biol Chem.* (2005) 280:11059–66. doi: 10.1074/jbc.M413382200
43. Adhikari AS, Singh BN, Rao KS, Rao Ch M. alphaB-crystallin, a small heat shock protein, modulates NF-kappaB activity in a phosphorylation-dependent manner and protects muscle myoblasts from TNF-alpha induced cytotoxicity. *Biochim Biophys Acta.* (2011) 1813:1532–42. doi: 10.1016/j.bbamcr.2011.04.009

44. Xu F, Yu H, Liu J, Cheng L. αB-crystallin regulates oxidative stress-induced apoptosis in cardiac H9c2 cells via the PI3K/AKT pathway. *Mol Biol Rep*. (2012) 40:2517–26. doi: 10.1007/s11033-012-2332-2
45. Kamradt MC, Chen F, Cryns VL. The small heat shock protein alpha B-crystallin negatively regulates cytochrome c- and caspase-8-dependent activation of caspase-3 by inhibiting its autoproteolytic maturation. *J Biol Chem*. (2001) 276:43435–45. doi: 10.1074/jbc.C100107200
46. Hu WF, Gong L, Cao Z, Ma H, Ji W, Deng M, et al. αA- and αB-crystallins interact with Caspase-3 and bax to guard mouse lens development. *Curr Mol Med*. (2012) 12:177–87. doi: 10.2174/156652412798889036

Conflict of Interest: The authors declare that the research was conducted in the absence of any commercial or financial relationships that could be construed as a potential conflict of interest.

frontiers in Immunology

ORIGINAL RESEARCH
published: 02 June 2021
doi: 10.3389/fimmu.2021.678354

Stabilization of Hypoxia-Inducible Factor Promotes Antimicrobial Activity of Human Macrophages Against *Mycobacterium tuberculosis*

*Sebastian F. Zenk, Sebastian Hauck, Daniel Mayer, Mark Grieshober and Steffen Stenger**

Institute of Medical Microbiology and Infection Control, University Hospital Ulm, Ulm, Germany

Hypoxia-inducible factor (HIF) is a key oxygen sensor that controls gene expression patterns to adapt cellular metabolism to hypoxia. Pharmacological inhibition of prolyl-hydroxylases stabilizes HIFs and mimics hypoxia, leading to increased expression of more than 300 genes. Whether the genetic program initialized by HIFs affects immune responses against microbial pathogens, is not well studied. Recently we showed that hypoxia enhances antimicrobial activity against *Mycobacterium tuberculosis* (*Mtb*) in human macrophages. The objective of this study was to evaluate whether the oxygen sensor HIF is involved in hypoxia-mediated antimycobacterial activity. Treatment of *Mtb*-infected macrophages with the prolyl-hydroxylase inhibitor Molidustat reduced the release of TNFα and IL-10, two key cytokines involved in the immune response in tuberculosis. Molidustat also interferes with the p38 MAP kinase pathway. HIF-stabilization by Molidustat also induced the upregulation of the Vitamin D receptor and human β defensin 2, which define an antimicrobial effector pathway in human macrophages. Consequently, these immunological effects resulted in reduced proliferation of virulent *Mtb* in human macrophages. Therefore, HIFs may be attractive new candidates for host-directed therapies against infectious diseases caused by intracellular bacteria, including tuberculosis.

Keywords: tuberculosis, hypoxia, HIF, human, macrophages, Molidustat

OPEN ACCESS

Edited by:
Rosane M. B. Teles, University of California, Los Angeles, United States

Reviewed by:
Luciana Silva Rodrigues, Rio de Janeiro State University, Brazil
Evgeniya V. Nazarova, Genentech, United States

***Correspondence:**
Steffen Stenger
steffen.stenger@uniklinik-ulm.de

Specialty section:
This article was submitted to Microbial Immunology, a section of the journal Frontiers in Immunology

Received: *09 March 2021*
Accepted: *18 May 2021*
Published: *02 June 2021*

Citation:
Zenk SF, Hauck S, Mayer D, Grieshober M and Stenger S (2021) Stabilization of Hypoxia-Inducible Factor Promotes Antimicrobial Activity of Human Macrophages Against Mycobacterium tuberculosis. Front. Immunol. 12:678354. doi: 10.3389/fimmu.2021.678354

INTRODUCTION

Tuberculosis is an airborne infectious disease caused by *Mycobacterium tuberculosis* (*Mtb*), which primarily affects human lungs. Active tuberculosis is treated with a combination of isoniazid, rifampin, pyrazinamide and ethambutol for at least 6 months to achieve clearance of the pathogen and prevent the selection of drug resistant mutants (1). Drug resistance against *Mtb* was already

Abbreviations: CFU, colony forming units; hBD2, human ß defensin 2; HIF, Hypoxia inducible factor; MOI, multiplicity of infection; *Mtb*, *Mycobacterium tuberculosis*; PBMC, peripheral blood mononuclear cells; VDR, Vitamin D receptor.

described in 1948 when the very first human TB therapy trial using Streptomycin was conducted (2). In 2014 (3) *Mtb* isolated from approximately 1.9 million patients were isoniazid mono-resistant (13.3%) and multidrug resistant (MDR, 5.3%). 9.7% of individuals with MDR-TB had extensively drug-resistant (XDR) tuberculosis, which was reported by 105 countries (WHO, 2020). Infection with drug resistant *Mtb* requires longer and more-toxic treatment and is only moderately effective. Hence there is an urgent need for the development of novel strategies to treat tuberculosis (4). Modern concepts include host-targeted therapies to promote immune responses without toxicity and development of drug resistance.

HIFs are not only sensors for cellular hypoxia, but also control key functions of immune cells required for protection against microbial pathogens (5, 6). Though several HIF isoforms exist, HIF-1α is the most prominent and detected nearly in all innate immune populations (7). Under normoxia (20% O_2) HIF-1α is rapidly degraded by prolyl-hydroxylases, von Hippel-Lindau tumor suppressor protein and the proteasome (8). Hypoxia (pO_2 ≤1%) deactivates prolyl hydroxylases and consequently HIF-1α is stabilized and translocated into the nucleus. Here, the transcription of multiple target genes responsible for angiogenesis (e.g. vascular endothelial growth factor), cellular proliferation (e.g. erythropoietin), glucose metabolism (e.g. glucose transporters) as well as inflammation (e.g. inflammatory cytokines) are induced (9, 10).

Recently, others and we demonstrated that hypoxia is beneficial for the control of *Mtb* in macrophages obtained from humans and non-human primates (11, 12). Furthermore, pharmacological induction of hypoxia by VEGF-signaling in a *Mycobacterium marinum* zebrafish model reduced bacterial growth *in vivo* (13). There is evidence that HIF-1α plays an important role in innate immune responses directed against a wide variety of pathogens including group A and B streptococci, *Staphylococcus aureus*, *Salmonella typhimurium*, *Pseudomonas aeruginosa* and Mycobacteria (14). The myeloid HIF-response influences metabolism (cellular ATP pool), production of granule proteases (neutrophil elastase, cathepsin G), expression of antimicrobial peptides (cathelicidin), inducible nitric oxide and cytokines (TNFα, IL-1, IL-4, IL-6, IL-12) (7, 15–17). Recently we demonstrated that hypoxia upregulates an antimicrobial effector pathway mediated by the vitamin D receptor (VDR) and human β defensin 2 (hBD2) (12).

Proly hydroxylase inhibitors can be applied to stabilize HIFs in normoxic atmosphere and induce downstream antimicrobial effector functions. The HIF-stabilizers L-Mimosine and AKB-4924 showed therapeutic benefit in mouse models of *Staphylococcus aureus* skin infection (18, 19), and dimethyloxaloylglycine supported host defense in a *Mycobacterium marinum* zebrafish model (17). Currently several prolyl hydroxylase-inhibitors (FG-2216, Roxadustat, Daprodust, Molidustat and AKB-6548) are under evaluation in clinical trials or already approved for the treatment of renal anemia (20–23).

Given the complex downstream events orchestrated by HIF, any pharmacological manipulation of this pathway must consider potential harmful effects for the host, including susceptibility to microbial pathogens. Here, we investigated whether HIF-stabilization by the prolyl-hydroxylase inhibitor Molidustat modulates the immune response of human macrophages against the major human pathogen *Mtb*. Our results demonstrate a differential effect of Molidustat on the release of cytokines (reduction) and the VitD-mediated antimicrobial effector pathway (induction) ultimately resulting in reduced intracellular growth of virulent *Mtb*. These findings suggest that HIF-stabilization promotes the antimicrobial function of human macrophages and this pathway may provide a new target for host-directed therapies against tuberculosis.

MATERIALS AND METHODS

Cell Culture and Reagents

Primary human cells were cultured in RPMI 1640 (Life Technologies) supplemented with 2 mM glutamine (Sigma), 10 mM HEPES, 13 mM $NaHCO_3$, 100 µg/ml streptomycin, 60 µg/ml penicillin (all from Biochrom) and 5% heat-inactivated human AB serum (Sigma) (complete medium). For THP-1 cells (ATCC® TIB-202™, Institute for Medical Microbiology and Hygiene, Ulm University) heat-inactivated human AB serum was replaced by 20% fetal calf serum ([FCS] Sigma). For experiments involving the virulent laboratory strain *Mtb* H37Rv (ATCC® 27294™, Institute for Medical Microbiology and Hygiene, Ulm University) the medium was modified to optimize phagocytosis (non-heat-inactivated serum) and allow multiplication of the bacteria (no streptomycin). In order to prevent fungal growth 5.6 µg/ml Amphotericin B and 60 µg/ml Penicillin G were added. *Mtb*-extract was used as source for soluble mycobacterial antigens in a final concentration of 10 µg/ml. These antigens were generated by collecting the ultracentrifuged supernatant of mycobacterial cells that were repeatedly sonicated. Afterwards cell wall components and intracellular antigens were extracted (24). Molidustat (BAY 85-3934, Selleckchem) is a HIF-stabilizer (prolyl-hydroxylase inhibitor), which was dissolved in DMSO and serially diluted in PBS.

Hypoxia Chamber

A hypoxia chamber was tailor-made for the specific requirements of a biological safety level 3 facility (Toepffer Laboratories). The chamber represents a closed system that is accessible from the outside through aerosol tight gloves. Outgoing air is filtered through a high-efficiency particulate air (HEPA Class 14) filter to permit experiments with virulent *Mtb*. Materials and reagents are shuttled into the chamber *via* a sluice, such that the atmosphere remains constant at all times during the experiments. Temperature (37°C), CO_2 (5%), and humidity were constant, and O_2 and N_2 were adjusted according to the experimental requirements. All parameters were monitored by digital sensors.

Preparation of Macrophages and THP-1 Cells

Peripheral blood mononuclear cells (PBMC) were isolated by density gradient centrifugation of buffy coat preparations from anonymous donors (Institute of Transfusion Medicine, Ulm

University). Macrophages were generated from plastic-adherent PBMC cultured in the presence of granulocyte-macrophage colony-stimulating factor (GM-CSF, 10 ng/ml, Miltenyi) for 7 days. Macrophages were stored in liquid nitrogen if required. THP-1 cells (ATCC, TIB-202™) were differentiated to macrophages by treatment with phorbol 12-myristate 13-acetate (10ng/ml) for 18hrs.

Culture of Mycobacterium Tuberculosis

Mtb H37Rv was grown in suspension with gentle rotation in roller bottles containing Middlebrook 7H9 broth (BD Biosciences) supplemented with 1% glycerol (Roth), 0.05% Tween 80 (Sigma), and 10% Middlebrook oleic acid, albumin, dextrose, and catalase enrichment (BD Biosciences). Aliquots from logarithmically growing cultures were frozen in PBS/10% glycerol, and representative vials were thawed and enumerated for viable colony forming units (CFU). *Mtb* were sonicated in a pre-heated (37°C) water bath for 10 min prior to use.

Quantification of Extracellular and Intracellular Mycobacterial Growth

To determine the effects of Molidustat on extracellular *Mtb*, bacteria were cultured in 96 well plates in 7H9 broth. Iron supplementation was accomplished by addition of filtered (0.2 µm pores, Millipore) iron (II) sulfate heptahydrate ($FeSO_4$ * 7 H_2O, Sigma). *Mtb* were then incubated for 5 days. Subsequently extracellular bacteria were harvested by vigorous re-suspension, transferred into screw caps, and sonicated in a preheated (37°C) water bath for 10 min. Aliquots of the sonicate were serially diluted (1:10, 1:100, 1:1000) in cell culture medium without streptomycin. Four dilutions of each sample were plated on 7H11 agar plates (BD Biosciences) and incubated for 14 days before determining the number of CFU. To analyze the effects of Molidustat on intracellular *Mtb*, macrophages were infected with single-cell suspensions of *Mtb* at a multiplicity of infection (MOI) of 10 as bulk infection. After 18 hrs macrophages were washed with PBS to remove extracellular bacteria. Viability of macrophages was verified with the LIVE/DEAD® Kit (Invitrogen) and was approximately 95%. The percentage of infected macrophages was controlled regularly by acid-fast stain and was between 31 ± 17% with 1-10 bacilli per infected cell. Infected macrophages were then equally distributed into the wells of a culture plate before adding the stimuli which secures an equal bacillary burden in all samples at the beginning of the incubation period. After 5 days of culture, the number of viable bacilli was determined by plating cell lysates (0.3% saponin; Sigma) on 7H11 agar plates as described above.

Viability Assays

Annexin V/propidium iodide staining was performed using the "FITC Annexin V Apoptosis Detection Kit I" from BD Biosciences following the manufacturer's protocol. Data were analyzed by flow cytometry (FACSCalibur, BD) using FlowJo, version 10.1 (Tree Star Inc., Ashland, Oregon, USA).

Measurement of Cytokine Concentrations

Supernatants were harvested, and stored at -70°C. Supernatants from *Mtb*-infected cultures were filtered (0.2 µm) and sterility was confirmed by culture of filtered aliquots on 7H11 agar plates. The concentration of tumor necrosis factor α (TNF-α) and interleukin-10 (IL-10) was determined by enzyme linked immunosorbent assay (ELISA, R&D Systems) exactly as suggested by the manufacturer. Sensitivity of the ELISAs was regularly 32 pg/ml.

Western Blot Analysis

Macrophages (5-10 x 10^6/ml) were incubated with Molidustat and *Mtb*-extract for 16 ± 2 hrs. Subsequently cells were harvested with ice-cold PBS 1 mM EDTA and centrifuged (4°C, 16.000 g for 20 s). Pellets were lysed using CER I buffer (NE-PER™, Thermo Scientific), protease inhibitor cocktail tablets as well as phosphatase-inhibitor cocktail tablets (both from Roche). For HIF-1α detection proteins were purified directly from CER I buffer lysates containing nuclear and cytoplasmic protein fractions. Deferoxamine (DFO, Sigma) was used in a final concentration of 50 µM in order to prevent Prolylhydroxylase II mediated degradation of HIF-1α by Fe^{2+} chelation. Protein concentrations of lysates were adjusted to equal levels according to BCA Protein Assay (Pierce). Lysates containing 25–100 µg protein were boiled (10 min, 95°C) in Laemmli sample buffer (2 mM SDS (Roth); 0.3% Glycerol (Sigma); 63 mM Tris-HCl (Sigma), pH 6; 0.03% bromophenol blue (Biomol); 0.15% mercaptoethanol (Sigma)) and analyzed by SDS-Page (12%) and western blot. Membranes were probed overnight with HIF-1α mAb mouse (BD Biosciences) (1:1000), respectively. Afterwards donkey anti mouse alkaline phosphatase conjugated antibody (1:10.000, Jackson ImmunoResearch Laboratories) was used as secondary antibody. Proteins were detected by chemiluminescence (CDP Star, Roche) following the manufacturer's protocol. The same membrane was stripped (0.2 M Glycine (AppliChem GmbH); 3.5 mM SDS (Roth); 0.1% Tween 20 (Sigma), pH 2.2) and re-probed using β-Actin rabbit mAb (Cell Signaling Technology) (1:1000).

Phosphorylated p 38 (pp38) detection was performed with 7 x 10^5 THP-1 macrophages after 16 ± 2 hrs treatment as indicated. Processing of lysates was performed as described above. Membranes were probed overnight with pp38 rabbit polyclonal Ab (Cell Signaling Technology) (1:1000). Band intensity was measured by using Image J software (Version 1.50i).

Quantitative RT- PCR

Macrophages (2,5 - 5 x 10^6/ml) were incubated with Molidustat in presence or absence of *Mtb*-extract for 48 h. Cells were lysed and RNA was prepared using the RNeasy purification kit (Qiagen) according to the manufacturer's instructions. cDNA was prepared by reverse transcription (Fermentas). LightCycler PCR was performed using SYBR Green PCR Master Mix (Roche). The following primers were used: forward

β-actin, 5'-GGCCACGGGCTGCTTC-3'; reverse β-actin, 5' GTTGGCGTACAGGTCTTTGC-3'; forward vitamin D receptor (VDR), 5'-AAGGACAACCGACGCCACT-3'; reverse VDR, 5'-ATCATGCCGATGTCCACACA-3'; forward hBD2, 5' GGTGTTTTTGGTGGTATAGGCG-3'; reverse hBD2, 5'-AGGGCAAAAGACTGGATGACA-3'. The cycles were performed as follows: 1 cycle 95°C, 10 min; 40 cycles: 95°C, 15 s; 60°C, 10 s; 72°C, 20 s. The mRNA levels for VDR and hBD2 were normalized to the amount of β-actin, which was measured

simultaneously. A comparative threshold cycle was used to determine gene expression relative to untreated cells cultured at 20% O_2. Relative expression levels were calculated using the delta-delta CT method (ΔΔCT) as described previously (25).

Statistical Analysis

Experiments were performed 5-11 times as indicated in the respective legends. For each experiment macrophages were derived from independent anonymous blood donors. Results are presented as mean ± standard error of the mean (SEM). Statistical significance was calculated using the Student's *t* test for paired samples or one tailed Wilcoxon test as indicated. Differences were considered significant if $p \leq 0.05$.

RESULTS

Molidustat Is Not Toxic for Primary Human Macrophages

To rule out that stabilization of HIF by the prolyl hydroxylase inhibitor Molidustat affects the viability of macrophages, cells were incubated overnight in the presence of increasing concentrations of Molidustat (0.1 μM to 10 μM). Viability was evaluated by Annexin-FITC/Propidium Iodide staining and analyzed by flow cytometry (**Figure 1A**). Cell viability in general was slightly reduced (70%) due to the purification- and culture conditions. Importantly, Molidustat had no effect on the viability of macrophages as compared to untreated cells generated from 7 independent donors at all concentrations tested (**Figure 1B**).

Molidustat Stabilizes HIF-1α in *Mtb*-Treated Macrophages

To ascertain that Molidustat-mediated prolyl-hydroxylase inhibition increases HIF-1α expression in the specific cell population used in our study, macrophages were incubated overnight with 0.1 μM, 1μM and 10 μM Molidustat. HIF-1α expression was determined by Western Blot analysis. HIF-1α expression was increased by Molidustat in a dose dependent manner (**Figures 2A, B**). Since the major objective of this study was to investigate the effect of HIF-1α-stabilization on *Mtb*-mediated immune responses, we next stimulated macrophages with mycobacterial antigens (*Mtb*-extract) in the absence or presence of Molidustat. *Mtb*-extract alone stabilized HIF-1α and the expression was further enhanced in a dose-dependent manner by treatment with Molidustat (**Figures 2A, B**) and reached levels beyond deferoxamine, which prevents prolyl hydroxylase II mediated degradation of HIF-1α by Fe^{2+} chelation and was therefore used as a positive control for HIF-1α stabilization. These results demonstrate that microbial antigens stabilize HIF-1α in human macrophages and this effect is enhanced by the prolyl hydroxylase inhibitor Molidustat.

HIF-Stabilization Reduces *Mtb*-Mediated Cytokine-Release and Leads to an Interference With p38 MAP Kinase Activation

Since HIF-1α is stabilized by mycobacterial antigens, we hypothesized that pharmacological manipulation of HIF-

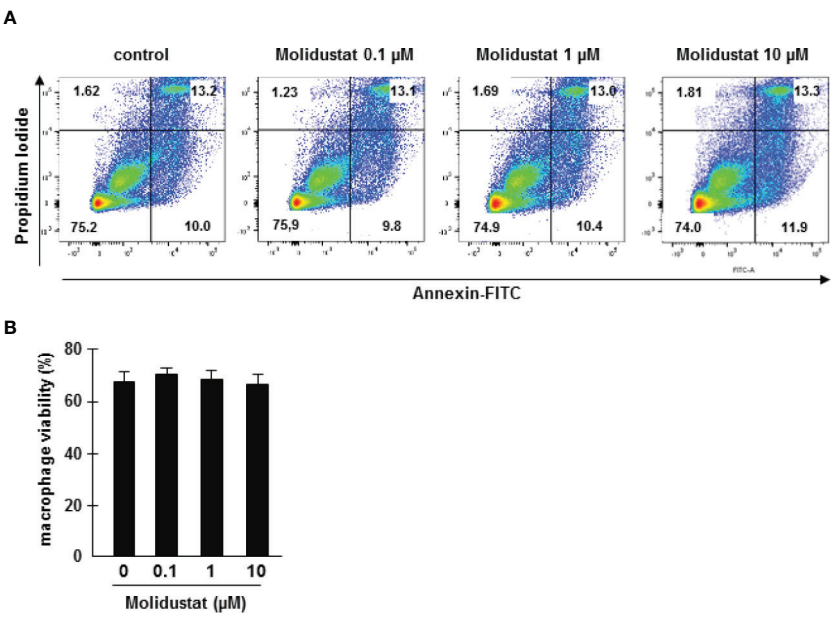

FIGURE 1 | Molidustat is not toxic for primary human macrophages. **(A)** $1x10^6$ macrophages were incubated with medium alone or increasing levels of Molidustat as indicated. After 16 ± 2 hrs incubation apoptotic and necrotic cells were detected by annexin V-FITC and PI-staining. The panel shows a representative result of seven independent donors. **(B)** The diagram gives the average percentage ± SEM of annexin V and PI negative macrophages of seven independent donors. There were no statistical differences as calculated with a Wilcoxon test.

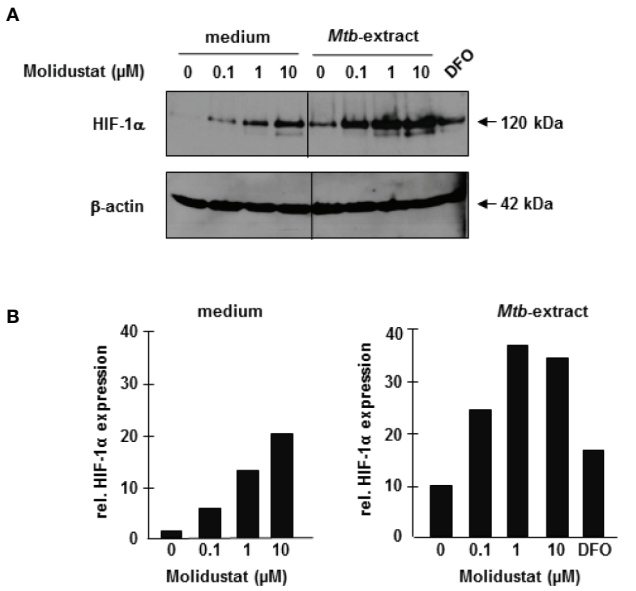

FIGURE 2 | Molidustat stabilizes HIF-1α in *Mtb*-stimulated macrophages 2×10^6 macrophages were stimulated for 16 ± 2hrs with Molidustat in the absence or presence of *Mtb*-extract (10 μg/ml) or Deferoxamine (DFO, 50 μM). Cell lysates were probed with a HIF-1α antibody (1:1000). **(A)** The upper panel shows a representative result of three independent experiments. The lower panel shows the blots after stripping and detection of β-actin (1:1000). **(B)** The graphs show the relative HIF-1α expression calculated by measuring the integrated densities as compared to un-treated samples (defined as 1).

expression by Molidustat might affect *Mtb*-mediated macrophage activation. Since cytokine release is an essential function of macrophages in the immune response against intracellular bacteria, we analyzed the effects of HIF-stabilization on the *Mtb*-induced release of the TNFα and IL-10. We selected TNFα and IL-10 because both are key mediators for orchestrating the immune response in human tuberculosis (26). Molidustat alone did not induce the release of TNF-a or IL-10 (not shown). *Mtb*-extract induced high levels of TNFα-release by macrophages (19 ng/ml ± 7 ng/ml) (**Figure 3A**). Treatment with Molidustat (10 μM) reduced *Mtb*-extract-mediated TNFα-release by 26% (n=10). Importantly, Molidustat also inhibited the release of TNFα by macrophages infected with virulent *Mtb* to background levels (**Figure 3B**). Similarly, the *Mtb*-extract induced release of IL-10 was inhibited by Molidustat (61 ± 16%; 7 donors, **Figure 3C**). Furthermore, Molidustat reduced IL-10 secretion induced by viable *Mtb* in a dose-dependent manner and suppressed the cytokine release to background levels at a concentration of 10 μM (7 donors, **Figure 3D**). Therefore, the stabilization of HIF-1α by Molidustat results in the reduced secretion of TNFα and IL-10, supporting our hypothesis that HIF-1α is a potential target for the modulation of innate immune responses in *Mtb*-infection.

To investigate the molecular mechanism underlying Molidustat-mediated inhibition of TNFα and IL-10, we considered p38 mitogen activated protein (MAP) kinase activation because prolyl-hydroxylase inhibitors were previously implicated in *Escherichia coli*-mediated p38 MAPK activation (27). For this set of experiments, we used a human macrophage-like cell line (THP-1), since GM-CSF required for the maturation of peripheral blood monocytes already activates the MAP kinase pathway precluding studies on *Mtb*-specific regulation (28). THP-1 cells were stimulated with *Mtb*-extract in the presence or absence of Molidustat and cell lysates were analyzed for the expression of phospho-p38. The stabilization of HIF-1α by Molidustat- as shown for primary macrophages- could not be experimentally demonstrated for THP-1 cells due to technical obstacles. *Mtb*-extract induced a profound up-regulation of p38 phosphorylation (**Figure 4**). Molidustat (10 μM) reduced the *Mtb*-mediated up-regulation of phospho-p38 to the levels observed in the untreated control (**Figures 4A, B**).

Taken together these results demonstrate that pharmacological HIF-stabilization inhibits the *Mtb*-induced release of immune-modulatory cytokines and this effect may be associated with an inhibition of the p38 MAP kinase signaling pathway.

Molidustat Induces the Up-Regulation of the VDR and hBD-2

One important effector pathway of human macrophages is initiated by Toll like receptor ligation and involves the up-regulation of the VDR and the subsequent production of the antimicrobial peptide hBD-2 (29). Recently we and others demonstrated that hypoxia similarly up-regulates the VDR and hBD-2 (12, 30, 31). To evaluate whether mimicking hypoxia by pharmacological HIF-1 stabilization has comparable effects, macrophages were incubated with Molidustat and VDR- and hBD2 mRNA levels were determined by quantitative PCR after 48 hrs. In 6 independent experiments Molidustat significantly enhanced VDR (3.5 ± 0.8-fold, p=0.02)- and hBD-2 (5.2 ± 1.8-fold; p=0.008) expression as compared to un-treated control cultures (**Figure 5A**). To relate this finding to *Mtb*-infection we co-incubated macrophages with *Mtb*-extract and Molidustat. Again, Molidustat strongly enhanced the expression of VDR (4.6 ± 1.8-fold, p =0.03) as well as hBD-2 mRNA-expression (11.1 ± 2.9-fold; p=0.008) as compared to samples that were treated with *Mtb*-extract alone (**Figure 5B**). Taken together we demonstrated Molidustat results in an increased expression of two molecules (VDR and hBD2) which define an antimicrobial pathway in human macrophages.

Molidustat Reduces the Growth of Intracellular *Mtb*

The differential effects of Molidustat on cytokine release (inhibition) and the expression of the antimicrobial peptide hBD2 (increase) in macrophages raised the question on the effect on the intracellular growth of *Mtb*. First, we investigated the effect of Molidustat on the proliferation of extracellular *Mtb* in liquid culture. Molidustat (0.1 μM to 10 μM) did not affect the viability of extracellular *Mtb* as measured by comparing the metabolic activity (**Figure 6A**) and growth (colony forming units, **Figure 6B**) in treated and un-treated control cultures. To evaluate the effect on the growth of intracellular *Mtb*, macrophages were infected with virulent *Mtb* and cultured in the presence of Molidustat for 5 days. As observed in un-infected cells (**Figure 1**) Molidustat did not affect the viability of *Mtb*-

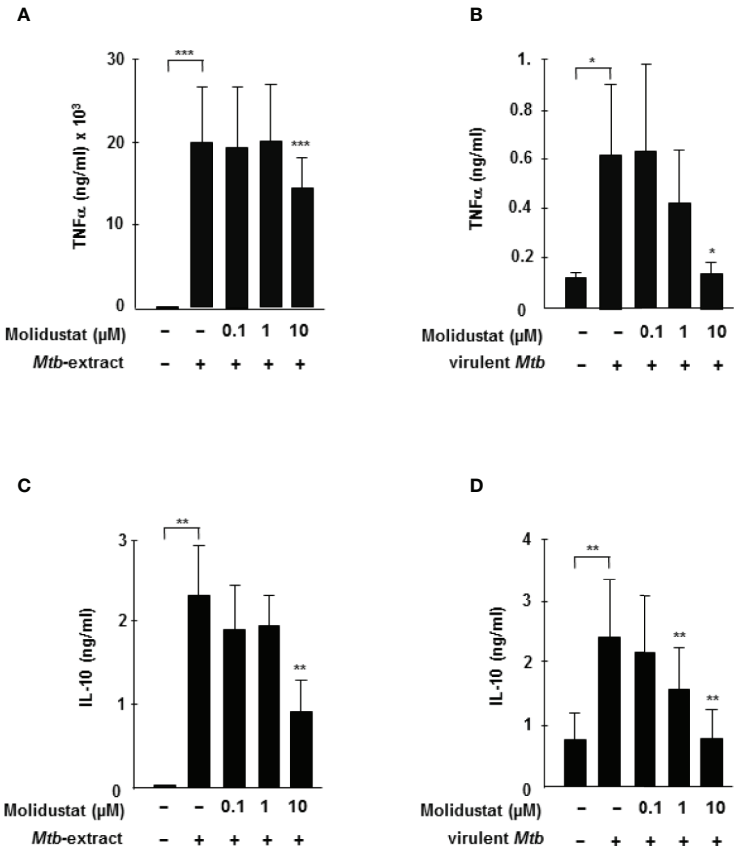

FIGURE 3 | HIF-stabilization reduces *Mtb*-mediated TNFα and IL-10 release **(A, C)** 3 x 10^5 macrophages were either left untreated or stimulated with *Mtb*-extract (10μg/ml) and incubated with increasing concentrations Molidustat for 16 ± 2 hrs. The release of TNFα or IL-10 in the supernatant was determined by Elisa. The figures present the cytokine release (mean ± SEM) of 10 (TNF-α) and 5 (IL-10) independent donors. **(B, D)** 3 × 10^5 macrophages were infected with virulent *Mtb* at an MOI of 10. TNFα and IL-10 concentrations in the supernatants were determined by ELISA after 16hrs of infection. The figures present the cytokine release (mean ± SEM) of 7 independent donors. Asterisks indicate statistical significance as calculated by Wilcoxon test. *$p \leq 0.05$; **$p \leq 0.01$; ***$p \leq 0.001$.

infected macrophages after 5 d of infection and was in a range between 64-79% (data not shown). The number of viable bacilli was significantly lower in Molidustat- treated macrophages in all 11 donors included in the study (79 ± 5%; $p = 0.0005$) (**Figure 7A**) and this effect was dose dependent (n=9) (**Figure 7B**). The extent of growth inhibition induced by Molidustat closely correlated with the levels of growth inhibition induced by hypoxia (1%) in the same donors

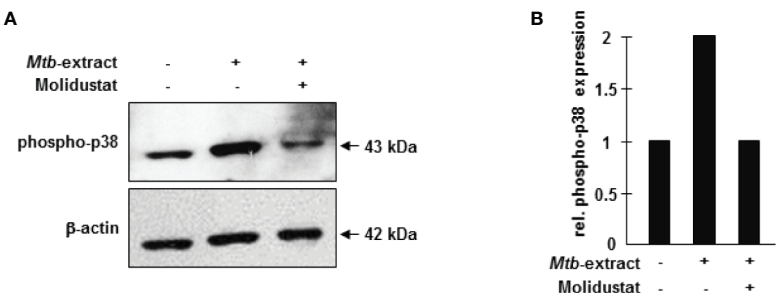

FIGURE 4 | HIF-stabilization interferes with p38 MAP kinase activation. **(A)** 7x10^5 THP-1 macrophages were either left untreated or stimulated with 10 μg/ml *Mtb*-extract in absence or presence of 10 μM Molidustat. After 16 ± 2 hrs cells were harvested and lysed. 30 μg cell extract were separated on a 12% SDS PAGE gel and analyzed by western blot. Samples were probed with a polyclonal antibody directed against phospho-p38 (1:1000). The lower panel shows the blot after stripping and detection of β-actin (1:1000) as a loading control. The panel shows a representative blot of three with similar results. **(B)** The graph shows the relative phosphor-p38 expression calculated by measuring the integrated densities as compared to un-treated samples (defined as 1).

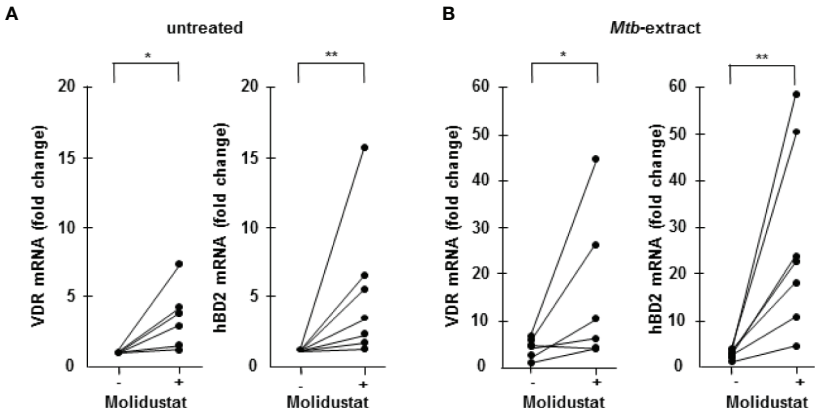

FIGURE 5 | Molidustat induces the up-regulation of the Vitamin D receptor and hBD2 6 x 10^5 Macrophages were either left untreated or incubated with 10 µM Molidustat for 48 h. Vitamin D receptor (VDR) and human β defensin 2 (hBD2) mRNA levels were measured by LightCycler PCR in **(A)** unstimulated as well as **(B)** *Mtb*-extract- (10 µg/ml) stimulated macrophages. VDR and hBD2 mRNA levels in all probes were compared to levels of unstimulated macrophages without Molidustat treatment, which were defined as 1. The graph shows the mRNA levels for 6 (VDR) or 7 (hBD2) independent donors, respectively. Asterisks indicate statistically significant differences as determined by Wilcoxon test. *$p \leq 0.05$; **$p \leq 0.01$.

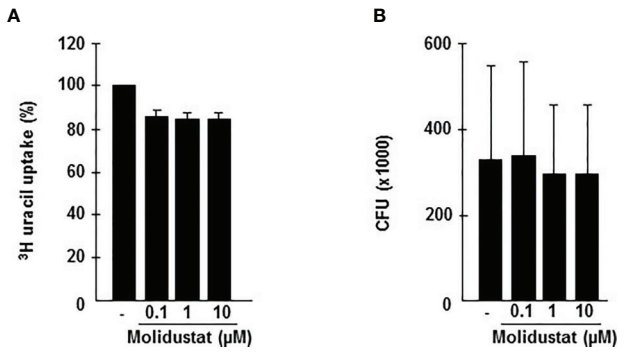

FIGURE 6 | Molidustat does not affect viability of extracellular *Mtb*. **(A)** 1 x 10^5 *Mtb* H37Rv were grown in 7H9 broth in absence or presence of increasing concentrations Molidustat (0.1, 1, 10 µM) for 5 days at 37°C. Subsequently mycobacteria were harvested and 10 µl of the sonicate were plated on 7H11 agar plates. After 14 d incubation at 37°C CFU were determined. **(B)** The graph shows the results for 5 independent experiments using the identical *Mtb* H37Rv stock.

(**Figure 7C**). Hypoxia did not influence the viability of macrophages as shown previously (12). By inference this supports our hypothesis that Molidustat enhances macrophage activity against *Mtb* by stabilization of HIF, thereby mimicking an oxygen-restricted environment.

In summary, our experiments demonstrate that pharmacological HIF-stabilization by Molidustat has profound effects on macrophage functions (summarized in **Figure 8**). The skewing of the expression of cytokines and antimicrobial peptides ultimately results in reduced growth of intracellular *Mtb*. These findings highlight the potential of HIF-stabilizers to serve – in addition to the established benefit for ameliorating renal anemia – as host-targeted therapy to treat tuberculosis when classical antibiotic regimes fail as a result of antibiotic resistance.

DISCUSSION

Treatment of tuberculosis remains a major challenge due to the emergence of drug-resistance strains, severe side effects of first-line drugs and lack of compliance related to the 6-months duration of treatment. Host-directed therapies that support the immune system rather than directly acting on the pathogen provide an attractive alternative treatment strategy. Here, we demonstrate that pharmacological stabilization of hypoxia-induced factor by Molidustat, a compound already tested in phase III clinical trials for the treatment of renal anemia, modulates *Mtb*-associated macrophage functions resulting in reduced growth of the pathogen. Our results provide preclinical evidence that the hypoxia-triggered signal transduction pathway is a potential target for host-directed therapies against intracellular bacteria, specifically *Mtb*.

HIF-1α is an essential environmental and metabolic sensor that acts as a transcription factor thereby affecting multiple immune cell functions. Physiologically HIF-1α is stabilized at low oxygen tension (14, 32). However, HIF-1α stabilization may also occur at physiological oxygen levels, when target cells are stimulated, for example by *Mtb*-derived trehalose dimycolate (33) or TLR4 ligation (16). Stabilization is linked to the transcription factor NF-κB, which activates the downstream target HIF-1α (34). Accordingly, the human HIF-1α promotor contains a canonical NF-κB binding site 197/188 bp upstream of the transcription start site (35). Here, we demonstrate that the prolyl hydroxylase inhibitor Molidustat increases HIF-1α levels

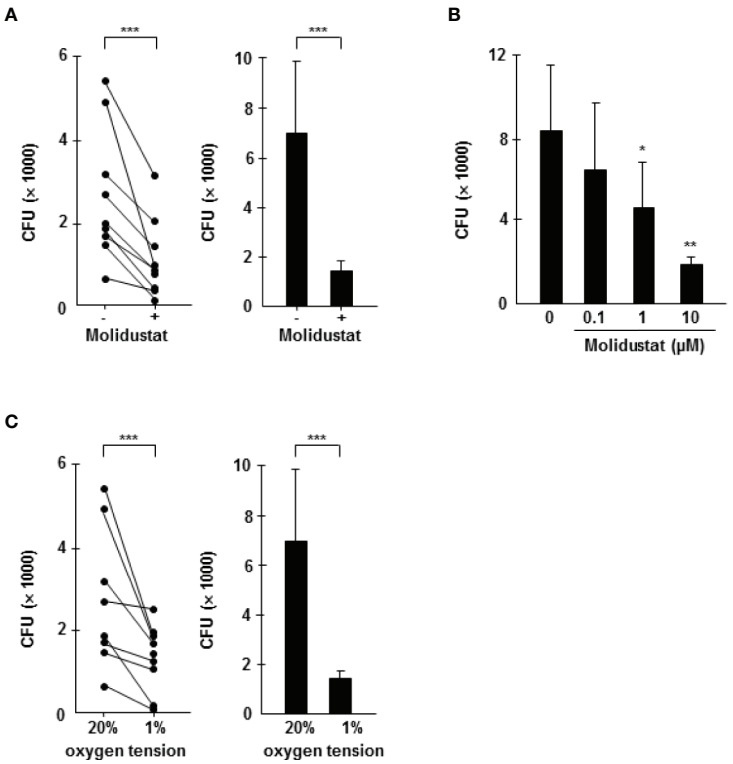

FIGURE 7 | Molidustat mimics hypoxia and inhibits the proliferation of intracellular *Mtb* in a dose dependent manner. Macrophages were infected in bulk culture overnight (MOI 10), harvested, and replated in 24-well plates (2 x 10^5/300 µl). Infected cells were cultured for 5 days in absence or presence of Molidustat **(A, B)** or under hypoxia **(C)**. The number of viable bacilli was determined after 2 weeks by plating cell lysates on 7H11 agar plates. **(A)** Effect of 10 µM Molidustat on the intracellular growth of viable *Mtb*. *Left panel*: Individual results of 9 out of 11 donors. *Right panel*: Summary of the results of all 11 donors (mean ± SEM). **(B)** Dose dependent effects of 0.1, 1 and 10 µM Molidustat on the intracellular growth of viable *Mtb*. The graph shows the summary of the results of 9 independent donors (mean ± SEM). **(C)** Effect of hypoxia (pO_2 = 1%) on the intracellular growth of viable *Mtb*. *Left panel*: Individual results of 9 out of 11 donors. *Right panel*: Summary of the results of all 11 donors (mean ± SEM). Asterisks indicate statistically significant differences as determined by Wilcoxon test. $^*p \leq 0.05$, $^{**}p \leq 0.005$, $^{***}p \leq 0.0005$.

in human macrophages stimulated with mycobacterial antigens. Molidustat also upregulates HIF-2α in epithelial (HeLa)-, adenonocarcinoma (A549)- and hepatoma (Hep3B) cell lines. Since Molidustat stabilizes both HIF isotypes, the effects observed in this study cannot definitively be attributed to HIF-1α. However, HIF-2α is most abundantly expressed in vascular endothelial cells, plays an important role in embryogenesis and is closely related to VEGF mRNA expression (36, 37). Therefore, it is likely that the effects of Molidustat on macrophages are mediated by HIF-1α.

HIF-1α activation switches energy metabolism to glycolysis to provide continuous ATP supply, when oxygen is limited (38). As compared to lymphoid cell lines, which predominantly use oxidative phosphorylation for their energy metabolism and therefore rely on the presence of high levels of oxygen, myeloid cells (neutrophils, macrophages) favor glycolysis (39). This is in accordance with our observation that macrophages tolerate high concentrations of Molidustat (10µM) (**Figure 1**), resulting in a "hypoxia-like" microenvironment.

In response to microbial stimuli macrophages release a broad panel of inflammatory mediators. In tuberculosis macrophage-derived TNFα and IL-10 play a special role and the balance between these mediators affect the outcome of tuberculosis infection. p38 – a key kinase of the MAP-kinase pathway – regulates TNFα and IL-10 release (40). In addition, restriction of local oxygen supply increases the production of cytokines and chemokines (41, 42). In our study Molidustat decreased both *Mtb*-induced TNFα and IL-10 secretion by macrophages (**Figure 3**). Similarly, AKB-4924, another pharmacological HIF-1α stabilizing compound, dampened the host inflammatory response (27). Intriguingly this effect was also attributed to the inhibition of p38 MAPK activation (27). Hence inhibition of p38 phosphorylation seems to be a common effect of pharmacological HIF-stabilizers.

At first glance the differential regulation of immune molecules appears contradictory. However, HIF-1-α is a ubiquitous transcription factor which is expressed in all myeloid cells including macrophages. The genes responding to HIF-1-α are highly diverse and include the regulation of metabolism, cell division and immune functions (6). The functional impact of gene regulation does not follow a predictable pattern and the understanding of biological end points (e.g. cytokine release or

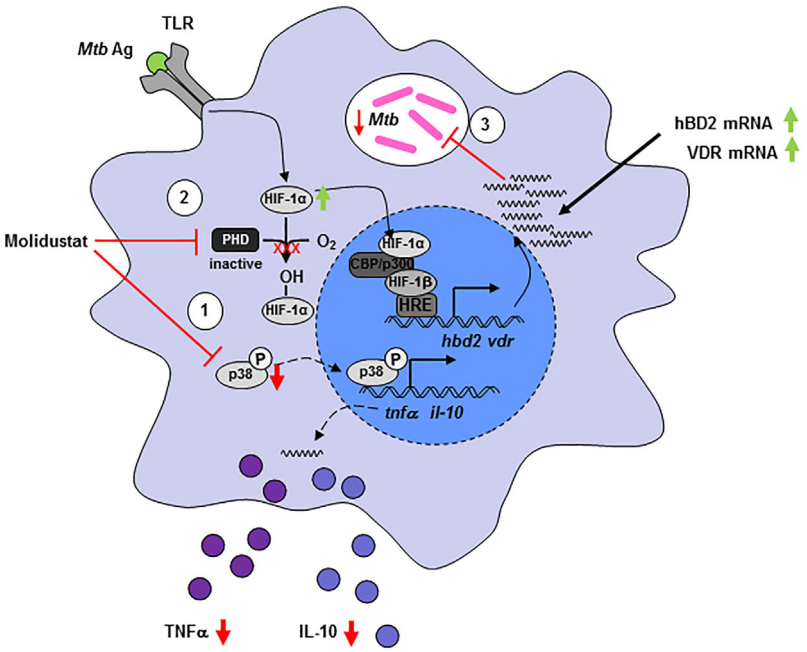

FIGURE 8 | Molidustat directly reduces viability of intracellular *Mtb* and increases the expression of VDR and hBD2, which inhibits growth of *Mtb* in human macrophages. Molidustat interferes in the interplay between *Mtb* and macrophages on several different levels. (1) Application of Molidustat reduces the release of pro- (TNF-α) and anti-inflammatory (IL-10) cytokines released by *Mtb* antigen stimulated macrophages. This effect is a result of interference with the MAPK pathway *via* inhibition of p38 phosphorylation. (2) Inhibition of Prolylhydroxylases by Molidustat prevents degradation of HIF-1α and stabilizes *Mtb* antigen mediated induction of HIF-1α *via* TLR-signaling. (3) HIF-1α is subsequently translocated into the nucleus and induces the expression of an antimicrobial pathway involving VDR and hBD2, which leads to a significant inhibition of intracellular *Mtb* proliferation.

expression of antimicrobial peptides) requires specific experimental approaches. We believe that the differential effects on cytokine release and VDR/hBD2 reflects the complexity of biological effects governed by HIF-1-α.

Our study was not designed to define the molecular mechanism of Molidustat/HIF-1α-mediated growth inhibition of *Mtb*. We hypothesize that HIF-1α-mediated modifications of the energy metabolism in macrophages interfere with the multiplication of *Mtb*. First, increased intracellular HIF-1α levels promote glycolysis resembling the Warburg effect in tumors (43). Increased glucose consumption results in increased formation of lactate (44). Several reports indicate that lactic acid monomers activate macrophages and enhance their ability to kill intracellular *Mtb* (45). Second, increased levels of HIF-1α induce a metabolic reprogramming of the citric acid cycle that affects the production of critical metabolites such as succinate (46) and itaconic acid (47). Succinate serves as an inflammatory signal which also stabilizes HIF-1α (48). Itaconic acid, which is formed *via* decarboxylation from the tricarboxylic acid cycle intermediate cis-aconitate directly inhibits growth of *Mtb*. Mechanistically this effect is mediated by inhibition of the bacterial isocitrate lyase, a key enzyme of the glyoxylate shunt responsible for bacterial growth (47). In mice HIF-1α upregulation and glucose metabolism were shown to be essential for macrophage migratory activity (7, 49). Alternative mechanisms for HIF-1α mediated antimicrobial activity could be the induction of antimicrobial peptides (CRAMP), granule proteases (Cathepsin G) as well as iNOS producing nitric oxide in mice. These mechanisms contributed to HIF-1α- dependent bactericidal activity and systemic spread of group A streptococci, *Salmonella Typhimurium* and *Pseudomonas aeruginosa* (15). Similarly, indirect (Molidustat)- or direct exposure to hypoxia (hypoxia chamber) triggered the expression of VDR and its downstream target hBD2 thereby enhancing the antimicrobial activity against intracellular *Mtb* (**Figure 5**) (12). Notably hBD2 has been directly associated with growth restriction of intracellular *Mtb* (50).

Although Molidustat did not affect the growth of *Mtb* (**Figure 6**), direct effects of HIF-1 stabilizers on *Mtb* cannot be excluded. Even though the precise mode of action for inhibiting Prolylhydroxylase II by HIF-1α stabilizers is unknown, two major principles are currently discussed: Blocking the active site of the enzyme (e.g. FG-4497) or chelate Fe^{2+} (e.g. Deferoxamine), which is essential for the activity of prolyl hydroxylase. In case of L-Mimosine, a Molidustat-related HIF-1α stabilizer, both mechanisms are active (51, 52). Intriguingly iron chelating agents such as deferoxamine significantly decrease the viability of extracellular *Mtb* (53). Since Molidustat, as compared to deferoxamine, is able to permeate cellular membranes, direct effects on intracellular *Mtb* mediated by partial Fe^{2+}-chelation may be possible.

Our results support an emerging concept of a role for HIF-1α in protection against bacterial infections. Other studies demonstrated that HIF-1α supports the clearance of bacterial infections in mouse keratinocytes infected with Group A streptococci, a *Mycobacterium marinum* zebrafish model or infection of murine bladders with uropathogenic *Escherichia coli* (17, 27, 54). Accordingly, the HIF-1α stabilizer (AKB-4924) supported the clearance of *Escherichia coli* (27). Even though our results do not provide direct proof for a causative link between reduced cytokine release and p38 MAP kinase expression, we suggest that the "hypoxia-HIF-1α-p38 Map kinase axis" is a novel and intriguing target for host directed therapy of bacterial infections. Appropriate compounds, such as Molidustat used in this study, are well tolerated *in vivo*, currently investigated in Phase II/III clinical trials (20, 55) or – such as Roxadustat – already prescribed (22) to treat renal anemia. Our study should therefore encourage clinical studies to extend the clinical application of HIF-1α stabilizers for the treatment of severe bacterial infections.

DATA AVAILABILITY STATEMENT

The raw data supporting the conclusions of this article will be made available by the authors, without undue reservation.

ETHICS STATEMENT

PBMC were isolated from buffy coat preparations from anonymous donors (Institute of Transfusion Medicine, Ulm University) which cannot be tracked. The ethics committee of the University Hospital in Ulm declared that no formal ethical approval is required for this study.

AUTHOR CONTRIBUTIONS

SZ: planned and conducted experiments, wrote the manuscript. SH: conducted experiments. DM: conducted experiments. MG: conducted experiments. SS: concepted and supervised the study, wrote the manuscript. All authors contributed to the article and approved the submitted version.

FUNDING

This work was supported by the German Research Foundation (STE 925/4-1 and CRC1279) and the Landesstiftung Baden-Württemberg (Förderprogramm Biotechnologie).

REFERENCES

1. Connolly LE, Edelstein PH, Ramakrishnan L. Why is Long-Term Therapy Required to Cure Tuberculosis? *PloS Med* (2007) 4:e120. doi: 10.1371/journal.pmed.0040120
2. Daniels M, Hill AB. Chemotherapy of Pulmonary Tuberculosis in Young Adults; an Analysis of the Combined Results of Three Medical Research Council Trials. *Br Med J* (1952) 1:1162–8. doi: 10.1136/bmj.1.4769.1162
3. Ahmad A, Sharif-Askari E, Fawaz L, Menezes J. Innate Immune Response of the Human Host to Exposure With Herpes Simplex Virus Type 1: In Vitro Control of the Virus Infection by Enhanced Natural Killer Activity Via interleukin-15 Induction. *J Virol* (2000) 74:7196–203. doi: 10.1128/JVI.74.16.7196-7203.2000
4. Pai M, Behr MA, Dowdy D, Dheda K, Divangahi M, Boehme CC, et al. Tuberculosis. *Nat Rev Dis Primers* (2016) 2:16076. doi: 10.1038/nrdp.2016.76
5. Bhandari T, Nizet V. Hypoxia-Inducible Factor (HIF) as a Pharmacological Target for Prevention and Treatment of Infectious Diseases. *Infect Dis Ther* (2014) 3:159–74. doi: 10.1007/s40121-014-0030-1
6. Hayek I, Schatz V, Bogdan C, Jantsch J, Lührmann A. Mechanisms Controlling Bacterial Infection in Myeloid Cells Under Hypoxic Conditions. *Cell Mol Life Sci CMLS* (2020) 78:887–907. doi: 10.1007/s00018-020-03684-8
7. Cramer T, Yamanishi Y, Clausen BE, Forster I, Pawlinski R, Mackman N, et al. Hif-1alpha is Essential for Myeloid Cell-Mediated Inflammation. *Cell* (2003) 112:645–57. doi: 10.1016/S0092-8674(03)00154-5
8. Palazon A, Goldrath AW, Nizet V, Johnson RS. HIF Transcription Factors, Inflammation, and Immunity. *Immunity* (2014) 41:518–28. doi: 10.1016/j.immuni.2014.09.008
9. Hong SS, Lee H, Kim KW. Hif-1alpha: A Valid Therapeutic Target for Tumor Therapy. *Cancer Res Treat Off J Korean Cancer Assoc* (2004) 36:343–53. doi: 10.4143/crt.2004.36.6.343
10. Braverman J, Sogi KM, Benjamin D, Nomura DK, Stanley SA. HIF-1alpha Is an Essential Mediator of IFN-gamma-Dependent Immunity to Mycobacterium Tuberculosis. *J Immunol* (2016) 197:1287–97. doi: 10.4049/jimmunol.1600266
11. Gautam US, Mehra S, Ahsan MH, Alvarez X, Niu T, Kaushal D. Role of TNF in the Altered Interaction of Dormant Mycobacterium Tuberculosis With Host Macrophages. *PloS One* (2014) 9:e95220. doi: 10.1371/journal.pone.0095220
12. Nickel D, Busch M, Mayer D, Hagemann B, Knoll V, Stenger S. Hypoxia Triggers the Expression of Human Beta Defensin 2 and Antimicrobial Activity Against Mycobacterium Tuberculosis in Human Macrophages. *J Immunol* (2012) 188:4001–7. doi: 10.4049/jimmunol.1100976
13. Oehlers SH, Cronan MR, Scott NR, Thomas MI, Okuda KS, Walton EM, et al. Interception of Host Angiogenic Signalling Limits Mycobacterial Growth. *Nature* (2015) 517:612–5. doi: 10.1038/nature13967
14. Nizet V, Johnson RS. Interdependence of Hypoxic and Innate Immune Responses. *Nat Rev Immunol* (2009) 9:609–17. doi: 10.1038/nri2607
15. Peyssonnaux C, Datta V, Cramer T, Doedens A, Theodorakis EA, Gallo RL, et al. Hif-1alpha Expression Regulates the Bactericidal Capacity of Phagocytes. *J.Clin.Invest* (2005) 115:1806–15. doi: 10.1172/JCI23865
16. Peyssonnaux C, Cejudo-Martin P, Doedens A, Zinkernagel AS, Johnson RS, Nizet V. Cutting Edge: Essential Role of Hypoxia Inducible factor-1alpha in Development of Lipopolysaccharide-Induced Sepsis. *J Immunol* (2007) 178:7516–9. doi: 10.4049/jimmunol.178.12.7516
17. Elks PM, Brizee S, van der Vaart M, Walmsley SR, van Eeden FJ, Renshaw SA, et al. Hypoxia Inducible Factor Signaling Modulates Susceptibility to Mycobacterial Infection Via a Nitric Oxide Dependent Mechanism. *PloS Pathog* (2013) 9:e1003789. doi: 10.1371/journal.ppat.1003789
18. Zinkernagel AS, Peyssonnaux C, Johnson RS, Nizet V. Pharmacologic Augmentation of Hypoxia-Inducible factor-1alpha With Mimosine Boosts the Bactericidal Capacity of Phagocytes. *J Infect Dis* (2008) 197:214–7. doi: 10.1086/524843
19. Okumura CY, Hollands A, Tran DN, Olson J, Dahesh S, von Kockritz-Blickwede M, et al. A New Pharmacological Agent (AKB-4924) Stabilizes Hypoxia Inducible Factor-1 (HIF-1) and Increases Skin Innate Defenses Against Bacterial Infection. *J Mol Med (Berlin Germany)* (2012) 90:1079–89. doi: 10.1007/s00109-012-0882-3
20. Brigandi RA, Johnson B, Oei C, Westerman M, Olbina G, de Zoysa J, et al. A Novel Hypoxia-Inducible Factor-Prolyl Hydroxylase Inhibitor (GSK1278863) for Anemia in CKD: A 28-Day, Phase 2a Randomized Trial. *Am J Kidney Dis Off J Natl Kidney Foundation* (2016) 67:861–71. doi: 10.1053/j.ajkd.2015.11.021
21. Maxwell PH, Eckardt KU. HIF Prolyl Hydroxylase Inhibitors for the Treatment of Renal Anaemia and Beyond. *Nat Rev Nephrol* (2016) 12:157–68. doi: 10.1038/nrneph.2015.193
22. Dhillon S. Roxadustat: First Global Approval. *Drugs* (2019) 79:563–72. doi: 10.1007/s40265-019-01077-1
23. Yamamoto H, Taguchi M, Matsuda Y, Iekushi K, Yamada T, Akizawa T. Molidustat for the Treatment of Renal Anaemia in Patients With non-

Dialysis-Dependent Chronic Kidney Disease: Design and Rationale of Two Phase III Studies. *BMJ Open* (2019) 9:e026704. doi: 10.1136/bmjopen-2018-026704
24. Beckman EM, Melian A, Behar SM, Sieling PA, Chatterjee D, Furlong ST, et al. CD1c Restricts Responses of Mycobacteria-Specific T Cells. Evidence for Antigen Presentation by a Second Member of the Human CD1 Family. *J Immunol* (1996) 157:2795–803.
25. Livak KJ, Schmittgen D. Analysis of Relative Gene Expression Data Using Real-Time Quantitative PCR and the 2(-Delta Delta C(T)) Method. *Methods* (2001) 25:402–8. doi: 10.1006/meth.2001.1262
26. Bruns H, Stenger S. New Insights Into the Interaction of Mycobacterium Tuberculosis and Human Macrophages. *Future Microbiol* (2014) 9:327–41. doi: 10.2217/fmb.13.164
27. Lin AE, Beasley FC, Olson J, Keller N, Shalwitz RA, Hannan TJ, et al. Role of Hypoxia Inducible Factor-1alpha (Hif-1alpha) in Innate Defense Against Uropathogenic Escherichia Coli Infection. *PloS Pathog* (2015) 11:e1004818. doi: 10.1371/journal.ppat.1004818
28. Wang Y, Zhou C, Huo J, Ni Y, Zhang P, Lu C, et al. TRAF6 is Required for the GM-CSF-induced Jnk, p38 and Akt Activation. *Mol Immunol* (2015) 65:224–9. doi: 10.1016/j.molimm.2015.01.012
29. Liu PT, Stenger S, Li H, Wenzel L, Tan BH, Krutzik SR, et al. Toll-Like Receptor Triggering of a Vitamin D-mediated Human Antimicrobial Response. *Science* (2006) 311:1770–3. doi: 10.1126/science.1123933
30. Xu H, Lu A, Sharp FR. Regional Genome Transcriptional Response of Adult Mouse Brain to Hypoxia. *BMC Genomics* (2011) 12:499. doi: 10.1186/1471-2164-12-499
31. Kelly CJ, Glover LE, Campbell EL, Kominsky DJ, Ehrentraut SF, Bowers BE, et al. Fundamental Role for HIF-1alpha in Constitutive Expression of Human Beta Defensin-1. *Mucosal Immunol* (2013) 6:1110–8. doi: 10.1038/mi.2013.6
32. Eltzschig HK, Carmeliet P. Hypoxia and Inflammation. *N.Engl.J.Med* (2011) 364:656–65. doi: 10.1056/NEJMra0910283
33. Schoenen H, Huber A, Sonda N, Zimmermann S, Jantsch J, Lepenies B, et al. Differential Control of Mincle-dependent Cord Factor Recognition and Macrophage Responses by the Transcription Factors C/EBPbeta and HIF1alpha. *J Immunol* (2014) 193:3664–75. doi: 10.4049/jimmunol.1301593
34. Frede S, Stockmann C, Freitag P, Fandrey J. Bacterial Lipopolysaccharide Induces HIF-1 Activation in Human Monocytes Via P44/42 MAPK and NF-Kappab. *Biochem J* (2006) 396:517–27. doi: 10.1042/BJ20051839
35. Rius J, Guma M, Schachtrup C, Akassoglou K, Zinkernagel AS, Nizet V, et al. NF-Kappab Links Innate Immunity to the Hypoxic Response Through Transcriptional Regulation of HIF-1alpha. *Nature* (2008) 453:807–11. doi: 10.1038/nature06905
36. Ema M, Taya S, Yokotani N, Sogawa K, Matsuda Y, Fujii-Kuriyama Y. A Novel bHLH-PAS Factor With Close Sequence Similarity to Hypoxia-Inducible Factor 1alpha Regulates the VEGF Expression and is Potentially Involved in Lung and Vascular Development. *Proc Natl Acad Sci USA* (1997) 94:4273–8. doi: 10.1073/pnas.94.9.4273
37. Talks KL, Turley H, Gatter KC, Maxwell PH, Pugh CW, Ratcliffe PJ, et al. The Expression and Distribution of the Hypoxia-Inducible Factors HIF-1alpha and HIF-2alpha in Normal Human Tissues, Cancers, and Tumor-Associated Macrophages. *Am J Pathol* (2000) 157:411–21. doi: 10.1016/S0002-9440(10)64554-3
38. Denko NC. Hypoxia, HIF1 and Glucose Metabolism in the Solid Tumour. *Nat Rev Cancer* (2008) 8:705–13. doi: 10.1038/nrc2468
39. Kominsky DJ, Campbell EL, Colgan SP. Metabolic Shifts in Immunity and Inflammation. *J Immunol* (2010) 184:4062–8. doi: 10.4049/jimmunol.0903002
40. Song CH, Lee JS, Lee SH, Lim K, Kim HJ, Park JK, et al. Role of Mitogen-Activated Protein Kinase Pathways in the Production of Tumor Necrosis Factor-Alpha, interleukin-10, and Monocyte Chemotactic Protein-1 by Mycobacterium Tuberculosis H37Rv-infected Human Monocytes. *J Clin Immunol* (2003) 23:194–201. doi: 10.1023/a:1023309928879
41. Lewis JS, Lee JA, Underwood JC, Harris AL, Lewis CE. Macrophage Responses to Hypoxia: Relevance to Disease Mechanisms. *J Leukoc Biol* (1999) 66:889–900. doi: 10.1002/jlb.66.6.889
42. Bosco MC, Puppo M, Blengio F, Fraone T, Cappello P, Giovarelli M, et al. Monocytes and Dendritic Cells in a Hypoxic Environment: Spotlights on Chemotaxis and Migration. *Immunobiology* (2008) 213:733–49. doi: 10.1016/j.imbio.2008.07.031
43. Kelly B, O'Neill LA. Metabolic Reprogramming in Macrophages and Dendritic Cells in Innate Immunity. *Cell Res* (2015) 25:771–84. doi: 10.1038/cr.2015.68
44. Appelberg R, Moreira D, Barreira-Silva P, Borges M, Silva L, Dinis-Oliveira RJ, et al. The Warburg Effect in Mycobacterial Granulomas is Dependent on the Recruitment and Activation of Macrophages by Interferon-Gamma. *Immunology* (2015) 145:498–507. doi: 10.1111/imm.12464
45. Lawlor C, O'Connor G, O'Leary S, Gallagher PJ, Cryan SA, Keane J, et al. Treatment of Mycobacterium Tuberculosis-Infected Macrophages With Poly (Lactic-Co-Glycolic Acid) Microparticles Drives NFkappaB and Autophagy Dependent Bacillary Killing. *PloS One* (2016) 11:e0149167. doi: 10.1371/journal.pone.0149167
46. Tannahill GM, Curtis AM, Adamik J, Palsson-McDermott EM, McGettrick AF, Goel G, et al. Succinate is an Inflammatory Signal That Induces IL-1beta Through HIF-1alpha. *Nature* (2013) 496:238–42. doi: 10.1038/nature11986
47. Michelucci A, Cordes T, Ghelfi J, Pailot A, Reiling N, Goldmann O, et al. Immune-Responsive Gene 1 Protein Links Metabolism to Immunity by Catalyzing Itaconic Acid Production. *Proc Natl Acad Sci USA* (2013) 110:7820–5. doi: 10.1073/pnas.1218599110
48. Jha AK, Huang SC, Sergushichev A, Lampropoulou V, Ivanova Y, Loginicheva E, et al. Network Integration of Parallel Metabolic and Transcriptional Data Reveals Metabolic Modules That Regulate Macrophage Polarization. *Immunity* (2015) 42:419–30. doi: 10.1016/j.immuni.2015.02.005
49. Semba H, Takeda N, Isagawa T, Sugiura Y, Honda K, Wake M, et al. Hif-1alpha-PDK1 Axis-Induced Active Glycolysis Plays an Essential Role in Macrophage Migratory Capacity. *Nat Commun* (2016) 7:11635. doi: 10.1038/ncomms11635
50. Rivas-Santiago B, Schwander SK, Sarabia C, Diamond G, Klein-Patel ME, Hernandez-Pando R, et al. Human {Beta}-Defensin 2 is Expressed and Associated With Mycobacterium Tuberculosis During Infection of Human Alveolar Epithelial Cells. *Infect Immun* (2005) 73:4505–11. doi: 10.1128/IAI.73.8.4505-4511.2005
51. Fraisl P, Aragones J, Carmeliet P. Inhibition of Oxygen Sensors as a Therapeutic Strategy for Ischaemic and Inflammatory Disease. *Nat Rev Drug Discovery* (2009) 8:139–52. doi: 10.1038/nrd2761
52. Flagg SC, Martin CB, Taabazuing CY, Holmes BE, Knapp MJ. Screening Chelating Inhibitors of HIF-prolyl Hydroxylase Domain 2 (PHD2) and Factor Inhibiting HIF (Fih). *J Inorganic Biochem* (2012) 113:25–30. doi: 10.1016/j.jinorgbio.2012.03.002
53. Cronje L, Edmondson N, Eisenach KD, Bornman L. Iron and Iron Chelating Agents Modulate Mycobacterium Tuberculosis Growth and Monocyte-Macrophage Viability and Effector Functions. *FEMS Immunol Med Microbiol* (2005) 45:103–12. doi: 10.1016/j.femsim.2005.02.007
54. Peyssonnaux C, Boutin AT, Zinkernagel AS, Datta V, Nizet V, Johnson RS. Critical Role of HIF-1alpha in Keratinocyte Defense Against Bacterial Infection. *J Invest Dermatol* (2008) 128:1964–8. doi: 10.1038/jid.2008.27
55. Provenzano R, Besarab A, Wright S, Dua S, Zeig S, Nguyen P, et al. Roxadustat (Fg-4592) Versus Epoetin Alfa for Anemia in Patients Receiving Maintenance Hemodialysis: A Phase 2, Randomized, 6- to 19-Week, Open-Label, Active-Comparator, Dose-Ranging, Safety and Exploratory Efficacy Study. *Am J Kidney Dis Off J Natl Kidney Foundation* (2016) 67:912–24. doi: 10.1053/j.ajkd.2015.12.020

Conflict of Interest: The authors declare that the research was conducted in the absence of any commercial or financial relationships that could be construed as a potential conflict of interest.

frontiers in Immunology

REVIEW
published: 24 June 2021
doi: 10.3389/fimmu.2021.687962

The Role of microRNAs and Long Non-Coding RNAs in the Regulation of the Immune Response to *Mycobacterium tuberculosis* Infection

Manikuntala Kundu * *and Joyoti Basu* *

Department of Chemistry, Bose Institute, Kolkata, India

OPEN ACCESS

Edited by:
Rosane M. B. Teles, University of California, Los Angeles, United States

Reviewed by:
Shamila D. Alipoor, National Institute for Genetic Engineering and Biotechnology, Iran
Chul-Su Yang, Hanyang University, South Korea
Esmaeil Mortaz, National Research Institute of Tuberculosis and Lung Diseases (NRITLD), Iran

***Correspondence:**
Manikuntala Kundu
manikuntala.kundu@gmail.com
Joyoti Basu
joyotibasu@gmail.com

Specialty section:
This article was submitted to Microbial Immunology, a section of the journal Frontiers in Immunology

Received: *30 March 2021*
Accepted: *09 June 2021*
Published: *24 June 2021*

Citation:
Kundu M and Basu J (2021) The Role of microRNAs and Long Non-Coding RNAs in the Regulation of the Immune Response to Mycobacterium tuberculosis Infection. Front. Immunol. 12:687962. doi: 10.3389/fimmu.2021.687962

Non-coding RNAs have emerged as critical regulators of the immune response to infection. MicroRNAs (miRNAs) are small non-coding RNAs which regulate host defense mechanisms against viruses, bacteria and fungi. They are involved in the delicate interplay between *Mycobacterium tuberculosis*, the causative agent of tuberculosis (TB), and its host, which dictates the course of infection. Differential expression of miRNAs upon infection with *M. tuberculosis*, regulates host signaling pathways linked to inflammation, autophagy, apoptosis and polarization of macrophages. Experimental evidence suggests that virulent *M. tuberculosis* often utilize host miRNAs to promote pathogenicity by restricting host-mediated antibacterial signaling pathways. At the same time, host- induced miRNAs augment antibacterial processes such as autophagy, to limit bacterial proliferation. Targeting miRNAs is an emerging option for host-directed therapies. Recent studies have explored the role of long non-coding RNA (lncRNAs) in the regulation of the host response to mycobacterial infection. Among other functions, lncRNAs interact with chromatin remodelers to regulate gene expression and also function as miRNA sponges. In this review we attempt to summarize recent literature on how miRNAs and lncRNAs are differentially expressed during the course of *M. tuberculosis* infection, and how they influence the outcome of infection. We also discuss the potential use of non-coding RNAs as biomarkers of active and latent tuberculosis. Comprehensive understanding of the role of these non-coding RNAs is the first step towards developing RNA-based therapeutics and diagnostic tools for the treatment of TB.

Keywords: *Mycobacterium tuberculosis*, microRNAs, long non-coding RNAs, immune response, autophagy, apoptosis, inflammation

INTRODUCTION

Tuberculosis (TB) is a global health problem. About one third of the world's population is infected with *Mycobacterium tuberculosis*, the causative agent of TB. Of these, about 5 to 10% of infected individuals develop active disease. Around 10 million new TB infections and 1.4 million deaths were reported in 2019 (1). In latent TB (LTBI), *M. tuberculosis* remains walled off within a granuloma in

the lung for long periods of time in a dormant state with no symptoms of disease and without a marked immune response. The bacilli then reactivate under favorable conditions, most notably when the host is immunocompromised as in the case of HIV infection. A reduction in the global burden of TB, requires a means of diagnosing as well as treating latent TB. The problems of TB are further exacerbated by the growing increase in multidrug-resistant (MDR), extensively drug-resistant (XDR) and totally drug resistant TB. With this background, it is evident that there is an increasing need to develop newer approaches towards therapy of TB. Host-directed therapies (HDTs) provide the option of manipulating the host immune response to thwart disease, without the development of drug-resistant bacilli. Effective HDTs require a detailed knowledge of the immune response to infection.

MicroRNAs (miRNAs) are non-coding RNAs which are conserved across species and phyla and are typically 20 to 22 nucleotides in length (2). In recent years it has become evident that miRNAs regulate the interactions between hosts and pathogens (3–5). They play important roles in regulating the immune response to bacterial pathogens such as *Listeria monocytogenes*, *Helicobacter pylori*, *Pseudomonas aeruginosa*, *Salmonella typhimurium* and *M. tuberculosis* (5). miRNAs regulate the response of innate immune cells such as macrophages, to infection. Macrophages are the sentinels of the host immune defense system. One of the first steps of bacterial infection is the sensing of the pathogen associated molecular patterns (PAMPs) by host pattern recognition receptors (PRRs) expressed on macrophages. This triggers a cascade of signaling events which culminate in reprogramming of the host transcriptome so that the bacterium is effectively thwarted. The bacterium responds by remodeling its own transcriptome to adjust metabolism and to express virulence genes. Bacteria also hijack the innate immune pathways of the host for their own benefit (6). In the case of *M. tuberculosis* infection, the host-pathogen interaction impacts processes such as apoptosis, autophagy, cytokine production, macrophage polarization and MHC class II expression. Recent studies have shown that many of these processes are regulated by miRNAs (7–9). Long noncoding RNAs (lncRNAs) are transcripts that are longer than 200 nucleotides, but do not code for proteins (10–12). LncRNAs interact with proteins such as chromatin remodelers and are regulators of innate immunity (13, 14). Differential regulation of lncRNAs modulates the response of immune cells to mycobacterial infection (15, 16).

In addition to the potential use of miRNA or lncRNA-targeted drugs in HDT, several studies have explored the potential of miRNAs (17) and lncRNAs (18) as biomarkers for active TB as well as LTBI, thus underscoring the translational potential of miRNAs as markers of disease. Here, we will focus on regulation of the macrophage immune response to *M. tuberculosis* infection by miRNAs and lncRNAs, and touch upon their potential as biomarkers of disease. We will restrict our discussion primarily to how these ncRNAs rewire the innate immune response to regulate inflammation, apoptosis, macrophage polarization and autophagy, which determine the outcome of *M. tuberculosis* infection. The immune responses to other pathogenic mycobacteria, have not been discussed in detail in this review.

BIOGENESIS OF miRNAs

miRBase, an online repository of miRNAs, lists 4885 mature miRNAs in 271 species (release 22, March 2018). miRNA genes are transcribed by RNA polymerase II, as 5'-capped and 3'-polyadenylated precursors of 200 to 300 nucleotides (19). They are processed by nuclear RNase Drosha and the RNA binding protein DiGeorge syndrome critical region 8 (DGCR8) into 60-70 nucleotide premiRNAs with hairpin structures and exported to the cytoplasm with the help of Exportin 5 and RAN GTPase. In the cytoplasm, the pre-miRNA is cleaved by the RNase III Dicer in combination with the HIV TAR RNA-binding protein (TRBP) or Protein Activator of PKR (PACT) RNA-binding proteins into 16-24 bp double stranded RNA. The guide RNA strand then associates with a protein of the Argonaute (AGO) family while the passenger strand is degraded. The AGO-associated miRNA strand is a part of the RNA-induced silencing complex (RISC). It interacts with mRNA *via* base pairing. The AGO proteins along with other partners recruit other players such as the deadenylase complexes PAN2-PAN3 and CCR4-NOT to repress translation and promote degradation of target mRNAs (20). miRNA biogenesis is regulated at the post-translational level through modifications such as phosphorylation and sumoylation (19).

MAMMALIAN TOLL-LIKE RECEPTORS AND RLRS

MiRNAs regulate innate immune responses by targeting inflammatory pathways. PRRs recognize PAMPS to trigger inflammatory signaling. The role of Toll-like receptors (TLRs) has been extensively studied in the context of *M. tuberculosis* infection (21). The cytosolic sensors cyclic GMP-AMP synthase (cGAS), interferon-activable protein 204 (IFI204), and absent in melanoma 2 (AIM2) recognize *M. tuberculosis* DNA, while retinoic acid-inducible gene-I (RIG-I), melanoma differentiation-associated protein 5 (MDA5), and protein kinase R (PKR) detect RNA (22). Nucleotide-binding oligomerization domain (NOD) 2 recognizes muramyl dipeptide and regulates inflammatory cytokine production during *M. tuberculosis* infection (23).

The best studied pathway inhibited by miRNAs involves signaling through TLRs. TLRs are expressed on the plasma membrane [TLRS 1, 2, 5, 6; and 11 (expressed in mice but not in humans)] or on endosomes [TLRs 3, 7-8, 9; and 13 (expressed in mice but not in humans)] (24). Each TLR (or a combination of TLRs) senses PAMPs such as tricayllipopeptides (TLR1/2), diacyllipopeptides (TLR2/TLR6), lipopolysaccharide (LPS) (TLR4), flagellin (TLR5), dsRNA (TLR3), ssRNA (TLRs 7 and 8) or CpG DNA and hemozoin (TLR9). Once a ligand binds to the extracellular domain of a TLR, the intracellular Toll-IL-1-resistance (TIR) domains dimerize and recruit adaptor proteins such as myeloid differentiating factor 88 (MyD88) and TIR domain-containing adaptor inducing interferon-β (TRIF), followed by the sequential recruitment and activation of IL-1R-associated kinase (IRAK)-4, IRAK-1 and IRAK-2. Subsequently, there is engagement of downstream adaptor molecules such as

TNF receptor-associated factors (TRAFs), which then undergo K63-linked ubiquitination to activate the IκB kinase (IKK) complex (25). The IKK complex phosphorylates IκB-α, triggering its ubiquitination and proteasomal degradation, release of nuclear factor κ-light-chain-enhancer of activated B cells (NF-κB) p65, its translocation to the nucleus, and regulation of gene transcription, including those associated with inflammation (26). TLR3- or TLR4-mediated TRIF-dependent signaling leads to activation of the non-canonical IKKs Tank-binding protein kinase 1 (TBK1) and IKKε, and the phosphorylation and nuclear translocation of IFN regulatory factor (IRF) 3. miRNAs limit inflammation by targeting intermediates in this pathway.

RIG-I receptors (RLRs) are RNA sensors localized in the cytosol (27–29). There are three members, RIG-I, MDA5 and laboratory of genetics and physiology 2 (LGP2). RIG-I and MDA5 have two amino-terminal caspase activation and recruitment domains (CARDs), which mediate downstream signal transduction. RIG-I and MDA5 are essential for antiviral defense and type I interferon induction (30, 31). Interaction of RIG-I with mitochondrial anti-viral signaling protein (MAVS) is followed by activation of TBK1 and IKKε, which in turn activate IRF3 and IRF7 (32).

miRNAs TARGET THE INNATE IMMUNE RESPONSE DURING *M. TUBERCULOSIS* INFECTION

Phagocytosis and maturation of the phagosome are key steps in the clearance of bacterial pathogens by macrophages. Pathogenic mycobacteria evade maturation of the phagosome where they reside at least in part by blocking actin assembly. Early during infection of macrophages with *M. tuberculosis* there is an increase in miR-142-3p which directly targets N-Wiskott-Aldrich syndrome protein (N-WASp) to inhibit actin assembly (33). This demonstrates the miRNA-mediated regulation of phagocytosis during *M. tuberculosis* infection. MiR-146a/b, miR-155 and miR-21, form a trinity of miRNAs which regulate multiple steps of the TLR and RLR pathways (34–38) to regulate inflammation. These miRNAs are regulated upon activation of TLRs. miR-21 upregulation during *Mycobacterium leprae* infection is a bacterial strategy to escape the vitamin D-dependent induction of antimicrobial peptides (39). Downregulation of let-7 family members is also characteristic of the response of macrophages to bacterial infection (40, 41). Phosphatidylinositol-3,4,5-trisphosphate 5-phosphatase (SHIP1) is a negative regulator of NF-κB signaling. miR-155 targets SHIP1 in *M. tuberculosis*-infected macrophages (42), leading to the activation of the serine/threonine kinase Akt, likely facilitating the survival of *M. tuberculosis* in macrophages. miR-155 also targets BTB and CNC homology 1 (Bach1), a transcriptional repressor of heme oxygenase-1 (HO-1) and inhibits expression of interleukin-6 (*Il6*) to emerge as a regulator of the macrophage response to *M. tuberculosis*. miR-155 plays a dual role during *M. tuberculosis* infection *in vivo*. It enhances survival of macrophages as well as *M. tuberculosis*-specific T cells, providing on the one hand a niche for bacterial replication and on the other hand enabling an effective immune response (43). In support of this, miR-155$^{-/-}$ mice control infection at the initial stages, but fail to do so after the onset of adaptive immunity. Overall, the knockout of miR-155 exacerbates infection. This has also been borne out by the studies of Iwai et al. (44) using miR-155$^{-/-}$ mice challenged with *M. tuberculosis*. miRNA-mediated repression of the NF-κB pathway prevents exacerbated immune responses to infection. *M. tuberculosis*-induced miR-21-5p attenuates the secretion of IL-1β, IL-6 and TNF-α in RAW264.7 and THP-1 macrophages (45), whereas miR-27a directly targets IRAK4 to attenuate the production of IFN-γ, IL-β, IL-6, and TNF-α (46). There have been few studies on the regulation of miRNAs during infection of alveolar macrophages. In *M. bovis* BCG-infected alveolar macrophages, miR-124 negatively regulates inflammatory responses by directly targeting multiple components of the TLR pathways including MyD88, TRAF6 and TNF-α (47). miR-203, miR-30a and miR-149 target MyD88 in infected murine or human macrophages to downregulate proinflammatory cytokines as well as nitric oxide (NO) production (48–50). miR-20b inhibits *M. tuberculosis*-induced inflammation by directly targeting the NLRP3/casapase1/IL1β pathway (51). Further, miRNA-mediated NF-κB repression promotes the survival of *M. tuberculosis* in macrophages. The downregulation of let-7f during infection increases the expression of the A20 deubiquitinase. A20 targets the K63-linked ubiquitination of TRAF6 (52, 53), thereby negatively regulating the NF-κB pathway, and inhibiting inflammatory cytokine and nitric oxide production thereby facilitating the survival of *M. tuberculosis* in macrophages (40). MiRNA-125a targets TRAF6 during *M. tuberculosis* infection, to repress NF-κB (54). The TLR4/miRNA-32-5p/FSTL1 (follistin like protein 1) axis attenuates IL-1β, IL-6 and TNF-α in THP-1 and U937 cells after *M. tuberculosis* infection (55). *M. tuberculosis*-induced miR-1178 targets TLR4 and attenuates release of IFN-γ, IL-6, IL-1β, and TNF-α in human macrophages (56). miR-378d targets Rab10. It is downregulated in *M. tuberculosis*-infected THP-1 and RAW264.7 macrophages leading to enhanced production of IL-6, IL-1β and TNF-α (57). miR-206 targets tissue inhibitor of metalloproteinase 3 (TIMP3) (58). leading to increased production of MMP9 as well as inflammatory cytokines during *M. tuberculosis* infection. miR-99b expression is highly upregulated in infected macrophages as well as in dendritic cells. It targets TNF-α and TNFRSF-4 receptor genes to attenuate IL-12, IL-1β, IL-6 and TNF-α (59). miR-125b targets TNF-α, whereas miR-155 enhances TNF-α production by increasing TNF mRNA half-life and limiting expression of SHIP1, a negative regulator of the PI3K/Akt pathway. Rajaram et al. (60) have shown that human macrophages infected with *M. tuberculosis* induce high miR-125b expression and low miR-155 expression with correspondingly low TNF-α production. miR-140 is upregulated in human peripheral blood mononuclear cells (PBMCs) from patients with TB. It dampens the production of IL-1β, IL-6 and TNF-α in THP-1 macrophages infected with *M. tuberculosis* (61). In *M. bovis* BCG-infected macrophages, miR-142-3p targets IRAK1 (62) and miR-146a targets IRAK-1 and TRAF-6 (63) to dampen the production

of proinflammatory cytokines TNF-α, IL-6, IL-1β and the chemokine MCP-1. miR-223 targets the chemoattractants CXCL2, CCL3, and IL-6 in myeloid cells to regulate recruitment of myeloid cells to the lungs and as a result, neutrophil-driven inflammation (64). MiR-223 is upregulated in the blood and lung parenchyma of tuberculosis patients. From the above, it is evident that miRNAs play a central role in the attenuation of inflammatory responses during *M. tuberculosis* infection. **Table 1** summarizes the role of miRNAs in regulating inflammatory responses in *M. tuberculosis*-infected macrophages.

Depending on the stimulus, macrophages can be directed towards distinct phenotypes in a process termed macrophage polarization. In the simplest scenario, macrophage polarization results in M1 (classically activated macrophages, proinflammatory state) or M2 (alternatively activated macrophages, anti-inflammatory state) phenotypes, a molecular event crucial for inflammation. M1 macrophages produce proinflammatory cytokines TNF-α, IL-1β, IL-12, IL-6 and IL-23 along with reactive oxygen species (ROS) and nitric oxide. They recruit other immune cells including neutrophils through the production of chemokines such as CXCL8, CCL2, CXCL11, CXCL9 and CXCL10. M2 macrophages produce anti-inflammatory cytokines such as IL-10 and TGF-β, as well as arginase which represses nitric oxide production. M2 macrophages express the mannose receptor (MR) which signals production of cytokines such as CCL17, CCL18, CCL22 and CCL24 that recruit Th2 lymphocytes, eosinophils, basophils and T regulatory (Treg) cells (68). M1 polarized macrophages efficiently clear *M. tuberculosis*, whereas M2 polarization enhances survival of the bacterium in macrophages. Virulent strains of *M. tuberculosis* drive M2 polarization (69). Macrophage polarization is influenced by miRNAs. For example, *M. tuberculosis* infection of murine macrophages, decreases miR-26a-5p, consequently derepressing the transcription factor Kruppel-like factor 4 (KLF4), favoring M2 macrophage polarization in murine macrophages (65). However, in human macrophages miR-26a and miR-132 have been reported to be upregulated (66). These target p300 to attenuate IFNγ responses. In contrast, miR-20b directly targets nucleotide-binding oligomerization domain, leucine rich repeat and pyrin domain containing (NLRP) 3, and its downregulation during *M. tuberculosis* infection favors M1 polarization through activation of the NLRP3/IL-1β/caspase-1 axis (51). It is evident that inflammatory responses in the macrophage can be regulated by targeting miRNAs which interfere with pathways linked to macrophage polarization.

TABLE 1 | MicroRNAs that target signaling in myeloid cells during *M. tuberculosis* infection to regulate phagocytosis, cytokines, chemokines, macrophage polarization and glycolysis.

MicroRNA	Target	Reference
miR-142-3p	N-Wasp	(33)
miR-155	Ship1, Bach1	(42)
miR-21-5p	Bcl-2, Tlr4	(45)
miR-27a	Irak4	(46)
miR-203, miR-30a, miR-149	Myd88	(48–50)
miR-124	Myd88, Traf6, Tnfα	(47)
miR-20b	Nlrp3	(51)
Let-7f	A20 (Tnfaip3)	(40)
miR-125a	Traf6	(54)
miR-32-5p	Fstl1	(55)
miR-1178	Tlr4	(56)
miR-378d	Rab10	(57)
miR-206	Timp3	(58)
miR-99b	Tnfα, Tnfrsf4	(59)
miR-125b	Tnfα	(60)
miR-26a-5p	Klf4	(65)
miR-132	p300	(66)
miR-20b	Nlrp3	(51)
miR-223	Cxcl2, Ccl3, Il6	(64)
miR-21	Pfk-M	(67)

THE REGULATION OF METABOLIC REPROGRAMMING BY miRNAs

The phenotype of the macrophage is intimately linked to its metabolism (70). The relationship between metabolic pathways and macrophage polarization, is more complex than previously thought, However, in a broad sense, M1 macrophages rely on glycolysis (71). They present two breaks in the tricarboxylic acid (TCA) cycle which lead to accumulation of itaconate and succinate, which directly impact macrophage functions (72). Succinate stabilizes hypoxia inducible factor 1-α (HIF1-α). This activates the transcription of glycolytic genes and enhances glycolysis. M2 macrophages, on the other hand, are more dependent on oxidative phosphorylation (OXPHOS), their TCA cycle being intact. Evidence for the prevalence of glycolysis during *M. tuberculosis* infection was obtained by RNA-sequencing of the infected mouse lung tissue at 12, 18 and 30 days (73). It showed the upregulation of glycolytic genes including hexokinases (*Hk2* and *3*), phosphofructokinase (*Pfk*) family 1 and 2, glyceraldehye-3-phosphate dehydrogenase (*Gapdh*), phosphoglycerate kinase (*Pgk1*), enolase (*Eno1*), and lactate dehydrogenase A (*Ldha*); glucose transporters (*Glut1, 3* and *6*); a transporter for lactate (*Mct4*); an H^+-ATPase involved in cytosolic pH homeostasis; and *Hif-1α* (regulatory unit of HIF-1, a transcriptional activator of several glycolytic genes which regulates inflammatory processes under normoxia (74). Treating *M. tuberculosis*-infected mice with 2-deoxyglucose depleted the highly glycolytic subset of infiltrating macrophages and increased the burden of *M. tuberculosis*. The importance of glycolysis in host defense against *M. tuberculosis* has been documented in several studies (75–78). Hackett et al. (67) have shown that persistent *M. tuberculosis* infection of macrophages is associated with miR-21-dependent negative regulation of host glycolysis. Dampening of glycolysis is mediated through targeting of phosphofructokinase muscle (PFK-M) isoform which in turn facilitates bacterial growth by limiting pro-inflammatory mediators such as IL-1β. *M. tuberculosis*-infected *MiR-21*$^{-/-}$ bone marrow derived macrophages (BMDMs) showed increased levels of pro-inflammatory mediators including nitric oxide synthase 2 (*Nos2*) mRNA, arginase 1 (*Arg1*), and ROS with concomitant containment of *M. tuberculosis*. Increased containment of bacteria in *MiR-21*$^{-/-}$ BMDMs is lost when expression of PFK-M is silenced by specific siRNA. In summary, metabolic reprogramming as a consequence of infection, can be influenced by targeting miRNA-regulated pathways. In this context, it is important to evaluate how

much information obtained from experiments with mice, can be extrapolated to human infection.

REGULATION OF AUTOPHAGY BY miRNAs

Autophagy is regarded as a homeostatic process by which the eukaryotic cell delivers cytosolic cargo such as misfolded proteins or damaged organelles to the lysosomes for degradation. It can be classified into macroautophagy, chaperone-mediated autophagy and microautophagy. For this review, the term autophagy will refer to macroautophagy. Autophagy impacts diseases linked to inflammation such as infections, cancer, metabolic disorders, autoimmunity, neurodegeneration, cardiovascular and liver diseases (79). In brief, autophagy requires the capture of cargo destined for the lysosomes in double-membrane organelles termed autophagosomes. This occurs through the induction of a signal followed by membrane targeting, vesicle expansion and autophagosome formation. A range of signals such as starvation triggers formation of an isolation membrane usually derived from the endoplasmic reticulum (80). The Unc-51-like kinase 1 (ULK1) is released from the mammalian target of rapamycin complex 1 (mTORC1). Phosphorylated AMP-activated protein kinase (AMPK) phosphorylates ULK1 which in turn forms a complex with the 200 kDa focal adhesion kinase family-interacting protein (FIP200) and autophagy related gene (ATG) 13 to induce autophagy (81). The ULK1 complex recruits Beclin-1 (BECN1) and phosphoinositide 3-kinase regulatory subunit 4 (PIK3R4) in the phagophore membrane nucleation step. The engagement of PtdIns3-kinase class III (PtdIns3KC3) results in the production of PtdIns3P at the phagophore, recruitment of PtdIns3P binding proteins such as WD-repeat protein interacting with phosphoinositides (WIPI) 1 and WIPI2, finally leading to phagophore assembly. The tumor suppressor protein, UV-radiation resistance associated gene (UVRAG) interacts with Beclin-1 and promotes Beclin-1–PI3KC3-mediated autophagy by functioning as an adaptor (82, 83). Autophagosome elongation involves two ubiquitin-like conjugation systems, ATG12-ATG5 which is activated by ATG7 and ATG10 (E1 like and E2 like enzymes respectively) and light chain 3 (LC3 or MAP1LC3B)-phosphatidylethanolamine (PE) which is activated by ATG7 and ATG3 (E2 like enzyme) (84). ATG12-ATG5 complex directs LC3 to the target membrane where it is cleaved by the cysteine protease ATG4B, followed by conjugation of PE to the exposed glycine residue (**Figure 1**). Eventually, the autophagosomes are directed to lysosomes in a process requiring small GTPases such as Rab7 and soluble N-ethylmaleimide-sensitive factor attachment protein receptor proteins (SNAREs). In a variation of autophagy termed xenophagy, intracellular bacteria and viruses are captured with the help of autophagy adaptors for targeting to lysosomes (85, 86). Adaptors such as sequestosome 1 (SQSTM1/p62), nuclear dot protein 52 (NDP52), optineurin (OPTN), and neighbor of BRCA1 gene 1 (NBR1) form a bridge between the cargo and LC3 (87). For a more detailed understanding of autophagy and its role in the immune response to bacteria and viruses, the reader may refer to several excellent reviews (85, 86, 88–90).

Autophagy has long been recognized as a defense against *M. tuberculosis* (91–93). *M. tuberculosis* employs a range of factors to evade autophagy. For example, "enhanced intracellular survival" (eis) gene inhibits host autophagy (94). MiRNAs play a role in the regulation of autophagy during *M. tuberculosis* infection (95). Differentially regulated miR-23a-5p induction by *M. tuberculosis* inhibits autophagy in murine RAW264.7 macrophages by targeting TLR2 (96). Induction of Ca^{2+} acts as a major regulator of autophagy. Upon stimulation, entry of Ca^{2+} into the cytoplasm activates Ca^{2+}/calmodulin-dependent

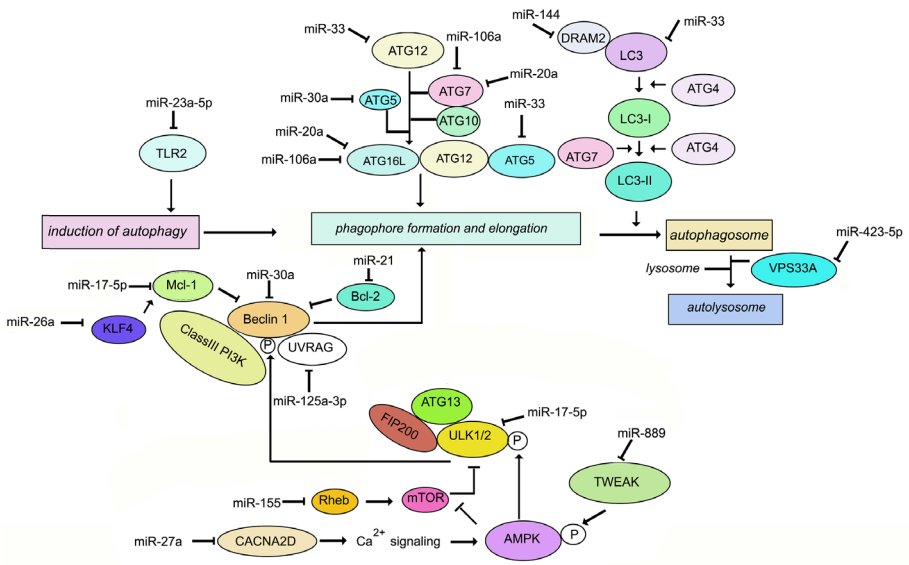

FIGURE 1 | Schematic representation of the key molecules of autophagy targeted by miRNAs during *M. tuberculosis* infection.

serine/threonine kinase leading to activation of AMPK and phosphorylation of ULK1. Therefore downregulation of Ca^{2+} signaling inhibits autophagy promoting the intracellular survival of *M. tuberculosis* in macrophages. miR-27a targets the Ca^{2+} transporter voltage-dependent calcium channel subunit alfa2delta (CACNA2D) to limit Ca^{2+} entry into the cytoplasm and downregulate Ca^{2+} signaling (97). Mycobacterial infection induces TNF-like weak inducer of apoptosis (TWEAK) in the early phase of infection. TWEAK induces autophagy and promotes mycobacterial autophagosome maturation through activation of AMPK. *M. tuberculosis* induces MiR-889 which inhibits autophagy *via* post-transcriptional suppression of TWEAK expression to maintain mycobacterial survival in granulomas (98). The Bcl-2 family member Mcl-1 sequesters Beclin-1 to inhibit autophagy (99). *M. tuberculosis* inhibits miR17-5p and upregulates its targets Mcl-1 and STAT3, which is a transcriptional activator of Mcl-1 (100), thereby inhibiting autophagy during *M. tuberculosis* infection. miR-125a-3p regulates autophagy by targeting UVRAG (101). *M. tuberculosis* induces miR106-a in THP1 macrophages. miR-106-a could inhibit autophagy by targeting ULK1, ATG7, and ATG16L1 (102). Infection of macrophages with *M. bovis* BCG results in enhanced expression of miR-20a, which inhibits autophagy by targeting ATG7 and ATG16L1 (103). A negative correlation has been demonstrated between miR-30a expression and levels of Beclin-1 as well as ATG5 in *M. tuberculosis*-infected THP-1 cells (104). Ouimet et al. (8) have reported that miR-33 inhibits autophagy flux through repression of ATG5, ATG12 and LC3B in *M. tuberculosis*-infected macrophages. *M. tuberculosis* infection upregulates miR-144 which targets DNA damage-regulated autophagy modulator (DRAM2). DRAM2 releases Beclin-1 from the BECN1 inhibitory complex by directly interacting with Beclin1 (105). Vacuolar protein sorting 33A(VPS33A) is a direct target of miR-423-5p which is upregulated in the serum of TB patients (106). It is therefore plausible that upregulation of miR-423-5p suppresses autophagosome-lysosome fusion during active tuberculosis. Upregulation of miR-26a has been demonstrated to modulate autophagy and *M. tuberculosis* survival in human and murine macrophages by targeting Mcl-1 (65). In summary, during *M. tuberculosis* infection, multiple miRNAs target intermediates which are involved in autophagy. There are fewer reports of miRNA-mediated induction of autophagy during *M. tuberculosis* infection. One report is the induction of miR-155 in *M. tuberculosis*-infected macrophages, which leads to repression of the negative regulator of autophagy, RHEB, ultimately inducing autophagy and compromised bacterial survival (107). On the contrary, *M. bovis* BCG reportedly inhibits IFNγ-induced autophagy by induction of miR-155 and miR-31 which target the protein phosphatase 2A (PP2A) regulatory subunit, PPP2R5A (108). These differences could be due to miR-155 functioning differently in resting macrophages *vs*. IFNγ-activated macrophages, or due to differences in cell types infected. The role of miRNAs in the regulation of autophagy during *M. tuberculosis* infection, is summarized in **Figure 1**. Exploiting miRNA-directed therapeutics to augment autophagy, is a plausible option for the management of TB.

REGULATION OF APOPTOSIS BY miRNAs

There are principally two major pathways leading to apoptosis that are characterized by the activation of caspases 3 and 7 (109, 110). The extrinsic apoptotic pathway involves death receptors, such as Fas and TNFR1, which are membrane-bound. Upon binding of their ligands FasL and TNFR1, they oligomerize and initiate a cascade of signaling events involving assembly of a death-inducing signaling complex (DISC) on the cytoplasmic side of the membrane. The Fas/FasL pair recruits the adaptor protein Fas-associated protein with death domain (FADD), while the TNFR1/TNF pair, recruits tumor necrosis factor receptor type 1-associated death domain protein (TRADD). This is followed by formation of the death inducing complex (DISC) which causes the self-cleavage of procaspase 8 into its active form. Caspase 8 then activates downstream caspases -3, -6 and -7. Intrinsic apoptosis occurs when the cell experiences intracellular stress such as DNA damage or oxidative stress, leading to damage of the mitochondrial outer membrane, and mitochondrial outer membrane permeability (MOMP). Cytochrome c is released into the cytosol, where it associates with the adaptor protein apoptosis protease activating factor 1 (Apaf-1) to trigger its oligomerization and formation of the apoptosome complex. The apoptosome recruits and activates caspase 9, finally leading to the activation of caspase 3. The release of cytochrome c is regulated by the Bcl-2 family of proteins that are either pro- or anti-apoptotic (111). Pro-apoptotic members such as Bax and Bak bind directly to the mitochondrial outer membrane forming pores. Anti-apoptotic members such as Mcl-1 and Bcl-2 bind and sequester the proapoptotic Bcl-2 proteins. The BH3 only proteins such as Bim, p53 upregulated modulator of apoptosis (PUMA), Bid and Bad, bind to the pro-survival Bcl-2 family proteins to sequester them (112) (**Figure 2**). Unlike apoptosis, necrotic cells undergo swelling of organelles and rupturing of cytoplasmic content into the extracellular space. The necrotic debris and damage-associated molecular pattern molecules (DAMPs) trigger inflammation and tissue damage (113). *M. tuberculosis* initiates apoptosis or necrosis in the infected host. Apoptosis protects the host and kills the bacteria through efferocytosis of the apoptotic vesicles (114). Apoptosis of infected macrophages is required for dendritic cells to acquire mycobacterial antigens for cross priming. Necrosis, on the other hand, benefits the pathogen. It releases the intracellular bacteria into the extracellular milieu to promote dissemination, and triggers inflammation. Virulent strains of *M. tuberculosis* induce necrosis (115, 116) and evade apoptosis (117). The differential regulation of apoptosis and necrosis by virulent as opposed to avirulent *M. tuberculosis* or members of the *M. tuberculosis* complex, depends at least in part, on the differential expression of miRNAs. For example, *M. bovis* BCG induces IFNγ by inhibiting miR-29 (118), whereas *M. tuberculosis* H37Rv upregulates miR-99b expression in murine dendritic cells and macrophages to decrease their targets TNF and TNFRSF45 (TNFR1) (59). Cytokine expression in the cells is altered to affect activation of the host immune response and the survival of intracellular mycobacteria. miR-20a-5p targets JNK2 to repress Bim expression and apoptosis in macrophages. Downregulation of miR-20a-5p in THP-1 macrophages triggers apoptosis and facilitates clearance of *M. tuberculosis* (119). miR-20b-5p on the other hand,

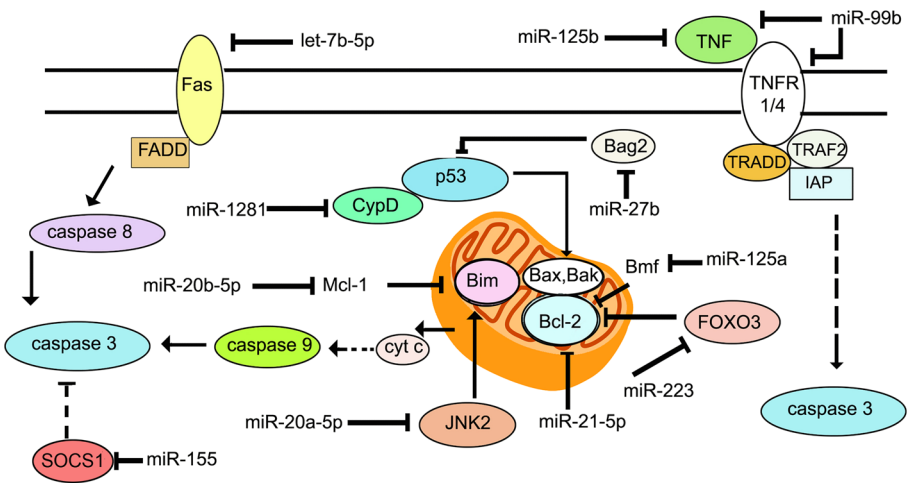

FIGURE 2 | Schematic representation of the key molecules of apoptosis targeted by miRNAs during *M. tuberculosis* infection.

targets Mcl-1 (120), and miR-21-5p targets Bcl-2 (45) to activate apoptosis in *M. tuberculosis*-infected macrophages. Cyclophilin D (CyPD) associates with p53 to induce apoptosis (121). Overexpression of miRNA-1281 which targets CyPD, protects human macrophages from *M. tuberculosis*-induced programmed necrosis and apoptosis (122). The nuclear body protein, Sp110 regulates miR-125a, miR-146a, miR-155, miR-21a and miR-99b expression in *M. tuberculosis*-infected RAW264.7 (123). It upregulates Bcl2 modifying factor (Bmf) by inhibiting miR-125a, thereby enhancing apoptosis. In primary human macrophages infected with *M. tuberculosis*, miR-579 induction downregulates its targets sirtuin 1 (SIRT1) and phosphoinositide-dependent protein kinase 1 (PDK1) and leads to macrophage apoptosis (124). miR-325-3p directly targets ligand of numb-protein X 1 (LNX1) (125), an E3 ubiquitin ligase of NIMA related kinase 6 (NEK6) which promotes NEK6 proteasomal degradation. The accumulation of NEK6 activates signal transducer and activator of transcription 3 (STAT3) signaling and inhibits apoptosis. On the other hand, Wu et al. (126) have shown that miR-21 is increased in alveolar macrophages of BCG-vaccinated mice, and miR-21 enhances apoptosis of bone marrow derived dendritic cells (BMDCs) from BCG-vaccinated mice most likely by targeting Bcl-2. 6 kDa early secretory antigenic target (ESAT-6)-driven miR-155 targets suppressor of cytokine signaling 1 (SOCS1) to augment macrophage apoptosis by elevating caspase 3 activity (127). TLR-2/MyD88/NF-κB dependent induction of miR-27b suppresses NF-κB (128). Further, miR-27b targets Bcl-2-associated athanogene 2 (Bag2) to regulate apoptosis. miR-27b increases p53-dependent apoptosis to lower bacterial burden. Induction of let-7b-5p in *M. tuberculosis* infected THP-1 macrophages leads to reduction in its target Fas, and inhibition of apoptosis (29). Activated Akt phosphorylates and inhibits the transcriptional activity of forkhead box O3 (FOXO3) (129). Upon Akt inactivation, dephosphorylated FOXO3 translocates to the nucleus where it activates transcription of multiple pro-apoptotic genes harboring the forkhead response elements (FRE) in their promoter regions (130). miR-223 targets FOXO3 (131). The upregulation of miR-223 during infection, therefore, likely plays a role in the attenuation of macrophage apoptosis. A list of miRNAs regulating apoptosis during *M. tuberculosis* infection is given in **Table 2**, and their roles are schematically presented in **Figure 2**. Manipulation of apoptosis by administration of miRNA agonists or antagonists deserves further exploration as a means of containing *M. tuberculosis in vivo*.

THE ROLE OF LONG NON-CODING RNAs IN REGULATING THE IMMUNE RESPONSE TO *M. TUBERCULOSIS*

The majority of lncRNAs are transcribed by RNA polymerase II (RNAPII) (133), although there are some that are transcribed by RNA polymerase III (RNAPIII) including the 7SL RNA genes (134). LncRNAs undergo transcriptional editing such as splicing and polyadenylation before finally adopting a stable structure. They are expressed in a manner that is dependent on cell and tissue types, the stage of development, and association with disease (10, 135). They show poor evolutionary conservation (136), although a small number of lncRNAs are well conserved (137). LncRNAs fall into different categories. Antisense lncRNAs are transcribed across the exons of protein coding genes, but from the opposite strand. The transcripts for long intergenic non-coding RNAs (lincRNAs) are located between protein coding genes. Enhancer RNA (eRNA) transcripts are bidirectionally expressed at active enhancer regions of the genome. These are mainly cis-acting and control interactions between promoters and enhancers to regulate gene expression. Intronic lncRNAs are transcribed from the introns of annotated protein coding genes. circRNAs interact with and interfere with the functions of miRNAs.

LncRNAs perform diverse functions among which is the regulation of immunity and host-pathogen interactions (138–140). They interact with other molecules through base pairing or

TABLE 2 | MicroRNAs involved in the regulation of apoptosis during *M. tuberculosis* infection.

MicroRNA	Target	Reference
miR-99b	Tnf, Tnfrsf45	(59)
miR-20a-5p	Jnk2	(119)
miR-20b-5p	Mcl-1	(120)
miR-21-5p	Bcl-2	(45)
miR-1281	Cyclophilin D	(121)
miR-125a	Bmf	(123)
miR-579	Sirt1, Pdk	(124)
miR-155	Socs1	(127)
miR-27b	Bag2	(128)
miR-223	Foxo3	(131)
Let-7b-5p	Fas	(132)
miR-325-3p	Lnx1	(125)

secondary structures (141). Nuclear lncRNAs interact with chromatin remodelers to regulate the expression of neighboring or distal genes. Cytoplasmic lncRNAs interfere with stability and translation of mRNA and signaling pathways (142). They also interact with a range of other molecules. In summary, they can act as protein scaffolds, regulators of transcription, antisense RNA or miRNA sponges (143–147). LncRNAs are now acknowledged as major players in maintaining homeostasis and in disease (148, 149). Transcriptomic data have shown the differential expression of hundreds of lncRNAs during PRR stimulation (150–153). Several of these lncRNAs are trans-acting regulators of protein-coding genes such as TNF and HNRNPL related immunoregulatory long non-coding RNAc(THRIL) which regulates TNF-α expression by forming a complex with the ribonucleoprotein (RNP) hnRNPL that acts at the TNF-α promoter (154), or the lincRNA-COX2 which regulates inflammatory gene expression in LPS-stimulated bone marrow-derived dendritic cells by interacting with hnRNP-A/B and hnRNP-A2/B1 (151) or the lincRNA-EPS which associates with chromatin and interacts with hnRNPL to repress immune-responsive gene-1 (IRG) expression (150).

LncRNA expression profiles have been documented by transcriptome analysis from pulmonary TB (PTB) patients *vs.* healthy individuals (155). PTB patients showed differential expression of 449 lncRNAs. The expression profiles of lncRNAs were investigated by transcriptome sequencing. Lnc-HNRNPU-1:7 and lnc-FAM76B-4:1 were the most upregulated and downregulated lncRNAs respectively, in PTB patients compared to healthy individuals. In separate studies (156), a comprehensive analysis has shown that compared to healthy volunteers, 1,429 and 2,040 lncRNAs are deregulated in the PBMCs from MDR-TB and drug-sensitive TB patients, respectively. However, these results have not been analyzed with respect to their relevance and implications in the context of infection. During TB infection, the expression of the lnc-TGS1–1 target miR-143, is increased due to elimination of the sponge effect of lnc-TGS1-1. This likely suppresses downstream innate immune signaling (157). Along similar lines, removal of the inhibitory effect of lnc-AC145676.2.1–6 results in upregulation of miR-29a and interference with the TLR pathway (158).

LncRNA nuclear paraspeckle assembly transcript 1 (NEAT1) is expressed at higher levels in PBMCs from patients with tuberculosis than in healthy individuals, and in infected THP1 cells compared to uninfected ones (159). Knockdown of NEAT1 increases bacterial CFUs in infected THP1 cells, suggesting that NEAT1 is required for mounting a bactericidal response against *M. tuberculosis*. Comprehensive expression profiles of murine RAW264.7 macrophages infected with *M. tuberculosis* showed differential regulation of 1,487 lncRNAs (791 up and 696 down) (160). LncRNA profiles have also been generated for human macrophages infected with *M. tuberculosis* (161). In a study involving 473 healthy individuals and 467 TB patients, lnc-AC145676.2.1-6 and lnc-TGS1-1 expression levels were lower in TB patients. LincRNA cyclooxygenase 2 (Cox2) is activated by the TLR signaling pathway in macrophages and mediates both activation and repression of genes (151). LincRNACox2 is increased in macrophages infected with *M. tuberculosis* (15). Knockdown of lincRNA Cox2 decreased NF-κB and STAT3 while increasing apoptosis in infected macrophages. LncRNA HOX Transcript Antisense RNA (HOTAIR) targets the H3K27 methylase complex polycomb repressive complex 2 (PRC2) to distinct loci to regulate H3K27 methylation at these loci (162). Subuddhi et al. (163) have shown that lncRNA HOTAIR is downregulated in *M. tuberculosis* H37Rv-infected THP-1 macrophages, but upregulated in *M. tuberculosis* H37Ra-infected macrophages, leading to differential association of H3K27 methylation marks at the dual specificity phosphatase 4 (DUSP4) and SATB homeobox 1 (SATB1) loci. Downregulation of HOTAIR, facilitated increased transcription of DUSP4 and SATB1, both of which favored the survival of *M. tuberculosis* H37Rv in macrophages. Li et al. (164) showed a significant reduction in PC-esterase domain containing 1B antisense RNA1 (PCED1B-AS1) expression in monocytes from patients with active TB compared with that in monocytes from healthy individuals. Suppression of PCED1B-AS1 in infected macrophages significantly attenuated TNF-α-induced apoptosis with decreased cleaved caspase-3 and a concomitant increase in Bcl-2. Further, PCED1B-AS1 serves a miR-155 sponge. Its knockdown leads to upregulation of miR-155 and inhibition of its targets RHEB and FOXO3, culminating in enhanced autophagy (107, 165). Sun et al. (166) have reported that LncRNA maternally expressed 3 (MEG3) is activated by vitamin D and plays a regulatory role in carcinogenesis (167). It is highly expressed in pulmonary tuberculosis (PTB) (166). Lnc-MEG3 binds miR-145-5p (168). The relationship between Lnc-MEG3, miR-145-5p and apoptosis has been strengthened by infecting RAW264.7 with *M. bovis* BCG under conditions of overexpression or knock down of MEG3 (166). The authors have shown that inhibition of Lnc-MEG3 is associated with increased miR-145-5p and decreased apoptosis. Lnc-MEG3 also induces autophagy in macrophages infected with *M. bovis* BCG (16).

LncRNAs regulate the response of T and B cells to *M. tuberculosis* by regulating chromatin modification states. During *M. tuberculosis* infection, CD244, a T cell-inhibitory molecule, mediates inhibition of IFN-γ and TNF-α expression by inducing lncRNA-CD244 which interacts with the H3K27 methylase enhancer of zeste homolog 2 (EZH2), and mediates modification of a more repressive chromatin

state at the *infg* and tnfa loci (169). Knock down of lncRNA-CD244 significantly enhances IFN-γ and TNF-α expression and improves protective immunity of CD8+ T cells.

Differentially expressed lncRNAs have been identified in CD4+ T cells in latent TB (170). Fu et al. (171) have reported that 844 lncRNAs were differentially expressed in B cells from individuals with TB. Concomitant with the dysregulation of several lncRNAs, adjacent protein-coding genes were also deregulated. For example, SOCS3 and its neighboring lncRNA XLOC_012582 were highly expressed in B cells from TB patients. The relevance of this observation in the context of TB, awaits further investigation. LncRNAs that regulate host signaling pathways during *M. tuberculosis* infection, are shown in **Figure 3**.

NON-CODING RNAS AS MARKERS OF ACTIVE TB AND LTBI

The potential use of miRNAs in the diagnosis of tuberculosis has been reviewed by Sabir et al. (172). In particular, the role of exosomal miRNAs as biomarkers of TB is of interest (173). MiRNAs miR-20a, miR-20b, miR-26a, miR-106a, miR-191, miR-486 are differentially expressed in exosomes from TB compared to healthy individuals (174). The overexpressed miRNAs showed reduction in expression after two months of anti-tuberculosis therapy. In a separate study, miR-484, miR-425, and miR-96-3-p were reported to be enriched in exosomes from patients with active TB (175). Some studies have specifically explored the potential of exosomal miRNAs as biomarkers of LTBI. Small RNA sequencing of serum exosomes from LTBI and TB patients showed that let-7e-5p, let-7d-5p, miR-450a-5p and miR-140-5p were specifically expressed in LTBI, whereas miR-1246, miR-2110, miR-370-3p, miR-28-3p and miR-193-5p, were specifically associated with active TB (176). In a separate study, miR-122-5p expression was observed to be significantly higher in the exosomes of LTBI than in active TB (177). On the other hand, let-7i-5p, miR-148a-3p, miR-21-5p and miR-423-5p showed higher expression in active TB than in LTBI. Independent miRNA profiling from PBMCs or serum suggest that a group of differentially regulated miRNAs distinguish active TB from latent TB (178, 179). miR-889 expression was increased in patients with latent TB compared to uninfected individuals (98). Latorre et al. (180) have identified whole blood-derived miRNA signatures that enable distinguishing active TB from latent TB. A systems biology approach has been adopted by Lin

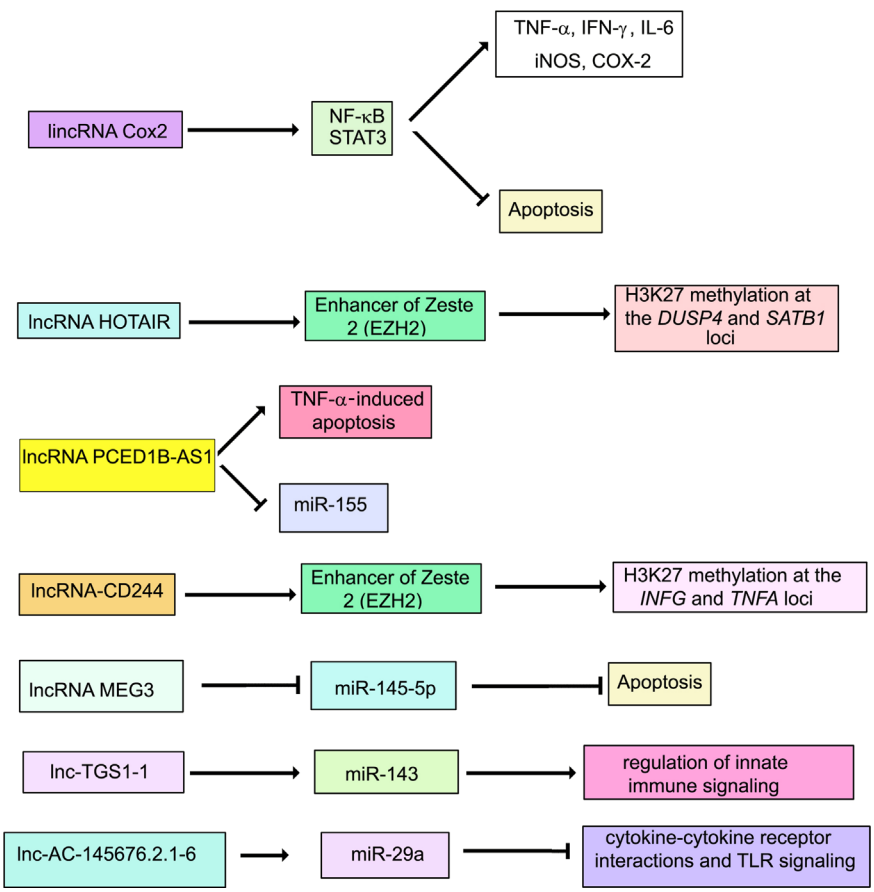

FIGURE 3 | Schematic representation of the role of lncRNAs during *M. tuberculosis* infection.

et al. (181) to generate a unique miRNA-gene regulatory network for LTBI by analyzing numerous microarray data sets. The miRNAs in this network were identified with the Hippo signaling pathway (miR-212-3p, miR-29a-5p, miR-29b-3p), ECM–receptor interaction (miR-432-5p, miR-148b-5p, miR-29b-3p, miR-532-5p), and the PI3K-Akt signaling pathway (miR-29b-3p). The reciprocal relationship between MAPK1 and miR-212-3p was validated. The authors suggest that the interaction of miR-212-3p with MAPK1 could regulate the PI3K-Akt signaling pathway to affect the transmission of *M. tuberculosis*.

In a similar vein, attempts have been made to use lncRNA expression as a means of TB diagnosis. Fang et al. (182) have analyzed the GEO dataset (GSE94907) and identified the differentially regulated lncRNAs NONHSAT101518.2, NONHSAT 067134.2, NONHSAT148822.1 and NONHSAT078957.2 which are downregulated in the plasma of active TB patient plasma compared with the healthy individuals, as potential biomarkers. In a separate study, a total of 163 upregulated lncRNAs and 348 downregulated lncRNAs were identified in the plasma of PTB patients (18). Four differentially expressed lncRNAs, NR_038221, NR_003142, ENST00000570366 and ENST00000422183 were confirmed by qRT-PCR. The potential target genes of NR_003142 in immune pathways were TLR6, nucleotide binding oligomerization domain containing 2 (NOD2), HLA-DQB and IL6ST suggesting that it could influence TB pathology. Hu et al. (183) have shown that three lncRNAs, ENST00000497872, n333737, and n335265 are differentially expressed in blood samples of active TB patients compared to healthy individuals and suggested that these may serve as potential biomarkers for clinically diagnosed PTB patients. Of these, lncRNA ENST00000497872 is located close to the immune related gene immunoglobulin heavy constant alfa 1 (IGHA1) and n333737 is located close to the immune related gene T cell receptor alfa variable 1-2 (TRAV1-2). Lnc-TGS1–1 and lnc-AC145676.2.1–6 are downregulated in TB patients (184). In separate studies, 41 lncRNAs have been reported to be deregulated in a comparison between healthy subjects, active TB and LTBI (170). These studies suggest that targeting miRNAs and lncRNAs for development of HDTs, and as biomarkers of TB, deserve detailed investigation.

CONCLUDING REMARKS

This review outlines the role of miRNAs and lncRNAs in regulating functions in myeloid cells that are critical in determining the outcome of *M. tuberculosis* infection such as inflammation, macrophage polarization, metabolism, autophagy and apoptosis. In spite of the extensive literature presently available, there are several roadblocks and contradictions along the path towards understanding the role of miRNAs in human tuberculosis, arising out of differences between animal infections and human disease and variations in methodology (such as strains used, multiplicity of infection, and time of infection) between different studies. One such example is the role of miR-21 in infection. Mir-21, on the one hand, inhibits glycolysis and the production of bactericidal effectors such as ROS and NO (67), providing a permissive milieu for the growth of *M. tuberculosis*. On the other hand, Zhao et al. (45) report that miR-21 targets Bcl-2, suggesting that it accelerates apoptosis. This would deprive *M. tuberculosis* of its niche within the host. As of now, there are no *in vivo* studies to resolve such contradictions on the actual role of miR-21 in infection.

Methods for rapid diagnosis of TB are urgently required. miRNAs have been explored for the diagnosis of a range of diseases such as cancer. Several studies have tested the potential of miRNAs as diagnostic markers for TB. Among the miRNAs that have been discussed here, at least four have been consistently associated with TB namely miR-144-3p, miR-144-5p, miR-146a and miR-155. miR-144-3p levels are higher in sputum and serum from patients with active TB compared to healthy uninfected individuals (185). miR-144-3p targets ATG4a to inhibit autophagy during *M. bovis* BCG infection. miR-144-5p levels are increased in PBMCs from active TB patients compared to healthy individuals (186). miR-144-5p targets DRAM2 to regulate autophagy. Alveolar macrophages from smear-positive patients show lower levels of miR-146a than those from smear-negative patients or healthy uninfected individuals (187). miR-146a targets IRAK1 and TRAF6. miR-155 levels are reportedly reduced in serum from patients with active TB (188), and increased after TB therapy. miR-155 has been reported to regulate inflammatory cytokines, autophagy and apoptosis, during infection of macrophages. miR-196b and miR-376c have been proposed as serum markers of active TB and LTBI (179). The differential expression of miRNAs in body fluids such as blood and sputum, distinguishes TB patients from healthy individuals, or LTBI; treated from untreated patients; and those infected with hypervirulent or drug-resistant strains (189). Serum exosomes have also been evaluated for the presence of miRNA biomarkers capable of distinguishing latent TB, active TB and healthy individuals. A recent study has suggested the differential expression of miR-625-3p in urine samples, as a marker for TB diagnosis (190). This highlights the pivotal role of miRNAs in TB. However, as of now miRNA signatures characteristic of tuberculosis disease states, remain to be defined (191). In particular, detailed investigation needs to be done in terms of identifying biomarkers for latent TB. There are obvious pitfalls in comparing miRNA levels during *in vitro* and *in vivo* infection across different studies, arising out of difficulties in pinning down different stages of the disease, choice of platform for miRNA identification, choice of strain of *M. tuberculosis*, age and sex of individuals, methods of RNA extraction, and sample size, to mention a few. However, there is substantial literature that underscores the need to explore development of miRNA delivery vehicles and miRNA-based therapeutics as possible strategies for shortening the duration of therapy (9). Some studies in animal models have shown promise. Lou et al. (51) have demonstrated that intravenous administration of miR-20b mimics could attenuate the inflammatory response in a mouse model of infection by inhibiting activation of the inflammosome. In a *M. marinum* model, transfection of microglia with miR-124-3p promoted apoptosis through targeting of STAT3 to decrease mycobacterial

proliferation (192). It is therefore important to devise efficient delivery methods for miRNAs that would protect them from circulating RNAse and target them to the site of infection. The available technologies for miRNA delivery include nanoparticles as vehicles, use of viral vectors, exosome-like vesicles and lipid-based delivery systems. A silica nanoparticle-based targeted delivery of miR-34a, to neuroblastoma tumors in a murine orthotopic xenograft model, has been demonstrated (193). It must be mentioned that nanoparticle based delivery platforms are associated with high cost of production, non-specific distribution and cytotoxicity. Administration of miR-26a in a mouse model of hepatocellular carcinoma using adeno-associated virus (AAV) inhibited cancer cell proliferation (194). However, viral delivery methods may elicit unwanted inflammatory responses. There are several reports that suggest that miRNA could probably be delivered to the lung for the treatment of TB. Mice treated with pre-miR-133b containing lipoplexes through the tail vein, showed 52-fold higher expression of miR-33b in the lungs compared to untreated mice (195). miRNA targeting drugs are in clinical trials for the treatment of hepatitis C virus infection *via* targeting miR-122, polycystic kidney disease *via* targeting miR-17, cutaneous T cell lymphoma *via* targeting miR-155 and keloids *via* targeting miR-19 (196). miRNA based therapeutic options need to be pursued in earnest for the management of TB.

The association of lncRNAs with tuberculosis, and their functions have been less extensively explored than the role of miRNAs. Much more work needs to carried out, before we understand their link to disease outcomes.

AUTHOR CONTRIBUTIONS

JB and MK reviewed the literature and wrote the manuscript. All authors contributed to the article and approved the submitted version.

FUNDING

JB is supported by funding from the J.C. Bose Fellowship (SB/S2/JCB-049/2016). MK is supported by the Council for Scientific and Industrial Research, Emeritus Scientist Scheme (21(1088)/19/EMR-II).

ACKNOWLEDGMENTS

The authors acknowledge the contributions of all the scientists in this area and apologize for failing to cite any work due to constraints of space.

REFERENCES

1. *Global Tuberculosis Report 2020*. Geneva: World Health Organization (2020).
2. Gurtan AM, Sharp PA. The Role of miRNAs in Regulating Gene Expression Networks. *J Mol Biol* (2013) 425:3582–600. doi: 10.1016/j.jmb.2013.03.007
3. Aguilar C, Mano M, Eulalio A. MicroRNAs at the Host-Bacteria Interface: Host Defense or Bacterial Offense. *Trends Microbiol* (2019) 27:206–18. doi: 10.1016/j.tim.2018.10.011
4. Skalsky RL, Cullen BR. Viruses, MicroRNAs, and Host Interactions. *Annu Rev Microbiol* (2010) 64:123–41. doi: 10.1146/annurev.micro.112408.134243
5. Staedel C, Darfeuille F. MicroRNAs and Bacterial Infection. *Cell Microbiol* (2013) 15:1496–507. doi: 10.1111/cmi.12159
6. Duval M, Cossart C, Lebretonde A. Mammalian MicroRNAs and Long Noncoding RNAs in the Host-Bacterial Pathogen Crosstalk. *Semin Cell Dev Biol* (2017) 65:11–9. doi: 10.1016/j.semcdb.2016.06.016
7. Das K, Garnica O, Dhandayuthapani S. Modulation of Host miRNAs by Intracellular Bacterial Pathogens. *Front Cell Infect Microbiol* (2016) 6:79. doi: 10.3389/fcimb.2016.00079
8. Ouimet M, Koster S, Sakowski E, Ramkelawon B, van Solingen C, Oldebeken S, et al. *Mycobacterium Tuberculosis* Induces mir-33 Locus to Reprogram Autophagy and Host Lipid Metabolism. *Nat Immunol* (2016) 6:677–86. doi: 10.1038/ni.3434
9. Singh AK, Ghosh M, Kumar V, Aggarwal S, Patil SA. Interplay Between miRNAs and *Mycobacterium Tuberculosis*: Diagnostic and Therapeutic Implications. *Drug Discov Today* (2021) 26:1245–55. doi: 10.1016/j/drudis.2021.01.021
10. Derrien T, Johnson R, Bussotti G, Tanzer A, Djebali S, Tilgner H, et al. The GENCODE V7 Catalog of Human Long Noncoding RNAs: Analysis of Their Gene Structure, Evolution, and Expression. *Genome Res* (2012) 22:1775–89. doi: 10.1101/gr.132159.111
11. Häfner SJ, Talvard TG, Lund AH. Long Noncoding RNAs in Normal and Pathological Pluripotency. *Semin Cell Dev . Biol* (2017) 65:1–10. doi: 10.1016/j.semcdb.2016.07.011
12. Rinn JL, Chang HY. Genome Regulation by Long Noncoding RNAs. *Annu Rev Biochem* (2012) 81:145–66. doi: 10.1146/annurev-biochem-051410-092902
13. Fathizadeh H, Hayat SMG, Dao S, Ganbarov K, Tanomand A, Asgharzadeh M, et al. Long Non-Coding RNA Molecules in Tuberculosis. *Int J Biol Macromol* (2020) 156:340–6. doi: 10.1016/j.ijbiomac.2020.04.030
14. Hadjicharalambous MR, Lindsay MA. Long Non-Coding RNAs and the Innate Immune Response. *Non-Coding RNA* (2019) 5:34. doi: 10.3390/ncrna5020034
15. Li D, Gao C, Zhao L, Zhang Y. Inflammatory Response Is Modulated by LincRNAcox2 *Via* the NF−κB Pathway in Macrophages Infected by *Mycobacterium Tuberculosis*. *Mol Med Rep* (2020) 21:2513–21. doi: 10.3892/mmr.2020.11053
16. Pawar K, Hanisch C, Vera SEP, Einspanier R, Sharbati S. Down Regulated lncRNA MEG3 Eliminates Mycobacteria in Macrophages Via Autophagy. *Sci Rep* (2016) 6:19416. doi: 10.1038/srep19416
17. Wang C, Yang S, Liu CM, Jiang TT, Chen ZL, Tu HH, et al. Screening and Identification of Four Serum miRNAs as Novel Potential Biomarkers for Cured Pulmonary Tuberculosis. *Tuberculosis* (2018) 10826:–34. doi: 10.1016/j.tube.2017.08.010
18. Chen Z-L, Wei L-L, Shi L-Y, Li M, Jiang T-T, Chen J, et al. Screening and Identification of lncRNAs as Potential Biomarkers for Pulmonary Tuberculosis. *Sci Rep* (2017b) 7:16751. doi: 10.1038/s41598-017-17146-y
19. Treiber T, Treiber N, Meister G. Regulation of MicroRNA Biogenesis and Its Crosstalk With Other Cellular Pathways. *Nat Rev Mol Cell Biol* (2019) 20:5–20. doi: 10.1038/s41580-018-0059-1
20. Huntzinger E, Izaurralde E. Gene Silencing by MicroRNAs: Contributions of Translational Repression and mRNA Decay. *Nat Rev Genet* (2011) 12:99–110. doi: 10.1038/nrg2936
21. Basu J, Shin D-M, Jo E-K. Mycobacterial Signaling Through Toll-Like Receptors. *Front Cell Infect Microbiol* (2012) 2:145. doi: 10.3389/fcimb.2012.00145
22. Chai Q, Wang L, Liu CH, Baoxue G. New Insights Into the Evasion of Host Innate Immunity by *Mycobacterium Tuberculosis*. *Cell Mol Immunol* (2020) 17:901–13. doi: 10.1038/s41423-020-0502-z

23. Brooks MN, Rajaram MVS, Azad AK, Amer AO, Valdivia-Arenas MA, Park J-H, et al. Nod2 Controls the Nature of the Inflammatory Response and Subsequent Fate of *Mycobacterium Tuberculosis* and *M. Bovis* BCG in Human Macrophages. *Cell Microbiol* (2011) 13:402–18. doi: 10.1111/j.1462-5822.2010.01544.x
24. Kawasaki T, Kawai T. Toll-Like Receptor Signaling Pathways. *Front Immunol* (2014) 5:461. doi: 10.3389/fimmu.2014.00461
25. Chen ZJ. Ubiquitin Signalling in the NF-κB Pathway. *Nat Cell Biol* (2005) 7:758–65. doi: 10.1038/ncb0805-758
26. Hayden MS, Ghosh S. Nf-κb, the First Quarter-Century: Remarkable Progress and Outstanding Questions. *Genes Dev* (2012) 26:203–34. doi: 10.1101/gad.183434.111
27. Goubau D, Deddouche S, Reis e Sousa C. Cytosolic Sensing of Viruses. *Immunity* (2013) 38:855–69. doi: 10.1016/j.immuni.2013.05.007
28. Hartmann G. Nucleic Acid Immunity. *Adv Immunol* (2017) 133:121–69. doi: 10.1016/bs.ai.2016.11.001
29. Yoneyama M, Kikuchi M, Natsukawa T, Shinobu N, Imaizumi T, Miyagishi M, et al. The RNA Helicase RIG-I Has An Essential Function in Double-Stranded RNA-Induced Innate Antiviral Responses. *Nat Immunol* (2004) 5:730–7. doi: 10.1038/ni1087
30. Gitlin L, Barchet W, Gilfillan S, Cella M, Beutler B, Flavell RA, et al. Essential Role of Mda-5 in Type I Ifn Responses to Polyriboinosinic:Polyribocytidylic Acid and Encephalomyocarditis PicoRNAvirus. *Proc Natl Acad Sci USA* (2006) 103:8459–64. doi: 10.1073/pnas.0603082103
31. Kato H, Takeuchi O, Sato S, Yoneyama M, Yamamoto M, Matsui K, et al. Differential Roles of MDA5 and RIG-I Helicases in the Recognition of RNA Viruses. *Nature* (2006) 441:101–5. doi: 10.1038/nature04734
32. Rehwinkel J, Gack MU. Rig-I-Like Receptors: Their Regulation and Roles in RNA Sensing. *Nat Rev Immunol* (2020) 20:537–51. doi: 10.1038/s41577-020-0288-3
33. Bettencourt P, Marion S, Pires D, Santos LF, Lastrucci C, Carmo N, et al. Actin-Binding Protein Regulation by MicroRNAs as a Novel Microbial Strategy to Modulate Phagocytosis by Host Cells: The Case of N-Wasp and Mir-142-3p. *Front Cell Infect Microbiol* (2013) 3:19. doi: 10.3389/fcimb.2013.00019
34. Hou J, Wang P, Lin L, Liu X, Ma F, An H, et al. MicroRNA-146a Feedback Inhibits RIG-I-Dependent Type I IFN Production in Macrophages by Targeting Traf6, IRAK1, and IRAK2. *J Immunol* (2009) 183:2150–8. doi: 10.4049/jimmunol.0900707
35. O'Connell RM, Taganov KD, Boldin MP, Cheng G, Baltimore D. MicroRNA-155 Is Induced During the Macrophage Inflammatory Response. *Prof Natl Acad Sci USA* (2007) 104:1604–9. doi: 10.1073/pnas.0610731104
36. Nejad C, Stunden HJ, Gantie MP. A Guide to miRNAs in Inflammation and Innate Immune Responses. *FEBS Lett* (2018) 285:3695–716. doi: 10.1111/febs.14482
37. Sheedy FJ, Palsson-McDermott E, Hennessy EJ, Martin C, O'Leary JJ, Ruan Q, et al. Negative Regulation of TLR4 *Via* Targeting of the Proinflammatory Tumor Suppressor PDCD4 by the MicroRNA Mir-21. *Nat Immunol* (2010) 11:141–7. doi: 10.1038/ni.1828
38. Taganov KD, Boldin MP, Chang KJ, Baltimore D. Nf-κB-Dependent Induction of MicroRNA Mir-146, An Inhibitor Target to Signaling Proteins of Innate Immune Responses. *Proc Natl Acad Sci USA* (2006) 103:12481–6. doi: 10.1073/pnas.0605298103
39. Liu PT, Wheelwright M, Teles R, Komisopoulos E, Edfeldt K, Ferguson B, et al. MicroRNA-21 Targets the Vitamin D-Dependent Antimicrobial Pathway in Leprosy. *Nat Med* (2012) 18:267–73. doi: 10.1038/nm.2584
40. Kumar M, Sahu SK, Kumar R, Subuddhi A, Maji RK, Jana K, et al. MicroRNA Let-7 Modulates the Immune Response to *Mycobacterium Tuberculosis* Infection Via Control of A20, an Inhibitor of the NF-κB Pathway. *Cell Host Microbe* (2015) 17:345–56. doi: 10.1016/j.chom.2015.01.007
41. Schulte LN, Eulalio A, Mollenkopf H-J, Reinhardt R, Vogel J. Analysis of the Host MicroRNA Response to Salmonella Uncovers the Control of Major Cytokines by the Let-7 Family. *EMBO J* (2011) 30:1977–89. doi: 10.1038/emboj.2011.94
42. Kumar R, Halder P, Sahu S, Kumar M, Kumari M, Jana K, et al. Identification of a Novel Role of ESAT-6-Dependent Mir-155 Induction During Infection of Macrophages With *Mycobacterium Tuberculosis*. *Cell Microbiol* (2012) 14:1620–31. doi: 10.1111/j.1462-5822.2012.01827.x
43. Rothchild AC, Sissons JR, Shafiani S, Plaisier C, Min D, Mai D, et al. Mir-155–Regulated Molecular Network Orchestrates Cell Fate in the Innate and Adaptive Immune Response to *Mycobacterium Tuberculosis*. *Proc Natl Acad Sci USA* (2016) 113:E6172–81. doi: 10.1073/pnas.1608255113
44. Iwai H, Funatogawa K, Matsumura K, Kato-Miyazawa M, Kirikae F, Kiga K, et al. MicroRNA-155 Knockout Mice Are Susceptible to *Mycobacterium Tuberculosis* Infection. *Tuberculosis* (2015) 95:246–50. doi: 10.1016/j.tube.2015.03.006
45. Zhao Z, Hao J, Li X, Chen Y, Qi X. Mir-21-5p Regulates Mycobacterial Survival and Inflammatory Responses by Targeting Bcl-2 and TLR4 in *Mycobacterium Tuberculosis*-Infected Macrophages. *FEBS Lett* (2019) 593:1326–35. doi: 10.1002/1873-3468.13438
46. Wang J, Jia Z, Wei B, Zhou Y, Niu C, Bai S, et al. MicroRNA-27a Restrains the Immune Response to *Mycobacterium Tuberculosis* Infection by Targeting IRAK4, a Promoter of the NF-κB Pathway. *Int J Clin Exp Pathol* (2017) 10:9894–901.
47. Maa C, Lia Y, Lia M, Deng G, Wu X, Zeng J, et al. MicroRNA-124 Negatively Regulates TLR Signaling in Alveolar Macrophages in Response to Mycobacterial Infection. *Mol Immunol* (2014) 62:150–8. doi: 10.1016/j.molimm.2014.06.014
48. Wei J, Huang Z, Zhang W, Jia Z, Zhao Z, Zhang Y, et al. Myd88 as a Target of MicroRNA-203 in Regulation of Lipopolysaccharide or Bacille Calmette-Guerin Induced Inflammatory Response of Macrophage Raw264.7 Cells. *Mol Immunol* (2013) 55:303–9. doi: 10.1016/j.molimm.2013.03.004
49. Wu Y, Sun Q, Dai L. Immune Regulation of Mir-30 on the *Mycobacterium Tuberculosis*-Induced TLR/Myd88 Signaling Pathway in THP-1 Cells. *Exp Ther Med* (2017) 14:3299–303. doi: 10.3892/etm.2017.4872
50. Xu G, Zhang Z, Xing Y, Wei J, Ge Z, Liu X, et al. MicroRNA-149 Negatively Regulates TLR-Triggered Inflammatory Response in Macrophages by Targeting Myd88. *J Cell Biochem* (2014) 115:919–27. doi: 10.1002/jcb.24734
51. Lou J, Wang Y, Zhang Z, Qiu W. Mir-20b Inhibits *Mycobacterium Tuberculosis* Induced Inflammation in the Lung of Mice Through Targeting Nlrp3. *Exp Cell Res* (2017) 358:120–8. doi: 10.1016/j.yexcr.2017.06.007
52. Boone DL, Turer EE, Lee EG, Ahmad C, Wheeler MT, Tsui C, et al. The Ubiquitin-Modifying Enzyme A20 Is Required for Termination of Toll-Like Receptor Response. *Nat Immunol* (2004) 5:1052–60. doi: 10.1038/ni1110
53. Liu YC, Penninger J, Karin M. Immunity by Ubiquitylation: A Reversible Process of Modification. *Nat Rev Immunol* (2005) 5:941–52. doi: 10.1038/nri1731
54. Niu W, Sun B, Li M, Cui J, Huang J, Zhang L. TLR-4/MicroRNA-125a/NF-κB Signaling Modulates the Immune Response to Mycobacterium Tuberculosis Infection. *Cell Cycle* (2018) 17:1931–45. doi: 10.1080/15384101.2018.1509636
55. Zhang Z-M, Zhang A-R, Xu M, Lou J, Qiu W-Q. TLR-4/miRNA-32-5p/FSTL1 Signaling Regulates Mycobacterial Survival and Inflammatory Responses in *Mycobacterium Tuberculosis*-Infected Macrophages. *Exp Cell Res* (2017) 352:313–21. doi: 10.1016/j.yexcr.2017.02.025
56. Shi G, Mao G, Xe K, Wu D, Wang W. Mir-1178 Regulates Mycobacterial Survival and Inflammatory Responses in *Mycobacterium Tuberculosis*-Infected Macrophages Partly *Via* Tlr4. *J. Cell Biochem* (2018) 119:7449–57. doi: 10.1002/jcb.27054
57. Zhu Y, Xiao Y, Kong D, Liu H, Chen X, Chen Y, et al. Down-Regulation of Mir-378d Increased Rab10 Expression to Help Clearance of *Mycobacterium Tuberculosis* in Macrophages. *Front Cell Infect Microbiol* (2020) 17:108. doi: 10.3389/fcimb.2020.00108
58. Fu X, Zeng L, Liu Z, Ke X, Lei L, Li G. MicroRNA-206 Regulates the Secretion of Inflammatory Cytokines and MMP9 Expression by Targeting TIMP3 in *Mycobacterium Tuberculosis*–Infected THP-1 Human Macrophages. *Biochim Biophys Acta* (2016) 477:167–73. doi: 10.1016/j.bbrc.2016.06.038
59. Singh Y, Kaul V, Mehra A, Chatterjee S, Tousif S, Dwivedi VP, et al. *Mycobacterium Tuberculosis* Controls MicroRNA-99b (Mir-99b) Expression in Infected Murine Dendritic Cells to Modulate Host Immunity. *J Biol Chem* (2013) 288:5056–61. doi: 10.1074/jbc.C112.439778

60. Rajaram MVS, Ni B, Morris JD, Brooks MN, Carlson TK, Bakthavachalu B, et al. *Mycobacterium Tuberculosis* Lipomannan Blocks TNF Biosynthesis by Regulating Macrophage MAPK-Activated Protein Kinase 2 (MK2) and MicroRNA miR-125b. *Proc Natl Acad Sci USA* (2011) 108:17408–13. doi: 10.1073/pnas.1112660108
61. Li X, Huang S, Yu T, Liang G, Liu H, Pu D, et al. Mir-140 Modulates the Inflammatory Responses of *Mycobacterium Tuberculosis*-Infected Macrophages by Targeting Traf6. *J Cell Mol Med* (2019) 23:5642–53. doi: 10.1111/jcmm.14472
62. Xu G, Zhang Z, Wei J, Zhang Y, Zhang Y, Guo L, et al. Micror-142-3p Down-Regulates IRAK-1 in Response to *Mycobacterium Bovis* BCG Infection in Macrophages. *Tuberculosis* (2013) 93:606–11. doi: 10.1016/j.tube.2013.08.006
63. Li S, Yue Y, Xu W, Xiong S. MicroRNA-146a Represses Mycobacteria-Induced Inflammatory Response and Facilitates Bacterial Replication *Via* Targeting IRAK-1 and TRAF-6. *PloS One* (2013) 8:e81438. doi: 10.1371/journal.pone.0081438
64. Dorhoi A, Iannaccone M, Farinacci M, Faé KC, Schreiber J, Moura-Alves P, et al. MicroRNA-223 Controls Susceptibility to Tuberculosis by Regulating Lung Neutrophil Recruitment. *J Clin Invest* (2013) 123:4386–848. doi: 10.1172/JCI67604
65. Sahu SK, Kumar M, Chakraborty S, Banerjee SK, Kumar R, Gupta P, et al. MicroRNA 26a (miR-26a)/KLF4 and CREB-C/Ebpβ Regulate Innate Immune Signaling, the Polarization of Macrophages and the Trafficking of *Mycobacterium Tuberculosis* to Lysosomes During Infection. *PloS Pathog* (2017) 13:e1006410. doi: 10.1371/journal.ppat.1006410
66. Ni B, Rajaram MVS, Lafuse WP, Landes MB, Schlesinger LS. Mycobacterium Tuberculosis Decreases Human Macrophage IFN-γ Responsiveness Through miR-132 and miR-26a. *J Immunol* (2014) 193:4537–47. doi: 10.4049/jimmunol.1400124
67. Hackett EE, Charles-Messance H, O'Leary SM, Gleeson LE, Munoz-Wolf N, Case S, et al. *Mycobacterium Tuberculosis* Limits Host Glycolysis and IL-1b by Restriction of PFK-M *Via* MicroRNA-21. *Cell Rep* (2020) 30:124–36. doi: 10.1016/j.celrep.2019.12.015
68. Thiriot JD, Martinez-Martinez YB, Endsley JJ, Torres AG. Hacking the Host: Exploitation of Macrophage Polarization by Intracellular Bacterial Pathogens. *Pathog Dis* (2020) 78:ftaa009. doi: 10.1093/femspd/ftaa009
69. Lim Y-J, Yi MH, Choi J-A, Lee J, Han J-Y, Jo S-H, et al. Roles of Endoplasmic Reticulum Stress-Mediated Apoptosis in M1-Polarized Macrophages During Mycobacterial Infections. *Sci Rep* (2016) 6:37211. doi: 10.1038/srep37211
70. Van den Bossche J, O'Neill LA, Menon D. Macrophage Immunometabolism: Where Are We Going? *Trends Immunol* (2017) 38:395–406. doi: 10.1016/j.it.2017.03.001
71. Viola A, Munari F, Sánchez-Rodríguez R, Scolaro T, Castegna A. The Metabolic Signature of Macrophage Responses. *Front Immunol* (2019) 10:1462. doi: 10.3389/fimmu.2019.01462
72. O'Neill LA, Pearce EJ. Immunometabolism Governs Dendritic Cell and Macrophage Function. *J Exp Med* (2016) 213:15–23. doi: 10.1084/jem.20151570
73. Shi L, Salamon H, Eugenin EA, Pine R, Cooper A, Gennaro ML. Infection With Mycobacterium Tuberculosis Induces the Warburg Effect in Mouse Lungs. *Sci Rep* (2015) 5:18176. doi: 10.1038/srep18176
74. Imtiyaz HZ, Simon MC. Hypoxia-Inducible Factors as Essential Regulators of Inflammation. *Curr Top Microbiol Immunol* (2010) 345:105–20. doi: 10.1007/82_2010_74
75. Gleeson LE, Sheedy FJ, McDermott P, Triglia D, O'Leary SM, O'Sullivan MP, et al. *Mycobacterium Tuberculosis* Induces Aerobic Glycolysis in Human Alveolar Macrophages That Is Required for Control of Intracellular Bacillary Replication. *J Immunol* (2016) 196:2444–9. doi: 10.4049/jimmunol.1501612
76. Gleeson LE, O'Leary SM, Ryan D, McLaughlin AM, Sheedy FJ, Keane J. Cigarette Smoking Impairs the Bioenergetic Immune Response to Mycobacterium Tuberculosis Infection. *Am J Respir Cell Mol Biol* (2018) 59:572–9. doi: 10.1165/rcmb.2018-0162OC
77. Lachmandas E, Beigier-Bompadre M, Cheng SC, Kumar V, van Laarhoven A, Wang X, et al. Rewiring Cellular Metabolism *Via* the AKT/Mtor Pathway Contributes to Host Defence Against *Mycobacterium Tuberculosis* in Human and Murine Cells. *Eur J Immunol* (2016a) 46:2574–86. doi: 10.1002/eji.201546259
78. Lachmandas E, Boutens L, Ratter JM, Hijmans A, Hooiveld GJ, Joosten LAB, et al. Microbial Stimulation of Different Toll-Like Receptor Signalling Pathways Induces Diverse Metabolic Programmes in Human Monocytes. *Nat Microbiol* (2016b) 2:16246. doi: 10.1038/nmicrobiol.2016.246
79. Deretic V. Autophagy in Inflammation, Infection, and Immunometabolism. *Immunity* (2021) 54:437–53. doi: 10.1016/j.immuni.2021.01.018
80. Hayashi-Nishino M, Fujita N, Noda T, Yamaguchi A, Yoshimori T, Yamamoto A. A Subdomain of the Endoplasmic Reticulum Forms a Cradle for Autophagosome Formation. *Nat Cell Biol* (2009) 11:1433–7. doi: 10.1038/ncb1991
81. Mizushima N. The Role of the Atg1/ULK1 Complex in Autophagy Regulation. *Curr Opin Cell Biol* (2010) 22:132–9. doi: 10.1016/j.ceb.2009.12.004
82. Liang C, Feng P, Ku B, Dotan I, Canaani D, Oh B-H, et al. Autophagic and Tumour Suppressor Activity of a Novel Beclin1-Binding Protein Uvrag. *Nat Cell Biol* (2006) 8:688–99. doi: 10.1038/ncb1426
83. Liang C, Lee J-S, Inn K-S, Gack MU, Li Q, Roberts EA, et al. Beclin1-Binding UVRAG Targets the Class C Vps Complex to Coordinate Autophagosome Maturation and Endocytic Trafficking. *Nat Cell Biol* (2008) 10:776–87. doi: 10.1038/ncb1740
84. Mizushima N, Noda T, Yoshimori T, Tanaka Y, Ishii T, George MD, et al. A Protein Conjugation System Essential for Autophagy. *Nature* (1998) 395:395–8. doi: 10.1038/26506
85. Levine B. Eating Oneself and Uninvited Guests: Autophagy-Related Pathways in Cellular Defense. *Cell* (2005) 120:159–62. doi: 10.1016/S0092-8674(05)00043-7
86. Levine B, Mizushima N, Virgin HW. Autophagy in Immunity and Inflammation. *Nature* (2011) 469:323–35. doi: 10.1038/nature09782
87. Shaid S, Brandts CH, Serve H, Dikic I. Ubiquitination and Selective Autophagy. *Cell Death Differ* (2013) 20:21–30. doi: 10.1038/cdd.2012.72
88. Deretic V. Autophagy in Tuberculosis. *Cold Spring Harb. Perspect Med* (2014) 4:a018481. doi: 10.1101/cshperspect.a018481
89. Jo EK, Yuk J-M, Shin DM, Sasakawa C. Roles of Autophagy in Elimination of Intracellular Bacterial Pathogens. *Front Immunol* (2013) 4:97. doi: 10.3389/fimmu.2013.00097
90. Siqueira MDS, Ribeiro RM, Travassos LH. Autophagy and Its Interaction With Intracellular Bacterial Pathogens. *Front Immunol* (2018) 9:935. doi: 10.3389/fimmu.2018.00935
91. Castillo EF, Dekonenko A, Arko-Mensah J, Mandell MA, Dupont N, Jiang S, et al. Autophagy Protects Against Active Tuberculosis by Suppressing Bacterial Burden and Inflammation. *Proc Natl Acad Sci USA* (2012) 109:E3168–76. doi: 10.1073/pnas.1210500109
92. Gutierrez MG, Master SS, Singh SB, Taylor GA, Colombo MI, Deretic V. Autophagy Is a Defense Mechanism Inhibiting BCG and Mycobacterium Tuberculosis Survival in Infected Macrophages. *Cell* (2004) 119:753–66. doi: 10.1016/j.cell.2004.11.038
93. Watson RO, Manzanillo PS, Cox JS. Extracellular M. Tuberculosis DNA Targets Bacteria for Autophagy by Activating the Host DNA-Sensing Pathway. *Cell* (2012) 150:803–15. doi: 10.1016/j.cell.2012.06.040
94. Shin DM, Jeon BY, Lee HM, Jin HS, Yuk JM, Song CH, et al. *Mycobacterium Tuberculosis* Eis Regulates Autophagy, Inflammation, and Cell Death Through Redox-Dependent Signaling. *PloS Pathog* (2010) 6:e1001230. doi: 10.1371/journal.ppat.1001230
95. Kim JK, Kim TS, Basu J, Jo E-K. MicroRNA in Innate Immunity and Autophagy During Mycobacterial Infection. *Cell Microbiol* (2017) 19:e12687. doi: 10.1111/cmi.12687
96. Gu X, Gao Y, Mu DG, Fu EQ. Mir-23a-5p Modulates Mycobacterial Survival and Autophagy During *Mycobacterium Tuberculosis* Infection Through Tlr2/Myd88/Nf-κb Pathway by Targeting Tlr2. *Exp Cell Res* (2017) 354:71–7. doi: 10.1016/j.yexcr.2017.03.039
97. Liu F, Chen J, Wang P, Li H, Zhou Y, Liu H, et al. MicroRNA-27a Controls the Intracellular Survival of *Mycobacterium Tuberculosis* by Regulating Calcium Associated Autophagy. *Nat Commun* (2018) 9:4295. doi: 10.1038/s41467-018-06836-4
98. Chen DY, Chen Y-M, Lin CF, Lo CM, Liu HJ, Liao TL. MicroRNA-889 Inhibits Autophagy to Maintain Mycobacterial Survival in Patients With Latent Tuberculosis Infection by Targeting Tweak. *mBio* (2020) 11:e03045–19. doi: 10.1128/mBio.03045-19

99. Germain M, Slack R. Mcl-1 Regulates the Balance Between Autophagy and Apoptosis. *Autophagy* (2011) 7:549–51. doi: 10.4161/auto.7.5.15098
100. Kumar R, Sahu S, Kumar M, Jana K, Gupta P, Gupta U, et al. MicroRNA 17-5p Regulates Autophagy in *Mycobacterium Tuberculosis*-Infected Macrophages by Targeting Mcl-1 and STAT3. *Cell Microbiol* (2016) 18:679–91. doi: 10.1111/cmi.12540
101. Kim J, Yuk JY, Kim S, Kim TS, Jin HS, Young CS, et al. MicroRNA-125a Inhibits Autophagy Activation and Antimicrobial Responses During Mycobacterial Infection. *J Immunol* (2015) 11:5355–65. doi: 10.4049/jimmunol.1402557
102. Liu K, Hong D, Zhang F, Li X, He M, Han X. MicroRNA-106a Inhibits Autophagy Process and Antimicrobial Responses by Targeting Ulk1, ATG7, and ATG16L1 During Mycobacterial Infection. *Front Immunol* (2021) 11:610021. doi: 10.3389/fimmu.2020.610021
103. Guo L, Zhao J, Qu Y, Yin R, Gao Q, Ding S, et al. MicroRNA-20a Inhibits Autophagic Process by Targeting ATG7 and ATG16L1 and Favors Mycobacterial Survival in Macrophage Cells. *Front Cell Infect Microbiol* (2016) 6:134. doi: 10.3389/fcimb.2016.00134
104. Chen Z, Wang T, Liu Z, Zhang G, Wang J, Feng S, et al. Inhibition of Autophagy by miR-30A Induced by Mycobacterium Tuberculosis as a Possible Mechanism of Immune Escape in Human Macrophages. *Japan J Infect Dis* (2015) 68:420–4. doi: 10.7883/yoken.JJID.2014.466
105. Kim J, Lee HM, Park KS, Shin DM, Kim TS, Kim YS, et al. MIR144* Inhibits Antimicrobial Responses Against Mycobacterium Tuberculosis in Human Monocytes and Macrophages by Targeting the Autophagy Protein Dram2. *Autophagy* (2017) 13:423–41. doi: 10.1080/15548627.2016.1241922
106. Tu H, Yang S, Jiang T, Wei L, Shi L, Liu C, et al. Elevated Pulmonary Tuberculosis Biomarker miR-423-5p Plays Critical Role in the Occurrence of Active TB by Inhibiting Autophagosome-Lysosome Fusion. *Emerg Microb Infect* (2019) 8:448–60. doi: 10.1080/22221751.2019.1590129
107. Wang J, Yang K, Zhou L, Wu M, Wu Y, Zhu M, et al. MicroRNA-155 Promotes Autophagy to Eliminate Intracellular Mycobacteria by Targeting Rheb. *PloS Pathog* (2013) 9:e1003697. doi: 10.1371/journal.ppat.1003697
108. Holla S, Kurowska-Stolarska M, Bayry J, Balaji KN. Selective Inhibition of IFNG-Induced Autophagy by Mir155- and Mir31- Responsive WNT5A and SHH Signalling. *Autophagy* (2014) 2:311–30. doi: 10.4161/auto.27225
109. Creagh EM, Conroy H, Martin SJ. Caspase Activation Pathways in Apoptosis and Immunity. *Immunol Rev* (2003) 193:10–21. doi: 10.1034/j.1600-065X.2003.00048.x
110. Hengartner MO. The Biochemistry of Apoptosis. *Nature* (2000) 407:770–6. doi: 10.1038/35037710
111. Youle RJ, Strasser A. The Bcl-2 Protein Family: Opposing Activities That Mediate Cell Death. *Nat Rev Mol Cell Biol* (2008) 9:47–59. doi: 10.1038/nrm2308
112. Giam M, Huang DCS, Bouillet P. Bh3-Only Proteins and Their Roles in Programmed Cell Death. *Oncogene* (2008) 27:S128–36. doi: 10.1038/onc.2009.50
113. Lamkanfi M, Dixit VM. Manipulation of Host Cell Death Pathways During Microbial Infections. *Cell Host Microbe* (2010) 8:44–54. doi: 10.1016/j.chom.2010.06.007
114. Martin CJ, Booty MG, Rosebrock TR, Nunes-Alves C, Desjardins DM, Keren I, et al. Efferocytosis Is an Innate Antibacterial Mechanism. *Cell Host Microbe* (2012) 12:289–300. doi: 10.1016/j.chom.2012.06.010
115. Divangahi M, Chen M, Gan H, Desjardins D, Hickman TT, Lee DM, et al. *Mycobacterium Tuberculosis* Evades Macrophage Defenses by Inhibiting Plasma Membrane Repair. *Nat Immunol* (2009) 10:899–906. doi: 10.1038/ni.1758
116. Park JS, Tamayo MH, Gonzalez-Juarrero M, Orme IM, Ordway DJ. Virulent Clinical Isolates of Mycobacterium Tuberculosis Grow Rapidly and Induce Cellular Necrosis But Minimal Apoptosis in Murine Macrophages. *J Leukocyte Biol* (2006) 79:80–6. doi: 10.1189/jlb.0505250
117. Keane J, Remold HG, Kornfeld H. VirulentMycobacterium Tuberculosis Strains Evade Apoptosis of Infected Alveolar Macrophages. *J Immunol* (2000) 164:2016–20. doi: 10.4049/jimmunol.164.4.2016
118. Ma F, Xu S, Liu X, Zhang Q, Xu X, Liu M, et al. The MicroRNA Mir-29 Controls Innate and Adaptive Immune Responses to Intracellular Bacterial Infection by Targeting Interferon-γ. *Nat Immunol* (2011) 12:861–9. doi: 10.1038/ni.2073
119. Zhang G, Liu X, Wang W, Cai Y, Li S, Chin Q, et al. Downregulation of miR-20a-5p Triggers Cell Apoptosis to Facilitate Mycobacterial Clearance Through Targeting JNK2 in Human Macrophages. *Cell Cycle* (2016) 15:2527–38. doi: 10.1080/15384101.2016.1215386
120. Zhang D, Yi Z, Fu Y. Downregulation of miR-20b-5p Facilitates *Mycobacterium Tuberculosis* Survival in RAW 264.7 Macrophages *Via* Attenuating the Cell Apoptosis by Mcl-1 Upregulation. *Cell Biochem* (2019) 120:5889–96. doi: 10.1002/jcb.27874
121. Qin LS, Jia PF, Zhang ZQ, Zhang SM. Ros-P53-Cyclophilin-D Signaling Mediates Salinomycin-Induced Glioma Cell Necrosis. *J Exp Clin Cancer Res* (2015) 34:57. doi: 10.1186/s13046-015-0174-1
122. Sun Q, Shen X, Wang P, Ma J, Sha W. Targeting Cyclophilin-D by miR-1281 Protects Human Macrophages From *Mycobacterium Tuberculosis*-Induced Programmed Necrosis and Apoptosis. *Aging* (2019) 11:12661–73. doi: 10.18632/aging.102593
123. Wu Y, Guo Z, Yao K, Miao Y, Liang S, Liu F, et al. The Transcriptional Foundations of Sp110-Mediated Macrophage (Raw264.7) Resistance to *Mycobacterium Tuberculosis* H37ra. *Sci Rep* (2016) 6:22041. doi: 10.1038/srep22041
124. Ma J, Chen X-L, Sun Q. MicroRNA-579 Upregulation Mediates Death of Human Macrophages With Mycobacterium Tuberculosis Infection. Biochem. Biophys. *Res Commun* (2019) 518:219–26. doi: 10.1016/j.bbrc.2019.08.035
125. Fu B, Xue W, Zhang H, Zhang R, Feldman K, Zhao Q, et al. MicroRNA-325-3p Facilitates Immune Escape of *Mycobacterium Tuberculosis* Through Targeting LNX1 *Via* NEK6 Accumulation to Promote Anti-Apoptotic STAT3 Signaling. *mBIO* (2020) 11:e00557–20. doi: 10.1128/mBio.00557-20
126. Wu Z, Lu H, Sheng J, Li L. Inductive MicroRNA-21 Impairs Anti-Mycobacterial Responses by Targeting IL-12 and Bcl-2. *FEBS Lett* (2012) 586:2459–67. doi: 10.1016/j.febslet.2012.06.004
127. Yang S, Li F, Jia S, Zhang K, Jiang W, Shang Y, et al. Early Secreted Antigen ESAT-6 of *Mycobacterium Tuberculosis* Promotes Apoptosis of Macrophages *Via* Targeting the MicroRNA155-SOCS1 Interaction. *Cell Physiol Biochem* (2015) 35:1276–88. doi: 10.1159/000373950
128. Liang S, Song Z, Wu Y, Gao Y, Gao M, Liu F, et al. MicroRNA-27b Modulates Inflammatory Response and Apoptosis During *Mycobacterium Tuberculosis* Infection. *J Immunol* (2018) 200:3506–18. doi: 10.4049/jimmunol.1701448
129. Tzivion G, Dobson M, Ramakrishnan G. Foxo Transcription Factors; Regulation by AKT and 14-3-3 Proteins. *Biochim Biophys Acta* (2011) 1813:1938– 1945. doi: 10.1016/j.bbamcr.2011.06.002
130. Gilley J, Coffer PJ, Ham J. Foxo Transcription Factors Directly Activate *Bim* Gene Expression and Promote Apoptosis in Sympathetic Neurons. *J Cell Biol* (2003) 162:613–22. doi: 10.1083/jcb.200303026
131. Xi X, Zhang C, Han W, Zhao H, Zhang H, Jiao J. MicroRNA-223 Is Upregulated in Active Tuberculosis Patients and Inhibits Apoptosis of Macrophages by Targeting Foxo3. *Genet Test Mol Biomark* (2015) 19:650–6. doi: 10.1089/gtmb.2015.0090
132. Tripathi A, Srivastava V, Singh BN. Hsa-Let-7b-5p Facilitates Mycobacterium Tuberculosis Survival in THP-1 Human Macrophages by Fas Downregulation. *FEMS Microbiol Lett* (2018) 365:1–7. doi: 10.1093/femsle/fny040
133. Guttman M, Amit I, Garber M, French C, Lin MF, Feldser D, et al. Chromatin Signature Reveals Over a Thousand Highly Conserved Large Non-Coding RNAs in Mammals. *Nature* (2009) 458:223–7. doi: 10.1038/nature07672
134. Englert M, Felis M, Junker V, Beier H. Novel Upstream and Intragenic Control Elements for the RNA Polymerase III-Dependent Transcription of Human 7sl RNA Genes. *Biochimie* (2004) 86:867–74. doi: 10.1016/j.biochi.2004.10.012
135. Cabili MN, Trapnell C, Goff L, Koziol M, Tazon-Vega B, Regev A, et al. Integrative Annotation of Human Large Intergenic Noncoding RNAs Reveals Global Properties and Specific Subclasses. *Genes Dev* (2011) 25:1915–27. doi: 10.1101/gad.17446611
136. Necsulea A, Necsulea A, Kaessmann H, Kaessmann H. Evolutionary Dynamics of Coding and Non-Coding Transcriptomes. *Nat Rev Genet* (2014) 15:734–48. doi: 10.1038/nrg3802
137. Johnsson P, Lipovich L, Grandér D, Morris KV. Evolutionary Conservation of Long Non-Coding RNAs; Sequence, Structure, Function. *Biochim Biophys Acta* (2014) 1840:1063–71. doi: 10.1016/j.bbagen.2013.10.035

138. Agliano F, Rathinam VA, Medvedev AE, Vanaja SK, Vella AT. Long Noncoding RNAs in Host–Pathogen Interactions. *Trends Immunol* (2019) 40:492–510. doi: 10.1016/j.it.2019.04.001
139. Chen YG, Satpathy AT, Chang HY. Gene Regulation in the Immune System by Long Noncoding RNAs. *Nat Immunol* (2017a) 18:962–72. doi: 10.1038/ni.3771
140. Zhang Q, Chao T-C, Patil VS, Qin Y, Tiwari SK, Chiou J, et al. The Long Noncoding RNA *ROCKI* Regulates Inflammatory Gene Expression. *EMBO J* (2019) 38:e100041. doi: 10.15252/embj.2018100041
141. Boon RA, Jaé N, Holdt L, Dimmeler S. Long Noncoding RNAs: From Clinical Genetics to Therapeutic Targets? *J Am Coll Cardiol* (2016) 67:1214–26. doi: 10.1016/j.jacc.2015.12.051
142. Statello L, Guo C-J, Chen L-L, Huarte M. Gene Regulation by Long Non-Coding RNAs and Its Biological Functions. *Nat Rev Mol Cell Biol* (2021) 22:96–118. doi: 10.1038/s41580-020-00315-9
143. Ebert MS, Sharp PA. Emerging Roles for Natural MicroRNA Sponges. *Curr Biol* (2010) 20:R858–861. doi: 10.1016/j.cub.2010.08.052
144. Liu P, Yang H, Zhang J, Peng X, Lu Z, Tong W, et al. The LncRNA MALAT1 Acts as a Competing Endogenous RNA to Regulate Kras Expression by Sponging Mir-217 in Pancreatic Ductal Adenocarcinoma. *Sci Rep* (2017) 7:5186. doi: 10.1038/s41598-017-05274-4
145. Wang SH, Zhang WJ, Wu XC, Weng MZ, Zhang MD, Cai Q, et al. The LncRNA Malat1 Functions as a Competing Endogenous RNA to Regulate Mcl-1 Expression by Sponging miR-363-3p in Gallbladder Cancer. *J Cell Mol Med* (2016) 20:2299–308. doi: 10.1111/jcmm.12920
146. Xiao H, Tang K, Liu P, Chen K, Hu J, Zeng J, et al. LncRNA MALAT1 Functions as a Competing Endogenous RNA to Regulate Zeb2 Expression by Sponging miR-200s in Clear Cell Kidney Carcinoma. *Oncotarget* (2015) 6:38005–15. doi: 10.18632/oncotarget.5357
147. Xi Y, Jiang T, Wang W, Yu J, Wang Y, Wu X, et al. Long Non-Coding HCG18 Promotes Intervertebral Disc Degeneration by Sponging miR-146a-5p and Regulating Traf6 Expression. *Sci Rep* (2017) 7:13234. doi: 10.1038/s41598-017-13364-6
148. Esteller M. Non-Coding RNAs in Human Disease. *Nat Rev Genet* (2011) 12:861–74. doi: 10.1038/nrg3074
149. Yan X, Hu Z, Feng Y, Hu X, Yuan J, Zhao SD, et al. Comprehensive Genomic Characterization of Long Non-Coding RNAs Across Human Cancers. *Cancer Cell* (2015) 28:529–40. doi: 10.1016/j.ccell.2015.09.006
150. Atianand MK, Hu W, Satpathy AT, Shen Y, Ricci EP, Alvarez-Dominguez JR, et al. A Long Noncoding RNA LincRNA-EPS Acts as a Transcriptional Brake to Restrain Inflammation. *Cell* (2016) 165:1672–85. doi: 10.1016/j.cell.2016.05.075
151. Carpenter S, Aiello D, Atianand MK, Ricci EP, Gandhi P, Hall LL, et al. A Long Noncoding RNA Mediates Both Activation and Repression of Immune Response Genes. *Science* (2013) 341:789–92. doi: 10.1126/science.1240925
152. Rapicavoli NA, Qu K, Zhang J, Mikhail M, Laberge RM, Chang HY. A Mammalian Pseudogene LncRNA at the Interface of Inflammation and Anti-Inflammatory Therapeutics. *Elife* (2013) 2:e00762. doi: 10.7554/eLife.00762
153. Wang P, Xue Y, Han Y, Lin L, Wu C, Xu S, et al. The STAT3-Binding Long Noncoding RNA lnc-DC Controls Human Dendritic Cell Differentiation. *Science* (2014) 344:310–3. doi: 10.1126/science.1251456
154. Li Z, Chao TC, Chang KY, Lin N, Patil VS, Shimizu C, et al. The Long Noncoding RNA Thril Regulates Tnfα Expression Through Its Interaction With Hnrnpl. *Proc Natl Acad Sci USA* (2014) 111:1002–7. doi: 10.1073/pnas.1313768111
155. Zhang X, Liang Z, Zhang Y, Min DD, Wang ZJ, Hu X. Comprehensive Analysis of Long Non-Coding RNAs Expression Pattern in the Pathogenesis of Pulmonary Tuberculosis. *Genomics* (2020) 112:1970–7. doi: 10.1016/j.ygeno.2019.11.009
156. Yan H, Xu R, Zhang X, Wang Q, Pang J, Zhang X, et al. Identifying Differentially Expressed Long Non−Coding RNAs in PBMC in Response to the Infection of Multidrug-Resistant Tuberculosis. *Infect Drug Resist* (2018) 11:945–59. doi: 10.2147/IDR.S154255
157. Zhou J, Chaudhry H, Zhong Y, Ali MM, Perkins LA, Owens WB, et al. Dysregulation in MicroRNA Expression in Peripheral Blood Mononuclear Cells of Sepsis Patients Is Associated With Immunopathology. *Cytokine* (2015) 71:89–100. doi: 10.1016/j.cyto.2014.09.003
158. Siddle KJ, Deschamps M, Tailleux L, Nedelec Y, Pothlichet J, Lugo-Villarino G, et al. A Genomic Portrait of the Genetic Architecture and Regulatory Impact of MicroRNA Expression in Response to Infection. *Genome Res* (2014) 24:85–859. doi: 10.1101/gr.161471.113
159. Huang S, Huang Z, Luo Q, Qing C. The Expression of LncRNA NEAT1 in Human Tuberculosis and Its Antituberculosis Effect. *Biomed Res Intl* (2018) 2018:9529072. doi: 10.1155/2018/9529072
160. Huang Z, Liu J, Li L, Guo Y, Luo Q, Li J. Long Non-Coding RNA Expression Profiling of Macrophage Line RAW264.7 Infected by *Mycobacterium Tuberculosis*. *Biotech Histochem* (2020) 95:403–10. doi: 10.1080/10520295.2019.1707874
161. Yang X, Yang J, Wang J, Wen Q, Wang H, He J, et al. Microarray Analysis of Long Noncoding RNA and mRNA Expression Profiles in Human Macrophages Infected With *Mycobacterium Tuberculosis*. *Sci Rep* (2016) 6:38963. doi: 10.1038/srep38963
162. Margueron R, Reinberg D. The Polycomb Complex PRC2 and Its Mark in Life. *Nature* (2011) 469:343–9. doi: 10.1038/nature09784
163. Subuddhi A, Kumar M, Majumder D, Sarkar A, Ghosh Z, Madavan V, et al. Unraveling the Role of H3K4 Trimethylation and LncRNA HOTAIR in SATB1 and DUSP4-Dependent Survival of Virulent *Mycobacterium Tuberculosis* in Macrophages. *Tuberculosis* (2020) 120:101897. doi: 10.1016/j.tube.2019.101897
164. Li M, Cui J, Niu W, Huang J, Feng T, Sun B, et al. Long Non-Coding PCED1B-AS1 Regulates Macrophage Apoptosis and Autophagy by Sponging Mir-155 in Active Tuberculosis. *Biochem Biophys Res Commun* (2019) 509:803–9. doi: 10.1016/j.bbrc.2019.01.005
165. Huang J, Jiao J, Xu W, Zhao H, Zhang C, Shi Y, et al. Mir-155 Is Upregulated in Patients With Active Tuberculosis and Inhibits Apoptosis of Monocytes by Targeting Foxo3. *Mol Med Rep* (2015) 12:7102–8. doi: 10.3892/mmr.2015.4250
166. Sun W, Lou H, Cao J, Wang P, Sha W, Sun Q. LncRNA MEG3 Controls Mycobacterium Tuberculosis Infection *Via* Controlled Mir-145-5p Expression and Modulation of Macrophage Proliferation. *Microbial Pathogenesis* (2020) 149:104550. doi: 10.1016/j.micpath.2020.104550
167. Zuo S, Wu L, Wang Y, Yuan X. Long Non-Coding RNA Meg3 Activated by Vitamin D Suppresses Glycolysis in Colorectal Cancer Via Promoting C-Myc Degradation. *Front Oncol* (2020) 10:274. doi: 10.3389/fonc.2020.00274
168. Liu D, Liu Y, Zheng X, Liu N. C-MYC-Induced Long Noncoding RNA Meg3 Aggravates Kidney Ischemia–Reperfusion Injury Through Activating Mitophagy by Upregulation of RTKN to Trigger the Wnt/β-Catenin Pathway. *Cell Death Dis* (2021) 12:191. doi: 10.1038/s41419-021-03466-5
169. Wang Y, Zhong H, Xie X, Chen CY, Huang D, Shen L, et al. Long Noncoding RNA Derived From CD244 Signaling Epigenetically Controls CD8+ T-Cell Immune Responses in Tuberculosis Infection. *Proc Natl Acad Sci USA* (2015) 112:E3883–92. doi: 10.1073/pnas.1501662112
170. Yi Z, Li J, Gao K, Fu Y. Identification of Differentially Expressed Long Non-Coding RNAs in $CD4^+$ T Cells Response to Latent Tuberculosis Infection. *J Infection* (2014) 69:558–68. doi: 10.1016/j.jinf.2014.06.016
171. Fu Y, Xu X, Xue J, Duan W, Yi Z. Deregulated LncRNAs in B Cells From Patients With Active Tuberculosis. *PloS One* (2017) 12:e0170712. doi: 10.1371/journal.pone.0170712
172. Sabir N, Hussain T, Shah SZA, Peramo A, Zhao D, Zhou X. miRNAs in Tuberculosis: New Avenues for Diagnosis and Host-Directed Therapy. *Front Microbiol* (2018) 9:602. doi: 10.3389/fmicb.2018.00602
173. Mirzaei R, Babakhani S, Ajorloo P, Ahmadi RH, Hosseini-Fard SR, Keyvani H, et al. The Emerging Role of Exosomal miRNAs as a Diagnostic and Therapeutic Biomarker in *Mycobacterium Tuberculosis* Infection. *Mol Med* (2021) 27:34. doi: 10.1186/s10020-021-00296-1
174. Hu X, Liao S, Bai H, Wu L, Wang M, Wu Q, et al. Integrating Exosomal MicroRNAs and Electronic Health Data Improved Tuberculosis Diagnosis. *EBioMedicine* (2019) 40:564–73. doi: 10.1016/j.ebiom.2019.01.023
175. Alipoor SD, Tabarsi P, Varahram M, Movassaghi M, Dizaji MK, Folkerts G. Serum Exosomal miRNAs Are Associated With Active Pulmonary Tuberculosis. *Dis Markers* (2019) 2019:1907426. doi: 10.1155/2019/1907426
176. Lyu L, Zhang X, Li C, Yang T, Wang J, Pan L, et al. Small RNA Profiles of Serum Exosomes Derived From Individuals With Latent and Active Tuberculosis. *Front Microbiol* (2019) 10:1174. doi: 10.3389/fmicb.2019.01174
177. Hashimoto S, Zhao H, Hayakawa M, Nakajima K, Taguchi Y-H, Murakami Y. Developing a Diagnostic Method for Latent Tuberculosis Infection Using Circulating MiRNA. *Trans Med Commun* (2020) 5:25. doi: 10.1186/s41231-020-00078-7

178. Wang C, Yang S, Sun G, Tang X, Lu S, Neyrolles O, et al. Comparative MiRNA Expression Profiles in Individuals With Latent and Active Tuberculosis. *PloS One* (2011) 6:e25832. doi: 10.1371/journal.pone.0025832
179. Zhang H, Sun Z, Wei W, Liu Z, Fleming J, Zhang S, et al. Identification of Serum MicroRNA Biomarkers for Tuberculosis Using RNA-Seq. *PloS One* (2014) 9:e88909. doi: 10.1371/journal.pone.0088909
180. Latorre I, Leidinger P, Backes C, Domínguez J, de Souza-Galvão ML, Maldonado J, et al. A Novel Whole-Blood MiRNA Signature for a Rapid Diagnosis of Pulmonary Tuberculosis. *Eur Respir J* (2015) 45:1173–6. doi: 10.1183/09031936.00221514
181. Lin Y, Zhang Y, Yue H, Tian R, Wang G, Li F. Identification of Unique Key Genes and miRNAs in Latent Tuberculosis Infection by Network Analysis. *Mol Immunol* (2019) 112:103–14. doi: 10.1016/j.molimm.2019.04.032
182. Fang Y, Zhao J, Wang X, Wang X, Wang L, Liu L, et al. Identification of Differentially Expressed LncRNAs as Potential Plasma Biomarkers for Active Tuberculosis. *Tuberculosis* (2021) 128:102065. doi: 10.1016/j.tube.2021.102065
183. Hu X, Liao S, Bai H, Gupta S, Zhou Y, Zhou J, et al. LncRNA and Predictive Model to Improve the Diagnosis of Clinically Diagnosed Pulmonary Tuberculosis. *J Clin Microbiol* (2020) 58:e01973–19. doi: 10.1128/JCM.01973-19
184. Bai H, Wu Q, Hu X, Wu T, Song J, Liu T, et al. Clinical Significance of lnc-AC145676.2.1-6 and lnc-TGS1-1 and Their Variants in Western Chinese Tuberculosis Patients. *Int J Infect Dis* (2019) 84:8–14. doi: 10.1016/j.ijid.2019.04.018
185. Lv Y, Guo S, Li XG, Chi JY, Qu YQ, Zhong HL. Sputum and Serum MicroRNA-144 Levels in Patients With Tuberculosis Before and After Treatment. *Int J Infect Dis* (2016) 43:68–73. doi: 10.1016/j.ijid.2015.12.014
186. Spinelli SV, Diaz A, D'Attilio L, Marchesini MM, Bogue C, Bay ML, et al. Altered MicroRNA Expression Levels in Mononuclear Cells of Patients With Pulmonary and Pleural Tuberculosis and Their Relation With Components of the Immune Response. *Mol Immunol* (2013) 53:265–9. doi: 10.1016/j.molimm.2012.08.008
187. Liu Z, Zhou G, Deng X, Yu Q, Hu Y, Sun H, et al. Analysis of MiRNA Expression Profiling in Human Macrophages Responding to *Mycobacterium* Infection: Induction of the Immune Regulator Mir-146a. *J Infect* (2014) 68:553–6. doi: 10.1016/j.jinf.2013.12.017
188. Wagh V, Urhekar A, Modi D. Levels of MicroRNA Mir-16 and Mir-155 Are Altered in Serum of Patients With Tuberculosis and Associate With Responses to Therapy. *Tuberculosis* (2017) 102:24–30. doi: 10.1016/j.tube.2016.10.007
189. Fu Y, Yi Z, Wu X, Li J, Xu F. Circulating MicroRNAs in Patients With Active Pulmonary Tuberculosis. *J Clin Microbiol* (2011) 49:4246– 4251. doi: 10.1128/JCM.05459-11
190. Wang J, Zhu X, Xiong X, Ge P, Liu H, Ren N, et al. Identification of Potential Urine Proteins and MicroRNA Biomarkers for the Diagnosis of Pulmonary Tuberculosis Patients. *Emerg Microbes Infect* (2018) 7:63. doi: 10.1038/s41426-018-0066-5
191. Ruiz-Tagle C, Naves R, Balcells ME. Unraveling the Role of MicroRNAs in Mycobacterium Tuberculosis Infection and Disease: Advances and Pitfalls. *Infect Immun* (2020) 88:e00649–19. doi: 10.1128/IAI.00649-19
192. Zhou YL, Zhang L, Zhou Z, Liu W, Lu Y, He S, et al. Antibody Modified Nanoparticle-Mediated Delivery of Mir-124 Regulates Apoptosis *Via* Repression the Stat3 Signal in Mycobacterial-Infected Microglia. *J Biomed Nanotechnol* (2018) 14:2185–97. doi: 10.1166/jbn.2018.2650
193. Tivnan A, Orr WS, Gubala V, Nooney R, Williams DE, McDonagh C, et al. Inhibition of Neuroblastoma Tumor Growth by Targeted Delivery of MicroRNA-34a Using Anti-Disialoganglioside GD2 Coated Nanoparticles. *PloS One* (2012) 7:e38129. doi: 10.1371/journal.pone.0038129
194. Kota J, Chivukula RR, O'Donnell KA, Wentzel EA, Montgomery CL, Hwang HW, et al. Therapeutic MicroRNA Delivery Suppresses Tumorigenesis in a Murine Liver Cancer Model. *Cell* (2009) 137:1005–17. doi: 10.1016/j.cell.2009.04.021
195. Wu Y, Crawford M, Yu B, Mao Y, Nana-Sinkam SP, Lee LJ. MicroRNA Delivery by Cationic Lipoplexes for Lung Cancer Therapy. *Mol Pharm* (2011) 8:1381–9. doi: 10.1021/mp2002076
196. Roberts TC, Langer R, Wood MJA. Advances in Oligonucleotide Drug Delivery. *Nat Rev Drug Discov* (2020) 19:673–94. doi: 10.1038/s41573-020-0075-7

Conflict of Interest: The authors declare that the research was conducted in the absence of any commercial or financial relationships that could be construed as a potential conflict of interest.

frontiers in Immunology

REVIEW
published: 28 June 2021
doi: 10.3389/fimmu.2021.703060

Understanding the Reciprocal Interplay Between Antibiotics and Host Immune System: How Can We Improve the Anti-Mycobacterial Activity of Current Drugs to Better Control Tuberculosis?

Hyun-Eui Park[1], *Wonsik Lee*[2], *Min-Kyoung Shin*[1]* *and Sung Jae Shin*[3]*

[1] Department of Microbiology and Convergence Medical Science, Institute of Health Sciences, College of Medicine, Gyeongsang National University, Jinju, South Korea, [2] School of Pharmacy, Sungkyunkwan University, Suwon, South Korea, [3] Department of Microbiology, Institute for Immunology and Immunological Diseases, Brain Korea 21 Project for Graduate School of Medical Science, Yonsei University College of Medicine, Seoul, South Korea

OPEN ACCESS

Edited by:
Veronica Schmitz,
Oswaldo Cruz Foundation (Fiocruz), Brazil

Reviewed by:
Dwayne R. Roach,
San Diego State University, United States
C Gopi Mohan,
Amrita Vishwa Vidyapeetham University, India

***Correspondence:**
Sung Jae Shin
sjshin@yuhs.ac
Min-Kyoung Shin
mkshin@gnu.ac.kr

Specialty section:
This article was submitted to Microbial Immunology, a section of the journal Frontiers in Immunology

Received: 30 April 2021
Accepted: 11 June 2021
Published: 28 June 2021

Citation:
Park H-E, Lee W, Shin M-K and Shin SJ (2021) Understanding the Reciprocal Interplay Between Antibiotics and Host Immune System: How Can We Improve the Anti-Mycobacterial Activity of Current Drugs to Better Control Tuberculosis? Front. Immunol. 12:703060. doi: 10.3389/fimmu.2021.703060

Tuberculosis (TB), caused by *Mycobacterium tuberculosis* (Mtb) infection, remains a global health threat despite recent advances and insights into host-pathogen interactions and the identification of diverse pathways that may be novel therapeutic targets for TB treatment. In addition, the emergence and spread of multidrug-resistant Mtb strains led to a low success rate of TB treatments. Thus, novel strategies involving the host immune system that boost the effectiveness of existing antibiotics have been recently suggested to better control TB. However, the lack of comprehensive understanding of the immunomodulatory effects of anti-TB drugs, including first-line drugs and newly introduced antibiotics, on bystander and effector immune cells curtailed the development of effective therapeutic strategies to combat Mtb infection. In this review, we focus on the influence of host immune-mediated stresses, such as lysosomal activation, metabolic changes, oxidative stress, mitochondrial damage, and immune mediators, on the activities of anti-TB drugs. In addition, we discuss how anti-TB drugs facilitate the generation of Mtb populations that are resistant to host immune response or disrupt host immunity. Thus, further understanding the interplay between anti-TB drugs and host immune responses may enhance effective host antimicrobial activities and prevent Mtb tolerance to antibiotic and immune attacks. Finally, this review highlights novel adjunctive therapeutic approaches against Mtb infection for better disease outcomes, shorter treatment duration, and improved treatment efficacy based on reciprocal interactions between current TB antibiotics and host immune cells.

Keywords: mycobacteria, tuberculosis, anti-TB drug, immune response, Mtb response

INTRODUCTION

Tuberculosis (TB) is a chronic infectious disease caused by an obligate pathogen, *Mycobacterium tuberculosis* (Mtb), in humans (1). According to the WHO report, in 2020, approximately 10 million people were newly diagnosed, and 1.3 million people died from this notorious disease (2). Moreover, the recent treatment success rate was 82% for drug-sensitive TB and 55% for multidrug-resistant (MDR)-TB (3). There has been a gradual increase in the incidence of MDR-TB, defined as resistance to isoniazid (INH) and rifampicin (RIF), and extensively drug-resistant (XDR)-TB, defined as *in vitro* drug resistance to not only INH and RIF, but also all fluoroquinolones and at least one injectable aminoglycoside (4).

The presence of a mycobacterial population with more than one bacterial phenotype has been observed in patients with TB, as indicated by bacterial populations with varying growth dynamics in sputum samples (3). TB treatment strategy involves long-term treatment with several drugs for at least six months, which may increase the risk of MDR- and XDR-Mtb emergence (4–6), which is attributed to residual bacteria that are sheltered from or unresponsive to antibiotic treatment in heterogenous mycobacterial populations in patients (3). Thus, enhancing treatment success rate, shortening treatment duration, and preventing MDR Mtb emergence are the most critical factors for successful TB treatment. In this review, we provide an understanding of the mechanism underlying the generation of persistent mycobacteria in heterogeneous mycobacteria populations under immune- or drug-induced stress and discuss the effects of anti-TB drugs on host immune responses as opposed to their effects on Mtb. This review provides insights that may contribute to the development of host immune-mediated therapeutic strategies to eliminate persistent mycobacteria more effectively, thereby enhancing treatment success and preventing the development of MDR-TB.

MYCOBACTERIAL PERSISTERS ADAPT TO STRESSES IN THE HOST AND EXHIBIT ANTIBIOTIC TOLERANCE

Antibiotic Tolerance

Host-related stresses, such as hypoxia, acidic conditions, nutrient starvation, oxidative stress, and cytokine responses, alter the metabolic state of pathogens and eventually induces a drug-tolerant phenotype termed "persister" (7–10). These persister cells can maintain an unreplicated status and simultaneously survive antibiotic treatment. After cessation of anti-TB therapy, the surviving persisters revive their metabolism for replication, subsequently causing a relapse. Thus, antibiotic-tolerant persisters are considered surviving bacteria that did not undergo genetic mutations even after long-term antibiotic treatment (11). Although antibiotic tolerance and antibiotic resistance share common characteristics, they differ in several aspects (12, 13). Antibiotic resistance is generally inheritable and occurs in a drug-specific manner, while antibiotic tolerance is not inheritable and functions broadly. Antibiotic resistance is accompanied by an increase in minimum inhibitory concentration (MIC) of drugs, while antibiotic-tolerant and susceptible subpopulations show identical MIC (13). Tolerance refers only to bactericidal antibiotics and not to bacteriostatic antibiotics, unlike resistance (12).

The mechanism of antibiotic tolerance through the formation of persisters in response to a variety of stresses, including nutrient deprivation, oxidative stress, acidic environment, osmotic conditions, and host immune-mediated stresses, has been described in many pathogenic bacteria, including *Escherichia coli*, *Staphylococcus aureus*, *Pseudomonas aeruginosa*, and Mtb (14–18). Several mechanisms underlying the generation of persisters in response to the stresses have been identified; these include metabolic regulation, such as toxin–antitoxin (TA) systems, stringent and SOS responses, and biofilm formation (19–24). Understanding the mechanisms of persister formation under various stresses and developing therapeutic strategies specifically targeting the mechanisms related to antibiotic tolerance are expected to contribute to TB control. Therefore, here, we review the detailed mechanism of persister formation induced by host-mediated stress in Mtb and its effect on antibiotic tolerance.

Mtb Adapts to Host-Mediated Stresses Through Metabolic Regulation

Regulation of Transcription Factors

Mtb encounters various stresses, such as acidic pH, oxidative stress, hypoxia, nutrient deprivation, and cytokine-mediated effectors, during infection. On detecting such a stressful environment, Mtb reprograms its metabolism, at the transcriptional level, to survive in the niche (25, 26). Bacteria combat environmental stress to induce changes in antibiotic resistance and toxicity through two-component systems (TCSs), consisting of a sensor histidine kinase and a modulator of cytoplasmic response integrated into the inner membrane, as a stress recognition and response system (27, 28). To date, 12 complete TCSs have been identified in Mtb, of which PhoPR, PrrAB, MprAB, NarL, and TcrXY are involved in response to stresses, including pH, macrophage infection, detergents, hypoxia, low iron levels, and starvation (27).

The phoPR TCS may be a critical factor for adaptation to a low pH environment (27). When PhoP detects low pH, it activates the transcriptional regulator whiB3, regulates the expression of pH-responsive gene clusters (*aprABC*, *icl*, *pks2*, *pks3*, *pks4*, and *lipF*), and is involved in the survival of Mtb in macrophages (29–33) (**Figure 1**). Indeed, *phoP* deletion mutants exhibit growth defects in murine bone marrow-derived

Abbreviations: AhR, aryl hydrocarbon receptor; AMPK, AMP-activated kinase; ARE, antioxidant response element; ARNT, AhR nuclear translocator; ESAT-6, early secretory antigenic target-6; HMG-CoA, β-Hydroxy β-methylglutaryl-CoA; NFκB, nuclear factor kappa B; HO-1, hemeoxygenase-1; ICL, isocitrate lyase; ILIs, intracellular lipophilic inclusions; MIC, minimum inhibitory concentration; Mtb, *M. tuberculosis*; mTOR, mechanistic target of rapamycin; Nrf2-Keap1, NF-E2-related factor 2 (Nrf2)-Kelch-like ECH-associated protein 1; Pht, phthiochol; ppGpp, guanosine pentaphosphate; TA, toxin–antitoxin; TAG, triacylglycerol; TCA, tricarboxylic acid; RNS, reactive nitrogen species; ROS, reactive oxygen species.

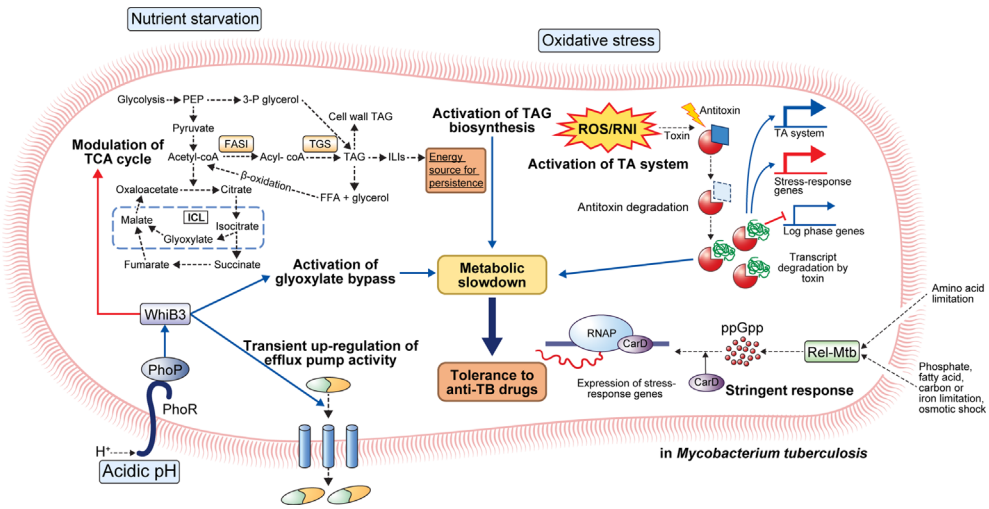

FIGURE 1 | General mechanisms for the establishment of antibiotic tolerance in *Mycobacterium tuberculosis*. Under host-mediated stresses, *M. tuberculosis* (Mtb) adapts to stress conditions via several mechanisms. Under acidic pH, the phoPR two-component system activates transcriptional regulator whiB3 that promotes suppression of the TCA cycle, activation of glyoxylate bypass, and transient upregulation of efflux pump activity. Activation of glyoxylate bypass is mediated by isocitrate lyase that converts isocitrate to glyoxylate under stress conditions. Nutrient starvation induces several changes in Mtb metabolism. Nutrient starvation also suppresses the TCA cycle and activates glyoxylate bypass, thereby enhancing the accumulation of triacylglycerol (TAG). The accumulated TAG is stored in the form of intracellular lipophilic inclusions (ILIs). The stored ILIs are used as an energy source in the persistence state. Additionally, the limitation of amino acids, phosphate, fatty acids, carbon, iron, and osmotic shock induces activation of stringent response through the production of ppGpp by Rel-Mtb. Production of ppGpp activates the expression of stress-response genes that causes a metabolic slowdown. Oxidative stress induces the activation of the TA system. Degradation of antitoxin occurs, and toxin degrades the transcript of log-phase genes. Further, upregulation of stress-response genes occurs, facilitating adaptation to stress conditions. Collectively, the adaptation of Mtb to stress conditions leads to metabolic modulation that results in antibiotic tolerance.

macrophages (BMDMs) as well as attenuated virulence with reduced bacterial burden in the lungs, liver, and spleen of a mouse Mtb infection model (34). Interestingly, transcriptional analyses revealed an overlapping of the repressed genes in H37Ra and *phoP* knockout mutant of H37Rv (35). Moreover, the incorporation of intact *phoP* into the H37Ra genome increased the bacterial persistence in murine BMDMs (35). In another study, the *phoP* mutant Mtb strain showed considerable attenuation in severe combined immunodeficient mice compared to the parental and BCG strains (32). Moreover, the Mtb *phoP* deletion mutant strain conferred protective anti-TB immunity in mouse and guinea pig models, indicating its potential as a live vaccine candidate (32). Liu et al. demonstrated that the expression of five regulons, DosR, MprA, PhoP, Rv1404, and Rv3058c, is responsible for the antibiotic tolerance of Mtb; these five regulons controlled the expression of over 50% of the upregulated genes after treatment with different anti-TB drugs, and their (DosR, PhoP, and MprA) deletion reduced drug tolerance under stress conditions (36).

Stringent Response

The stringent response is a conserved global signaling system that promotes bacterial survival in various environments, such as nutrient deprivation and other stresses (37). Particularly, stringent responses have been reportedly caused by amino acids, carbon, nitrogen, or phosphorus starvation, as well as UV exposure and fatty acid depletion (37). The stringent response is mediated by the hyperphosphorylated guanine nucleotides ppGpp and pppGpp, collectively referred to as [(p)ppGpp], and inorganic polyphosphate [poly(P)], and the synthesized signaling molecules regulate bacterial transcriptional changes under various stress conditions (38, 39). In Mtb, (p)ppGpp synthesis is induced by nutrient deprivation, long-term culture, and chronic infection in animal models, and it has been reported to be necessary for Mtb survival (37, 40, 41). Two proteins, RelA and SpoT, responsible for the synthesis of (p)ppGpp in gram-negative bacteria, have been identified, but many gram-positive bacteria, including mycobacteria, have only one protein (Rel) homologous to both RelA and SpoT (37). Accumulation of (p)ppGpp synthesized by Rel-Mtb and the transcription factor CarD in hostile environments, such as nutrient deficiency and oxidative stress, leads to transcription and translation of stress-responsive genes in Mtb (37) (**Figure 1**).

The protein Rel-Mtb modulates the intracellular (p)ppGpp content by regulating its synthesis and hydrolysis *via* an N-terminal hydrolase and synthetase domain (42). Nutrient starvation induces upregulation of *Rv2583c* (*Rel-Mtb*) that subsequently promotes the production of intracellular (p)ppGpp in Mtb (37). *Rel-Mtb* deletion mutant showed a growth defect in liquid media, and the disrupted growth rate was restored when citrate or phospholipid was used as the sole carbon source *in vitro* (37). A disrupted growth rate can induce antibiotic tolerance to drugs that kill actively growing cells. Recently, Dutta et al. showed that Rel-Mtb deficiency induces disruption of antibiotic tolerance under stress conditions, increasing susceptibility to INH (43). They reported that the nutrient-starved Rel-Mtb mutants

showed similar metabolic activity as wild type bacteria growing in nutrient-rich conditions (43). Disruption of Rel-Mtb induced increased susceptibility to INH *in vitro* nutrient starvation and BALB/c mouse models (43). Furthermore, they discovered a Rel-Mtb inhibitor through pharmaceutical library screening that showed a direct cytotoxic effect on antibiotic-tolerant Mtb and synergetic effect with INH activity (43). In Mtb, the polyphosphate kinase PPK1 is responsible for poly(P) synthesis, and the exopolyphosphatases, PPX1 and PPX2, and PPK2 are responsible for poly(P) hydrolysis, thereby regulating cellular poly(P) homeostasis (39). The *ppx1* or *ppk2* deletion mutant strains showed low glycerol-3-phosphate (G3P) and 1-deoxy-xylulose-5-phosphate expression levels in bacterial cells, suggesting downregulated G3P synthesis pathway (39). As a result, the *ppk2* and *ppx1* deletion mutant increased susceptibility to plumbagin and meropenem, and clofazimine, respectively (39). Similarly, the ppk1 deletion mutants showed increased susceptibility to INH, levofloxacin, and RIF (44). These results suggest that (p)ppGpp and poly(P) synthesis and their modulators play important roles in the development of antibiotic resistance *in vivo*.

Metabolic Modulation

Numerous acid-inducible genes induce a carbon metabolism shift for microbial persistence in the host macrophages. One such acid-inducible gene encodes isocitrate lyase that converts isocitrate to succinate and glyoxylate (45). Moreover, malate synthase catalyzes malate formation by the addition of acetyl-CoA to glyoxylate (45). Overexpression of isocitrate lyase causes the activation of the glyoxylate shunt, subsequently inducing metabolic shifting; pyruvate, succinate, fumarate, and malate levels were increased while the α-ketoglutarate level was decreased in macrophage infection and low pH culture model (46). The limitation of α-ketoglutarate-derived amino acids and oxaloacetate by glyoxylate shunt activation slows bacterial cell growth and metabolic activity (46). Antibiotics can induce growth and metabolic activity arrest in rapidly growing cells. For example, the antimicrobial effect of INH depends on INH conversion to isonicotinoyl by the catalase-peroxidase katG (3). Converted isonicotinoyl binds NAD^+ to make isonicotinoyl-NAD that inhibits mycolic acid synthesis, a bacterial cell wall component, subsequently interfering with mycobacterial cell wall integrity (3). Thus, reduced need for cell wall synthesis due to arrested growth and metabolic activity due to acidic stress induces tolerance to INH (3). RIF kills metabolically active cells by binding to RNA polymerase subunit B and interfering with transcription; RIF resistance is usually acquired through mutation in *rpoB* that encodes RNA polymerase B protein (47). However, transient antibiotic tolerance has also been reported in previous studies (48–50). In response to environmental stress, Mtb translates a mutated form of RNA polymerase with a lower affinity to RIF, thereby facilitating the acquisition of transient antibiotic tolerance during antibiotic treatment (50). Collectively, growing evidence suggests that metabolically arrested states induce antibiotic tolerance that prevents the complete sterilization of pathogens. Therefore, to eradicate the antibiotic-tolerant bacterial population, a treatment strategy that reactivates the metabolically arrested bacterial population is needed (**Figure 1**).

Modulation of Lipid Metabolism

Several host immune-mediated stresses induce intracellular triacylglycerol (TAG) droplet accumulation in Mtb by TAG synthase activity. For example, TAG synthase upregulation was confirmed in multiple-stress conditions, such as hypoxia, low pH, and low iron (51–54). Accelerated TAG synthesis induces a reduction in TCA flux and subsequently enhances the survival of Mtb in the presence of antibiotics, such as INH, streptomycin, ciprofloxacin, and ethambutol (EMB) (54). Interestingly, antibiotic tolerance due to TAG accumulation can be reversed by modulating carbon fluxes with complete inhibition of TAG synthase *in vitro* and *in vivo* (54). Furthermore, *tgs1* deletion mutants continue to grow under stress conditions while wild type strain stops replicating (54). Kapoor et al. developed an *in vitro* model of human granuloma for pulmonary tuberculosis and discovered unique characteristics of Mtb within the granuloma; Mtb showed dormant phenotypes, including the loss of acid-fastness, accumulation of lipid droplet, transcriptional change of lipid metabolism genes, and tolerance to RIF (51). Moreover, treatment with anti-tumor necrosis factor-alpha (TNF-α) monoclonal antibodies induced resuscitation of Mtb as previously described in human TB (51). Similarly, a multiple-stress model that included low oxygen, high CO_2, low nutrient, and acidic pH showed arrested growth, acid-fastness loss, TAG, and wax ester accumulation, along with the rise in antibiotic tolerance to INH and RIF in Mtb (52). Interestingly, antibiotic tolerance was diminished in the *tgs1* deletion mutant and restored with the addition of complementation. Furthermore, transcriptome analysis using microarray revealed the achievement of the dormant state showing repression of energy generation, transcription and translation machinery, and induction of stress-responsive genes (52). Recently, Santucci et al. identified the mechanism of TAG accumulation to involve intracytoplasmic lipid inclusions (ILI) induced by carbon excess and nitrogen starvation in *M. smegmatis* and *M. abscessus* (53). They also identified *tgs1*-mediated TAG formation and lipolytic enzyme-mediated TAG breakdown mechanisms. Moreover, they discovered that emergence of antibiotic tolerance against RIF and INH induced by low nitrogen and high ILI environment as previously described (53). Taken together, the importance of TAG synthesis in antibiotic tolerance of Mtb suggests the potential of lipid metabolism-related proteins, such as triacylglycerol synthase and fatty-acyl-CoA reductase, as therapeutic targets for abolishing antibiotic tolerance.

Toxin–Antitoxin (TA) System

The TA system comprises a stable toxin that interferes with indispensable cellular metabolism and an unstable antitoxin that blocks the toxin activity during persister formation (55, 56). The TA systems are generally divided into seven classes depending on their mechanism (57). In detail, type I and III antitoxin include an RNA antitoxin that interferes with translocation of the toxin as an antisense RNA (type I) or binding to toxin protein to neutralize the toxin activity (type III). Type II antitoxins are

proteins that interfere with the toxins by direct binding to the toxin protein. Type IV antitoxins inhibit toxin activity by attaching to the toxin target, while type V antitoxins degrade the toxin mRNA target directly. Type VI antitoxins bind to the toxin; they do not directly degrade the toxin itself but promote its degradation by ClpXP (56). In the type VII TA system, antitoxin acts as an enzyme for the chemical modification of the toxin and subsequently neutralizes the toxin (57). As a representative example, in the HipBA toxin/antitoxin module, HipA is a toxin that inhibits cell growth and induces persister formation, while HipB is an antitoxin that binds to HipA and acts as a transcription inhibitor of the hipBA operon. In particular, high HipA expression leads to multidrug resistance in *E. coli* (55). Characteristically, Mtb has many TA system-related loci in its genome, and at least 88 TAs have been identified (58). According to Keren et al., 10 TA modules were overexpressed in Mtb persister cells, suggesting that the TA system not only contributes to Mtb virulence but also the formation of bacterial persister cells (8). Further, Torrey et al. revealed that multiple pathways such as lipid biosynthesis, carbon metabolism, TA systems, and transcriptional regulators are involved in Mtb persister formation using transcriptional analysis and whole-genome sequencing of Mtb hip mutant (59). Notably, most of the identified Mtb TA systems were Type II, and these include VapBC, MazEF, YefM/YoeB, RelBE, HigBA, and ParDE (60).

Notably, the VapBC TA family is the most abundant type of TA system encoded by Mtb (60). Several studies have demonstrated that host-mediated stress, such as hypoxia and activated macrophages, induces transcriptional activation of multiple VapBC TA loci (61–63). Hudock et al. identified the transcriptional profile from granuloma samples of active and latent TB patients; the expression of eight dosR regulon members (Rv0080, Rv0081, Rv1736c, Rv1737c, Rv2032, Rv2625c, and Rv2630) along with the induction of four pairs of toxin/antitoxin (vapBC19, vapBC21, vapBC33, and vapBC34) were observed within the granulomas of active and latent TB patients (61). Sharma et al. demonstrated that VapC21 overexpression hinders mycobacterial growth, and co-expression of antitoxin VapB21 reverses this effect (62). Moreover, VapC21 overexpression mutant and Mtb cultured in stress conditions, such as nutrient deprivation and hypoxia, exhibited similar transcriptional profiles (62). Furthermore, VapC21 overexpression resulted in upregulated WhiB7 regulon, inducing antibiotic tolerance to aminoglycosides and EMB (62). Talwar et al. identified the role of VapBC12 TA in persister formation under cholesterol-rich conditions; VapC12 RNase toxin targets *proT* transcript that is indispensable for Mtb growth regulation in a cholesterol-rich environment (63). Therefore, the expression of VapC12 RNase toxin induced the generation of a slow-growing population, and this phenotype occurrence was increased in the presence of cholesterol (63). Interestingly, co-expressing of antitoxin *vapB12* disrupted the vapC12-induced phenotype, while *vapC12* deletion enhanced the immunopathologic severity and lung bacterial burden compared with the wild type strain (63). Recently, Yu et al. demonstrated a phosphorylation-dependent TA system in Mtb (58). Specifically, phosphorylation of TgIT by TakA induces toxicity neutralization and allows bacterial growth (58). In stressful conditions, TgIT activation *via* dephosphorylation promotes bacterial growth inhibition, leading to a non-replicating but viable state (58).

SOS Response

Various host-mediated stresses, such as reactive oxygen and nitrogen species, result in DNA damage and subsequently induce a DNA repair mechanism called SOS response (64). The SOS response is controlled by two regulator proteins, RecA and LexA. RecA recognizes damaged single-stranded DNA and induces the proteolysis of LexA repressor leading to the activation of SOS genes (64). Völzing and Brynildsen discovered that DNA repair was essential for the survival of ofloxacin-induced persisters and that delayed DNA repair occurred after ofloxacin treatment (65). Another study indicated that the timing of DNA repair was a key factor for the complete recovery of persisters after ofloxacin treatment. Additionally, nutrient starvation increased the survival rate of *E. coli* to approximately 100%, following ofloxacin treatment (66). These results indicate that changes in post-antibiotic treatment recovery time are critical to the formation of persister and support the notion that interference of DNA damage repair systems could be an effective strategy to eradicate the persister population.

Previous studies showed that stress-response regulons, including SOS response genes, were upregulated in Mtb persisters (8, 67). In mycobacteria, the DNA damage repair system comprises LexA-mediated and ClpR factor-mediated mechanisms (67). Further, DnaE2 polymerase, induced by ROS and NOS produced in the host immune response, contributes to mutations during the DNA repair process (68). Recently, inhibition of DNA gyrase by fluoroquinolone was found to modulate Mtb growth in intracellular and extracellular environments (69). Interestingly, inhibition of DNA gyrase contributes to the drug tolerance *via* RecA/LexA-mediated SOS response (69). Choudhary et al. demonstrated that DNA gyrase knockdown Mtb mutant showed decreased drug susceptibility to RIF 24 and 48 h post-treatment, and a similar pattern was observed following INH and EMB treatment (69). Taken together, these findings indicate that changes in post-antibiotic treatment recovery time are critical to the formation of persisters and support the notion that interference by DNA damage repair systems could be an effective strategy to eradicate the persister population.

Mtb Biofilm Formation Contributes to Antibiotic Tolerance

Biofilm is a three-dimensionally organized multicellular bacterial community that grows on surfaces *in vitro* and *in vivo* (70). Biofilm induces persistent bacterial infection by protecting bacteria from antibiotics (71). Therefore, the formation of biofilms has been closely linked to antibiotic tolerance in various bacterial pathogens, including *E. coli*, *S. aureus*, *P. aeruginosa*, and Mtb (72–76). Host-mediated stress conditions, such as prolonged hypoxia, oxidative stress, and nutrient starvation, induce biofilm formation leading to the development of antibiotic tolerance (77–81).

Ackart et al. showed that human leukocyte lysis enhanced biofilm formation, subsequently inducing antibiotic tolerance to several anti-TB drugs, such as INH, RIF, and pyrazinamide (PZA) (77). Interestingly, treatment with DNase I or tween scattered the established biofilm. It reversed the antibiotic tolerance, indicating that biofilm formation induced by host-mediated stress provides antibiotic tolerance that leads to persistent infection, and targeting the biofilm enhances drug sensitivity in Mtb (77). Another study induced Mtb biofilm formation *in vitro* through thiol reductive stress (TRS), resulting in drug-tolerant (INH, RIF, and EMB) phenotypes in which metabolic activity was maintained with the same levels of ATP/ADP, NAD+/NADH, and NADP+/NADPH (78). Furthermore, the TRS-induced biofilm formation was not interrupted by cell wall biosynthesis inhibitor antibiotics (INH and ETB), while DNA synthesis (levofloxacin and ofloxacin), RNA transcription (RIF), and protein synthesis (tetracycline) inhibitors disrupted its formation (78). Recently, Richards et al. identified several indispensable genes for Mtb adaptation during biofilm formation induced by host-mediated stresses, but not in dispersed culture using detergent (79). They observed that the formation of biofilm enhances the enrichment of antibiotic-tolerant cells and subsequently inducing RIF tolerance. Importantly, they established that isonitrile lipopeptide is essential for the structural formation of Mtb biofilm under stress conditions (79). In another study, modulation of trehalose metabolism was observed in antibiotic-tolerant Mtb population isolated from a biofilm; antibiotic-tolerant Mtb utilize trehalose to synthesize central carbon metabolism intermediates required to sustain mandatory cellular functions, whereas planktonic cells use cell-surface glycolipids (81). Moreover, drug-susceptible and MDR Mtb showed similar alteration after antibiotic therapy, suggesting the role of trehalose in both transient and permanent antibiotic tolerance (81). Tripathi et al. showed that ClpB is essential for Mtb survival under host-mediated stress conditions; they demonstrated that ClpB is required for bacterial survival during hypoxia and nutrient starvation (80). The clpB deletion mutant showed abnormal cellular morphology, disrupted biofilm formation, and reduced rate of intracellular survival in THP-1 cells (80). In addition, they showed that ClpB induces the secretion of inflammatory cytokines, such as TNF-α and IL-6, controlled by MAPK and NF-κB pathways (80). Taken together, various virulence factors involved in Mtb biofilm formation may be a potential novel drug target for the elimination of drug-tolerant bacteria.

ANTIBIOTICS CAN AFFECT HOST IMMUNITY AND INFLUENCE CLINICAL OUTCOMES

Host Metabolic Changes Induced by Antibiotics

Antibiotic activities against bacterial pathogens have traditionally been considered only in terms of their direct killing effects (82). However, growing evidence indicates indirect effects of antibiotics through interaction with host innate immunity that can alter clinical outcomes (83–85). Yang et al. identified antibiotic-induced host metabolic changes during infection and found that antibiotic treatment directly induced the host cells to produce metabolites that reduce drug efficacy and amplify phagocytic killing (86). After ciprofloxacin treatment, the systemic alteration of metabolites was confirmed in mouse tissues, including the peritoneum, plasma, and lungs. On the contrary, *E. coli* infection induced local changes in the peritoneum alone, not in the plasma or lungs (86). Further, most of the antibiotic-induced metabolic changes were not reliant on the intestinal microbiome and were most likely caused by the direct action of antibiotics on local host cells (86).

Above all, advanced host types of machinery protect cells by detecting and preventing damage due to intrinsic and exogenous inferior substances, such as oxidative stress and toxins (87). These apparatuses are partially responsible for microbial pathogenesis by detecting endogenous factors induced by Mtb infection or exogenous Mtb factors; however, they are responsible for detecting and detoxifying anti-TB drugs or drug-induced endogenous factors (88). These apparatuses may belong to the NRF2-KEAP1 and aryl hydrocarbon receptor (AhR) signaling pathways, whose dual action may be a double-edged sword in Mtb infection. This section evaluates the effect of such a system on Mtb infection and anti-TB treatment.

Keap1-Nrf2 Signaling Pathway

The Keap1-Nrf2 regulatory pathway is a key mechanism for preventing cell damage by detecting intrinsic and exogenous stresses, such as oxidative stress, chemotherapy, and radiation, regulating gene expression to modulate various subsequent antioxidant functions (87). Nrf2 is bound to the inhibitory protein Keap1 in the cytoplasm. When a stressor is detected, the Nrf2 protein is separated from Keap1, causing its cytoplasmic accumulation. Thereafter, it translocates to the cell nucleus, where it acts as a transcription factor, binds to the antioxidant reaction factor (ARE), and then binds to the antioxidant-related genes [e.g., hemeoxygenase-1 (HO-1), NAD(P)H:quinone redox enzyme-1 (NQO1), glutathione S-transferase (GST)] to promote their transcriptional expression (**Figure 2**) (87). Mtb factors, such as ESAT-6, can induce oxidative damage and apoptosis, counteracted by upregulating antioxidant enzymes *via* activation of the Keap1-Nrf2 signaling cascade (88, 89). Recent studies have shown that the antioxidant factor expressed by activation of the Keap1-Nrf2 system protects cells by removing infection and damage caused by drugs; however, it also inhibits T cell activation and rather hinders the removal of Mtb. Representatively, HO-1 is a cellular antioxidant enzyme expressed in response to various stress conditions, such as exposure to heavy metals, heat shock, hypoxia, starvation, and immune activation (90–95). HO-1 is the rate-limiting enzyme that degrades heme molecules into free iron, biliverdin, and carbon monoxide (CO) (96). Free iron inhibits nitric oxide (NO) production by acting on inducible NO synthase (iNOS) and, thereby, could improve the survival of intracellular Mtb.

In addition, bactericidal antibiotics cause mitochondrial dysfunction and oxidative damage in mammalian cells (97). A dose- and time-dependent upregulation of intracellular ROS

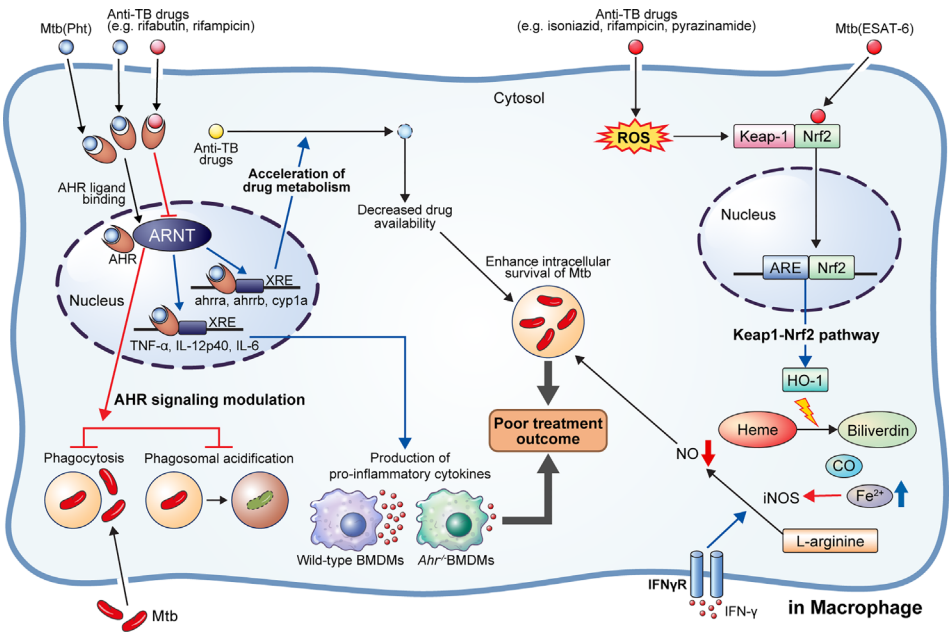

FIGURE 2 | AhR modulation by anti-TB drugs and downstream events. NRF2-KEAP1 signaling and AhR signaling pathways generally protect cells by detecting and preventing damage to endogenous and exogenous substances such as oxidative stress and toxins. They can also detect *M. tuberculosis* (Mtb) infection or anti-TB drugs and affect host defense and drug metabolism. 1,4-naphthoquinone phthiochol (Pht) produced by Mtb and anti-TB drugs can attach to AhR present in the cytoplasm across the cell membrane. The combined ligand and receptor complex transfers into the nucleus and heterodimerizes with AhR nuclear translocator (ARNT). The ligand, receptor, and ARNT complex binds to xenobiotic response elements (XRE) that are specific DNA sequences found in the target gene promoter region. Activation of the AhR by Pht and anti-TB drugs (e.g., rifabutin, bedaquiline) in macrophages induces impaired phagocytosis of Mtb H37Rv, and phagosome acidification, and production of pro-inflammatory cytokines. Furthermore, activation of AhR facilitates the hepatic metabolism of drugs, ultimately reducing drug availability. Meanwhile, some drugs (e.g., rifampicin) act as AhR inhibitors, inducing impairment of phagocytosis and phagosome acidification, consequently improving the intracellular survival of Mtb in macrophage and zebrafish models. On the other hand, Mtb ESAT-6 and anti-tuberculosis drugs (e.g., isoniazid, rifampicin, pyrazinamide) act on Nrf2-Keap1 signaling to induce the translocation of Nrf2 to the nucleus by degradation of Keap-1. The translocated Nrf2 binds to the antioxidant response element (ARE) and upregulates antioxidant enzymes. Production of hemeoxygenase-1 (HO-1), a representative antioxidant enzyme, is activated, which subsequently induces catabolism of heme to biliverdin, CO, and Fe^{2+}. Elevated Fe^{2+} inhibits the production of nitric oxide from L-arginine mediated by IFN-γ signaling. Thus, activation of heme catabolism by HO-1 induces the reduction of intracellular bacterial killing. Taken together, activation of AhR signaling and HO-1 production induces a pathogen-beneficial effect that enables persistent infection.

production was confirmed in different human cell lines after treatment with bactericidal antibiotics (ciprofloxacin, ampicillin, and kanamycin) belonging to different classes. Moreover, mitochondrial potential, ATP levels, and metabolic activity were considerably decreased after this treatment, suggesting impairment of mitochondrial function (97). Furthermore, treating human sinonasal epithelial cells with the bactericidal antibiotics, amoxicillin and levofloxacin, leads to increased ROS production, antioxidant gene expression, and cell death (98).

Bactericidal anti-TB drugs, such as RIF, INH, and PZA, can similarly cause mitochondrial dysfunction and oxidative damage in host cells, leading to apoptosis, in addition to their effect on Mtb. Simultaneously, antioxidant mechanisms, such as the Keap1-Nrf2 signaling pathway, may interfere with the removal of Mtb. Interestingly, ROS-mediated damage induced by antibiotics could be rescued by N-acetyl-l-cysteine (NAC) without affecting the antibiotic's killing ability (97). In addition, an HO-1 inhibitor showed the same effect in the lungs of Mtb-infected mice as anti-TB drugs (99). Thus, the long-term use of bactericidal anti-TB drugs can induce cell death due to ROS production and mitochondrial dysfunction, while simultaneously, the produced ROS act as antioxidants and interfere with the removal of Mtb. These ambivalences need to be more clearly elucidated with respect to the pathogenesis of Mtb. The aforementioned adjuvant treatments are described in detail in section 4.

AhR Signaling Pathway

The AhR is a transcription factor that detects both endogenous and exogenous ligands (100). Initially, AhR function was associated with the detoxification of heterologous ligands, such as benzo[a]pyrene and the highly toxic 2,3,7,8-tetrachlorodibenzo-p-dioxin (TCDD); subsequently, endogenous molecules, such as tryptophan (Trp), kynurenine, or formindolo [3,2-b] carbazole (FICZ), dietary components, and bacterial-derived ligands, were identified as AhR ligands, broadening the understanding of their function (100).

Particularly, bacterial pigment proteins such as phenazine produced by *P. aeruginosa* and 1,4-naphthoquinone phthiochol (Pht) produced by Mtb have been identified as bacterial-derived

AhR ligands (101). AhR is widely expressed in almost all cell types; in particular, both innate and adaptive immune cells express AhR, suggesting its potential broad-range effects on host immunity (102). AhR is present in the cytoplasm and is activated upon binding to a ligand. Activated AhR binds to the AhR nuclear translocator (ARNT) and regulates the transcription of several target genes, including cytochrome P450 monooxygenases (*CYP1A1* and *CYP1B1*), AhR inhibitor, and pro-inflammatory cytokines (102) (**Figure 2**).

Ligand-activated AhR translocates to the nucleus from the cytosol and induces immunosuppressive or pro-inflammatory downstream effects depending on the ligand property (102). Further, AhR can modulate macrophage immune response. Shinde et al. showed that phagocytosis of apoptotic cells through toll-like receptor (TLR)9-dependent sensing of the apoptotic cell DNA induces the activation of the AhR pathway (103).

The ligand-activated AhR binds to TB virulence factors and regulates antibacterial responses (104). Puyskens et al. demonstrated that anti-TB drugs, such as RIF and rifabutin bind to AhR and induce modulation of host immune response (104). However, AhR signaling inhibition by a synthetic AhR inhibitor, CH-223191, impairs phagocytosis in THP-1 macrophages. Further, they demonstrated that the rate of internalized zymosan was decreased following RIF treatment, while phagosome acidification was also impaired after RIF as well as CH-223191 treatment (104). In addition to this *in vitro* study, they confirmed AhR modulation during *M. marinum* infection in a zebrafish model; a higher bacterial burden was observed in zebrafish embryo following AhR inhibition with CH-223191 than in the untreated control group (104). Similarly, Moura-Alves et al. demonstrated significantly increased bacterial burden in the lungs, liver, and spleen of $AhR^{-/-}$ mice than wild type mice after aerosol Mtb infection (101). Moreover, the production of pro-inflammatory cytokines, such as TNF-α, IL-12p40, and IL-6, were hindered in $AhR^{-/-}$ bone marrow-derived macrophages (101). Furthermore, Memari et al. demonstrated that AhR induced expression of IL-23 and IL-1β, thereby stimulating the production of IL-17 and 22 by specific T cell subsets (Th17, Th22, and ILC3 cells) (105). Upregulation of IL-17 activates parenchymal cells and subsequently induces an influx of polymorphonuclear cells to the infection site mediated by CXCL1, CXCL3, and CXCL5 (106). Further, phagocytosis of apoptotic polymorphonuclear cells by macrophages promotes a phenotypic change of macrophage from M0 to M2c, thereby contributing to inflammation resolution (106).

Modulation of Host Immunity by Anti-TB Drugs

Antibiotics can modulate host immunity either indirectly or directly (107). First, antibiotics alter the host immune system indirectly by affecting the host microbiota composition (108). Second, antibiotics affect the host immune system directly by altering the functions of immune cells (86, 97, 109). Therefore, the interaction between antibiotics and host immunity may influence the clinical outcomes or treatment duration. Several studies have reported the modulation of host immune response by anti-TB drugs. For example, INH induces the apoptosis of activated $CD4^+$ T cells in Mtb-infected mice (110) as well as impairs the production of Mtb-specific interferon (IFN)-γ and anti-CFP10 antibody in household contacts of latent TB patients (111). Similarly, RIF reportedly exerts a mild immunosuppression effect, as indicated by its inhibition of human lymphocytes (112) and significant suppression of T cells compared to that in TB patients without RIF treatment (113). Moreover, RIF partially suppressed the phagocytosis of zymosan by macrophages and moderately suppressed the expression of TNF-α at high doses (114). it was reported to significantly inhibit the secretion of IL-1β and TNF-α while increasing the secretion of IL-6 and IL-10 (115). Furthermore, RIF suppressed LPS-induced production of iNOs, cyclooxygenase-2, IL-1β, TNF-α, and prostaglandin E2 in microglial cells, subsequently improving neuron survival (116). Manca et al. demonstrated that PZA treatment reduces the secretion of pro-inflammatory cytokines and chemokines, such as IL-1β, IL-6, TNF-α, and MCP-1, in Mtb-infected human monocytes and mice (117). Additionally, PZA treatment elevated the expression of adenylate cyclase and peroxisome-proliferator activated receptor in the lungs of Mtb-infected mice (117).

Bedaquiline (BDQ) specifically disrupts intracellular ATP production in bacteria by inhibiting the activity of bacterial ATP synthase, resulting in depleted energy production (118, 119). Recently, a genome-wide transcriptional analysis demonstrated that BDQ promotes the formation of lysosomes, phagocytic vesicle membrane, vacuolar lumen, hydrolase activity, and lipid homeostasis in naïve and Mtb-infected macrophages (120). Moreover, it suppressed basal glycolysis, reduced glycolytic capacity in heat-killed-Mtb-stimulated macrophages, and triggered anti-mycobacterial mechanisms, such as phagosome–lysosome fusion and autophagy (120). Further, BDQ treatment induced the activation of the lysosomal pathway through transcription factor EB and calcium signaling. Interestingly, other classical anti-TB drugs, such as amikacin, EMB, and INH, did not activate the lysosomal pathway. Additionally, BDQ potentiated the anti-mycobacterial activity of PZA but did not show synergistic effects with bactericidal activities of EMB, INH, and RIF (120).

Clofazimine (CFZ) is a riminophenazine compound used for the standard treatment of leprosy (121). In addition to its antimicrobial activity, CFZ has an immune-modulatory activity; CFZ forms biocrystal and modulates innate immune response after phagocytosis as demonstrated by the intracellular CFZ crystal-induced activation of the Akt pathway and enhancement of IL-1RA production in RAW 264.7 cells (122). Moreover, CFZ treatment inhibited TLR2-and TLR4-mediated NF-κB activation and TNF-α production (122). Fukutomi et al. demonstrated that CFZ induces apoptosis of macrophages; representative features of apoptosis, such as decreased metabolic activity, diminished cell size, nuclear condensation, and fragmentation, were observed in CFZ-treated human monocyte-derived macrophages (123). Further, caspase-3 activity was significantly increased in CFZ-treated macrophages (123). Recently, Ahmad et al. showed that BCG revaccination with CFZ treatment induces the differentiation of the stem cell-like memory T (Tsm) cells in mice (124). Differentiation of Tsm cells recovered long-lasting central

memory T cells and T effector memory cells to provide enhanced vaccine efficacy in mice (124).

ADJUNCTIVE HOST-DIRECTED THERAPIES IMPROVE ANTI-TB DRUG ACTIVITY

Anti-TB therapy involves the combination of several drugs and has a long treatment duration of treatment, resulting in the frequent occurrence of side effects (125, 126). Side effects range from minor ones that disappear spontaneously to serious ones that require treatment (126). The strategies for developing new treatments to control Mtb can be divided into two broad categories: developing novel efficient antibiotics and using existing therapeutic drugs to achieve faster and more effective treatments in a host-specific manner (127, 128). The development of host-directed therapy maximizes treatment efficiency by using the adjunct to elicit a response (127). Essentially, these treatments do not directly target pathogens, thus avoiding the occurrence of drug resistance and reducing drug side effects, thereby making this a promising strategy (127). In this section, we have proposed several such strategies, including various host targets that affect Mtb susceptibility, and discussed the corresponding drugs and their mechanisms of action. A summary of the proposed adjunctive host-directed therapies that improving anti-TB drug activity is presented in **Table 1**.

Autophagy-Modulating Drugs

Autophagy is an intracellular self-degradation system that transfers cytoplasmic components or specific cytosolic targets to the lysosome for cellular homeostasis maintenance (153). Autophagy is induced by various stress conditions, such as nutrient starvation, hypoxia, and microbial infection (153). Furthermore, diverse pathophysiological conditions, such as aging, autoimmune disease, neurodegeneration, cancer, and inflammation-associated metabolic disorders, are involved in autophagy (154). Autophagy is an essential part of the host immune system against diverse intracellular pathogens, such as *Salmonella*, *Listeria monocytogenes*, and Mtb, *via* the activation of phagolysosome formation (155–157). Therefore, activating autophagy is a promising strategy for eradicating Mtb, especially in the case of MDR-TB.

Rapamycin

Rapamycin (RAP) is a potent antifungal agent produced by *Streptomyces hygroscopicus* and is used to suppress transplant rejection reactions due to its immunosuppressive property (158, 159). RAP also enhances the T helper 1-driven immune response when co-administered with the BCG vaccine (129). Further, RAP-loaded nanoparticles were efficiently phagocytosed by THP-1 macrophages, significantly reducing the intracellular Mtb load at a concentration of 100 μg/mL (130). In addition to the *in vitro* results, Gupta et al. showed that inhaled RAP particles reduced pulmonary Mtb loads as well as activated autophagy and phagosome–lysosome fusion in a mouse model (131) (**Figure 3**). Another study showed that a low dose of RAP (<10 μM) was sufficient to increase autophagy in RAW264.7 cells; however, intracellular mycobacteria killing was only observed at a high concentration of RAP (10 μM) (160). In contrast, Andersson et al. demonstrated that RAP facilitates the increase of Mtb burden in both single and human immunodeficiency virus (HIV) co-infected human monocyte-derived macrophages (161). They suggested that autophagy induction disrupts intracellular killing during a low dose infection. However, they used HIV co-infected human macrophages for their experiment that exhibit impaired immunity and, therefore, are not suitable for investigating the effect of RAP on autophagy.

Metformin

Metformin (MET) is the most commonly used medication for diabetes and has been suggested as an adjunctive agent for host-directed TB therapy (132). Singhal et al. discovered that the MET disrupts the intracellular Mtb growth, reduces immunopathological severity, and increases the efficacy of anti-TB drugs (132). In detail, MET treatment reduced the bacterial load (in terms of CFU) 35 days post-infection in Mtb-infected mice (132). The combination of MET and anti-TB drugs, such as INH and ethionamide, significantly decreased lung Mtb load in the mouse model, indicating synergism between MET and anti-TB drugs (132). Additionally, reduction of lung tissue pathology was confirmed in the MET-treated mice, and the number of lung $CD8^+$ IFN-γ^+ cells was increased in MET-treated mice in both unstimulated and Mtb-stimulated groups, suggesting an enhanced immune response to TB (132). Similarly, the protective effect of MET was confirmed in a chronically Mtb-infected guinea pig model in which reduced lung legions and Mtb CFU were observed in the MET-treated group compared to those in the untreated group (135). Further, the MET-treated animals showed a higher proportion of lymphocytes in the acute and subacute stages and well-encapsulated granulomas (135). MET reportedly reduces the immunopathological severity by reprogramming T cell metabolism (162, 163). MET-induced oxidative phosphorylation and glycolysis enhanced the host resistance to Mtb infection in the guinea pig model (135). Moreover, Degner et al. demonstrated that MET treatment reduces mortality during TB therapy in a retrospective cohort study in Taiwan (133). Another study reported that MET enhances anti-TB immune responses by altering host responses in humans (134). Additionally, MET induced a significant reduction in TNF-α, IL-1β, IL-6, IFN-γ, and IL-17 release in response to Mtb lysate (134). These studies indicate that MET protects against Mtb infection *via* modulation of inflammation and metabolism (133–135). Indeed, MET reduces the type I IFN response and pathological severity of TB while enhancing anti-TB immunity, such as autophagy, ROS production, and phagocytosis (132, 164, 165) (**Figure 3**). In contrast, Dutta et al. showed that MET-treated mice had similar lung Mtb CFU compared to control mice, and the percentage of mice with Mtb culture relapse was similar between the two groups (166). This result was contradictory to a previous *in vivo* study that used the same MET dose (250 mg/kg) (132). The major difference between the two studies is the co-injection of multiple

TABLE 1 | Effect of TB representative adjunctive therapeutic agents of anti-TB drugs on host immunity.

Therapeutic agent	Mechanism of action	Role in TB	Model	Therapeutic effect or outcome	References
Rapamycin	Inhibits mTOR complex	Enhances autophagy and antigen presentation	Mouse (C57BL/6)	Increased Ag85B-specific T cell responses	(129)
			Macrophage (THP-1)	Inhibition of Mtb growth	(130)
			Mouse (BALB/c)	Reduced pathological lesion and Mtb burden	(131)
Metformin	Activates the AMPK	Enhances autophagy and reduces inflammation	Mouse (C57BL/6)	Reduced pathological lesion and enhanced Th1 immune response	(132)
			Clinical trial	Decreased mortality during TB treatment in diabetes patients	(133)
			PBMCs	Lowered TNF-α, IFN-γ, and IL-1β Increased phagocytosis and ROS production	(134)
			Guinea pigs	Decreased pathological severity	(135)
Statins	Inhibits HMG-CoA reductase	Enhancing autophagy and phagosome maturation	MDM	Decreased intracellular Mtb survival by statin monotherapy	(136)
	Increase intracellular Ca^{2+}		Mouse (C57BL/6)	Decreased intracellular Mtb survival Decreased pathological severity	
			Macrophage (J774)	Decreased intracellular Mtb survival	(137)
			Mouse (BALB/c)	Enhanced bactericidal activity of anti-TB drugs	
			Macrophage (THP-1)	Decreased intracellular Mtb survival	(138)
			Mouse (BALB/c)	Decreased intracellular Mtb survival Reduced TB relapse rates	
			PBMCs	Decreased intracellular Mtb survival	(139)
			Macrophage (THP-1)	Reduced Mtb growth	(140)
			Mouse (C3HeB/FeJ)	Enhanced bactericidal activity of anti-TB drugs	
NAC	ROS scavenging Increase intracellular GSH	Reduces oxidative stress/inflammation	Randomized clinical trial	Reduction of anti-TB drug-induced hepatotoxicity	(141)
			Guinea pig	Decreased intracellular Mtb survival Decreased pathological severity	(142)
			Macrophage (THP-1)	Decreased intracellular Mtb survival	(143)
			Mouse (C57BL/6) (*gp91Phox*$^{-/-}$)	Decreased intracellular Mtb survival by NAC monotherapy	
			Randomized clinical trial	Clearing of lung infiltration Reduction of cavity size	(144)
			Human granuloma	Decreased intracellular Mtb survival Formation of solid stable granuloma	(145)
			Macrophage (THP-1)	Synergistic effect on bactericidal activity of anti-TB drugs	(146)
			Randomized clinical trial in TB/HIV co-infected patients	No significant change between NAC-treated and non-treated groups	(147)
			In vitro	NAC potentiates the activity of anti-TB drugs	(148)
			Macrophage (THP-1/J774)	Reduced intracellular Mtb survival in THP1, but not in J774	
			Mouse (CBA/J)	Co-treatment of NAC potentiates the activity of anti-TB drugs, but disappeared at the later time point	
Verapamil	Inhibits the calcium ion channel	Inhibits the drug efflux pump of Mtb	Mouse (C3HeB/FeJ)	Co-treatment of verapamil with anti-TB drugs significantly lowered lung bacterial loads and relapse rates compared to standard therapy alone	(149)
			Mouse (BALB/c)	Co-treatment of verapamil with a combination regimen of moxifloxacin and linezolid showed a significant reduction in lung mycobacterial load	(150)
		Disrupts membrane potential of Mtb	*In vitro*	VP kills exponentially growing, stationary-phase and nutrient-starved non-replicating Mtb	(151)
		Increase drug bioavailability and efficacy	Mouse (CD-1)	VP increases plasma concentration of RIF	(151)
			Mouse (BALB/c)	Co-treatment of BDQ with VP increased the plasma exposure for BDQ	(152)

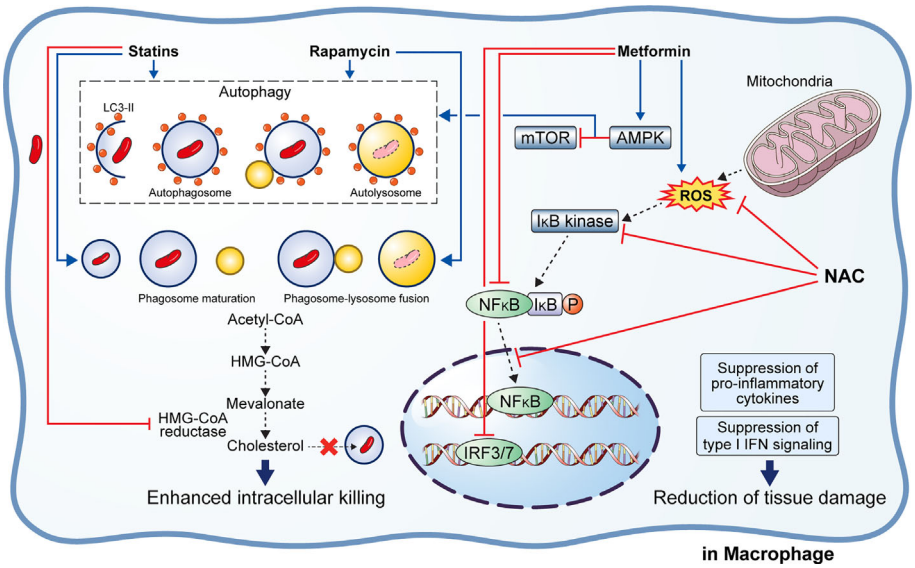

FIGURE 3 | Effect of adjunctive therapeutic agents of anti-TB drugs on host immunity. Various adjunctive drugs aid TB treatment by modulating the host immune response. *M. tuberculosis* (Mtb) can accumulate cholesterol for use as a source of carbon and energy. Statins bind to the active site of HMG-CoA reductase, thereby inhibiting cholesterol biosynthesis. In addition, statins induce autophagy and phagosome maturation to promote the removal of Mtb. Similarly, rapamycin induces autophagy and phagosome–lysosome fusion to enhance the intracellular killing of Mtb. Metformin inhibits the mTOR complex via AMPK activation in the mitochondria to promote autophagy. Metformin also inhibits ROS production, NFκB signaling, and type I interferon signaling. Similarly, N-acetyl-l-cysteine eliminates the generated ROS and inhibits NFκB signaling. Suppression of pro-inflammatory immune response and type I interferon signaling lead to reduced immunopathological severity that beneficial to the host.

anti-TB drugs (RIF, INH, PZA, and EMB) in the *in vivo* model compared with the single anti-TB drug (INH or EMB) used *in vitro* (132, 166). In addition to its antimicrobial activity, RIF promotes liver metabolism by activating hepatic cytochrome P450 enzymes, such as CYP2D6 and CYP3A4, thereby accelerating the drug metabolism and clearance by the liver (167). However, MET is not metabolized in the liver and is excreted *via* the urine in its unchanged form (168). Another potential explanation is that MET and RIF compete for the same drug target, namely the AMP-activated protein kinase (AMPK) in the liver (109, 169). Therefore, the combination with RIF reduces the effect of MET in the host.

Statin

Statins are anti-hyperlipidemic drugs that block 3-hydroxy-3-methylglutaryl coenzyme A reductase in the cholesterol synthesis pathway, thereby lowering the risk of stroke and cardiovascular diseases (170) (**Figure 3**). As cholesterol is an essential intracellular energy source for Mtb, elevated cholesterol level is a risk factor for TB (171). Statins also have immunomodulatory effects, such as the production of natural killer T cells, downregulation of MHC II expression, elevated secretion of IL-1β and IFN-γ, and increased caspase-1 enzyme activity, and thereby promote apoptosis and autophagy (172) (**Figure 3**). Both retrospective clinical trials and animal model studies have reported that statins are effective in the treatment and prevention of TB (136, 173, 174). Decreased bacterial burden was confirmed in peripheral blood mononuclear cells and monocyte-derived macrophages from patients with familial hypercholesterolemia during statin treatment compared to healthy donors (136). Further, statin treatment reduced the Mtb burden and histopathological severity in the lungs of Mtb-infected mice (136). Lobato et al. evaluated the effects of two statins (atorvastatin and simvastatin) alone and in combination with RIF on *M. leprae* and Mtb in THP-1 macrophages (175). Both statins showed bactericidal effects on intracellular mycobacteria 72 h post-infection and synergism with RIF at a concentration of 0.2 μM for reducing the viability of intracellular Mtb (175). Skerry et al. investigated the bactericidal activity of simvastatin alone and in combination with anti-TB drugs (RIF, INH, and PZA) in macrophages and a mouse model and found that the addition of 5 mM simvastatin significantly enhanced the bacterial killing of INH in Mtb-infected J774 macrophages (137). In contrast, the addition of 25 mg/kg simvastatin to the standard TB treatment regimen significantly reduced the lung bacterial burden in BALB/c mice (137). Similarly, Dutta et al. found that the addition of simvastatin (60 mg/kg) to the TB treatment regimen (INH/RIF/PZA) shortened the duration required to attain culture-negative results from 4.5 to 3.5 months, i.e., shortened the treatment duration (138). Simvastatin significantly improved the bactericidal activities of anti-TB drugs against intracellular Mtb while having no effect on intracellular RIF concentrations (138). The same research group further showed that various statins, including pravastatin, simvastatin, and Fluvastatin, improved the antimicrobial activity of INH, RIF, and PZA in THP-1 cells and the C3HeB/FeJ mouse model

(140). Additionally, pravastatin induced phagosome–lysosome fusion and macrophage activation observed in IFN-γ- and LPS-activated macrophages (140). Interestingly, Guerra-De-Blas et al. demonstrated that simvastatin alone significantly reduced bacterial load in Mtb-infected PBMCs *via* enhanced production of natural killer T cells, upregulation of co-stimulatory molecules in monocytes, increased the secretion of IL-1β and IL-12p70, and promotion of apoptosis and autophagy in monocytes (139).

ROS Modulating Drugs

ROS and reactive nitrogen species (RNS) are critical host defense mechanisms to eradicate pathogens during infection (176). The ROS and RNS react with the phagosomes and efficiently eliminate intracellular bacteria. However, excessive ROS production may cause mitochondrial damage and cell apoptosis, leading to severe immunopathologic outcomes (177). Therefore, appropriately balanced cellular ROS levels are critical for eliminating intracellular Mtb without causing a detrimental effect in the host.

N-Acetyl-Cysteine (NAC)

Multiple studies have shown that reducing ROS accumulation in the Mtb-infected host by NAC inhibited the Mtb growth and reduced the immunopathological severity despite the contradictory views on the Mtb killing ability of NAC (142, 143, 145, 148, 178–182) (**Figure 3**). Several studies have demonstrated that NAC ameliorates aminoglycoside-induced ototoxicity (183–185). Venketaraman et al. found that glutathione level was significantly reduced in PBMCs and RBCs isolated from TB patients (181). Further, reduced secretion of IL-10, IL-6, TNF-α, and IL-1 was confirmed in blood cultures of TB patients after NAC treatment (181). Similarly, Palanisamy et al. showed that NAC treatment moderately increased blood glutathione level and the serum antioxidant capacity in Mtb-infected guinea pigs, reduced the bacterial burden in the spleen, and decreased the immunopathological severity in the lungs and spleen of animals (142). Subsequently, Guerra et al. demonstrated that increased glutathione level due to NAC treatment inhibits the intracellular growth of Mtb by causing an increase in the levels of IL-2, IL-12, and IFN-γ secreted by T cells (180). Furthermore, NAC attenuates liver injury induced by anti-TB drugs by promoting free radical scavenging and glutathione synthesis (141).

Similarly, Amaral et al. demonstrated that NAC inhibits the growth of diverse pathogenic mycobacteria such as Mtb, *M. bovis*, and *M. avium* (143). The mycobacterial loads in the lungs of NAC-treated animals were significantly reduced compared to that in the untreated animals in both wild type and *gp91Phox*$^{-/-}$ macrophages, suggesting that the anti-TB activity of NAC is independent of the host NADPH oxidase system (143). Lamprecht et al. showed that NAC potentiates the bactericidal activity of BDQ, Q203, and CFZ in an *in vitro* macrophage model (179). They found that the addition of NAC significantly improved bactericidal activity of the three anti-TB drugs, leading to complete Mtb sterilization (179). In another study, NAC treatment caused a 50% reduction in bacterial load (in terms of CFU) in THP-1 macrophages and potentiated the bactericidal effect of anti-TB drugs, such as INH, RIF, EMB, or PZA (146). Moreover, NAC treatment can modulate TNF-α levels to maintain granuloma structure without inducing detrimental cell damage to the host (146). Similarly, Teskey et al. showed that incubation of Mtb Erdman strain with NAC significantly inhibited the bacterial growth, while incubation with a combination of NAC and anti-TB drugs (INH, RIF, and EMB) completely sterilized the Mtb culture (145). In addition, NAC treatment significantly increased the IFN-γ level while decreasing that of TNF-α as well as significantly enhanced the phagosome acidification in human granulomas, which indicates improved intracellular killing (145). On the contrary, NAC alone did not kill Mtb in macrophages, whereas INH and NAC combined showed an improved bactericidal activity than INH alone (178). However, Khameneh et al. demonstrated that the combination of anti-TB drugs (RIF and INH) and vitamin C, but not NAC, induced synergistic effects for bacterial killing (182). However, there were a few inconsistencies in their results. For instance, in the presence of 20 μg/mL RIF, treatment with 0.05 mg/mL NAC showed 10% CFU, whereas treatment with 0.1 mg/mL NAC showed 150% CFU compared to untreated controls (182). Recently, Vilchèze et al. showed that NAC improves the sterilizing activity of first and second-line anti-TB drugs *in vitro* against drug-susceptible and drug-resistant Mtb strains (148). However, a synergistic effect between NAC and anti-TB drugs was not observed in Mtb-infected mice (148). Moreover, although NAC initially inhibited Mtb growth, the NAC-induced growth inhibition was not significant and was lost after the first week of treatment (148). The major difference between the controversial studies is the host species. The direct killing effect of NAC was not seen in studies using *in vivo* or *in vitro* mouse models. Similarly, clinical trials on the adjunct effect of NAC on TB therapy in TB patients showed contradictory results (144, 147). Mahakalkar et al. showed that NAC treatment significantly shortened the duration of anti-TB therapy in TB patients (144). On the contrary, a recent clinical trial in Brazil demonstrated that NAC addition to a standard TB regimen did not reduce the duration required to achieve a negative sputum culture, nor did it reduce radiological severity in hospitalized patients with severe TB and HIV co-infection (147) (**Table 1**). However, these trials did not include a sufficiently large study population. Therefore, a large-scale clinical study is needed to determine the safety and efficacy of NAC treatment in TB.

Vitamin C

Vitamin C (VC) is an essential nutrient for humans that possesses reducing and antioxidant abilities associated with its ability to donate electrons (186). Several studies have investigated the host beneficial or detrimental roles of VC in the pathogenesis of TB (187–192). Vilchèze et al. demonstrated that VC kills drug-susceptible and drug-resistant Mtb *via* Fenton reaction in a dose-dependent manner *in vitro*, and 4 mM of VC completely sterilized Mtb culture at three weeks after treatment (187). VC is assumed to kill Mtb by increasing the intracellular ROS level, and this process depends on the intracellular iron concentration (187). The same research group also showed that a combination of VC and anti-TB drugs sterilizes Mtb cultures faster than monotherapy with anti-TB drugs (190). Further, Susanto et al.

revealed that administration of VC improves the sputum conversion culture rate in RIF-susceptible Mtb-infected patients (189). On the contrary, Sikri et al. suggested that VC induces Mtb dormancy leading to a viable but non-culturable state (188). VC-treated Mtb showed antibiotic tolerance, thereby exhibiting a higher survival rate than untreated Mtb culture in the presence of anti-TB drugs (188). Similarly, Nandi et al. demonstrated that VC induces the activation of multiple transcriptional regulators for the temporal adaptation to VC, leading to a dormancy response (191). In summary, VC sterilizes Mtb culture by generating ROS *via* Fenton reaction and promoting oxygen consumption, thus eradicating bacterial persisters. However, several studies report that VC promotes the generation of bacterial persisters in TB. Therefore, further research is needed to elucidate the role of VC in the pathogenesis of TB.

HO-1 Inhibitor

In section 3, we discussed that Mtb and bactericidal anti-TB drugs cause mitochondrial dysfunction and oxidative damage in host cells, consequently ROS-mediated apoptosis as well as simultaneous activation of antioxidant mechanisms, such as the Keap1-Nrf2 signaling pathway, that may interfere with the removal of Mtb (88, 89) A major factor involved in this mechanism is HO-1 (95, 192). However, the detailed role of host HO-1 during the onset and pathogenesis of TB remains controversial and has not been fully elucidated (95, 99, 192–195). HO-1 exerts anti-inflammatory and cytoprotective effects, although the underlying mechanisms are not fully understood (196). Several studies have investigated the host beneficial or detrimental roles of HO-1 during TB infection (95, 99, 192–195). Andrade et al. showed that active TB patients show a negative correlation between plasma levels of HO-1 and MMP-1 (95). Notably, the TB patients with high plasma levels of HO-1 or MMP-1 demonstrated unique clinical presentation and inflammatory cytokine profiles (95). Moreover, a high HO-1 level was induced by the infection of virulent Mtb strain in human or murine macrophages, and MMP-1 expression was inhibited by CO by suppressing c-Jun/AP-1 signaling (95). Costa and colleagues demonstrated that the administration of tin protoporphyrin IX (SnPPIX), an HO-1 enzymatic inhibitor, decreases pulmonary Mtb loads comparable to that accomplished by anti-TB drug therapy as well as improves the bactericidal activity of anti-TB drugs (RIF, INH, and PZA) (192). Interestingly, host T cell immune response was needed to inhibit HO-1 by SnPPIX, and SnPPIX failed to reduce bacterial growth and activity of Mtb HO-1 enzyme in broth culture (192). Rockwood et al. reported HO-1 upregulation in Mtb-infected rabbits, mice, and non-human primates, and anti-TB therapy reduced the HO-1 plasma levels (193). Similar upregulation of HO-1 was observed in the plasma of untreated HIV-1 co-infected TB patients. In these patients, the plasma HO-1 levels positively and negatively correlated with the HIV-1 viral load and $CD4^+$ T cell count, respectively (193). Further, early secreted antigen ESAT-6-mediated nuclear translocation of transcription factor NRF-2 is required for Mtb-induced HO-1 expression (193). Recently, Costa et al. discovered that HO-1 inhibition improves IFN-γ-induced NOS2-dependent bacterial killing by murine macrophages (99). Additionally, HO-1 inhibition induced low intracellular non-protein bound iron in Mtb-infected macrophages and reduced iron deposition in the lungs of Mtb-infected mice (99). Taken together, HO-1 expression inhibits T cell-mediated IFN-γ-induced NOS2-dependent control of Mtb by producing free iron. Therefore, inhibition of HO-1 expression potentiates the anti-TB therapy and improves clinical outcomes.

Calcium Channel Blocker

Verapamil (VP) is a calcium channel blocker used for hypertension treatment that also acts as an inhibitor of drug efflux protein. Several studies have proposed that VP can potentially improve the bactericidal activity of anti-TB drugs, such as RIF, INH, EMB, BDQ, and CFZ (151, 197–199). Machado et al. demonstrated that VP disrupts the heightened antibiotic resistance induced by repetitive exposure to INH (197). Similarly, Gupta et al. showed that VP potentiates the bactericidal activity of BDQ in reference strain H37Rv and eight clinical Mtb isolates (198). Similarly, Li et al. suggested that the addition of VP improves RIF susceptibility in RIF-resistant Mtb isolates (199). Chen et al. suggested that VP monotherapy kills exponentially growing, stationary-phase, nutrient-starved, non-replicating Mtb by disrupting membrane energetics without affecting the physical integrity of the membrane (151). Further, VP potentiates the bactericidal effects of BDQ and CFZ *in vitro* and in a RIF mouse model without changing the intracellular concentration of the drugs (151). Similarly, Xu et al. demonstrated that VP potentiates the efficacy of BDQ and CFZ against Mtb clinical isolates (152). However, VP increased bioavailability and efficacy of BDQ but not CFZ in Mtb-infected mice (152). Collectively, synergistic activity of VP *in vivo* may be attributed to improved systemic exposure to co-treated drugs by modulating mammalian transporters without inhibiting bacterial efflux pumps (152). Thus, the combination of VP and anti-TB drugs may be an effective therapy for TB.

Cytokines

Cytokines are small soluble proteins with multifaced aspects of host protective and detrimental effects (200). Excessive TB-induced inflammation interferes with normal lung function and may increase the risk of TB relapse (201). Comprehensive insight into host-pathogen interaction in TB would aid in designing host-directed therapies to shorten antibiotic treatment duration and relieve immunopathology. Immunotherapy with several cytokines protects the host and boosts bacterial clearance (**Table 2**).

IFN-γ and IL-12

IL-12/IFN-γ axis plays a critical role in host immune response for controlling TB, and IFN-γ is the key cytokine in the innate immune response during Mtb infection (219). IFN-γ is responsible for enhancing bactericidal activity through the upregulation of ROS, RNI, and autophagy (155, 228, 229). IFN-γ reverses the blockade of phagosome–lysosome fusion caused

TABLE 2 | Effect of cytokines on host immunity in TB.

Cytokine	Role in TB	Model	Therapeutic effect or outcome	References
GM-CSF	Restriction of Mtb burden Lymphocyte recruitment Formation of normal granulomas	Mouse (C57BL/6)	Prevented weight loss and enhanced pulmonary Mtb clearance	(202)
		Mouse (BALB/c)	Exogenous administration GM-CSF induced significant reduction of pulmonary bacterial loads	(203)
		Mouse (BALB/c)	Exogenous administration GM-CSF induced significant reduction of pulmonary bacterial loads and pneumonic area	(204)
		Mouse (C57BL/6)	GM-CSF neutralization reduces acute lung inflammation and neutrophil recruitment	(205)
		Mouse (C57BL/6)	GM-CSF neutralization induces increased pathological lesion, necrosis, inflammation, and pulmonary Mtb burden	(206)
IFN-γ	Mediator of macrophage activation	Randomized clinical trial	Increased rate of Mtb clearance Significant reduction of prevalence of clinical symptoms such as fever, sneeze, and night sweats	(207)
		Mouse (BALB/c)	Exogenous administration of IFN-γ reduced bacterial loads and tissue damage in the lung	(208)
		Macrophage (MDM)	Pretreatment of IFN-γ impaired immune response of MDM from MDR-TB patients	(209)
Type I interferons (IFN-α/IFN-β)	Suppression of pro-inflammatory cytokines and Th1 responses	Mouse (C57BL/6)	Overexpression of type I interferons induced increased pulmonary Mtb loads	(210)
		Mouse (C57BL/6)	*Ifnar*$^{-/-}$/*Ifngr*$^{-/-}$ mice showed decreased survival rate and increased Mtb loads in the lung	(211)
		Mouse (C57BL/6)	*Ifnar*$^{-/-}$ mice showed similar Mtb loads in the lung	(206)
		Mouse (129S2)	Suppression of type I IFN signaling significantly enhanced the bactericidal activity of RIF which leading to reduced bacterial loads and improved survival	(212)
		Mouse (C57BL/6)	*Il1r1*$^{-/-}$ mice showed decreased survival rate and increased pulmonary Mtb loads	(213)
TNF-α	Macrophage activation, critical for granuloma formation and maintenance	Analysis of reports	Infliximab therapy induced the reactivation of latent tuberculosis	(214)
		Mouse (B6D2F1)	Exogenous administration of TNF-α induced significant reduction of bacterial load and pneumonic area	(215)
		3D cell culture model	TNF-α neutralization reverses augmented Mtb growth caused by anti-PD-1 treatment	(216)
		In vitro granuloma model	TNF-α antagonists induced resuscitation of dormant Mtb	(217)
IL-2	Promotes the expansion of the antigen-specific T cells	Clinical trials	Exogenous administration of IL-2 reduced bacterial loads in sputum	(218)
		Mouse (C57BL/6)	Exogenous administration of IL-2 restored T cell dysfunction induced by persistent Mtb infection	(219)
IL-12	Proliferation and activation of T lymphocytes, NK cells, and NKT cells	Mouse (C57BL/6)	IL-12 improved survival and reduced bacterial loads of Mtb-infected *CD4*$^{-/-}$ mice	(220)
		Mouse (BALB/c)	IL-12 reduced bacterial loads and immunopathological severity	(221)
IL-22	Production of inflammatory mediators and recruitment of pathologic effector cells	Mouse (C57BL/6)	*Il22*$^{-/-}$ mice showed increased bacterial loads in the lung and spleen	(222)
		Macrophage (MDM)	Exogenous administration of IL-22 induced significant reduction of intracellular growth of Mtb	(223)
IL-17	Affect neutrophil homeostasis and survival	Mouse (C57BL/6)	*Il17*$^{-/-}$ mice showed increased lung bacterial burden compared to wild type	(224)
IL-23	Induces the IFN-γ and IL-17 response in the lung and enhances host protection	Mouse (C57BL/6)	*Il23*$^{-/-}$ mice showed moderately enhanced immunopathological response in the lung	(225)
		Mouse (C57BL/6)	Exogenous administration of IL-23 significantly reduced the pulmonary Mtb loads, and the lung inflammation levels	(226)
IL-24	Induces IFN-γ production by $CD8^+$ T cells	Mouse (BALB/c)	Exogenous administration of IL-24 significantly reduced the Mtb loads in the lung and spleen. Also, survival was improved in IL-24 treated group	(227)

by Mtb (230). Moreover, IFN-γ stimulates the production of IL-12 in Mtb-infected macrophages, while IL-12 stimulates the production of IFN-γ by T cells and NK cells, thus activating macrophages that lead to intracellular bacterial killing (231). Dawson et al. reported a significant increase in $CD4^+$ lymphocyte response and significantly reduced Mtb load in the sputum of the recombinant IFN-γ1b-treated group (207). Mata-Espinosa et al. demonstrated that exogenous administration of IFN-γ reduces bacterial loads and tissue damage in the lungs of Mtb-infected mice (208). Along similar lines, Khan et al. showed

that treatment with exogenous IFN-γ restored defective immune response of MDMs isolated from MDR-TB patients (209). Exogenous administration of IL-12 improved survival and reduced the bacterial loads of Mtb-infected $CD4^{-/-}$ mice (220). Similarly, treatment with recombinant adenovirus encoding IL-12 (AdIL-12) significantly reduced the bacterial loads in a progressive pulmonary TB mouse model (221). AdIL-12-treated mice showed significantly higher levels of IFN-γ, TNF-α, and iNOS compared with the untreated group. In addition, AdIL-12-treated mice showed less severe pathological legions than the untreated mice (221).

TNF-α

TNF-α plays an important role in controlling TB in both the initial and late stages (232). TNF-α activates macrophages and contributes to the formation and maintenance of granulomas to suppress the dissemination of Mtb; however, it also induces tissue damage due to the excessive immune responses (233). Keane et al. demonstrated that treatment with TNF-α inhibitor induces the reactivation of latent TB (234). Similarly, treatment with several TNF-α antagonists differentially induced resuscitation of dormant Mtb in a 3D microgranuloma model (214). Adalimumab, a TNF-α antagonist, showed a greater resuscitation rate than etanercept through the TGF-β1-dependent pathway (214). Furthermore, exogenous administration of TNF-α significantly decreased the bacterial load and pneumonic area in Mtb-infected mice (217). In contrast, Tereza et al. demonstrated that excessive TNF-α secretion *via* PD-1 inhibition facilitated Mtb growth in a micro granuloma model (215).

IL-24

IL-24 plays an immune-regulatory role to induce Th1 cytokines, such as IFN-γ, IL-6, and TNF-α, during TB infection (216). Upregulated IL-24 expression was observed in BCG-vaccinated newborns, suggesting the host protective role of IL-24 during TB infection (235). Wu et al. demonstrated that administration of exogenous IL-24 induces IFN-γ upregulation, whereas IL-24 neutralization causes IFN-γ downregulation (216). Similarly, IL-24 stimulation results in the upregulation of IFN-γ-inducing cytokines, such as IL-12, IL-23, and IL-27 (216). Furthermore, Ma et al. demonstrated that administration of IL-24 induced IFN-γ production and activated $CD8^+$ T cells in mice, indicating its host protective effect in TB (227). Huang et al. found that IL-24 family cytokines, such as IL-19, IL-20, and IL-22, are elevated in BCG-vaccinated non-human primates as well (236). Treatment with exogenous IL-24 significantly increased the survival rate and significantly reduced the bacterial burden compared to the control group (**Table 2**).

IL-2

IL-2 plays a critical regulatory role during T cell differentiation *via* induction of the transcription factor eomesodermin and perforin (237). During chronic viral infection, the production of memory T cells and memory T cell-associated molecules, such as CD127 and CD44, was observed after stimulation with low-dose IL-2 (238). IL-2 administration is proven to exert host protective effects in TB infection; it reduced or cleared bacterial burden and increased the number of $CD25^+$ and $CD56^+$ cells (239). A similar protective effect of exogenous IL-2 was reported by Shen et al., who showed that the IL-2-treated group showed decreased sputum smear-positive rates, whereas the control group showed increased sputum smear-positive rates (218). The IL-2-treated group also demonstrated less severe legions than the control group during TB treatment (218). Liu et al. showed that persistent stimulation with Mtb antigen induces disrupted cytokine production by T cells, and IL-2 restores the T cell dysfunction (219). Their findings suggested that administration of exogenous IL-2 leads to maintenance of immune homeostasis in the bone marrow and reactivation of the disrupted hematopoiesis by persistent Mtb infection (219).

Granulocyte-Macrophage Colony-Stimulating Factor (GM-CSF)

Previous studies showed that GM-CSF exerts a host protective role during TB infection (202–205, 240–242). It mediates the formation of granuloma and promotes bacterial clearance in the host (241), and induces classical activation of macrophage to M1 polarization state (242).

Treatment with recombinant adenoviruses encoding GM-CSF significantly reduced the bacterial burden in the lungs, increased the number of activated DCs, and elevated the levels of TNF-α, IFN-γ, and iNOS (203). The same group further demonstrated that exogenous administration of GM-CSF significantly reduced the pulmonary Mtb loads and pneumonic area in Mtb-infected mice (202). Similarly, Pasula et al. demonstrated that exogenous keratinocyte growth factor administration protects against Mtb infection through GM-CSF-dependent macrophage activation and phagosome–lysosome fusion (204). Moreover, neutralization of GM-CSF induced higher bacterial burden and increased immunopathologic severity with necrotic granulomatous lesions during INH/RIF treatment in TNF-α-deficient mice (205). Furthermore, GM-CSF blocking by monoclonal antibody enhanced host susceptibility and immunopathological severity in Mtb-infected mice (206). Moreover, the absence of GM-CSF signaling results in type I IFN-induced neutrophil extracellular trap formation that aggravates lung mycobacterial burden and lung pathology (206). In addition, neutrophil extracellular traps were abundant in the lung lesions of Mtb-infected C3HeB/FeJ mice and TB patients who showed impaired response to anti-TB therapy (206).

Type I IFNs

Type I IFNs include IFN-α, IFN-β, and several other IFNs that interact with IFNAR1 and IFNAR2 to activate a range of IFN-stimulated genes *via* STAT1 and STAT2 signaling (243, 244). Type I IFNs play a complex role in mediating beneficial and detrimental effects in the host during TB infection (244). Whole blood transcriptional profiling of active TB patients revealed that upregulation of type I IFN-αβ-inducible transcripts correlated with radiographic severity of the lungs that was restored to the

level of healthy controls after anti-TB therapy (245). Recent studies have demonstrated that type I IFN-inducible blood transcriptional signature, including upregulation of *STAT1*, *IFITs*, *GBPs*, *MX1*, *OAS1*, and *IRF1*, was associated with active TB disease (246–248).

Antonelli et al. demonstrated that overexpression of type I IFNs increased pulmonary bacterial loads and extensively distributed necrotic legions in the poly-l-lysine and carboxymethylcellulose (poly-ICLC)-treated Mtb-infected mice (210). Further, a significant increase of $CD11b^{+}F4/80^{+}Gr1int$ cells that showed diminished MHC II expression was confirmed in their lungs (210). Similarly, Mayer-Barber et al. showed IL-1-dependent host protection by producing eicosanoids that suppress immoderate type I IFN production and control bacterial loads (213). The *Il1r1*$^{-/-}$ mice showed a significantly decreased survival rate and increased bacterial loads in the lungs compared with the wild type mice (213) (**Table 2**). Similarly, induction of type I IFN due to loss of GM-CSF signaling or genetic susceptibility facilitated Mtb growth and increased disease severity (206). Interestingly, the same group demonstrated host protective effect of type I IFN in the lungs of Mtb-infected mice lacking IFN-γ signaling; the pulmonary bacterial loads were significantly higher in the *Ifnar*$^{-/-}$/*Ifngr*$^{-/-}$ mice compared with that in the *Ifngr*$^{-/-}$ and *Ifnar*$^{-/-}$ mice on post-infection days 24 and 28 (211). Recently, Zhang et al. demonstrated a correlation between type I IFN signaling and cell death of Mtb-infected mouse macrophage (212). Further, suppression of type I IFN signaling significantly enhanced the bactericidal activity of RIF in Mtb-infected mice, leading to reduced bacterial loads and improved survival (212). Collectively, these results provide strong evidence that modulation of type I IFN signaling determines the disease severity and susceptibility of immunopathologic lesions in TB.

Th17 Cytokines

Th17 cytokines secreted by Th17 and Th22 cells may play a regulatory role in the immune response during Mtb infection (249). Th17 cytokines play a protective role in Mtb infection but are also involved in pathology due to excessive immune response (250). IL-22 promotes the production of inflammatory mediators and the recruitment of pathologic effector cells in TB (250). IL-22 also promotes tissue repair and healing in lung epithelial cells (251). Treerat et al. demonstrated a significantly increased bacterial burden in the lungs and spleen of *Il22*$^{-/-}$ mice (222). Similarly, exogenous administration of IL-22 significantly inhibited intracellular Mtb growth by inducing calgranulin A expression (223). Modulation of Th17 responses is essential to promote anti-TB immunity and block immense immunopathology, leading to a detrimental effect on the host (**Table 2**). Gopal et al. showed that *Il17*$^{-/-}$ mice demonstrate increased lung bacterial burden compared to that in wild type mice; however, IL-17 overexpression improved the resistance to TB in Mtb-infected *Il17*$^{-/-}$ mice (224). IL-23 induces the production of IFN-γ and IL-17 response that promotes anti-TB immunity. Khader et al. observed increased immunopathological severity in the lungs of *Il23*$^{-/-}$ mice (225). The exogenous administration of IL-23 induced significant reduction of the pulmonary Mtb loads and the immunopathological severity in a mouse model *via* enhanced local T cell immunity (226). Taken together, appropriate modulation of Th-17 cytokines is critical to control TB with minimal detrimental effects to the host.

CONCLUSION AND FUTURE PERSPECTIVE

Understanding bacterial adaptation to host-mediated stress contributing to antibiotic tolerance is a critical factor in improving disease outcomes and shortening treatment duration. In addition to eliminating the pathogen, effective TB therapy should relieve the associated clinical symptoms by controlling immune-mediated inflammatory responses and minimize damage to the host, thereby minimizing the sequelae. Within the host, Mtb undergoes metabolic reprogramming by drugs or host-mediated stress, resulting in a drug-tolerant state across drug classes. Representative examples of metabolic reprogramming include metabolic stagnation, activation of metabolic bypass, accumulation of triacylglycerol, biofilm formation, and stringent response. The host metabolism is modulated by Mtb infection or the anti-TB drugs, leading to the critical point that determines the treatment success. Therefore, if the host metabolism can be regulated to induce a host-favorable state, the treatment period can be drastically reduced, and side effects can be minimized, dramatically improving clinical outcomes.

AUTHOR CONTRIBUTIONS

H-EP, WL, M-KS, and SS wrote the manuscript. M-KS and SS conceived the study, supervised the team, and critically revised the manuscript. All authors contributed to the article and approved the submitted version.

FUNDING

This work was supported by the National Research Foundation of Korea (NRF) grant (NRF-2019R1A2C2003204 and NRF-2021R1C1C2012177) and the Bio & Medical Technology Development Program of NRF (NRF-2020M3A9H5104234) funded by the Korean Government (MSIT), Republic of Korea. The funders had no role in study design, data collection and analysis, decision to publish, or manuscript preparation.

ACKNOWLEDGMENTS

The authors thank MID (Medical Illustration & Design), a part of the Medical Research Support Services of Yonsei University College of Medicine, for all artistic support related to this work.

REFERENCES

1. Floyd K, Glaziou P, Zumla A, Raviglione M. The Global Tuberculosis Epidemic and Progress in Care, Prevention, and Research: An Overview in Year 3 of the End TB Era. *Lancet Respir Med* (2018) 6(4):299–314. doi: 10.1016/S2213-2600(18)30057-2
2. World Health Organization. *Global Tuberculosis Report 2020*. Geneva: World Health Organization (2020).
3. Goossens SN, Sampson SL, van Rie A. Mechanisms of Drug-Induced Tolerance in *Mycobacterium tuberculosis*. *Clin Microbiol Rev* (2021) 34(1): e00141–20. doi: 10.1128/CMR.00141-20
4. Nasiri MJ, Haeili M, Ghazi M, Goudarzi H, Pormohammad A, Fooladi AAI, et al. New Insights in to the Intrinsic and Acquired Drug Resistance Mechanisms in Mycobacteria. *Front Microbiol* (2017) 8:681. doi: 10.3389/fmicb.2017.00681
5. Mandal S, Njikan S, Kumar A, Early JV, Parish T. The Relevance of Persisters in Tuberculosis Drug Discovery. *Microbiology (United Kingdom)* (2019) 165(5):492–9. doi: 10.1099/mic.0.000760
6. Zhang Y, Yew WW, Barer MR. Targeting Persisters for Tuberculosis Control. *Antimicrob Agents Chemother* (2012) 56(5):2223–30. doi: 10.1128/AAC.06288-11
7. Fauvart M, de Groote VN, Michiels J. Role of Persister Cells in Chronic Infections: Clinical Relevance and Perspectives on Anti-Persister Therapies. *J Med Microbiol* (2011) 60(Pt 6):699–709. doi: 10.1099/jmm.0.030932-0
8. Keren I, Minami S, Rubin E, Lewis K. Characterization and Transcriptome Analysis of *Mycobacterium tuberculosis* Persisters. *mBio* (2011) 2(3): e00100–11. doi: 10.1128/mBio.00100-11
9. Sebastian J, Swaminath S, Nair RR, Jakkala K, Pradhan A, Ajitkumar P. De Novo Emergence of Genetically Resistant Mutants of *Mycobacterium tuberculosis* From the Persistence Phase Cells Formed Against Antituberculosis Drugs In Vitro. *Antimicrob Agents Chemother* (2017) 61 (2):e01343–16. doi: 10.1128/AAC.01343-16
10. Sebastian J, Swaminath S, Ajitkumar P. Reduced Permeability to Rifampicin by Capsular Thickening as a Mechanism of Antibiotic Persistence in *Mycobacterium tuberculosis*. *bioRxiv* (2019). doi: 10.1101/624569
11. Balaban NQ, Helaine S, Lewis K, Ackermann M, Aldridge B, Andersson DI, et al. Definitions and Guidelines for Research on Antibiotic Persistence. *Nat Rev Microbiol* (2019) 17(7):441–8. doi: 10.1038/s41579-019-0196-3
12. Brauner A, Fridman O, Gefen O, Balaban NQ. Distinguishing Between Resistance, Tolerance and Persistence to Antibiotic Treatment. *Nat Rev Microbiol* (2016) 14(5):320–30. doi: 10.1038/nrmicro.2016.34
13. Levin-Reisman I, Brauner A, Ronin I, Balaban NQ. Epistasis Between Antibiotic Tolerance, Persistence, and Resistance Mutations. *Proc Natl Acad Sci USA* (2019) 116(29):14734–9. doi: 10.1073/pnas.1906169116
14. Ma D, Mandell JB, Donegan NP, Cheung AL, Ma W, Rothenberger S, et al. The Toxin-Antitoxin mazEF Drives Staphylococcus Aureus Biofilm Formation, Antibiotic Tolerance, and Chronic Infection. *mBio* (2019) 10 (6):e01658–19. doi: 10.1128/mBio.01658-19
15. Rowe SE, Wagner NJ, Li L, Beam JE, Wilkinson AD, Radlinski LC, et al. Reactive Oxygen Species Induce Antibiotic Tolerance During Systemic Staphylococcus Aureus Infection. *Nat Microbiol* (2020) 5(2):282–90. doi: 10.1038/s41564-020-0679-z
16. Matern WM, Rifat D, Bader JS, Karakousis PC. Gene Enrichment Analysis Reveals Major Regulators of *Mycobacterium tuberculosis* Gene Expression in Two Models of Antibiotic Tolerance. *Front Microbiol* (2018) 9:610. doi: 10.3389/fmicb.2018.00610
17. Secor PR, Michaels LA, Ratjen A, Jennings LK, Singh PK. Entropically Driven Aggregation of Bacteria by Host Polymers Promotes Antibiotic Tolerance in *Pseudomonas Aeruginosa*. *Proc Natl Acad Sci USA* (2018) 115(42):10780–5. doi: 10.1073/pnas.1806005115
18. Meylan S, Andrews IW, Collins JJ. Targeting Antibiotic Tolerance, Pathogen by Pathogen. *Cell* (2018) 172(6):1228–38. doi: 10.1016/j.cell.2018.01.037
19. Vega NM, Allison KR, Khalil AS, Collins JJ. Signaling-Mediated Bacterial Persister Formation. *Nat Chem Biol* (2012) 8(5):431–3. doi: 10.1038/nchembio.915
20. Helaine S, Cheverton AM, Watson KG, Faure LM, Matthews SA, Holden DW. Internalization of Salmonella by Macrophages Induces Formation of Nonreplicating Persisters. *Science* (2014) 343(6167):204–8. doi: 10.1126/science.1244705
21. Kaiser P, Regoes RR, Dolowschiak T, Wotzka SY, Lengefeld J, Slack E, et al. Cecum Lymph Node Dendritic Cells Harbor Slow-Growing Bacteria Phenotypically Tolerant to Antibiotic Treatment. *PloS Biol* (2014) 12(2): e1001793. doi: 10.1371/journal.pbio.1001793
22. Manina G, Dhar N, McKinney JD. Stress and Host Immunity Amplify *Mycobacterium tuberculosis* Phenotypic Heterogeneity and Induce Nongrowing Metabolically Active Forms. *Cell Host Microbe* (2015) 17 (1):32–46. doi: 10.1016/j.chom.2014.11.016
23. Mouton JM, Helaine S, Holden DW, Sampson SL. Elucidating Population-Wide Mycobacterial Replication Dynamics at the Single-Cell Level. *Microbiology (United Kingdom)* (2016) 162(6):966–78. doi: 10.1099/mic.0.000288
24. Brown DR. Nitrogen Starvation Induces Persister Cell Formation in Escherichia Coli. *J Bacteriol* (2019) 201(3):e00622–18. doi: 10.1128/JB.00622-18
25. Schnappinger D, Ehrt S, Voskuil MI, Liu Y, Mangan JA, Monahan IM, et al. Transcriptional Adaptation of *Mycobacterium tuberculosis* Within Macrophages: Insights Into the Phagosomal Environment. *J Exp Med* (2003) 198(5):693–704. doi: 10.1084/jem.20030846
26. Flentie K, Garner AL, Stallings CL. *Mycobacterium tuberculosis* Transcription Machinery: Ready to Respond to Host Attacks. *J Bacteriol* (2016) 198 (9):1360–73. doi: 10.1128/JB.00935-15
27. Parish T. Two-Component Regulatory Systems of Mycobacteria. *Microbiol Spectr* (2014) 2(1):MGM2-0010-2013. doi: 10.1128/microbiolspec.MGM2-0010-2013
28. Beceiro A, Tomas M, Bou G. Antimicrobial Resistance and Virulence: A Successful or Deleterious Association in the Bacterial World? *Clin Microbiol Rev* (2013) 26(2):185–230. doi: 10.1128/CMR.00059-12
29. Galagan JE, Minch K, Peterson M, Lyubetskaya A, Azizi E, Sweet L, et al. The *Mycobacterium tuberculosis* Regulatory Network and Hypoxia. *Nature* (2013) 499(7457):178–83. doi: 10.1038/nature12337
30. Walters SB, Dubnau E, Kolesnikova I, Laval F, Daffe M, Smith I. The *Mycobacterium tuberculosis* PhoPR Two-Component System Regulates Genes Essential for Virulence and Complex Lipid Biosynthesis. *Mol Microbiol* (2006) 60(2):312–30. doi: 10.1111/j.1365-2958.2006.05102.x
31. Asensio JG, Maia C, Ferrer NL, Barilone N, Laval F, Soto CY, et al. The Virulence-Associated Two-Component PhoP-PhoR System Controls the Biosynthesis of Polyketide-Derived Lipids in *Mycobacterium tuberculosis*. *J Biol Chem* (2006) 281(3):1313–6. doi: 10.1074/jbc.C500388200
32. Martin C, Williams A, Hernandez-Pando R, Cardona PJ, Gormley E, Bordat Y, et al. The Live *Mycobacterium tuberculosis* Phop Mutant Strain Is More Attenuated Than BCG and Confers Protective Immunity Against Tuberculosis in Mice and Guinea Pigs. *Vaccine* (2006) 24(17):3408–19. doi: 10.1016/j.vaccine.2006.03.017
33. Cimino M, Thomas C, Namouchi A, Dubrac S, Gicquel B, Gopaul DN. Identification of DNA Binding Motifs of the *Mycobacterium tuberculosis* Phop/Phor Two-Component Signal Transduction System. *PloS One* (2012) 7 (8):e42876. doi: 10.1371/journal.pone.0042876
34. Pérez E, Bordas Y, Guilhot C, Gicquel B, Martı C, Samper S, et al. An Essential Role for Phop in *Mycobacterium tuberculosis* Virulence. *Mol Microbiol* (2001) 41(1):179–87. doi: 10.1046/j.1365-2958.2001.02500.x
35. Lee JS, Krause R, Schreiber J, Mollenkopf HJ, Kowall J, Stein R, et al. Mutation in the Transcriptional Regulator PhoP Contributes to Avirulence of *Mycobacterium Tuberculosis* H37Ra Strain. *Cell Host Microbe* (2008) 3 (2):97–103. doi: 10.1016/j.chom.2008.01.002
36. Liu Y, Tan S, Huang L, Abramovitch RB, Rohde KH, Zimmerman MD, et al. Immune Activation of the Host Cell Induces Drug Tolerance in *Mycobacterium Tuberculosis* Both In Vitro and In Vivo. *J Exp Med* (2016) 213(5):809–25. doi: 10.1084/jem.20151248
37. Primm TP, Andersen SJ, Mizrahi V, Avarbock D, Rubin H, Barry CE. The Stringent Response of *Mycobacterium tuberculosis* Is Required for Long-Term Survival. *J Bacteriol* (2000) 182(17):4889–98. doi: 10.1128/JB.182.17.4889-4898.2000
38. Avarbock D, Salem J, Li LS, Wang ZM, Rubin H. Cloning and Characterization of a Bifunctional RelA/SpoT Homologue From *Mycobacterium tuberculosis*. *Gene* (1999) 233(1–2):261–9. doi: 10.1016/S0378-1119(99)00114-6

39. Chuang YM, Dutta NK, Hung CF, Wu TC, Rubin H, Karakousis PC. Stringent Response Factors PPX1 and PPK2 Play an Important Role in *Mycobacterium tuberculosis* Metabolism, Biofilm Formation, and Sensitivity to Isoniazid In Vivo. *Antimicrob Agents Chemother* (2016) 60(11):6460–70. doi: 10.1128/AAC.01139-16
40. Dalebroux ZD, Svensson SL, Gaynor EC, Swanson MS. ppGpp Conjures Bacterial Virulence. *Microbiol Mol Biol Rev* (2010) 74(2):171–99. doi: 10.1128/MMBR.00046-09
41. Trastoy R, Manso T, Fernández-García L, Blasco L, Ambroa A, Pérez Del Molino ML, et al. Mechanisms of Bacterial Tolerance and Persistence in the Gastrointestinal and Respiratory Environments. *Clin Microbiol Rev* (2018) 31(4):e00023–18. doi: 10.1128/CMR.00023-18
42. Avarbock A, Avarbock D, Teh JS, Buckstein M, Wang ZM, Rubin H. Functional Regulation of the Opposing (p)ppGpp Synthetase/Hydrolase Activities of RelMtb From *Mycobacterium tuberculosis*. *Biochemistry* (2005) 44(29):9913–23. doi: 10.1021/bi0505316
43. Dutta NK, Klinkenberg LG, Vazquez MJ, Segura-Carro D, Colmenarejo G, Ramon F, et al. Inhibiting the Stringent Response Blocks *Mycobacterium tuberculosis* Entry Into Quiescence and Reduces Persistence. *Sci Adv* (2019) 5(3):eaav2104. doi: 10.1126/sciadv.aav2104
44. Singh R, Singh M, Arora G, Kumar S, Tiwari P, Kidwai S. Polyphosphate Deficiency in *Mycobacterium tuberculosis* Is Associated With Enhanced Drug Susceptibility and Impaired Growth in Guinea Pigs. *J Bacteriol* (2013) 195(12):2839–51. doi: 10.1128/JB.00038-13
45. Sharma V, Sharma S, Hoener Zu Bentrup K, McKinney JD, Russell DG, Jacobs WR, et al. Structure of Isocitrate Lyase, a Persistence Factor of *Mycobacterium tuberculosis*. *Nat Struct Biol* (2000) 7(8):663–8. doi: 10.1038/77964
46. Nandakumar M, Nathan C, Rhee KY. Isocitrate Lyase Mediates Broad Antibiotic Tolerance in *Mycobacterium tuberculosis*. *Nat Commun* (2014) 5:4306. doi: 10.1038/ncomms5306
47. Nguyen L. Antibiotic Resistance Mechanisms in *M. Tuberculosis*: An Update. *Arch Toxicol* (2016) 90(7):1585–604. doi: 10.1007/s00204-016-1727-6
48. Zhu JH, Wang BW, Pan M, Zeng YN, Rego H, Javid B. Rifampicin can Induce Antibiotic Tolerance in Mycobacteria Via Paradoxical Changes in Rpob Transcription. *Nat Commun* (2018) 9(1):4218. doi: 10.1038/s41467-018-06667-3
49. Hu Y, Mangan JA, Dhillon J, Sole KM, Mitchison DA, Butcher PD, et al. Detection of mRNA Transcripts and Active Transcription in Persistent *Mycobacterium tuberculosis* Induced by Exposure to Rifampin or Pyrazinamide. *J Bacteriol* (2000) 182(22):6358–65. doi: 10.1128/JB.182.22.6358-6365.2000
50. Javid B, Sorrentino F, Toosky M, Zheng W, Pinkham JT, Jain N, et al. Mycobacterial Mistranslation Is Necessary and Sufficient for Rifampicin Phenotypic Resistance. *Proc Natl Acad Sci USA* (2014) 111(3):1132–7. doi: 10.1073/pnas.1317580111
51. Kapoor N, Pawar S, Sirakova TD, Deb C, Warren WL, Kolattukudy PE. Human Granuloma In Vitro Model, for TB Dormancy and Resuscitation. *PloS One* (2013) 8(1):e53657. doi: 10.1371/journal.pone.0053657
52. Deb C, Lee CM, Dubey VS, Daniel J, Abomoelak B, Sirakova TD, et al. A Novel In Vitro Multiple-Stress Dormancy Model for *Mycobacterium tuberculosis* Generates a Lipid-Loaded, Drug-Tolerant, Dormant Pathogen. *PloS One* (2009) 4(6):e6077. doi: 10.1371/journal.pone.0006077
53. Santucci P, Johansen MD, Point V, Poncin I, Viljoen A, Cavalier JF, et al. Nitrogen Deprivation Induces Triacylglycerol Accumulation, Drug Tolerance and Hypervirulence in Mycobacteria. *Sci Rep* (2019) 9(1):8667. doi: 10.1038/s41598-019-45164-5
54. Baek SH, Li AH, Sassetti CM. Metabolic Regulation of Mycobacterial Growth and Antibiotic Sensitivity. *PloS Biol* (2011) 9(5):e1001065. doi: 10.1371/journal.pbio.1001065
55. Correia FF, D'Onofrio A, Rejtar T, Li L, Karger BL, Makarova K, et al. Kinase Activity of Overexpressed HipA Is Required for Growth Arrest and Multidrug Tolerance in *Escherichia coli*. *J Bacteriol* (2006) 188(24):8360–7. doi: 10.1128/JB.01237-06
56. Page R, Peti W. Toxin-Antitoxin Systems in Bacterial Growth Arrest and Persistence. *Nat Chem Biol* (2016) 12(4):208–14. doi: 10.1038/nchembio.2044
57. Wang X, Yao J, Sun YC, Wood TK. Type VII Toxin/Antitoxin Classification System for Antitoxins That Enzymatically Neutralize Toxins. *Trends Microbiol* (2020) 29(5):388–93. doi: 10.1016/j.tim.2020.12.001
58. Yu X, Gao X, Zhu K, Yin H, Mao X, Wojdyla JA, et al. Characterization of a Toxin-Antitoxin System in *Mycobacterium tuberculosis* Suggests Neutralization by Phosphorylation as the Antitoxicity Mechanism. *Commun Biol* (2020) 3(1):216. doi: 10.1038/s42003-020-0941-1
59. Torrey HL, Keren I, Via LE, Lee JS, Lewis K. High Persister Mutants in *Mycobacterium tuberculosis*. *PloS One* (2016) 11(5):e0155127. doi: 10.1371/journal.pone.0155127
60. Slayden RA, Dawson CC, Cummings JE. Toxin-Antitoxin Systems and Regulatory Mechanisms in *Mycobacterium tuberculosis*. *Pathog Dis* (2018) 76(4). doi: 10.1093/femspd/fty039
61. Hudock TA, Foreman TW, Bandyopadhyay N, Gautam US, Veatch AV, LoBato DN, et al. Hypoxia Sensing and Persistence Genes Are Expressed During the Intragranulomatous Survival of *Mycobacterium tuberculosis*. *Am J Respir Cell Mol Biol* (2017) 56(5):637–47. doi: 10.1165/rcmb.2016-0239OC
62. Sharma A, Chattopadhyay G, Chopra P, Bhasin M, Thakur C, Agarwal S, et al. VapC21 Toxin Contributes to Drug-Tolerance and Interacts With non-Cognate vapB32 Antitoxin in *Mycobacterium tuberculosis*. *Front Microbiol* (2020) 11:2037. doi: 10.3389/fmicb.2020.02037
63. Talwar S, Pandey M, Sharma C, Kutum R, Lum J, Carbajo D, et al. Role of vapBC12 Toxin-Antitoxin Locus in Cholesterol-Induced Mycobacterial Persistence. *mSystems* (2020) 5(6):e00855–20. doi: 10.1128/mSystems.00855-20
64. Podlesek Z, Zgur Bertok D. The DNA Damage Inducible Sos Response Is a Key Player in the Generation of Bacterial Persister Cells and Population Wide Tolerance. *Front Microbiol* (2020) 11:1785. doi: 10.3389/fmicb.2020.01785
65. Völzing KG, Brynildsen MP. Stationary-Phase Persisters to Ofloxacin Sustain DNA Damage and Require Repair Systems Only During Recovery. *mBio* (2015) 6(5):e00731–15. doi: 10.1128/mBio.00731-15
66. Mok WWK, Brynildsen MP. Timing of DNA Damage Responses Impacts Persistence to Fluoroquinolones. *Proc Natl Acad Sci USA* (2018) 115(27):E6301–9 doi: 10.1073/pnas.1804218115
67. Smollett KL, Smith KM, Kahramanoglou C, Arnvig KB, Buxton RS, Davis EO. Global Analysis of the Regulon of the Transcriptional Repressor LexA, a Key Component of SOS Response in *Mycobacterium tuberculosis*. *J Biol Chem* (2012) 287(26):22004–14. doi: 10.1074/jbc.M112.357715
68. Boshoff HIM, Reed MB, Barry CE, Mizrahi V. DnaE2 Polymerase Contributes to In Vivo Survival and the Emergence of Drug Resistance in *Mycobacterium tuberculosis*. *Cell* (2003) 113(2):183–93. doi: 10.1016/S0092-8674(03)00270-8
69. Choudhary E, Sharma R, Kumar Y, Agarwal N. Conditional Silencing by CRISPRi Reveals the Role of DNA Gyrase in Formation of Drug-Tolerant Persister Population in *Mycobacterium Tuberculosis*. *Front Cell Infect Microbiol* (2019) 9:70. doi: 10.3389/fcimb.2019.00070
70. Hall-Stoodley L, Costerton JW, Stoodley P. Bacterial Biofilms: From the Natural Environment to Infectious Diseases. *Nat Rev Microbiol* (2004) 2(2):95–108. doi: 10.1038/nrmicro821
71. Stewart PS, Costerton JW. Antibiotic Resistance of Bacteria in Biofilms. *Lancet* (2001) 358(9276):135–8. doi: 10.1016/S0140-6736(01)05321-1
72. Drenkard E, Ausubel FM. Pseudomonas Biofilm Formation and Antibiotic Resistance Are Linked to Phenotypic Variation. *Nature* (2002) 416(6882):740–3. doi: 10.1038/416740a
73. Hall CW, Mah TF. Molecular Mechanisms of Biofilm-Based Antibiotic Resistance and Tolerance in Pathogenic Bacteria. *FEMS Microbiol Rev* (2017) 41(3):276–301. doi: 10.1093/femsre/fux010
74. Yan J, Bassler BL. Surviving as a Community: Antibiotic Tolerance and Persistence in Bacterial Biofilms. *Cell Host Microbe* (2019) 26(1):15–21. doi: 10.1016/j.chom.2019.06.002
75. Esteban J, García-Coca M. Mycobacterium Biofilms. *Front Microbiol* (2018) 8:2651. doi: 10.3389/fmicb.2017.02651
76. Basaraba RJ, Ojha AK. Mycobacterial Biofilms: Revisiting Tuberculosis Bacilli in Extracellular Necrotizing Lesions. *Microbiol Spectr* (2017) 5(3):10.1128/microbiolspec.TBTB2-0024-2016. doi: 10.1128/microbiolspec.TBTB2-0024-2016

77. Ackart DF, Hascall-Dove L, Caceres SM, Kirk NM, Podell BK, Melander C, et al. Expression of Antimicrobial Drug Tolerance by Attached Communities of *Mycobacterium tuberculosis*. *Pathog Dis* (2014) 70(3):359–69. doi: 10.1111/2049-632X.12144
78. Trivedi A, Mavi PS, Bhatt D, Kumar A. Thiol Reductive Stress Induces Cellulose-Anchored Biofilm Formation in *Mycobacterium tuberculosis*. *Nat Commun* (2016) 7:11392. doi: 10.1038/ncomms11392
79. Richards JP, Cai W, Zill NA, Zhang W, Ojha AK. Adaptation of *Mycobacterium tuberculosis* to Biofilm Growth Is Genetically Linked to Drug Tolerance. *Antimicrob Agents Chemother* (2019) 63(11):e01213–19. doi: 10.1128/AAC.01213-19
80. Tripathi P, Singh LK, Kumari S, Hakiem OR, Batra JK. Clpb Is an Essential Stress Regulator of *Mycobacterium tuberculosis* and Endows Survival Advantage to Dormant Bacilli. *Int J Med Microbiol* (2020) 310(3):151402. doi: 10.1016/j.ijmm.2020.151402
81. Lee JJ, Lee SK, Song N, Nathan TO, Swarts BM, Eum SY, et al. Transient Drug-Tolerance and Permanent Drug-Resistance Rely on the Trehalose-Catalytic Shift in *Mycobacterium tuberculosis*. *Nat Commun* (2019) 10 (1):2928. doi: 10.1038/s41467-019-10975-7
82. Aminov RI. A Brief History of the Antibiotic Era: Lessons Learned and Challenges for the Future. *Front Microbiol* (2010) 1:134. doi: 10.3389/fmicb.2010.00134
83. Bode C, Diedrich B, Muenster S, Hentschel V, Weisheit C, Rommelsheim K, et al. Antibiotics Regulate the Immune Response in Both Presence and Absence of Lipopolysaccharide Through Modulation of Toll-Like Receptors, Cytokine Production and Phagocytosis In Vitro. *Int Immunopharmacol* (2014) 18(1):27–34. doi: 10.1016/j.intimp.2013.10.025
84. Benoun JM, Labuda JC, McSorley SJ. Collateral Damage: Detrimental Effect of Antibiotics on the Development of Protective Immune Memory. *mBio* (2016) 7(6):e01520–16. doi: 10.1128/mBio.01520-16
85. Berti A, Rose W, Nizet V, Sakoulas G. Antibiotics and Innate Immunity: A Cooperative Effort Toward the Successful Treatment of Infections. *Open Forum Infect Dis* (2020) 7(8):ofaa302. doi: 10.1093/ofid/ofaa302
86. Yang JH, Bhargava P, McCloskey D, Mao N, Palsson BO, Collins JJ. Antibiotic-Induced Changes to the Host Metabolic Environment Inhibit Drug Efficacy and Alter Immune Function. *Cell Host Microbe* (2017) 22 (6):757–65.e3. doi: 10.1016/j.chom.2017.10.020
87. Suzuki T, Yamamoto M. Molecular Basis of the Keap1-Nrf2 System. *Free Radical Biol Med* (2015) 88(Pt B):93–100. doi: 10.1016/j.freeradbiomed.2015.06.006
88. Sun Q, Shen X, Ma J, Lou H, Zhang Q. Activation of Nrf2 Signaling by Oltipraz Inhibits Death of Human Macrophages With *Mycobacterium tuberculosis* Infection. *Biochem Biophys Res Commun* (2020) 531(3):312–9. doi: 10.1016/j.bbrc.2020.07.026
89. Rothchild AC, Olson GS, Nemeth J, Amon LM, Mai D, Gold ES, et al. Alveolar Macrophages Generate a Noncanonical NRF2-driven Transcriptional Response to *Mycobacterium tuberculosis* In Vivo. *Sci Immunol* (2019) 4(37):eaaw6693. doi: 10.1126/sciimmunol.aaw6693
90. Menzel DB, Rasmussen RE, Lee E, Meacher DM, Said B, Hamadeh H, et al. Human Lymphocyte Home Oxygenase 1 as a Response Biomarker to Inorganic Arsenic. *Biochem Biophys Res Commun* (1998) 250(3):653–6. doi: 10.1006/bbrc.1998.9363
91. Chang SH, Barbosa-Tessmann I, Chen C, Kilberg MS, Agarwal A. Glucose Deprivation Induces Heme Oxygenase-1 Gene Expression by a Pathway Independent of the Unfolded Protein Response. *J Biol Chem* (2002) 277 (3):1933–40. doi: 10.1074/jbc.M108921200
92. Tsuchihashi S, Zhai Y, Fondevila C, Busuttil RW, Kupiec-Weglinski JW. HO-1 Upregulation Suppresses Type 1 IFN Pathway in Hepatic Ischemia/Reperfusion Injury. *Transplant Proc* (2005) 37(4):1677–8. doi: 10.1016/j.transproceed.2005.03.080
93. Wang L, Weng CY, Wang YJ, Wu MJ. Lipoic Acid Ameliorates Arsenic Trioxide-Induced HO-1 Expression and Oxidative Stress in THP-1 Monocytes and Macrophages. *Chem Biol Interact* (2011) 190(2–3):129–38. doi: 10.1016/j.cbi.2011.02.001
94. Neubauer JA, Sunderram J. Heme Oxygenase-1 and Chronic Hypoxia. *Respir Physiol Neurobiol* (2012) 184(2):178–85. doi: 10.1016/j.resp.2012.06.027
95. Andrade BB, Pavan Kumar N, Amaral EP, Riteau N, Mayer-Barber KD, Tosh KW, et al. Heme Oxygenase-1 Regulation of Matrix Metalloproteinase-1 Expression Underlies Distinct Disease Profiles in Tuberculosis. *J Immunol* (2015) 195(6):2763–73. doi: 10.4049/jimmunol.1500942
96. Willis D, Moore AR, Frederick R, Willoughby DA. Heme Oxygenase: A Novel Target for the Modulation of the Inflammatory Response. *Nat Med* (1996) 2(1):87–90. doi: 10.1038/nm0196-87
97. Kalghatgi S, Spina CS, Costello JC, Liesa M, Morones-Ramirez JR, Slomovic S, et al. Bactericidal Antibiotics Induce Mitochondrial Dysfunction and Oxidative Damage in Mammalian Cells. *Sci Trans Med* (2013) 5 (192):192ra85. doi: 10.1126/scitranslmed.3006055
98. Kohanski MA, Tharakan A, Lane AP, Ramanathan M. Bactericidal Antibiotics Promote Reactive Oxygen Species Formation and Inflammation in Human Sinonasal Epithelial Cells. *Int Forum Allergy Rhinol* (2016) 6(2):191–200. doi: 10.1002/alr.21646
99. Costa DL, Amaral EP, Namasivayam S, Mittereder LR, Fisher L, Bonfim CC, et al. Heme Oxygenase-1 Inhibition Promotes IFNγ- and NOS2-Mediated Control of *Mycobacterium tuberculosis* Infection. *Mucosal Immunol* (2021) 14(1):253–66. doi: 10.1038/s41385-020-00342-x
100. Rothhammer V, Quintana FJ. The Aryl Hydrocarbon Receptor: An Environmental Sensor Integrating Immune Responses in Health and Disease. *Nat Rev Immunol* (2019) 19(3):184–97. doi: 10.1038/s41577-019-0125-8
101. Moura-Alves P, Faé K, Houthuys E, Dorhoi A, Kreuchwig A, Furkert J, et al. AhR Sensing of Bacterial Pigments Regulates Antibacterial Defence. *Nature* (2014) 512(7515):387–92. doi: 10.1038/nature13684
102. Lamorte S, Shinde R, McGaha TL. Nuclear Receptors, the Aryl Hydrocarbon Receptor, and Macrophage Function. *Mol Aspects Med* (2021) 78:100942. doi: 10.1016/j.mam.2021.100942
103. Shinde R, Hezaveh K, Halaby MJ, Kloetgen A, Chakravarthy A, Da Silva Medina T, et al. Apoptotic Cell-Induced AhR Activity Is Required for Immunological Tolerance and Suppression of Systemic Lupus Erythematosus in Mice and Humans Article. *Nat Immunol* (2018) 19 (6):571–82. doi: 10.1038/s41590-018-0107-1
104. Puyskens A, Stinn A, van der Vaart M, Kreuchwig A, Protze J, Pei G, et al. Aryl Hydrocarbon Receptor Modulation by Tuberculosis Drugs Impairs Host Defense and Treatment Outcomes. *Cell Host Microbe* (2020) 27 (2):238–48.e7. doi: 10.1016/j.chom.2019.12.005
105. Memari B, Bouttier M, Dimitrov V, Ouellette M, Behr MA, Fritz JH, et al. Engagement of the Aryl Hydrocarbon Receptor in *Mycobacterium tuberculosis* –Infected Macrophages Has Pleiotropic Effects on Innate Immune Signaling. *J Immunol* (2015) 195(9):4479–91. doi: 10.4049/jimmunol.1501141
106. Mourik BC, Lubberts E, de Steenwinkel JEM, Ottenhoff THM, Leenen PJM. Interactions Between Type 1 Interferons and the Th17 Response in Tuberculosis: Lessons Learned From Autoimmune Diseases. *Front Immunol* (2017) 8:294. doi: 10.3389/fimmu.2017.00294
107. Willing BP, Russell SL, Finlay BB. Shifting the Balance: Antibiotic Effects on Host-Microbiota Mutualism. *Nat Rev Microbiol* (2011) 9(4):233–43. doi: 10.1038/nrmicro2536
108. Ubeda C, Pamer EG. Antibiotics, Microbiota, and Immune Defense. *Trends Immunol* (2012) 33(9):459–66. doi: 10.1016/j.it.2012.05.003
109. Lee EH, Baek SY, Park JY, Kim YW. Rifampicin Activates AMPK and Alleviates Oxidative Stress in the Liver as Mediated With Nrf2 Signaling. *Chem Biol Interact* (2020) 315:108889. doi: 10.1016/j.cbi.2019.108889
110. Tousif S, Singh DK, Ahmad S, Moodley P, Bhattacharyya M, Van Kaer L, et al. Isoniazid Induces Apoptosis of Activated CD4+ T Cells: Implications for Post-Therapy Tuberculosis Reactivation and Reinfection. *J Biol Chem* (2014) 289(44):30190–5. doi: 10.1074/jbc.C114.598946
111. Biraro IA, Egesa M, Kimuda S, Smith SG, Toulza F, Levin J, et al. Effect of Isoniazid Preventive Therapy on Immune Responses to *Mycobacterium tuberculosis*: An Open Label Randomised, Controlled, Exploratory Study. *BMC Infect Dis* (2015) 15(1):438. doi: 10.1186/s12879-015-1201-8
112. Nilsson BS. Rifampicin: An Immunosuppressant? *Lancet* (1971) 298 (7720):374. doi: 10.1016/S0140-6736(71)90087-0
113. Gupta S, Grieco MH, Siegel I. Suppression of T Lymphocyte Rosettes by Rifampin. Studies in Normals and Patients With Tuberculosis. *Ann Internal Med* (1975) 82(4):484–8. doi: 10.7326/0003-4819-82-4-484
114. Mlambo G, Sigola LB. Rifampicin and Dexamethasone Have Similar Effects on Macrophage Phagocytosis of Zymosan, But Differ in Their Effects on

Nitrite and TNF-α Production. *Int Immunopharmacol* (2003) 3(4):513–22. doi: 10.1016/S1567-5769(03)00022-5
115. Ziglam HM, Daniels I, Finch RG. Immunomodulating Activity of Rifampicin. *J Chemother* (2004) 16(4):357–61. doi: 10.1179/joc.2004.16.4.357
116. Bi W, Zhu L, Wang C, Liang Y, Liu J, Shi Q, et al. Rifampicin Inhibits Microglial Inflammation and Improves Neuron Survival Against Inflammation. *Brain Res* (2011) 1395:12–20. doi: 10.1016/j.brainres.2011.04.019
117. Manca C, Koo MS, Peixoto B, Fallows D, Kaplan G, Subbian S. Host Targeted Activity of Pyrazinamide in *Mycobacterium tuberculosis* Infection. *PloS One* (2013) 8(8):e74082. doi: 10.1371/journal.pone.0074082
118. Koul A, Dendouga N, Vergauwen K, Molenberghs B, Vranckx L, Willebrords R, et al. Diarylquinolines Target Subunit C of Mycobacterial ATP Synthase. *Nat Chem Biol* (2007) 3(6):323–4. doi: 10.1038/nchembio884
119. Andries K, Verhasselt P, Guillemont J, Göhlmann HWH, Neefs JM, Winkler H, et al. A Diarylquinoline Drug Active on the ATP Synthase of *Mycobacterium tuberculosis*. *Science* (2005) 307(5707):223–7. doi: 10.1126/science.1106753
120. Giraud-Gatineau A, Coya JM, Maure A, Biton A, Thomson M, Bernard EM, et al. The Antibiotic Bedaquiline Activates Host Macrophage Innate Immune Resistance to Bacterial Infection. *eLife* (2020) 9:e55692. doi: 10.7554/eLife.55692
121. Cholo MC, Steel HC, Fourie PB, Germishuizen WA, Anderson R. Clofazimine: Current Status and Future Prospects. *J Antimicrob Chemother* (2012) 67(*2*):290–8. doi: 10.1093/jac/dkr444
122. Yoon GS, Sud S, Keswani RK, Baik J, Standiford TJ, Stringer KA, et al. Phagocytosed Clofazimine Biocrystals can Modulate Innate Immune Signaling by Inhibiting TNF-α and Boosting IL-1RA Secretion. *Mol Pharm* (2015) 12(7):2517–27. doi: 10.1021/acs.molpharmaceut.5b00035
123. Fukutomi Y, Maeda Y, Makino M. Apoptosis-Inducing Activity of Clofazimine in Macrophages. *Antimicrob Agents Chemother* (2011) 55(9):4000–5. doi: 10.1128/AAC.00434-11
124. Ahmad S, Bhattacharya D, Gupta N, Rawat V, Tousif S, van Kaer L, et al. Clofazimine Enhances the Efficacy of BCG Revaccination Via Stem Cell-Like Memory T Cells. *PloS Pathog* (2020) 16(5):e1008356. doi: 10.1371/journal.ppat.1008356
125. Yang TW, Park HO, Jang HN, Yang JH, Kim SH, Moon SH, et al. Side Effects Associated With the Treatment of Multidrug-Resistant Tuberculosis at a Tuberculosis Referral Hospital in South Korea. *Medicine (United States)* (2017) 96(28):e7482. doi: 10.1097/MD.0000000000007482
126. Yee D, Valiquette C, Pelletier M, Parisien I, Rocher I, Menzies D. Incidence of Serious Side Effects From First-Line Antituberculosis Drugs Among Patients Treated for Active Tuberculosis. *Am J Respir Crit Care Med* (2003) 167(11):1472–7. doi: 10.1164/rccm.200206-626OC
127. Kilinç G, Saris A, Ottenhoff THM, Haks MC. Host-Directed Therapy to Combat Mycobacterial Infections*. *Immunol Rev* (2021) 301(1):62–83. doi: 10.1111/imr.12951
128. Oh S, Trifonov L, Yadav VD, Barry CE, Boshoff HI. Tuberculosis Drug Discovery: A Decade of Hit Assessment for Defined Targets. *Front Cell Infect Microbiol* (2021) 11:611304. doi: 10.3389/fcimb.2021.611304
129. Jagannath C, Lindsey DR, Dhandayuthapani S, Xu Y, Hunter RL, Eissa NT. Autophagy Enhances the Efficacy of BCG Vaccine by Increasing Peptide Presentation in Mouse Dendritic Cells. *Nat Med* (2009) 15(3):267–76. doi: 10.1038/nm.1928
130. Gupta A, Pant G, Mitra K, Madan J, Chourasia MK, Misra A. Inhalable Particles Containing Rapamycin for Induction of Autophagy in Macrophages Infected With *Mycobacterium tuberculosis*. *Mol Pharm* (2014) 11(4):1201–7. doi: 10.1021/mp4006563
131. Gupta A, Sharma D, Meena J, Pandya S, Sachan M, Kumar S, et al. Preparation and Preclinical Evaluation of Inhalable Particles Containing Rapamycin and Anti-Tuberculosis Agents for Induction of Autophagy. *Pharm Res* (2016) 33(8):1899–912. doi: 10.1007/s11095-016-1926-0
132. Singhal A, Jie L, Kumar P, Hong GS, Leow MKS, Paleja B, et al. Metformin as Adjunct Antituberculosis Therapy. *Sci Trans Med* (2014) 6(263):263ra159. doi: 10.1126/scitranslmed.3009885
133. Degner NR, Wang JY, Golub JE, Karakousis PC. Metformin Use Reverses the Increased Mortality Associated With Diabetes Mellitus During Tuberculosis Treatment. *Clin Infect Dis* (2018) 66(2):198–205. doi: 10.1093/cid/cix819
134. Lachmandas E, Eckold C, Böhme J, Koeken VACM, Marzuki MB, Blok B, et al. Metformin Alters Human Host Responses to *Mycobacterium tuberculosis* in Healthy Subjects. *J Infect Dis* (2019) 220(1):139–50. doi: 10.1093/infdis/jiz064
135. Frenkel JDH, Ackart DF, Todd AK, DiLisio JE, Hoffman S, Tanner S, et al. Metformin Enhances Protection in Guinea Pigs Chronically Infected With *Mycobacterium tuberculosis*. *Sci Rep* (2020) 10(1):16257. doi: 10.1038/s41598-020-73212-y
136. Parihar SP, Guler R, Khutlang R, Lang DM, Hurdayal R, Mhlanga MM, et al. Statin Therapy Reduces the *Mycobacterium tuberculosis* Burden in Human Macrophages and in Mice by Enhancing Autophagy and Phagosome Maturation. *J Infect Dis* (2014) 209(5):754–63. doi: 10.1093/infdis/jit550
137. Skerry C, Pinn ML, Bruiners N, Pine R, Gennaro ML, Karakousis PC. Simvastatin Increases the In Vivo Activity of the First-Line Tuberculosis Regimen. *J Antimicrob Chemother* (2014) 69(9):2453–7. doi: 10.1093/jac/dku166
138. Dutta NK, Bruiners N, Pinn ML, Zimmerman MD, Prideaux B, Dartois V, et al. Statin Adjunctive Therapy Shortens the Duration of TB Treatment in Mice. *J Antimicrob Chemother* (2016) 71(6):1570–7. doi: 10.1093/jac/dkw014
139. Guerra-De-Blas PDC, Bobadilla-Del-Valle M, Sada-Ovalle I, Estrada-García I, Torres-González P, López-Saavedra A, et al. Simvastatin Enhances the Immune Response Against *Mycobacterium tuberculosis*. *Front Microbiol* (2019) 10:2097. doi: 10.3389/fmicb.2019.02097
140. Dutta NK, Bruiners N, Zimmerman MD, Tan S, Dartois V, Gennaro ML, et al. Adjunctive Host-Directed Therapy With Statins Improves Tuberculosis-Related Outcomes in Mice. *J Infect Dis* (2020) 221(7):1079–87. doi: 10.1093/infdis/jiz517
141. Baniasadi S, Eftekhari P, Tabarsi P, Fahimi F, Raoufy MR, Masjedi MR, et al. Protective Effect of N-Acetylcysteine on Antituberculosis Drug-Induced Hepatotoxicity. *Eur J Gastroenterol Hepatol* (2010) 22(10):1235–8. doi: 10.1097/MEG.0b013e32833aa11b
142. Palanisamy GS, Kirk NM, Ackart DF, Shanley CA, Orme IM, Basaraba RJ. Evidence for Oxidative Stress and Defective Antioxidant Response in Guinea Pigs With Tuberculosis. *PloS One* (2011) 6(10):e26254. doi: 10.1371/journal.pone.0026254
143. Amaral EP, Conceição EL, Costa DL, Rocha MS, Marinho JM, Cordeiro-Santos M, et al. N-Acetyl-Cysteine Exhibits Potent Anti-Mycobacterial Activity in Addition to Its Known Anti-Oxidative Functions. *BMC Microbiol* (2016) 16(1):251. doi: 10.1186/s12866-016-0872-7
144. Mahakalkar S, Nagrale D, Gaur S, Urade C, Murhar B, Turankar A. N-Acetylcysteine as an Add-on to Directly Observed Therapy Short-I Therapy in Fresh Pulmonary Tuberculosis Patients: A Randomized, Placebo-Controlled, Double-Blinded Study. *Perspect Clin Res* (2017) 8(3):132–6. doi: 10.4103/2229-3485.210450
145. Teskey G, Cao R, Islamoglu H, Medina A, Prasad C, Prasad R, et al. The Synergistic Effects of the Glutathione Precursor, NAC and First-Line Antibiotics in the Granulomatous Response Against *Mycobacterium tuberculosis*. *Front Immunol* (2018) 9:2069. doi: 10.3389/fimmu.2018.02069
146. Cao R, Teskey G, Islamoglu H, Abrahem R, Munjal S, Gyurjian K, et al. Characterizing the Effects of Glutathione as an Immunoadjuvant in the Treatment of Tuberculosis. *Antimicrob Agents Chemother* (2018) 62(11):e01132–18. doi: 10.1128/AAC.01132-18
147. Safe IP, Lacerda MVG, Printes VS, Marins AFP, Rabelo ALR, Costa AA, et al. Safety and Efficacy of N-Acetylcysteine in Hospitalized Patients With HIV-Associated Tuberculosis: An Open-Label, Randomized, Phase II Trial (RIPENACTB Study). *PloS One* (2020) 15(6):e0235381. doi: 10.1371/journal.pone.0235381
148. Vilchèze C, Jacobs WR. The Promises and Limitations of N-acetylcysteine as a Potentiator of First-Line and Second-Line Tuberculosis Drugs. *Antimicrob Agents Chemother* (2021) 65(5):e01703–20. doi: 10.1128/AAC.01703-20
149. Gupta S, Tyagi S, Almeida DV, Maiga MC, Ammerman NC, Bishai WR. Acceleration of Tuberculosis Treatment by Adjunctive Therapy With Verapamil as an Efflux Inhibitor. *Am J Respir Crit Care Med* (2013) 188(5):600–7. doi: 10.1164/rccm.201304-0650OC
150. Pieterman ED, te Brake LHM, de Knegt GJ, van der Meijden A, Alffenaar JWC, Bax HI, et al. Assessment of the Additional Value of Verapamil to a

Moxifloxacin and Linezolid Combination Regimen in a Murine Tuberculosis Model. *Antimicrob Agents Chemother* (2018) 62(9):e01354–18. doi: 10.1128/AAC.01354-18
151. Chen C, Gardete S, Jansen RS, Shetty A, Dick T, Rhee KY, et al. Verapamil Targets Membrane Energetics in *Mycobacterium tuberculosis*. *Antimicrob Agents Chemother* (2018) 62(5):e02107–17. doi: 10.1128/AAC.02107-17
152. Xu J, Tasneen R, Peloquin CA, Almeida DV, Li SY, Barnes-Boyle K, et al. Verapamil Increases the Bioavailability and Efficacy of Bedaquiline But Not Clofazimine in a Murine Model of Tuberculosis. *Antimicrob Agents Chemother* (2018) 62(1):e01692–17. doi: 10.1128/AAC.01692-17
153. Levine B, Mizushima N, Virgin HW. Autophagy in Immunity and Inflammation. *Nature* (2011) 469(7330):323–35. doi: 10.1038/nature09782
154. Jiang P, Mizushima N. Autophagy and Human Diseases. *Cell Res* (2014) 24(1):69–79. doi: 10.1038/cr.2013.161
155. Gutierrez MG, Master SS, Singh SB, Taylor GA, Colombo MI, Deretic V. Autophagy Is a Defense Mechanism Inhibiting BCG and *Mycobacterium tuberculosis* Survival in Infected Macrophages. *Cell* (2004) 119(6):753–66. doi: 10.1016/j.cell.2004.11.038
156. Manzanillo PS, Ayres JS, Watson RO, Collins AC, Souza G, Rae CS, et al. The Ubiquitin Ligase Parkin Mediates Resistance to Intracellular Pathogens. *Nature* (2013) 501(7468):512–6. doi: 10.1038/nature12566
157. Kim YS, Silwal P, Kim SY, Yoshimori T, Jo EK. Autophagy-Activating Strategies to Promote Innate Defense Against Mycobacteria. *Exp Mol Med* (2019) 51(12):1–10. doi: 10.1038/s12276-019-0290-7
158. Saunders RN, Metcalfe MS, Nicholson ML. Rapamycin in Transplantation: A Review of the Evidence. *Kidney Int* (2001) 59(1):3–16. doi: 10.1046/j.1523-1755.2001.00460.x
159. Dumont FJ, Su Q. Mechanism of Action of the Immunosuppressant Rapamycin. *Life Sci* (1995) 58(5):373–95. doi: 10.1016/0024-3205(95)02233-3
160. Zullo AJ, Jurcic Smith KL, Lee S. Mammalian Target of Rapamycin Inhibition and Mycobacterial Survival Are Uncoupled in Murine Macrophages. *BMC Biochem* (2014) 15(1):4. doi: 10.1186/1471-2091-15-4
161. Andersson AM, Andersson B, Lorell C, Raffetseder J, Larsson M, Blomgran R. Autophagy Induction Targeting mTORC1 Enhances *Mycobacterium tuberculosis* Replication in HIV Co-Infected Human Macrophages. *Sci Rep* (2016) 6:28171. doi: 10.1038/srep28171
162. Son HJ, Lee J, Lee SY, Kim EK, Park MJ, Kim KW, et al. Metformin Attenuates Experimental Autoimmune Arthritis Through Reciprocal Regulation of Th17/Treg Balance and Osteoclastogenesis. *Mediators Inflamm* (2014) 2014:973986. doi: 10.1155/2014/973986
163. Kang KY, Kim YK, Yi H, Kim J, Jung HR, Kim IJ, et al. Metformin Downregulates Th17 Cells Differentiation and Attenuates Murine Autoimmune Arthritis. *Int Immunopharmacol* (2013) 16(1):85–92. doi: 10.1016/j.intimp.2013.03.020
164. Titov AA, Baker HV, Brusko TM, Sobel ES, Morel L. Metformin Inhibits the Type 1 IFN Response in Human $CD4^+$ T Cells. *J Immunol* (2019) 203 (2):338–48. doi: 10.4049/jimmunol.1801651
165. Saenwongsa W, Nithichanon A, Chittaganpitch M, Buayai K, Kewcharoenwong C, Thumrongwilainet B, et al. Metformin-Induced Suppression of IFN-α Via mTORC1 Signalling Following Seasonal Vaccination Is Associated With Impaired Antibody Responses in Type 2 Diabetes. *Sci Rep* (2020) 10(1):3229. doi: 10.1038/s41598-020-60213-0
166. Dutta NK, Pinn ML, Karakousis PC. Metformin Adjunctive Therapy Does Not Improve the Sterilizing Activity of the First-Line Antitubercular Regimen in Mice. *Antimicrob Agents Chemother* (2017) 61(8):e00652–17. doi: 10.1128/AAC.00652-17
167. Hedrich WD, Hassan HE, Wang H. Insights Into CYP2B6-Mediated Drug-Drug Interactions. *Acta Pharm Sin B* (2016) 6(5):413–25. doi: 10.1016/j.apsb.2016.07.016
168. Hardie DG. AMP-Activated Protein Kinase as a Drug Target. *Annu Rev Pharmacol Toxicol* (2007) 47:185–200. doi: 10.1146/annurev.pharmtox.47.120505.105304
169. Zhou G, Myers R, Li Y, Chen Y, Shen X, Fenyk-Melody J, et al. Role of AMP-Activated Protein Kinase in Mechanism of Metformin Action. *J Clin Invest* (2001) 108(8):1167–74. doi: 10.1172/JCI13505
170. Oesterle A, Laufs U, Liao JK. Pleiotropic Effects of Statins on the Cardiovascular System. *Circ Res* (2017) 120(1):229–43. doi: 10.1161/CIRCRESAHA.116.308537
171. Lee W, VanderVen BC, Fahey RJ, Russell DG. Intracellular *Mycobacterium tuberculosis* Exploits Host-Derived Fatty Acids to Limit Metabolic Stress. *J Biol Chem* (2013) 288(10):6788–800. doi: 10.1074/jbc.M112.445056
172. Tahir F, Bin Arif T, Ahmed J, Shah SR, Khalid M. Anti-Tuberculous Effects of Statin Therapy: A Review of Literature. *Cureus* (2020)12(3):e7404. doi: 10.7759/cureus.7404
173. Liao KF, Lin CL, Lai SW. Population-Based Case-Control Study Assessing the Association Between Statins Use and Pulmonary Tuberculosis in Taiwan. *Front Pharmacol* (2017) 8:597. doi: 10.3389/fphar.2017.00597
174. Su VYF, Su WJ, Yen YF, Pan SW, Chuang PH, Feng JY, et al. Statin Use Is Associated With a Lower Risk of TB. *Chest* (2017) 152(3):598–606. doi: 10.1016/j.chest.2017.04.170
175. Lobato LS, Rosa PS, Da Silva Ferreira J, Da Silva Neumann A, Da Silva MG, Nascimento DC, et al. Statins Increase Rifampin Mycobactericidal Effect. *Antimicrob Agents Chemother* (2014) 58(10):5766–74. doi: 10.1128/AAC.01826-13
176. Vatansever F, de Melo WCMA, Avci P, Vecchio D, Sadasivam M, Gupta A, et al. Antimicrobial Strategies Centered Around Reactive Oxygen Species - Bactericidal Antibiotics, Photodynamic Therapy, and Beyond. *FEMS Microbiol Rev* (2013) 37(6):955–89. doi: 10.1111/1574-6976.12026
177. Forrester SJ, Kikuchi DS, Hernandes MS, Xu Q, Griendling KK. Reactive Oxygen Species in Metabolic and Inflammatory Signaling. *Circ Res* (2018) 122(6):877–902. doi: 10.1161/CIRCRESAHA.117.311401
178. Vilchèze C, Hartman T, Weinrick B, Jain P, Weisbrod TR, Leung LW, et al. Enhanced Respiration Prevents Drug Tolerance and Drug Resistance in *Mycobacterium tuberculosis*. *Proc Natl Acad Sci USA* (2017) 114(17):4495–500. doi: 10.1073/pnas.1704376114
179. Lamprecht DA, Finin PM, Rahman MA, Cumming BM, Russell SL, Jonnala SR, et al. Turning the Respiratory Flexibility of *Mycobacterium tuberculosis* Against Itself. *Nat Commun* (2016) 7:12393. doi: 10.1038/ncomms12393
180. Guerra C, Morris D, Sipin A, Kung S, Franklin M, Gray D, et al. Glutathione and Adaptive Immune Responses Against *Mycobacterium tuberculosis* Infection in Healthy and HIV Infected Individuals. *PloS One* (2011) 6(12): e28378. doi: 10.1371/journal.pone.0028378
181. Venketaraman V, Millman A, Salman M, Swaminathan S, Goetz M, Lardizabal A, et al. Glutathione Levels and Immune Responses in Tuberculosis Patients. *Microb Pathog* (2008) 44(3):255–61. doi: 10.1016/j.micpath.2007.09.002
182. Khameneh B, Fazly Bazzaz BS, Amani A, Rostami J, Vahdati-Mashhadian N. Combination of Anti-Tuberculosis Drugs With Vitamin C or NAC Against Different *Staphylococcus Aureus* and *Mycobacterium tuberculosis* Strains. *Microb Pathog* (2016) 93:83–7. doi: 10.1016/j.micpath.2015.11.006
183. Ejigu DA, Abay SM. N-Acetyl Cysteine as an Adjunct in the Treatment of Tuberculosis. *Tuberc Res Treat* (2020) 2020:5907839. doi: 10.1155/2020/5907839
184. Vural A, Koçyiğit İ, Şan F, Eroğlu E, Ketenci İ, Ünal A, et al. Long-Term Protective Effect of N-Acetylcysteine Against Amikacin-Induced Ototoxicity in End-Stage Renal Disease: A Randomized Trial. *Perit Dialysis Int* (2018) 38 (1):57–62. doi: 10.3747/pdi.2017.00133
185. Kocyigit I, Vural A, Unal A, Sipahioglu MH, Yucel HE, Aydemir S, et al. Preventing Amikacin Related Ototoxicity With N-Acetylcysteine in Patients Undergoing Peritoneal Dialysis. *Eur Arch Otorhinolaryngol* (2015) 272 (10):2611–20. doi: 10.1007/s00405-014-3207-z
186. Carr AC, Maggini S. Vitamin C and Immune Function. *Nutrients* (2017) 9 (11):1211. doi: 10.3390/nu9111211
187. Vilchèze C, Hartman T, Weinrick B, Jacobs WR. *Mycobacterium tuberculosis* Is Extraordinarily Sensitive to Killing by a Vitamin C-induced Fenton Reaction. *Nat Commun* (2013) 4:1881. doi: 10.1038/ncomms2898
188. Sikri K, Duggal P, Kumar C, Batra SD, Vashist A, Bhaskar A, et al. Multifaceted Remodeling by Vitamin C Boosts Sensitivity of *Mycobacterium tuberculosis* Subpopulations to Combination Treatment by Anti-Tubercular Drugs. *Redox Biol* (2018) 15:452–66. doi: 10.1016/j.redox.2017.12.020
189. Susanto L, Siregar Y, Kusumawati L. Vitamin C Supplementation Improve the Sputum Conversion Culture Rate in Pulmonary Tuberculosis Treatment While Rifampicin Susceptible. *Iop Conf Ser: Earth Environ Sci* (2018) 125:012140. doi: 10.1088/1755-1315/125/1/012140

190. Vilchèze C, Kim J, Jacobs WR. Vitamin C Potentiates the Killing of *Mycobacterium tuberculosis* by the First-Line Tuberculosis Drugs Isoniazid and Rifampin in Mice. *Antimicrob Agents Chemother* (2018) 62(3):e02165–17. doi: 10.1128/AAC.02165-17
191. Nandi M, Sikri K, Chaudhary N, Mande SC, Sharma RD, Tyagi JS. Multiple Transcription Factors Co-Regulate the *Mycobacterium tuberculosis* Adaptation Response to Vitamin C. *BMC Genomics* (2019) 20(1):887. doi: 10.1186/s12864-019-6190-3
192. Costa DL, Namasivayam S, Amaral EP, Arora K, Chao A, Mittereder LR, et al. Pharmacological Inhibition of Host Heme Oxygenase-1 Suppresses *Mycobacterium tuberculosis* Infection In Vivo by a Mechanism Dependent on T Lymphocytes. *mBio* (2016) 7(5):e01675–16. doi: 10.1128/mBio.01675-16
193. Rockwood N, Costa DL, Amaral EP, du Bruyn E, Kubler A, Gil-Santana L, et al. *Mycobacterium tuberculosis* Induction of Heme Oxygenase-1 Expression Is Dependent on Oxidative Stress and Reflects Treatment Outcomes. *Front Immunol* (2017) 8:542. doi: 10.3389/fimmu.2017.00542
194. Chinta KC, Rahman MA, Saini V, Glasgow JN, Reddy VP, Lever JM, et al. Microanatomic Distribution of Myeloid Heme Oxygenase-1 Protects Against Free Radical-Mediated Immunopathology in Human Tuberculosis. *Cell Rep* (2018) 25(7):1938–52.e5. doi: 10.1016/j.celrep.2018.10.073
195. Chinta KC, Pacl HT, Agarwal A, Steyn AJC. Heme Oxygenase-1 as a Pharmacological Target for Host-Directed Therapy to Limit Tuberculosis Associated Immunopathology. *Antioxidants* (2021) 10(2):177. doi: 10.3390/antiox10020177
196. Canesin G, Hejazi SM, Swanson KD, Wegiel B. Heme-Derived Metabolic Signals Dictate Immune Responses. *Front Immunol* (2020) 11:66. doi: 10.3389/fimmu.2020.00066
197. Machado D, Couto I, Perdigão J, Rodrigues L, Portugal I, Baptista P, et al. Contribution of Efflux to the Emergence of Isoniazid and Multidrug Resistance in *Mycobacterium tuberculosis*. *PloS One* (2012) 7(4):e34538. doi: 10.1371/journal.pone.0034538
198. Gupta S, Cohen KA, Winglee K, Maiga M, Diarra B, Bishai WR. Efflux Inhibition With Verapamil Potentiates Bedaquiline in *Mycobacterium tuberculosis*. *Antimicrob Agents Chemother* (2014) 58(1):574–6. doi: 10.1128/AAC.01462-13
199. Li G, Zhang J, Guo Q, Wei J, Jiang Y, Zhao X, et al. Study of Efflux Pump Gene Expression in Rifampicin-Monoresistant *Mycobacterium tuberculosis* Clinical Isolates. *J Antibiot* (2015) 68(7):431–5. doi: 10.1038/ja.2015.9
200. Domingo-Gonzalez R, Prince O, Cooper A, Khader SA. Cytokines and Chemokines in *Mycobacterium tuberculosis* Infection. *Microbiol Spectr* (2016) 4(5):10.1128/microbiolspec.TBTB2-0018-2016. doi: 10.1128/microbiolspec.TBTB2-0018-2016
201. Verver S, Warren RM, Beyers N, Richardson M, van der Spuy GD, Borgdorff MW, et al. Rate of Reinfection Tuberculosis After Successful Treatment Is Higher Than Rate of New Tuberculosis. *Am J Respir Crit Care Med* (2005) 171(12):1430–5. doi: 10.1164/rccm.200409-1200OC
202. Francisco-Cruz A, Mata-Espinosa D, Ramos-Espinosa O, Marquina-Castillo B, Estrada-Parra S, Xing Z, et al. Efficacy of Gene-Therapy Based on Adenovirus Encoding Granulocyte-Macrophage Colony-Stimulating Factor in Drug-Sensitive and Drug-Resistant Experimental Pulmonary Tuberculosis. *Tuberculosis* (2016) 100:5–14. doi: 10.1016/j.tube.2016.05.015
203. Francisco-Cruz A, Mata-Espinosa D, Estrada-Parra S, Xing Z, Hernández-Pando R. Immunotherapeutic Effects of Recombinant Adenovirus Encoding Granulocyte-Macrophage Colony-Stimulating Factor in Experimental Pulmonary Tuberculosis. *Clin Exp Immunol* (2013) 171(3):283–97. doi: 10.1111/cei.12015
204. Pasula R, Azad AK, Gardner JC, Schlesinger LS, McCormack FX. Keratinocyte Growth Factor Administration Attenuates Murine Pulmonary *Mycobacterium tuberculosis* Infection Through Granulocyte-Macrophage Colony-Stimulating Factor (GM-CSF)-Dependent Macrophage Activation and Phagolysosome Fusion. *J Biol Chem* (2015) 290(11):7151–9. doi: 10.1074/jbc.M114.591891
205. Benmerzoug S, Marinho FV, Rose S, Mackowiak C, Gosset D, Sedda D, et al. GM-CSF Targeted Immunomodulation Affects Host Response to M. Tuberculosis Infection. *Sci Rep* (2018) 8(1):8652. doi: 10.1038/s41598-018-26984-3
206. Moreira-Teixeira L, Stimpson PJ, Stavropoulos E, Hadebe S, Chakravarty P, Ioannou M, et al. Type I IFN Exacerbates Disease in Tuberculosis-Susceptible Mice by Inducing Neutrophil-Mediated Lung Inflammation and Netosis. *Nat Commun* (2020) 11(1):5566. doi: 10.1038/s41467-020-19412-6
207. Dawson R, Condos R, Tse D, Huie ML, Ress S, Tseng CH, et al. Immunomodulation With Recombinant Interferon-γ1b in Pulmonary Tuberculosis. *PloS One* (2009) 4(9):e6984. doi: 10.1371/journal.pone.0006984
208. Mata-Espinosa DA, Mendoza-Rodríguez V, Aguilar-León D, Rosales R, López-Casillas F, Hernández-Pando R. Therapeutic Effect of Recombinant Adenovirus Encoding Interferon-γ in a Murine Model of Progressive Pulmonary Tuberculosis. *Mol Ther* (2008) 16(6):1065–72. doi: 10.1038/mt.2008.69
209. Khan TA, Mazhar H, Saleha S, Tipu HN, Muhammad N, Abbas MN. Interferon-Gamma Improves Macrophages Function Against *M. Tuberculosis* in Multidrug-Resistant Tuberculosis Patients. *Chemother Res Pract* (2016) 2016:7295390. doi: 10.1155/2016/7295390
210. Antonelli LRV, Rothfuchs AG, Gonçalves R, Roffê E, Cheever AW, Bafica A, et al. Intranasal poly-IC Treatment Exacerbates Tuberculosis in Mice Through the Pulmonary Recruitment of a Pathogen-Permissive Monocyte/Macrophage Population. *J Clin Invest* (2010) 120(5):1674–82. doi: 10.1172/JCI40817
211. Moreira-Teixeira L, Sousa J, McNab FW, Torrado E, Cardoso F, Machado H, et al. Type I IFN Inhibits Alternative Macrophage Activation During *Mycobacterium tuberculosis* Infection and Leads to Enhanced Protection in the Absence of IFN-γ Signaling. *J Immunol* (2016) 197(12):4714–26. doi: 10.4049/jimmunol.1600584
212. Zhang L, Jiang X, Pfau D, Ling Y, Nathan CF. Type I Interferon Signaling Mediates *Mycobacterium tuberculosis*–Induced Macrophage Death. *J Exp Med* (2021) 218(2):e20200887. doi: 10.1084/jem.20200887
213. Mayer-Barber KD, Andrade BB, Oland SD, Amaral EP, Barber DL, Gonzales J, et al. Host-Directed Therapy of Tuberculosis Based on Interleukin-1 and Type I Interferon Crosstalk. *Nature* (2014) 511(7507):99–103. doi: 10.1038/nature13489
214. Arbués A, Brees D, Chibout SD, Fox T, Kammüller M, Portevin D. TNF-α Antagonists Differentially Induce TGFβ1-Dependent Resuscitation of Dormant-Like *Mycobacterium tuberculosis*. *PloS Pathog* (2020) 16(2):e1008312. doi: 10.1371/journal.ppat.1008312
215. Tezera LB, Bielecka MK, Ogongo P, Walker NF, Ellis M, Garay-Baquero DJ, et al. Anti-PD-1 Immunotherapy Leads to Tuberculosis Reactivation Via Dysregulation of TNF-α. *eLife* (2020) 9:e52668. doi: 10.7554/eLife.52668
216. Wu B, Huang C, Kato-Maeda M, Hopewell PC, Daley CL, Krensky AM, et al. IL-24 Modulates IFN-γ Expression in Patients With Tuberculosis. *Immunol Lett* (2008) 117(1):57–62. doi: 10.1016/j.imlet.2007.11.018
217. Ramos-Espinosa O, Hernández-Bazán S, Francisco-Cruz A, Mata-Espinosa D, Barrios-Payán J, Marquina-Castillo B, et al. Gene Therapy Based in Antimicrobial Peptides and Proinflammatory Cytokine Prevents Reactivation of Experimental Latent Tuberculosis. *Pathog Dis* (2016) 74(7):ftw075. doi: 10.1093/femspd/ftw075
218. Shen H, Min R, Tan Q, Xie W, Wang H, Pan H, et al. The Beneficial Effects of Adjunctive Recombinant Human Interleukin-2 for Multidrug Resistant Tuberculosis. *Arch Med Sci* (2015) 11(3):584–90. doi: 10.5114/aoms.2015.52362
219. Liu X, Li F, Niu H, Ma L, Chen J, Zhang Y, et al. IL-2 Restores T-cell Dysfunction Induced by Persistent *Mycobacterium tuberculosis* Antigen Stimulation. *Front Immunol* (2019) 10:2350. doi: 10.3389/fimmu.2019.02350
220. Nolt D, Flynn JAL. Interleukin-12 Therapy Reduces the Number of Immune Cells and Pathology in Lungs of Mice Infected With *Mycobacterium tuberculosis*. *Infect Immun* (2004) 72(5):2976–88. doi: 10.1128/IAI.72.5.2976-2988.2004
221. Mata-Espinosa DA, Francisco-Cruz A, Marquina-Castillo B, Barrios-Payan J, Ramos-Espinosa O, Bini EI, et al. Immunotherapeutic Effects of Recombinant Adenovirus Encoding Interleukin 12 in Experimental Pulmonary Tuberculosis. *Scand J Immunol* (2019) 89(3):e12743. doi: 10.1111/sji.12743
222. Treerat P, Prince O, Cruz-Lagunas A, Muñoz-Torrico M, Salazar-Lezama MA, Selman M, et al. Novel Role for IL-22 in Protection During Chronic *Mycobacterium tuberculosis* HN878 Infection. *Mucosal Immunol* (2017) 10(4):1069–81. doi: 10.1038/mi.2017.15
223. Dhiman R, Venkatasubramanian S, Paidipally P, Barnes PF, Tvinnereim A, Vankayalapati R. Interleukin 22 Inhibits Intracellular Growth of

Mycobacterium tuberculosis by Enhancing Calgranulin a Expression. *J Infect Dis* (2014) 209(4):578–87. doi: 10.1093/infdis/jit495
224. Gopal R, Monin L, Slight S, Uche U, Blanchard E, A. Fallert Junecko B, et al. Unexpected Role for IL-17 in Protective Immunity Against Hypervirulent *Mycobacterium tuberculosis* HN878 Infection. *PloS Pathog* (2014) 10(5): e1004099. doi: 10.1371/journal.ppat.1004099
225. Khader SA, Pearl JE, Sakamoto K, Gilmartin L, Bell GK, Jelley-Gibbs DM, et al. IL-23 Compensates for the Absence of IL-12p70 and Is Essential for the IL-17 Response During Tuberculosis But Is Dispensable for Protection and Antigen-Specific IFN-γ Responses if IL-12p70 Is Available. *J Immunol* (2005) 175(2):788–95. doi: 10.4049/jimmunol.175.2.788
226. Happel KI, Lockhart EA, Mason CM, Porretta E, Keoshkerian E, Odden AR, et al. Pulmonary Interleukin-23 Gene Delivery Increases Local T-Cell Immunity and Controls Growth of *Mycobacterium tuberculosis* in the Lungs. *Infect Immun* (2005) 73(9):5782–8. doi: 10.1128/IAI.73.9.5782-5788.2005
227. Ma Y, Chen HD, Wang Y, Wang Q, Li Y, Zhao Y, et al. Interleukin 24 as a Novel Potential Cytokine Immunotherapy for the Treatment of *Mycobacterium tuberculosis* Infection. *Microbes Infect* (2011) 13(12–13):1099–110. doi: 10.1016/j.micinf.2011.06.012
228. Chan J, Xing Y, Magliozzo RS, Bloom BR. Killing of Virulent *Mycobacterium tuberculosis* by Reactive Nitrogen Intermediates Produced by Activated Murine Macrophages. *J Exp Med* (1992) 175(4):1111–22. doi: 10.1084/jem.175.4.1111
229. Liu CH, Liu H, Ge B. Innate Immunity in Tuberculosis: Host Defense vs Pathogen Evasion. *Cell Mol Immunol* (2017) 14(12):963–75. doi: 10.1038/cmi.2017.88
230. MacMicking JD. Cell-Autonomous Effector Mechanisms Against *Mycobacterium tuberculosis*. *Cold Spring Harb Perspect Med* (2014) 4(10): a018507. doi: 10.1101/cshperspect.a018507
231. Ramirez-Alejo N, Santos-Argumedo L. Innate Defects of the IL-12/IFN-γ Axis in Susceptibility to Infections by Mycobacteria and Salmonella. *J Interferon Cytokine Res* (2014) 34(5):307–17. doi: 10.1089/jir.2013.0050
232. Roach DR, Bean AGD, Demangel C, France MP, Briscoe H, Britton WJ. TNF Regulates Chemokine Induction Essential for Cell Recruitment, Granuloma Formation, and Clearance of Mycobacterial Infection. *J Immunol* (2002) 168 (9):4620–7. doi: 10.4049/jimmunol.168.9.4620
233. Pagán AJ, Ramakrishnan L. Immunity and Immunopathology in the Tuberculous Granuloma. *Cold Spring Harb Perspect Med* (2015) 5(9): a018499. doi: 10.1101/cshperspect.a018499
234. Keane J, Gershon S, Wise RP, Mirabile-Levens E, Kasznica J, Schwieterman WD, et al. Tuberculosis Associated With Infliximab, a Tumor Necrosis Factor α–Neutralizing Agent. *N Engl J Med* (2001) 345(15):1098–104. doi: 10.1056/NEJMoa011110
235. Wu B, Huang C, Garcia L, De Leon AP, Osornio JS, Bobadilla-del-Valle M, et al. Unique Gene Expression Profiles in Infants Vaccinated With Different Strains of *Mycobacterium Bovis* Bacille Calmette-Guérin. *Infect Immun* (2007) 75(7):3658–64. doi: 10.1128/IAI.00244-07
236. Huang D, Qiu L, Wang R, Lai X, Du G, Seghal P, et al. Immune Gene Networks of Mycobacterial Vaccine-Elicited Cellular Responses and Immunity. *J Infect Dis* (2007) 195(1):55–69. doi: 10.1086/509895
237. Pipkin ME, Sacks JA, Cruz-Guilloty F, Lichtenheld MG, Bevan MJ, Rao A. Interleukin-2 and Inflammation Induce Distinct Transcriptional Programs That Promote the Differentiation of Effector Cytolytic T Cells. *Immunity* (2010) 32(1):79–90. doi: 10.1016/j.immuni.2009.11.012
238. West EE, Jin HT, Rasheed AU, Penaloza-MacMaster P, Ha SJ, Tan WG, et al. PD-L1 Blockade Synergizes With IL-2 Therapy in Reinvigorating Exhausted T Cells. *J Clin Invest* (2013) 123(6):2604–15. doi: 10.1172/JCI67008
239. Johnson B, Bekker LG, Ress S, Kaplan G. Recombinant Interleukin 2 Adjunctive Therapy in Multidrug-Resistant Tuberculosis. *Novartis Found Symp* (1998) 217:99–106; discussion 106–11. doi: 10.1002/0470846526.ch7
240. Robinson RT. T Cell Production of GM-CSF Protects the Host During Experimental Tuberculosis. *mBio* (2017) 8(6):e02087–17. doi: 10.1128/mBio.02087-17
241. Szeliga J, Daniel DS, Yang CH, Sever-Chroneos Z, Jagannath C, Chroneos ZC. Granulocyte-Macrophage Colony Stimulating Factor-Mediated Innate Responses in Tuberculosis. *Tuberculosis* (2008) 88(1):7–20. doi: 10.1016/j.tube.2007.08.009
242. Bhattacharya P, Budnick I, Singh M, Thiruppathi M, Alharshawi K, Elshabrawy H, et al. Dual Role of GM-CSF as a Pro-Inflammatory and a Regulatory Cytokine: Implications for Immune Therapy. *J Interferon Cytokine Res* (2015) 35(8):585–99. doi: 10.1089/jir.2014.0149
243. Ivashkiv LB, Donlin LT. Regulation of Type I Interferon Responses. *Nat Rev Immunol* (2014) 14(1):36–49. doi: 10.1038/nri3581
244. Moreira-Teixeira L, Mayer-Barber K, Sher A, O'Garra A. Type I Interferons in Tuberculosis: Foe and Occasionally Friend. *J Exp Med* (2018) 215 (5):1273–85. doi: 10.1084/jem.20180325
245. Berry MPR, Graham CM, McNab FW, Xu Z, Bloch SAA, Oni T, et al. An Interferon-Inducible Neutrophil-Driven Blood Transcriptional Signature in Human Tuberculosis. *Nature* (2010) 466(7309):973–7. doi: 10.1038/nature09247
246. Zak DE, Penn-Nicholson A, Scriba TJ, Thompson E, Suliman S, Amon LM, et al. A Blood RNA Signature for Tuberculosis Disease Risk: A Prospective Cohort Study. *Lancet* (2016) 387(10035):2312–22. doi: 10.1016/S0140-6736(15)01316-1
247. Sambarey A, Devaprasad A, Mohan A, Ahmed A, Nayak S, Swaminathan S, et al. Unbiased Identification of Blood-Based Biomarkers for Pulmonary Tuberculosis by Modeling and Mining Molecular Interaction Networks. *EBioMedicine* (2017) 15:112–26. doi: 10.1016/j.ebiom.2016.12.009
248. Esmail H, Lai RP, Lesosky M, Wilkinson KA, Graham CM, Horswell S, et al. Complement Pathway Gene Activation and Rising Circulating Immune Complexes Characterize Early Disease in HIV-associated Tuberculosis. *Proc Natl Acad Sci USA* (2018) 115(5):E964–73. doi: 10.1073/pnas.1711853115
249. Papotto PH, Ribot JC, Silva-Santos B. IL-17^{+}γδ T Cells as Kick-Starters of Inflammation. *Nat Immunol* (2017) 18(6):604–11. doi: 10.1038/ni.3726
250. Shen H, Chen ZW. The Crucial Roles of Th17-Related Cytokines/Signal Pathways in M. Tuberculosis Infection. *Cell Mol Immunol* (2018) 15(3):216–25. doi: 10.1038/cmi.2017.128
251. Pociask DA, Scheller EV, Mandalapu S, McHugh KJ, Enelow RI, Fattman CL, et al. IL-22 Is Essential for Lung Epithelial Repair Following Influenza Infection. *Am J Pathol* (2013) 182(4):1286–96. doi: 10.1016/j.ajpath.2012.12.007

Conflict of Interest: The authors declare that the research was conducted in the absence of any commercial or financial relationships that could be construed as a potential conflict of interest.

frontiers in Immunology

ORIGINAL RESEARCH
published: 03 August 2021
doi: 10.3389/fimmu.2021.712678

Granzyme A Produced by $\gamma_9\delta_2$ T Cells Activates ER Stress Responses and ATP Production, and Protects Against Intracellular Mycobacterial Replication Independent of Enzymatic Activity

Valerio Rasi[1,2], *David C. Wood*[3], *Christopher S. Eickhoff*[2], *Mei Xia*[2], *Nicola Pozzi*[3], *Rachel L. Edwards*[2], *Michael Walch*[4], *Niels Bovenschen*[5,6] *and Daniel F. Hoft*[1,2]*

[1] Department of Molecular Microbiology and Immunology, Saint Louis University School of Medicine, Saint Louis, MO, United States, [2] Department of Internal Medicine, Saint Louis University School of Medicine, Saint Louis, MO, United States, [3] Department of Biochemistry and Molecular Biology, Saint Louis University School of Medicine, Saint Louis, MO, United States, [4] Anatomy Unit, Department of Oncology, Microbiology and Immunology, Faculty of Science and Medicine, University of Fribourg, Fribourg, Switzerland, [5] Department of Pathology, University Medical Center Utrecht, Utrecht, Netherlands, [6] Center for Translational Immunology, University Medical Center Utrecht, Utrecht, Netherlands

OPEN ACCESS

Edited by:
Veronica Schmitz, Oswaldo Cruz Foundation (Fiocruz), Brazil

Reviewed by:
Frank Verreck, Biomedical Primate Research Centre (BPRC), Netherlands
Lu Huang, University of Arkansas for Medical Sciences, United States

***Correspondence:**
Daniel F. Hoft
Daniel.Hoft@health.slu.edu

Specialty section:
This article was submitted to Microbial Immunology, a section of the journal Frontiers in Immunology

Received: *21 May 2021*
Accepted: *12 July 2021*
Published: *03 August 2021*

Citation:
Rasi V, Wood DC, Eickhoff CS, Xia M, Pozzi N, Edwards RL, Walch M, Bovenschen N and Hoft DF (2021) Granzyme A Produced by $\gamma_9\delta_2$ T Cells Activates ER Stress Responses and ATP Production, and Protects Against Intracellular Mycobacterial Replication Independent of Enzymatic Activity. Front. Immunol. 12:712678. doi: 10.3389/fimmu.2021.712678

Mycobacterium tuberculosis (Mtb), the pathological agent that causes tuberculosis (TB) is the number one infectious killer worldwide with one fourth of the world's population currently infected. Data indicate that $\gamma_9\delta_2$ T cells secrete Granzyme A (GzmA) in the extracellular space triggering the infected monocyte to inhibit growth of intracellular mycobacteria. Accordingly, deletion of *GZMA* from $\gamma_9\delta_2$ T cells reverses their inhibitory capacity. Through mechanistic studies, GzmA's action was investigated in monocytes from human PBMCs. The use of recombinant human GzmA expressed in a mammalian system induced inhibition of intracellular mycobacteria to the same degree as previous human native protein findings. Our data indicate that: 1) GzmA is internalized within mycobacteria-infected cells, suggesting that GzmA uptake could prevent infection and 2) that the active site is not required to inhibit intracellular replication. Global proteomic analysis demonstrated that the ER stress response and ATP producing proteins were upregulated after GzmA treatment, and these proteins abundancies were confirmed by examining their expression in an independent set of patient samples. Our data suggest that immunotherapeutic host interventions of these pathways may contribute to better control of the current TB epidemic.

Keywords: Granzyme A, *Mycobacterium tuberculosis*, BCG, ER stress response, ATP production, 2D-DIGE, human monocyte, GZMA

INTRODUCTION

Mycobacterium tuberculosis (Mtb), the etiological agent that causes tuberculosis (TB), is the number one infectious killer worldwide causing 1.4 million deaths in 2019 alone (1). In recent years, there has been an increase in the number of multidrug resistant (MDR), as well as extensively drug resistant (XDR) TB cases, highlighting the urgent need to develop new therapeutics to eradicate this disease. While several clinical trials have evaluated host-directed therapies for TB (2), current treatment regimens only target antimicrobial pathways, which engenders antimicrobial resistance to emerge.

Despite WHO eradication efforts, the only licensed TB vaccine is the Bacillus Calmette–Guerin (BCG), which is an attenuated strain of *Mycobacterium bovis* that causes disease in cattle. While the BCG vaccine protects children from acute meningitis and miliary TB, it is less protective against adult pulmonary disease and aerosol transmission. Therefore, new strategies must be employed, including novel immunotherapies that trigger host responses capable of inhibiting mycobacterial growth *in vivo*.

Our lab has previously shown that $\gamma_9\delta_2$ T cells develop a memory response after BCG vaccination (3), potently inhibit the intracellular replication of mycobacteria (4), and produce Granzyme A (GzmA), a key mediator for this inhibition (5). Since mice lack $\gamma_9\delta_2$ T cells specifically, studies are underway in non-human primates (NHP) to evaluate the protective role of $\gamma_9\delta_2$ T cells *in vivo*. Further, data indicate that Mtb-derived 6-O-methylglucose–containing lipopolysaccharides (mGLP) induces potent $\gamma_9\delta_2$ T cell-expansion, higher frequencies of $\gamma_9\delta_2$ T cells producing GzmA, and mycobacterial inhibition (6). Preliminary data suggest that rhesus macaques vaccinated with mGLP have lower bacterial load at the site of inoculation, no dissemination to other lung lobes, and lower pathological disease burden than controls (manuscript in preparation). Thus, $\gamma_9\delta_2$ T cells are an attractive target for novel TB vaccine design and GzmA-mediated mechanism of inhibition requires more investigation.

GzmA is a serine protease released from secretory granules by activated NK cells and T cells. Recently, GzmA has been shown to induce a pro-inflammatory profile in monocytes and macrophages (7–11). Our group has previously shown that $\gamma_9\delta_2$ T cells secrete GzmA upon contact with mycobacteria-infected macrophages and importantly concentrations of GzmA correlate with mycobacterial inhibition. Accordingly, *GZMA* gene knockdown in $\gamma_9\delta_2$ T cell clones reversed this inhibitory activity whereas native human GzmA added exogenously to infected macrophages leads to inhibition of intracellular mycobacterial growth (5). Transcriptional analyses have failed to uncover the pathways responsible for mycobacterial growth inhibition. However, due to the protease activity harbored by this family of enzymes, GzmA-mediated control of intracellular mycobacterial was postulated to occur at the protein level.

Global proteomics experiments were performed to elucidate how GzmA activates monocytes to kill intracellular mycobacteria. We report here that GzmA added to BCG-infected monocytes activates the ER stress response and ATP producing proteins and leads to intracellular inhibition of mycobacteria. Site-directed mutagenesis demonstrates that enzymatic activity is not necessary to mediate mycobacterial growth inhibition. Since GzmA is internalized in infected cells, we speculate that key features within the protein structure activate target cells to induce the ER stress response and ATP-producing proteins to control mycobacteria infection.

MATERIALS AND METHODS

Human Samples

Healthy adult volunteers were recruited according to protocols approved by the Saint Louis University Institutional Review Board #26646 and #26645. Written consent from the volunteers was obtained according to the principles expressed in the Declaration of Helsinki. Ficoll-Paque (GE Healthcare, Piscataway, NJ) was used to obtain PBMC from leukapheresed samples. Adherent monocytes were isolated by plastic adherence as previously described (12).

Preparation of Mycobacteria Infection

Connaught strain BCG was grown to mid-logarithmic phase in Middlebrook 7H9 media supplemented with 10% albumin, dextrose, catalase (ADC; Cat # 211887 BD Diagnostics, Franklin Lakes, NJ) + 0.05% Tween-80. Stocks were aliquoted in media without Tween -80 and frozen at -80°C. The concentration of the bacterial stock was determined after thawing by CFU plating performed in triplicate. Thawed aliquots were sonicated to generate single-cell suspensions before dilution and infection of monocytes.

Mycobacterial Growth Inhibition Assay (MGIA)

The assay was performed as previously published with slight modifications (12). Briefly, thawed PBMC were plated on round-bottom 96-well plates in RPMI-1640 (Gibco Cat #11875, Thermofisher, Wantham, MA) supplemented with 10% Human AB serum (Sigma, St. Louis, MO) and 1% L-glutamine (Sigma, St. Louis, MO) (without antibiotics); complete media is termed R+2. After 2 h, cells were gently washed with warmed R+2 media at 37°C to remove non-adherent cells. The monocytes (mostly $CD14^+$) attached to the plate were then infected with Connaught BCG (Multiplicity of Infection=3) and treated with 200 nM Granzyme A (GzmA). After 1 h, cells were gently washed with R+2 media three times to remove extracellular BCG and resuspended in R+2 media containing 200 nM GzmA. After 72 h co-culture, cells were lysed 0.2% saponin (Cat # S7900, Sigma, St. Louis, MO) solution in RPMI-1640, and the reaction quenched after 2 h with 100 µL 7H9+ADC containing 1 µCi 5,6-^{3}H-uridine. After 72 h, plates were harvested onto glass fiber filter papers (filtermats). Filtermats received Illumina Gold F scintillation fluid (Cat # 6013321, PerkinElmer, Waltham, MA) and were imaged using a MicroBeta^2 liquid scintillation counter (PerkinElmer, Waltham, MA) measuring Disintegration Per Minute (DPM). The % inhibition was calculated as: 100 – 100 x (DPM from

wells treated with GzmA and infected with BCG/DPM from wells infected with BCG).

GzmA Purification

Native GzmA was purchased from TheraTest (Lombard, IL), which utilized previously published techniques (13). Recombinant GzmA was purified after transient transfection of HEK293T cells (ATCC® CRL11268TM; ATCC, Manassas, VA) with *GZMA* encoded within the pHL-sec plasmid (14). Dr. Walch kindly provided the plasmids that were then amplified in endotoxin-free Giga-kits (Qiagen, Germany). GzmA-S195A was obtained by submitting GzmA-WT pHL-sec plasmid to Genewiz (South Plainfield, NJ), which performed site directed mutagenesis at position 212 (195 using tryptase numbering) and substituted Ala to Ser. Genewiz also verified successful mutagenesis and released report. For RhGzmA-WT and Rh-GzmA-S195A purification, HEK293T cells were incubated at 37°C for 7-11 h with plasmid in FBS-containing DMEM media using Lipofectamine 3000 [instead of Calcium Phosphate transfection as in (14)]) and following the recommended concentrations (Cat # L3000008, Thermofisher, Waltham, MA). Supernatant-containing GzmA was then harvested 72-96 h after transfection [improved method by not switching to serum-free media compared to (14)]. The purification protocol was modified to maintain buffers in either isotonic or hypertonic solution, as protein precipitation occurred in hypotonic buffers. Purification of supernatant was performed at 4°C first using Ni-IMAC column (Cat # 17531806, GE Healthcare, Chicago, IL), activation of GzmA after enterokinase (Cat # SRP3032, Sigma, St. Louis, MO) treatment at room temperature (RT), and final MonoS column (Cat # 17516801, GE Healthcare, Chicago, IL) purification at 4°C. All steps were completed with single-use plastic bottles and endotoxin-free reagents and the final protein was run over an Endotrap column (Lionex Gmbh, Germany) to remove any residual endotoxin contamination. Homodimerization was verified by non-reducing SDS gel electrophoresis, and protein was verified by western blot with a GzmA 1:500 antibody (R&D, Clone #356422) and further, by the lack of interaction with Granzyme K 1:100 antibody (Cat # SAB2103935, Sigma, MO). WT and GzmA-S195A were tested using MALDI-TOF, which confirmed protein purification as well as site-directed mutagenesis (data not shown). Protein was stored at -80°C in 10 µL aliquots and thawed and diluted the day of the experiment.

BLT Esterase Assay

The substrate Z-L-Lys-SBzl hydrochloride (Sigma, St. Louis, MO) was added at different concentrations (19.5-2,500 µM to measure Vmax and Km, and 2,500 µM for GzmA-S195A experiments) and diluted in assay buffer (50 mM Tris, 154 mM NaCl, pH 7.5) in presence of 0.55 M (5,5-dithio-bis-(2-nitrobenzoic acid) (DTNB) (Sigma, St. Louis, MO) chromophore. 120 pM of protein was added per well and substrate hydrolysis was quantified by measuring the absorbance at 405 nm using an SLT Rainbow plate reader (Tecan, Männedorf, Switzerland). Esterolytic activity was reported as rate of hydrolysis using extinction coefficient of 13,100 $M^{-1}cm^{-1}$ for the 3-carboxy-4-nitrophenoxide ion. Specific activity measured as nM product/min/nM of enzyme present.

DCI Experiments

150 µM of 3,4-dichloroisocoumarin (DCI) (Cat# D7910, Sigma, St. Louis, MO) was incubated with GzmA (7.5 µM) for 30 min at RT. DCI-treated GzmA was then dialyzed against 50 mM Hepes, 150 mM NaCl, pH 7.4, and its inactivation was confirmed by BLT assay.

GzmA Internalization and Confocal Microscopy Experiments

To monitor GzmA internalization, monocytes were first blocked with True Stain Fc blocker (Cat. # 426101, Biolegend, San Diego, CA), and then incubated with anti-GzmA antibody conjugated with PE (Cat. #558904, BD Biosciences, San Diego, CA). Permeabilization solution was used to study GzmA internalization (Cat. #554715, BD Biosciences, San Diego, CA). For confocal microscopy experiments, cells were incubated on Lab-tek tissue culture-treated wells (Cat. #154941, Nunc, Denmark). At the time of fixation, cells were washed twice with 1x RT PBS, and fixed in 4% paraformaldehyde for 15 min at 37°C. Then slides were washed thrice for 5 min with RT 1x PBS, and then blocked with 5% donkey serum [52-000-121] with 0.25% Tween-20 (Cat. #P9416, Sigma, St. Louis, MO). Cells were then incubated overnight at 4°C with primary antibody anti-GzmA (Cat. # MAB29051, R&D, Minneapolis, MN) at 1:20 (12.5 µg/mL) in blocking buffer. To remove unbound antibody, cells were washed four times with 1x PBS at RT, and then incubated in the dark for 1 h with secondary antibody conjugated with Alexa Fluor 594 (Cat. # 715-545-150, Jackson Immunoresearch, West Grove, PA) at 1:100. Cells were then washed thrice with 1x PBS at RT and incubated with 2.86 µM DAPI (Cat. #5748, Tocris, Bristol, UK) for 5 min at RT. Slides were finally mounted using Prolong Diamond antifade mountant (Cat. #P36965, Life Technologies, OR, USA) overnight, and then stored at -20°C until visualized using instrument at Saint Louis University Research Microscopy Core.

2D DIGE Analysis and MALDI-TOF

Cells were washed twice with sterile 1x PBS, then lysed in buffer compatible for 2D separation (8 M urea, 2 M thiourea, 4% CHAPS, 50 mM Tris, pH 8.5) in presence of 1:100 HALT phosphatase and protease inhibitor (HALT phosphatase and protease inhibitor (Cat # 78442, Thermo-Fisher, Waltham, MA). Samples underwent ReadyPrep 2Dclean-up kit (BioRad, Hercules, CA). Protein concentrations were quantified using Pierce 660 nm protein assay (Cat # 23236, Thermo-Fisher, Waltham, MA). Prior to carrying out DIGE substoichiometric CyDye labeling, an equal protein quantity was taken from each lysate to create a pool for normalization of fluorescence intensity for all analytical 2D gels. This pool was labeled with Cy2 dye, and individual samples were labeled with either Cy3 or Cy5 (Lumiprobe, Hunt Valley, MD) using a dye ratio of 8 pmol per µg protein. Samples were incubated on ice in dark for 30 min. The reaction was quenched by adding 10 mM lysine and incubating on ice for 10 min. Samples were pooled (Cy2, Cy3,

and Cy5) on a immobiline dry strip immobilized pH gradient (IPG) pH 3-11 Non-Linear (NL) (GE Healthcare, Chicago, IL), 7 cm, rehydrated overnight in rehydration buffer (30 mM Tris, pH 8.5, 2 M thiourea, 7 M urea, 2% dithiothreitol (DTT), 4% CHAPS, and 0.5% IPG buffer) at 30 V. Isoelectric Focusing (IEF) separation was performed according to manufacturer instructions (total 11 kW). IEF strip was reduced in 10 mg/mL DTT and then alkylated in 25 mg/mL iodoacetamide in reducing buffer (100 mM Tris, pH 8.8, 6 M urea, 30% glycerol, 2% SDS). Proteins were separated by SDS-PAGE using Criterion XT 4-12% SDS-PAGE gels (BioRad, Hercules, CA) and applying 100 V for 45 min. Gels were fixed in 30% methanol, 7% acetic acid, and then washed twice in distilled water. CyDyed spots were detected with a Typhoon 9410 scanner (GE Healthcare, Chicago, IL) with PMT voltage adjusted to a maximum intensity between 80,000-95,000 and with <15% variation between Cy2, Cy3, and Cy5. Melanie software V.9.1.1 (GE Healthcare, Chicago, IL) analysis was used to overlap gels from different subjects and conditions to find identical protein spots across gels, normalization of Cy3 and Cy5 to Cy2, and fold change of relative abundance after BCG infection and/or GzmA treatment. The average fold change of a spot in two subjects that was >1.3 in Group 4 relative to Group 3 and Group 1 was isolated for identification. Spots corresponding to differentially abundant proteins were identified using MALDI-TOF mass spectrometry. Following in-gel tryptic digestion (15), we used an Axima Resonance MALDI-TOF mass spectrometer (Shimadzu, Kyoto, Japan) to identify the differentially abundant protein spots. Spots that had a MALDI score of at least 60 were chosen indicating that there is less than 1 in $1e^6$ chances that this protein was discovered by a random coincidence.

Protein-Protein Interaction Network

To construct protein-protein interactions for GmzA-associated proteins, the Search Tool for the Retrieval of Interacting Genes/Proteins (16) database version 10.5. was used (17).

Statistical Analysis

For generation of graphs and statistical analysis we used GraphPad Prism version 9.0.0 for Windows, GraphPad Software, San Diego, California USA, www.graphpad.com.

RESULTS

Recombinant Human GzmA Phenocopies Native Protein

Our previous studies that confirmed the mycobacterial growth inhibition in infected macrophages were conducted using native human GzmA (NhGzmA). However, due to the low yield (50 μg from the purification of $1x10^9$ NK92MI cells-data not shown) that is obtained and the potential co-elution with other granzymes, we decided to compare commercially available NhGzmA to recombinant human (RhGzmA). RhGzmA was purified from transiently transfected HEK293T cells with an improved purification method that allowed us to produce 20 mg of highly purified GzmA protein, which is 10 fold higher than previously reported methods (14), and can be utilized for large global proteomic studies. RhGzmA was shown to form homodimers (~50 kDa) similar to NhGzmA by silver stain and western blot (**Figure 1A**) as well as polymers of the 50 kDa protein as previously reported (11). RhGzmA has a slightly higher molecular weight because of the presence of a His-tag at the C-terminus of the protein. To compare the specific enzymatic activities of recombinant and native GzmA, we analyzed their ability to cleave the chromogenic substrate, Z-L-Lys-SBzl hydrochloride (BLT). Data indicate that the recombinant protein is similar to the native protein in that both can efficiently cleave BLT (**Figure 1B**). It is important to note that substrate cleavage efficiencies were found to be similar between independently purified batches of recombinant GzmA, demonstrating the reproducibility of our purification method (**Figure 1C**). To confirm whether RhGzmA and NhGzmA induce similar protective effects against mycobacteria, monocytes were infected with BCG and treated with either recombinant or native human GzmA and the degree of mycobacterial growth inhibition was measured. As expected, RhGzmA inhibited almost 80% of the intracellular replication of mycobacteria, and no significant difference was detected between the recombinant protein and the native form (**Figure 1D**).

To verify that the inhibitory activity is independent of endotoxin, RhGzmA was heated at 95°C for 10 min to denature the recombinant protein while retaining the activity of a potential endotoxin contaminant as reviewed in (18). The ability of the heat-treated protein was then assayed for its ability to inhibit mycobacterial growth. As demonstrated in **Supplementary Figure 1A**, heat denaturation of RhGzmA abolished the intracellular growth inhibition suggesting that endotoxin contamination did not explain the protective effects of RhGzmA. To further rule out whether endotoxin contributes to the robust growth inhibition displayed by the recombinant protein, RhGzmA was passed through an Endotrap column to remove any residual endotoxin and then tested for its ability to inhibit growth. Data indicate that when purified RhGzmA is treated for endotoxin removal, the protein retains its capacity to restrict intracellular growth (**Supplementary Figure 1B**). Taken together, these data indicate that RhGzmA recapitulates the effects of native GzmA, and accordingly, can be used for large scale applications such as global proteomic studies to help identify molecular mechanisms of protection.

Enzymatic Activity Is Dispensable to Mediate Mycobacterial Growth Inhibition

GzmA is a trypsin-like serine protease, cleaving substrates after positively charged lysine and arginine residues (19). GzmA possesses the canonical serine protease catalytic triad formed by His57, Asp102, and Ser195. To determine whether its enzymatic activity is necessary to mediate mycobacterial growth inhibition, Ala was substituted for Ser195 and the protein variant was purified similar to the wild-type (WT) RhGzmA (**Supplementary Figure 2**) (10, 11, 20). The S195A mutant was then evaluated for its ability to cleave BLT. The single amino acid substitution abolished catalytic activity

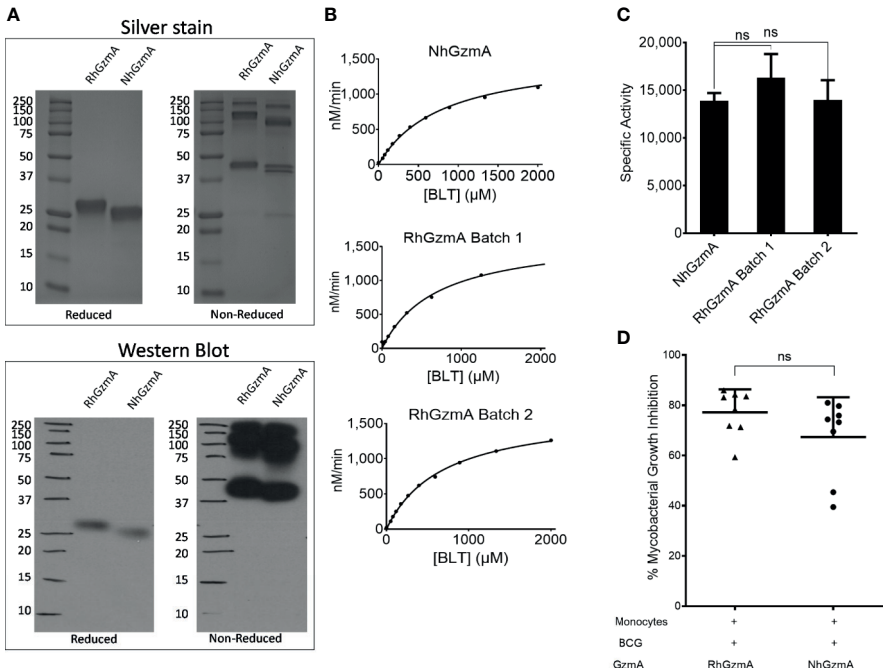

FIGURE 1 | Recombinant human GzmA phenocopies native protein. **(A)** RhGzmA and NhGzmA homodimerize (~50 kDa, some monomer at ~25 kDa in NhGzmA) and are pure as shown by silver stain (top figure) and western blot (bottom figure). Under reducing conditions, GzmA assumes the monomer form, while under non-reducing conditions homodimer and polymers of GzmA are the predominant forms. RhGzmA has a His-tag at the C-terminus of the protein, which accounts for the slightly heavier MW. **(B, C)** RhGzmA and NhGzmA cleave BLT substrate at similar rates, and different lots of RhGzmA have similar enzymatic activity in the BLT esterase assay. Results are plotted using the Michaelis-Menten equation **(B)** and fitted to produce specific activity **(C)**. Commercially obtained native protein, and two different lots of purified recombinant protein are shown. Negative control results (BLT alone) were subtracted from results for each experiment (unpaired t-test, experiment repeated at least three times). **(D)** Recombinant human GzmA recapitulates mycobacterial growth inhibition as native protein measured in the Mycobacterial Growth Inhibition Assay (n=8; data representative of two independent experiments; means and SEM; Wilcoxon matched-pairs signed rank test) (*$p < 0.05$, **$p < 0.01$, ***$p < 0.001$; ns, not significant).

(**Figures 2A, B**). The catalytically inactive S195A GzmA protein was then tested in the mycobacterial growth inhibition assay (**Figure 2C**), which revealed similar mycobacterial inhibitory activity comparing WT and S195A, implying that a catalytically active enzyme is not required to inhibit intracellular growth. To confirm that catalytic activity is unnecessary for mycobacterial growth inhibition, WT GzmA was incubated with the serine protease inhibitor 3,4 Dichloroisocoumarin (DCI), and then tested for its ability to restrict growth. While WT GzmA treated with DCI was unable to cleave the BLT substrate (**Figure 2D**) similar to the S195A mutant (**Figure 2A**), its ability to mediate mycobacterial growth inhibition was not affected indicating that enzymatic activity is dispensable (**Figure 2D**).

GzmA Is Internalized in Infected Monocytes

There are conflicting reports as to whether GzmA elicits its physiological effect intracellularly or at the cell surface (10, 11). To investigate this possibility, we performed flow cytometry studies using both surface and intracellular staining. Anti-human GzmA-PE was used either with or without cell permeabilization reagents to investigate GzmA localization. After overnight infection and treatment, higher frequencies of monocytes internalized GzmA compared to the protein levels adhered to the cell surface (**Figure 3A**). This internalization is also evident by confocal microscopy as GzmA is detected adjacent and surrounding the nucleus (**Figure 3B**). To further explore the timing and localization of GzmA in relation to mycobacteria, we performed a series of immunocytochemistry experiments during infection. There was evidence of mycobacterial control as early as 2 h post-infection as seen in (**Figure 3C**) and quantified as integrated density of BCG-GFP comparing untreated cells to GzmA-WT and GzmA-S195A treated cells (**Figure 3D**). At 16 h post-infection it appears that the smaller proportions of cells that would become infected after GzmA treatment had not internalized GzmA (**Figure 3E**). The merged image on the left was split so that BCG-GFP$^+$ areas could be isolated (center) and overlapped with GzmA signal (right). In the lower panel, integrated density analyses quantified the amount of GzmA signal withing BCG-GFP$^+$ areas, which were minimal, and compared the GzmA$^+$ areas, which had very little BCG-GFP signal. The visualization and quantification further confirmed that there is no overlap between infection and GzmA, hinting at the possibility that those cells that do not internalize GzmA appear to be more prone to higher bacterial burden.

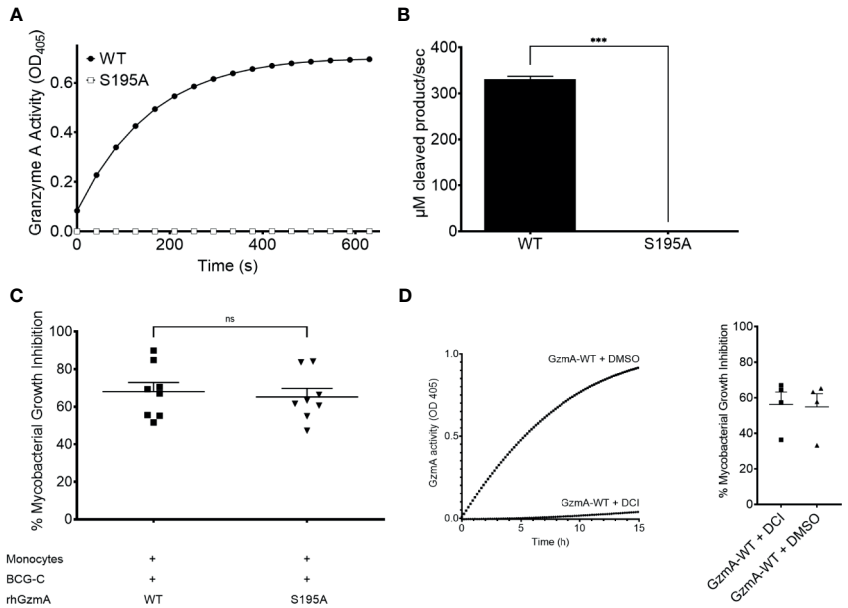

FIGURE 2 | Enzymatic activity is dispensable to mediate mycobacterial growth inhibition. **(A)** GzmA of wild-type (WT) and S195A variant proteins' activity over time measured by the BLT assay of three independent experiments performed as triplicates per condition. **(B)** For statistics, the rate of initial reaction was compared between WT and S195A variant (means and SD; paired t-test). **(C)** MGIA comparing WT and S195A enzymatically inactive variant, displayed as % of inhibition (n=8 in at least two independent experiments. Mean and SEM, Wilcoxon matched-pairs signed rank test). **(D)** GzmA treated with DCI inhibits intracellular replication as GzmA-DMSO in MGIA (left) and BLT assay (right) showing that inhibited GzmA retains inhibitory activity (n=4, Mean and SEM) (*p < 0.05, **p < 0.01, ***p < 0.001; ns, not significant).

Global Proteomic Analysis Uncovers Several Differentially Abundant Proteins

To better understand the mechanism of mycobacterial growth inhibition, we employed proteomics to identify differentially abundant proteins using the two-dimensional difference gel electrophoresis (2D-DIGE) platform. We studied each subject's monocytes with four experimental groups, each with its own CyDye label that Melanie software (21) utilized to understand which protein spots were upregulated or downregulated with BCG infection or GzmA treatment (**Supplementary Figure 3**). The four groups studied are summarized in **Table 1**: 1) Monocytes alone, 2) Monocytes treated with GzmA, 3) Monocytes infected with BCG, 4) Monocytes infected with BCG and treated with GzmA. We focused on spots that were differentially abundant (>1.3-fold change in Group 4 *vs.* Group 1/2/3) in cells from Group 4 (BCG+GzmA), while the other groups served as controls. An example of a matched spot of interest is spot #431, shown in **Supplementary Figure 3**, which was upregulated in Group 4 and not in the other groups. Next, MALDI-TOF studies were employed to identify the differentially abundant protein spots (**Table 2**). Of these spots, ten were found using the human Mascot database (22). As a validation of our method, we investigated the identity of a protein that was not differentially abundant, and we identified cytoskeletal protein Tubulin 5 (TBB5). To the best of our knowledge, TBB5 has not been associated with differential expression in monocytes following mycobacterial infection or GzmA treatment, corroborating our investigation.

ER Stress Response and ATP Synthesis Are Involved in GzmA-Mediated Mycobacterial Control

To understand the relationship between the identified proteins and the growth inhibition displayed by GzmA, we used the Search Tool for the Retrieval of Interacting Genes/Proteins (STRING) (16) database since it interrogates protein interactions on a global scale including stable physical associations, transient binding, substrate chaining, and information relay (17). After analyzing the results of all discovered spots, we focused on the Gene Ontology (GO) category of STRING and selected those pathways with a False Discovery Rate (FDR) ≤0.001. We identified two pathways associated with GzmA-mediated inhibition of intracellular mycobacteria: 1) the response to endoplasmic reticulum (ER) stress, and 2) mitochondrial ATP synthesis coupled proton transport. Protein Disulfide Isomerase A1 and A3 (PDIA1 and PDIA3), Binding immunoglobulin Protein (BiP), and Endoplasmin (HSP90B1) were identified as part of the ER stress pathway (**Supplementary Figure 4**). For the ATP synthesis pathway, we probed the STRING database using proteins that had a fold change >1.5 by both Group 4/Group 3 and Group 4/Group 1. This search alone did not yield a pathway, so additional nodes were created in STRING (increased from 5 original nodes to 10 machine-generated nodes), which identified ATP5H as a key protein (**Supplementary Figure 5**). Importantly, both the ER stress response (23–26) and ATP production leading to P2X7 receptor activation (27–35) have

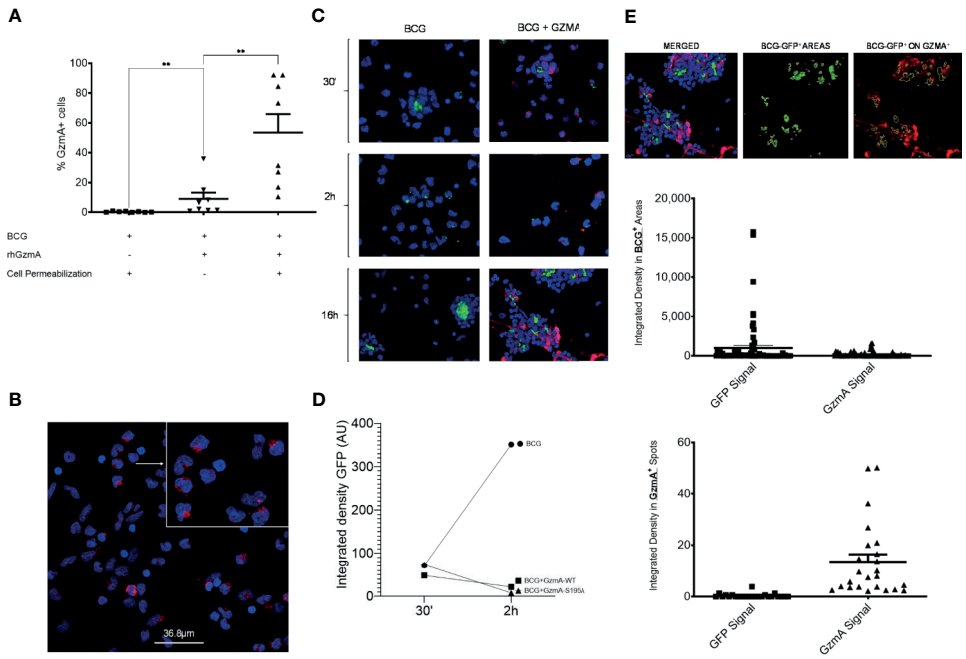

FIGURE 3 | GzmA is internalized in infected monocytes. **(A)** In flow cytometry studies comparing surface *vs.* intracellular staining, the majority of GzmA is inside the monocytes after treatment (n=8 in at least two independent experiments; means and SEM; Wilcoxon matched-pairs signed rank test). Similarly, GzmA is shown to be adjacent to the nucleus of treated monocytes as seen by confocal microscopy. **(B)** Representative confocal microscopy image showing GzmA in red and DAPI (nuclear stain) in blue. **(C)** Representative confocal microscopy images from three separate experiments showing GzmA in red, DAPI (nuclear stain) in blue, and BCG-GFP in green. Comparing 30 min and 2 h post-infection, GzmA-treated cells show lower bacterial burden. **(D, E)** Image analysis isolating BCG-GFP+ areas at 16 h post-infection: superimposition of areas where BCG is present and GzmA. GzmA and BCG are not found in the same cells as visually represented in images and measured in graphs by looking at integrated density signal of BCG and its overlap with GzmA **(E)** (mean, at least three independent experiments) (*$p < 0.05$, **$p < 0.01$, ***$p < 0.001$; ns, not significant).

TABLE 1 | Groups for proteomic analysis.

Group #	Infection and/or Treatment
1	Media-rested Monocvtes (DN)
2	GzmA-treated Monocytes
3	BCG-infected Monocytes
4	BCG-infected and GzmA-treated Monocvtes (DP)

The four groups studied are summarized here: 1) Monocytes alone, 2) Monocytes treated with GzmA, 3) Monocytes infected with BCG, 4) Monocytes infected with BCG and treated with GzmA.

been implicated in mycobacterial control, consistent with our findings.

Differentially Abundant Proteins Discovered With 2D-DIGE Are Also Differentially Abundant as Measured With Quantitative Western Blot Analysis

To validate our global proteomic data, we quantified the levels of three ER stress response proteins BiP, PDIA1, and Endoplasmin

TABLE 2 | Global proteomic analysis uncovers several differentially abundant proteins.

#	ID	UNIPROT #	MALDI Score	Fold change (DP *vs.* DN)	Fold change (BCG+GzmA *vs.* BCG)
431	FBF1	Q8TES7	74	2.16	1.82
273	ACTB/G	P60709	66	2.18	1.80
272	CH60	P10809	84	1.69	1.58
43	ATP5H	O75947	80	1.62	1.54
323	BIP	P11021	240	1.77	1.54
280	INVO	P07476	70	2.24	1.47
268	PDIA1	P07237	65	1.90	1.46
374	Endoplasmin	P14625	97	1.71	1.44
259	PDIA3	P30101	103	1.31	1.39
332	GLU2B	P14314	114	1.70	1.34
228	TBB5	P07437	122	1.02	1.01

After software analysis Melanie identified 18 protein spots differentially abundant in 2 subjects, 10 proteins were identified using MALDI-TOF. # is the matched spot number for these proteins across subjects, their identity, UNIPROT#, MALDI score (which marks confidence of identification; i.e. score of 60 is the chance that 1 in a million that protein identified is a random event), Fold change Double Positive group (DP) vs Double Negative (DN) (group 4 abundancy/group 1 abundancy), Fold change DP vs BCG (group 4 abundancy/group 3 abundancy).

as well as the key protein involved in ATP production, ATP5H, in an independent set of volunteer samples. As displayed in (**Figure 4**) and as an example in (**Supplementary Figure 6**), the levels of these proteins were upregulated in Group 4 compared to the other control groups, confirming the increased protein levels observed by 2D-DIGE (**Table 2**).

DISCUSSION

$\gamma_9\delta_2$ T cells are attractive candidates for novel vaccines against TB, because they are not MHC I restricted, and thus, can be broadly stimulated in the target population (36). GzmA is a key mediator employed by $\gamma_9\delta_2$ T cells to control mycobacteria, but the mechanism by which it elicits an effect is unclear. While data in mice demonstrated that GzmA has no impact on TB control, it is important to note that $\gamma_9\delta_2$ T cells are absent in mice and that TB pathology is markedly different than that in NHP or humans (37). Moreover, the mouse family of granzymes is larger than the human counterpart (9 *vs* 5 respectively), and biological redundancies between granzymes have been reported suggesting that mice are likely a poor model for studying the molecular mechanism of GzmA-mediated control of TB (38).

To perform global proteomic experiments, large quantities of human GzmA were required. Traditionally, NhGzmA is purified from the human NK cell line NK92MI encoding a constitutively expressed IL-2 transduced gene. However, this purification method requires more than four weeks to grow a sufficient number of cells to purify GzmA from their cytotoxic granules, and only yields approximately 50 μg of purified protein [data not shown and (14, 39)]. We demonstrate that RhGzmA phenocopies NhGzmA by assessing protein purity and formation of homodimer, enzymatic activity, and mycobacteria growth inhibition; our results also confirm previous reports that RhGzmA and NhGzmA have similar effects (10, 11). RhGzmA provides the key advantage of being able to generate large amounts of protein. Further, this recombinant construct may better reflect the native conformation than other commercially available or published constructs as the protein is expressed in a mammalian system to maintain full glycosylation of the protein.

GzmA-S195A induces mycobacterial killing similar to WT GzmA. As previously reported, GzmA-WT as well as GzmA-S195A are both able to mediate a synergic action with bacterial ligands to produce a pro-inflammatory profile in human monocytes (10), Thus, our studies confirm similar biological findings and create the opportunity for this pro-inflammatory phenotype to translate into an anti-mycobacterial role. As

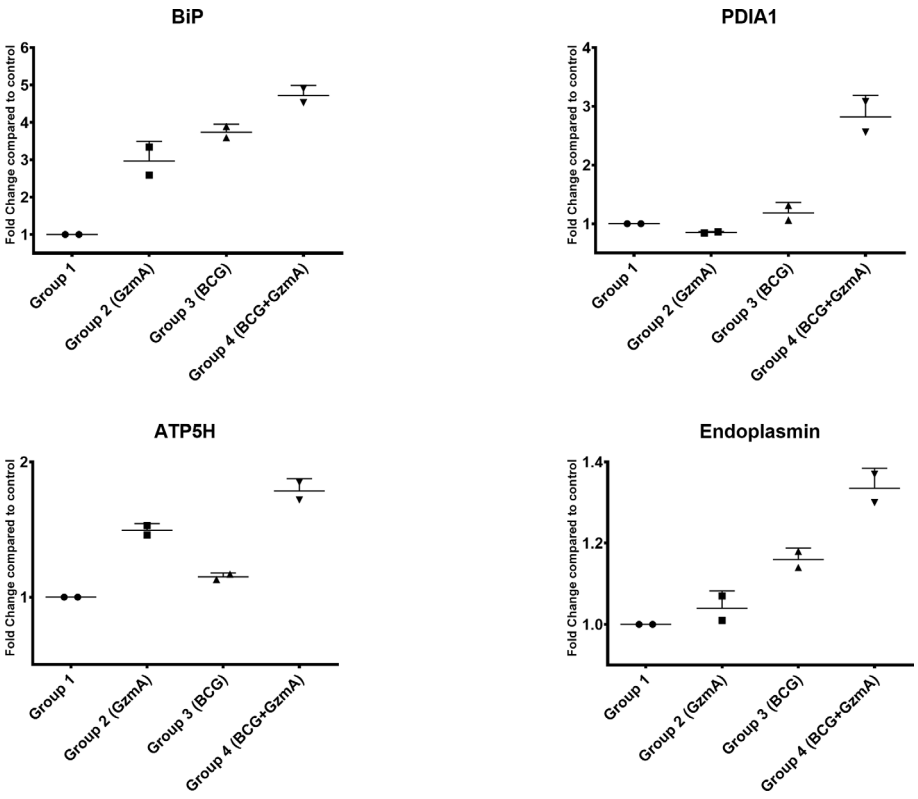

FIGURE 4 | ER stress response and ATP producing proteins are involved in GzmA-mediated mycobacterial control. Graphs show four proteins that were selected from **Table 1**. Using Odyssey CLx near-infrared platform and total protein for normalization, data confirms 2D-DIGE results. Protein lysate obtained from 2 additional subjects that were not included in original 2D-DIGE analysis. Experiments done in triplicates per group, means ± SEM.

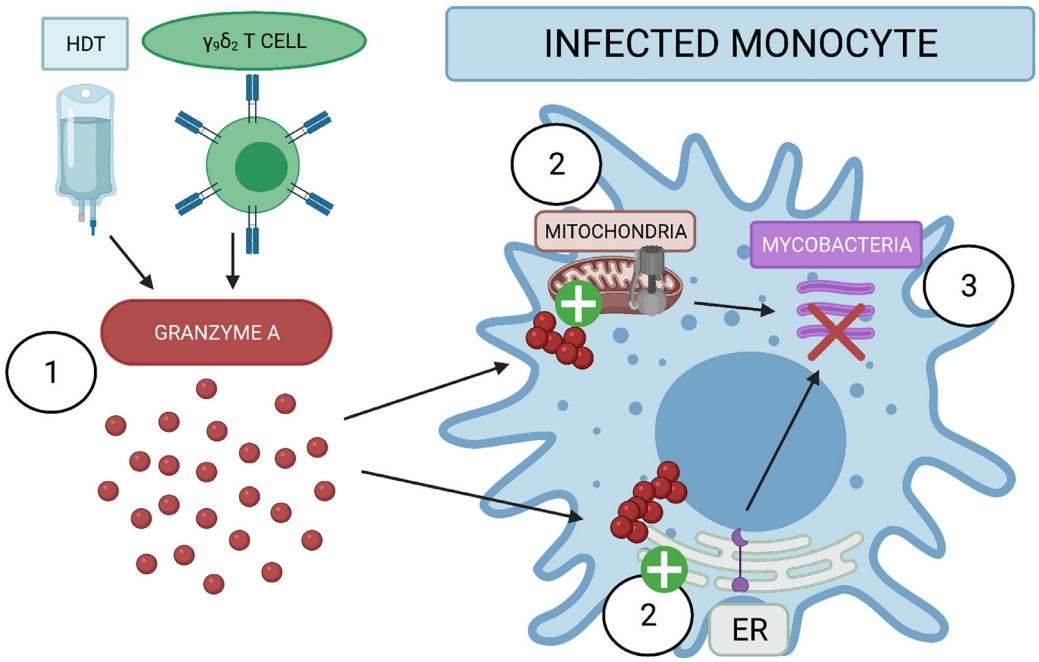

FIGURE 5 | Extracellular GzmA added to infected monocyte induce mycobacterial inhibition by activating ER stress response and ATP producing proteins. (1) GzmA protein is released into the extracellular environment of infected monocytes either as an Host Directed Therapy (HDT) or from secretion of $\gamma_9\delta_2$. GzmA is internalized and does not appear to cleave any cellular substrate. (2) GzmA instead activates ATP producing proteins and the ER stress response to induce (3) the inhibition of intracellular mycobacterial growth. Created with BioRender.com

evidenced in (10), CD14 binding may be a key mediator for this action, and future studies will be required to investigate its role in the context of TB. Similarly, in a mouse model it has been shown that GzmA augments the response of plasmacytoid Dendritic Cells (pDC) through TLR9 to train adaptive immune cells (40), showing that GzmA could facilitate the activation of innate immune cells. More recently, it has been shown that GzmA cleaves Gasdermin B (GSDMB) to trigger pyroptosis of target cancer cells (41). However, this reported mechanism was triggered by 1) an intact active site, and 2) the use of perforin. Thus, while we did not investigate the role of GSDMB in our study, it is unlikely that the mycobactericidal role relies on this pathway. Similarly, it has been shown that patients and mice infected with arboviruses have increased levels of GzmA in the serum, and the use of a specific mouse GzmA inhibitor (Serpinb6b) can reverse the overactive inflammatory response (42); however, this mechanism was also reliant on an intact active site. The finding that GzmA-S195A also mediates mycobacterial inhibition opens the possibility that other key structural determinants are needed in this context such as homodimerization and/or glycosylation.

GzmA is internalized within one hour at steady state (11), and is detected inside cells after infection and treatment (**Figure 3**). Internalization of GzmA suggests that GzmA may be trafficked through an endocytic process after binding to a putative receptor. However, it is unclear whether intracellular GzmA is required for mycobacterial inhibition. In (11), GzmA was modified to more readily enter the cytosol of the target cell, and similar approaches could be explored. Other examples include site-directed mutagenesis of asparagine 170, which is glycosylated (43) and may affect the internalization rate by substituting it with glutamine. Cysteine residue at position 93, which is necessary for homodimerization, could be substituted to serine, as previously reported (44). Monomeric GzmA could lose the ability to bind to the putative receptor that is necessary for internalization, and/or GzmA ability to bind to bacteria and LPS as shown in (10).

Data indicate that an unbiased global proteomic analysis in primary cells is critical for uncovering novel substrates, since cell lines may identify substrates that lack biological relevance (45–47). Accordingly, when we compared our GzmA substrate data generated from primary human cells with previous reports that used cell lines, we found no information that would inform our studies (46, 47). There is evidence that GzmA is selective in the protein substrates that it cleaves due to its homodimeric configuration, and further, GzmA may only use a few substrates *in vivo* emphasizing the importance of the model system employed (44). Our model uses primary monocytes infected with mycobacteria and cells that are treated with physiological amounts of GzmA. As shown in (11), sub-micromolar concentrations of GzmA do not mediate pro-apoptotic events, but instead promote a different phenotype

characterized with pro-inflammatory sequelae in human monocytes. Our studies were conducted at less than 200 nM concentrations, not noting an advantage of using higher concentrations of GzmA. Thus, our model may more closely resemble the natural immunological response after Mtb infection of alveolar macrophages (48). Future experiments are required to discern whether primary alveolar macrophages infected with Mtb recapitulate our findings. Our experiments were performed using mycobacteria BCG strain as we have previously shown that $\gamma_9\delta_2$ T cells inhibit intracellular replication of Mtb as well as BCG through GzmA, and BCG has the advantage of being less biohazardous for our proteomic strategy (5).

The pathways uncovered in our proteomic analysis are supported by previous data regarding host control of mycobacteria. For example, the ER stress response has been associated with M1 macrophage polarization, which leads to better host control of Mtb infection (26). While the precise mechanism has yet to be elucidated, this may be due to stimulation of the TLR2 pathway which triggers fusion of the lysosomal compartment with Mtb-containing phagosomes and induction of iNOS. Moreover, preliminary data indicate that antibiotics that induce ER-stress mediated autophagy, such as thiostrepton, are potential therapies for recently infected patients (23, 24). Thus, further studies are required to understand the potential treatment window in NHP. ATP-producing proteins such as ATP5H may help infected cells during energy-intensive processes such as protein production, protein folding, and cell metabolism (49). Future studies will investigate the ATP levels of GzmA-treated and infected monocytes; mycobacteria has been shown to reprogram host cell metabolism as shown in (50–52), and it is possible that GzmA is capable of switching cellular metabolism to favor the host. Moreover, the P2X7 receptor was recently shown to be important for mycobacterial control (27–35). This purinergic channel senses extracellular ATP and the cell responds to this stimulus by activating an inflammatory response and phagosome-lysosomal maturation. Further studies will be required to investigate the concentration of extracellular ATP and the involvement of the P2X7 receptor. As summarized in **Figure 5**, GzmA either used as Host Directed Therapy (HDT) or secreted from activated $\gamma_9\delta_2$ T cells is internalized inside monocytes. In turn the treated monocyte activates the production of ATP producing proteins and the ER stress response pathway, leading to the inhibition of the intracellular mycobacterial growth. While these two pathways have been previously identified as important for mycobacterial control, to the best of our knowledge this is the first time that GzmA has been reported to induce these pathways for mycobacterial control and pathogen immunity. Future studies will investigate the necessity of these pathways for the induction of mycobacterial inhibition through gene alterations and pharmaceutical interventions to better describe GzmA mechanistic effects. These studies could lead to novel targets for host-directed therapies, as well as detection of important immune markers during future vaccine trials. Together, these strategies will contribute to the world health community's goal of TB eradication.

DATA AVAILABILITY STATEMENT

The original contributions presented in the study are included in the article/**Supplementary Material**. Further inquiries can be directed to the corresponding author.

ETHICS STATEMENT

The studies involving human participants were reviewed and approved by Institutional Review Board, Saint Louis University. The patients/participants provided their written informed consent to participate in this study.

AUTHOR CONTRIBUTIONS

VR, DW, CE, MX, RE, and DH designed key experiments. VR and DW performed global proteomics experiments. VR, NP, CE, MX, and DH designed GzmA-S195A, and VR tested enzymatically inactive GzmA. VR, RE, and DH designed confocal microscopy experiments, and VR executed them. MW and NB collaborated by providing key reagents, guidance through execution, and feedback on major experiments. All authors reviewed draft before submission. All authors contributed to the article and approved the submitted version.

FUNDING

Research reported in this publication was supported by the National Heart, Lung, And Blood Institute under Award Number F30HL151136 to VR and National Institute of Allergy and Infectious Diseases of the National Institutes of Health under Award Number R01AI048391 to DH. NP was in part supported by a grant (R01 HL150146) from the National Heart, Lung and Blood Institute.

ACKNOWLEDGMENTS

We would like to thank Dr. Grant R. Kolar from the Saint Louis University Research Microscopy Core for help in obtaining the images from the confocal microscopy experiments.

SUPPLEMENTARY MATERIAL

The Supplementary Material for this article can be found online at: https://www.frontiersin.org/articles/10.3389/fimmu.2021.712678/full#supplementary-material

Supplementary Figure 1 | RhGzmA acts independent of endotoxin. RhGzmA heated at 95°C for 10 min loses inhibitory activity, and RhGzmA passed through Endotrap column retains it. (n=4 in at least two independent experiments. Mean and SEM, paired t test).

Supplementary Figure 2 | RhGzmA-S195A protein is pure and is detectable by western blot. Transient transfection of HEK293T cells expressing plasmid for RhGzmA-S195A yields a pure product without co-purification of other proteins.

Anti-human GzmA binds to RhGzmA-S195A like RhGzmA-WT (**Figure 1A**) with a preference for the homodimer (Non-Reduced) conformation.

Supplementary Figure 3 | Workflow diagram of global proteomic experiment and rationale for protein of interest. PBMC were treated or not with GzmA, and infected or not with BCG for 36 h. Cells were then washed with PBS, lysed with protease and phosphatase inhibitors, and downstream 2D-DIGE workflow. Example of matched spot #431. Melanie software analysis discovered this protein spot that was differentially abundant only in group 4 (BCG-infected, GzmA-treated monocytes) in two volunteers. Each labeled spot was normalized with CyDye2 labeling.

Supplementary Figure 4 | STRING-DB enrichment pathways highlights ER stress response pathway involved in GzmA-mediated mycobacterial control. STRING database enriches protein for their relation to each other by known literature reports. Response to ER stress was upregulated when all the 10 proteins were interrogated.

Supplementary Figure 5 | STRING-DB enrichment pathways highlights ATP synthesis pathway involved in GzmA-mediated mycobacterial control. STRING database enriches protein for their relation to each other by known literature reports. ATP synthesis was found after interrogating proteins with ≥1.5-fold change paired with machine-generated additional nodes.

Supplementary Figure 6 | Example of BiP protein validated by Odyssey platform (quantitative western blot). On the left, protein was normalized using total protein stain, while on the right software analyzed signal and validated upregulation in BCG + GzmA group.

REFERENCES

1. World Health Organization. *Global Tuberculosis Report*. (2019). Available at: https://apps.who.int/iris/bitstream/handle/10665/329368/9789241565714-eng.pdf.
2. Lee A, Xie YL, Barry CE, Chen RY. Current and Future Treatments for Tuberculosis. *BMJ* (2020) 368:m216. doi: 10.1136/bmj.m216
3. Hoft DF, Brown RM, Roodman ST. Bacille Calmette-Guérin Vaccination Enhances Human γδ T Cell Responsiveness to Mycobacteria Suggestive of a Memory-Like Phenotype. *J Immunol* (1998) 161:1045–54.
4. Spencer CT, Abate G, Blazevic A, Hoft DF. Only a Subset of Phosphoantigen-Responsive $\gamma_9\delta_2$ T Cells Mediate Protective Tuberculosis Immunity. *J Immunol* (2008) 181:4471–84. doi: 10.4049/jimmunol.181.7.4471
5. Spencer CT, Abate G, Sakala IG, Xia M, Truscott SM, Eickhoff CS, et al. Granzyme A Produced by $\gamma_9\delta_2$ T Cells Induces Human Macrophages to Inhibit Growth of an Intracellular Pathogen. *PloS Pathog* (2013) 9:e1003119. doi: 10.1371/journal.ppat.1003119
6. Xia M, Hesser DC, De P, Sakala IG, Spencer CT, Kirkwood JS, et al. A Subset of Protective γ9δ2 T Cells Is Activated by Novel Mycobacterial Glycolipid Components. *Infect Immun* (2016) 84:2449–62. doi: 10.1128/IAI.01322-15
7. Arias MA, Jimenez de Bagues MP, Aguilo N, Menao S, Hervas-Stubbs S, de Martino A, et al. Elucidating Sources and Roles of Granzymes A and B During Bacterial Infection and Sepsis. *Cell Rep* (2014) 8:420–9. doi: 10.1016/j.celrep.2014.06.012
8. van Eck JA, Shan L, Meeldijk J, Hack CE, Bovenschen N. A Novel Proinflammatory Role for Granzyme a. *Cell Death Dis* (2017) 8:e2630. doi: 10.1038/cddis.2017.56
9. Campbell RA, Franks Z, Bhatnagar A, Rowley JW, Manne BK, Supiano MA, et al. Granzyme A in Human Platelets Regulates the Synthesis of Proinflammatory Cytokines by Monocytes in Aging. *J Immunol* (2018) 200:295–304. doi: 10.4049/jimmunol.1700885
10. Wensink AC, Kok HM, Meeldijk J, Fermie J, Froelich CJ, Hack CE, et al. And K Differentially Potentiate LPS-Induced Cytokine Response. *Cell Death Discovery* (2016) 2:16084. doi: 10.1038/cddiscovery.2016.84
11. Metkar SS, Menaa C, Pardo J, Wang B, Wallich R, Freudenberg M, et al. Human and Mouse Granzyme A Induce a Proinflammatory Cytokine Response. *Immunity* (2008) 29:720–33. doi: 10.1016/j.immuni.2008.08.014
12. Worku S, Hoft DF. *In Vitro* Measurement of Protective Mycobacterial Immunity: Antigen-Specific Expansion of T Cells Capable of Inhibiting Intracellular Growth of Bacille Calmette-Guerin. *Clin Infect Dis* (2000) 30 (Suppl 3):S257–61. doi: 10.1086/313887
13. Hanna WL, Zhang X, Turbov J, Winkler U, Hudig D, Froelich CJ. Rapid Purification of Cationic Granule Proteases: Application to Human Granzymes. *Protein Expression Purification* (1993) 4:398–404. doi: 10.1006/prep.1993.1052
14. Dotiwala F, Fellay I, Filgueira L, Martinvalet D, Lieberman J, Walch M. A High Yield and Cost-Efficient Expression Aystem of Human Granzymes in Mammalian Cells. *J Vis Exp* (2015) 100:e52911. doi: 10.3791/52911
15. Shevchenko A, Tomas H, Havlis J, Olsen JV, Mann M. In-Gel Digestion for Mass Spectrometric Characterization of Proteins and Proteomes. *Nat Protoc* (2006) 1:2856–60. doi: 10.1038/nprot.2006.468
16. Esin S, Batoni G, Counoupas C, Stringaro A, Brancatisano FL, Colone M, et al. Direct Binding of Human NK Cell Natural Cytotoxicity Receptor NKp44 to the Surfaces of Mycobacteria and Other Bacteria. *Infect Immun* (2008) 76:1719–27. doi: 10.1128/IAI.00870-07
17. Szklarczyk D, Franceschini A, Wyder S, Forslund K, Heller D, Huerta-Cepas J, et al. String v10: Protein-Protein Interaction Networks, Integrated Over the Tree of Life. *Nucleic Acids Res* (2015) 43:D447–52. doi: 10.1093/nar/gku1003
18. Vetten MA, Yah CS, Singh T, Gulumian M. Challenges Facing Sterilization and Depyrogenation of Nanoparticles: Effects on Structural Stability and Biomedical Applications. *Nanomedicine* (2014) 10:1391–9. doi: 10.1016/j.nano.2014.03.017
19. Odake S, Kam CM, Narasimhan L, Poe M, Blake JT, Krahenbuhl O, et al. Human and Murine Cytotoxic T Lymphocyte Serine Proteases: Subsite Mapping With Peptide Thioester Substrates and Inhibition of Enzyme Activity and Cytolysis by Isocoumarins. *Biochemistry* (1991) 30:2217–27. doi: 10.1021/bi00222a027
20. Beresford PJ, Kam CM, Powers JC, Lieberman J. Recombinant Human Granzyme A Binds to Two Putative HLA-Associated Proteins and Cleaves One of Them. *Proc Natl Acad Sci U.S.A.* (1997) 94:9285–90. doi: 10.1073/pnas.94.17.9285
21. Righetti PG, Castagna A, Antonucci F, Piubelli C, Cecconi D, Campostrini N, et al. Critical Survey of Quantitative Proteomics in Two-Dimensional Electrophoretic Approaches. *J Chromatogr A* (2004) 1051:3–17. doi: 10.1016/j.chroma.2004.05.106
22. Perkins DN, Pappin DJ, Creasy DM, Cottrell JS. Probability-Based Protein Identification by Searching Sequence Databases Using Mass Spectrometry Data. *Electrophoresis* (1999) 20:3551–67. doi: 10.1002/(SICI)1522-2683(19991201)20:18<3551::AID-ELPS3551>3.0.CO;2-2
23. Zheng Q, Wang Q, Wang S, Wu J, Gao Q, Liu W. Thiopeptide Antibiotics Exhibit a Dual Mode of Action Against Intracellular Pathogens by Affecting Both Host and Microbe. *Chem Biol* (2015) 22:1002–7. doi: 10.1016/j.chembiol.2015.06.019
24. Paik S, Kim JK, Chung C, Jo EK. Autophagy: A New Strategy for Host-Directed Therapy of Tuberculosis. *Virulence* (2019) 10:448–59. doi: 10.1080/21505594.2018.1536598
25. Rekha RS, Mily A, Sultana T, Haq A, Ahmed S, Mostafa Kamal SM, et al. Immune Responses in the Treatment of Drug-Sensitive Pulmonary Tuberculosis With Phenylbutyrate and Vitamin D3 as Host Directed Therapy. *BMC Infect Dis* (2018) 18:303. doi: 10.1186/s12879-018-3203-9
26. Lim YJ, Yi MH, Choi JA, Lee J, Han JY, Jo SH, et al. Roles of Endoplasmic Reticulum Stress-Mediated Apoptosis in M1-polarized Macrophages During Mycobacterial Infections. *Sci Rep* (2016) 6:37211. doi: 10.1038/srep37211
27. Songane M, Kleinnijenhuis J, Netea MG, van Crevel R. The Role of Autophagy in Host Defence Against *Mycobacterium tuberculosis* Infection. *Tuberculosis (Edinb)* (2012) 92:388–96. doi: 10.1016/j.tube.2012.05.004
28. Humphreys BD, Rice J, Kertesy SB, Dubyak GR. Stress-Activated Protein Kinase/JNK Activation and Apoptotic Induction by the Macrophage P2X7 Nucleotide Receptor. *J Biol Chem* (2000) 275:26792–8. doi: 10.1016/S0021-9258(19)61445-6
29. Lammas DA, Stober C, Harvey CJ, Kendrick N, Panchalingam S, Kumararatne DS. ATP-Induced Killing of Mycobacteria by Human Macrophages Is Mediated by Purinergic P2Z(P2X7) Receptors. *Immunity* (1997) 7:433–44. doi: 10.1016/S1074-7613(00)80364-7
30. Santos AA Jr, Rodrigues-Junior V, Zanin RF, Borges TJ, Bonorino C, Coutinho-Silva R, et al. Implication of Purinergic P2X7 Receptor in *M. tuberculosis* Infection and Host Interaction Mechanisms: A Mouse Model Study. *Immunobiology* (2013) 218:1104–12. doi: 10.1016/j.imbio.2013.03.003

31. Ramachandra L, Qu Y, Wang Y, Lewis CJ, Cobb BA, Takatsu K, et al. *Mycobacterium tuberculosis* Synergizes With ATP to Induce Release of Microvesicles and Exosomes Containing Major Histocompatibility Complex Class II Molecules Capable of Antigen Presentation. *Infect Immun* (2010) 78:5116–25. doi: 10.1128/IAI.01089-09
32. Placido R, Auricchio G, Falzoni S, Battistini L, Colizzi V, Brunetti E, et al. P2X (7) Purinergic Receptors and Extracellular ATP Mediate Apoptosis of Human Monocytes/Macrophages Infected With *Mycobacterium tuberculosis* Reducing the Intracellular Bacterial Viability. *Cell Immunol* (2006) 244:10–8. doi: 10.1016/j.cellimm.2007.02.001
33. Fernando SL, Saunders BM, Sluyter R, Skarratt KK, Goldberg H, Marks GB, et al. A Polymorphism in the P2X7 Gene Increases Susceptibility to Extrapulmonary Tuberculosis. *Am J Respir Crit Care Med* (2007) 175:360–6. doi: 10.1164/rccm.200607-970OC
34. Fernando SL, Saunders BM, Sluyter R, Skarratt KK, Wiley JS, Britton WJ. Gene Dosage Determines the Negative Effects of Polymorphic Alleles of the P2X7 Receptor on Adenosine Triphosphate-Mediated Killing of Mycobacteria by Human Macrophages. *J Infect Dis* (2005) 192:149–55. doi: 10.1086/430622
35. Saunders BM, Fernando SL, Sluyter R, Britton WJ, Wiley JS. A Loss-of-Function Polymorphism in the Human P2X7 Receptor Abolishes ATP-mediated Killing of Mycobacteria. *J Immunol* (2003) 171:5442–6. doi: 10.4049/jimmunol.171.10.5442
36. Peng G, Guo Z, Kiniwa Y, Voo KS, Peng W, Fu T, et al. Toll-Like Receptor 8-Mediated Reversal of $CD4^+$ Regulatory T Cell Function. *Science* (2005) 309:1380–4. doi: 10.1126/science.1113401
37. Uranga S, Marinova D, Martin C, Pardo J, Aguilo N. Granzyme A Is Expressed in Mouse Lungs During *Mycobacterium tuberculosis* Infection But Does Not Contribute to Protection *In Vivo*. *PloS One* (2016) 11: e0153028. doi: 10.1371/journal.pone.0153028
38. Kaiserman D, Bird CH, Sun J, Matthews A, Ung K, Whisstock JC, et al. The Major Human and Mouse Granzymes Are Structurally and Functionally Divergent. *J Cell Biol* (2006) 175:619–30. doi: 10.1083/jcb.200606073
39. Thiery J, Walch M, Jensen DK, Martinvalet D, Lieberman J. Isolation of Cytotoxic T Cell and NK Granules and Purification of Their Effector Proteins. *Curr Protoc Cell Biol Chapter* (2010) 3:Unit3 37. doi: 10.1002/0471143030.cb0337s47
40. Shimizu K, Yamasaki S, Sakurai M, Yumoto N, Ikeda M, Mishima-Tsumagari C, et al. Granzyme A Stimulates pDCs to Promote Adaptive Immunity *Via* Induction of Type I Ifn. *Front Immunol* (2019) 10:1450. doi: 10.3389/fimmu.2019.01450
41. Zhou Z, He H, Wang K, Shi X, Wang Y, Su Y, et al. Granzyme A From Cytotoxic Lymphocytes Cleaves GSDMB to Trigger Pyroptosis in Target Cells. *Science* (2020) 368(6494):eaaz7548. doi: 10.1126/science.aaz7548
42. Schanoski AS, Le TT, Kaiserman D, Rowe C, Prow NA, Barboza DD, et al. Granzyme A in Chikungunya and Other Arboviral Infections. *Front Immunol* (2019) 10:3083. doi: 10.3389/fimmu.2019.03083
43. Chen R, Jiang X, Sun D, Han G, Wang F, Ye M, et al. Glycoproteomics Analysis of Human Liver Tissue by Combination of Multiple Enzyme Digestion and Hydrazide Chemistry. *J Proteome Res* (2009) 8:651–61. doi: 10.1021/pr8008012
44. Bell JK, Goetz DH, Mahrus S, Harris JL, Fletterick RJ, Craik CS. The Oligomeric Structure of Human Granzyme A Is a Determinant of its Extended Substrate Specificity. *Nat Struct Biol* (2003) 10:527–34. doi: 10.1038/nsb944
45. Joeckel LT, Bird PI. Blessing or Curse? Proteomics in Granzyme Research. *Proteomics Clin Appl* (2014) 8:351–81. doi: 10.1002/prca.201300096
46. Van Damme P, Maurer-Stroh S, Hao H, Colaert N, Timmerman E, Eisenhaber F, et al. The Substrate Specificity Profile of Human Granzyme a. *Biol Chem* (2010) 391:983–97. doi: 10.1515/bc.2010.096
47. Plasman K, Maurer-Stroh S, Gevaert K, Van Damme P. Holistic View on the Extended Substrate Specificities of Orthologous Granzymes. *J Proteome Res* (2014) 13:1785–93. doi: 10.1021/pr401104b
48. Radloff J, Heyckendorf J, van der Merwe L, Sanchez Carballo P, Reiling N, Richter E, et al. Mycobacterium Growth Inhibition Assay of Human Alveolar Macrophages as a Correlate of Immune Protection Following *Mycobacterium bovis* Bacille Calmette-Guerin Vaccination. *Front Immunol* (2018) 9:1708. doi: 10.3389/fimmu.2018.01708
49. Bussi C, Gutierrez MG. Mycobacterium Tuberculosis Infection of Host Cells in Space and Time. *FEMS Microbiol Rev* (2019) 43:341–61. doi: 10.1093/femsre/fuz006
50. Cumming BM, Addicott KW, Adamson JH, Steyn AJ. *Mycobacterium tuberculosis* Induces Decelerated Bioenergetic Metabolism in Human Macrophages. *Elife* (2018) 7:e39169. doi: 10.7554/eLife.39169
51. Somashekar BS, Amin AG, Tripathi P, MacKinnon N, Rithner CD, Shanley CA, et al. Metabolomic Signatures in Guinea Pigs Infected With Epidemic-Associated W-Beijing Strains of *Mycobacterium tuberculosis*. *J Proteome Res* (2012) 11:4873–84. doi: 10.1021/pr300345x
52. Sheedy FJ, Divangahi M. Targeting Immunometabolism in Host Defence Against *Mycobacterium tuberculosis*. *Immunology* (2021) 162:145–59. doi: 10.1111/imm.13276

Author Disclaimer: The content is solely the responsibility of the authors and does not necessarily represent the official views of the National Institutes of Health.

Conflict of Interest: The authors declare that the research was conducted in the absence of any commercial or financial relationships that could be construed as a potential conflict of interest.

Publisher's Note: All claims expressed in this article are solely those of the authors and do not necessarily represent those of their affiliated organizations, or those of the publisher, the editors and the reviewers. Any product that may be evaluated in this article, or claim that may be made by its manufacturer, is not guaranteed or endorsed by the publisher.

frontiers in Immunology

MINI REVIEW
published: 06 September 2021
doi: 10.3389/fimmu.2021.728742

Autophagy and Host Defense in Nontuberculous Mycobacterial Infection

Prashanta Silwal[1,2], *In Soo Kim*[1,2] *and Eun-Kyeong Jo*[1,2]*

[1] Department of Microbiology, Chungnam National University College of Medicine, Daejeon, South Korea, [2] Infection Control Convergence Research Center, Chungnam National University College of Medicine, Daejeon, South Korea

Autophagy is critically involved in host defense pathways through targeting and elimination of numerous pathogens *via* autophagic machinery. Nontuberculous mycobacteria (NTMs) are ubiquitous microbes, have become increasingly prevalent, and are emerging as clinically important strains due to drug-resistant issues. Compared to *Mycobacterium tuberculosis* (Mtb), the causal pathogen for human tuberculosis, the roles of autophagy remain largely uncharacterized in the context of a variety of NTM infections. Compelling evidence suggests that host autophagy activation plays an essential role in the enhancement of antimicrobial immune responses and controlling pathological inflammation against various NTM infections. As similar to Mtb, it is believed that NTM bacteria evolve multiple strategies to manipulate and hijack host autophagy pathways. Despite this, we are just beginning to understand the molecular mechanisms underlying the crosstalk between pathogen and the host autophagy system in a battle with NTM bacteria. In this review, we will explore the function of autophagy, which is involved in shaping host–pathogen interaction and disease outcomes during NTM infections. These efforts will lead to the development of autophagy-based host-directed therapeutics against NTM infection.

Keywords: autophagy, nontuberculous mycobacteria, host defense, innate immunity, infection

OPEN ACCESS

Edited by:
Malcolm Scott Duthie, HDT Biotech Corporation, United States

Reviewed by:
Gian Maria Fimia, Sapienza University of Rome, Italy
Meng Rui Lee, National Taiwan University, Taiwan

***Correspondence:**
Eun-Kyeong Jo
hayoungj@cnu.ac.kr

Specialty section:
This article was submitted to Microbial Immunology, a section of the journal Frontiers in Immunology

Received: *22 June 2021*
Accepted: *16 August 2021*
Published: *06 September 2021*

Citation:
Silwal P, Kim IS and Jo E-K (2021) Autophagy and Host Defense in Nontuberculous Mycobacterial Infection. Front. Immunol. 12:728742. doi: 10.3389/fimmu.2021.728742

INTRODUCTION

Around 200 species of nontuberculous mycobacteria (NTMs) have been identified as the causal pathogens of pulmonary and ulcerative human diseases in both immunocompromised and immunocompetent subjects. The *Mycobacterium avium* complex (MAC) group including *M. intracellulare*, *M. avium* subsp. *hominissuis*, and *M. intracellulare* subsp. *chimaera* are the most common causes of NTM pulmonary diseases (NTM-PD), which are more emerging (1–3). *Mycobacteroides abscessus* (Mabc) is another frequently encountered pathogen that causes NTM-PD (4–6). The prevalence and incidence of NTM infections are increasing worldwide, and the risk of antibiotics resistance is often challenging and complex in the treatment of NTM diseases (7). Despite this, we have a lack of understanding of the virulence factors and host–pathogen interactions in terms of NTM infection.

Autophagy is an intracellular process for the maintenance of homeostasis upon stress conditions through lysosomal degradation of cytoplasmic cargos (8, 9). During a variety of infections,

autophagy plays a cell-autonomous and/or a non-autonomous function to protect the hosts from infectious hazards and harmful inflammation (10). Recent studies highlighted multiple layered crosstalks of autophagy with several important processes, including innate immunity, immunometabolism, and mitochondrial function, to prevent harmful inflammation and to augment host protective function (10, 11). Therefore, autophagy-activating strategies are becoming promising not only for the development of host-directed therapeutics but also for the design of potential vaccines against mycobacterial infection (3). However, intracellular pathogens are able to develop sophisticated strategies of exploitation and subvert autophagy in order to enhance their survival in the host cells (12–14). Compared with *Mycobacterium tuberculosis* (Mtb), an extensively studied pathogen, much less is known about the function of autophagy pathways against NTM infection. In addition, the individual picture of NTM interaction with host autophagy machinery and how each NTM escapes from host autophagic responses remain uncharacterized. In this review, we focus on the recent progress of our understanding of autophagy functions in the context of host defense against NTM infections.

OVERVIEW OF HOST–PATHOGEN INTERACTION DURING NTM INFECTIONS

NTM bacteria are diverse species that grow in the environment and are opportunistic pathogens that cause a wide spectrum of diseases in humans. The prevalence, morbidity, and mortality of NTM diseases are increasing worldwide, particularly in developed countries, associated with several predisposing factors such as aging, immunosuppressive therapy or conditions, and relevant comorbidity with chronic pulmonary diseases (15–21). NTM-PD is common in immunocompetent persons, whereas immunocompromised patients primarily suffer from disseminated diseases (16, 18). The most important human pathogens causing NTM-PD include MAC, Mabc, and *Mycobacterium kansasii*. In addition, the infections caused by NTMs also vary by geographic distribution (22, 23). NTM-PD also can be organized into clinical phenotypes (24). For example, "Lady Windermere's syndrome" usually occurs in elderly females with a fibronodular radiographic pattern of NTM-PD (25, 26). Besides NTM-PD, NTM causes extrapulmonary diseases, including skin and soft-tissue infections, musculoskeletal infections, lymphadenitis, and disseminated disease (27, 28). Importantly, NTM treatment is often toxic and difficult because of intrinsic multidrug resistance, limited treatment options, and lengthy duration (24, 29, 30).

After infection, NTMs are found in different types of cells but extensively studied in macrophages as the primary host cells where a vast number of NTMs are able to arrest phagosomal maturation and persist, form biofilms, and even replicate (31–34). Thus, innate immune signaling activated by numerous pathogen-associated molecular patterns may contribute to host immune defense against NTM infection (32). Although the exact nature of host protective factors is uncertain, it has been long thought that T helper 1 (Th1) responses induced by interferon (IFN)-γ and interleukin (IL)-12 are crucial in the defense against NTM infection (31, 35). In addition, several genetic factors, including cystic fibrosis transmembrane conductance regulator mutations, vitamin D receptors, and polymorphisms of solute carrier 11A1 (or natural resistance-associated macrophage protein 1), are associated with NTM-PD (35, 36), although these are not specific to NTM infections. Moreover, anti-tumor necrosis factor (TNF)-α therapy during autoimmune diseases may lead to the increased risk of NTM diseases as well as tuberculosis, suggesting that TNF-α is also crucial for host defense against NTM infection (37, 38). Recent studies highlight the function of autophagy and apoptosis as another key factor for controlling mycobacteria (1, 3). In this review, we primarily discuss the current understanding of host cell autophagy in terms of host defense and controlling immunopathology during NTM infection.

OVERVIEW OF AUTOPHAGY IN TERMS OF MYCOBACTERIAL INFECTIONS

Although this session covers a general understanding of the autophagy/xenophagy pathways and their interaction with intracellular Mtb, much uncertainty remains on the specific function of autophagy in the context of each NTM infection. In Mtb infection, there are at least three types of autophagy pathways participating in the antibacterial host defense (39). Xenophagy involves the cytoplasmic escape of Mtb through the ESAT-6 secretion (ESX)-1 system, thereby being subjected to ubiquitination system and recognized by selective cargo receptors, i.e., p62 and NDP52, for lysosomal degradation (40). Although the ESX-1 system is required for early autophagy induction, it functions in a late inhibition of autophagy flux in human primary dendritic cells (41). Xenophagy involves the core autophagy-related genes (Atg), including ULK1, Atg14, Beclin-1, and Atg5-12, which are important in the initiation of autophagosome formation and elongation step of autophagy (42). Another type of noncanonical autophagy, LC3-associated phagocytosis (LAP), involves Rubicon, NADPH oxidase 2, Beclin-1, and Atg5-12, which is also crucial for combating intracellular Mtb, which resists this process through its own effector, the LCP protein CpsA (43). In recent years, we have made considerable progress in revealing the signaling pathways that regulate xenophagy against Mtb infection. The cytosolic DNA sensor cyclic GMP-AMP synthase (cGAS)-STING signaling pathway is critically required to recognize cytosolic Mtb DNA to induce autophagy (44). A recent study showed that xenophagy could be triggered by the direct ubiquitination of Mtb surface protein Rv1468c, which contains a eukaryotic-like ubiquitin-associated domain (45). In addition, xenophagic clearance of Mtb is mediated by various E3 ubiquitin ligases, including PARK2 (46), Smurf1 *via* K48-linked ubiquitination (47), and TRIM16 through interaction with galectin-3 (48). Moreover, the lysosomal damage recognized by galectin-8 and -9 signaling promotes autophagy and antimicrobial responses

against Mtb infection (49). However, it is largely unclear whether these or other signaling pathways are involved in regulating autophagy defense against NTM bacteria, which may operate different strategies compared to Mtb to survive within host cells.

So far, numerous autophagy-activating agents/drugs have been reported to enhance the activation of autophagy and phagosomal maturation through colocalization of bacterial phagosomes with autophagosomes/lysosomes (50–52). Accumulating evidence suggests that a wide range of antimicrobial strategies can be applied to promote antimicrobial activities for infectious diseases through autophagy modulation (50–53). These strategies include multiple biological pathways such as targeting selective autophagy through adaptors, regulation of posttranslational modification of key proteins, modulation of inflammatory responses, etc. (10, 52, 53).

Earlier studies showed that both *Mycolicibacterium smegmatis* and *Mycolicibacterium fortuitum* exhibit strong autophagy induction, whereas *M. kansasii* induces less induction of autophagy in macrophages (54). In addition, autophagy induced by *M. smegmatis* is independent of mTOR activity, and lipid components of *M. smegmatis* activate mTOR signaling (54). Because mTOR inhibition by rapamycin results in decreasing intracellular bacterial burden (55), simultaneous activation of both autophagy and mTOR signaling might be another immune escaping strategy manipulated by bacteria. Mabc smooth (Mabc S) variant exhibits pathogenesis mainly through the suppression of phagosomal maturation and induction of phagosome-cytosol communications. However, the Mabc rough (Mabc R) variant enhances autophagy and apoptosis and can form extracellular cords, thereby evading phagocytosis (56, 57). However, it remains largely unknown how various NTM microbes induce or suppress host cell autophagy in different tissues/cells and whether it exerts to modify host defensive system during infection. In the next session, we discuss the recent advances and perspectives on the roles of host cell autophagy in the context of infection with each NTM pathogen and explore in brief the potential autophagy-activating strategies against NTM infections.

AUTOPHAGY IN NTM INFECTIONS

MAC and Autophagy

M. avium complex (MAC), among other NTMs, is the most commonly isolated species in the world (58). *M. avium* infection leads to the increase in numerous microRNAs, including miR-125a-5p that is required for autophagy activation and suppression of intracellular survival of *M. avium* in macrophages (59). MiR-125a-5p-mediated autophagy activation is induced by targeting of signal transducers and activators of transcription 3 (STAT3) in macrophages (59).

Alpha-1-antitrypsin (AAT) deficiency is closely related to the increased risk of emphysema and bronchiectasis (60), which are important predisposing factors for NTM-PD (36). Previous studies reported that AAT treatment results in the control of intracellular growth of *M. abscessus* and *M. intracellulare* in human macrophages (61, 62). Interestingly, human primary monocyte-derived macrophage culture with plasma obtained from patients with post-AAT infusion significantly increases the autophagosome formation during *M. intracellulare* infection (61). These studies may provide potential clinical significance because AAT-based, autophagy-related, adjunctive therapy could be beneficial for treatment of NTM-PD patients who have underlying diseases such as bronchiectasis along with AAT deficiency.

M. abscessus and Autophagy

Mabc is the rapidly growing NTM strain and unique in the characteristics for survival inside macrophages (56). Mabc is classified into two morphotypes, i.e., S and R forms, depending on the presence of glycopeptidolipids (GPL) (56, 63–65). Mabc ESX-4 locus that encodes an ESX-4 type VII secretion system is crucial for the growth and survival within host cells through blockade of phagosomal acidification and the ability to damage phagosomes (66).

Mabc S variants reside within more intact phagosomes and are surrounded by an electron translucent zone (ETZ), whereas Mabc R variants possess a loose phagosomal membrane and lack ETZ (63). Thus, it is thought that Mabc S strains are capable of successful phagosome-cytosol communication and are more resistant to phagosomal acidification. In addition, the nature of Mabc S to favor phagosome-cytosol communication is associated with less induction of autophagy and apoptosis than those by Mabc R morphotype (63). In accordance with this, Mabc S infection of macrophages upregulates the LC3-II and p62 levels in a time-dependent manner, suggesting that Mabc S inhibits autophagic flux (67). Earlier studies suggest that the use of antibiotics such as azithromycin aggravates the impairment of autophagy during Mabc infection, thus predisposing patients with cystic fibrosis to NTM infections. Mechanistically, long-term use of macrolide drug azithromycin results in an inhibition of intracellular clearance of Mabc in human macrophages, at least due to defective autophagy and prevention of lysosomal acidification of NTM bacteria (68). Furthermore, the virulent clinical strain UC22 of Mabc, the R variant, robustly inhibits autophagic flux, thereby escaping from the clearance by host defense (69).

However, recent reports showed that treatment of the autophagy inhibitor and activator (chloroquine and rapamycin, respectively) does not affect antimycobacterial effects against Mabc R and S infection in neutrophils (70). These data suggest that autophagy is not critically involved in neutrophil antimicrobial pathways against Mabc infection. Future studies are warranted to discover the exact roles and mechanisms by which autophagy activation regulates the virulence or protective responses in different cell types and tissues during infection with Mabc and their related strains.

Mycobacterium marinum and Autophagy

M. marinum is a natural pathogen of ectotherms to cause systemic tuberculosis-like disease and is widely used as a model organism of Mtb (71–73). *M. marinum* usually grows at 25 to 35°C and causes extrapulmonary infections at cooler surfaces like skin in humans (71, 73). The genomes of Mtb and *M. marinum* are closely related at a high degree of homology and share amino acid identity averages of 85% (72, 74).

A microscopic imaging approach through zebrafish injection of mycobacteria has lighted on tracking an *in vivo* autophagic process related to Mtb and NTM infectious diseases (75). Earlier studies reported that *M. marinum*, a model NTM for tuberculosis-like disease in zebrafish, can induce autophagosome formation *via* the ESX-1 secretion system but simultaneously actively block the autophagic flux to escape from xenophagic degradation during infection (76, 77). In *M. marinum*–infected macrophages, phagosomal escape and bacterial ubiquitination are followed by targeting the lysosome-like organelle through the autophagy-independent pathway, which does not involve atg5 or LC3 association (78). Another study showed that *M. marinum* mimG, an orthologue of Mtb Rv3242c that contains phosphoribosyltransferase, enhances intracellular bacterial survival and virulence in zebrafish. *M. marinum* mimG-induced pathogenesis is at least partly mediated due to the inhibition of autophagy in macrophages (79). Future studies are warranted to identify other bacterial effectors that alter host cell autophagy to exert immune evasion during infection. These efforts will facilitate the presentation of attractive targets for potential host-directed drug therapies during NTM infection.

M. marinum is targeted by selective autophagy through autophagic adaptors optineurin and p62/SQSTM1 for bacterial clearance (80). DNA damage regulated autophagy modulator 1 (DRAM1), a critical regulator of autophagy and cell death, is activated by Toll-like receptor signaling and plays an essential function in selective autophagic defense against *M. marinum* infection (81). The selective autophagy activation by DRAM1 is mediated through cytosolic DNA sensor STING and the adaptor p62/SQSTM1 (81). Indeed, DRAM1 functions through autophagic targeting and phagosomal maturation of *M. marinum*, thereby restricting bacteria during the early phase of infection. Dissemination of *M. marinum* infection is associated with defective autophagy and gasdermin Eb-mediated pyroptotic cell death in dram1 mutant zebrafish larvae (82). However, it remains to be characterized whether DRAM1 plays a crucial role in host defense to other NTM strains through activation of autophagy and prevention of cell death.

Moreover, *M. marinum* infection of microglial cells induces autophagy that can limit the intracellular replication of *M. marinum* (83). Notably, rapamycin-induced autophagy activation inhibits the intracellular survival of *M. marinum*, suggesting the role of autophagy in microglial defense against *M. marinum* (83). Because *M. marinum* is genetically closely related to Mtb in a high degree of homology (74), autophagy activation may provide a new strategy for the treatment of tubercular meningitis.

Drosophila melanogaster is another model host for *M. marinum* and is widely used for innate immune defense and xenophagy during mycobacterial infection (46, 84–86). In the Drosophila model, autophagy-related gene *Atg2* is required to inhibit intracellular mycobacterial growth and lipid droplets in phagocytes without changing bulk autophagy during *M. marinum* infection (85). By using atg7 mutant Drosophila, autophagy activation *in vivo* was found to contribute to antibiotic-mediated antimicrobial effects during *M. marinum* infection (87). Using unicellular eukaryote *Dictyostelium discoideum*, another model host for *M. marinum*, transcriptome analysis identified that *M. marinum* induces transcriptional activation of autophagy genes and endosomal sorting complexes required for transport (ESCRT) (88). Another study showed that the *Mycobacterium*-containing vacuole (MCV) damage induced by the ESX-1 system of *M. marinum* is recognized and repaired by the ESCRT component Tsg101, thereby leading to the containment of *M. marinum* in an intact compartment (89). In this process, autophagy and ESCRT pathways function in separate membrane repair processes in parallel for the restriction of mycobacterial growth in the cytosols during *M. marinum* infection (89). However, it is yet to be elucidated how ESCRT components are recruited to vacuolar damage sites in *D. discoideum* and whether ubiquitination system is involved in the ESCRT recruitment for membrane repair.

M. smegmatis and Autophagy

Nonpathogenic *M. smegmatis* is well known to induce autophagy in macrophages through the upregulation of several autophagy-related genes and TLR2 activation. However, autophagy targeting of *M. smegmatis* is not dependent on membrane damage and ubiquitination of bacteria (90). In addition, a high dose of rapamycin treatment leads to antimicrobial activities to *M. smegmatis*, presumably due to autophagy-independent modality, because bacterial growth is also inhibited in autophagy-deficient macrophages (91). Thus, there might be an alternative mechanism by which the autophagy pathway is functional in the recognition of mycobacteria to enhance phagosomal maturation and antimicrobial responses during infection.

M. smegmatis infection of PC12 and C17.2 cells induces neural differentiation through an autophagy-independent pathway *via* IFN-γ and PI3K-Akt signaling pathways (92). Vitamin D3, known as a protective factor for human tuberculosis, increases intracellular *M. smegmatis* clearance and restricts host cell cytotoxicity (93). Because vitamin D3 induces the activation of antibacterial autophagy and cathelicidin to inhibit intracellular Mtb survival (94), vitamin D3-mediated *M. smegmatis* clearance is presumably mediated through autophagy and antimicrobial proteins. Future studies are warranted to clarify the roles of autophagy in antimicrobial host defense against *M. smegmatis* infection.

Mycobacterium ulcerans and Autophagy

Buruli ulcer, the third most common mycobacterial disease and destructive necrotizing skin infection caused by *M. ulcerans*, is common in West and Central Africa and becoming increasingly common in southeastern Australia (95, 96). Several studies have highlighted the genetic susceptibility of *M. ulcerans* infection in the context of autophagy. Recent genetic studies showed the protective effect of the minor allele G of ATG16L1 (rs2241880) from the ulcer phenotype in Buruli ulcer (97, 98). In addition, several autophagy genes, including PRKN, NOD2, and ATG16L1, are related to susceptibility to severe Buruli ulcer (98). Importantly, the missense variant T300A (rs2241880) of the *ATG16L1* gene is associated with the development of Buruli ulcer (98). A mechanistic study showed that knock-in mice (*Atg16L1*^{T316A})

harboring the human ATG16L1 variant (T300A) functions in a decrease in bacterial autophagy, thereby protective to *Citrobacter rodentium* infection through type I interferon response, similar to hypomorphic ATG16L1 mice (99). However, it is still unclear whether a certain allele of ATG16L1 (T300A) functions in the suppression of autophagy against *M. ulcerans* to confer host protection against Buruli ulcer.

A proteomics study showed that mycolactone, the potent exotoxin of *M. ulcerans*, significantly increases autophagosome formation and protein ubiquitination (100). These data strongly suggest that toxin affects host cell homeostasis, although the molecular mechanisms underlying these phenomena have not been elucidated. A genome-wide association study (GWAS) identified two variants in LncRNA genes (rs9814705 and rs76647377) in association with Buruli ulcer (97), suggesting the potential roles for LncRNAs in the pathogenesis of Buruli ulcer. Given the findings that the expression of long intergenic noncoding RNA erythroid prosurvival (lincRNA-EPS) is downregulated in primary monocytes from patients with active pulmonary tuberculosis and silencing of lincRNA-EPS enhances autophagy in macrophages during bacillus Calmette-Guérin (BCG) infection (101, 102), the LncRNA variant may play a role in the autophagy activation to modulate antimicrobial responses during Buruli ulcer further. Future studies are warranted to determine the exact role of autophagy and its related function of the identified variants of LncRNAs in Buruli ulcer. Such an effort will facilitate the development of new strategies against Buruli ulcer.

Mycolicibacter terrae and Autophagy

M. terrae is a member of the *M. terrae* complex and slow-growing NTM and can cause antibiotic-resistant debilitating diseases, including tenosynovitis and pulmonary disease (103). Interestingly, IL-17A and IL-17F are capable of activating autophagosome formation and autophagic flux, thereby restricting the intracellular growth of *M. terrae* in RAW264.7 cells (104). The autophagic responses during several NTM infections are summarized in **Table 1**.

A Comparative Analysis of Autophagy Among NTMs

Because different mycobacterial species have distinct virulence mechanisms for their pathogenesis, numerous NTMs and Mtb may possess differential activities and strategies to regulate host autophagy. Although there remain many gaps in the knowledge to address differential regulation of various NTMs as well as Mtb in the host defensive pathways, a recent finding reported differential immune and autophagic responses induced by Mtb and four different NTMs (Mabc, *M. smegmatis*, *M. intracellulare*, and *M. avium*) in human THP-1 cells (105). Compared to the autophagy-inducing activities by *M. smegmatis* and Mabc, the levels of autophagy induction are less in the infection with MAC

TABLE 1 | Bacterial virulent and host defense responses in autophagy process during NTM infections.

Factors	Origin	Autophagic response	Mechanism	Study model	Ref.
***Mycobacterium avium* complex**					
miR-125a-5p	Host	↑	Autophagy induction by MiR-125a-5p *via* repression of STAT3 expression	THP-1 cells	(59)
Mycobacteroides abscessus					
Smooth type	Bacteria	Weak	Prevention of phagosomal maturation and acidification	BMDMs, THP-1 cells	(63)
Smooth type	Bacteria	↓	Upregulation of LC3-II and p62 level to inhibit autophagic flux	BMDMs	(67)
Rough type	Bacteria	Strong	Escapes from phagocytosis and induces more autophagy than S morphotype	BMDMs, THP-1 cells	(63)
UC22 (R variant)	Bacteria	↓	Increased autophagy response but inhibition of autophagic flux	RAW cells, BMDMs	(69)
Mycobacterium marinum					
ESX-1	Bacteria	↓	ESX-1 mediated induction of early autophagic responses but blockage of autophagic flux	*Dictyostelium discoideum*	(76)
Rv3242c	Bacteria	↓	Rv3242c-mediated inhibition of LC3-II and induction of p62 through MAPK/ERK	RAW264.7, THP-1 cells	(79)
DRAM1	Host	↑	Dram1-mediated p62-dependent autophagy flux and lysosomal maturation	Zebrafish, human macrophages	(81)
ATG2	Host	↑	Activation of JAK-STAT signaling leading to inhibition of Atg2 expression and formation of lipid droplets	Drosophila	(85)
ESCRT	Host	↑	Recruitment of Vps32 and Atg8 in MCVs for membrane repair	Drosophila	(89)
Mycolicibacterium smegmatis					
TLR2	Host	↑	TLR2 mediated activation of autophagy	THP-1 cells	(90)
Mycobacterium ulcerans					
Mycolactone	Bacteria	↓	Inhibition of autophagosome–lysosome fusion	L929 cells	(100)
Mycolicibacter terrae					
IL-17A and IL-17F	Host	↑	Increase in number and size of autophagosome	RAW264.7 cells	(104)

BMDM, bone marrow-derived macrophage; DRAM1, DNA damage regulated autophagy modulator 1; ESCRT, endosomal sorting complexes required for transport; ESX-1, early secreted antigenic target of 6 kDa (ESAT-6) secretion system 1; JAK-STAT, Janus kinases (JAKs), signal transducer and activator of transcription proteins; LC3, microtubule-associated protein 1 light chain 3; MAPK/ERK, mitogen-activated protein kinase/extracellular-signal-regulated kinase; MCV, Mycobacterium-containing vacuole; STAT3, signal transducer and activator of transcription 3; TLR2, Toll-like receptor 2; Vps32, vacuolar protein sorting protein 32; ↑, increase/activation; ↓, decrease/inhibition.

and Mtb (105). Another study in RAW264.7 cells also has shown that autophagy induction by mycobacteria differs in magnitude among several species, including Mtb, BCG, and NTM (*M. smegmatis*, *M. foruitum*, and *M. kansasii*); and autophagy induction was minimal with the *M. kansasii* infection (54). Although a study suggested that long incubation of *M. kansasii* with Rapamycin could reduce the growth rate of bacteria (91), the exact role of autophagy in the regulation of *M. kansasii* infection is yet to be identified. A better understanding of the differential activities that regulate host autophagy pathways could offer a new insight for controlling a variety of mycobacterial infections.

AUTOPHAGY-ACTIVATING STRATEGIES FOR ANTIMICROBIAL EFFECTS AGAINST NTM INFECTIONS

Several reports have highlighted the antimicrobial roles of autophagy-activating agents against NTM. Recent studies showed that trehalose treatment results in the activation of the xenophagic flux to inhibit intracellular bacterial survival of various NTM strains as well as Mtb. Importantly, trehalose-mediated autophagy promotes the eradication of intracellular Mtb or NTMs, even in the status with co-infection with human immunodeficiency virus (HIV) (106). Trehalose-induced autophagy is mediated through the activation of TFEB, the key transcriptional factor for autophagy and lysosomal biogenesis (107), in macrophages (106). In addition, the autophagy induction by trehalose is dependent on lysosomal calcium release *via* MCOLN1 (106). These findings are corroborative with our recent data showing that the activation of nuclear receptor peroxisome proliferator-activated receptor α (PPARα) by gemfibrozil suppresses *in vitro* and *in vivo* bacterial growth of Mabc through TFEB activation (67). During Mabc infection, PPARα activation promotes nuclear translocation of TFEB and colocalization of bacterial phagosomes with lysosomes in macrophages (67).

Autophagy activation by vitamin D treatment induces autophagy to facilitate antimicrobial function through CAMP production in macrophages infected with *M. marinum* (108). In addition, the blockade of glycolysis by inhibitors such as 2-deoxyglucose (2-DG) prior to infection inhibits the proliferation of *M. marinum* in macrophages and zebrafishes (109). Thiostrepton (TSR) is an antibiotic harboring a quinaldic acid (QA) moiety that targets bacterial ribosome and induces ER stress-mediated autophagy to promote antimicrobial host defense during *M. marinum* infection (110). Similarly, rifampicin and amikacin also have antimicrobial activities against *M. marinum* in *Drosophila melanogaster* through the activation of the autophagic flux (87). Ohmyungsamycins, the cyclic peptides harboring autophagy activity, have antimicrobial activities against *M. marinum* in *D. melanogaster* (84). Moreover, autophagy activation by rapamycin exhibits a defense against *M. marinum* in microglial cells (83). These data strongly suggest that several antibiotics exhibit both direct antimicrobial and indirect host-targeting ability to enhance their effects to eliminate intracellular NTM strains. Future studies are warranted to clarify the dual mode of actions mediated by several drugs that possess potential host defense activities.

Through selective targeting intracellular pathogens, the autophagy pathway functions in the activation of antimicrobial responses, regulation of immunologic balance, and anti-inflammatory effects during infection (42, 111). Recent studies showed that the NTM-PD patients with Mabc or *Mycobacteroides abscessus* subsp. *massiliense* have pathological inflammatory responses in their peripheral blood mononuclear cells (112). In addition, resveratrol, an agonist of sirtuin 1 and 3 (113, 114), exerts a beneficial role through controlling excessive inflammation and mitochondrial homeostasis upon Mabc infection *in vivo* (115). Combined with resveratrol-induced antibacterial autophagy effects during Mtb infection (116), these data strongly suggest that autophagy-activating agents provide potential candidates for host-directed therapeutics during NTM infection. Antimicrobial responses of autophagy-activating exogenous agents against various NTM infections are summarized in **Table 2**.

Additionally, BCG vaccination currently in use for immunization against Mtb could be exploited against NTM (117, 118). However, BCG vaccine interference by NTM mycobacterial species is thought to be a potential cause of its reduced efficacy against Mtb (119). In addition, several vaccine candidates with autophagy activation as a major element have been tested against Mtb in animal models (120, 121), but there are currently no recommended vaccine protocols established to study the vaccine efficacy against NTM infections. Using autophagy-related strategies

TABLE 2 | Antimicrobial and autophagic responses of exogenous agents against various NTM infections.

Agents	NTM	Mechanism	Study model	Ref.
Trehalose	*M. avium, M. fortuitum*	Induction of xenophagic flux *via* lysosomal Ca^{2+} release and TFEB activation	PBMCs, U937 and U1.1 cells	(106)
Gemfibrozil	*M. abscessus*	Increase in TFEB nuclear translocation	BMDMs, MDMs	(67)
Resveratrol	*M. abscessus*	Inhibition of inflammation by controlling mitochondrial ROS	Mice, BMDMs, Zebrafish	(115)
Vitamin D	*M. marinum*	Increased CAMP production and induction of autophagolysosome	THP-1, U927 and MEF cells	(108)
2-Deoxy-D-glucose	*M. marinum*	Increased autophagolysosome development and LC3-II	RAW264.7 cells, Zebrafish	(109)
Thiostrepton	*M. marinum*	Activation of PERK/eIF2a pathway mediated autophagy	RAW264.7 cells	(110)
Ohmyungsamycins	*M. marinum*	Activation of autophagy *via* AMPK pathway	Drosophila	(84)
Rifampicin, Amikacin	*M. marinum*	Increased colocalization of LC3 with lysosome	Drosophila	(87)
Rapamycin	*M. marinum*	Increased LC3 puncta formation	BV2 cells, Zebrafish	(83)

AMPK, 5'-adenosine monophosphate (AMP)-activated protein kinase; BMDM, bone marrow-derived macrophages; CAMP, cathelicidin antimicrobial peptide; eIF2a, eukaryotic translation initiation factor 2A; LC3, microtubule-associated protein 1 light chain 3; MDM, monocyte-derived macrophages; PBMC, peripheral blood mononuclear cell; PERK, protein kinase R-like endoplasmic reticulum kinase; ROS, reactive oxygen species; TFEB, transcription factor EB.

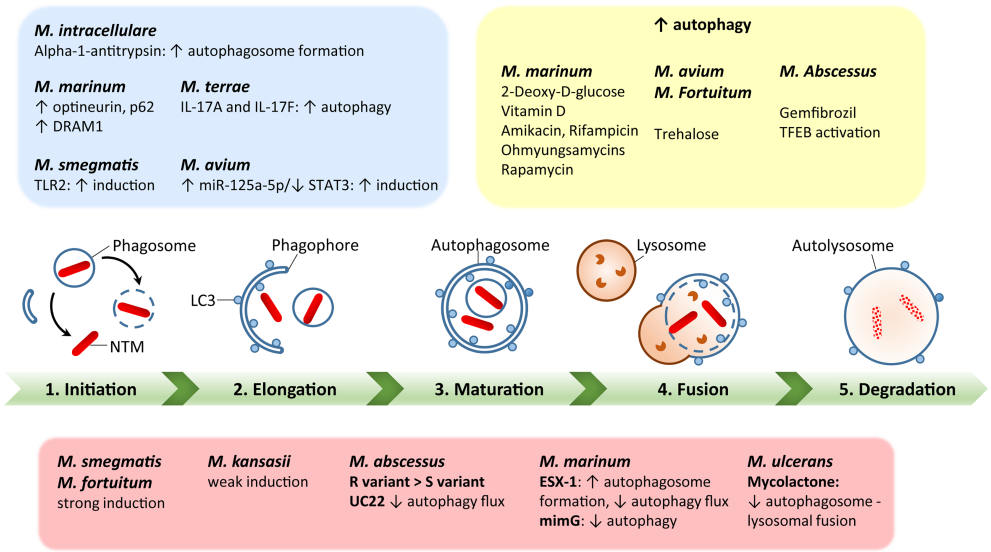

FIGURE 1 | A schematic diagram of autophagy regulation by each nontuberculous mycobacterial infection. Green bar depicts the steps of autophagy, including initiation, elongation, maturation, fusion with lysosomes, and degradation. The red box summarizes each NTM response to regulate host autophagy processes. The blue box represents host factors to regulate autophagy during NTM infection. The yellow box shows the effects of autophagy-regulating agents for modulation of autophagy in the context of each NTM infection. The detailed mechanisms have been described in the text.

to develop effective vaccinations against NTM could be a huge advance in the fight against NTM infections (3). A schematic representation of the autophagy process during several NTM infections is shown in **Figure 1**.

CONCLUSION

Compared with the autophagy activation against Mtb infection, it remains to be largely uncharacterized in the roles for host autophagy/xenophagy in the context of infection caused by a variety of NTM bacteria. However, autophagy modulation seems to be a potential pathway to provide novel adjunctive therapeutics based on autophagy against various NTM infections. Future studies are warranted to understand differential roles for autophagy to regulate a complex layer of host–pathogen interaction during NTM infection.

Current knowledge is very limited on how various NTMs circumvent the autophagy process during infection. Future studies are warranted to elucidate the mechanisms by which each NTM strain induces and/or manipulates the host autophagy signaling pathway during pulmonary or extrapulmonary manifestation. Such an effort to understand autophagy functions upon NTM infection will advance the development of potential host-directed therapeutics against NTM infection.

AUTHOR CONTRIBUTIONS

E-KJ: designed. E-KJ, PS, and ISK: wrote and reviewed the manuscript. PS: summarized the tables. ISK: drew the figure. All authors contributed to the article and approved the submitted version.

FUNDING

This work was supported by the National Research Foundation of Korea (NRF) grant funded by the Korea government (MSIT) (No. 2017R1A5A2015385) and a grant of the Korea Health Technology R&D Project through the Korea Health Industry Development Institute (KHIDI), funded by the Ministry of Health & Welfare, Republic of Korea (HI 20C0017).

ACKNOWLEDGMENTS

We are indebted to current and past members of our Medical Research Center (*i*-MRC) for discussions and investigations that contributed to this article. We apologize to colleagues whose work and publications could not be cited due to space limitations.

REFERENCES

1. Kilinc G, Saris A, Ottenhoff THM, Haks MC. Host-Directed Therapy to Combat Mycobacterial Infections. *Immunol Rev* (2021) 301(1):62–83. doi: 10.1111/imr.12951
2. Crilly NP, Ayeh SK, Karakousis PC. The New Frontier of Host-Directed Therapies for Mycobacterium Avium Complex. *Front Immunol* (2020) 11:623119. doi: 10.3389/fimmu.2020.623119
3. Strong EJ, Lee S. Targeting Autophagy as a Strategy for Developing New Vaccines and Host-Directed Therapeutics Against Mycobacteria. *Front Microbiol* (2020) 11:614313. doi: 10.3389/fmicb.2020.614313

4. Johansen MD, Herrmann JL, Kremer L. Non-Tuberculous Mycobacteria and the Rise of Mycobacterium Abscessus. *Nat Rev Microbiol* (2020) 18 (7):392–407. doi: 10.1038/s41579-020-0331-1
5. van Ingen J, Wagner D, Gallagher J, Morimoto K, Lange C, Haworth CS, et al. Poor Adherence to Management Guidelines in Nontuberculous Mycobacterial Pulmonary Diseases. *Eur Respir J* (2017) 49(2):1601855. doi: 10.1183/13993003.01855-2016
6. Park IK, Olivier KN. Nontuberculous Mycobacteria in Cystic Fibrosis and non-Cystic Fibrosis Bronchiectasis. *Semin Respir Crit Care Med* (2015) 36 (2):217–24. doi: 10.1055/s-0035-1546751
7. Falkinham JO3rd. Challenges of NTM Drug Development. *Front Microbiol* (2018) 9:1613. doi: 10.3389/fmicb.2018.01613
8. Deretic V, Saitoh T, Akira S. Autophagy in Infection, Inflammation and Immunity. *Nat Rev Immunol* (2013) 13(10):722–37. doi: 10.1038/nri3532
9. Mizushima N, Levine B. Autophagy in Mammalian Development and Differentiation. *Nat Cell Biol* (2010) 12(9):823–30. doi: 10.1038/ncb0910-823
10. Deretic V. Autophagy in Inflammation, Infection, and Immunometabolism. *Immunity* (2021) 54(3):437–53. doi: 10.1016/j.immuni.2021.01.018
11. Rao L, Eissa NT. Autophagy in Pulmonary Innate Immunity. *J Innate Immun* (2020) 12(1):21–30. doi: 10.1159/000497414
12. Pareja ME, Colombo MI. Autophagic Clearance of Bacterial Pathogens: Molecular Recognition of Intracellular Microorganisms. *Front Cell Infect Microbiol* (2013) 3:54. doi: 10.3389/fcimb.2013.00054
13. Jo EK, Yuk JM, Shin DM, Sasakawa C. Roles of Autophagy in Elimination of Intracellular Bacterial Pathogens. *Front Immunol* (2013) 4:97. doi: 10.3389/fimmu.2013.00097
14. Ogawa M, Yoshikawa Y, Mimuro H, Hain T, Chakraborty T, Sasakawa C. Autophagy Targeting of *Listeria Monocytogenes* and the Bacterial Countermeasure. *Autophagy* (2011) 7(3):310–4. doi: 10.4161/auto.7.3.14581
15. Pereira AC, Ramos B, Reis AC, Cunha MV. Non-Tuberculous Mycobacteria: Molecular and Physiological Bases of Virulence and Adaptation to Ecological Niches. *Microorganisms* (2020) 8(9):1380. doi: 10.3390/microorganisms8091380
16. Swenson C, Zerbe CS, Fennelly K. Host Variability in NTM Disease: Implications for Research Needs. *Front Microbiol* (2018) 9:2901. doi: 10.3389/fmicb.2018.02901
17. Jeon D. Infection Source and Epidemiology of Nontuberculous Mycobacterial Lung Disease. *Tuberc Respir Dis (Seoul)* (2019) 82(2):94–101. doi: 10.4046/trd.2018.0026
18. Koh WJ. Nontuberculous Mycobacteria-Overview. *Microbiol Spectr* (2017) 5 (1). doi: 10.1128/microbiolspec.TNMI7-0024-2016
19. Wassilew N, Hoffmann H, Andrejak C, Lange C. Pulmonary Disease Caused by Non-Tuberculous Mycobacteria. *Respiration* (2016) 91(5):386–402. doi: 10.1159/000445906
20. Kwon YS, Koh WJ. Diagnosis and Treatment of Nontuberculous Mycobacterial Lung Disease. *J Korean Med Sci* (2016) 31(5):649–59. doi: 10.3346/jkms.2016.31.5.649
21. Honda JR, Knight V, Chan ED. Pathogenesis and Risk Factors for Nontuberculous Mycobacterial Lung Disease. *Clin Chest Med* (2015) 36 (1):1–11. doi: 10.1016/j.ccm.2014.10.001
22. Davidson RM. A Closer Look at the Genomic Variation of Geographically Diverse *Mycobacterium Abscessus* Clones That Cause Human Infection and Disease. *Front Microbiol* (2018) 9:2988. doi: 10.3389/fmicb.2018.02988
23. Zweijpfenning SMH, Ingen JV, Hoefsloot W. Geographic Distribution of Nontuberculous Mycobacteria Isolated From Clinical Specimens: A Systematic Review. *Semin Respir Crit Care Med* (2018) 39(3):336–42. doi: 10.1055/s-0038-1660864
24. Holt MR, Miles JJ, Inder WJ, Thomson RM. Exploring Immunomodulation by Endocrine Changes in Lady Windermere Syndrome. *Clin Exp Immunol* (2019) 196(1):28–38. doi: 10.1111/cei.13265
25. Kartalija M, Ovrutsky AR, Bryan CL, Pott GB, Fantuzzi G, Thomas J, et al. Patients With Nontuberculous Mycobacterial Lung Disease Exhibit Unique Body and Immune Phenotypes. *Am J Respir Crit Care Med* (2013) 187 (2):197–205. doi: 10.1164/rccm.201206-1035OC
26. Kim RD, Greenberg DE, Ehrmantraut ME, Guide SV, Ding L, Shea Y, et al. Pulmonary Nontuberculous Mycobacterial Disease: Prospective Study of a Distinct Preexisting Syndrome. *Am J Respir Crit Care Med* (2008) 178 (10):1066–74. doi: 10.1164/rccm.200805-686OC
27. Wi YM. Treatment of Extrapulmonary Nontuberculous Mycobacterial Diseases. *Infect Chemother* (2019) 51(3):245–55. doi: 10.3947/ic.2019.51.3.245
28. Piersimoni C, Scarparo C. Extrapulmonary Infections Associated With Nontuberculous Mycobacteria in Immunocompetent Persons. *Emerg Infect Dis* (2009) 15(9):1351–8; quiz 544. doi: 10.3201/eid1509.081259
29. Nasiri MJ, Haeili M, Ghazi M, Goudarzi H, Pormohammad A, Imani Fooladi AA, et al. New Insights in to the Intrinsic and Acquired Drug Resistance Mechanisms in Mycobacteria. *Front Microbiol* (2017) 8:681. doi: 10.3389/fmicb.2017.00681
30. Griffith DE, Aksamit TR. Therapy of Refractory Nontuberculous Mycobacterial Lung Disease. *Curr Opin Infect Dis* (2012) 25(2):218–27. doi: 10.1097/QCO.0b013e3283511a64
31. Abe Y, Fukushima K, Hosono Y, Matsumoto Y, Motooka D, Ose N, et al. Host Immune Response and Novel Diagnostic Approach to NTM Infections. *Int J Mol Sci* (2020) 21(12):4351. doi: 10.3390/ijms21124351
32. Prasla Z, Sutliff RL, Sadikot RT. Macrophage Signaling Pathways in Pulmonary Nontuberculous Mycobacteria Infections. *Am J Respir Cell Mol Biol* (2020) 63(2):144–51. doi: 10.1165/rcmb.2019-0241TR
33. Sousa S, Borges V, Joao I, Gomes JP, Jordao L. Nontuberculous Mycobacteria Persistence in a Cell Model Mimicking Alveolar Macrophages. *Microorganisms* (2019) 7(5):113. doi: 10.3390/microorganisms7050113
34. Sousa S, Bandeira M, Carvalho PA, Duarte A, Jordao L. Nontuberculous Mycobacteria Pathogenesis and Biofilm Assembly. *Int J Mycobacteriol* (2015) 4(1):36–43. doi: 10.1016/j.ijmyco.2014.11.065
35. Sexton P, Harrison AC. Susceptibility to Nontuberculous Mycobacterial Lung Disease. *Eur Respir J* (2008) 31(6):1322–33. doi: 10.1183/09031936.00140007
36. Chan ED, Iseman MD. Underlying Host Risk Factors for Nontuberculous Mycobacterial Lung Disease. *Semin Respir Crit Care Med* (2013) 34(1):110–23. doi: 10.1055/s-0033-1333573
37. Brode SK, Jamieson FB, Ng R, Campitelli MA, Kwong JC, Paterson JM, et al. Increased Risk of Mycobacterial Infections Associated With Anti-Rheumatic Medications. *Thorax* (2015) 70(7):677–82. doi: 10.1136/thoraxjnl-2014-206470
38. Yoo JW, Jo KW, Kang BH, Kim MY, Yoo B, Lee CK, et al. Mycobacterial Diseases Developed During Anti-Tumour Necrosis Factor-Alpha Therapy. *Eur Respir J* (2014) 44(5):1289–95. doi: 10.1183/09031936.00063514
39. Silwal P, Paik S, Kim JK, Yoshimori T, Jo EK. Regulatory Mechanisms of Autophagy-Targeted Antimicrobial Therapeutics Against Mycobacterial Infection. *Front Cell Infect Microbiol* (2021) 11:633360. doi: 10.3389/fcimb.2021.633360
40. Watson RO, Manzanillo PS, Cox JS. Extracellular M. Tuberculosis DNA Targets Bacteria for Autophagy by Activating the Host DNA-Sensing Pathway. *Cell* (2012) 150(4):803–15. doi: 10.1016/j.cell.2012.06.040
41. Romagnoli A, Etna MP, Giacomini E, Pardini M, Remoli ME, Corazzari M, et al. ESX-1 Dependent Impairment of Autophagic Flux by Mycobacterium Tuberculosis in Human Dendritic Cells. *Autophagy* (2012) 8(9):1357–70. doi: 10.4161/auto.20881
42. Bah A, Vergne I. Macrophage Autophagy and Bacterial Infections. *Front Immunol* (2017) 8:1483. doi: 10.3389/fimmu.2017.01483
43. Koster S, Upadhyay S, Chandra P, Papavinasasundaram K, Yang G, Hassan A, et al. *Mycobacterium Tuberculosis* is Protected From NADPH Oxidase and LC3-Associated Phagocytosis by the LCP Protein CpsA. *Proc Natl Acad Sci U S A* (2017) 114(41):E8711–E20. doi: 10.1073/pnas.1707792114
44. Watson RO, Bell SL, MacDuff DA, Kimmey JM, Diner EJ, Olivas J, et al. The Cytosolic Sensor cGAS Detects *Mycobacterium Tuberculosis* DNA to Induce Type I Interferons and Activate Autophagy. *Cell Host Microbe* (2015) 17 (6):811–9. doi: 10.1016/j.chom.2015.05.004
45. Chai Q, Wang X, Qiang L, Zhang Y, Ge P, Lu Z, et al. A *Mycobacterium Tuberculosis* Surface Protein Recruits Ubiquitin to Trigger Host Xenophagy. *Nat Commun* (2019) 10(1):1973. doi: 10.1038/s41467-019-09955-8
46. Manzanillo PS, Ayres JS, Watson RO, Collins AC, Souza G, Rae CS, et al. The Ubiquitin Ligase Parkin Mediates Resistance to Intracellular Pathogens. *Nature* (2013) 501(7468):512–6. doi: 10.1038/nature12566

47. Franco LH, Nair VR, Scharn CR, Xavier RJ, Torrealba JR, Shiloh MU, et al. The Ubiquitin Ligase Smurf1 Functions in Selective Autophagy of *Mycobacterium Tuberculosis* and Anti-Tuberculous Host Defense. *Cell Host Microbe* (2017) 21(1):59–72. doi: 10.1016/j.chom.2016.11.002
48. Chauhan S, Kumar S, Jain A, Ponpuak M, Mudd MH, Kimura T, et al. TRIMs and Galectins Globally Cooperate and TRIM16 and Galectin-3 Co-Direct Autophagy in Endomembrane Damage Homeostasis. *Dev Cell* (2016) 39(1):13–27. doi: 10.1016/j.devcel.2016.08.003
49. Jia J, Abudu YP, Claude-Taupin A, Gu Y, Kumar S, Choi SW, et al. Galectins Control mTOR in Response to Endomembrane Damage. *Mol Cell* (2018) 70 (1):120–35.e8. doi: 10.1016/j.molcel.2018.03.009
50. Maphasa RE, Meyer M, Dube A. The Macrophage Response to *Mycobacterium Tuberculosis* and Opportunities for Autophagy Inducing Nanomedicines for Tuberculosis Therapy. *Front Cell Infect Microbiol* (2020) 10:618414. doi: 10.3389/fcimb.2020.618414
51. Kim YS, Silwal P, Kim SY, Yoshimori T, Jo EK. Autophagy-Activating Strategies to Promote Innate Defense Against Mycobacteria. *Exp Mol Med* (2019) 51(12):1–10. doi: 10.1038/s12276-019-0290-7
52. Paik S, Kim JK, Chung C, Jo EK. Autophagy: A New Strategy for Host-Directed Therapy of Tuberculosis. *Virulence* (2019) 10(1):448–59. doi: 10.1080/21505594.2018.1536598
53. Rubinsztein DC, Bento CF, Deretic V. Therapeutic Targeting of Autophagy in Neurodegenerative and Infectious Diseases. *J Exp Med* (2015) 212(7):979–90. doi: 10.1084/jem.20150956
54. Zullo AJ, Lee S. Mycobacterial Induction of Autophagy Varies by Species and Occurs Independently of Mammalian Target of Rapamycin Inhibition. *J Biol Chem* (2012) 287(16):12668–78. doi: 10.1074/jbc.M111.320135
55. Gutierrez MG, Master SS, Singh SB, Taylor GA, Colombo MI, Deretic V. Autophagy Is a Defense Mechanism Inhibiting BCG and *Mycobacterium Tuberculosis* Survival in Infected Macrophages. *Cell* (2004) 119(6):753–66. doi: 10.1016/j.cell.2004.11.038
56. Viljoen A, Herrmann JL, Onajole OK, Stec J, Kozikowski AP, Kremer L. Controlling Extra- and Intramacrophagic *Mycobacterium Abscessus* by Targeting Mycolic Acid Transport. *Front Cell Infect Microbiol* (2017) 7:388. doi: 10.3389/fcimb.2017.00388
57. Bernut A, Herrmann JL, Kissa K, Dubremetz JF, Gaillard JL, Lutfalla G, et al. *Mycobacterium Abscessus* Cording Prevents Phagocytosis and Promotes Abscess Formation. *Proc Natl Acad Sci U S A* (2014) 111(10):E943–52. doi: 10.1073/pnas.1321390111
58. Daley CL, Winthrop KL. Mycobacterium Avium Complex: Addressing Gaps in Diagnosis and Management. *J Infect Dis* (2020) 222(Suppl 4):S199–211. doi: 10.1093/infdis/jiaa354
59. Wang Y, Chen C, Xu XD, Li H, Cheng MH, Liu J, et al. Levels of miR-125a-5p are Altered in *Mycobacterium Avium*-Infected Macrophages and Associate With the Triggering of an Autophagic Response. *Microbes Infect* (2020) 22(1):31–9. doi: 10.1016/j.micinf.2019.07.002
60. Parr DG, Guest PG, Reynolds JH, Dowson LJ, Stockley RA. Prevalence and Impact of Bronchiectasis in Alpha1-Antitrypsin Deficiency. *Am J Respir Crit Care Med* (2007) 176(12):1215–21. doi: 10.1164/rccm.200703-489OC
61. Bai X, Bai A, Honda JR, Eichstaedt C, Musheyev A, Feng Z, et al. Alpha-1-Antitrypsin Enhances Primary Human Macrophage Immunity Against Non-Tuberculous Mycobacteria. *Front Immunol* (2019) 10:1417. doi: 10.3389/fimmu.2019.01417
62. Chan ED, Kaminska AM, Gill W, Chmura K, Feldman NE, Bai X, et al. Alpha-1-Antitrypsin (AAT) Anomalies are Associated With Lung Disease Due to Rapidly Growing Mycobacteria and AAT Inhibits *Mycobacterium Abscessus* Infection of Macrophages. *Scand J Infect Dis* (2007) 39(8):690–6. doi: 10.1080/00365540701225744
63. Roux AL, Viljoen A, Bah A, Simeone R, Bernut A, Laencina L, et al. The Distinct Fate of Smooth and Rough Mycobacterium Abscessus Variants Inside Macrophages. *Open Biol* (2016) 6(11):1601. doi: 10.1098/rsob.160185
64. Awuh JA, Flo TH. Molecular Basis of Mycobacterial Survival in Macrophages. *Cell Mol Life Sci* (2017) 74(9):1625–48. doi: 10.1007/s00018-016-2422-8
65. Howard ST, Rhoades E, Recht J, Pang X, Alsup A, Kolter R, et al. Spontaneous Reversion of Mycobacterium Abscessus From a Smooth to a Rough Morphotype Is Associated With Reduced Expression of Glycopeptidolipid and Reacquisition of an Invasive Phenotype. *Microbiol (Reading)* (2006) 152(Pt 6):1581–90. doi: 10.1099/mic.0.28625-0
66. Laencina L, Dubois V, Le Moigne V, Viljoen A, Majlessi L, Pritchard J, et al. Identification of Genes Required for *Mycobacterium Abscessus* Growth In Vivo With a Prominent Role of the ESX-4 Locus. *Proc Natl Acad Sci U S A* (2018) 115(5):E1002–E11. doi: 10.1073/pnas.1713195115
67. Kim YS, Kim JK, Hanh BTB, Kim SY, Kim HJ, Kim YJ, et al. The Peroxisome Proliferator-Activated Receptor Alpha- Agonist Gemfibrozil Promotes Defense Against *Mycobacterium Abscessus* Infections. *Cells* (2020) 9 (3):648. doi: 10.3390/cells9030648
68. Renna M, Schaffner C, Brown K, Shang S, Tamayo MH, Hegyi K, et al. Azithromycin Blocks Autophagy and may Predispose Cystic Fibrosis Patients to Mycobacterial Infection. *J Clin Invest* (2011) 121(9):3554–63. doi: 10.1172/JCI46095
69. Kim SW, Subhadra B, Whang J, Back YW, Bae HS, Kim HJ, et al. Clinical Mycobacterium Abscessus Strain Inhibits Autophagy Flux and Promotes Its Growth in Murine Macrophages. *Pathog Dis* (2017) 75(8). doi: 10.1093/femspd/ftx107
70. Pohl K, Grimm XA, Caceres SM, Poch KR, Rysavy N, Saavedra M, et al. *Mycobacterium Abscessus* Clearance by Neutrophils Is Independent of Autophagy. *Infect Immun* (2020) 88(8):e00024–20. doi: 10.1128/IAI.00024-20
71. Aubry A, Mougari F, Reibel F, Cambau E. Mycobacterium Marinum. *Microbiol Spectr* (2017) 5(2). doi: 10.1128/microbiolspec.TNMI7-0038-2016
72. Stinear TP, Seemann T, Harrison PF, Jenkin GA, Davies JK, Johnson PD, et al. Insights From the Complete Genome Sequence of *Mycobacterium Marinum* on the Evolution of *Mycobacterium Tuberculosis*. *Genome Res* (2008) 18(5):729–41. doi: 10.1101/gr.075069.107
73. Clark HF, Shepard CC. Effect of Environmental Temperatures on Infection With *Mycobacterium Marinum* (Balnei) of Mice and a Number of Poikilothermic Species. *J Bacteriol* (1963) 86:1057–69. doi: 10.1128/jb.86.5.1057-1069.1963
74. Tobin DM, Ramakrishnan L. Comparative Pathogenesis of Mycobacterium Marinum and *Mycobacterium Tuberculosis*. *Cell Microbiol* (2008) 10 (5):1027–39. doi: 10.1111/j.1462-5822.2008.01133.x
75. Hosseini R, Lamers GE, Hodzic Z, Meijer AH, Schaaf MJ, Spaink HP. Correlative Light and Electron Microscopy Imaging of Autophagy in a Zebrafish Infection Model. *Autophagy* (2014) 10(10):1844–57. doi: 10.4161/auto.29992
76. Cardenal-Munoz E, Arafah S, Lopez-Jimenez AT, Kicka S, Falaise A, Bach F, et al. *Mycobacterium Marinum* Antagonistically Induces an Autophagic Response While Repressing the Autophagic Flux in a TORC1- and ESX-1-Dependent Manner. *PLoS Pathog* (2017) 13(4):e1006344. doi: 10.1371/journal.ppat.1006344
77. Lerena MC, Colombo MI. *Mycobacterium Marinum* Induces a Marked LC3 Recruitment to its Containing Phagosome That Depends on a Functional ESX-1 Secretion System. *Cell Microbiol* (2011) 13(6):814–35. doi: 10.1111/j.1462-5822.2011.01581.x
78. Collins CA, De Maziere A, van Dijk S, Carlsson F, Klumperman J, Brown EJ. Atg5-Independent Sequestration of Ubiquitinated Mycobacteria. *PLoS Pathog* (2009) 5(5):e1000430. doi: 10.1371/journal.ppat.1000430
79. Mohanty S, Jagannathan L, Ganguli G, Padhi A, Roy D, Alaridah N, et al. A Mycobacterial Phosphoribosyltransferase Promotes Bacillary Survival by Inhibiting Oxidative Stress and Autophagy Pathways in Macrophages and Zebrafish. *J Biol Chem* (2015) 290(21):13321–43. doi: 10.1074/jbc.M114.598482
80. Zhang R, Varela M, Vallentgoed W, Forn-Cuni G, van der Vaart M, Meijer AH. The Selective Autophagy Receptors Optineurin and P62 are Both Required for Zebrafish Host Resistance to Mycobacterial Infection. *PLoS Pathog* (2019) 15(2):e1007329. doi: 10.1371/journal.ppat.1007329
81. van der Vaart M, Korbee CJ, Lamers GE, Tengeler AC, Hosseini R, Haks MC, et al. The DNA Damage-Regulated Autophagy Modulator DRAM1 Links Mycobacterial Recognition via TLR-MYD88 to Autophagic Defense [Corrected]. *Cell Host Microbe* (2014) 15(6):753–67. doi: 10.1016/j.chom.2014.05.005
82. Zhang R, Varela M, Forn-Cuni G, Torraca V, van der Vaart M, Meijer AH. Deficiency in the Autophagy Modulator Dram1 Exacerbates Pyroptotic Cell

Death of Mycobacteria-Infected Macrophages. *Cell Death Dis* (2020) 11 (4):277. doi: 10.1038/s41419-020-2477-1
83. Chen Z, Shao XY, Wang C, Hua MH, Wang CN, Wang X, et al. *Mycobacterium Marinum* Infection in Zebrafish and Microglia Imitates the Early Stage of Tuberculous Meningitis. *J Mol Neurosci* (2018) 64(2):321–30. doi: 10.1007/s12031-018-1026-1
84. Kim TS, Shin YH, Lee HM, Kim JK, Choe JH, Jang JC, et al. Ohmyungsamycins Promote Antimicrobial Responses Through Autophagy Activation via AMP-Activated Protein Kinase Pathway. *Sci Rep* (2017) 7(1):3431. doi: 10.1038/s41598-017-03477-3
85. Pean CB, Schiebler M, Tan SW, Sharrock JA, Kierdorf K, Brown KP, et al. Regulation of Phagocyte Triglyceride by a STAT-ATG2 Pathway Controls Mycobacterial Infection. *Nat Commun* (2017) 8:14642. doi: 10.1038/ncomms14642
86. Floto RA, Sarkar S, Perlstein EO, Kampmann B, Schreiber SL, Rubinsztein DC. Small Molecule Enhancers of Rapamycin-Induced TOR Inhibition Promote Autophagy, Reduce Toxicity in Huntington's Disease Models and Enhance Killing of Mycobacteria by Macrophages. *Autophagy* (2007) 3 (6):620–2. doi: 10.4161/auto.4898
87. Kim JJ, Lee HM, Shin DM, Kim W, Yuk JM, Jin HS, et al. Host Cell Autophagy Activated by Antibiotics Is Required for Their Effective Antimycobacterial Drug Action. *Cell Host Microbe* (2012) 11(5):457–68. doi: 10.1016/j.chom.2012.03.008
88. Kjellin J, Pranting M, Bach F, Vaid R, Edelbroek B, Li Z, et al. Investigation of the Host Transcriptional Response to Intracellular Bacterial Infection Using Dictyostelium Discoideum as a Host Model. *BMC Genomics* (2019) 20 (1):961. doi: 10.1186/s12864-019-6269-x
89. Lopez-Jimenez AT, Cardenal-Munoz E, Leuba F, Gerstenmaier L, Barisch C, Hagedorn M, et al. The ESCRT and Autophagy Machineries Cooperate to Repair ESX-1-Dependent Damage at the Mycobacterium-Containing Vacuole But Have Opposite Impact on Containing the Infection. *PLoS Pathog* (2018) 14(12):e1007501. doi: 10.1371/journal.ppat.1007501
90. Bah A, Lacarriere C, Vergne I. Autophagy-Related Proteins Target Ubiquitin-Free Mycobacterial Compartment to Promote Killing in Macrophages. *Front Cell Infect Microbiol* (2016) 6:53. doi: 10.3389/fcimb.2016.00053
91. Zullo AJ, Jurcic Smith KL, Lee S. Mammalian Target of Rapamycin Inhibition and Mycobacterial Survival Are Uncoupled in Murine Macrophages. *BMC Biochem* (2014) 15:4. doi: 10.1186/1471-2091-15-4
92. Feng X, Lu J, He Z, Wang Y, Qi F, Pi R, et al. *Mycobacterium Smegmatis* Induces Neurite Outgrowth and Differentiation in an Autophagy-Independent Manner in PC12 and C17.2 Cells. *Front Cell Infect Microbiol* (2018) 8:201. doi: 10.3389/fcimb.2018.00201
93. Gough ME, Graviss EA, May EE. The Dynamic Immunomodulatory Effects of Vitamin D3 During Mycobacterium Infection. *Innate Immun* (2017) 23 (6):506–23. doi: 10.1177/1753425917719143
94. Yuk JM, Shin DM, Lee HM, Yang CS, Jin HS, Kim KK, et al. Vitamin D3 Induces Autophagy in Human Monocytes/Macrophages via Cathelicidin. *Cell Host Microbe* (2009) 6(3):231–43. doi: 10.1016/j.chom.2009.08.004
95. Buultjens AH, Vandelannoote K, Meehan CJ, Eddyani M, de Jong BC, Fyfe JAM, et al. Comparative Genomics Shows That Mycobacterium Ulcerans Migration and Expansion Preceded the Rise of Buruli Ulcer in Southeastern Australia. *Appl Environ Microbiol* (2018) 84(8):e02612–17. doi: 10.1128/AEM.02612-17
96. Capela C, Sopoh GE, Houezo JG, Fiodessihoue R, Dossou AD, Costa P, et al. Clinical Epidemiology of Buruli Ulcer From Benin (2005-2013): Effect of Time-Delay to Diagnosis on Clinical Forms and Severe Phenotypes. *PLoS Negl Trop Dis* (2015) 9(9):e0004005. doi: 10.1371/journal.pntd.0004005
97. Manry J, Vincent QB, Johnson C, Chrabieh M, Lorenzo L, Theodorou I, et al. Genome-Wide Association Study of Buruli Ulcer in Rural Benin Highlights Role of Two LncRNAs and the Autophagy Pathway. *Commun Biol* (2020) 3 (1):177. doi: 10.1038/s42003-020-0920-6
98. Capela C, Dossou AD, Silva-Gomes R, Sopoh GE, Makoutode M, Menino JF, et al. Genetic Variation in Autophagy-Related Genes Influences the Risk and Phenotype of Buruli Ulcer. *PLoS Negl Trop Dis* (2016) 10(4):e0004671. doi: 10.1371/journal.pntd.0004671
99. Martin PK, Marchiando A, Xu R, Rudensky E, Yeung F, Schuster SL, et al. Autophagy Proteins Suppress Protective Type I Interferon Signalling in Response to the Murine Gut Microbiota. *Nat Microbiol* (2018) 3(10):1131–41. doi: 10.1038/s41564-018-0229-0
100. Gama JB, Ohlmeier S, Martins TG, Fraga AG, Sampaio-Marques B, Carvalho MA, et al. Proteomic Analysis of the Action of the *Mycobacterium Ulcerans* Toxin Mycolactone: Targeting Host Cells Cytoskeleton and Collagen. *PLoS Negl Trop Dis* (2014) 8(8):e3066. doi: 10.1371/journal.pntd.0003066
101. Manry J. Human Genetics of Buruli Ulcer. *Hum Genet* (2020) 139(6-7):847–53. doi: 10.1007/s00439-020-02163-1
102. Ke Z, Lu J, Zhu J, Yang Z, Jin Z, Yuan L. Down-Regulation of lincRNA-EPS Regulates Apoptosis and Autophagy in BCG-Infected RAW264.7 Macrophages via JNK/MAPK Signaling Pathway. *Infect Genet Evol* (2020) 77:104077. doi: 10.1016/j.meegid.2019.104077
103. Smith DS, Lindholm-Levy P, Huitt GA, Heifets LB, Cook JL. *Mycobacterium Terrae*: Case Reports, Literature Review, and In Vitro Antibiotic Susceptibility Testing. *Clin Infect Dis* (2000) 30(3):444–53. doi: 10.1086/313693
104. Orosz L, Papanicolaou EG, Seprenyi G, Megyeri K. IL-17A and IL-17F Induce Autophagy in RAW 264.7 Macrophages. *BioMed Pharmacother* (2016) 77:129–34. doi: 10.1016/j.biopha.2015.12.020
105. Feng Z, Bai X, Wang T, Garcia C, Bai A, Li L, et al. Differential Responses by Human Macrophages to Infection With *Mycobacterium Tuberculosis* and Non-Tuberculous Mycobacteria. *Front Microbiol* (2020) 11:116. doi: 10.3389/fmicb.2020.00116
106. Sharma V, Makhdoomi M, Singh L, Kumar P, Khan N, Singh S, et al. Trehalose Limits Opportunistic Mycobacterial Survival During HIV Co-Infection by Reversing HIV-Mediated Autophagy Block. *Autophagy* (2021) 17(2):476–95. doi: 10.1080/15548627.2020.1725374
107. Settembre C, Di Malta C, Polito VA, Garcia Arencibia M, Vetrini F, Erdin S, et al. TFEB Links Autophagy to Lysosomal Biogenesis. *Science* (2011) 332 (6036):1429–33. doi: 10.1126/science.1204592
108. Sato E, Imafuku S, Ishii K, Itoh R, Chou B, Soejima T, et al. Vitamin D-Dependent Cathelicidin Inhibits *Mycobacterium Marinum* Infection in Human Monocytic Cells. *J Dermatol Sci* (2013) 70(3):166–72. doi: 10.1016/j.jdermsci.2013.01.011
109. Kan Y, Meng L, Xie L, Liu L, Dong W, Feng J, et al. Temporal Modulation of Host Aerobic Glycolysis Determines the Outcome of *Mycobacterium Marinum* Infection. *Fish Shellfish Immunol* (2020) 96:78–85. doi: 10.1016/j.fsi.2019.11.051
110. Zheng Q, Wang Q, Wang S, Wu J, Gao Q, Liu W. Thiopeptide Antibiotics Exhibit a Dual Mode of Action Against Intracellular Pathogens by Affecting Both Host and Microbe. *Chem Biol* (2015) 22(8):1002–7. doi: 10.1016/j.chembiol.2015.06.019
111. Sharma V, Verma S, Seranova E, Sarkar S, Kumar D. Selective Autophagy and Xenophagy in Infection and Disease. *Front Cell Dev Biol* (2018) 6:147. doi: 10.3389/fcell.2018.00147
112. Kim HJ, Kim IS, Lee SG, Kim YJ, Silwal P, Kim JY, et al. MiR-144-3p is Associated With Pathological Inflammation in Patients Infected With *Mycobacteroides Abscessus*. *Exp Mol Med* (2021) 53(1):136–49. doi: 10.1038/s12276-020-00552-0
113. Bagul PK, Katare PB, Bugga P, Dinda AK, Banerjee SK. SIRT-3 Modulation by Resveratrol Improves Mitochondrial Oxidative Phosphorylation in Diabetic Heart Through Deacetylation of TFAM. *Cells* (2018) 7(12):235. doi: 10.3390/cells7120235
114. Howitz KT, Bitterman KJ, Cohen HY, Lamming DW, Lavu S, Wood JG, et al. Small Molecule Activators of Sirtuins Extend Saccharomyces Cerevisiae Lifespan. *Nature* (2003) 425(6954):191–6. doi: 10.1038/nature01960
115. Kim YJ, Lee SH, Jeon SM, Silwal P, Seo JY, Hanh BTB, et al. Sirtuin 3 is Essential for Host Defense Against *Mycobacterium Abscessus* Infection Through Regulation of Mitochondrial Homeostasis. *Virulence* (2020) 11 (1):1225–39. doi: 10.1080/21505594.2020.1809961
116. Kim TS, Jin YB, Kim YS, Kim S, Kim JK, Lee HM, et al. SIRT3 Promotes Antimycobacterial Defenses by Coordinating Mitochondrial and Autophagic Functions. *Autophagy* (2019) 15(8):1356–75. doi: 10.1080/15548627.2019.1582743
117. Rampacci E, Stefanetti V, Passamonti F, Henao-Tamayo M. Preclinical Models of Nontuberculous Mycobacteria Infection for Early Drug Discovery and Vaccine Research. *Pathogens* (2020) 9(8):641. doi: 10.3390/pathogens9080641

118. Kwon BE, Ahn JH, Park EK, Jeong H, Lee HJ, Jung YJ, et al. B Cell-Based Vaccine Transduced With ESAT6-Expressing Vaccinia Virus and Presenting Alpha-Galactosylceramide Is a Novel Vaccine Candidate Against ESAT6-Expressing Mycobacterial Diseases. *Front Immunol* (2019) 10:2542. doi: 10.3389/fimmu.2019.02542
119. Verma D, Chan ED, Ordway DJ. Non-Tuberculous Mycobacteria Interference With BCG-Current Controversies and Future Directions. *Vaccines (Basel)* (2020) 8(4):688. doi: 10.3390/vaccines8040688
120. Hu D, Wu J, Zhang R, Chen L, Chen Z, Wang X, et al. Autophagy-Targeted Vaccine of LC3-LpqH DNA and its Protective Immunity in a Murine Model of Tuberculosis. *Vaccine* (2014) 32(20):2308–14. doi: 10.1016/j.vaccine.2014.02.069
121. Meerak J, Wanichwecharungruang SP, Palaga T. Enhancement of Immune Response to a DNA Vaccine Against *Mycobacterium Tuberculosis* Ag85B by Incorporation of an Autophagy Inducing System. *Vaccine* (2013) 31(5):784–90. doi: 10.1016/j.vaccine.2012.11.075

Conflict of Interest: The authors declare that the research was conducted in the absence of any commercial or financial relationships that could be construed as a potential conflict of interest.

Publisher's Note: All claims expressed in this article are solely those of the authors and do not necessarily represent those of their affiliated organizations, or those of the publisher, the editors and the reviewers. Any product that may be evaluated in this article, or claim that may be made by its manufacturer, is not guaranteed or endorsed by the publisher.

frontiers in Immunology

ORIGINAL RESEARCH
published: 21 September 2021
doi: 10.3389/fimmu.2021.727580

Changes in B Cell Pool of Patients With Multibacillary Leprosy: Diminished Memory B Cell and Enhanced Mature B in Peripheral Blood

Otto Castro Nogueira[1†], Mariana Gandini[1†], Natasha Cabral[1], Vilma de Figueiredo[1], Rodrigo Nunes Rodrigues-da-Silva[2], Josué da Costa Lima-Junior[2], Roberta Olmo Pinheiro[3], Geraldo Moura Batista Pereira[1], Maria Cristina Vidal Pessolani[1] and Cristiana Santos de Macedo[1,4]*

[1] Cellular Microbiology Laboratory, Oswaldo Cruz Institute, Oswaldo Cruz Foundation, Rio de Janeiro, Brazil, [2] Immunoparasitology Laboratory, Oswaldo Cruz Institute, Oswaldo Cruz Foundation, Rio de Janeiro, Brazil, [3] Leprosy Laboratory, Oswaldo Cruz Institute, Oswaldo Cruz Foundation, Rio de Janeiro, Brazil, [4] Center for Technological Development in Health, Oswaldo Cruz Foundation, Rio de Janeiro, Brazil

OPEN ACCESS

Edited by:
Maria Teresa Ochoa, University of Southern California, United States

Reviewed by:
Andre Talvani, Universidade Federal de Ouro Preto, Brazil
Yean Kong Yong, Xiamen University, Malaysia

***Correspondence:**
Cristiana Santos de Macedo
cristiana.macedo@cdts.fiocruz.br

†These authors have contributed equally to this work and share first authorship

Specialty section:
This article was submitted to Microbial Immunology, a section of the journal Frontiers in Immunology

Received: 18 June 2021
Accepted: 31 August 2021
Published: 21 September 2021

Citation:
Nogueira OC, Gandini M, Cabral N, de Figueiredo V, Rodrigues-da-Silva RN, Lima-Junior JdC, Pinheiro RO, Pereira GMB, Pessolani MCV and de Macedo CS (2021) Changes in B Cell Pool of Patients With Multibacillary Leprosy: Diminished Memory B Cell and Enhanced Mature B in Peripheral Blood. Front. Immunol. 12:727580. doi: 10.3389/fimmu.2021.727580

Despite being treatable, leprosy still represents a major public health problem, and many mechanisms that drive leprosy immunopathogenesis still need to be elucidated. B cells play important roles in immune defense, being classified in different subgroups that present distinct roles in the immune response. Here, the profile of B cell subpopulations in peripheral blood of patients with paucibacillary (TT/BT), multibacillary (LL/BL) and erythema nodosum leprosum was analyzed. B cell subpopulations (memory, transition, plasmablasts, and mature B cells) and levels of IgG were analyzed by flow cytometry and ELISA, respectively. It was observed that *Mycobacterium leprae* infection can alter the proportions of B cell subpopulations (increase of mature and decrease of memory B cells) in patients affected by leprosy. This modulation is associated with an increase in total IgG and the patient's clinical condition. Circulating B cells may be acting in the modulation of the immune response in patients with various forms of leprosy, which may reflect the patient's ability to respond to *M. leprae*.

Keywords: *Mycobacterium leprae*, B lymphocytes, B cell differentiation, active immune response, erythema nodosum leprosum

INTRODUCTION

Leprosy is a chronic infectious disease caused by the intracellular pathogen *Mycobacterium leprae*, which is endemic in many countries: in 2019, WHO reported 202,185 new cases worldwide (1, 2). The disease presents a complex clinical and immunopathological spectrum: at one end, tuberculoid leprosy (TT), in which skin lesions are characterized by a classical epithelioid cell granuloma formation, with a strong pro-inflammatory Th1/Th17 cellular immune response and consequent bacterial growth control. On the opposite side, lepromatous leprosy (LL), is characterized by a

complete absence of granuloma and epithelioid cells in active lesions, the presence of humoral immune response and high bacillary load. Between these poles, there are unstable borderline forms: borderline tuberculoid (BT), borderline borderline (BB), and borderline lepromatous (BL) (3). For clinical diagnosis and treatment, WHO implemented an operational classification according to the number of skin lesions: paucibacillary (PB), patients with leprosy who present less than five lesions (tuberculoid); and multibacillary (MB), with five or more lesions (lepromatous) (4).

Patients with leprosy may present peripheral nerve demyelination and axonal loss, resulting in an impaired neural function, disfiguration, and deformities (5, 6). Leprosy reactions are acute inflammatory episodes that may occur at any stage of the clinical course of the disease (these reactions may affect 30–50% of all patients with leprosy). The most common episodes are Type I reaction (or reversal reaction-RR) and Type II reaction (also known as erythema nodosum leprosum-ENL). Expression levels of immunoglobulin receptors and B cell receptors during RR and ENL, evaluated by a transcriptomic analysis of peripheral blood mononuclear cells (PBMCs), support an antibody-mediated immune response during both RR and ENL (7). ENL is frequently associated with an intense infiltrate of neutrophils in the profound dermis and hypodermis, accompanied by macrophages, but skin fragments collected after 72 h of the reaction demonstrated the presence of lymphocytes, plasma cells, and mast cells (8).

The bacillus, and presumably similar breakdown products, are involved in the onset of the reactional episodes. Phospholipids are found in lepromatous tissues, as well as other bacillary breakdown products (9, 10) which could contribute to the stimuli of humoral responses in patients with LL. B-cells are activated by microorganisms *via* antigen-specific B-cell receptors (BCR) or non-specific pattern recognition receptors. The main mechanisms leading to antibody production by B cells are largely known and, Toll-like receptor (TLR) stimulation in B cells are associated with the regulation of the magnitude of the antibody response and the amount of antigen required for initiating BCR signaling (11, 12).

Antibody responses to specific *M. leprae* antigens have been used to diagnose patients affected by leprosy. The antibody titers generally increase as the disease progresses across the spectrum, from the TT to LL form. Patients affected by ENL also present higher titers of antibodies. In addition, the bacterial index is positively correlated with the antibody titers (13, 14).

The study of immune cells involved in leprosy immunopathogenesis is fundamental to understanding the phenomena that drive the evolution of subclinical to active leprosy (15), and several studies demonstrated that there is a significant increase in the risk of leprosy in contacts with an anti-PGL-I (anti-phenolic glycolipid-I) seropositivity (16, 17). PGL-I, despite its extreme lipophilicity due to its inherent phthiocerol dimycocerosyl component, is highly antigenic evoking high title IgM antibodies in patients affected by LL, attributable largely to the unique 3,6-di-O-methyl-beta-D-glucosyl entity at the non-reducing terminus of its trisaccharide (18). In the LL form of the disease higher titers of antibodies, complement and B-cell-derived IL-10 are observed, although it is not clear if it is responsible for the increased susceptibility in patients affected by LL (19–21). Additionally, IgG immune complexes are associated with the pathogenesis of ENL (22).

Although the relevance of innate and cellular immune responses in the pathogenesis of leprosy, several data suggest the involvement of B cells (humoral response) not only in reactional episodes, but in the pathogenesis of the disease. There are only a few publications about phenotypic analysis of peripheral B cells, restricted to some clinical presentations: Negera et al. studied the total count and frequencies of naïve, mature, and memory (resting, activated, and tissue-like) B cells in patients with ENL (23). Other authors compared the percentage of total B and of B1a cells, which are associated with autoimmune diseases, between patients with LL and uninfected subjects, and found that both are higher in the former (24). Tarique et al. found a higher frequency of B regulatory cells in antigen-stimulated PBMC of MB patients in comparison to PB and uninfected subjects (25). The pathways leading to B cell activation in leprosy are still unknown. Here, we analyzed and compared different B cell phenotypes in leprosy (multibacillary, paucibacillary and erythema nodosum leprosum) to elucidate a possible role of these B cells in the pathology of the disease.

MATERIALS AND METHODS

Patients With Leprosy and Uninfected Subjects

Patients with leprosy were recruited from Souza Araújo Leprosy Outpatient Unit (Oswaldo Cruz Foundation, Rio de Janeiro-RJ, Brazil) from 2016 through 2019. Uninfected subjects, all residents in the city of Rio de Janeiro (State of Rio de Janeiro, Brazil), were selected according to the similarity of age (18 to 65) and gender patient's cohort. The patients were classified on the leprosy spectrum clinically and histologically based on Ridley-Jopling classification schemes (26). The present study comprised 55 voluntary participants divided into four groups of donors: i) Patients with paucibacillary-PB (TT/BT) leprosy recruited before the start of multidrug therapy (MDT); ii) Patients with multibacillary-MB (LL/BL) recruited before the start of MDT with no signs of leprosy reactions at the time of leprosy diagnosis; iii) Patients clinically diagnosed with erythema nodosum leprosum-ENL (diagnosed - without treatment); iv) Uninfected subjects (**Table 1**; detailed information about patients and assays on **SI Table 1**). Patients and uninfected subjects with chronic or acute diseases unrelated to leprosy, diagnosed with other infectious diseases, using immunosuppressive drugs, or during pregnancy were excluded.

Ethics Statement

The use of samples was approved by the FIOCRUZ Research Ethics Committee (CAAE 01247418.8.0000.5248). All participants, including parents of minors, provided informed written consent.

TABLE 1 | Baseline characteristics of patients and uninfected individuals whose B cells were analyzed by flow cytometry.

Characteristics	Leprosy N = 35	PB N = 13	MB N = 12	ENL N = 10	Uninfected individuals N = 20
Mean age (Years)	47.9	48.7	47.5	45.8	36.53
Gender, males (%)	21 (60)	5 (38)	8 (66)	8 (80)	14 (70)
Gender, females (%)	14 (40)	8 (62)	4 (34)	2 (20)	6 (30)
Mean Logarithmic Index of Bacilli (LIB)	–	0	4,61	3,66	–
Mean Bacilloscopic Index (BI)	–	0	4,15	3,95	–

Groups included in this study: Leprosy: All patients, PB, Paucibacillary; MB, Multibacillary; ENL, erythema nodosum leprosum; and uninfected individuals.

Isolation of the Peripheral Blood Mononuclear Cells and Flow Cytometry Staining

Blood samples were layered on Ficoll-Hypaque (Sigma Aldrich, USA) and mononuclear cells were isolated by centrifugation at 900 x *g* for 30 min, then stained with surface antibodies anti-human -CD3 (ALX 700, clone:UCHT1, Biolegend); -CD19 (APCCy7, clone SJ25C1, BD); -CD38 (PerCP-C5.5, clone HIT2, BD); -CD24 (FITC, clone ML5, BD); -CD27 (PECY7, clone 1A4CD27, Beckman Coulter); -CD21 (PECY7, clone B-ly4, BD); -IgM (BV510, clone g20-127, BD) and- IgD (PE, clone IA6-2, Beckman Coulter) for 30 min at 4°C in the dark. Cells were fixed with 2% paraformaldehyde and stored at 4°C. Data were collected using FACSAria IIup (BD Biosciences) and analyzed using FlowJo software (BD Biosciences) (17).

ELISA

The IgG levels were determined in all plasma samples using an in-house ELISA. Briefly, MaxiSorp 96-well-plates (Nunc, Rochester, NY, USA) were coated with PBS containing 1.5 μg/ml of anti-human IgG (A0170, Sigma). After overnight incubation at 4°C, the plates were then washed three times with phosphate-buffered saline-0.05% Tween 20 (PBS-Tween) and blocked for 1 h at 37°C with PBS-Tween containing 5% nonfat-dried milk (PBS-Tween-M). Plasma samples diluted 1:1000 in PBS-Tween-M were added in duplicate wells containing 5% nonfat-dried milk (PBS-Tween-M) were added in duplicate wells. After 1 h at 37°C and three washings, specific antibodies were detected by goat peroxidase-conjugated anti-human IgG (Sigma, St. Louis) and followed by the addition of 3,3′,5,5′-tetramethylbenzidine (TMB) for 30 minutes. The reaction was stopped with HCl 1M (Merck) and optical density was measured at 450 nm using a SpectraMax microplate spectrophotometer (Molecular Devices, Sunnyvale, CA, USA). The IgG level in each sample was calculated interpolating the mean optical density value of the sample on a linear regression graphic of recombinant IgG (ref. 15260) standard curve dilution (ranging from 0.500 to 0.031 μg/mL) performed using the same conditions described above (27).

Statistical Analysis

Differences in percentages of B cells, B cell subsets, and ELISA were analyzed using the Kruskal-Wallis test. Graphs were produced by GraphPad Prism version 8.0 for Mac (GraphPad Software, CA, USA). The statistical significance level was set at $p<0.05$; $p<0.005$; $p<0.0005$.

RESULTS

Frequency of Different B Cell Subpopulations in PBMCs From Patients With Leprosy

To study peripheral B cell subpopulations, initially, lumps and monocytes were excluded using the parameters of frontal dispersion measured by area (FSC-A, forward scatter-area), versus frontal dispersion measured by height (FSC-H, forward scatter-height). Next, the lymphocyte region was selected by FSC-A and lateral dispersion measured by SSC-A area (side scatter), and in this region B cells (CD3-CD19+) were detected. The B cell subpopulation gate strategies were applied to different leprosy manifestations and uninfected subjects. No difference between the different clinical forms and uninfected subjects was observed (**Figure 1A**). Using this strategy, it was possible to identify four B cell subpopulations: memory B cells (CD24++CD38-/+), transitional B cells (CD24hiCD38hi), plasmablasts (CD24-CD38+) and mature B cells (CD24intCD38int) (**Figure 1B**).

The transitional B cells and plasmablasts can also produce IL-10 and regulate CD4+ T cell proliferation and differentiation toward T helper (Th) effector cells (28). Our results showed that there were no significant differences between patients and uninfected subjects in both transitional and plasmablast B cells (**Figures 1C, D**). Besides that, a larger frequency of mature B cells was observed in patients with MB leprosy (mean_79.70; range_30.10; p=0.0032) and ENL (mean_79.40; range_31.10; p=0.0030) in comparison to uninfected subjects. Patients with PB leprosy (mean_62.20; range_ 41.80; p=0.0450) in comparison to ENL patients (differences between MB e PB were not statistically significant) (**Figure 1E**). Memory B cells are formed within the germinal centers from mature cells. These cells also express higher affinity B cell receptors, which not only strengthens the effector functions of the antibodies secreted by their plasma cell progeny but also allows memory B cells to sense very low antigen levels. A decrease in the frequency of memory B cells in patients with MB leprosy, who present a higher bacillary load (mean_9.37; range_31.98; p=0.0002) and ENL (mean_10.50; range_29.90; p=0.0035) was observed in comparison to uninfected subjects. This decrease was also seen in patients with MB leprosy compared to those with PB leprosy (p=0.0163) (**Figure 1F**).

Frequency of Memory B Cells in PBMCs From Patients With Leprosy

Unswitched memory B cells (CD19+CD27+IgD+) are important in the first line of defense against infections because of the quick

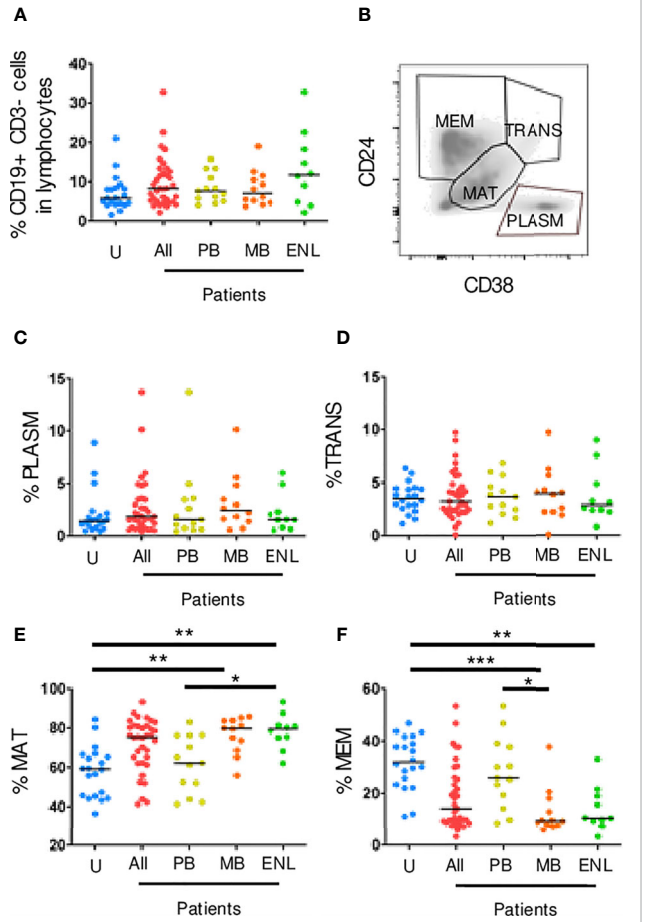

FIGURE 1 | Circulating CD19+ B cell subpopulations sorted by CD24 and CD38 expression. PBMC of uninfected individuals (U), paucibacillary patients (PB), multibacillary patients in type II reaction (ENL) or not (MB) were freshly stained and analyzed by flow cytometry. **(A)** Frequency of CD19+ CD3- B cells among lymphocytes for all groups described above in which All represents PB, MB, and ENL. **(B)** Density plot profile for B cell subpopulations based on CD24 and CD38 expression in which memory B cells (MEM), transitional B cells (TRANS), mature B cells (MAT), and plasmablasts (PLASM) are depicted. Percentage of plasmablasts **(C)**, transitional B cells **(D)**, mature B cells **(E)**, and memory B cells **(F)** among CD19+ CD3- B cells. Each dot represents one donor and lines represent median values for each group. Significant values (*) were calculated by Kruskal-Wallis tests with Dunn's multiple comparisons test. *$p < 0.05$; **$p < 0.005$; ***$p < 0.0005$.

production of low-affinity IgM (29). **Figure 2A** is a gating strategy for selecting circulating memory B cells sorted by CD27 and IgD. Our results showed that there was a decrease in the frequency of unswitched memory B cells both in CD19+ B cells (CD27+IgD+) of patients with MB leprosy (p=0.0064)/ENL (p=0.0095) in comparison to uninfected subjects and patients with MB leprosy (p=0.0007)/ENL (p=0.0010) in comparison to patients with PB leprosy. This decrease was also seen within B memory cells (CD19+CD24+CD38+) in patients with MB leprosy (p=0.0308)/ENL (p=0.0222) in comparison to uninfected subjects and patients with MB leprosy (p=0.0036)/ENL (p=0.0026) in comparison to patients with PB leprosy (**Figures 2B, E**).

We did not observe differences in switched memory B cells between the different clinical profiles of the disease (**Figures 2C, D, F, G**). Resting memory B cells (CD19+CD21+CD27+) can produce antibodies in absence of T cell help, are highly proliferative, and have increased cell turnover compared to other B cell memory subpopulations (atypical memory and activated memory).

Figure 3A shows the gating strategy for selecting circulating memory B cells sorted by CD27 and CD21 (30). Our data did not show significant differences between clinical forms and uninfected subjects in both B cells total and B memory cells (**Figures 3B, E**). We observed a reduced frequency in patients with MB leprosy and with ENL both in total B cells (CD19+) and in memory cells (CD19+CD24+CD38+/-) (**Figures 3C, F**) (23). No significant differences on atypical memory B cells (CD19+CD21-CD27-) in total B cells (CD3-CD19+) were observed (**Figure 3D**). However, we observed an increase in expression (CD19+CD21-CD27-) within memory B cells in patients with MB leprosy (p=0.0194) and with ENL (p= 0.0173) in comparison to uninfected subjects (**Figure 3G**).

Lastly, total IgG levels were assessed to corroborate the distinct profile of IgG antibody production in different clinical scenarios. The median of IgG levels in the uninfected subject group was 442.5 (range _ 966.1), 1539 in MB (range _ 3179), 319.7 in PB (IQ range _ 419.5), and 438.5 in ENL (range _ 589.4). Despite the relatively low number of analyzed donors, a significantly higher level of circulating IgG in patients with MB leprosy compared to PB (p=0.0004) and patients with ENL (p=0.0164) was observed (**Figure 4**). Moreover, all other groups included in our study (PB, ENL, and uninfected subjects) presented very similar levels of circulating IgG.

DISCUSSION

Leprosy is a complex and multifactorial disease in which the immune system is pivotal for determining the clinical course of the disease. Although several studies reinforce the importance of T cells in the pathogenesis of the disease, as well as genetic factors and the innate immune cells, the pathogenesis of leprosy is still not fully understood.

M. leprae-specific immunoglobulin G1 (IgG1) antibodies in patients with leprosy show a direct correlation with bacterial load suggesting that IgG1 B-cell responses may be surrogate markers of disease progression, although the role of B cells in the different clinical forms of the disease needs to be elucidated. There are still only few reports about the role of B cells in active leprosy lesions in different spectral forms of the disease, although there are several evidences of the involvement of B cells not only in the onset of reactional episodes but also in the course of non-reactional leprosy.

Fabel and colleagues (31) have suggested that B cells might be implicated in tuberculoid granuloma formation and type 1 reactions. They demonstrated that tuberculoid leprosy shows more B cells and less plasma cells than lepromatous leprosy. Here, we observed that there were no significant differences between patients and uninfected subjects in both transitional and plasmablast B cells, but a higher frequency of mature B cells was observed in both groups of patients with MB and ENL.

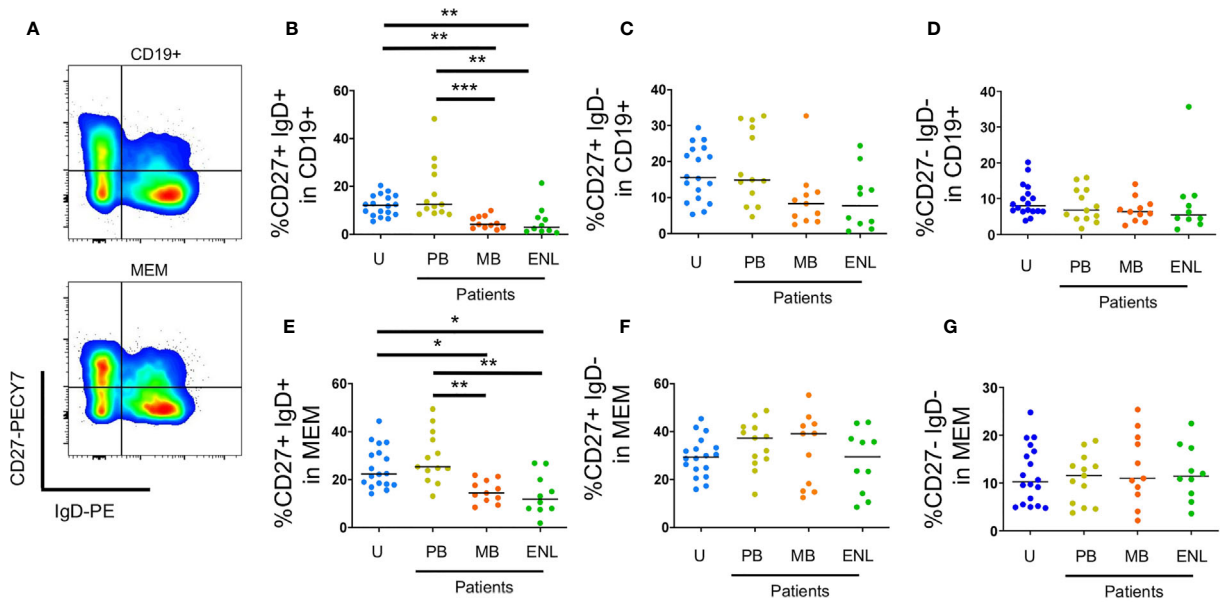

FIGURE 2 | Circulating memory B cells sorted by CD27 and IgD. PBMC of uninfected individuals (U), paucibacillary patients (PB), multibacillary patients in type II reaction (ENL) or not (MB) were freshly stained and analyzed by flow cytometry. **(A)** Pseudocolor plot profile for CD19+ B cells (top) and MEM B cells (bottom) for CD27 and IgD expression. Percentage of CD27+IgD+ **(B)**, CD27+IgD- **(C)** and CD27-IgD- **(D)** cells among CD19+ B cell subpopulation or MEM B cell subpopulation (**E–G**, respectively). Each dot represents one donor and lines represent median values for each group. Significant values (*) were calculated by Kruskal-Wallis tests with Dunn's multiple comparisons test. *$p < 0.05$; **$p < 0.005$; ***$p < 0.0005$.

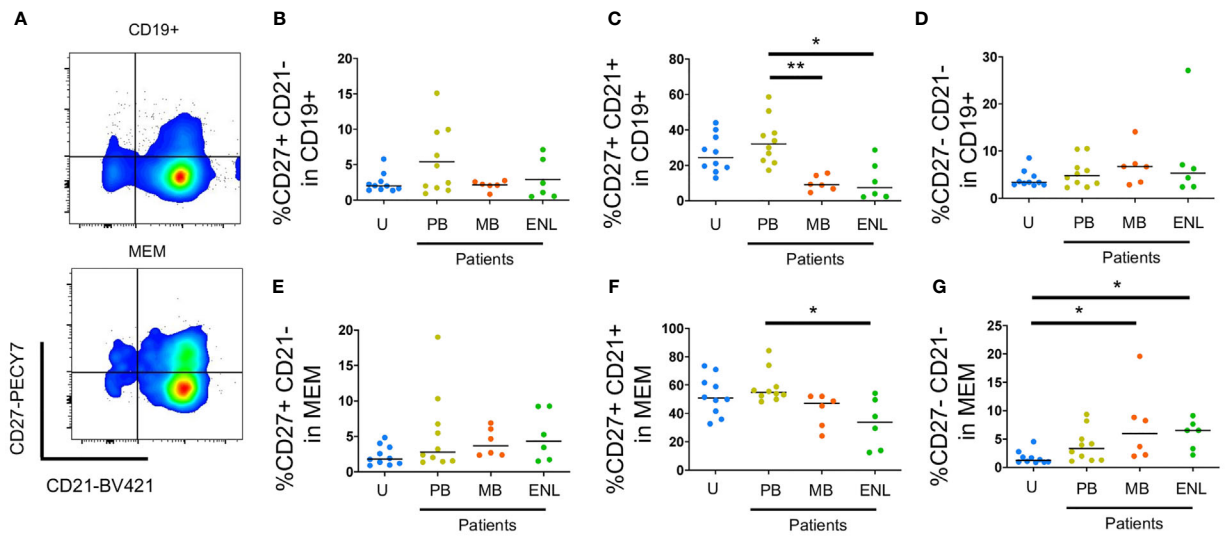

FIGURE 3 | Circulating B cells sorted by CD21 and CD27. PBMC of uninfected individuals (U), paucibacillary patients (PB), multibacillary patients in type II reaction (ENL) or not (MB) were freshly stained and analyzed by flow cytometry. **(A)** Pseudocolor plot profile for CD19+ B cells (top) and MEM B cells (bottom) for CD21 and CD27 expression. Percentage of CD27+CD21- **(B)**, CD27+CD21+ **(C)**, and CD27-CD21- **(D)** cells among CD19+ B cell subpopulation or MEM B cell subpopulation (**E–G**, respectively). Each dot represents one donor and lines represent median values for each group. Significant values (*) were calculated by the Kruskal-Wallis test with Dunn's multiple comparisons test. *$P < 0.05$; **$p < 0.005$; ***$p < 0.0005$.

We acknowledge that one limitation of the present study is the absence of functional analysis but a previous morphometric analysis of B cells and plasma cells in ENL demonstrated a positive correlation with CD3-positive pan T cells in the biopsy and a negative correlation with T regulatory – T cell ratio (32).

Negera and colleagues reported that mature and memory B cells on patients with MB leprosy have no different frequencies

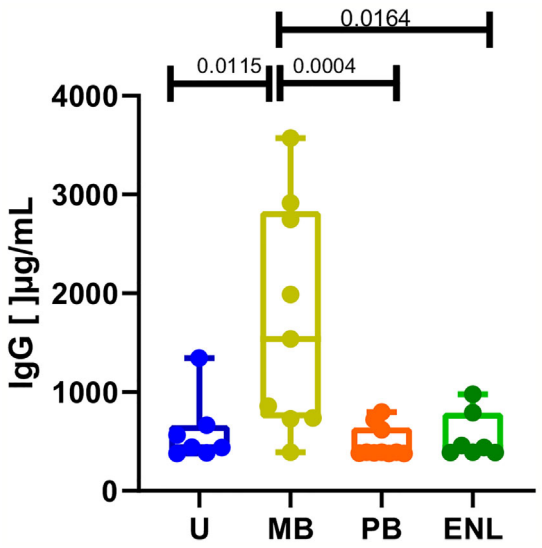

FIGURE 4 | Total IgG levels measured by ELISA in sera from uninfected individuals (U), paucibacillary patients (PB), multibacillary patients in type II reaction (ENL) or not (MB). Significant values were calculated by the Kruskal-Wallis test with Dunn's multiple comparisons test. A p-value < 0.05 was considered statistically significant.

from the ones in ENL (23). However, our data showed that, during ENL, atypical B cells (CD27-CD21-) decreased whereas activated B cells (CD27+CD21) increased in frequency. Despite the lack of consensus, those two subpopulations of memory B cells differ in function: activated B cells are readily prone to BCR reactivation and atypical B cells may represent an exhausted/anergic phenotype or a normal lineage of B cells with repeated antigen encounters (33).

In addition, CD27+CD21+ resting memory B cells were diminished in patients with MB leprosy, with only a slight significant increase in atypical memory B cells. Several reports point toward an increased subpopulation of atypical memory B cells in diseases with chronic antigen stimulation and many display a robust circulation of proinflammatory mediators (34, 35). However, multibacillary leprosy displays several anti-inflammatory mechanisms that favor pathogen persistence (15). It is well established that lipid mediators derived from the metabolism of ω3 and ω6 polyunsaturated fatty acids (PUFAs) are present in leprosy and its reactions and may play important roles in the modulation of the innate and adaptive immune responses (15, 36): patients with MB leprosy have higher levels of lipid mediators (prostaglandin E_2, leukotriene B_4, lipoxin A_4) when compared to PB, and these substances can inhibit B cell activation (37–39). Furthermore, it is known that lipoxin A_4 can inhibit the production of specific memory B cell antibodies (38). Because only a slight increase in the frequency of atypical memory B among the pool of total memory B cells was observed, we hypothesize that these anti-inflammatory mechanisms may impact memory B cell activation counterbalancing a high antigen availability with low or refractory T cell help. Also, the expansion of mature B cells may be the reason why atypical memory B cells were only statistically significant when analyzed in the memory cell pool. Our future studies will aim at the identification of which memory B cells are diminished or whether all phenotypes are equally diminished in patients with MB leprosy.

CD27+IgD+IgM+ memory B cells are also called marginal zone B cells and are pivotal to the response against encapsulated bacteria (40). Here, a great reduction in this subpopulation was observed in the multibacillary group. Indeed, some authors report that *M. leprae* (41) and cell wall components (42) are present in the blood. This high antigen availability may promote an enhanced plasma cell differentiation chronically in a manner that no great impact is immediately observed on plasmablast frequencies, for changes in this compartment are transient and detected easily during acute infections or vaccination (40).

Circulating memory B cells may also undergo apoptosis or be redistributed to other compartments. For instance, B cells are detected frequently in LL/BL lesions but sporadically observed in BT granulomas (43), in which both mature and plasma cells were found. Another hypothesis for the reduced frequencies of circulating memory B cells could be inferred from the high levels of total IgG observed in patients with MB leprosy. A state of polyclonal activation would activate memory B cell clones both nonspecific and *M. leprae*-specific to differentiate into plasma cells and increase the production of antibodies by the bone marrow resident cells. Indeed, the hypothesis of hypergammaglobulinemia in leprosy was already suggested by other groups (44, 45), although no specific antigen was implicated. Recently, our group showed that bacterial histone-like protein (hlp) and human DNA were increased in patients with MB leprosy when B cells also had increased levels of TLR9 expression (46). One of the mechanisms of maintenance of antibody levels is the induced recall by small quantities of bacterial DNA which promotes antibody production of all specificities and all subclasses (47). This serological memory is kept by bone marrow-resident plasma cells and by memory B cells, which are constantly restimulated by bystander cytokines and TLR-triggering on B cells in an antigen-independent way (48). Furthermore, both memory and naïve B cells could acquire plasma-cell phenotype *in vitro* after CpG stimulation (49). However, the persistence of *M. leprae*-derived circulating antigens, especially the bacterial DNA-histone complex, could impact memory and naïve B cell subpopulations. Therefore, we hypothesized that a state of polyclonal B cell activation by bacterial compounds would promote mature B cell expansion and migration of memory B cells to bone marrow or infection sites, reflected in increased numbers of the former and diminished numbers of the latter in the circulating pool.

B cell homeostasis is a highly regulated process, in which bone marrow is constantly producing B cells. Circulating B cells and soluble factors are responsible for B cell frequency maintenance in the peripheral tissues (50). Patients with MB leprosy have increased circulating mature B cells, however, no impact in transitional B cells was reported. Because the latter represents recent egress cells from bone marrow, higher production of B cells

would impact transitional B cell frequency (51). Therefore, we cannot exclude the hypothesis that an increased production of survival factors in the periphery may diminish naïve B cell death.

Type II reaction or ENL is a pathological process that may be related to the break of *M. leprae* tolerance caused by MDT treatment and viral infections, for example (52). It results in a systemic inflammation to the bacillus which is often recurrent or chronic and is treated with corticosteroid or thalidomide (22). Negera et al. demonstrated that memory B cells are impacted after ENL treatment in paired samples, suggesting that a controlled inflammation has a role in B cell pool frequencies. As bacterial killing is enhanced in patients with ENL (53), there is a consequent increase in antigen availability, however, no differences in all B cell frequencies among patients with MB and ENL were observed here, but in total IgG levels. Those could be explained by the increased formation of immune complexes during ENL because of the high antigen availability (54).

The presence of different functionally active B-cell stages within lesions of patients with leprosy, including BT patients, which could secrete anti-*M*. leprae-specific antibodies were described (43). Our data suggest that antigen availability that occurs in patients with high bacillary load (MB and ENL) may be associated with alterations in the frequency and function of B-cell subpopulations (mature and memory B cells). It remains to be clarified whether the impact on the B cell pool is directly contributing to the clinical state of patients with MB leprosy or is simply a consequence of a failure in the interferon gamma (IFN-γ) efficient response in those patients, especially because patients with PB leprosy who can contain bacterial spread show similar B cell frequencies as uninfected subjects. To the best of our knowledge, it is the first study that demonstrates these different B cell phenotypes in polar forms of leprosy and in ENL, which can contribute to elucidate the role of B cell phenotypes in the disease.

DATA AVAILABILITY STATEMENT

The raw data supporting the conclusions of this article will be made available by the authors, without undue reservation.

ETHICS STATEMENT

The studies involving human participants were reviewed and approved by FIOCRUZ Research Ethics Committee (CAAE 01247418.8.0000.5248). Written informed consent to participate in this study was provided by the participants' legal guardian/next of kin.

AUTHOR CONTRIBUTIONS

ON and MG designed the analyses, collected, and analyzed data, and wrote the manuscript. VF and NC contributed with data collection. RR-d-S and JL contributed with analysis tools. RP, GP, and MP designed the analyses and supervised experimental work. CM supervised and wrote the manuscript. All authors contributed to the article and approved the submitted version.

FUNDING

This work was supported by The New York Community Trust/ Heiser Program for Research on Leprosy and The National Institute of Allergy and Infectious Diseases of the National Institutes of Health (NIAID/NIH) under the award number RO1AI129835.

ACKNOWLEDGMENTS

ON and NC received scholarships from CAPES, Brazil.

SUPPLEMENTARY MATERIAL

The Supplementary Material for this article can be found online at: https://www.frontiersin.org/articles/10.3389/fimmu.2021.727580/full#supplementary-material

REFERENCES

1. World Health Organization. *Organisation Mondiale De La S. Weekly Epidemiological Record*, Vol. 95. World Health Organization. (2020). p. 36.
2. Daumerie D. *Elimination of Leprosy as a Public Health Problem – Current Status and Challenges Ahead*. Geneva: World Health Organization (2002).
3. Scollard DM, Adams LB, Gillis TP, Krahenbuhl JL, Truman RW, Williams DL. The Continuing Challenges of Leprosy. *Clin Microbiol Rev* (2006) 19 (2):338–81. doi: 10.1128/CMR.19.2.338-381.2006
4. WHO. *Chemotherapy for Leprosy Control Programmes*. World Health Organization. (1982).
5. Scollard DM. The Biology of Nerve Injury in Leprosy. *Leprosy Rev* (2008) 79 (3):242–53. doi: 10.47276/lr.79.3.242
6. Scollard DM, Truman RW, Ebenezer GJ. Mechanisms of Nerve Injury in Leprosy. *Clinics Dermatol* (2015) 33(1):46–54. doi: 10.1016/j.clindermatol.2014.07.008
7. Dupnik KM, Bair TB, Maia AO, Amorim FM, Costa MR, Keesen TS, et al. Transcriptional Changes That Characterize the Immune Reactions of Leprosy. *J Infect Dis* (2015) 211(10):1658–76. doi: 10.1093/infdis/jiu612
8. Mabalay MC, Helwig EB, Tolentino JG, Binford CH. The Hispatology and Histochemisty of Erythema Nodosum Leprosum. *Int J Lepr* (1965) 33:28–49.
9. de Macedo CS, Anderson DM, Pascarelli BM, Spraggins JM, Sarno EN, Schey KL, et al. MALDI Imaging Reveals Lipid Changes in the Skin of Leprosy Patients Before and After Multidrug Therapy (MDT). *J Mass Spectrometry JMS* (2015) 50(12):1374–85. doi: 10.1002/jms.3708
10. Sakurai I, Skinsnes OK. Lipids in Leprosy. 2. Histochemistry of Lipids in Human Leprosy. *Int J Leprosy Other Mycobacterial Dis Off Organ Int Leprosy Assoc* (1970) 38(4):389–403.
11. DeFranco AL, Rookhuizen DC, Hou B. Contribution of Toll-Like Receptor Signaling to Germinal Center Antibody Responses. *Immunol Rev* (2012) 247 (1):64–72. doi: 10.1111/j.1600-065X.2012.01115.x
12. Freeman SA, Jaumouillé V, Choi K, Hsu BE, Wong HS, Abraham L, et al. Toll-Like Receptor Ligands Sensitize B-Cell Receptor Signalling by Reducing Actin-Dependent Spatial Confinement of the Receptor. *Nat Commun* (2015) 6:6168. doi: 10.1038/ncomms7168
13. Duthie MS, Hay MN, Rada EM, Convit J, Ito L, Oyafuso LK, et al. Specific IgG Antibody Responses may be Used to Monitor Leprosy Treatment Efficacy and

as Recurrence Prognostic Markers. *Eur J Clin Microbiol Infect Dis Off Publ Eur Soc Clin Microbiol* (2011) 30(10):1257–65. doi: 10.1007/s10096-011-1221-2
14. Paula Vaz Cardoso L, Dias RF, Freitas AA, Hungria EM, Oliveira RM, Collovati M, et al. Development of a Quantitative Rapid Diagnostic Test for Multibacillary Leprosy Using Smart Phone Technology. *BMC Infect Dis* (2013) 13:497. doi: 10.1186/1471-2334-13-497
15. de Macedo CS, Lara FA, Pinheiro RO, Schmitz V, de Berredo-Pinho M, Pereira GM, et al. New Insights Into the Pathogenesis of Leprosy: Contribution of Subversion of Host Cell Metabolism to Bacterial Persistence, Disease Progression, and Transmission. *F1000Research* (2020) 9:1–9. doi: 10.12688/f1000research.21383.1
16. Hacker MA, Sales AM, Duppre NC, Sarno EN, Moraes MO. Leprosy Incidence and Risk Estimates in a 33-Year Contact Cohort of Leprosy Patients. *Sci Rep* (2021) 11(1):1947. doi: 10.1038/s41598-021-81643-4
17. Düppre NC, Camacho LA, Sales AM, Illarramendi X, Nery JA, Sampaio EP, et al. Impact of PGL-I Seropositivity on the Protective Effect of BCG Vaccination Among Leprosy Contacts: A Cohort Study. *PloS Negl Trop Dis* (2012) 6(6):e1711. doi: 10.1371/journal.pntd.0001711
18. Spencer JS, Brennan PJ. The Role of Mycobacterium Leprae Phenolic Glycolipid I (PGL-I) in Serodiagnosis and in the Pathogenesis of Leprosy. *Leprosy Rev* (2011) 82(4):344–57. doi: 10.47276/lr.82.4.344
19. Moura DF, de Mattos KA, Amadeu TP, Andrade PR, Sales JS, Schmitz V, et al. CD163 Favors Mycobacterium Leprae Survival and Persistence by Promoting Anti-Inflammatory Pathways in Lepromatous Macrophages. *Eur J Immunol* (2012) 42(11):2925–36. doi: 10.1002/eji.201142198
20. Lahiri R, Sandoval FG, Krahenbuhl JL, Shannon EJ. Activation of Complement by Mycobacterium Leprae Requires Disruption of the Bacilli. *Leprosy Rev* (2008) 79(3):311–4. doi: 10.47276/lr.79.3.311
21. Gomes GI, Nahn EPJr., Santos RK, Da Silva WD, Kipnis TL. The Functional State of the Complement System in Leprosy. *Am J Trop Med Hygiene* (2008) 78(4):605–10. doi: 10.4269/ajtmh.2008.78.605
22. Polycarpou A, Walker SL, Lockwood DNJ. A Systematic Review of Immunological Studies of Erythema Nodosum Leprosum. *Front Immunol* (2017) 8:233. doi: 10.3389/fimmu.2017.00233
23. Negera E, Walker SL, Bekele Y, Dockrell HM, Lockwood DN. Increased Activated Memory B-Cells in the Peripheral Blood of Patients With Erythema Nodosum Leprosum Reactions. *PloS Negl Trop Dis* (2017) 11(12):e0006121. doi: 10.1371/journal.pntd.0006121
24. Kotb A, Ismail S, Kimito I, Mohamed W, Salman A, Mohammed AA. Increased CD5+ B-Cells are Associated With Autoimmune Phenomena in Lepromatous Leprosy Patients. *J Infect Public Health* (2019) 12(5):656–9. doi: 10.1016/j.jiph.2019.03.001
25. Tarique M, Naz H, Kurra SV, Saini C, Naqvi RA, Rai R, et al. Interleukin-10 Producing Regulatory B Cells Transformed CD4(+)CD25(-) Into Tregs and Enhanced Regulatory T Cells Function in Human Leprosy. *Front Immunol* (2018) 9:1636. doi: 10.3389/fimmu.2018.01636
26. Ridley DS, Jopling WH. Classification of Leprosy According to Immunity. A Five-Group System. *Int J Leprosy Other Mycobacterial Dis Off Organ Int Leprosy Assoc* (1966) 34(3):255–73.
27. Matos ADS, Rodrigues-da-Silva RN, Soares IF, Baptista BO, de Souza RM, Bitencourt-Chaves L, et al. Antibody Responses Against Plasmodium Vivax TRAP Recombinant and Synthetic Antigens in Naturally Exposed Individuals From the Brazilian Amazon. *Front Immunol* (2019) 10:2230. doi: 10.3389/fimmu.2019.02230
28. Simon Q, Pers JO, Cornec D, Le Pottier L, Mageed RA, Hillion S. In-Depth Characterization of CD24(high)CD38(high) Transitional Human B Cells Reveals Different Regulatory Profiles. *J Allergy Clin Immunol* (2016) 137 (5):1577–84.e10. doi: 10.1016/j.jaci.2015.09.014
29. Carsetti R, Rosado MM, Donnanno S, Guazzi V, Soresina A, Meini A, et al. The Loss of IgM Memory B Cells Correlates With Clinical Disease in Common Variable Immunodeficiency. *J Allergy Clin Immunol* (2005) 115 (2):412–7. doi: 10.1016/j.jaci.2004.10.048
30. Das A, Xu H, Wang X, Yau CL, Veazey RS, Pahar B. Double-Positive CD21 +CD27+ B Cells are Highly Proliferating Memory Cells and Their Distribution Differs in Mucosal and Peripheral Tissues. *PloS One* (2011) 6 (1):e16524. doi: 10.1371/journal.pone.0016524
31. Fabel A, Giovanna Brunasso AM, Schettini AP, Cota C, Puntoni M, Nunzi E, et al. Pathogenesis of Leprosy: An Insight Into B Lymphocytes and Plasma Cells. *Am J Dermatopathology* (2019) 41(6):422–7. doi: 10.1097/DAD.0000000000001310
32. Biswas D, Sethy M, Behera B, Palit A, Mitra S. Image Morphometric Analysis of B Cells and Plasma Cells in Erythema Nodosum Leprosum With Clinicopathological Correlation. *Am J Dermatopathology* (2020). doi: 10.1097/DAD.0000000000001860
33. Sutton HJ, Aye R, Idris AH, Vistein R, Nduati E, Kai O, et al. Atypical B Cells are Part of an Alternative Lineage of B Cells That Participates in Responses to Vaccination and Infection in Humans. *Cell Rep* (2021) 34(6):108684. doi: 10.1016/j.celrep.2020.108684
34. Portugal S, Obeng-Adjei N, Moir S, Crompton PD, Pierce SK. Atypical Memory B Cells in Human Chronic Infectious Diseases: An Interim Report. *Cell Immunol* (2017) 321:18–25. doi: 10.1016/j.cellimm.2017.07.003
35. Portugal S, Tipton CM, Sohn H, Kone Y, Wang J, Li S, et al. Malaria-Associated Atypical Memory B Cells Exhibit Markedly Reduced B Cell Receptor Signaling and Effector Function. *eLife* (2015) 4:1–21. doi: 10.7554/eLife.07218
36. Silva CAM, Belisle JT. Host Lipid Mediators in Leprosy: The Hypothesized Contributions to Pathogenesis. *Front Immunol* (2018) 9:134. doi: 10.3389/fimmu.2018.00134
37. Murn J, Alibert O, Wu N, Tendil S, Gidrol X. Prostaglandin E2 Regulates B Cell Proliferation Through a Candidate Tumor Suppressor, Ptger4. *J Exp Med* (2008) 205(13):3091–103. doi: 10.1084/jem.20081163
38. Ramon S, Bancos S, Serhan CN, Phipps RP. Lipoxin A_4 Modulates Adaptive Immunity by Decreasing Memory B-Cell Responses via an ALX/FPR2-Dependent Mechanism. *Eur J Immunol* (2014) 44(2):357–69. doi: 10.1002/eji.201343316
39. Liu A, Claesson HE, Mahshid Y, Klein G, Klein E. Leukotriene B4 Activates T Cells That Inhibit B-Cell Proliferation in EBV-Infected Cord Blood-Derived Mononuclear Cell Cultures. *Blood* (2008) 111(5):2693–703. doi: 10.1182/blood-2007-08-102319
40. Palm AE, Henry C. Remembrance of Things Past: Long-Term B Cell Memory After Infection and Vaccination. *Front Immunol* (2019) 10:1787. doi: 10.3389/fimmu.2019.01787
41. Drutz DJ, Chen TSN, Lu W-H. The Continuous Bacteremia of Lepromatous Leprosy. *New Engl J Med* (1972) 287(4):159–64. doi: 10.1056/NEJM197207272870402
42. Cho SN, Cellona RV, Fajardo TTJr., Abalos RM, dela Cruz EC, Walsh GP, et al. Detection of Phenolic Glycolipid-I Antigen and Antibody in Sera From New and Relapsed Lepromatous Patients Treated With Various Drug Regimens. *Int J Leprosy Other Mycobacterial Dis Off Organ Int Leprosy Assoc* (1991) 59(1):25–31.
43. Iyer AM, Mohanty KK, van Egmond D, Katoch K, Faber WR, Das PK, et al. Leprosy-Specific B-Cells Within Cellular Infiltrates in Active Leprosy Lesions. *Hum Pathol* (2007) 38(7):1065–73. doi: 10.1016/j.humpath.2006.12.017
44. Bonomo L, Dammacco F, Gillardi U. Hypergammaglobulinemia, Secondary Macroglobulinemia and Paraproteinemia in Leprosy. *Int J Leprosy Other Mycobacter Dis Off Organ Int Leprosy Assoc* (1969) 37 (3):280–7.
45. Jha P, Balakrishnan K, Talwar GP, Bhutani LK. Status of Humoral Immune Responses in Leprosy. *Int J Leprosy Other Mycobacterial Dis Off Organ Int Leprosy Assoc* (1971) 39(1):14–9.
46. Dias AA, Silva CO, Santos JP, Batista-Silva LR, Acosta CC, Fontes AN, et al. DNA Sensing via TLR-9 Constitutes a Major Innate Immunity Pathway Activated During Erythema Nodosum Leprosum. *J Immunol (Baltimore Md 1950)* (2016) 197(5):1905–13. doi: 10.4049/jimmunol.1600042
47. Capolunghi F, Cascioli S, Giorda E, Rosado MM, Plebani A, Auriti C, et al. CpG Drives Human Transitional B Cells to Terminal Differentiation and Production of Natural Antibodies. *J Immunol (Baltimore Md 1950)* (2008) 180 (2):800–8. doi: 10.4049/jimmunol.180.2.800
48. Dorner M, Brandt S, Tinguely M, Zucol F, Bourquin JP, Zauner L, et al. Plasma Cell Toll-Like Receptor (TLR) Expression Differs From That of B Cells, and Plasma Cell TLR Triggering Enhances Immunoglobulin Production. *Immunology* (2009) 128(4):573–9. doi: 10.1111/j.1365-2567.2009.03143.x

49. Huggins J, Pellegrin T, Felgar RE, Wei C, Brown M, Zheng B, et al. CpG DNA Activation and Plasma-Cell Differentiation of CD27- Naive Human B Cells. *Blood* (2007) 109(4):1611–9. doi: 10.1182/blood-2006-03-008441
50. Crowley JE, Scholz JL, Quinn WJ3rd, Stadanlick JE, Treml JF, Treml LS, et al. Homeostatic Control of B Lymphocyte Subsets. *Immunologic Res* (2008) 42(1-3):75–83. doi: 10.1007/s12026-008-8036-y
51. Bemark M. Translating Transitions - How to Decipher Peripheral Human B Cell Development. *J Biomed Res* (2015) 29(4):264–84. doi: 10.7555/JBR.29.20150035
52. Schmitz V, Tavares IF, Pignataro P, Machado AM, Pacheco FDS, Dos Santos JB, et al. Neutrophils in Leprosy. *Front Immunol* (2019) 10:495. doi: 10.3389/fimmu.2019.00495
53. Vieira LM, Sampaio EP, Nery JA, Duppre NC, Albuquerque EC, Scheinberg MA, et al. Immunological Status of ENL (Erythema Nodosum Leprosum) Patients: Its Relationship to Bacterial Load and Levels of Circulating IL-2r. *Rev Inst Med Trop Sao Paulo* (1996) 38(2):103–11. doi: 10.1590/S0036-46651996000200004
54. Amorim FM, Nobre ML, Nascimento LS, Miranda AM, Monteiro GRG, Freire-Neto FP, et al. Differential Immunoglobulin and Complement Levels in Leprosy Prior to Development of Reversal Reaction and Erythema Nodosum Leprosum. *PloS Negl Trop Dis* (2019) 13(1):e0007089. doi: 10.1371/journal.pntd.0007089

Conflict of Interest: The authors declare that the research was conducted in the absence of any commercial or financial relationships that could be construed as a potential conflict of interest.

Publisher's Note: All claims expressed in this article are solely those of the authors and do not necessarily represent those of their affiliated organizations, or those of the publisher, the editors and the reviewers. Any product that may be evaluated in this article, or claim that may be made by its manufacturer, is not guaranteed or endorsed by the publisher.

frontiers in Immunology

ORIGINAL RESEARCH
published: 23 September 2021
doi: 10.3389/fimmu.2021.687044

A Bumpy Ride of Mycobacterial Phagosome Maturation: Roleplay of Coronin1 Through Cofilin1 and cAMP

*Saradindu Saha[1], Arnab Hazra[1], Debika Ghatak[1], Ajay Vir Singh[2], Sadhana Roy[1] and Somdeb BoseDasgupta[1]**

[1] Molecular Immunology and Cellular Microbiology Laboratory, Department of Biotechnology, Indian Institute of Technology Kharagpur, Kharagpur, India, [2] Department of Microbiology and Molecular Biology, ICMR-National JALMA Institute of Leprosy and Other Mycobacterial Diseases, Agra, India

OPEN ACCESS

Edited by:
Rosane M. B. Teles, University of California, Los Angeles, United States

Reviewed by:
Kindra Kelly-Scumpia, University of California, Los Angeles, United States
Hridayesh Prakash, Amity University, India

***Correspondence:**
Somdeb BoseDasgupta
somdeb@iitkgp.ac.in

Specialty section:
This article was submitted to Microbial Immunology, a section of the journal Frontiers in Immunology

Received: *28 March 2021*
Accepted: *17 August 2021*
Published: *23 September 2021*

Citation:
Saha S, Hazra A, Ghatak D, Singh AV, Roy S and BoseDasgupta S (2021) A Bumpy Ride of Mycobacterial Phagosome Maturation: Roleplay of Coronin1 Through Cofilin1 and cAMP. Front. Immunol. 12:687044. doi: 10.3389/fimmu.2021.687044

Phagosome-lysosome fusion in innate immune cells like macrophages and neutrophils marshal an essential role in eliminating intracellular microorganisms. In microbe-challenged macrophages, phagosome-lysosome fusion occurs 4 to 6 h after the phagocytic uptake of the microbe. However, live pathogenic mycobacteria hinder the transfer of phagosomes to lysosomes, up to 20 h post-phagocytic uptake. This period is required to evade pro-inflammatory response and upregulate the acid-stress tolerant proteins. The exact sequence of events through which mycobacteria retards phagolysosome formation remains an enigma. The macrophage coat protein Coronin1 (Cor1) is recruited and retained by mycobacteria on the phagosome membrane to retard its maturation by hindering the access of phagosome maturation factors. Mycobacteria-infected macrophages exhibit an increased cAMP level, and based on receptor stimulus, Cor1 expressing cells show a higher level of cAMP than non-Cor1 expressing cells. Here we have shown that infection of bone marrow-derived macrophages with H37Rv causes a Cor1 dependent rise of intracellular cAMP levels at the vicinity of the phagosomes. This increased cAMP fuels cytoskeletal protein Cofilin1 to depolymerize F-actin around the mycobacteria-containing phagosome. Owing to reduced F-actin levels, the movement of the phagosome toward the lysosomes is hindered, thus contributing to the retarded phagosome maturation process. Additionally, Cor1 mediated upregulation of Cofilin1 also contributes to the prevention of phagosomal acidification, which further aids in the retardation of phagosome maturation. Overall, our study provides first-hand information on Cor1 mediated retardation of phagosome maturation, which can be utilized in developing novel peptidomimetics as part of host-directed therapeutics against tuberculosis.

Keywords: mycobacteria, BMDM, Coronin1, cAMP, Cofilin1

INTRODUCTION

Tuberculosis (TB) caused by *Mycobacterium tuberculosis* (*M. tb*) affects a quarter of the globe and has mortality over 1.5 million every year (1). Lack of an environmental reservoir causes *M.tb* to be an obligate intracellular parasite that predominantly chooses alveolar macrophages as its host and evades the host immune system. A significant setback in tuberculosis treatment is the emergence of extreme and total drug-resistant *M. tb* arising out of unregulated and discontinuous use of anti-mycobacterial in socioeconomically backward populations (2). Host-directed therapeutics are coming of age. Therefore, the need of the hour is to identify new drug targets for which one must comprehend the molecular intricacies between the host defense system and mycobacterium. Mycobacterial pathogenesis involves the secretion of several virulence factors (PknG, SapM, PtpA, Eis) and the hijacking of host factors (Coronin1, Calcineurin, SOCS1, CISH, LRG47, Gbp5) to establish its niche within the macrophages (3). Evolutionarily, Coronins are a family of actin-binding proteins that regulate several cellular functions such as cell migration, cytokinesis, phagocytosis, cytoskeletal reprogramming, etc. (4, 5).

Cor1 is a 57-kDa, trimeric protein in mammals, explicitly expressed in the hematopoietic cells and brain. The interaction of Cor1 with F-actin has been established, but whether this interaction has any role in mycobacterial pathogenesis remains to be elucidated (6). Cofilin1 is another protein, which is activated through dephosphorylation followed by F-actin depolymerization by cooperatively binding along the sides of actin filaments and inducing conformational changes in filament structure (7). Cor1 is known to activate Cofilin1 by activating the phosphatase Slingshot and thereby affecting actin dynamics (8). Deletion of Cor1 affects actin reorganization dynamics, thus influencing phagocytosis (9). Trimeric Cor1 being a cortical protein is recruited and retained by live pathogenic mycobacteria and it hinders phagolysosome formation (6). Knockout of Cor1 does not affect phagocytosis, but mycobacteria-containing phagosomes in these cells are rapidly acidified and fuse with lysosomes. Macrophage Cor1 gets upregulated in active TB patients (10), while ectopic Cor1 expression in Cor1 non-expressing cells has increased intracellular cAMP levels (11). Mycobacterial infection of macrophages raises the intracellular cAMP levels, which then impacts pathogenesis through yet unknown mechanisms. Therefore, it remains to be revealed whether Cor1 mediated activation of Cofilin1 and Cor1 mediated increase in threshold levels of cAMP are two different events or part of an interlinked signaling cascade promoting mycobacterial pathogenesis.

When immortalized bone-marrow-derived macrophages (BMDM) were infected with live mycobacteria, the intracellular cAMP levels were raised, but the same did not occur in Cor1 knockout macrophages. A mycobacterial infection-induced nascent overexpression of Cor1 was also observed, which then led to the activation of Cofilin1, which then increasingly depolymerized F-actin at the vicinity of the phagosomes. Consequently, phagosomal acidification was hindered, thus hindering phagosome-lysosome fusion. Conversely, Cor1 knockout macrophages failed to activate Cofilin1 upon mycobacterial infection, thus causing F-actin accumulation at the phagosomes that then promoted its acidification. For the first time, this study elucidates the mechanism of Cor1 mediated hindrance to phagosome maturation upon mycobacterial infection. We ascribe that mycobacterial infection causes Cor1 mediated elevation of intracellular cAMP, followed by activation of Cofilin1 and thereafter depolymerization of F-actin to hinder phagosomal acidification and thus its maturation.

MATERIALS AND METHODS

Cell Lines

Immortalized murine BMDM (WT and Cor1$^{-/-}$) as described in Reference 12 were used in this study unless otherwise stated. All macrophages were maintained in DMEM (Sigma-Aldrich) supplemented with 10% heat-inactivated FBS (Gibco) at 37°C in a humidified incubator with 5% CO_2. Cells were microscopically checked after every 24 hours and routinely split into new cultures when they reach 70% confluence.

Mycobacterial Culture

M. tb H37Rv, *M. bovis BCG* (*BCG*), and *M. smeg* were grown on 7H9 liquid medium (Sigma) containing 0.08% Tween 80 and supplemented with 10% OADC enrichment. Parallel sets of mycobacterial cultures were maintained, and subcultures were given from those with little to no mycobacterial clumps. *M. tb* H37Rv cultures were carried out in a biosafety level 3 facility of National Jalma Institute of Leprosy and Other Mycobacterial Diseases (NJILOMD), Agra, and National Institute for Research on Tuberculosis (NIRT), Chennai. All experiments with *M. tb* were carried out according to institutional guidelines of NJILOMD and NIRT. *M. bovis BCG* and *M. smeg* were cultured inside biosafety class 2 type A2 cabinets at IIT Kharagpur as per the institutional guidelines. Dead mycobacteria were prepared by heating mycobacteria-containing cultures at 65°C for 30 min followed by washing and resuspension in DMEM containing 2% FBS.

Reagents

Competitive cAMP-ELISA kits were procured from Cayman, rabbit monoclonal anti-LAMP1, anti-EEA1, and anti-Coronin1 antibody was from cell signaling technology (CST), mouse monoclonal anti-Cofilin1 antibody, rabbit monoclonal LAMP1, and rabbit monoclonal anti-phospho Cofilin1 antibody was from Sigma-Aldrich, and anti-cAMP antibody was from Santa Cruz Biotechnology. Mouse monoclonal anti-αtubulin antibody was from Novus Biologicals. Secondary antibodies conjugated with fluorophores AlexaFlour488 and 568 were from Life Technologies, DRAQ5 from CST. KH7, Rolipram, Slingshot inhibitor D3 were from Sigma-Aldrich. Protease inhibitor cocktail and phosphatase inhibitor were from Roche. 5x Bradford Reagent was from Bio-Rad, Supersignal West Pico chemiluminescent reagent, and ProLong Gold Antifade was from Life Technologies.

Isolation of Total RNA, Preparation of cDNA, and Real-Time PCR Analysis

Total RNA was isolated from untreated or different inhibitor treated BMDM with or without mycobacterial infection using Roche Total RNA isolation kit as per manufacturers protocol. The quality of total RNA was analyzed using a microvolume spectrophotometer to 260/280 ratio. First-strand cDNA synthesis was carried out using oligo dT (Roche) and Superscript II RT (Thermo) as per manufacturers protocol. PCR amplification was initially standardized before real-time analysis using the sense and antisense primers TCGGACC TGTTCCAGGAGGA CTGGG CTCTGGTGTAGC TCTT for Cor1 and CATCACTGCCA CCCAGAAGACTG and ATGCCA GTGAGCTTCCCGTTCAG for GAPDH, respectively. Next, real-time PCR was carried out using BioRad SSO advanced master mix and in a BioRad CFX96 system. Relative mRNA expression was quantified using the ΔΔCt method (12).

To analyze Th1/Th2 response inside BMDM macrophages upon infection with non-pathogenic *M. smegmatis* or pathogenic *M. tb (H37Rv)* at 0-h and 3-h chase times, the cells were pelleted, lysed, and total RNA was prepared and cDNA generated as described previously. Next, sense and antisense oligonucleotides for TNFa (GGTGCCTATGTCTCAGCCTCTT and GCCATAG AACTGATGAGAGGGAG), IL-10 (CGGGAAGACAA TAACTGCACCC and CGGTTAGCAGTATGTTGTCCAGC), $iNOS_2$ (GAGACAGGGAAGTCTGAAGCAC and CCAGC AGTAGTTGCTCCTCTTC), and Arginase1 (AACACTCC CCTGACAACCAG and CCAGCAGGTAGCTGAAGGTC) were used for qPCR analysis having GAPDH as the housekeeping gene and using BioRad SSO advanced master mix and in a BioRad CFX96 system. Relative mRNA expression was quantified using the ΔΔCt method. The fold change in expression over the GAPDH expression level was plotted. The experiments were carried out in triplicate with each sample set being in duplicate for each of the experiments.

Mycobacterial Infection

Mycobacterial infection of BMDM macrophages was carried out as described elsewhere (13). Before infection, cells were plated in a 10-cm dish or 6-well plates at 2.2 $\times 10^6$ or 3×10^5 cells, respectively. Log phase mycobacterial culture was taken in a 15-ml tube and centrifuged at 1000 g for 5 min to remove clumped mycobacteria. After that, the supernatant was taken in a fresh tube, centrifuged again at 4500 g for 5 min, followed by three washes using DMEM containing 2% FBS, and finally resuspended in it before adding it to BMDM cells and thereafter kept at 37°C incubator with 5% CO_2 for 1 h. Next, mycobacteria were removed, and the cells were washed with DMEM containing 10% FBS and incubated similarly for the different time periods as indicated. Unless otherwise stated, an MOI of 1:20 was used in our experiments, since at this MOI we obtained appreciable viability as well as infectivity as compared to MOI 1:10 where cell viability was higher but infectivity was lower, while at MOI 1:40 the infectivity was higher but cell viability was lower (**Supplementary Figure 1A**). Likewise, measurements of cAMP levels showed that for different MOI that were used, cells where an MOI of 1:20 was used for infection appropriate levels of cAMP were observed, which also increased with time of infection (**Supplementary Figure 1B**).

Cloning and Transfection

Total RNA isolated from wildtype BMDM cells was used to generate cDNA as described earlier. Using the sense and antisense primers AGGCGCGCCTATGAGCCGGCA GGTG GTTCG and CGGCTCGAGCTACTTGGCCTGAAC AGTCT, respectively, Coronin1 was amplified and cloned in the AscI and XhoI sites of pCMV6-entry. The purified pCMV6-entry-Cor1 plasmid was mixed with $Cor1^{-/-}$ BMDM in Buffer E1 of the Neon Transfection System, and transfection was carried out as per manufacturers protocol using the 100-µl kit. The expression of Cor1 in these transfectants was further confirmed through immunoblot analysis (**Supplementary Figure 2**).

Competitive ELISA for Measurement of Intracellular cAMP

Wildtype, $Cor1^{-/-}$, or Cor1 transfected $Cor1^{-/-}$ BMDM cells (5×10^5 cells/well of 6-well plates) were seeded for 24 h, after which they were either left untreated or pretreated with KH7 or Rolipram for 2 h. These cells were either kept uninfected or infected with *M. tb* (H37Rv), *M. bovis* BCG, or *M. smegmatis (M. smeg)* at different MOI (1:10, 1:20, 1:40) and chased for different time periods as indicated. After this, cells were washed with PBS three times to remove extracellular bacteria. After that, cells were lysed, and cAMP ELISA was carried out as per manufacturer's protocol (Cayman). The indicated is an average of three independent experiments.

Immunoblot Analysis

BMDM cells seeded at 5×10^5 cells/well of a 6-well plate for 24 h were inhibitor-treated and thereafter infected with mycobacteria at MOI of 1:20 for different time periods as indicated. In one set of experiments, macrophages were pretreated with MG132 (5uM) for 1 h and infected with *M. tb* in the presence of the same concentration of MG132 for indicated time points and thereafter lysed and immunoblotted. Differentially treated and infected macrophages were next washed with ice-cold 1X PBS and subsequently incubated with RIPA lysis buffer containing protease inhibitor cocktail for 20 min on ice. The lysed cells were centrifuged at 16000 g for 20 min at 4°C, and the supernatant was taken in a new tube. Protein estimation was done, and equal amounts (30 µg) of protein corresponding to each sample were electrophoresed in 10% SDS-PAGE, transferred to PVDF membrane, blocked, and immunoblotted with different antibodies as indicated. Primary antibodies of different dilutions as standardized in 5% FBS containing PBS were used. The membranes were washed with PBS-T three times before incubation of species-specific secondary antibodies. The membranes were thereafter rewashed three times with PBS-T, followed by developing the membranes using Supersignal WestPico chemiluminescent reagent (Thermo) and analyzed under a LAS500 imager (GE). The best image out of three independent experiments has been represented, while densitometry analysis was carried out for the three experiments and the average

data was plotted. The phospho-Cofilin1 specific densitometry values were generated after normalization with respective total Cofilin1 protein intensity.

Immunofluorescence Microscopy

BMDM cells were seeded on Teflon-coated 10-well chamber slides for 2 h before mycobacterial infection at an MOI of 1:20 was carried out. Cells were incubated with mycobacteria for 60 min followed by a chase period as indicated. These infected cells were fixed using 4% paraformaldehyde for 15 min followed by permeabilization with 0.02% saponin (Sigma-Aldrich) and then blocked using 5% FBS in PBS for 1 h. After that, incubation in primary antibody, diluted in 5% FBS containing PBS, was carried out for 4 h, washed with PBS, incubated with respective AlexaFluor conjugated secondary antibody for 1 h, and washed again with PBS. The cells were counterstained with DRAQ5 (CST) when required to stain the nucleus. For staining mycobacteria, rabbit anti-mycobacteria antibody and AF488 conjugated donkey anti-rabbit were used. For labelling LAMP1 or LAMP2 and Cor1, rat anti-LAMP1 or LAMP2 and goat anti-Cor1 were used followed by counterstaining with AF568 conjugated donkey anti-rat and AF647 conjugated donkey anti-goat antibodies, respectively. The cells were mounted using ProLong Gold Antifade reagent and imaged under an FV3000 confocal microscope (Olympus).

Measurement of Phagosomal Acidification Upon Mycobacterial Infection

For phagosomal pH measurement, mycobacteria were double-stained sequentially with 25 mM pH-sensitive pHrodo succinimidyl ester (Invitrogen) for 60 min at 37°C and 20 µg/mL pH insensitive Alexa Fluor 488 carboxylic acid (Invitrogen) as per manufacturers protocol. Thereafter, stained mycobacteria were washed three times with DMEM and resuspended in DMEM containing 2% FBS. BMDM cells were next infected using these labeled mycobacteria at an MOI of 1:20 for indicated time points. Non-internalized mycobacteria were removed by washing with PBS. Next, pH calibration was carried out by incubating infected cells in 10 mM phospho-citrate buffer with predetermined pH of 5 to 8. Finally, infected cells were fixed with 4% paraformaldehyde, and phagosomal pH was measured by monitoring the change in fluorescence of pH-sensitive dye pHrodo in a Cytation5 multimode reader (BioTek) against the fluorescent Alexa Fluor 488 fluorescence. For calculation of phagosomal pH, mean fluorescence intensity ratio of pHrodo and Alexa Fluor 488 was considered. Three independent experiments were carried out, and the average data were plotted.

Quantification of Nascent Coronin1 Upon Infection

BMDM cells were cultured in L-methionine-free DMEM medium containing 10% dialyzed FBS for 2 h to deplete intracellular methionine level. After that, L-AZA (4-Azido-L-homoalanine, ortho analog of L-methionine) was added to the medium and incubated for another 2 h before infection with mycobacteria at MOI of 1:20. The presence of L-AZA instead of methionine causes nascent expressed proteins to harbor L-AZA. After infection for indicated time points for labelling of nascent proteins, the cells were washed three times with PBS and lysed with ice-cold lysis buffer containing 1% Triton-X-100. The lysate was incubated with biotin-alkyne. By exploiting the "click reaction" between Azide and alkyne, all the nascent expressed proteins that had been L-AZA labelled were biotin-alkylated (14). These proteins were next precipitated with Streptavidin-agarose and, after that, electrophoresed and immunoblotted using anti-Cor1 or anti-b-tubulin antibodies and processed as described earlier.

Quantification of Mycobacterial Degradation

Macrophages can degrade pathogens by rapidly transferring them to lysosomes through the fusion of the phagosome and lysosome. Pathogenic mycobacteria are known to hinder phagosome maturation and fusion with lysosome while non-pathogenic mycobacteria are rapidly transferred to the lysosomes and degraded. Hence, in the context of our study we correlated phagolysosome formation to mycobacterial degradation and therefore the extent of phagolysosomes formation quantitated based on colocalized green, fluorescent mycobacteria and red fluorescent LAMP1 or LAMP2 stained lysosomes was observed and represented as a percentage of infected cells that were counted (n=100). The experiments were done in triplicate and the averaged values were plotted.

Quantification of Phagosome Associated F-Actin

Both WT and Cor1$^{-/-}$ BMDM were infected with mycobacteria at an MOI of 1:20 for indicated time periods followed by treatment with 1% formaldehyde to crosslink all complexes as well as phagosome-associated F-actin. After that, the cells were lysed using a hypotonic lysis buffer and passed through a 22-gauge needle to disrupt the large membrane complexes. This lysate was layered on top of a discontinuous sucrose gradient, and the F-actin crosslinked, mycobacteria-containing phagosomes were isolated as described earlier (15). These phagosomes were further processed for F-actin solubilization and immunoblotting, as mentioned in Jayachandran et al. (16).

To stain intracellular F-actin, Alexa Fluor 488 conjugated phalloidin was used. In order to obtain the extent of F-actin polymerization around the mycobacteria-containing phagosomes, a fixed line (denoted in red) specific fluorescence intensity measurement was carried out both from infected WT and Cor1$^{-/-}$ BMDM. Fluorescence intensity values corresponding to two fixed lines were recorded from each image (n=50) and thereafter these recorded arbitrary fluorescence units were averaged and plotted for WT and Cor1$^{-/-}$ either untreated or pretreated with slingshot inhibitor D3 prior to infection with *M. tb*.

Transmission Electron Microscopy

Wild type and Cor1$^{-/-}$ BMDM cells were infected with mycobacteria having an MOI of 1:20 for 2 h. After that, the cells were fixed in 2% glutaraldehyde in 0.2 M sodium cacodylate buffer containing 0.12 M

sucrose for 1 h at 41°C. After washing, the cells were post-fixed in osmium tetroxide (1.5%, w/v) and stained in 0.5% uranyl acetate. Next, dehydration was carried out in ethanol, clearing in propylene oxide, and embedding in Epon 812 was performed according to standard procedures (17). Sections were stained in 5% (w/v) uranyl acetate and 0.4% (w/v) lead citrate. These sections were taken on copper grids by the floatation method.

Labelling was performed on the section by floating the grids (section side down) on droplets of labelling reagent on Parafilm M inside a humid chamber. Blocking was done with 0.5% BSA containing PBS for 5 min, followed by incubation with biotinylated-phalloidin for 1 h at RT. Next, the grids were washed with blocking buffer 6 times with 2 min for each wash, followed by incubation with streptavidin colloidal gold conjugate for 40 min at RT (18). The grids were rewashed 4 times with 2 min for each wash using blocking buffer. The grids were thereafter inserted into a Zeiss Orion TEM and visualized. In case of immunogold transmission electron microscopy, gold nanoparticle labelled target proteins appear as dense dots against the background of stained cells.

Statistical Analysis

Results were analyzed with one-way ANOVA and *post hoc* multiple comparison test (Tukey HSD). Data are represented as mean ± SEM. $p \leq 0.05$ was statistically significant. Significance was shown as follows: *$p \leq 0.05$, **$p \leq 0.01$, NS, non significant, graph plotted and statistical significance were shown using Origin8 and GraphPad Prism 5 software.

RESULTS

Mycobacteria Infected Macrophages Exhibit an Increased Level of cAMP in Comparison to Uninfected Macrophages

Increased intracellular cAMP is known to suppress the innate immune response and hinder phagosome maturation by interfering with phagosomal actin assembly (19–21). Nevertheless, whether this rise of intra-macrophage cAMP upon mycobacterial infection was caused by mycobacteria alone (22) or if macrophage signaling plays a role remained undeciphered. To investigate this, we infected BMDM with mycobacteria and thereafter measured intracellular cAMP by competitive ELISA. It was observed for uninfected macrophages that there was no rise in cAMP levels with time but when these BMDM were infected with *M. tb* there was an initial burst of cAMP at 30 min, which increased significantly after 180 min of infection (**Figure 1A**). A similar observation was also seen in the case of *M. bovis BCG*. When BMDM were infected with heat-killed mycobacteria, the initial level of cAMP at 30 min was slightly higher than the uninfected control, but it declined to levels similar to uninfected BMDM after 180 min of infection. This initial surge of cAMP after 30 min was generated by macrophages alone as the infecting mycobacteria were heat-killed, thus indicating that macrophages do contribute toward the increased level of intracellular cAMP upon mycobacterial infection. Next, when we carried out infection with non-pathogenic *M. smeg*, a similar initial surge of cAMP at 30 min was observed and the levels were between that of heat-killed mycobacteria and live pathogenic mycobacteria, since *M. smeg* although being non-pathogenic does contribute partly to the intracellular cAMP level. Non-pathogenic, *M. smeg* containing phagosomes fuse with lysosomes by 180 min post-infection. Hence, the cAMP levels also fall considerably at this time.

Compared to live *M. tb* or *M. bovis BCG*, heat-killed *M. tb* or *M. smeg* fails to retain the Cor1 coat on the phagosome membrane (23). When we infected BMDM with live pathogenic and heat-killed *M. tb*, it was observed that both live and heat-killed *M. tb* had Cor1 recruited to the respective phagosomes at the 0-h time point but only live *M. tb* containing phagosomes could retain the Cor1 coat after 3 h of infection and heat-killed *M. tb* containing phagosomes fused with lysosomes as it failed to retain the Cor1 coat around the phagosome (**Figure 1B**). Therefore, the decrease of cAMP with increasing time of infection in the case of heat-killed pathogenic mycobacteria or non-pathogenic mycobacteria could be attributed to its failure in retaining the Cor1 coat on the phagosome membrane because Cor1 has earlier been shown to increase cAMP levels (11).

Next, we pre-incubated cells with the adenylate cyclase antagonist, KH7, and thereafter measured cAMP levels with or without mycobacterial infection. The cAMP levels of KH7 pretreated BMDM at 30 min were lower than that in untreated cells (**Figure 1C**). Although infection of KH7 pretreated BMDM with *M. tb* and *M. bovis BCG* exhibited a rise of cAMP levels compared to uninfected macrophages at 30 min, the levels were much lower than that observed in untreated cells. A similar trend was observed in the case of infection with heat-killed mycobacteria or non-pathogenic *M. smeg* (**Figure 1C**). After 180 min of infection of KH7 pretreated BMDM with *M. tb* and *M. bovis BCG*, the cAMP values did increase due to gradual reactivation of inhibited ACs with time, but the levels were not sufficient in preventing phagolysosome formation (**Supplementary Figure 1C**). Infection with heat-killed mycobacteria or *M. smeg* at 30 min of infection exhibited reduced cAMP levels compared to KH7 untreated cells but infected BMDM, and the difference remained even after 180 min of infection. This can be attributed to the lack of mycobacterial contribution toward an increase of cAMP both for heat-killed mycobacteria or non-pathogenic *M. smeg* (24–26). Concomitant to decreased levels of cAMP after 180 min of infection, the heat-killed mycobacteria or *M. smeg* containing phagosomes fused with the lysosomes (**Supplementary Figure 1C**). This could also be attributed to the failure in retaining the Cor1 coat on the phagosome membrane.

BMDM cells exhibit a higher level of cAMP in Rolipram treated cells owing to its inhibition of PDE4 (27), but the levels reduced after 3 h due to reactivation of PDE4 (**Figure 1D**). Infection of these Rolipram pretreated cells with *M. tb* or *M. bovis BCG* exhibited a higher level of cAMP at 30 min, which increases further after 3 h of infection (**Figure 1D**). Infection with heat-killed mycobacteria or non-pathogenic *M. smeg* exhibited cAMP levels slightly higher than that observed for Rolipram treated but uninfected cells at 30 min, and the cAMP level decreases considerably after 3 h of infection to levels lower

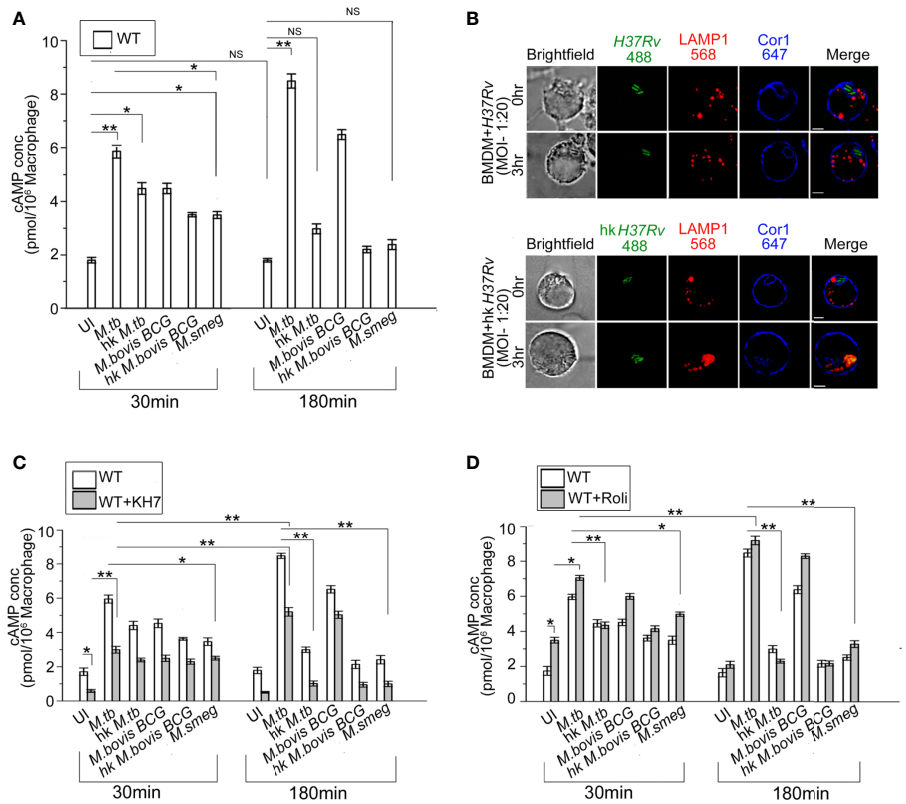

FIGURE 1 | **(A)** Intracellular cAMP concentration in uninfected and live *M. tb*, *M. bovis BCG*, *M. smeg*, heat-killed *M. tb*, and heat-killed *M. bovis BCG* infected BMDM after the indicated time points using competitive ELISA. **(B)** Immunofluorescence analysis of mycobacteria-infected macrophages. WT-BMDM infected with live *M. tb* or hk *M. tb* for indicated time points were stained for mycobacteria (green), lysosomes (LAMP1 in red), and Cor1 (blue). In the case of live *M. tb*-infected macrophages Cor1, recruited around phagosomes at 0-h time point was retained even after 3 h of infection, while for hk *M. tb*-infected macrophages Cor1 was not retained after 3 h of infection (scale:10 μm). **(C, D)** Competitive ELISA-based measurement of intracellular cAMP concentration in uninfected or live *M. tb*, *M. bovis BCG*, *M. smeg*, heat-killed *M. tb*, and heat-killed *M. bovis BCG* infected BMDM for the indicated time points without and after pretreatment with **(C)** adenylate cyclase inhibitor KH7 or **(D)** phosphodiesterase inhibitor Rolipram (n = 3). Data represents mean ± SEM; $^{*}p < 0.05$, $^{**}p < 0.01$, NS, non-significant.

than untreated levels for heat-killed mycobacteria but slightly higher in *M. smeg* infected cells (**Figure 1D**). But these levels were not sufficient to hinder phagolysosome formation (**Supplementary Figure 1C**). This fall in cAMP levels and concomitant phagolysosome formation could be attributed to the inability of heat-killed *M. tb* or *M. smeg* to retain the initial phagosome membrane-recruited Cor1. To ascertain this hypothesis, we carried out similar cAMP assays in Cor1 knockout BMDM.

Apart from LAMP1, LAMP2 is another lysosomal marker and sometimes a better determining factor in terms of phagolysosome formation. Hence, we carried out colocalization studies of mycobacteria with LAMP2 at indicated chase time points after infection with non-pathogenic *M. smeg* or pathogenic *M. tb*. Representative images as shown in **Supplementary Figure 1D** show that lysosomes are located close to mycobacteria-containing phagosomes at 0-h time point for *M. smeg* infected BMDM, and at 3 h phagosome-lysosome fusion has occurred in these cells. In contrast, for *M. tb* infected cells from 0-h timepoint itself the Cor1 scaffold around the phagosome is observed and it stays at the 3-h time point as well, thus hindering LAMP2 stained lysosomes to fuse with these phagosomes. To further analyze the role of AC inhibitor KH7 and PDE4 inhibitor Rolipram in the context of phagolysosome formation with respect to decrease or increase in the levels of intracellular cAMP, we pretreated cells with these inhibitors prior to infection with non-pathogenic *M. smeg* or pathogenic *M. bovis BCG* or *M. tb*. It was observed that phagolysosome formation majorly occurred in the case of *M. smeg* infection, and inhibition of PDE4 by Rolipram to increase intracellular cAMP to some extent could not prevent this phagolysosome formation (**Supplementary Figure 1E**). Infection with pathogenic mycobacteria by virtue of its ability to retain the Cor1 coat on the phagosome membrane could increase the cAMP levels and together with mycobacteria-generated cAMP could reach an above threshold level to hinder phagosome maturation. But KH7 treatment hindered the Cor1-induced macrophage cAMP production, thus reducing the intracellular cAMP level to be below the required threshold and hence causing the phagosomes to mature and fuse with lysosomes in the *M. bovis BCG* and *M. tb* infected macrophages.

Coronin1 Knockout Macrophages Exhibit a Lower Level of cAMP

Cor1, being a cortical macrophage protein, gets automatically recruited to mycobacterial phagosomes (16), but only live pathogenic mycobacteria can retain it on the phagosomal membrane through its secretion of lipoamide dehydrogenase (23). Ectopic expression of Cor1 in Cor1 non-expressing cells is known to exhibit increased cAMP levels upon GPCR triggering (11). Results from **Figures 1A, C, D** show that apart from mycobacteria, macrophages also contribute to the increase in intracellular cAMP levels upon mycobacterial infection (24). Hence, infection of Cor1$^{-/-}$ BMDM with live *M. tb* or *M. bovis BCG* resulted in cAMP levels that were lower than that of WT BMDM at 30 min. After 180 min of infection, Cor1$^{-/-}$ BMDM did not exhibit any rise in cAMP levels while there was a significant rise in cAMP levels of WT-BMDM infected macrophages (**Figure 2A**). The difference in cAMP levels between WT and Cor1$^{-/-}$ macrophages after 30 min of infection is indicative of the initial contribution of Cor1 toward cAMP production upon mycobacterial infection. The continued generation of cAMP owing to the presence of phagosome membrane bound Cor1 along with the mycobacteria-generated cAMP results in the high level of cAMP at 180 min post-infection. Thus, it was evident that the phagosome retained Cor1 contributes toward cAMP production with increasing time of infection and mycobacteria-generated cAMP only helps to keep the cAMP level at a higher threshold and static with increasing time of infection. Infection of Cor1$^{-/-}$ BMDM with heat-killed mycobacteria did not produce any appreciable amount of cAMP as compared to infected WT-BMDM or live mycobacteria infected Cor1$^{-/-}$ BMDM, and non-pathogenic *M. smeg* did not produce any appreciable amount of cAMP compared to infection of Cor1$^{-/-}$ BMDM with live mycobacteria or with infection of WT-BMDM with heat killed *M. tb*. The difference in the cAMP levels between Cor1$^{-/-}$ BMDM infected with live or heat-killed mycobacteria remained similar after 180 min of infection, but the difference in cAMP levels between WT and Cor1$^{-/-}$ BMDM infected with heat-killed mycobacteria reduced after 180 min of infection. Similarly, infection of Cor1$^{-/-}$ BMDM with non-pathogenic *M. smeg* after 30 min of infection exhibited a slightly lower level of cAMP compared to infection of WT-BMDM and the difference was non-significant after 180 min of infection.

Infection of KH7 pretreated Cor1$^{-/-}$ BMDM exhibited higher levels of cAMP at 30 min compared to untreated and uninfected Cor1$^{-/-}$ cells (**Figure 2B**), and this cAMP level increased considerably after 180 min of infection. The cAMP levels of untreated Cor1$^{-/-}$BMDM when infected with live pathogenic mycobacteria did not exhibit any increase, but there was a significant rise in the cAMP levels from 30 to 180 min after infection, between KH7 pretreated Cor1$^{-/-}$. This could be attributed to reduced initial level of cAMP in KH7 pretreated Cor1$^{-/-}$ cells as compared to untreated Cor1$^{-/-}$ and thereafter a

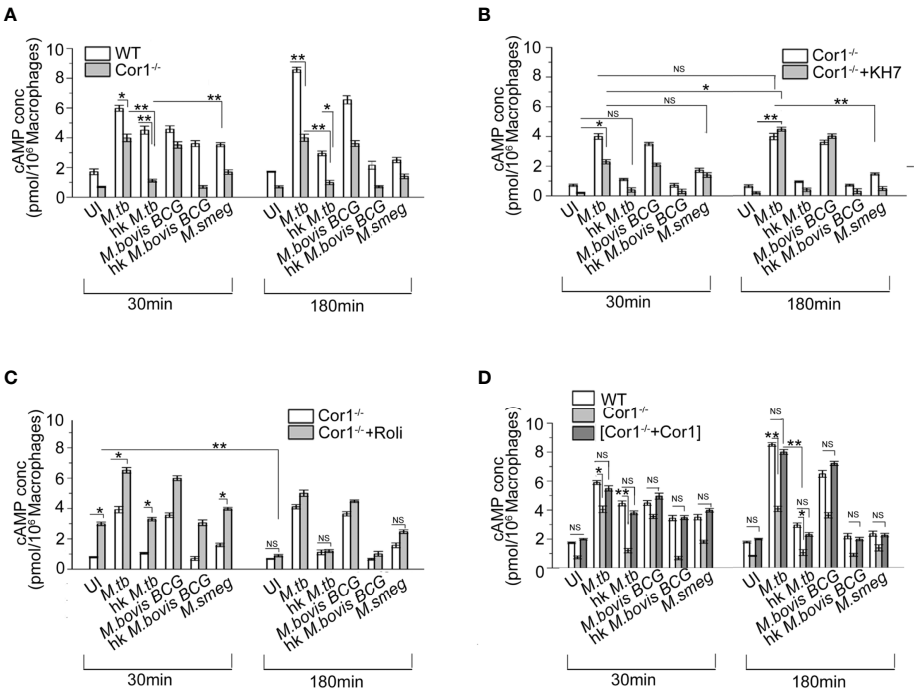

FIGURE 2 | Competitive ELISA-based measurement of intracellular cAMP concentration in uninfected and live *M. tb*, live *M. bovis BCG*, live *M. smeg*, heat-killed *M. tb*, and heat-killed *M. bovis BCG* infected **(A)** WT and Cor1$^{-/-}$ BMDM, **(B)** Cor1$^{-/-}$ BMDM without or after pretreatment with adenylate cyclase inhibitor KH7, and **(C)** Cor1$^{-/-}$ BMDM without or after pretreatment with phosphodiesterase inhibitor Roliparm or **(D)** transfected with pCMV6-Coronin1 for indicated time points (n = 3). Data represents mean ± SEM; *$p < 0.05$, **$p < 0.01$, NS, non-significant.

gradual cAMP production by adenylate cyclase with time due to the absence of KH7. The cAMP levels in KH7 pretreated $Cor1^{-/-}$ BMDM, upon infection with heat-killed mycobacteria, were similar to uninfected KH7 treated $Cor1^{-/-}$ BMDM. Interestingly, KH7 pretreated $Cor1^{-/-}$ BMDM when infected with *M. smeg* exhibited cAMP levels closer to KH7 pretreated $Cor1^{-/-}$ BMDM infected with live *M. tb* or *M. bovis BCG* at 30 min, but the cAMP levels fell for the former and rose for the later after 180 min of infection. This indicated that the initial level of cAMP at 30 min was contributed through infection in general but *M. smeg* being non-pathogenic failed to contribute toward cAMP production, which in contrast was carried out by live *M. tb* or *M. bovis BCG*.

Next, when $Cor1^{-/-}$ BMDM were treated with Rolipram, the cAMP level at 30 min was slightly elevated, and it decreased significantly after 180 min and became similar to untreated cells (**Figure 2C**). Since mycobacterial ACs generate an appreciable amount of cAMP, the live mycobacteria-infected macrophages in the Rolipram pretreated $Cor1^{-/-}$ BMDM exhibit a higher amount of cAMP at 30 min compared to untreated but infected cells. The cAMP level falls thereafter and becomes closely similar to that of untreated but infected cells (**Figure 2C**). Similarly, significant difference exists between the cAMP levels of untreated and Rolipram treated $Cor1^{-/-}$ BMDM after 30 min of infection with heat-killed mycobacteria or non-pathogenic *M. smeg*, but the cAMP levels become similar after 180 min of infection. Therefore, it is evident that the mycobacterial ACs, although capable of holding the cAMP level, are not enough to maintain it above the required threshold that is crucial for hindering phagosome maturation

Interestingly, when we expressed Cor1 inside $Cor1^{-/-}$ BMDM (**Supplementary Figure 2**) and measured the cAMP level in these transfectants with and without mycobacterial infection, it was observed that the cAMP values were close to that obtained from wild type BMDM, with and without mycobacterial infection (**Figure 2D**). The time-wise trend of increase or decrease of cAMP levels between that of ($Cor1^{-/-}$+Cor1) transfectant and $Cor1^{-/-}$ BMDM were similar to that observed in **Figure 2A** between WT-BMDM and Cor1 BMDM. This indicated that the differences observed in $Cor1^{-/-}$ were strictly due to the absence of Cor1-mediated cAMP production.

Mycobacterial Infection Induced Nascent Up-Regulation of Macrophage Coronin1

From the previous experiments, it is evident that mycobacterial infection-induced increased cAMP inside the macrophages is partly produced by mycobacteria and partly by the phagosome recruited Cor1 and the rise in cAMP level is due to retention of Cor1 on the phagosome by pathogenic mycobacteria. To understand the mechanism of Cor1-mediated rise of intracellular cAMP, we tested the transcript level of Cor1 in *M. tb*, *M. bovis BCG*, or *M. smeg*-infected macrophages after 3 h of infection using qRT PCR. Both live *M. tb* and *M. bovis BCG* infected macrophages exhibit a ~2.4-fold and 2-fold increase in Cor1 mRNA expression after 3 h of infection compared to uninfected macrophages, while there was no notable change in Cor1 expression upon infection with heat-killed mycobacteria or with *M. smeg* (**Figures 3A, B**). Next, we wanted to see if this increased level of Cor1 transcripts is also reflected at the protein level. Surprisingly, immunoblotting of mycobacteria-infected macrophage lysates did not exhibit any significant change in expression of Cor1 (**Supplementary Figure 3A**).

We assumed that the subtle difference in Cor1 level upon infection could be masked due to the long half-life of the abundant level of existing Cor1 in the cell or part of Cor1 could exist in a state of dynamic equilibrium of expression and degradation, and the increased expression of Cor1 is required to replenish the continuously degrading Cor1. If Cor1 gets degraded continuously, the hint for the same would be obtained by immunoblotting mycobacteria-infected macrophages that had been pretreated and also in the presence of the proteasomal degradation inhibitor MG132. Such an experiment exhibited a gradual increase in the level of Cor1 above that of the constitutive gene control. Pre-incubation as well as the presence of MG132 inhibited the 26S proteasome thus hindering degradation of both Cor1 as well as the constitutive gene b-tubulin. If mycobacterial infection increased the nascent expression of Cor1, then inhibition of the 26S proteasome would be exhibited by a greater increase in Cor1 level over the increase observed for the constitutive b-tubulin. From **Supplementary Figure 3B** we observed that a similar result was obtained and the nascent expression of Cor1 over control was plotted in the densitometry analysis. We next decided to study the nascent changes in Cor1 expression upon infection, using a non-radioactive L-AZA mediated assay as described in the *Materials and Methods* section. From this experiment, the difference in the expression level of nascent Cor1 was evident in the case of live mycobacteria and not heat-killed mycobacteria-infected macrophages (**Figures 3C, D**). Therefore, it can be stated that macrophages infected with live pathogenic mycobacteria not only recruit and retain Cor1 onto the phagosomal membrane but also bring about a nascent increase in Cor1 expression. This nascent increase of Cor1 expression is required to replenish the decreasing level of Cor1 on the phagosome membrane and thereby initiate cAMP production. Thus, the cumulative effect of retained Cor1 and increased Cor1 expression contributes toward the rise in cAMP levels above threshold values required to hinder phagosome maturation.

From the above data it is evident that mycobacterial infection leads to nascent overexpression of Cor1, which is essential to maintain the macrophage-generated cAMP essential to reach a threshold level of cAMP along with mycobacterial cAMP to hinder phagosome maturation. Whether such nascent overexpression has any implication in the Th1/Th2 response of the macrophage, when pretreated with AC inhibitor KH7 or PDE4 inhibitor Rolipram prior to infection with *M. smeg* or *M. tb*, must be determined. As markers of Th1 or pro-inflammatory response, we chose to monitor TNFa and iNOS2 expression, while markers chosen for Th2 or anti-inflammatory response were IL-10 and Arginase1 (Arg1). Indeed, it was observed that infection with *M. smeg* had higher levels of TNFa and iNOS2, which is indicative of a pro-inflammatory Th1 response in the context of the infected macrophages while infection with *M. tb* exhibited a higher IL-10 and Arg1 levels, which is indicative of a Th2 or anti-inflammatory response in the context of the macrophages (**Supplementary Figure 4**). Interestingly, BMDMs

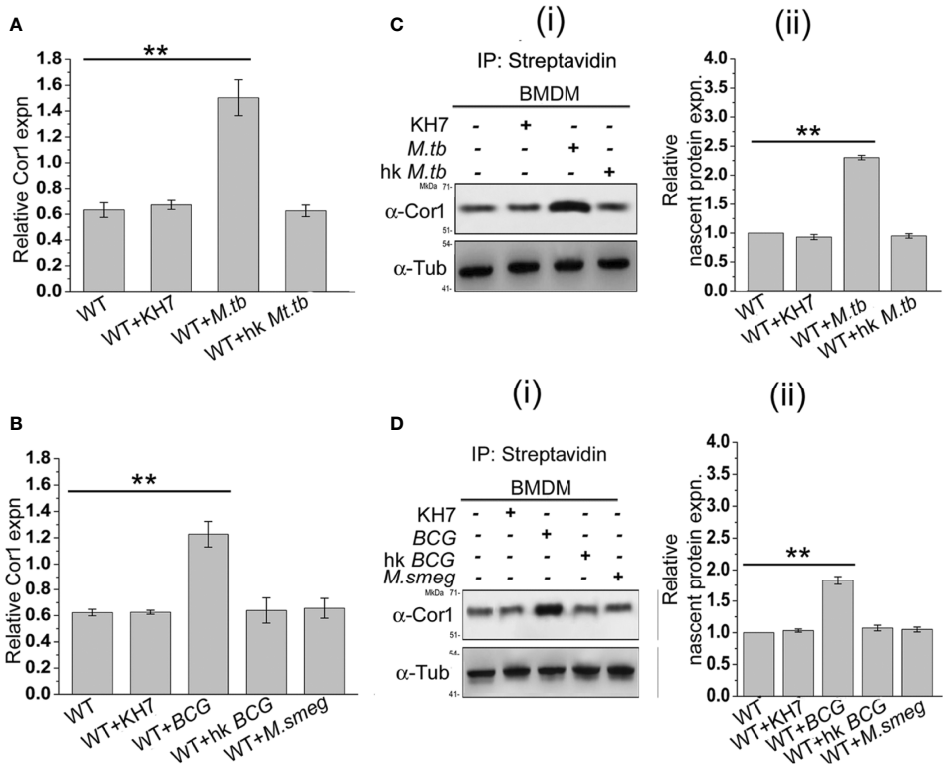

FIGURE 3 | **(A)** Relative Cor1 expression against control b-tubulin expression in BMDM when kept uninfected, KH7 treated or **(A)** live *M. tb*, heat-killed *M. tb* infected or **(B)** live *M. bovis BCG*, heat-killed *M. bovis BCG*, or live *M. smeg* infected BMDM. Infection was carried out with MOI of 1:20 for 3 h (n = 3). **(C)** Nascent proteins labelled with L-AZA and thereafter biotinylated were immunoprecipitated using streptavidin=agarose and then immunoblotted with anti-Cor1. Immunoblots and their corresponding densitometric analysis were carried out for BMDM, which were either untreated or treated with KH7 or **(C)** (i), (ii) infected with live *M. tb*, heat-killed *M. tb*, or **(D)** (i), (ii) infected with live *M. bovis BCG*, heat-killed *M. bovis BCG*, or live *M. smeg*, respectively (n = 3). Data represents mean ± SEM; $^{**}p < 0.01$.

pretreated with KH7 prior to *M. tb* infection shifted the balance from Th2 to Th1 response as evident from higher TNFa and iNOS2 levels in comparison to IL-10 and Arg1 levels. This could be the reason behind the phagosomal maturation and lysosomal fusion in these cells irrespective of infection with pathogenic *M. tb*. Although Rolipram is known to downregulate TNFa levels and dampen Th1 response (28), pretreatment of BMDM with Rolipram, although increasing the cAMP levels in *M. smeg* infected BMDMs, could not achieve a Th1 to Th2 switch. Hence, phagolysosome formation was not hindered in these cells. The inability of *M. smeg* to retain Cor1 on the phagosome could be playing a role as well. Therefore, we wanted to understand the role of Cor1-induced increased level of cAMP at the vicinity of the phagosome.

Cofilin1 Is Activated by Mycobacterial Infection-Induced Overexpressed Coronin1

The role of Cor1 is essential in hindering phagosome-lysosome fusion (29). Our data suggest that Cor1 has a significant contribution to the rise of cAMP inside macrophages upon mycobacterial infection. Previous literature suggests an increase in intracellular cAMP level activates the actin-binding protein Cofilin1 by dephosphorylating it (30). Ubiquitous Coronin2 is known to activate Cofilin1 by inducing its dephosphorylation through the engagement of the phosphatase Slingshot, and general activation of Cofilin1 occurs through its dephosphorylation by protein phosphatase 2A (8). Considering all these data, we hypothesized that mycobacterial infection-induced phagosome recruited Cor1 causes a rise in intracellular cAMP, which then activates a phosphatase to dephosphorylate Cofilin1 and thereby activate it. To address this possibility, we studied Cofilin1 dephosphorylation through immunoblotting. A continuous decrease in the level of phospho-Cof1 with increasing time of infection with *M. tb* was observed, where there was no decrease in phospho-Cof1 in the uninfected BMDM (**Figure 4A**). Densitometry analysis shows an ~80% decrease in the level of phospho-Cof1 after 3 h of macrophage infection with mycobacteria (**Figure 4B**). Contrary to this, no reduction of phosphor-Cof1 was observed in mycobacteria infected $Cor1^{-/-}$ BMDM cells (**Figure 4A**), and densitometry analysis also shows the same (**Figure 4B**). Total Cof1 remains constant both in the case of mycobacteria-infected WT and $Cor1^{-/-}$ BMDM cells, thus indicating that mycobacterial infection-induced activation of Cof1 occurs only in WT BMDM.

Next we pretreated wild type BMDM with Slingshot Inhibitor D3 and thereafter either kept them uninfected or infected them with *M. tb* for the indicated time points. Immunoblot analysis showed

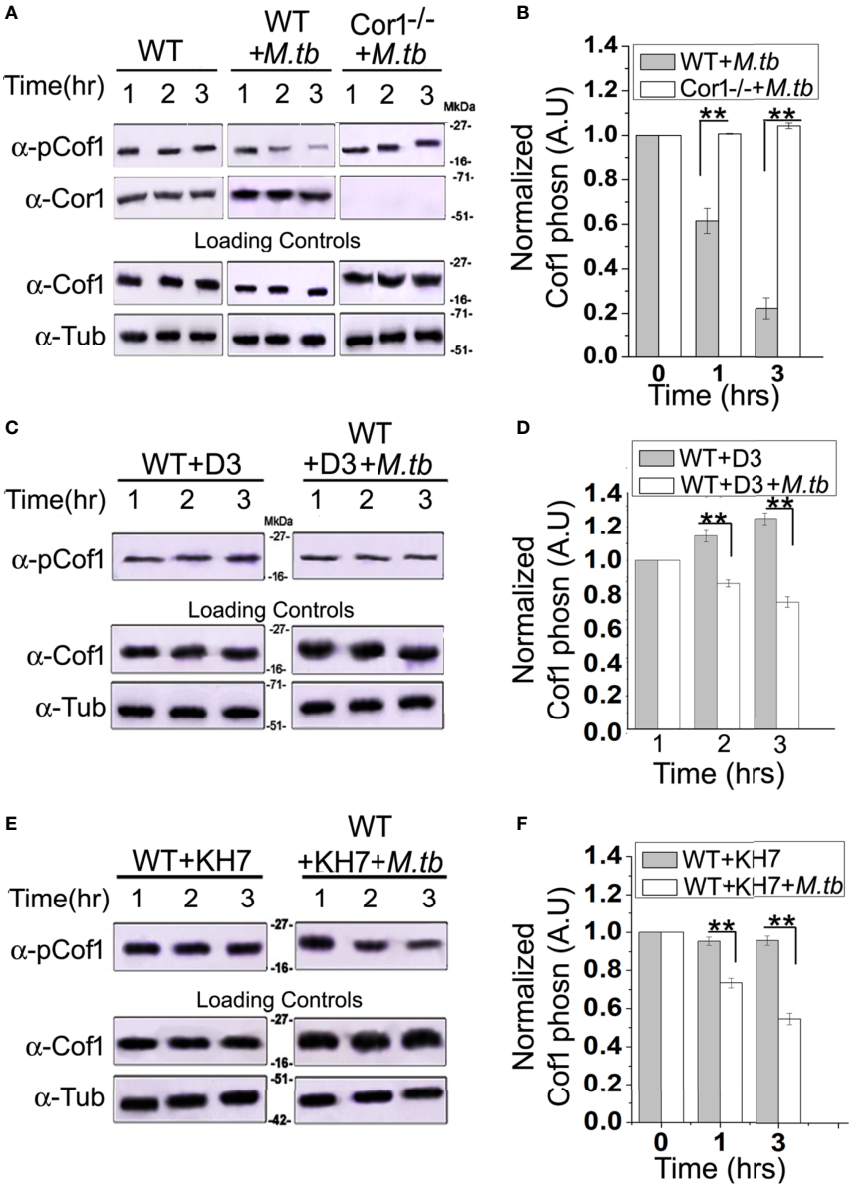

FIGURE 4 | Immunoblot analysis **(A, C, E)** and its corresponding densitometric analysis **(B, D, F)** for Cofilin1 phosphorylation that were carried out in **(A)** untreated and uninfected BMDM (left panel), **(A, B)** untreated but *M. tb* infected WT (middle panel) or Cor1$^{-/-}$ (right panel) BMDM, **(C, D)** D3 pretreated (left panel) or D3 pretreated and *M. tb* infected (right panel), **(E, F)** KH7 pretreated (left panel) or KH7 pretreated and *M. tb* infected wild-type BMDM, respectively (n = 3). Infections were carried out at an MOI of 1:20 for indicated time points. Immunoblots of Cofilin1 and b-tubulin served as loading control for these experiments. Data represents mean ± SEM; $^{**}p < 0.01$.

that the level of phosphor-Cof1 in uninfected but D3 pretreated macrophages remained constant. In contrast, D3 pretreated and infected macrophages exhibited only a negligible increase in infection time (**Figure 4C**), and the same is also observed in the densitometry analysis (**Figure 4D**). These results indicated that mycobacteria recruited Cor1 leads to the activation of the phosphatase, Slingshot, to dephosphorylate Cof1, thereby activating it. Pretreatment with Slingshot Inhibitor D3 prevented this dephosphorylation and thereby the activation of Cof1 upon infection.

Mycobacterial infection recruits and retains Cor1 on the phagosome membrane, contributing to the rise of intracellular cAMP. We next wanted to study whether this increased level of cAMP is required to activate Cof1. For this, we pretreated BMDM cells with adenylate cyclase inhibitor KH7 and then either kept them uninfected or infected them with mycobacteria for the indicated time periods. Immunoblot analysis showed that the KH7 treatment does not exhibit any change in the level of phosphor-Cof1. Simultaneously, there was an appreciable

reduction in the extent of Cof1 dephosphorylation with time upon KH7 pretreatment before mycobacterial infection (**Figure 4E**), thus indicating that hindering cAMP production does impede the activation of Slingshot, which then reduces the extent of Cof1 dephosphorylation and thereby its activation. Densitometry analysis shows that after 3 h of mycobacterial infection, there is only an ~40% decrease in phospho-Cof1 level in KH7 pretreated cells compared to untreated cells where an ~80% decrease was observed (**Figure 4F**). These data indicate that the mycobacteria-containing phagosome retained Cor1 increases the intracellular cAMP level, leading to the activation of Slingshot, which then dephosphorylates Cof1 and activates it. Hence, next we wanted to study the consequence of Cof1 activation upon infection.

Activated Cofilin1 Depolymerizes F-Actin at the Vicinity of Mycobacteria-Containing Phagosome

Fusion of mycobacteria-containing phagosomes with lysosomes requires F-actin tracks that guide the phagosome toward the lysosome (31). Activated Cof1 is known to associate with F-actin filaments and induce its depolymerization (19, 21). Hence, we wanted to check if Cor1 induced cAMP production upon mycobacterial infection results in activation of Cof1, which prevents phagosome lysosome fusion by causing F-actin depolymerization at the vicinity of the phagosomes. For this, we infected WT and Cor1$^{-/-}$ BMDM with mycobacteria for the indicated time points, followed by crosslinking of cellular protein, lysis of these cells, phagosome isolation, and thereafter immunoblotting. The obtained results showed a slight decrease in F-actin level for the wild-type infected macrophages with increasing time of infection (**Figure 5A**). In contrast, in the case of Cor1$^{-/-}$ macrophages, an increased amount of F-actin was observed on the phagosomes with increasing infection time. Since lack of Cor1$^{-/-}$ failed to increase intracellular cAMP, Cof1 remains phosphorylated and at the vicinity of the phagosomes, thus getting crosslinked and isolated along with the phagosomes. This then allowed F-actin polymerization. The presence of Cor1 on the phagosomes of *M. tb* infected WT-BMDM resulted in an increased level of cAMP that then led to dephosphorylation of Cof1. Hence, the dephosphorylated form of Cof1 was isolated along with the phagosomes as the same could prevent actin polymerization. Interestingly, immunoblotting with lysosomal marker LAMP1 shows that only in Cor1$^{-/-}$ macrophages phagolysosome fusion occurs due to increased F-actin polymerization at the vicinity of the phagosome.

This F-actin polymerization at the vicinity of the phagosome was further studied using immunogold transmission electron microscopy, where biotin-conjugated phalloidin was used to bind F-actin and gold nanoparticle conjugated streptavidin was used to label the F-actin that had bound by biotinylated phalloidin. In the case of immunogold transmission electron microscopy, gold nanoparticle-labelled target proteins appear as dense dots against the background of stained cells. Since we targeted F-actin, which is an abundant protein in the cell, there were numerous dense dots corresponding to intracellular, polymerized F-actin visible through immunogold electron microscopy. But an increased amount of dense dots corresponding to gold nanoparticle-labelled polymerized F-actin was observed at the vicinity of the mycobacteria-containing phagosome of Cor1$^{-/-}$ BMDM (**Figure 5C**) as compared to mycobacteria-containing phagosomes inside WT BMDM (**Figure 5B**) after 2 h of infection. This clearly indicated that an appreciable amount of F-actin polymerization was occurring around the mycobacteria-containing phagosomes of Cor1$^{-/-}$ macrophages, which was due to the failure of Cor1$^{-/-}$ macrophages to increase intracellular level of cAMP, thus causing Cof1 to stay phosphorylated and therefore no hindrance to F-actin polymerization. When similar studies were carried out with Alexa Fluor 488 conjugated phalloidin, similar F-actin polymerization was observed only around the mycobacteria-containing phagosomes inside Cor1$^{-/-}$ BMDM, not around the mycobacteria-containing phagosomes inside WT BMDM (**Figure 5D**). Fluorescence intensity calculations were next carried out, where intensity of Alexa Fluor 488 fluorescence corresponding to the presence of polymerized F-actin around the mycobacteria-containing phagosome was measured using a fixed line (denoted in red in **Figure 5D**). Such arbitrary fluorescence units that were obtained from 50 cells were averaged and plotted. It was observed that compared to mycobacteria infected WT BMDM, mycobacteria infected Cor1$^{-/-}$ BMDM exhibited significantly higher levels of fluorescence intensity values (**Figure 5E**). This indicated that after 2 h of mycobacterial infection there was considerable amount of F-actin polymerization around the mycobacteria-containing phagosomes of Cor1$^{-/-}$ BMDM alone (**Figure 5E**). When both WT and Cor1$^{-/-}$ BMDM were pretreated with Slingshot Inhibitor D3 before mycobacterial infection, there was a considerable increase in F-actin polymerization around the phagosomes of WT BMDM macrophages in comparison to untreated but mycobacteria infected WT BMDM, but there was no significant increase in F-actin polymerization in the D3 pretreated Cor1$^{-/-}$ BMDM upon mycobacterial infection compared to the untreated but mycobacteria infected Cor1$^{-/-}$ BMDM (**Figure 5E**). From these data, it is evident that Cor1-induced increase of cAMP-mediated activation of Cof1 through its dephosphorylation by Slingshot is required to prevent F-actin polymerization at the vicinity of the mycobacteria-containing phagosome, which thereby prevents its fusion with the lysosome and allows mycobacterial survival.

Coronin1 Activated Cofilin1 Also Hinders Phagosome Acidification

Prevention of lysosomal delivery is essentially associated with inhibition of phagosome acidification (31). Cor1 mediated activation of Cofilin1, through the rise of intracellular cAMP, hinders lysosomal delivery of mycobacteria-containing phagosome. We asked whether it is solely due to inhibition of F-actin polymerization or does Cofilin1 prevent the acidification of mycobacteria-containing phagosomes? For this, mycobacteria were dual-labelled with pH-sensitive, pHrodo, and pH insensitive Alexa Fluor 488, followed by infection of macrophages and analysis of phagosome pH in a multimode reader. A pH standard curve

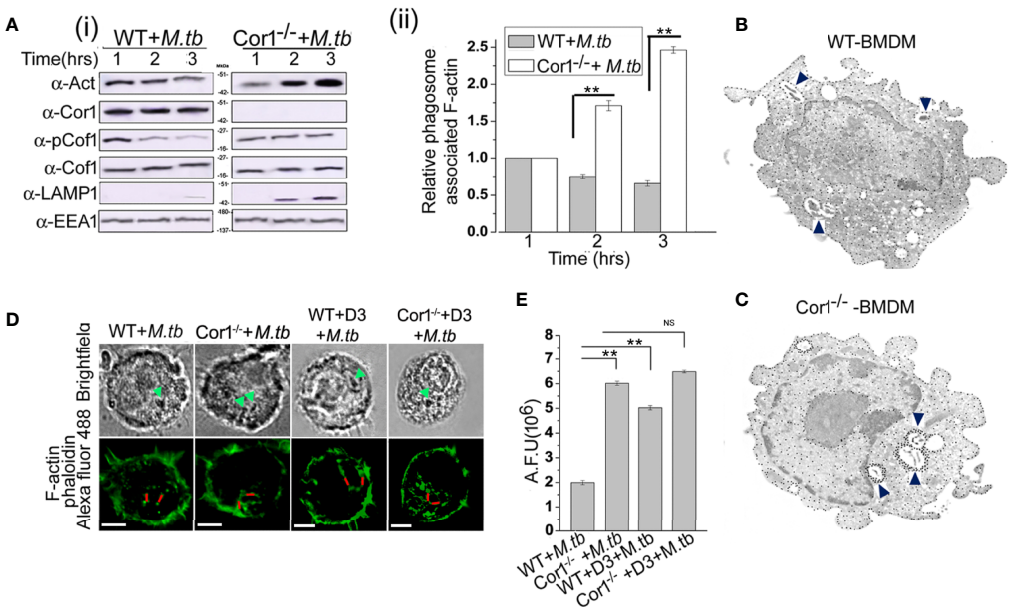

FIGURE 5 | **(A)** (i) Immunoblot of F-actin, Cor1, pCof1, LAMP1, and EEA1 and (ii) densiometric analysis of F-actin, all crosslinked to isolated phagosomes from *M. tb* infected [**A** (i) left panel] wild type and [**A** (i) right panel] Cor1$^{-/-}$ BMDM. Infection was carried out at MOI 1:20 for indicated time points. **(B, C)** Immunogold transmission electron microscopy for F-actin was carried out in *M. tb* infected **(B)** WT and **(C)** Cor1$^{-/-}$ BMDM. Infection was carried out at MOI 1:20 for 90 min. Blue arrows indicate *M. tb*-containing phagosomes in both cell types with dense dots corresponding to F-actin around mycobacteria-containing phagosomes in Cor1$^{-/-}$ BMDM. **(D)** Immunofluorescence analysis of F-actin (phalloidin-Alexa Fluor 488-green) around mycobacteria-containing phagosomes in *M. tb* infected WT (left panel) and Cor1$^{-/-}$ (right panel) BMDM. Green arrows in the brightfield indicate mycobacteria-containing phagosomes, while the red line corresponds to the arbitrary fluorescence units (AFU) corresponding to polymerized F-actin around phagosomes (scale: 10 μm). **(E)** AFU values corresponding to the number of 50 cells were averaged and plotted. Representation for wild type or Cor1$^{-/-}$ BMDM either untreated or pretreated with D3 and after that infected with *M. tb* at MOI of 1:20 for 90 min was carried out. Data represents mean ± SEM; $^{**}p < 0.01$, NS, non-significant.

(**Supplementary Figure 5**) was generated following the protocol stated in the *Materials and Methods* section. The pH of mycobacteria-containing phagosomes remains 6.4 after 3 h of infection, while in the case of Cor1$^{-/-}$ BMDM, the mycobacteria-containing phagosome pH falls to 5.3 at a similar time point after infection (**Figure 6A**). In terms of phagosome acidification and fusion with lysosomes, this fall of pH to 5.3 is significantly high. Further pretreatment of WT BMDM with Slingshot Inhibitor D3 before infection resulted in acidification of the mycobacteria-containing phagosomes in 3 h post-infection. Hence, the pH falls from 6.4 to 5.6. In the case of the Cor1$^{-/-}$ BMDM, D3 pretreatment prior to mycobacterial infection results in a further drop of phagosomal pH compared to untreated cells. The fall in pH in both WT and Cor1$^{-/-}$ BMDM upon pretreatment with D3 prior to mycobacterial infection was similar to that observed in the case of the untreated cells. Additionally, pretreatment of macrophages with vacuolar H+-ATPase inhibitor Concanamycin A (ConA) maintains mycobacteria-containing phagosome pH above 7 for WT and above 6 for Cor1$^{-/-}$ BMDM, respectively, which is significantly higher than the pH values of the untreated but infected cells (**Figure 6B**). This indicated that ConA, by inhibiting the vacuolar H+-ATPase, can prevent the pumping of H+ ions into the phagosome and thereby hinder phagosome acidification. To check if F-actin polymerization plays a role in phagosome acidification, next we pretreated macrophages with actin-depolymerizing agent Latrunculin B (LatB) before mycobacterial infection. After that, when phagosome pH was monitored (**Figure 6B**), it was observed that for LatB treated WT BMDM macrophages infected with mycobacteria, the phagosome pH rose to ~6.7 from ~6.3 for that of untreated WT BMDM macrophages infected with mycobacteria, while for LatB treated Cor1$^{-/-}$ BMDM macrophages infected with mycobacteria the phagosome pH rose to ~5.9 from ~5.4 for that of untreated Cor1$^{-/-}$ BMDM macrophages infected with mycobacteria. Thus, by inducing actin depolymerization, LatB could hinder the acidification of the phagosome as evident from a higher phagosome pH value upon LatB treatment. Therefore, the above data show that Cor1 activated Cof1 prevents phagosome acidification and thereby hinders phagosome-lysosome fusion.

DISCUSSION

With the turn of every century, there has been a rise and fall of one pandemic or another. Tuberculosis continues to plague humanity and is a leading cause of mortality worldwide. The success of its causative agent, mycobacteria, lies in its ability to continuously adapt to its ever-changing environment, leading to several paradigm shifts in its pathogenesis (3). Previously, it was believed that mycobacteria could recruit the macrophage coat

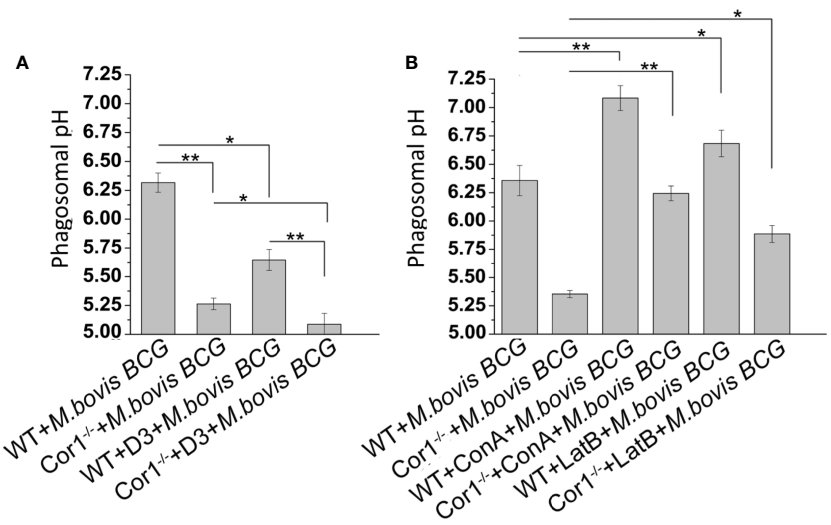

FIGURE 6 | Phagosome pH was monitored using pHrodo in WT and Cor1$^{-/-}$ BMDM upon being either **(A)** kept untreated or D3 pretreated before infection with *M. bovis BCG* for 3 h. **(B)** Similarly, WT or Cor1$^{-/-}$ macrophages were either kept untreated or pretreated with either ConA or LatB before infection with *M. bovis* for 3 h, followed by measurement of phagosome pH. The phagosome pH values were obtained from the standard curve generated using pHrodo in different pH buffers. Data represents mean ± SEM; *$p < 0.05$, **$p < 0.01$.

protein Cor1 on the phagosome membrane and thereby prevent its maturation. Recent studies show that in active TB, mycobacteria hinder the process of phagosome maturation until it can overexpress proteins that enable it to withstand acid stress of the lysosome (32). Contrary to this, perhaps when mycobacteria fail to hinder phagosome maturation, it secretes proteins that disrupt the phagosome membrane and allows the cytosolic escape of the infected mycobacteria. Once in the cytosol, mycobacteria engage the autophagic pathway, whereinafter autophagosomes and autophagolysosomes are formed gradually, thus providing time for mycobacteria to overexpress their acid-tolerant proteins (33).

Ensuing mycobacterial infection, macrophage Cor1 acts as the sentinel, and by being a cortical protein is present on the phagosome coat. Through its secretion of lipoamide dehydrogenase, mycobacteria can retain Cor1 on the phagosome membrane (23). Cor1-induced rise of intracellular Ca^{2+} upon mycobacterial infection causes the phosphatase calcineurin activation and thereby hinders phagosome maturation (16). However, this study did not explain how Cor1 directly or indirectly through calcineurin can delay phagosome maturation. It has also been shown that cAMP induces actin depolymerization at the vicinity of mycobacteria-containing phagosomes (21) thus preventing actin tracts from forming. Such actin tracts are required for the process of phagosome acidification by fusing with vacuolar H+-ATPase containing vesicles and also thereafter for fusing with lysosomes. However, this study did not state the varied source for this increasing cAMP concentration and the mechanism through which cAMP prevents actin polymerization at the vicinity of the phagosome. To answer these questions, we carried out our study where we first found that apart from the soluble adenylate cyclases secreted by mycobacteria, macrophages also contribute primarily toward the increasing intracellular cAMP concentration upon infection. This cAMP production is dependent on macrophage Cor1 as the same is absent in Cor1$^{-/-}$ macrophages. Cor1 has been implicated in increased cAMP production upon stimulation of GPCRs (11). The intracellular cAMP level in the uninfected condition is not high. Still, it rises only upon mycobacterial infection, thus indicating that like GPCR signaling, mycobacterial infection and its concomitant recruitment and retention of the Cor1 coat on the phagosome membrane act as triggers for Cor1 induced cAMP production inside the macrophage. Such Cor1 mediated rise of intracellular cAMP levels can be prevented by pretreatment of cells with AC inhibitor KH7 prior to mycobacterial infection. This then leads to a Th2 to Th1 conversion and phagosome maturation to predominantly eliminate the intracellular mycobacteria. Intracellular cAMP levels are known to be increased by inhibition of PDE4 (34). Hence, pretreatment with PDE4 inhibitor Rolipram prior to mycobacterial infection, although generated a higher level of cAMP, was not sufficient to prevent phagosome maturation of *M. smeg* containing phagosomes, possibly due to the inability of *M. smeg* to retain Cor1 on its phagosome and thus lacking Cor1 mediated cAMP production at the vicinity of the phagosome. Additionally, mycobacterial infection is known to increase intracellular Ca^{2+} level in a Cor1 dependent manner at the vicinity of the phagosome membrane, and this increased Ca^{2+} after that activates the phosphatase calcineurin. Increased Ca^{2+} can also activate phospholipase C (PLC) and diacylglycerol, of which PLC is known to trigger cAMP production. So, whether a mycobacterial infection-induced increase in intracellular cAMP is generated directly and indirectly through Cor1 remains to be determined.

An increased intracellular cAMP would activate the cAMP/PKA pathway, which then would induce phosphorylation

mediated activation of MAPK to induce IFNg secretion by T-cells upon mycobacterial infection of macrophages (35, 36). But *M. tb via* its LAM is known to activate SOCS and CISH proteins that dampen IFNg signaling inside mycobacteria infected macrophages. Hence, activated MAPK in *M. tb* infected cells fails to induce a Th1 response as compared to that in *M. smeg* infected cells. Hence, despite the MAPK activation in both *M. tb* and *M. smeg* infected cells, the former has means to prevent the Th1 response of the macrophages while the later exhibits the same.

We also observed that mycobacterial infection retains Cor1 on the phagosome membrane and induces its overexpression. The burning question that arose was why Cor1 expression would increase and, if so, why does immunofluorescence or immunoblotting analysis with increasing time of infection not exhibit this? We postulated that phagosome retained Cor1 gets degraded continuously, and to replenish this degrading Cor1, an increased expression of Cor1 was observed. Thus, Cor1 could be in a state of dynamic equilibrium where it is constantly getting degraded and replenished. Previous studies have shown that mycobacterial infection induces Cor1 mediated influx of Ca2+, which activates calcineurin, PLC, and DAG. The latter is known to activate PKC and activated PKC has been shown to delocalize Cor1 from the cortical surface by phosphorylating it at the C-terminus (37). PKC-mediated phosphorylation renders Cor1 monomeric, which then is scaffolded by RACK1 and shuttled by cargo carrier protein 14-3-3ζ (38). The monomeric Cor1 might be getting degraded in a condition where the macrophage is infected with mycobacteria, and semblance to this is observed when pretreatment with proteasomal inhibitor MG132 before infection exhibited an increase in Cor1 concentration. Additionally, studies of nascent protein expression could also indicate increased Cor1 expression with increasing infection time. The natural question would be if Cor1 is getting phosphorylated and degraded, and therefore to maintain its concentration around the phagosome, it must be overexpressed. Then what induces its overexpression? Our yet unpublished data show that calcineurin triggers this overexpression of Cor1 and thus maintains it in a dynamic equilibrium around the phagosome.

This Cor1 induced, increased intracellular cAMP levels upon mycobacterial infection causes a concomitant activation of Cofilin 1 through its dephosphorylation by activated phosphatase Slingshot. Cof1 is known to prevent actin polymerization in its active dephosphorylated form, while cAMP has been shown to induce F-actin depolymerization at the vicinity of mycobacteria-containing phagosomes (**Figure 7**). So, it had to be determined whether the increased intracellular cAMP can directly influence the depolymerization of F-actin or the phosphatase, Slingshot-mediated activation of Cof1 causes F-actin depolymerization. Adenylate cyclase inhibitor-treated cells failed to dephosphorylate Cof1, thus indicating that increased intracellular cAMP was required for the dephosphorylation mediated activation of Cof1. Additionally, cells pretreated with Slingshot Inhibitor D3 also hindered Cof1 activation, thereby indicating the activation of Slingshot as the phosphatase for Cof1. Maturing phagosomes require continuously polymerizing F-actin tracts that bring them in proximity to vacuolar H^+-ATPase containing vesicles for acidification and also in proximity to lysosomes to enable fusion and phagolysosome formation. Phagolysosome formation is hindered in the absence of such F-actin tracts. Previously, it was shown that increased intracellular cAMP could delay F-actin polymerization and thus prevent such tract formation (21), but the mechanism behind this was unknown. Here we show that cAMP, by activating Cof1, increases actin depolymerization, thereby hindering phagosome acidification and phagolysosome formation.

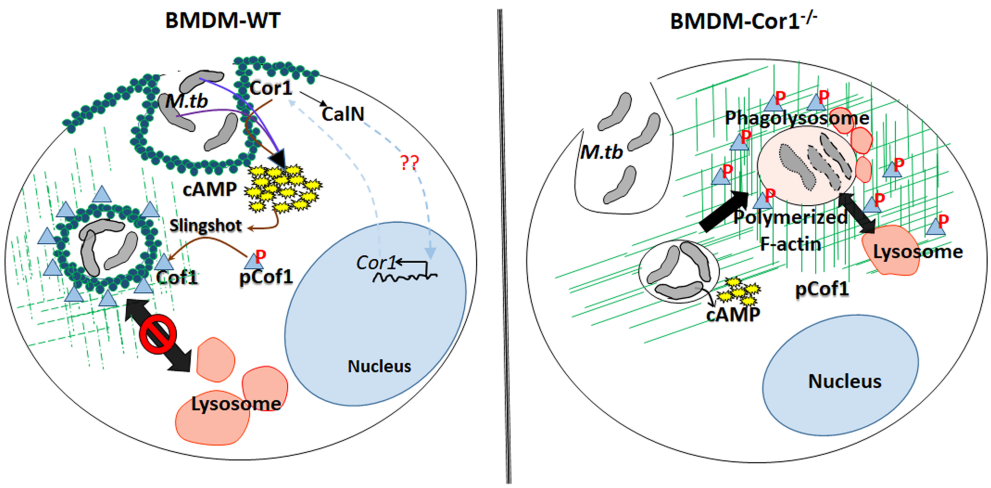

FIGURE 7 | Schematic representation of Cor1-mediated increase of intracellular cAMP upon mycobacterial infection leading to activation of the phosphatase Slingshot and thereby dephosphorylation mediated activation of Cofilin1 to induce the depolymerization of F-actin to hinder the phagosome maturation and the absence of such pathway in Cor1$^{-/-}$ macrophages.

Thus, phagosome retained Cor1 increases the intracellular cAMP levels and thereby activates the phosphatase Slingshot, which then dephosphorylates Cof1 and activates it, such that it can depolymerize F-actin tracts presumably more at the vicinity of the phagosome and to some extent on other intracellular vesicles and organelles thus hindering phagosomal acidification as well as its maturation. Based on the present paradigm, the goal of infected mycobacteria is to delay phagosome acidification and its maturation to provide it with the required time to express the acid stress-tolerant proteins. Our study provides a mechanism through which mycobacteria achieve this. Mycobacteria retained Cor1 scaffold on the phagosome membrane is in a state of dynamic equilibrium, and it also induces F-actin depolymerization around the phagosome, thereby enabling very slow acidification where a semblance of F-actin brings in V-H+-ATPase to the phagosome membrane and allows its access in between the phase of degradation of phosphorylated Cor1 and replenishment by newly synthesized Cor1. This slow and gradual access would retard the acidification process considerably, thus enabling mycobacteria to get adapted to the acid stress, such that it can later thrive inside the phagolysosome.

Taken together, this study, for the first time, explicitly provides knowledge on the missing links in the context of Cor1 mediated hindrance to phagosome maturation and the role of cAMP in the context of retarded phagosome maturation. It brings to light the sequence of events that leads to the bumpy ride of mycobacteria-containing phagosome and thereby retards its maturation. It also provides an insight into the objective behind this event. Such studies on the causes and consequences of hindered phagosome maturation in the context of mycobacterial pathogenesis would enable us to curb the TB menace by purporting host-directed immunomodulatory therapeutics through the use of peptidomimetics.

DATA AVAILABILITY STATEMENT

The original contributions presented in the study are included in the article/**Supplementary Material**. Further inquiries can be directed to the corresponding author.

ETHICS STATEMENT

The Institute Biosafety Committee approved the work, and for the use of *M. tb*, the work was permitted under the Biosafety Committee overseeing the use of the BSL3 facility at NJILOMD.

AUTHOR CONTRIBUTIONS

SS performed most of the experiments and wrote the manuscript. AH carried out some of the experiments. DG and SR helped SS execute some experiments and provided input toward the writing of the manuscript. AS provided the BSL3 facility and facilitated the execution of some experiments. SB planned the project and the course of the investigations and supervised manuscript writing. All authors contributed to the article and approved the submitted version.

FUNDING

We would like to thank DBT, India (BT/RLF/Re-entry/33/2014), and DST-SERB (YSS/2015/000471 and CRG/2020/000748) for providing financial assistance for conducting the research. SS, AH, DG, and SR were provided financial assistance through a fellowship from IIT Kharagpur under MoE.

ACKNOWLEDGMENTS

We would like to thank Jean Pieters of the Department of Biochemistry, Biozentrum, Switzerland, for kindly providing the WT and Cor1$^{-/-}$ BMDM. Our sincere acknowledgments to Dr. Rajesh Mondal, NIRT, Chennai, Dr. Vimal Kumar, NJILOMD, Agra, for their help and support.

SUPPLEMENTARY MATERIAL

The Supplementary Material for this article can be found online at: https://www.frontiersin.org/articles/10.3389/fimmu.2021.687044/full#supplementary-material

Supplementary Figure 1 | (A) Analyzing the extent of infectivity corresponding to viability. WT-BMDM were infected with *M. tb* at indicated MOI followed by analysis of cell viability and extent of *M. tb* infection in these viable cells (n = 50). **(B)** Competitive ELISA-based measurement of cAMP production of BMDM at indicated MOI of *M. tb* infection at indicated time points. **(C)** Extent of phagolysosome formation in live *M. tb, M. bovis BCG, M. smeg*, heat-killed *M. tb*, and heat-killed *M. bovis BCG* infected BMDM after 3 h of infection, without and after pretreatment with KH7 or Rolipram (n = 50). Data represents mean ± SEM; $*p < 0.05$, $**p < 0.01$, NS, non significant. **(D)** Immunofluorescence analysis of mycobacteria-infected macrophages. BMDM were infected with live *M. smeg* or *M. tb* for indicated time points and thereafter stained for mycobacteria (green), lysosomes (LAMP2 in red), and Cor1 (blue). In case of *M. smeg*, Cor1 fails to form a scaffold around the phagosome, which leads to phagosome-lysosome fusion at 3 h, while for *M. tb*-infected macrophages, the Cor1 scaffold around the phagosome hinders its maturation and hence it does not fuse with lysosomes (scale: 10 μm). **(E)** Extent of phagolysosome formation in *M. smeg* or *M. tb* infected BMDM after 3 h of infection and without and with pretreatment with KH7 or Rolipram (n = 100). Data represents mean of triplicates ± SEM.

Supplementary Figure 2 | Immunoblotting of WT, Cor1$^{-/-}$, and c-myc tagged Cor1 transfected Cor1$^{-/-}$ BMDM with anti-Cor1 and anti-c-myc antibodies exhibits expression of Cor1 in WT and Cor1$^{-/-}$ transfected with Cor1 and band corresponding to c-myc was observed only in Cor1 expressing Cor1$^{-/-}$ cells, indicating successful transfection. b-tub was used as loading control.

Supplementary Figure 3 | (A) Immunoblot of Cor1 from BMDM whole-cell lysates that were either kept uninfected or infected with live or heat-killed *M. tb*, *M. bovis BCG*, or live *M. smeg* did not exhibit the apparent increase of Cor1 expression upon infection. **(B)** Immunoblot and its corresponding densitometry analysis for Cor1 expression in WT-BMDM infected with *M. tb* after being pretreated and in the presence of MG132. Gradual increase in Cor1 expression normalized over that of b-tub control is observed (n = 3). Data represents mean ± SEM; $*p < 0.05$, $**p < 0.01$.

Supplementary Figure 4 | qPCR analysis of Th1/Th2 response in BMDMs upon infection with *M. smeg* or *M. tb*, without and with pretreatment with KH7 and Rolipram. Based on the overexpression of **(A)** TNFa and **(C)** iNOS2, Th1 response

was evident in *M. smeg* infected macrophages without or with KH7 or Rolipram pretreatment and partly in KH7 pretreated and *M. tb* infected macrophages. Overexpression of **(B)** IL-10 and **(D)** Arg1 in *M. tb* infected cells without and with Rolipram pretreatment is indicative of Th2 response in these macrophages.

Supplementary Figure 5 | Mycobacteria labelled with pH-sensitive pHrodo and pH-insensitive Alexa Fluor 488 were grown in 7H9 buffer of pH 4.5-8.5. The ratio of pHrodo to Alexa Fluor 488 fluorescence in different buffers was plotted to obtain the pH standard curve and used to measure phagosomal pH upon mycobacterial infection (n = 3).

REFERENCES

1. Sousa J, Cá B, Maceiras AR, Simões-Costa L, Fonseca KL, Fernandes AI, et al. *Mycobacterium Tuberculosis* Associated With Severe Tuberculosis Evades Cytosolic Surveillance Systems and Modulates IL-1β Production. *Nat Commun* (2020) 11:1949. doi: 10.1038/s41467-020-15832-6
2. Wang J, Ge P, Qiang L, Tian F, Zhao D, Chai Q, et al. The Mycobacterial Phosphatase PtpA Regulates the Expression of Host Genes and Promotes Cell Proliferation. *Nat Commun* (2017) 8:244. doi: 10.1038/s41467-017-00279-z
3. Saha S, Das P, BoseDasgupta S. "It Takes Two to Tango": Role of Neglected Macrophage Manipulators Coronin 1 and Protein Kinase G in Mycobacterial Pathogenesis. *Front Cell Infect Microbiol* (2020) 10:582563. doi: 10.3389/fcimb.2020.582563
4. Punwani D, Pelz B, Yu J, Arva NC, Schafernak K, Kondratowicz K, et al. Coronin-1A: Immune Deficiency in Humans and Mice. *J Clin Immunol* (2015) 35:100–7. doi: 10.1007/s10875-015-0130-z
5. Siegmund K, Klepsch V, Hermann-Kleiter N, Baier G. Proof of Principle for a T Lymphocyte Intrinsic Function of Coronin 1a. *J Biol Chem* (2016) 291:22086–92. doi: 10.1074/jbc.M116.748012
6. Bosedasgupta S, Pieters J. Coronin 1 Trimerization Is Essential to Protect Pathogenic Mycobacteria Within Macrophages From Lysosomal Delivery. *FEBS Lett* (2014) 588:3898–905. doi: 10.1016/j.febslet.2014.08036
7. Mikati MA, Breitsprecher D, Jansen S, Reisler E, Goode BL. Coronin Enhances Actin Filament Severing by Recruiting Cofilin to Filament Sides and Altering F-Actin Conformation. *J Mol Biol* (2015) 427:3137–47. doi: 10.1016/j.jmb.2015.08.011
8. Cai L, Marshall TW, Uetrecht AC, Schafer DA, Bear JE. Coronin 1B Coordinates Arp2/3 Complex and Cofilin Activities at the Leading Edge. *Cell* (2007) 128:915–29. doi: 10.1016/j.cell.2007.01.031
9. Kurita S, Watanabe Y, Gunji E, Ohashi K, Mizuno K. Molecular Dissection of the Mechanisms of Substrate Recognition and F-Actin-Mediated Activation of Cofilin-Phosphatase Slingshot-1. *J Biol Chem* (2008) 283:32542–52. doi: 10.1074/jbc.M804627200
10. Constantoulakis P, Filiou E, Rovina N, Chras G, Hamhougia A, Karabela S, et al. *In Vivo* Expression of Innate Immunity Markers in Patients With *Mycobacterium Tuberculosis* Infection. *BMC Infect Dis* (2010) 10:243. doi: 10.1186/1471-2334-10-243
11. Jayachandran R, Liu X, BoseDasgupta S, Müller P, Zhang CL, Moshous D, et al. Coronin 1 Regulates Cognition and Behavior Through Modulation of cAMP/Protein Kinase A Signaling. *PloS Biol* (2014) 12:e1001820. doi: 10.1371/journal.pbio.1001820
12. Livak KJ, Schmittgen TD. Analysis of Relative Gene Expression Data Using Real-Time Quantitative PCR and the 2-ΔΔCT Method. *Methods* (2001) 25:402–8. doi: 10.1006/meth.2001.1262
13. Kumar D, Nath L, Kamal MA, Varshney A, Jain A, Singh S, et al. Genome-Wide Analysis of the Host Intracellular Network That Regulates Survival of Mycobacterium Tuberculosis. *Cell* (2010) 140:731–43. doi: 10.1016/j.cell.2010.02.012
14. Ullrich M, Liang V, Chew YL, Banister S, Song X, Zaw T, et al. Bio-Orthogonal Labeling as a Tool to Visualize and Identify Newly Synthesized Proteins in *Caenorhabditis Elegans*. *Nat Protoc* (2014) 9:2237–55. doi: 10.1038/nprot.2014.150
15. Anes E, Kühnel MP, Bos E, Moniz-Pereira J, Habermann A, Griffiths G. Selected Lipids Activate Phagosome Actin Assembly and Maturation, Resulting in the Killing of Pathogenic Mycobacteria. *Nat Cell Biol* (2003) 5:793–802. doi: 10.1038/ncb1036
16. Jayachandran R, Sundaramurthy V, Combaluzier B, Mueller P, Korf H, Huygen K, et al. Survival of Mycobacteria in Macrophages Is Mediated by Coronin 1-Dependent Activation of Calcineurin. *Cell* (2007) 130:37–50. doi: 10.1016/j.cell.2007.04.043
17. Glauert AM, Butterworth AE, Sturrock RF, Houba V. The Mechanism of Antibody-Dependent, Eosinophil-Mediated Damage to Schistosomula of *Schistosoma Mansoni In Vitro*: A Study by Phase-Contrast and Electron Microscopy. *J Cell Sci* (1978) 34:173–92. doi: 10.1242/jcs.34.1.173
18. Abdellatif MEA, Hipp L, Plessner M, Walther P, Knoll B. Indirect Visualization of Endogenous Nuclear Actin by Correlative Light and Electron Microscopy (CLEM) Using an Actin-Directed Chromobody. *Histochem Cell Biol* (2019) 152:133–43. doi: 10.1007/s00418-019-01795-3
19. McDonough KA, Rodriguez A. The Myriad Roles of Cyclic AMP in Microbial Pathogens: From Signal to Sword. *Nat Rev Microbiol* (2012) 10:27–38. doi: 10.1038/nrmicro2688
20. Agarwal N, Bishai WR. cAMP Signaling in *Mycobacterium Tuberculosis*. *Indian J Exp Biol* (2009) 47:393–400.
21. Kalamidas SA, Kuehnel MP, Peyron P, Rybin V, Rauch S, Kotoulas OB, et al. cAMP Synthesis and Degradation by Phagosomes Regulate Actin Assembly and Fusion Events: Consequences for Mycobacteria. *J Cell Sci* (2006) 119:3686–94. doi: 10.1242/jcs.03091
22. Dey B, Bishai WR. Crosstalk Between *Mycobacterium Tuberculosis* and the Host Cell. *Semin Immunol* (2014) 26:486–96. doi: 10.1016/j.smim.2014.09.002
23. Deghmane AE, Soualhine H, Bach H, Sendide K, Itoh S, Tam A, et al. Lipoamide Dehydrogenase Mediates Retention of Coronin-1 on BCG Vacuoles, Leading to Arrest in Phagosome Maturation. *J Cell Sci* (2007) 120:2796–806. doi: 10.1242/jcs.022335
24. Agarwal N, Lamichhane G, Gupta R, Nolan S, Bishai WR. Cyclic AMP Intoxication of Macrophages by a *Mycobacterium Tuberculosis* Adenylate Cyclase. *Nature* (2009) 460:98–102. doi: 10.1038/nature08123
25. Bai G, Schaak DD, Mcdonough KA. cAMP Levels Within *Mycobacterium Tuberculosis* and *Mycobacterium Bovis* BCG Increase Upon Infection of Macrophages. *FEMS Immunol Med Microbiol* (2009) 55:68–73. doi: 10.1111/j.1574-695X.2008.00500.x
26. Lowrie DB, Jackett PS, Ratcliffe NA. *Mycobacterium Microti* may Protect Itself From Intracellular Destruction by Releasing Cyclic AMP Into Phagosomes. *Nature* (1975) 254:600–2. doi: 10.1038/254600a0
27. Kim HK, Hwang SH, Oh E, Abdi S. Rolipram, a Selective Phosphodiesterase 4 Inhibitor, Ameliorates Mechanical Hyperalgesia in a Rat Model of Chemotherapy-Induced Neuropathic Pain Through Inhibition of Inflammatory Cytokines in the Dorsal Root Ganglion. *Front Pharmacol* (2017) 8:885. doi: 10.3389/fphar.2017.00885
28. Ross SE, Williams RO, Mason LJ, Mauri C, Marinova-Mutafchieva L, Maini RN, et al. Suppression of TNF-Alpha Expression, Inhibition of Th1 Activity, and Amelioration of Collagen-Induced Arthritis by Rolipram. *J Immunol* (1997) 159(12):6253–59.
29. Nguyen L, Pieters J. The Trojan Horse: Survival Tactics of Pathogenic Mycobacteria in Macrophages. *Trends Cell Biol* (2005) 15:269–76. doi: 10.1016/j.tcb.2005.03.009
30. Ramachandran C, Patil RV, Sharif NA, Srinivas SP. Effect of Elevated Intracellular cAMP Levels on Actomyosin Contraction in Bovine Trabecular Meshwork Cells. *Investig Ophthalmol Vis Sci* (2011) 52:1474–85. doi: 10.1167/iovs.10-6241
31. Hmama Z, Pena-Diaz S, Joseph S, Av-Gay Y. Immunoevasion and Immunosuppression of the Macrophage by *Mycobacterium tuberculosis*. *Immunol Rev* (2015) 264:220–32. doi: 10.1111/imr.122
32. Ehrt S, Schnappinger D. Mycobacterial Survival Strategies in the Phagosome: Defense Against Host Stresses. *Cell Microbiol* (2009) 11:1170–8. doi: 10.1111/j.1462-5822.2009.01335.x
33. Watson RO, Manzanillo PS, Cox JS. Extracellular *M. Tuberculosis* DNA Targets Bacteria for Autophagy by Activating the Host DNA-Sensing Pathway. *Cell* (2012) 150:803–15. doi: 10.1016/j.cell.2012.06.040
34. Oehrl S, Prakash H, Ebling A, Trenkler N, Wölbing P, Kunze A, et al. The Phosphodiesterase 4 Inhibitor Apremilast Inhibits Th1 But Promotes Th17 Responses Induced by 6-Sulfo LacNAc (Slan) Dendritic Cells. *J Dermatol Sci* (2017) 87(2):110–15. doi: 10.1016/j.jdermsci.2017.04.005
35. Pasquinelli V, Rovetta AI, Alvarez IB, Jurado JO, Musella RM, Palmero DJ, et al. Phosphorylation of Mitogen-Activated Protein Kinases Contributes to Interferon γ Production in Response to *Mycobacterium Tuberculosis*. *J Infect Dis* (2013) 207(2):340–50. doi: 10.1093/infdis/jis672
36. Yadav M, Roach SK, Schorey JS. Increased Mitogen-Activated Protein Kinase Activity and TNF-Alpha Production Associated With Mycobacterium Smegmatis- But Not

Mycobacterium Avium-Infected Macrophages Requires Prolonged Stimulation of the Calmodulin/Calmodulin Kinase and Cyclic AMP/protein Kinase A Pathways. *J Immunol* (2004) 172(9):5588–97. doi: 10.4049/jimmunol.172.9.5588

37. BoseDasgupta S, Pieters J. Inflammatory Stimuli Reprogram Macrophage Phagocytosis to Macropinocytosis for the Rapid Elimination of Pathogens. *PloS Pathog* (2014) 10:e1003879. doi: 10.1371/journal.ppat.1003879
38. BoseDasgupta S, Moes S, Jenoe P, Pieters J. Cytokine-Induced Macropinocytosis in Macrophages Is Regulated by 14-3-3ζ Through Its Interaction With Serine-Phosphorylated Coronin 1. *FEBS J* (2015) 282:1167–81. doi: 10.1111/febs.13214

Conflict of Interest: The authors declare that the research was conducted in the absence of any commercial or financial relationships that could be construed as a potential conflict of interest.

Publisher's Note: All claims expressed in this article are solely those of the authors and do not necessarily represent those of their affiliated organizations, or those of the publisher, the editors and the reviewers. Any product that may be evaluated in this article, or claim that may be made by its manufacturer, is not guaranteed or endorsed by the publisher.

frontiers in Immunology

ORIGINAL RESEARCH
published: 28 October 2021
doi: 10.3389/fimmu.2021.738070

Type I Interferons Are Involved in the Intracellular Growth Control of *Mycobacterium abscessus* by Mediating NOD2-Induced Production of Nitric Oxide in Macrophages

*Jae-Hun Ahn[1], Ji-Yeon Park[1], Dong-Yeon Kim[1], Tae-Sung Lee[1], Do-Hyeon Jung[1], Yeong-Jun Kim[1], Yeon-Ji Lee[1], Yun-Ji Lee[1], In-Su Seo[1], Eun-Jung Song[1], Ah-Ra Jang[1], Soo-Jin Yang[2], Sung Jae Shin[3] and Jong-Hwan Park[1]**

[1] Laboratory Animal Medicine, College of Veterinary Medicine and BK21 FOUR Program, Chonnam National University, Gwangju, South Korea, [2] Department of Veterinary Microbiology, College of Veterinary Medicine and Research Institute for Veterinary Science, Seoul National University, Seoul, South Korea, [3] Department of Microbiology, Institute for Immunology and Immunological Diseases, Brain Korea 21 PLUS Project for Medical Science, Yonsei University College of Medicine, Seoul, South Korea

Mycobacterium abscessus (MAB) is one of the rapidly growing, multidrug-resistant non-tuberculous mycobacteria (NTM) causing various diseases including pulmonary disorder. Although it has been known that type I interferons (IFNs) contribute to host defense against bacterial infections, the role of type I IFNs against MAB infection is still unclear. In the present study, we show that rIFN-β treatment reduced the intracellular growth of MAB in macrophages. Deficiency of IFN-α/β receptor (IFNAR) led to the reduction of nitric oxide (NO) production in MAB-infected macrophages. Consistently, rIFN-β treatment enhanced the expression of iNOS gene and protein, and NO production in response to MAB. We also found that NO is essential for the intracellular growth control of MAB within macrophages in an inhibitor assay using iNOS-deficient cells. In addition, pretreatment of rIFN-β before MAB infection in mice increased production of NO in the lungs at day 1 after infection and promoted the bacterial clearance at day 5. However, when alveolar macrophages were depleted by treatment of clodronate liposome, rIFN-β did not promote the bacterial clearance in the lungs. Moreover, we found that a cytosolic receptor nucleotide-binding oligomerization domain 2 (NOD2) is required for MAB-induced TANK binding kinase 1 (TBK1) phosphorylation and IFN-β gene expression in macrophages. Finally, increase in the bacterial loads caused by reduction of NO levels was reversed by rIFN-β treatment in the lungs of NOD2-deficient mice. Collectively, our findings suggest that type I IFNs act as an intermediator of NOD2-induced NO production in macrophages and thus contribute to host defense against MAB infection.

Keywords: ***Mycobacterium abscessus*, type I IFN, NOD2, nitric oxide, macrophage**

OPEN ACCESS

Edited by:
Rosane M. B. Teles, University of California, Los Angeles, United States

Reviewed by:
Paulo R. Z. Antas, Oswaldo Cruz Foundation (Fiocruz), Brazil
Chaouki Benabdessalem, Pasteur Institute of Tunis, Tunisia, in collaboration with Leandro Pontes

***Correspondence:**
Jong-Hwan Park
jonpark@jnu.ac.kr

Specialty section:
This article was submitted to Microbial Immunology, a section of the journal Frontiers in Immunology

Received: *08 July 2021*
Accepted: *30 September 2021*
Published: *28 October 2021*

Citation:
Ahn J-H, Park J-Y, Kim D-Y, Lee T-S, Jung D-H, Kim Y-J, Lee Y-J, Lee Y-J, Seo I-S, Song E-J, Jang A-R, Yang S-J, Shin SJ and Park J-H (2021) Type I Interferons Are Involved in the Intracellular Growth Control of Mycobacterium abscessus by Mediating NOD2-Induced Production of Nitric Oxide in Macrophages. Front. Immunol. 12:738070. doi: 10.3389/fimmu.2021.738070

INTRODUCTION

Mycobacterium abscessus (MAB) is one of the rapidly growing non-tuberculous mycobacteria (NTM) causing chronic pulmonary infection and skin and soft tissue infection (SSTI) in immunosuppressed patients (1). MAB has been well-known for being multidrug resistant, and cases of recurrent infection have been reported despite macrolide, amikacin, cefoxitin, and imipenem treatment (2). Recent Canadian studies have shown that the number of patients infected with MAB is increasing every year and about four times higher than the incidence of tuberculosis (3). As an intracellular pathogen, MAB can survive within innate immune cells such as macrophages and escape host immune response. Thus, understanding the exact molecular mechanism of antimicrobial effect within macrophages against MAB infection is essential for prevention and treatment of MAB infection (4).

Type I interferons (IFNs) are well-known cytokines that play an important role in host antiviral responses, and there are 13 different type I IFN subfamilies (5). The genes encoding type I IFNs are located in the same chromosomal locus; and the IFN-β gene, one of the subfamily, is known as a primordial gene of type I IFN family (6). Microbial pathogen or damage-associated molecular pattern (DAMP) stimulates pattern recognition receptor (PRR), and this stimulation produces type I IFNs through TANK binding kinase 1 (TBK1)–IFN regulatory factor (IRF) signaling cascade (7). Consequently, type I IFNs, including IFN-β, is recognized by the IFN-α/β receptor (IFNAR), and this recognition leads to the transcription of various IFN-stimulated gene (ISG) mediating antiviral effects and various immune responses (6). Nucleotide-binding oligomerization domain 2 (NOD2) is a member of cytosolic nucleotide-binding oligomerization domain (NOD)-like receptor family (8). Upon detecting muramyl dipeptide (MDP) or bacterial peptidoglycan component, NOD2 initiates innate immune response against various microbial pathogens (9). Unlike other bacterial pathogens, mycobacteria produce characteristic enzyme called *N*-acetyl muramic acid hydroxylase (NamH) that converts the *N*-acetylated glycan chain of MDP to *N*-glycolylated chain (10). Moreover, *N*-glycolyl MDP exerts higher NOD2 activity than *N*-acetyl MDP and induces more potent immune response (11). For this reason, the essential role of NOD2 in host innate and adaptive immune responses against infections with *Mycobacterium* spp. has been extensively studied (12–15). Furthermore, we previously identified that NOD2 enhances the antimicrobial effect of macrophage against MAB infection by amplifying NO production, through *in vitro* and *in vivo* experiments (16).

Recently, several studies have been reported on the role of type I IFNs in host immune responses against bacterial infection (17). Interestingly, the role of type I IFNs in the aspect of antimicrobial effect is still controversial depending on bacterial species. In the case of systemic infection of *Streptococcus pneumoniae* and *Escherichia coli*, IFNAR-deficient mice maintained higher bacterial load in blood than did wild-type (WT) mice, which means that type I IFN signaling enhances bacterial clearance (18). Similarly, in case of *Helicobacter pylori* oral infection, IFNAR-deficient mice exhibited higher bacterial load in the stomach than did WT mice (19), correlating with the higher mortality in IFNAR-deficient mice in cecal ligation puncture-induced mouse sepsis model (20). On the contrary, IFNAR- or IFN-β-deficient mice exhibited lower bacterial load than did WT mice in the cases of *Francisella tularensis*, *Salmonella typhimurium*, and *Listeria monocytogenes* infection (21), indicating that type I IFNs exerted detrimental effects on host antimicrobial responses. In the case of mycobacterial infection, though belonging to the same genus, each species showed different phenotypes depending on the presence or absence of type I IFN signaling. INFAR-deficient mice infected with *Mycobacterium tuberculosis* exhibited lower bacterial loads in lung than the WT mice (22). On the other hand, the bacterial load of *Mycobacterium avium* complex and *Mycobacterium smegmatis* remained higher in IFNAR-deficient mice than WT mice (23). Even for the studies on *M. tuberculosis* infection, the impact of type I IFNs on bacterial clearance is different from study to study (24). For these reasons, it is important to identify the varying roles of type I IFN in host defense in the context of different experimental conditions such as bacterial species, infection dose, and infection route.

Likewise, the controversial roles of type I IFNs in MAB infection have been reported in two recent publications (25, 26). These two studies provided the conflicting results in antimicrobial responses of macrophages depending on the presence and absence of type I IFN signal. The first study reported that type I IFNs augment the cell-to-cell spread of MAB by increasing cytotoxicity of infected macrophages resulting in IFNAR-deficient macrophages that exhibited lower bacterial load as compared with the WT macrophages (26). The other reported that type I IFNs increased the production of NO in MAB-infected macrophages and that, consequently, IFNAR-deficient macrophages showed higher bacterial load than the WT macrophages in their study (25). Furthermore, there has been no study that elucidates the role of type I IFNs in *in vivo* model of MAB infection.

In this study, we aimed to i) clarify the antimicrobial mechanism of type I IFNs during MAB infection in macrophages and ii) elucidate the role of type I IFNs in *in vivo* MAB pulmonary infection model.

MATERIALS AND METHODS

Cell Culture and Medium

Bone marrow-derived macrophages (BMDMs) were derived from murine femur–tibia bone marrow and prepared as previously described (27). In summary, isolated BMDMs were incubated at 5% CO_2, 37°C in complete Iscove's modified Dulbecco's medium (IMDM; Gibco, Grand Island, NY, USA) supplemented with 12.5 ng/ml of recombinant mouse M-CSF Protein (R&D Systems, Minneapolis, MN, USA), 10% fetal bovine serum (FBS), 1% sodium pyruvate, 1% MEM Non-Essential Amino Acids (MEM NEAA), and 1% penicillin/streptomycin (P/S). After 3 days, 5 ml of fresh same medium

was added, and the cells were cultured under the same conditions for 3 days and then used in the experiment. For the treatment of bacteria and reagents, medium (hereafter referred to as treat medium) was supplied to IMDM with 2% FBS, 1% MEM NEAA, and 1% sodium pyruvate without antibiotics.

MH-S mouse alveolar macrophage (AM) cells purchased from American Type Culture Collection (ATCC, Manassas, VA, USA) were cultured in Roswell Park Memorial Institute (RPMI) 1640 (WELGENE, Gyeongsan, Republic of Korea) supplemented with 10% FBS, 50 μM of 2-mercaptoethanol, and 1% P/S at 37°C in 5% CO_2 conditions. Treat medium was supplied to RPMI 1640 with 2% FBS and 50 μM of 2-mercaptoethanol without antibiotics.

Murine primary AMs were cultured as previously described (28). Briefly, 8- to 15-week-old male mice with C57BL/7 background were anesthetized, and bronchoalveolar lavage fluid (BALF) was obtained by flushing 1 ml of cold Dulbecco's phosphate-buffered saline (D-PBS, WELGENE, Gyeongsan, Korea) containing 1 mM of EDTA. Collected BALFs from each mouse were pooled and centrifuged with 4°C and 250 relative centrifugal force (RCF). After the supernatant was discarded, pellets were dissolved with red blood cell (RBC) lysis buffer and incubated at room temperature for 10 min. After being washed twice with D-PBS, AMs were dissolved with DMEM high-glucose medium containing 10% FBS, 1% P/S, 1% HEPES, and 1% sodium pyruvate. AMs were seeded on a 48-well plate, 200 μl per well, with a concentration of 5×10^5 cell/ml. After 12 h, the time to stabilize cells after attaching to plate, intracellular bacterial growth assay was performed with the same method of BMDMs and MH-S cells. Treat medium was supplied to DMEM high-glucose medium with 2% FBS, 1% HEPES, and 1% sodium pyruvate without antibiotics.

Reagents

The following reagents were used. Mouse recombinant IFN-β (PBL Biomedical Laboratories, Piscataway, NJ, USA; Cat# 12401-1). Ultrapure lipopolysaccharide from *E. coli* O111:B4 (LPS; InvivoGen, San Diego, CA; Cat# tlrl-eblps), N^G-Nitro-L-arginine methyl ester (L-NAME; Sigma Aldrich, St. Louis, MO, USA, Cat# 51298-62-5), and BX795 (InvivoGen, San Diego, CA, USA, Cat# tlrl-bx7).

Mice

WT, *Ifnar*$^{-/-}$, *Inos*$^{-/-}$, and *Nod2*$^{-/-}$ mice on a C57BL/6 background were purchased from The Jackson Laboratory (Bar Harbor, ME, USA). Female mice aged 8–10 weeks were used for animal experiments. Animal experiments were performed under protocols approved by the Institutional Animal Care and the Use Committee of Chonnam National University (Approval No. CNU IACUC-YB-2017-56 and 2019-31).

Bacterial Culture and *In Vitro* Infection Dose

Bacterial culture of the isogenic rough variant of *M. abscessus* ATCC19977T (Manassas, VA, USA) were prepared as previously described (29). Briefly, the bacterium was cultivated in 7H9 broth supplemented with 0.5% glycerol, 10% oleic acid, dextrose, albumin, and catalase (OADC; BD Biosciences, San Jose, CA, USA). For seed culture, 1 ml of frozen bacterial stock (3×10^8 CFU) was added in 10 ml of culture medium, and the cells were allowed to grow for 7 days at 37°C with shaking at 130 rpm. For main culture, the entire cells from seed culture were added to 200 ml of culture medium and incubated for three more days. The cells were centrifuged at 4,500 RCF and washed three times with D-PBS. For single-cell suspension, the cells were dissolved in D-PBS and sonicated for 1 s at 40 kHz, 100 W. The cells aggregated by sonication were removed by passing through 40-μm mesh. This process was repeated three times. The seed lots dissolved in D-PBS (contained 40% glycerol) were kept at −80°C until use. In all *in vitro* experiments, the number of macrophages to the number of bacteria was set as 1:25 multiplicity of infection (MOI). This infection dose was determined in our previous study (16). Except the assessment of TBK1 phosphorylation (Western blotting), extracellular MAB was washed out after 1 h post infection, and cells were incubated with gentamicin (Sigma Aldrich, St. Louis, MO, USA) containing fresh medium for indicated times in all experiments

Intracellular Bacterial Growth Assay and Colony-Forming Unit Measurement

BMDMs and MH-S cells were seeded on a 48-well plate, 200 μl per well, with a concentration of 1×10^6 cell/ml. After 12 h, the time to stabilize cells after attaching to plate, MAB diluted in treat medium was infected for 200 μl per well with MOI 25. After 1 h, which is a sufficient time for phagocytosis, cell culture supernatant was washed out by D-PBS and replaced with fresh treated medium containing 100 μg/ml of gentamicin. Cell culture supernatant was washed out by D-PBS on indicated time, and attached cells were lysed with 100 μl of 1% Triton X-100. The bacterial colony-forming unit (CFU) of cell lysate was determined by the spread plate technique, as follows. The cell lysate or lung lysate (*in vivo*) samples containing bacteria were diluted with D-PBS as proper detectable levels. Fifty microliters of diluted samples was uniformly spread through glass beads on the Middlebrook 7H10 agar (Difco, Detroit, MI, USA) plate containing ampicillin, and plates were incubated for 96 h at 37°C. The number of colony was counted and converted to log value. The CFU value of the tissue sample was normalized to tissue weight (g).

Real-Time Quantitative Polymerase Chain Reaction

BMDMs and MH-S cells were seeded on a 6-well plate, 2 ml per well, with a concentration of 1×10^6 cell/ml. After 12 h, the time to stabilize cells after attaching to plate, infection and reagent treatment were performed with each indicated conditions. RNA was extracted using 1 ml of easy-BLUETM Total RNA Extraction Kit (iNtRON Biotechnology, Seongnam, Korea). cDNA was synthesized from 1 μg of RNA using ReverTra Ace® qPCR RT Master Mix (TOYOBO Biotechnology, Osaka, Japan). Real-time qPCR samples were prepared using the SYBR Green PCR Kit (Qiagen GmbH, Hilden, Germany). The primer sequences were as follows: iNOS; sense, 5′-GCATTGGAAGTGAAGCGTTTC-3′ and antisense, 5′-GGCAGCCTGTGAGACCTTTG-3′. IFN-β; sense 5′-ATGAACTCCACCAGCAGACAG-3′, and antisense,

5′-ACCACCATCCAGGCGTAGC-3′. CRAMP; sense 5′-AAGGAACAGGGGGTGGTG-3′ and antisense, 5′-CC GGGAAATTTTCTTGAACC-3′. NOX2; sense 5′-ACTCCTTGGAGCACTGG and antisense 5′-GT TCCTGTCCAGTTGTCTTC-3′. β-Actin; sense 5′-AGGCCCAGAGCAAGAGAG-3′ and antisense, 5′-TC AACATGATCTGGGTCAT-3′. PCR was conducted by a Rotor-Gene Q real-time PCR system (Qiagen) using a two-step protocol of 40 cycles of 95°C for 10 s followed by 60°C for 45 s. Normalized gene expression levels were indicated as the ratio between the mean value for the target gene and that for the β-actin.

Western Blotting

BMDMs were seeded on a 12-well plate, 1 ml per well, with a concentration of 1×10^6 cell/ml. After 12 h, the time to stabilize cells after attaching to plate, infection and reagent treatment were performed with each indicated conditions. Cells were lysed using lysis buffer containing Nonidet P-40, complete protease inhibitor cocktail (Roche, Mannheim, Germany), and 2 mM of dithiothreitol. Cell lysates were separated using sodium dodecyl sulfate–polyacrylamide gel electrophoresis (SDS-PAGE) and transferred to nitrocellulose membranes. The membranes were incubated at 4°C with anti-iNOS (1:2,000 dilution) (BD Biosciences, San Jose, CA, USA), anti-phospho-TBK1 (1:1,000 dilution) (Cell Signaling Technology, Beverly, MA, USA), anti-total-TBK1 (1:1,000 dilution) (Cell Signaling Technology, Beverly, MA, USA), and anti-β-actin (1:2,000 dilution) (Santa Cruz Biotechnology, Santa Cruz, CA) for 24 h. After the primary antibody is attached, the relevant secondary antibodies were attached at room temperature for 2 h. Proteins were detected by an enhanced chemiluminescence reagent (iNtRON Biotechnology, Seongnam, Korea).

Measurement of Nitric Oxide Levels in Cell Culture Supernatants

BMDMs and MH-S cells were seeded on a 48-well plate, 200 μl per well, with a concentration of 1×10^6 cell/ml. After bacterial infection and reagent treatment according to each condition, cell culture supernatants were harvested, and NO concentrations were measured *via* the Griess reaction assay as previously described (30).

Enzyme-Linked Immunosorbent Assay

To investigate the difference in inflammatory cytokine production depending on the presence or absence of type I IFN signal in the lung of MAB-infected mice, IL-6 (assay range 15.6–1,000 pg/ml), TNF-α (assay range 31.2–2,000 pg/ml), IL-10 (assay range 31.2–2,000 pg/ml), and IL-1β (assay range 15.6–1,000 pg/ml) cytokines from the supernatant of lung lysate were measured by ELISA kits (R&D System, Minneapolis, MN, USA) according to the manufacturer's instructions. The cytokine value of the tissue sample was normalized to tissue weight (g).

Lactate Dehydrogenase Assay

To elucidate the difference in cytotoxicity depending on the presence or absence of type I IFN signal in the MAB infection, BMDMs and MH-S cells were seeded on a 48-well plate, 200 μl per well, with a concentration of 1×10^6 cell/ml. After bacterial infection and reagent treatment according to each condition, cell culture supernatant was harvested, and lactate dehydrogenase (LDH) levels were measured by CytoTox 96® Non-Radioactive Cytotoxicity Assay kits (Promega, Madison, WI, USA) according to the manufacturer's instructions.

Mouse Infection Model

For intranasal inoculation or administration, mice were anesthetized with combination of xylazine (10 mg/kg) and zoletil (30 mg/kg). Mice were inoculated with 2×10^7 CFU (in 40 μl of D-PBS) of MAB intranasally. Eight hundred units (in 40 μl of D-PBS) per mouse of rIFN-β was administered in the same way as bacterial inoculation. At indicated day post infection, mice were sacrificed, and lung tissues were harvested in a sterilized condition. The rest of the lobes except the left lobe were homogenized with 500 μl of D-PBS, and the lysate was used for CFU measurements. The remaining lysate was centrifuged for 10 min at 4,000 RCF, and the supernatant was harvested for NO measurement and cytokine analysis. NO concentrations were measured by the Griess reaction assay, and cytokines were analyzed by ELISA. The left lung lobe was used for the histological examination.

Clodronate Liposomes and Macrophage Depletion

Clodronate liposomes and control liposomes were purchased from LIPOSOMA (Amsterdam, Netherlands, Cat# CP-005-005). Animal experiments for the depletion of macrophages in the lungs were performed as follows: 50 μl of clodronate liposomes or control liposomes was administrated intranasally under anesthesia once a day for 3 days. The administration of rIFN-β and bacterial infection were performed according to the schedule indicated in diagram of result section.

Flow Cytometry

The left lobes of the lung tissue were pooled by each group and slightly chopped using a pair of scissors in cold RPMI 1640 containing 1 μg/ml of dipase II (Sigma Aldrich, St. Louis, MO, USA). Samples were incubated at 37°C, 1,100 RPM shaking chamber. After 1 h, samples were placed on 40-μm cell strainer and homogenized using syringe rubber to obtain the single cells. RBCs were lysed using RBC lysis buffer, and flow cytometry assay was performed as previously described (31). In briefly, cells were stained with anti-CD45-APC (BD Biosciences, San Jose, CA, USA), anti-CD11c-PE (BD Biosciences), and anti-F4/80-FITC (Invitrogen, Carlsbad, CA, USA). Analysis was performed by using MACSQuant Analyzer 10 (Miltenyi Biotec, Bergisch Gladbach, Germany).

Histopathological Examination

The left lobe of the lung was fixed in 10% neutral formalin for 24 h, followed by tissue processing and paraffin embedding. The paraffin blocks were sectioned at 2 μm and stained with H&E. Histopathological examination was performed under microscopy. Histopathological severity was scored blindly by two experts in a field of laboratory animal pathology with an arbitrary scoring index based on the degree of inflammatory cell infiltration and the extent of the lesion area (0, normal; 1, mild; 2, mild to moderate; 3, moderate; 4, moderate to severe; and 5, severe).

Statistical Analysis

The statistical significance of differences between two groups was determined by unpaired t-test. In case of more than three groups, the statistical significance was determined by one-way ANOVA followed by Tukey's post-hoc test for comparisons between groups (GraphPad Prism 5; GraphPad Software Inc., La Jolla, CA, USA). p-Values <0.05 were considered statistically significant.

RESULTS

Mycobacterium abscessus Induces Interferon-β Gene Expression of Macrophages in TANK Binding Kinase 1-Dependent Manner, Which Promotes Intracellular Bacterial Clearance

We first examined whether MAB induces gene expression of type I IFNs in macrophages. Consistent with previous studies (25, 26), MAB upregulated IFN-β gene expression approximately 125-fold compared with 0 h in BMDMs as well as fivefold in MH-S cells, a murine AM cell line, at 3 h after infection (**Figures 1A, B**). Various PRR signaling mediates type I IFN expression by activating TBK1 (5). As expected, infection with MAB induced phosphorylation of TBK1 in both BMDMs and MH-S cells (**Figures 1C, D**). Pretreatment with BX795, a TBK1-specific inhibitor, suppressed MAB-induced TBK1 phosphorylation and IFN-β gene expression in a dose-dependent manner in BMDMs (**Figures 1E, F**), indicating that MAB induces gene expression of type I IFNs in macrophages *via* TBK1-dependent manner.

There has been an extreme controversy on the role of type I IFNs in the intracellular survival of MAB within macrophages (25, 26). To clarify this, we examined the intracellular bacterial CFUs under various experimental conditions. Compared with WT BMDMs (6.05 log CFU/ml), the bacterial CFUs were higher in IFNAR-deficient BMDMs (6.32 log CFU/ml) at 72 h after

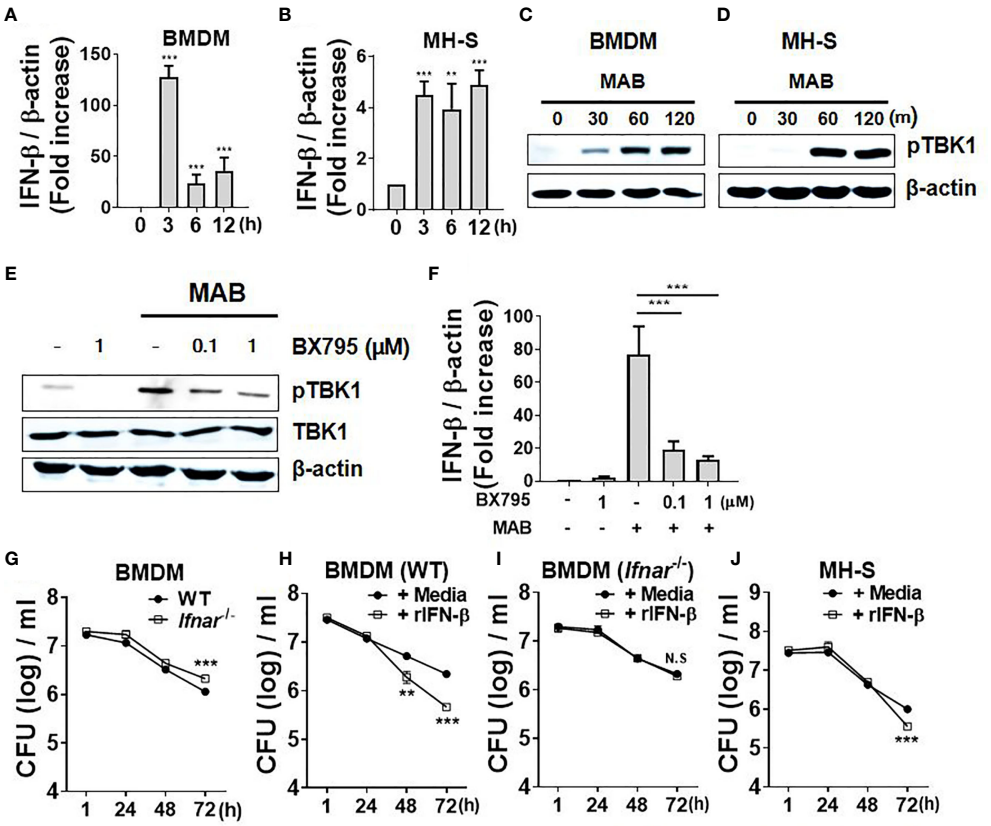

FIGURE 1 | MAB induces IFN-β gene expression of macrophages in TBK1-dependent manner, which promotes intracellular bacterial clearance. **(A, B)** BMDMs and mouse alveolar macrophage cell line MH-S cells were infected with MAB at multiplicity of infection (MOI) 1:25 for indicated times. mRNA was extracted, and the expression levels of IFN-β gene were determined by real-time PCR. **(C)** BMDMs and **(D)** MH-S cells were infected with MAB for indicated times. **(E)** BMDMs were infected with MAB for 1 h in the absence or presence of BX795 (2 h pretreated). **(C–E)** The levels of indicated proteins were determined by Western blotting. **(F)** BMDMs were infected with MAB for 6 h in the absence or presence of BX795 (2 h pretreated). The mRNA was extracted, and the expression levels of IFN-β gene were determined by real-time PCR. **(G–J)** Cells were infected with MAB in the absence or presence of recombinant IFN-β (1,000 units/ml, 2 h pretreated). Intracellular bacterial CFU on indicated times were evaluated by intracellular bacterial growth assay. **(A–J)** The results are from one representative experiment of two independent experiments (**p < 0.01, ***p < 0.001). MAB, *Mycobacterium abscessus*; IFN, interferon; TBK1, TANK binding kinase 1; BMDMs, bone marrow-derived macrophages; CFU, colony-forming unit. NS, Not Statistically Significant.

infection (**Figure 1G**). In addition, treatment of recombinant IFN-β (rIFN-β) enhanced the bacterial clearance from 6.34 log CFU/ml to 5.66 log CFU/ml in WT BMDMs, but not in IFNAR-deficient cells (**Figures 1H, I**) at 72 h after infection. In MH-S cells, the bacterial clearance was accelerated by rIFN-β from 6 log CFU/ml to 5.55 log CFU/ml at 72 h after infection (**Figure 1J**). These results suggest that type I IFNs inhibit the intracellular growth of MAB in macrophages.

Type I Interferons Augment *Mycobacterium abscessus*-Induced Production of Nitric Oxide in Macrophages

Antimicrobial peptides (AMPs), reactive oxygen species (ROS), and NO are the major factors involved in the removal of intracellular pathogens in macrophages (32). We sought to determine whether type I IFNs regulate expression of those factors in response to MAB in macrophages. IFNAR deficiency did not affect the gene expression of CRAMP and NOX2 (**Figures 2A, B**), whereas iNOS expression was mostly abolished in IFNAR-deficient BMDMs (**Figure 2C**). Treatment with rIFN-β also enhanced MAB-induced iNOS expression in WT BMDMs, but not in IFNAR-deficient BMDMs (**Figure 2D**). Moreover, rIFN-β also increased MAB-induced iNOS expression in MH-S cell (**Figure 2E**). The protein expression of iNOS induced by MAB was reduced in IFNAR-deficient macrophages *versus* the WT cells (**Figure 2F**), and rIFN-β enhanced MAB-induced expression of iNOS protein in BMDMs (**Figure 2G**) and MH-S cells (**Figure 2H**), but not in IFNAR-deficient BMDMs (**Figure 2G**). Our previous study revealed that MAB alone could not produce detectable level of NO in BMDMs, but at the presence of the type II IFN, IFN-γ, the bacterium led to substantial level of NO production (16). Consistently, at the presence of IFN-γ, MAB induced NO production in WT BMDMs, which were mostly abolished in IFNAR-deficient cells (**Figure 2I**). Unlike BMDMs, MAB alone could produce detectable levels of NO in MH-S cells, which were

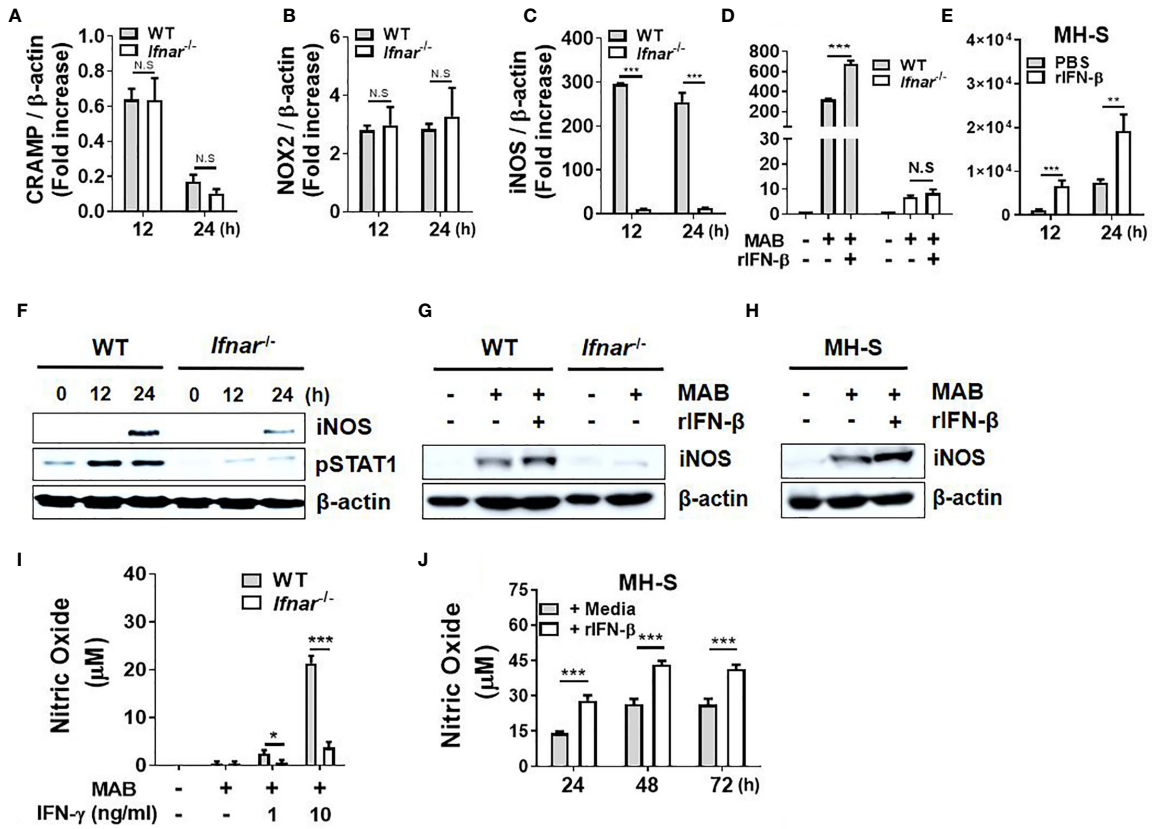

FIGURE 2 | Type I IFNs augment MAB-induced production of nitric oxide in macrophages. **(A–C)** WT and IFNAR-deficient BMDMs were infected with MAB at a MOI 1:25 for indicated times. **(D, E)** BMDMs and MH-S cells were pretreated with or without rIFN-β (1,000 units/ml) for 2 h and additionally infected with MAB for **(D)** 12 h or **(E)** indicated times. **(A–E)** mRNA was extracted, and the expression levels of each gene were determined by real-time PCR. **(F)** BMDMs were infected with MAB for indicated times. **(G)** BMDMs and **(H, J)** MH-S cells were pretreated with or without rIFN-β (1,000 units/ml) for 2 h and additionally infected with MAB for **(G, H)** 24 h or **(J)** indicated times. **(I)** BMDMs were incubated for 24 h with indicated conditions. **(F–H)** Cellular proteins were extracted, and the levels of indicated proteins were determined by Western blotting. **(I, J)** Nitric oxide concentration in cell culture supernatant was measured by Griess reaction. **(A–J)** The results are from one representative experiment of two independent experiments (*$p < 0.05$, **$p < 0.01$, ***$p < 0.001$). MAB, *Mycobacterium abscessus*; IFN, interferon; WT, wild type; IFNAR, interferon-α/β receptor; BMDMs, bone marrow-derived macrophages; MOI, multiplicity of infection. NS, Not Statistically Significant.

also enhanced by rIFN-β (**Figure 2J**). These results suggest that type I IFN signaling may contribute to MAB-induced NO production in macrophages.

Type I Interferons Inhibit the Intracellular *Mycobacterium abscessus* Growth in Macrophages by Regulating Nitric Oxide Production

It has been reported that NO is critical for the restriction of intracellular MAB growth in macrophages (16, 25, 33). As type I IFNs enhanced the intracellular MAB clearance and MAB-induced NO production in BMDMs at the presence of IFN-γ and MH-S cells, we sought to clarify whether NO is a key factor for type I IFN-mediated inhibition of the bacterial growth. In the presence of L-NAME, a non-selective nitric oxide synthase (NOS) inhibitor, there was no significant difference in the bacterial CFUs between WT and IFNAR-deficient BMDMs (**Supplementary Figure 1A**). Treatment of rIFN-β also did not affect the intracellular growth of MAB in L-NAME-treated or iNOS-deficient BMDMs (**Supplementary Figures 1B, C**). As shown in **Figure 3A**, L-NAME reduced MAB-induced or rIFN-β-enhanced NO production in MH-S cells. Treatment with L-NAME or rIFN-β did not affect the phagocytosis of MH-S cells (**Figure 3B**). Consistent with the result presented in **Figure 1J**, rIFN-β inhibited the MAB growth 3.8-fold compared with medium in MH-S cells, which was restored by L-NAME treatment (**Figure 3C**). This phenomenon was also confirmed in primary isolated murine AMs. The intracellular growth of MAB was 1.86-fold higher in L-NAME-treated AMs compared with medium-treated AMs at 72 h post infection (**Figure 3D**). Also, while rIFN-β inhibited the growth of MAB 1.91-fold compared with medium control, in the presence of L-NAME, rIFN-β did not suppress the intracellular growth of MAB in AMs, 72 h after infection (**Figure 3D**). These results indicate that type I IFNs suppress the intracellular survival of MAB by promoting NO production in macrophages.

Intranasal Pretreatment of rIFN-β Augments Nitric Oxide Production and Promotes the *Mycobacterium abscessus* Clearance in the Lungs of Mice

Next, we sought to determine *in vivo* role of type I IFNs against pulmonary infection of MAB by pre-exposure to rIFN-β. The experimental schedule is depicted in **Figure 4A**. NO levels in the lung homogenate of mice pretreated (i.n.) with rIFN-β were higher than those of the mice treated with PBS at day 1 after infection, although the difference between the two groups was not observed at day 5 (**Figure 4B**). Pretreatment of rIFN-β also reduced the bacterial CFUs in the lung homogenates of MAB-infected mice at day 5, but not at day 1 (**Figure 4C**). To determine the *in vivo* effect of type I IFN-induced NO on the growth control of MAB, we repeated the experiment using iNOS-deficient mice. As presented in **Figure 4D**, intranasal pretreatment with rIFN-β did not influence the MAB growth in the lungs of iNOS-deficient mice (**Figure 4D**), strongly supporting the notion that intranasal pre-exposure to rIFN-β contributes to *in vivo* growth control of MAB by promoting NO production in macrophages. However, administration of rIFN-β after MAB infection did not improve the bacterial clearance in the lungs of MAB-infected mice (**Supplementary Figures 2A, B**). To determine the impact of type I IFNs on host defense against MAB infection, we compared the bacterial CFUs in the lungs of WT and IFNAR-deficient mice. Unexpectedly, the bacterial CFUs at day 5 were significantly lower in IFNAR-deficient mice as compared with WT mice (**Supplementary Figures 3A, B**), suggesting that type I IFNs can exert a harmful effect in host defense against MAB infection, although prophylactic administration of type I IFNs improves *in vivo* growth control of MAB.

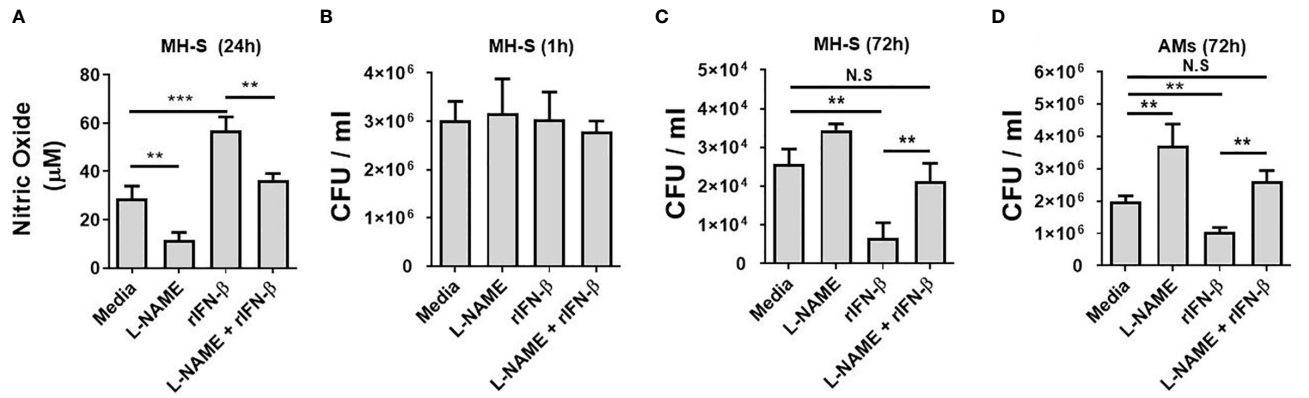

FIGURE 3 | Type I IFNs inhibits the intracellular MAB growth in macrophages by regulating NO production. **(A–C)** MH-S cells were incubated with MAB and indicated reagents (2 h pretreated). **(A)** Nitric oxide concentration in cell culture supernatant was measured by Griess reaction at 24 h post infection. Intracellular bacterial CFU on **(B)** 1 h and **(C)** 72 h were evaluated by intracellular bacterial growth assay. **(D)** AMs were incubated with MAB (MOI 1:25) and indicated reagents (2 h pretreated, L-NAME 1 mM, rIFN-β 1,000 units/ml). Intracellular bacterial CFU on 72 h was evaluated by intracellular bacterial growth assay. **(A–D)** The results are from one representative experiment of two independent experiments (**p < 0.01, ***p < 0.001). MAB, *Mycobacterium abscessus*; IFN, interferon; CFU, colony-forming unit; AMs, alveolar macrophages; MOI, multiplicity of infection. NS, Not Statistically Significant.

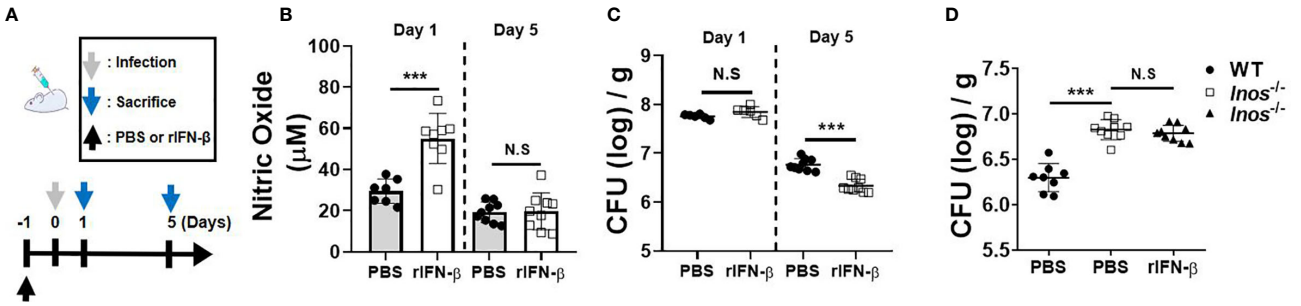

FIGURE 4 | Intranasal pretreatment of rIFN-β augments NO production and promotes the bacterial clearance in the lungs of mice infected with MAB. **(A)** The administration of rIFN-β and bacterial infection were performed according to the schedule indicated in the diagram. **(B–D)** WT or iNOS-deficient mice were administrated with PBS or rIFN-β (800 units per mouse) intranasally under anesthesia. After 1 day, mice were infected with 2×10^7 CFU of MAB per mouse intranasally; and the bacterial loads and nitric oxide levels in the lung lysate were determined at indicated days. **(B–D)** The results are merged data of two independent experiments (n = 4–6) (***p < 0.001). MAB, *Mycobacterium abscessus*; WT, wild type; PBS, phosphate-buffered saline; CFU, colony-forming unit. NS, Not Statistically Significant.

Macrophages Are Responsible for rIFN-β Response in *Mycobacterium abscessus*-Induced Nitric Oxide Production and the Bacterial Clearance *In Vivo*

We investigated whether macrophages are involved in the *in vivo* protective effect of rIFN-β against the pulmonary infection of MAB. Schedule of clodronate injection and MAB infection is depicted in **Figure 5A**. The bacterial CFUs in the lungs were examined at day 5 after infection and NO production at day 1. Flow cytometry analysis showed that MAB infection increased the ratio of the $CD45^+F4/80^+CD11c^+$ AM in the lungs from 4% to 18%, which was rescued to 4% by the treatment with clodronate liposome (**Figure 5A**). In mice treated with clodronate, rIFN-β treatment did not suppress the bacterial growth in the lungs, whereas the bacterial CFUs were decreased by rIFN-β treatment in mice with PBS liposome (**Figure 5B**). Moreover, rIFN-β treatment could not elicit NO production in mice treated with clodronate liposome (**Figure 5C**). Based on these data, it is likely that macrophages are essential for the protective effect of rIFN-β against MAB infection.

Type I Interferons Act as an Intermediator in a Cytosolic Receptor NOD2-Mediated Nitric Oxide Production in Response to *Mycobacterium abscessus*

Our previous study demonstrated that NOD2 contributes to *in vivo* and *in vitro* bacterial clearance against MAB infection by promoting NO production (16). In addition, Pandey et al. reported that NOD2-Ripk2 signaling is involved in induction of type I IFNs against *M. tuberculosis* infection through bacterial ESX-1- and host TBK1-IRFs-dependent pathways (34). Thus, we hypothesized that NOD2 mediates MAB-induced type I IFN expressions, which results in NO-mediated killing of MAB. NOD2 deficiency diminished MAB-induced phosphorylation of TBK1 in BMDMs (**Figure 6A**). In addition, the gene expression of IFN-β in response to MAB was significantly reduced in NOD2-deficient BMDMs as compared with WT cells (**Figure 6B**). The protein expression of iNOS was also decreased in NOD2-deficient BMDMs, which was restored by the addition of rIFN-β (**Figure 6C**). In an *in vivo* experiment, MAB-induced NO production was decreased in NOD2-deficient mice at day 1, which was also restored by rIFN-β (**Figure 6D**). The bacterial clearance in the lungs was impaired in NOD2-deficient mice at day 5 (**Figure 6E**). However, intranasal administration of rIFN-β reduced the bacterial CFUs in the lungs of NOD2-deficient mice, exhibiting comparable levels of CFUs as in WT mice (**Figure 6E**). These results suggest that NOD2 signaling contributes to the clearance of MAB by promoting type I IFN-mediated NO production in macrophages.

DISCUSSION

Macrophages play an essential role in host innate immune responses against intracellular bacterial infection (32). In the current investigation, we examined the impact of type I IFNs on bactericidal activity of macrophages and confirmed that IFNAR deficiency causes attenuation of bacterial clearance in macrophages under MAB infection. Moreover, pretreatment of mice with rIFN-β enhanced the bactericidal activity of macrophages. In fact, to evaluate the dose dependence of rIFN-β on MAB growth control, we used two doses of rIFN-β (500 and 1,000 units/ml). However, the 500 units/ml of rIFN-β inhibited the MAB growth at the same level of 1,000 units/ml in BMDMs (data not shown). As shown in **Figure 6C**, rIFN-β strongly increased iNOS protein expression even at a low dose (250 units/ml). Therefore, to see a dose-dependent response of rIFN-β on MAB growth inhibition, it seems that an experiment using much lower concentrations (below 250 units/ml) should be performed. In addition, our results suggested that type I IFNs promote production of NO against MAB infection and that MAB clearance is facilitated in a NO-dependent manner within macrophages. These results are consistent with the previous finding of the role of type I IFNs in

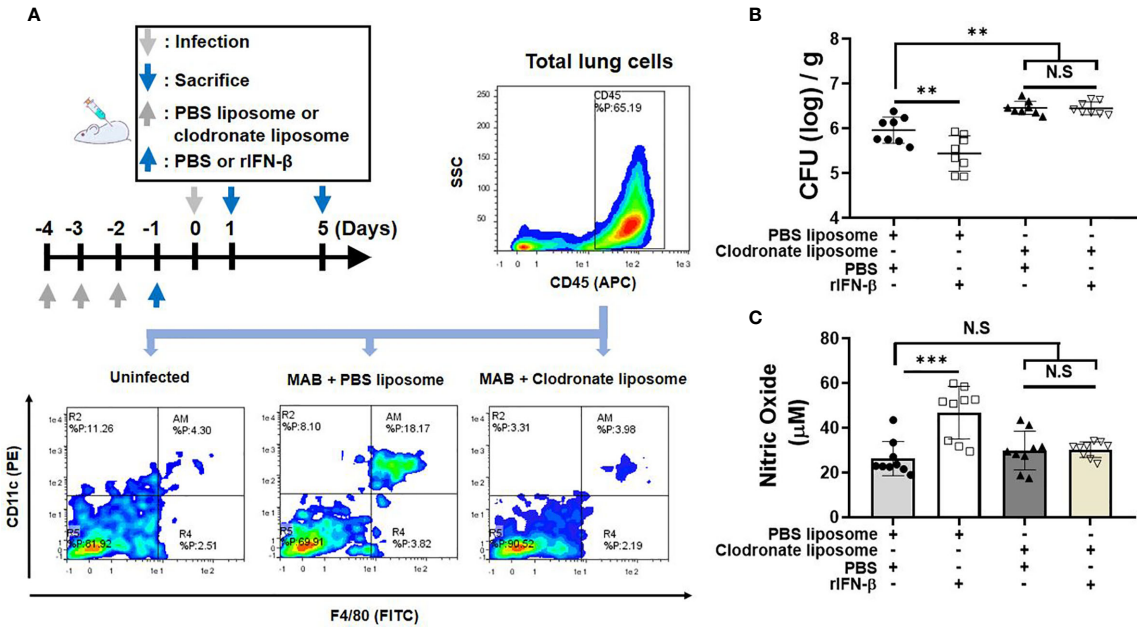

FIGURE 5 | Macrophages are responsible for rIFN-β response in MAB-induced NO production and the bacterial clearance *in vivo*. **(A)** The administration of reagents and bacterial infection were performed according to the schedule indicated in the diagram. Flow cytometric plot showing the population of $CD45^+CD11c^+F4/80^+$ alveolar macrophage in lung total cell at 1 day post infection. **(B)** Mice were administrated with indicated reagents intranasally under anesthesia. After 1 day, mice were infected with 2×10^7 CFU of MAB per mouse intranasally, and the bacterial loads in the lung lysate were determined at 5 days post infection. **(C)** Nitric oxide levels were measured on 1 day post infection in the lung lysate supernatant. **(A)** The results are one representative data of two independent experiments (n = 4). **(B, C)** The results are merged data of two independent experiments (n = 4–5) (**p < 0.01, ***p < 0.001). MAB, *Mycobacterium abscessus*; CFU, colony-forming unit. NS, Not Statistically Significant.

M. tuberculosis-infected macrophages (35). Interestingly, we found that type I IFN signaling engaged in the robust production of NO at the early stage of MAB infection. However, the difference in intracellular bacterial CFUs depending on the presence or absence of type I IFN signaling was observed at least 48 h post infection. These results are in line with previous studies (16) that showed bactericidal activity of macrophage by NO production after at least 48-h mycobacterial infection. This phenomenon may be related to the virulence mechanisms of *Mycobacterium* spp., which survive within phagosome as an immune evasion strategy (36).

Recently, controversial and complex roles of type I IFNs in MAB-infected macrophages have been reported from different research groups. MAB can lead to various types of cell death such as necrosis, apoptosis, and pyroptosis in macrophages (37–39). Previous studies revealed that rough morphotype of MAB (MAB-R), lacking cell surface glycopeptidolipids, is more proapoptotic than smooth morphotype (MAB-S) and releases more LDH (26, 38, 39). In addition, Kim et al. reported that type I IFNs augment the cell-to-cell spread of MAB by increasing cytotoxicity of infected macrophages (26). As a result, IFNAR-deficient macrophages exhibited lower levels of bacterial load compared with the WT macrophages (26). In this study, we also evaluated the effect of type I IFNs on cytotoxicity of MAB-infected macrophages by measuring LDH release. There was no significant difference in LDH release between the WT and IFNAR-deficient BMDMs in response to MAB (**Supplementary Figure 4A**) and pretreatment of the cells with rIFN-β slightly increased during the release of LDH only in WT BMDMs at 72 h post infection, but not in MH-S cells (**Supplementary Figure 4B**). Consistent with the results from our laboratory, Ruangkiattikul et al. reported that type I IFNs increased the production of NO in MAB-infected macrophages (25). Consequently, IFNAR-deficient macrophages showed higher bacterial load than the WT macrophages in their study (25). In this study, we confirmed that NO production is clearly amplified by type I IFNs, which correlated with the enhancement of bactericidal activity in MAB-infected macrophages.

Although the role of type I IFNs in MAB infection has been reported in several previous publications that utilized *in vitro* assays, none of these studies evaluated the role of type I IFNs in animal models (25, 26, 38). In the current study, the host defensive effect of type I IFNs against MAB pulmonary infection in mouse model was evaluated. Since administration of rIFN-β at 1 or 5 days post infection did not affect the bacterial load in the lungs, we established a model that employed administration of rIFN-β at 1 day before infection. Correlating with the *in vitro* results, rIFN-β-administered mice exhibited deceased bacterial loads in lung lysate samples compared with the PBS-administered control mice at 5 days post infection. Administration of rIFN-β also augmented production of NO in lung samples of MAB-infected mice at 1 day post infection. This host defensive effect of type I IFNs against MAB infection in mice was established in a NO-dependent manner evidenced by the inability to enhance bacterial clearance following

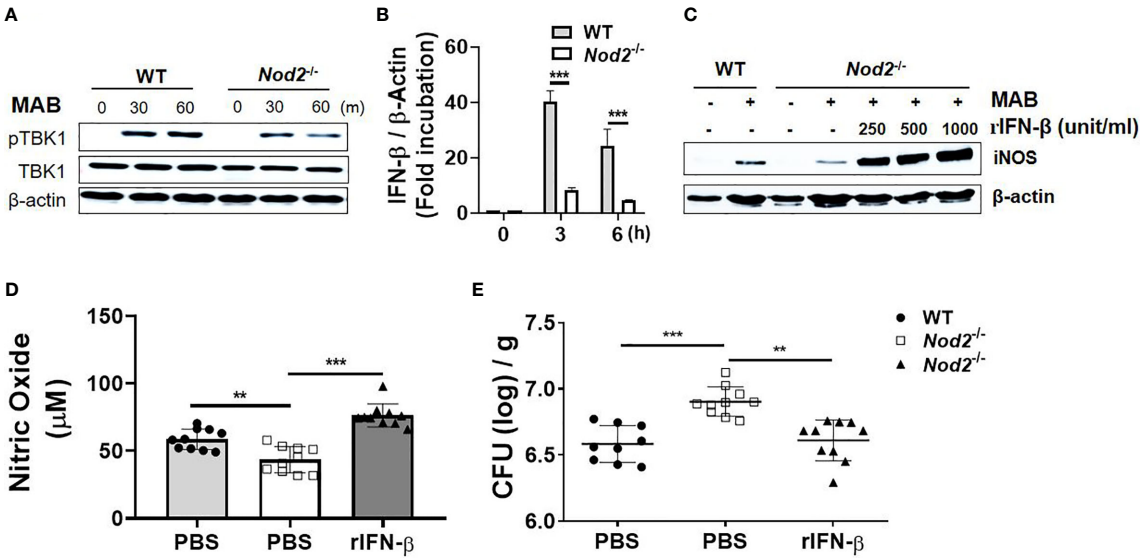

FIGURE 6 | Type I IFNs act as an intermediator of a cytosolic receptor NOD2-mediated NO production in response to MAB. **(A)** BMDMs were infected with MAB for indicated times. Cellular proteins were extracted, and the levels of each protein were determined by Western blotting. **(B)** BMDMs were infected with MAB for indicated time. mRNA was extracted, and the expression levels of IFN-β gene were determined by real-time PCR. **(C)** BMDMs were incubated for 24 h with indicated conditions. The levels of each protein were determined by Western blotting. **(D)** Nitric oxide levels were measured on 1 day post infection in the lung lysate (same conditions with **Figure 4**). **(E)** The bacterial load in the lung lysate was determined at 5 days post infection. **(A–C)** The results are from one representative experiment of two independent experiments. **(D, E)** The results are merged data of two independent experiments (n = 5) (**p < 0.01, ***p < 0.001). MAB, *Mycobacterium abscessus*; IFN, interferon; BMDMs, bone marrow-derived macrophages.

rIFN-β administration in iNOS-deficient mice. There was no difference in NO levels between rIFN-β and PBS-administered mice at 5 days post infection, and this is presumably due to the compensation mechanisms of immune homeostasis system such as anti-inflammatory response-mediated downward standardization (40–42).

From the perspective of host defense immune system against bacterial infection, enhancement of immune response can lead to fatal damage in host tissue (43). Hence, histological assessment was performed on lung samples from the MAB-infected mice. Although there was no significant difference in histological assessment *via* H&E staining (**Supplementary Figures 5D, E**), lung inflammatory cytokine levels were slightly diminished in rIFN-β-administered mice (**Supplementary Figures 5A–C**). It is presumed that the diminished lung bacterial load leads to the alleviation in the production of inflammatory cytokines.

Next, we confirmed that clodronate-induced macrophage depletion leads to the increase in the susceptibility to MAB pulmonary infection in mice. Moreover, rIFN-β did not enhance the bacterial clearance nor the production of NO within clodronate-administered mice. These findings suggest that the increased bactericidal activity by type I IFN–NO axis in AM is crucial for the host defense innate immune system against MAB infection. In fact, as significant efficacy was verified in several clinical trials (44–47), NO is a crucial host defense factor against MAB pulmonary infection in humans. Our results suggest that the administration of exogenous type I IFNs, at the early stage of infection, could be considered as a therapeutic candidate for MAB-infected patients. Meanwhile, interstitial macrophages as well as AMs are present in the lung tissue and exhibit various biological functions (48). According to previous reports, administration of clodronate liposomes does not eliminate interstitial macrophages (49, 50). In addition, it is known that interstitial macrophages exist with a lower proportion than AMs in the lung parenchyma and that their ability to produce ROS and NO is also much lower than that of AMs (51). Accordingly, the role of interstitial macrophages is not expected to be significant in type I IFN-induced NO production in the lungs, although we did not check the change of the population of interstitial macrophages by clodronate liposomes.

In contrast to our results, several previous studies reported that type I IFNs negatively affect *in vivo* antimicrobial response against most of intracellular bacterial infection (17). Indeed, we also verified the difference in bacterial loads in lung samples between WT and IFNAR-deficient mice. Interestingly, inconsistent with the observed phenotypes of rIFN-β administered mice, IFNAR-deficient mice displayed lower bacterial loads than did the WT mice at 5 days post infection (**Supplementary Figure 3B**). Our ongoing hypothesis is that, unlike the pre-exposure of rIFN-β, which is a single excessive stimulation, type I IFN signal is permanently blocked in IFNAR-deficient mice. Therefore, it could lead to a decrease in NO production in the incipient innate immune response. However, it would possible that the absence of type I IFN signal affects a certain adaptive immune response in the later phase of infection. In fact, several previous studies have reported that type I IFNs are associated with Th1-type adaptive immune response in *M. tuberculosis* infection (52–54).

Previously, our laboratory reported that NOD2 enhances the antimicrobial effect of macrophage against MAB infection by augmenting NO production (16). It has also been reported that NOD2 contributes to the induction of type I IFNs (34). In the current study, we identified the decrease in TBK1 phosphorylation and IFN-β gene expression in MAB-infected NOD2-deficient BMDMs compared with WT cells. In addition, as demonstrated in our previous study (16), NOD2-deficient mice showed higher bacterial load in lung lysates than did WT mice due to the reduced NO production. In the present study, we demonstrated that the administration of rIFN-β improves the impaired bacterial clearance of NOD2-deficient mice by increasing NO production. These results suggest the novel host defense mechanism mediated by NOD2-type I IFN–NO axis against bacterial infections.

Collectively, these data in combination with our hypothesis on IFNAR-deficient mice infection model and MAB-infected NOD2-deficient mice would also have to show lower bacterial load in lungs at 5 days post infection, because the attenuation of type I IFN signal in NOD2-deficient mice might also affect adaptive immune response, especially T-cell response (55). However, the production of type I IFNs by MAB infection is induced through not only NOD2 but also other PRRs such as toll-like receptor (TLR)2 and TLR4 (25). In fact, it has been reported that type I IFN signaling is critical for LPS-induced iNOS expression and NO production in macrophages (56) and that MAB possesses TLR-stimulating potential (25, 29, 57, 58). Therefore, it is likely that, in the early stage of infection, the attenuated type I IFN signal by the deficiency of NOD2 leads to the decrease in NO production and thus impairs the bacterial clearance. In mid-later stages of infection, however, the attenuated type I IFN signal by the NOD2 deficiency would be sufficiently compensated by the operation of other PRRs such as TLR2 and TLR4. Meanwhile, it was reported that type I IFN signaling exerts synergism in NO production through paracrine/autocrine effect of IFN-β (59). For this reason, NOD2-deficient mice would not show the same phenotypes as IFNAR-deficient mice. Currently, researches are ongoing in our laboratory to test this hypothesis.

In summary, we described here that MAB induces iNOS expression and NO production in macrophages *via* type I IFN-mediated signaling, which contribute to the intracellular growth control of the bacteria. In addition, a cytosolic receptor NOD2 is involved in MAB-induced expression of type I IFNs. The NOD2-type I IFN–NO axis may play an important role in host defense against MAB infection. However, there are several limitations in our study. Type I IFNs exert diverse biological functions on bacterial infection by modulating the expression of various cytokines as well as iNOS (5, 18). Several previous studies demonstrated that type I IFNs modulate the production of IL-10, IL-1, and TNF-α and that these cytokines influence the antimicrobial responses on *M. tuberculosis* infection by regulating the immune cell activation and recruitment (60–63). In fact, we evaluated cytokine production in the presence or absence of type I IFNs in MAB-infected BMDMs, and we confirmed that type I IFN amplified the production of TNF-α and IL-10 and inhibited the production of IL-1β (**Supplementary Figures 6A–C**). To date, the effect of TNF-α, IL-1β, and IL-10 on MAB infection is still unknown. It is necessary to further investigate the effect of these cytokines on host defense against MAB infection. In addition, although we clearly showed that the prophylactic administration of rIFN-β improves *in vivo* MAB clearance, the bacterial loads were rather lower in the lungs of IFNAR-deficient mice as compared with WT mice, suggesting that type I IFNs can exert a harmful effect on host defense against MAB infection. Further studies are strongly recommended to clarify the precise role of type I IFNs on MAB infection.

DATA AVAILABILITY STATEMENT

The datasets presented in this study can be found in online repositories. The names of the repository/repositories and accession number(s) can be found in the article/**Supplementary Material**.

ETHICS STATEMENT

The animal study was reviewed and approved by Institutional Animal Care and the Use Committee of Chonnam National University (Approval No. CNU IACUC-YB-2017-56 and 2019-31).

AUTHOR CONTRIBUTIONS

J-HP and J-HA provided substantial contributions to the conception of the work. J-HA performed substantially all the experiments and data analyses and wrote the manuscript. E-JS, A-RJ, J-YP, Ye-JL, Yu-JL, and I-SS contributed to the animal experiments. D-YK, T-SL, D-HJ, and Y-JK performed the histological analysis. SS performed the bacterial culture. S-JY wrote the manuscript. All authors approved the final version of this manuscript to be published and agreed to be accountable for all aspects of the work in ensuring that questions related to the accuracy or integrity of any part of the work are appropriately investigated and resolved.

FUNDING

This research was supported by the National Research Foundation of Korea (NRF) grant funded by the Korean government (MSIT) (Grant No: NRF-2018R1A2B3004143 and NRF-2017M3A9D5A0105244).

SUPPLEMENTARY MATERIAL

The Supplementary Material for this article can be found online at: https://www.frontiersin.org/articles/10.3389/fimmu.2021.738070/full#supplementary-material

REFERENCES

1. Liao C-H, Lai C-C, Ding L, Hou S, Chiu H-C, Chang S-C, et al. Skin and Soft Tissue Infection Caused by Non-Tuberculous Mycobacteria. *Int J Tuberc Lung Dis* (2007) 11(1):96–102.
2. Sanguinetti M, Ardito F, Fiscarelli E, La Sorda M, D'Argenio P, Ricciotti G, et al. Fatal Pulmonary Infection Due to Multidrug-Resistant *Mycobacterium Abscessus* in a Patient With Cystic Fibrosis. *J Clin Microbiol* (2001) 39(2):816–9. doi: 10.1128/JCM.39.2.816-819.2001
3. Koh WJ, Jeong BH, Kim SY, Jeon K, Park KU, Jhun BW, et al. Mycobacterial Characteristics and Treatment Outcomes in *Mycobacterium Abscessus* Lung Disease. *Clin Infect Dis* (2017) 64(3):309–16. doi: 10.1093/cid/ciw724
4. Kaufmann SH. Immunity to Intracellular Bacteria. *Annu Rev Immunol* (1993) 11(1):129–63. doi: 10.1146/annurev.iy.11.040193.001021
5. Kalliolias GD, Ivashkiv LB. Overview of the Biology of Type I Interferons. *Arthritis Res Ther* (2010) 12(1):S1. doi: 10.1186/ar2881
6. Honda K, Takaoka A, Taniguchi T. Type I Interferon [Corrected] Gene Induction by the Interferon Regulatory Factor Family of Transcription Factors. *Immunity* (2006) 25(3):349–60. doi: 10.1016/j.immuni.2006.08.009
7. Platanias LC. Mechanisms of Type-I- and Type-II-Interferon-Mediated Signalling. *Nat Rev Immunol* (2005) 5(5):375–86. doi: 10.1038/nri1604
8. Ting JP-Y, Lovering RC, Alnemri ES, Bertin J, Boss JM, Davis BK, et al. The NLR Gene Family: A Standard Nomenclature. *Immunity* (2008) 28(3):285–7. doi: 10.1016/j.immuni.2008.02.005
9. Moreira LO, Zamboni DS. NOD1 and NOD2 Signaling in Infection and Inflammation. *Front Immunol* (2012) 3:328. doi: 10.3389/fimmu.2012.00328
10. Raymond JB, Mahapatra S, Crick DC, Pavelka MS. Identification of the namH Gene, Encoding the Hydroxylase Responsible for the N-Glycolylation of the Mycobacterial Peptidoglycan. *J Biol Chem* (2005) 280(1):326–33. doi: 10.1074/jbc.M411006200
11. Coulombe F, Divangahi M, Veyrier F, de Léséleuc L, Gleason JL, Yang Y, et al. Increased NOD2-Mediated Recognition of N-Glycolyl Muramyl Dipeptide. *J Exp Med* (2009) 206(8):1709–16. doi: 10.1084/jem.20081779
12. Brooks MN, Rajaram MV, Azad AK, Amer AO, Valdivia-Arenas MA, Park JH, et al. NOD2 Controls the Nature of the Inflammatory Response and Subsequent Fate of Mycobacterium Tuberculosis and M. Bovis BCG in Human Macrophages. *Cell Microbiol* (2011) 13(3):402–18. doi: 10.1111/j.1462-5822.2010.01544.x
13. Ferwerda G, Girardin SE, Kullberg B-J, Le Bourhis L, De Jong DJ, Langenberg DM, et al. NOD2 and Toll-Like Receptors Are Nonredundant Recognition Systems of Mycobacterium Tuberculosis. *PloS Pathog* (2005) 1(3):e34. doi: 10.1371/journal.ppat.0010034
14. Landes MB, Rajaram MV, Nguyen H, Schlesinger LS. Role for NOD2 in Mycobacterium Tuberculosis-Induced iNOS Expression and NO Production in Human Macrophages. *J Leukoc Biol* (2015) 97(6):1111–9. doi: 10.1189/jlb.3A1114-557R
15. Divangahi M, Mostowy S, Coulombe F, Kozak R, Guillot L, Veyrier F, et al. NOD2-Deficient Mice Have Impaired Resistance to Mycobacterium Tuberculosis Infection Through Defective Innate and Adaptive Immunity. *J Immunol* (2008) 181(10):7157–65. doi: 10.4049/jimmunol.181.10.7157
16. Lee JY, Lee MS, Kim DJ, Yang SJ, Lee SJ, Noh EJ, et al. Nucleotide-Binding Oligomerization Domain 2 Contributes to Limiting Growth of *Mycobacterium Abscessus* in the Lung of Mice by Regulating Cytokines and Nitric Oxide Production. *Front Immunol* (2017) 8:1477. doi: 10.3389/fimmu.2017.01477
17. Boxx GM, Cheng G. The Roles of Type I Interferon in Bacterial Infection. *Cell Host Microbe* (2016) 19(6):760–9. doi: 10.1016/j.chom.2016.05.016
18. McNab F, Mayer-Barber K, Sher A, Wack A, O'Garra A. Type I Interferons in Infectious Disease. *Nat Rev Immunol* (2015) 15(2):87–103. doi: 10.1038/nri3787
19. Watanabe T, Asano N, Fichtner-Feigl S, Gorelick PL, Tsuji Y, Matsumoto Y, et al. NOD1 Contributes to Mouse Host Defense Against Helicobacter Pylori *via* Induction of Type I IFN and Activation of the ISGF3 Signaling Pathway. *J Clin Invest* (2010) 120(5):1645–62. doi: 10.1172/JCI39481
20. Kelly-Scumpia KM, Scumpia PO, Delano MJ, Weinstein JS, Cuenca AG, Wynn JL, et al. Type I Interferon Signaling in Hematopoietic Cells is Required for Survival in Mouse Polymicrobial Sepsis by Regulating CXCL10. *J Exp Med* (2010) 207(2):319–26. doi: 10.1084/jem.20091959
21. O'Connell RM, Saha SK, Vaidya SA, Bruhn KW, Miranda GA, Zarnegar B, et al. Type I Interferon Production Enhances Susceptibility to Listeria Monocytogenes Infection. *J Exp Med* (2004) 200(4):437–45. doi: 10.1084/jem.20040712
22. Dorhoi A, Yeremeev V, Nouailles G, Weiner J3rd, Jorg S, Heinemann E, et al. Type I IFN Signaling Triggers Immunopathology in Tuberculosis-Susceptible Mice by Modulating Lung Phagocyte Dynamics. *Eur J Immunol* (2014) 44(8):2380–93. doi: 10.1002/eji.201344219
23. Ruangkiattikul N, Nerlich A, Abdissa K, Lienenklaus S, Suwandi A, Janze N, et al. cGAS-STING-TBK1-IRF3/7 Induced Interferon-Beta Contributes to the Clearing of non Tuberculous Mycobacterial Infection in Mice. *Virulence* (2017) 8(7):1303–15. doi: 10.1080/21505594.2017.1321191
24. Moreira-Teixeira L, Mayer-Barber K, Sher A, O'Garra A. Type I Interferons in Tuberculosis: Foe and Occasionally Friend. *J Exp Med* (2018) 215(5):1273–85. doi: 10.1084/jem.20180325
25. Ruangkiattikul N, Rys D, Abdissa K, Rohde M, Semmler T, Tegtmeyer PK, et al. Type I Interferon Induced by TLR2-TLR4-MyD88-TRIF-IRF3 Controls *Mycobacterium Abscessus* Subsp. Abscessus Persistence in Murine Macrophages *via* Nitric Oxide. *Int J Med Microbiol* (2019) 309(5):307–18. doi: 10.1016/j.ijmm.2019.05.007
26. Kim B-R, Kim B-J, Kook Y-H, Kim B-J. Phagosome Escape of Rough *Mycobacterium Abscessus* Strains in Murine Macrophage *via* Phagosomal Rupture can Lead to Type I Interferon Production and Their Cell-to-Cell Spread. *Front Immunol* (2019) 10:125. doi: 10.3389/fimmu.2019.00125
27. Celada A, Gray PW, Rinderknecht E, Schreiber R. Evidence for a Gamma-Interferon Receptor That Regulates Macrophage Tumoricidal Activity. *J Exp Med* (1984) 160(1):55–74. doi: 10.1084/jem.160.1.55
28. Nayak DK, Mendez O, Bowen S, Mohanakumar T. Isolation and *In Vitro* Culture of Murine and Human Alveolar Macrophages. *J Vis Exp: JoVE* (2018) 134). doi: 10.3791/57287
29. Kim J-S, Kang M-J, Kim WS, Han SJ, Kim HM, Kim HW, et al. Essential Engagement of Toll-Like Receptor 2 in Initiation of Early Protective Th1 Response Against Rough Variants of *Mycobacterium Abscessus*. *Infect Immun* (2015) 83(4):1556–67. doi: 10.1128/IAI.02853-14
30. Green LC, Wagner DA, Glogowski J, Skipper PL, Wishnok JS, Tannenbaum SR. Analysis of Nitrate, Nitrite, and [15N] Nitrate in Biological Fluids. *Anal Biochem* (1982) 126(1):131–8. doi: 10.1016/0003-2697(82)90118-X
31. Choi J-H, Jo S-G, Jung S-K, Park W-T, Kim K-Y, Park Y-W, et al. Immunomodulatory Effects of Ethanol Extract of Germinated Ice Plant (Mesembryanthemum Crystallinum). *Lab Anim Res* (2017) 33(1):32–9. doi: 10.5625/lar.2017.33.1.32
32. Weiss G, Schaible UE. Macrophage Defense Mechanisms Against Intracellular Bacteria. *Immunol Rev* (2015) 264(1):182–203. doi: 10.1111/imr.12266
33. Chau T, da Silva J, Ghaffari A, Zelazny A, Olivier K. Synergistic Effect of Nitric Oxide With Antibiotics Against *Mycobacterium Abscessus In Vitro*. *B19 Adv IN THE Treat OF NTM: Am Thorac Society;* (2019) p:A2656–A. doi: 10.1164/ajrccm-conference.2019.199.1_MeetingAbstracts.A2656
34. Pandey AK, Yang Y, Jiang Z, Fortune SM, Coulombe F, Behr MA, et al. NOD2, RIP2 and IRF5 Play a Critical Role in the Type I Interferon Response to Mycobacterium Tuberculosis. *PloS Pathog* (2009) 5(7):e1000500. doi: 10.1371/journal.ppat.1000500
35. Banks DA, Ahlbrand SE, Hughitt VK, Shah S, Mayer-Barber KD, Vogel SN, et al. Mycobacterium Tuberculosis Inhibits Autocrine Type I IFN Signaling to Increase Intracellular Survival. *J Immunol* (2019) 202(8):2348–59. doi: 10.4049/jimmunol.1801303
36. Miller BH, Fratti RA, Poschet JF, Timmins GS, Master SS, Burgos M, et al. Mycobacteria Inhibit Nitric Oxide Synthase Recruitment to Phagosomes During Macrophage Infection. *Infect Immun* (2004) 72(5):2872–8. doi: 10.1128/IAI.72.5.2872-2878.2004
37. Bonay M, Roux A, Floquet J, Retory Y, Herrmann J, Lofaso F, et al. Caspase-Independent Apoptosis in Infected Macrophages Triggered by Sulforaphane *via* Nrf2/p38 Signaling Pathways. *Cell Death Discov* (2015) 1(1):1–10. doi: 10.1038/cddiscovery.2015.22
38. Kim B-R, Kim B-J, Kook Y-H, Kim B-J. *Mycobacterium Abscessus* Infection Leads to Enhanced Production of Type 1 Interferon and NLRP3 Inflammasome Activation in Murine Macrophages *via* Mitochondrial Oxidative Stress. *PloS Pathog* (2020) 16(3):e1008294. doi: 10.1371/journal.ppat.1008294

39. Whang J, Back YW, Lee K-I, Fujiwara N, Paik S, Choi CH, et al. *Mycobacterium Abscessus* Glycopeptidolipids Inhibit Macrophage Apoptosis and Bacterial Spreading by Targeting Mitochondrial Cyclophilin D. *Cell Death Dis* (2017) 8(8):e3012–e. doi: 10.1038/cddis.2017.420
40. Cobbold S, Waldmann H. Infectious Tolerance. *Curr Opin Immunol* (1998) 10 (5):518–24. doi: 10.1016/S0952-7915(98)80217-3
41. Couper KN, Blount DG, Riley EM. IL-10: The Master Regulator of Immunity to Infection. *J Immunol* (2008) 180(9):5771–7. doi: 10.4049/jimmunol.180.9.5771
42. Kotas ME, Medzhitov R. Homeostasis, Inflammation, and Disease Susceptibility. *Cell* (2015) 160(5):816–27. doi: 10.1016/j.cell.2015.02.010
43. Wallach D, Kang T-B, Kovalenko A. Concepts of Tissue Injury and Cell Death in Inflammation: A Historical Perspective. *Nat Rev Immunol* (2014) 14(1):51–9. doi: 10.1038/nri3561
44. Bogdanovski K, Chau T, Robinson CJ, MacDonald SD, Peterson AM, Mashek CM, et al. Antibacterial Activity of High-Dose Nitric Oxide Against Pulmonary *Mycobacterium Abscessus* Disease. *Access Microbiol* (2020) 2(9): acmi000154. doi: 10.1099/acmi.0.000154
45. Bentur L, Gur M, Ashkenazi M, Livnat-Levanon G, Mizrahi M, Tal A, et al. Pilot Study to Test Inhaled Nitric Oxide in Cystic Fibrosis Patients With Refractory *Mycobacterium Abscessus* Lung Infection. *J Cystic Fibrosis* (2020) 19(2):225–31. doi: 10.1016/j.jcf.2019.05.002
46. Yaacoby-Bianu K, Gur M, Toukan Y, Nir V, Hakim F, Geffen Y, et al. Compassionate Nitric Oxide Adjuvant Treatment of Persistent Mycobacterium Infection in Cystic Fibrosis Patients. *Pediatr Infect Dis J* (2018) 37(4):336–8. doi: 10.1097/INF.0000000000001780
47. Bentur L, Masarweh K, Livnat-Levanon G, Ashkenazi M, Dagan A, Mizrahi M, et al. Nitric Oxide Inhalations in CF Patients Infected With *Mycobacterium Abscessus* Complex: A Prospective, Open-Labeled, Multi-Center Pilot Study. *C96 Adv IN THE Manage OF Pulmonary NTM Dis: Am Thorac Society;* (2018) p:A5919–A.
48. Schyns J, Bureau F, Marichal T. Lung Interstitial Macrophages: Past, Present, and Future. *J Immunol Res* (2018) 2018:5160794. doi: 10.1155/2018/5160794
49. Sabatel C, Radermecker C, Fievez L, Paulissen G, Chakarov S, Fernandes C, et al. Exposure to Bacterial CpG DNA Protects From Airway Allergic Inflammation by Expanding Regulatory Lung Interstitial Macrophages. *Immunity* (2017) 46(3):457–73. doi: 10.1016/j.immuni.2017.02.016
50. Bedoret D, Wallemacq H, Marichal T, Desmet C, Calvo FQ, Henry E, et al. Lung Interstitial Macrophages Alter Dendritic Cell Functions to Prevent Airway Allergy in Mice. *J Clin Invest* (2009) 119(12):3723–38. doi: 10.1172/JCI39717
51. Franke-Ullmann G, Pförtner C, Walter P, Steinmüller C, Lohmann-Matthes M-L, Kobzik L. Characterization of Murine Lung Interstitial Macrophages in Comparison With Alveolar Macrophages *In Vitro*. *J Immunol* (1996) 157 (7):3097–104.
52. Manca C, Tsenova L, Bergtold A, Freeman S, Tovey M, Musser JM, et al. Virulence of a Mycobacterium Tuberculosis Clinical Isolate in Mice is Determined by Failure to Induce Th1 Type Immunity and is Associated With Induction of IFN-α/β. *Proc Natl Acad Sci* (2001) 98(10):5752–7. doi: 10.1073/pnas.091096998
53. Ordway D, Henao-Tamayo M, Harton M, Palanisamy G, Troudt J, Shanley C, et al. The Hypervirulent Mycobacterium Tuberculosis Strain HN878 Induces a Potent TH1 Response Followed by Rapid Down-Regulation. *J Immunol* (2007) 179(1):522–31. doi: 10.4049/jimmunol.179.1.522
54. Manca C, Tsenova L, Freeman S, Barczak AK, Tovey M, Murray PJ, et al. Hypervirulent M. Tuberculosis W/Beijing Strains Upregulate Type I IFNs and Increase Expression of Negative Regulators of the Jak-Stat Pathway. *J Interferon Cytokine Res* (2005) 25(11):694–701. doi: 10.1089/jir.2005.25.694
55. Mourik BC, Lubberts E, de Steenwinkel JE, Ottenhoff TH, Leenen PJ. Interactions Between Type 1 Interferons and the Th17 Response in Tuberculosis: Lessons Learned From Autoimmune Diseases. *Front Immunol* (2017) 8:294. doi: 10.3389/fimmu.2017.00294
56. Vadiveloo PK, Vairo G, Hertzog P, Kola I, Hamilton JA. Role of Type I Interferons During Macrophage Activation by Lipopolysaccharide. *Cytokine* (2000) 12(11):1639–46. doi: 10.1006/cyto.2000.0766
57. Sampaio EP, Elloumi HZ, Zelazny A, Ding L, Paulson ML, Sher A, et al. *Mycobacterium Abscessus* and M. Avium Trigger Toll-Like Receptor 2 and Distinct Cytokine Response in Human Cells. *Am J Respir Cell Mol Biol* (2008) 39(4):431–9. doi: 10.1165/rcmb.2007-0413OC
58. Shin DM, Yang CS, Yuk JM, Lee JY, Kim KH, Shin SJ, et al. *Mycobacterium Abscessus* Activates the Macrophage Innate Immune Response *via* a Physical and Functional Interaction Between TLR2 and Dectin-1. *Cell Microbiol* (2008) 10(8):1608–21. doi: 10.1111/j.1462-5822.2008.01151.x
59. Whitmore MM, DeVeer MJ, Edling A, Oates RK, Simons B, Lindner D, et al. Synergistic Activation of Innate Immunity by Double-Stranded RNA and CpG DNA Promotes Enhanced Antitumor Activity. *Cancer Res* (2004) 64 (16):5850–60. doi: 10.1158/0008-5472.CAN-04-0063
60. Novikov A, Cardone M, Thompson R, Shenderov K, Kirschman KD, Mayer-Barber KD, et al. Mycobacterium Tuberculosis Triggers Host Type I IFN Signaling to Regulate IL-1β Production in Human Macrophages. *J Immunol* (2011) 187(5):2540–7. doi: 10.4049/jimmunol.1100926
61. McNab FW, Ewbank J, Howes A, Moreira-Teixeira L, Martirosyan A, Ghilardi N, et al. Type I IFN Induces IL-10 Production in an IL-27–Independent Manner and Blocks Responsiveness to IFN-γ for Production of IL-12 and Bacterial Killing in Mycobacterium Tuberculosis–Infected Macrophages. *J Immunol* (2014) 193(7):3600–12. doi: 10.4049/jimmunol.1401088
62. Mayer-Barber KD, Andrade BB, Barber DL, Hieny S, Feng CG, Caspar P, et al. Innate and Adaptive Interferons \ress IL-1α and IL-1β Production by Distinct Pulmonary Myeloid Subsets During Mycobacterium Tuberculosis Infection. *Immunity* (2011) 35(6):1023–34. doi: 10.1016/j.immuni.2011.12.002
63. Bernut A, Nguyen-Chi M, Halloum I, Herrmann J-L, Lutfalla G, Kremer L. *Mycobacterium Abscessus*-Induced Granuloma Formation Is Strictly Dependent on TNF Signaling and Neutrophil Trafficking. *PloS Pathog* (2016) 12(11):e1005986. doi: 10.1371/journal.ppat.1005986

Conflict of Interest: The authors declare that the research was conducted in the absence of any commercial or financial relationships that could be construed as a potential conflict of interest.

frontiers in Immunology

MINI REVIEW
published: 09 November 2021
doi: 10.3389/fimmu.2021.752657

Progress of the Art of Macrophage Polarization and Different Subtypes in Mycobacterial Infection

*Gai Ge[1], Haiqin Jiang[1], Jingshu Xiong[1], Wenyue Zhang[1], Ying Shi[1], Chenyue Tao[2] and Hongsheng Wang[1,3,4]**

[1] Institute of Dermatology, Chinese Academy of Medical Sciences and Peking Union Medical College, Nanjing, China, [2] Imperial College London, London, United Kingdom, [3] National Center for Sexually Transmitted Disease and Leprosy Control, China Centers for Disease Control and Prevention, Nanjing, China, [4] Centre for Global Health, School of Public Health, Nanjing Medical University, Nanjing, China

OPEN ACCESS

Edited by:
Maria Teresa Ochoa, University of Southern California, United States

Reviewed by:
Lu Huang, University of Arkansas for Medical Sciences, United States
Nicola Ivan Lorè, Division of Immunology, Transplantation and Infectious Diseases, San Raffaele Scientific Institute (IRCCS), Italy

***Correspondence:**
Hongsheng Wang
whs33@vip.sina.com

Specialty section:
This article was submitted to Microbial Immunology, a section of the journal Frontiers in Immunology

Received: 03 August 2021
Accepted: 14 October 2021
Published: 09 November 2021

Citation:
Ge G, Jiang H, Xiong J, Zhang W, Shi Y, Tao C and Wang H (2021) Progress of the Art of Macrophage Polarization and Different Subtypes in Mycobacterial Infection. Front. Immunol. 12:752657. doi: 10.3389/fimmu.2021.752657

Mycobacteriosis, mostly resulting from *Mycobacterium tuberculosis* (MTb), nontuberculous mycobacteria (NTM), and *Mycobacterium leprae* (*M. leprae*), is the long-standing granulomatous disease that ravages several organs including skin, lung, and peripheral nerves, and it has a spectrum of clinical-pathologic features based on the interaction of bacilli and host immune response. Histiocytes in infectious granulomas mainly consist of infected and uninfected macrophages (Mφs), multinucleated giant cells (MGCs), epithelioid cells (ECs), and foam cells (FCs), which are commonly discovered in lesions in patients with mycobacteriosis. Granuloma Mφ polarization or reprogramming is the crucial appearance of the host immune response to pathogen aggression, which gets a command of endocellular microbe persistence. Herein, we recapitulate the current gaps and challenges during Mφ polarization and the different subpopulations of mycobacteriosis.

Keywords: mycobacteriosis, granuloma, macrophages, multinucleated giant cells, epithelioid cells, foam cells

INTRODUCTION

Mycobacteriosis is a contagious disease ravaging the skin tissue, respiratory system, and peripheral nerves, which results from *Mycobacterium tuberculosis* (MTb), nontuberculous mycobacteria (NTM), and *Mycobacterium leprae* (*M. leprae*). Tuberculosis (TB), caused by the MTb complex, has plagued humanity when it has killed billions of populations over the past two centuries (1). Cutaneous TB, including 1% to 2% of all cases, is a rare clinical manifestation of MTb or *M. bovis* infection. Rapidly growing mycobacteria, such as *M. abscessus* group, *M. fortuitum* group, *M. mucogenicum*, and *M. smegmatis* and slow-growing mycobacteria, such as *M. avium* complex, *M. kansasii*, and *M. marinum*, are compose of NTM (2). NTM cutaneous infection is unwonted, and predisposing factors, such as skin injury (such as gardening and fish-related injuries, injections, and surgery) or immunosuppression make up 95% of cases (3). Leprosy, Hansen's disease, is a remarkable public health problem, especially in countries such as Brazil, India, and Indonesia (4). Leprosy is a neglected tropical disease encountered by *M. leprae* or *M. lepromatosis*. At present, effective vaccines against infection and markers for beneficial immunity are not available (5, 6). The inability to eradicate the bacteria can result in infection in the immune system in a

granuloma structure. Macrophages (Mφs), primary effectors of inherited response, are considered essential pathophysiologic factors in wide-spread disease procedures involved with chronic inflammation. The heterogeneity of Mφs, either due to their developmental origin or their particular activation morphologies, is becoming increasingly distinct with regard to their diverse roles within infection of microbes (7). As a central part of the innate immunity and as the paramount host of infectious granuloma pathogens, Mφs have been the central focus of mycobacteriosis investigation.

INFECTIOUS GRANULOMA

Granuloma is a highly structured and organized collection of Mφs, often with phenotypic switches and other immune cells recruited, including multinucleated giant cells (MGCs), epithelioid cells (ECs), and foam cells (FCs). Someone claimed a new *ex vivo* granuloma culture technique to study granuloma consolidation (8). Mechanistically, Cronan et al. have found that in the existence of robust interferon-gamma (IFN-γ) signaling immune response, confronting interleukin (IL)-4 and IL-13 signals were associated with Mφ epithelial transition. IL-4/13 signaling, induced by *stat6*, was required for epithelioid transformation and granuloma architecture. Apart from *stat*6 function required in the new granuloma formation, persistent *stat*6 pathway was required to maintain the expression of E-cadherin and granuloma (9). MAB_4780, encoding a dehydratase, was required for intracellular *M. abscessus* growth and to avoid lysosome-mediated degradation, which compromises survival of ΔMAB_4780 in Mφs and granuloma formation (10). In granuloma transformation, IFN-γ and tumor necrosis factor-alpha (TNF-α) were deemed to be effective regulators, whereas IL-10 was a passive effector. Intriguingly, etanercept and adalimumab, the human monoclonal anti-TNF-α IgG1, exacerbated M1 polarization and delayed MGC generation in granuloma (11). Magically, there are two types of granulomas in leprosy. At one pole of leprosy, the presence of MGCs and granuloma configuration in tuberculoid leprosy (TT) contributes to the containment of *M. leprae* proliferation and transmission (**Figure 1A**). At the other pole, lepromatous leprosy (LL) has phagocytic FCs heavily parasitized with freely multiplying intracellular *M. leprae* (**Figure 1B**) (12). Ma et al. have constructed a map *via* integrating single-cell RNA sequencing with spatial sequencing to identify that the primary cell types, consisting of T cells, Mφs, keratinocytes, endothelial cells, and fibroblasts, were described to research the cellular composition and status discrepancies between reversal reactions and LL, and LGCs are more frequent in both lesions. IL-1β and IFN-γ were supposed to be important upstream effectors of the pseudo time trajectory and the activation of Mφs in granulomas to product genes contributing to antimicrobial responses in human leprosy granulomas (13).

Granuloma is a leading gateway for the host immune response to microorganisms and shape immune interplays, disease progression, and degeneration (14). The granuloma is a functional paradox, for example, it contains the bacilli in a local reservoir, preventing mycobacterial dissemination to near normal tissues of the host, or to shield itself from host's immunologic killing mechanisms and antimicrobial response (15).

Mφ PHENOTYPES IN MYCOBACTERIOSIS

Mφs show the increment of plasticity, and they can be differentiated into two contrary subsets: M1 Mφs and M2 Mφs. The network of molecular mediators is regulated in response to the diversity of stimulus. Binding of IFN-γ to its cellular surface receptor, for example, induces the activation of receptor-linked JAKs, which trigger STAT1 to dimerize and translocate to the nucleus where it initiates gene transcription that skew toward M1-correlated functions such as promoted microbicidal activity and proinflammatory cytokine production (**Figure 1C**). By contrast, IL-4 and IL-13 activate STAT6 to promote M2 profile inhibiting these effects (**Figure 1D**) (16). Furthermore, Yun–Ji et al. have shown that c-JUN N-terminal kinase (JNK)-mediated M1 plasticity was important in the elimination of bacilli *via* p53-mediated apoptosis by Mφs. Similarly, virulent MTb H37Rv infection can induce M2 Mφs and in turn restrain p53 by the activation of mouse double minute 2 (MDM2). These consequences elucidated that M2 population decreases p53-elicited cell death by MDM2 induction (17). In addition, early secreted antigenic target of 6 kDa (ESAT6), a prerequisite step to support the formation of granuloma, was one of the effectors used by MTb to facilitate the proinflammatory M1 Mφ at the primo-infection and then triggered the switch of M1 to M2 Mφ at a later infection phase (18). In particular, proinflammatory environment or bacterial product could perturb the classical M1 or M2 phenotypes. Bénard et al. recently showed that type I IFN hyperproduction by MTb-stimulated B cells drove an altered Mφs polarization toward a regulatory/anti-inflammatory profile, namely, M2 Mφ, during TB which associated with increased MTb burden in lungs (19). Moreover, Mφ polarization may augment antimicrobial response against MTb in the existence of vitamin D (20).

Furthermore, high-mobility group N2 (HMGN2) regulates anti-NTM-inherited response function of Mφ. In addition, HMGN2 is triggered in NTM and IFN-γ-primed M1-skewed subpopulation polarization (21). Yet, *M. abscessus* infection robustly induced p38 MAPK-dependent heme-oxygenase-1 (HO-1) induction in the THP-1 cells. HO-1 production was important for *M. abscessus* growth during the early stages of infection, and that the HO-1 producted bilirubin and biliverdin, perhaps through modulation of intracellular ROS levels, may be involved (22). Glycopeptidolipids limited the virulence of *M. abscessus* among Mφs by inhibition of apoptosis and spreading of bacteria (23). In TT, the activation of the classical signal by M1 Mφs results in the expression of TNF-α, IFN-γ, and iNOS, which trigger the multiplication of free radicals that remove *Bacillus* (24). Moreover, the LL shows a superiority of M2 Mφs that promotes the expression of IL-10, transforming growth factor-β, fibroblast growth factor-β, Arg-1, CD206, and CD163, causing immunosuppressive response and tissue

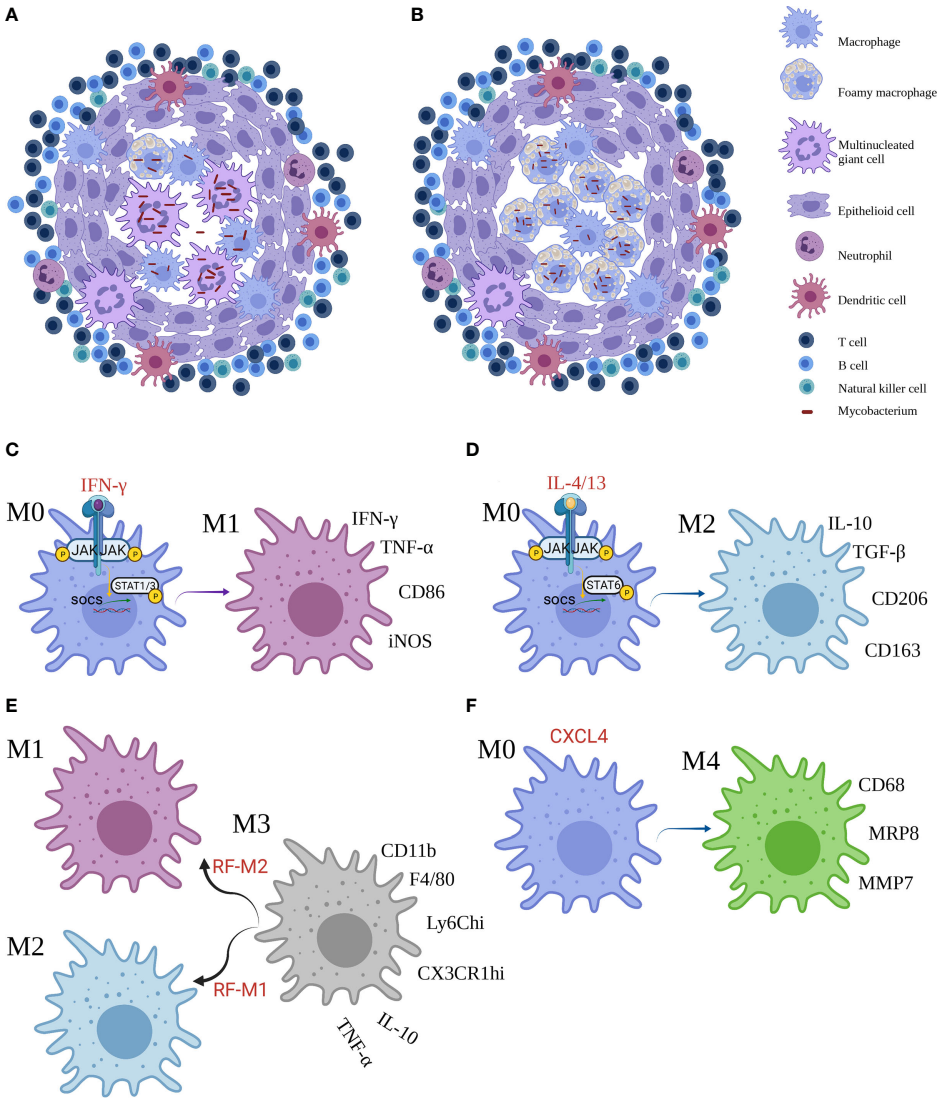

FIGURE 1 | The granuloma and macrophages subsets. **(A, B)** Two frameworks of mycobacterial infection granuloma. **(C–F)** Reprogramming of macrophages and main markers of M1, M2, M3 and M4 Mϕ. Created with BioRender.com.

repairment (25, 26). *M. leprae* could then utilize infected Mφs by two mechanisms: first, *M. leprae*-infected Mφs preferentially activated Treg but not Th1 or cytotoxic T-cell responses; second, *M. leprae*-infected Mφs were effective in escaping $CD8^+$ T-cell-primed cytotoxicity (27).

Other than the M1 and M2 subpopulations, a M3 switch profile exists. The M3 Mφ could be divided into two subsets such as the M1/2 paradigm, which in response to a reprogramming factor M1 (RF-M1) skews toward M2 Mφ, and the M2/1 dichotomy, which responding to RF-M2 favors M1 Mφ (28). In murine mesothelioma microenvironment, flow cytometry disclosed that the mixture of M1 and M2 phenotypes ($CD11b^+$ $F4/80^+$ $Ly6C^{hi}$ $CX3CR1^{hi}$), that was, M3 Mφ, secreted IL-10 and TNF-α. Jackaman et al. have suggested that the shifts of M1 to M2 Mφ and vice versa could occur through the M3 changing formation (**Figure 1E**) (29). The M3 mediator can be triggered by upregulation of M1-reprogramming signals with coinstantaneous suppression of the M2 Mφ transcription factors, STAT3, STAT6, and/or SMAD3 in Ehrlich ascites carcinoma (30). Nevertheless, the role of M3 Mφ in mycobacteriosis remains undetailed, and more studies are required for further investigation.

Unluckily, the part of M4 macrophages following M3 macrophages in Mφ phenotypes in mycobacteriosis notably, considerable evidence for another subpopulation of Mϕ, namely, M4 Mϕ, was frequently observed. In the presence of CXCL4, M0 Mϕ changed to M4 Mϕ, expressing CD206, CD68, matrix metallo proteinase (MMP) 7, myeloid-related protein 8 (MRP8) and S100A8, producing IL-6, TNF-α, MMP7, and MMP12 in atherosclerosis and cardiac remodeling (31–33).

At date, de Sousa et al. have also characterized the existence of M4 Mϕ in leprosy. Immunostaining determined that the expression of CD68, MRP8 and MMP7 was significantly higher, while IL-6 and TNF-α was significantly lower in the LL group compared with the TT group. The higher expression of M4 profile in LL lesions implied that the subpopulation was ineffective in the removal of bacilli, resulting in the development of multibacillary form and microbes replication (**Figure 1F**) (34). Further work is necessary to robustly establish this mechanism. Notwithstanding, the role of the new subset in TB and NTM is unclear.

MGCs IN MYCOBACTERIOSIS

Specific lineage of MΦs, particularly MGCs containing a horseshoe-shaped ring of nuclei, contributes to the core of granulomas. Previously, cells with three nuclei and the expression of iNOS were markers for MGC transformation (35). In addition, the formation of MGC, involving cell fusion (36), was a Mφ-specific, evolutionarily ancient program that proceeds in response to the persistence of extrinsic and intrinsic stimuli (37). Mφs or monocytes can be transformed into MGCs under several statuses, including cultivating with IL-4 or IL-13, GM-CSF combined with IL-4, IFN-γ bounding with IL-3, or bacterial glycolipids. E-cadherin is a necessary player in fusion, and its production can be stimulated by the activation of STAT6 through IL-4 or IL-13 pathway, similar to epithelialization under the circumstance of schistosome granulomas (38). However, the development of polyploid MGCs involves cell autonomous affliction of Toll-like receptor-elicited DNA damage, cell autonomous cell-cycle alterations, and impairment of p53 function by the potent antimicrobial effector, namely, NO, driving mitotic defects and multinucleation (35, 39). Wang et al. have corroborated experimental evidence that IL-15 primes M1 Mφ transformation, reprograms peripheral blood mononuclear cells in humans to transform into MGCs *via* direct activation of T cells and myeloid cells (40). Queval et al. have shown that out of the four infection combinations (blood-derived primary human and bovine Mϕs [hMϕ or bMϕ, respectively] infected with *M. bovis* and MTb), bMϕ infected with *M. bovis* promotes the formation of MGCs. Mechanistically, they have distinguished the functional differences between *M. bovis* and MTb host-pathogen interplay and demonstrated that MPB70 from *M. bovis* and extracellular vesicles released by *M. bovis*-infected bMϕ promote Mϕ multinucleation (41). Startlingly, local adaptive immune response, particularly programmed cell death ligand-1, fatty acid, and cholesterol metabolism could take part in containing granuloma progression in human lung TB (42, 43).

Unfortunately, the distinct role of MGCs in mycobacterial infection immune response remains as major gaps. MGCs may restrict mycobacterial cell-to-cell dissemination, involve in mycobacterial latency, or promote tissue destruction because of their high expression of extracellular matrix-degrading epithelioid macrophage marker molecules (EMMMs) (38, 43). The maturation of MGCs supplies a restrictive environment for *M. bovis*. The major lysosomal degradative signals remain functional within MGC transition. In addition, the increase of *M. bovis* in acidified compartments and correlation with LC3B in matured MGCs indicates that MGCs presented a restrictive milieu for microorganism replication (41). Nonetheless, the role of MGCs in NTM and leprosy remains an elusive issue.

ECs IN MYCOBACTERIOSIS

Microscopic analysis discloses that tightly interdigitated cell membranes are formed in zipper-like arrays to resemble epithelioid histiocytes. Nevertheless, none of the fusion molecules is strictly required to give rise to ECs, and the procedure is complicated. Epithelial differentiation can occur during days of granuloma transformation. Using the *M. marinum*-zebrafish model, Cronan et al. have found recently that granuloma Mφs undergo reprograming, which involves E-cadherin-dependent formation of fusogenic epithelial cell (44). In TB, ESAT6 plus TLR2 can activate iNOS/NO and ROS signaling to reduce the trimethylation of H3K27, thereby promoting the expression of EMMM that improved the transformation of Mφs into ECs (45).

The EC functions are amphibolous and nebulous from being repleted with organelles and strongly phagocytic and microbicidal to being nonphagocytic cells with secretory functions, which might be adjunctive in granuloma function. Notwithstanding, some people have demonstrated by electron microscopy that the ECs in TB are "primarily biosynthetic rather than phagocytic" (46). However, ECs control the multiplication of mycobacteria at least in one experimental model. Previous dates, therefore, have elucidated that interference to E-cadherin production, a tight junction protein among ECs, enhanced the transformation of untightly structured granuloma, resulting in unrestricted MTb motion and leads to MTb regeneration and dissemination (47). In NTM, EC surrogates restrain *M. avium* growth and serves as APCs *in vitro* and *in vivo*. ECs were commonly seen in TT and borderline tuberculoid leprosy (BT). Inconceivably, ECs from TT granulomas exhibited the M1 phenotype ($CD68^+$ $CD163^-$), whereas Mφs in LL granulomas showed the M2 phenotype ($CD68^+$ $CD163^+$) (48).

FCs IN MYCOBACTERIOSIS

FCs, with deregulated lipid metabolism, are a manifestation of maladaptive responses in chronic inflammatory statuses (49, 50). The biogenesis of FCs varies with underlying diseases. FC biogenesis is involved in the disruption of cholesterol homeostasis and consequent endocellular accumulation of cholesteryl esters in atherosclerosis, but it is linked to triglyceride accumulation in hMφs infected with MTb that is elicited by TNF receptor pathway *via* downstream activation of

the caspase cascade and mammalian target of rapamycin complex 1 (51). In comparison, Genoula et al. suggested that alternatively activated Mφs were loath to the accumulation of lipid droplets (LDs) *via* the STAT6, which facilitated the degradation of lipids. However, MTb offsets lipolysis *via* switching alternatively activated Mφ metabolism to accumulate LDs due to the HIF-1α activation (52). Similarly, the zebrafish-*M. marinum* granuloma contained FCs and the mycobacterial ESX1 pathogenicity locus thought to elicit the morphology switch of Mφs to FCs (53). The biogenesis of FCs in leprosy remains a challenging enigma.

Diverse, and in part controversial, we summarize the current findings in the role of FCs in mycobacteriosis. First, Mφ ontology may be a major paramount factor of the inherited response in the containment of MTb infection. LDs may take part in inherent immunity against MTb by directly eliminating intracellular MTb and modulate metabolism to infection (54). Strikingly, PPAR signaling is responsible for lots of adipocyte differentiation-correlated genes, leading to amassing of intracellular lipids to accommodate *M. leprae* parasitization in host FCs (55, 56). Furthermore, the formation of LD may support the host by averting access of MTb to host's fatty acids (FAs) while favoring native immune responses (54). In comparison, unlike other programs, FC formation reduced the avidity of host cell and the phagocytosis of MTb while protecting the cells from death. The protective effect is associated with enhanced inflammatory potential of FCs and cause slower proliferation of MTb. Also, the balance of TNF-a, IL-1β, IL-6, and NF-kB innate inflammatory responses was altered in response to MTb vs. LPS in FCs compared with uninfected controls (57). Additionally, FCs triggered the formation of necrotic core by releasing triglyceride-rich content into the caseum (51), resulting in progressive lung tissue destruction and pulmonary function loss in infected rabbits and marmosets and in individuals with active TB (50).

Lastly, FCs may result in TB pathogenesis by enhancing MTb persistence and drug resistance. Moreover, a lipid-rich diet rather than nutrient deprivation in caseum rewires the condition of MTb toward drug resistance (58). In addition, IL-10/STAT3 axis primed FC differentiation during MTb infection, favoring pathogen persistence (59). Palma et al. have shown that controlled caloric restriction protected murine model against pulmonary MTb infection by decreasing bacterial load and FC proliferation to reduce lung damage and limit MTb spreading (60). Thus, the reduction of LDs in MTb-infected FCs might restrain the endocellular survival of MTb (61). Likewise, ultrastructural analysis of demic leprosy tissue showed colocalization between cholesterol-laden lipid bodies and *M. leprae*-containing phagosomes in FCs. The mechanisms of leprosy indicate that lipid abundance has a pathophysiological effect on the persistence of microbes in the host. The function of FCs remains the unsolved mystery of NTM.

DISCUSSION

Mycobacterium-infected disease is an infectious granuloma disease with a spectrum of clinical and pathological features. Granuloma formation and immune mechanism are primarily observed in mycobacteriosis. Different cellular immune and clinical manifestations are primed by Mφ polarization or reprogramming. Different Mφ subphenotypes may be positively correlated with the number of germs and host immune response. The increment of M2 Mφs and FCs and a low degree of MGCs are more likely to attribute to the bacillary multiplies and impaired innate immune. Conversely, the results reveal a positive correlation between high-level M1 Mφs and MGCs, the diminution of FCs, and a limited bacterial load and immunocompetent innate immune response. Particularly, ECs are commonly seen in TT and borderline BT, FCs are mostly a commonly factor in leprosy, particularly LL. Now, we recapitulate the main findings of Mφs, MGCs, ECs, and FCs in mycobacterial infection (**Table 1**). Mφ reprogramming or markers can shed light on the cell immune response in mycobacteriosis. Moreover, the mycobacterial granuloma

TABLE 1 | Main findings described in Mφs, MGCs, ECs, and FCs.

Cell types	Stimulus	Main cyto/chemokines and enzymes	Functions/Immune responses	References
M1 Mφ	IFN-γ/STAT1, p53, ESAT6	iNOS, IFN-γ, TNF-α, CD86, IL-6, and HMGN2	Microbicidal activity and proinflammatory cytokine production	(16–18, 24)
M2 Mφ	IL-4 plus IL-13/STAT6, ESAT6, type I IFN	Arg-1, IL-10, TGF-β, fibroblast growth factor-β, CD206, CD163	Immunosuppressive response and tissue repairment	(16–19, 25, 26)
M3 Mφ	RF-M1/2	IL-10, TNF-α, CD11b, F4/80, Ly6C^{hi} CX3CR1^{hi}	Undetailed	(28, 29)
M4 Mφ	CXCL4	CD68, MRP8, MMP7	Weak phagocytosis, favoring bacillus regeneration	(35–38)
MGC	IL-4 or IL-13, GM-CSF plus IL-4, IFN-γ plus IL-3, E-cadherin, IL-15	iNOS, EMMMs, PD-L1	Inhibiting mycobacterial cell-to-cell spread or tissue destruction and mycobacterial latency	(39, 42, 45–47)
EC	ESAT6 plus TLR2	CD68^{+} CD163^{-}, CD68+ CD163+	Strongly phagocytic and microbicidal or nonphagocytic cells with secretory functions	(49, 52)
FC	PPAR, IL-10	TNF-a, IL-1β, IL-6	Favoring inherited response or pathogen persistence, Less-bactericidal, Less-phagocytic	(59–61)

Arg-1, arginase-1; CXCL, C-X-C motif ligand; ECs, epithelioid cells; EMMMs, extracellular matrix-degrading epithelioid macrophage marker molecules; ESAT6, early secreted antigenic target of 6-kDa; FCs, foamy cells; HMGN2, high-mobility group N2; IFN-γ, interferon-gamma; IL, interleukin; iNOS, inducible nitric oxide synthase; IRF, Interferon regulatory factors; Mφs, macrophages; MGCs, multinucleated giant cells; MMP, matrix metallo proteinase; MRP8, myeloid-related protein 8; PD-L1, programmed cell death ligand-1; RF-M1, reprogramming factor M1; STAT, signal transducer and activator of transcription; TGF-β, transforming growth factor beta; TNF-α, tumor necrosis factor-alpha.

model may delineate the development of alternative vaccines for mycobacteriosis. Accordingly, these researches prompt that Mφs, especially M1 Mφ and LGCs represent a therapeutic target for the emergence of antibacterial immunity. Together, therapies targeting some particular cells are being studied as novel therapies for TB, leprosy, and other bacterial infections.

AUTHOR CONTRIBUTIONS

HW, HJ, JX, WZ, and YS involved in supervision. CT and GG drafted figures. GG reviewed the literature and wrote the manuscript. All authors contributed to the article and approved the submitted version.

FUNDING

This study was supported by grants from the Science and Technology Planning Project of Jiangsu Province of China (BE2018619), Chinese Academy of Medical Science Innovation Fund for Medical Science (2017-I2M-B&R-14), and the National Natural Science Foundation of China (81972950).

ACKNOWLEDGMENTS

The authors acknowledge the contributions of all the scientists in this area and apologize for failing to cite any work due to constraints of space.

REFERENCES

1. Reid M, Arinaminpathy N, Bloom A, Bloom BR, Boehme C, Chaisson R, et al. Building a Tuberculosis-Free World: The Lancet Commission on Tuberculosis. *Lancet* (2019) 393(10178):1331–84. doi: 10.1016/S0140-6736(19)30024-8
2. Franco-Paredes C, Marcos LA, Henao-Martinez AF, Rodriguez-Morales AJ, Villamil-Gomez WE, Gotuzzo E, et al. Cutaneous Mycobacterial Infections. *Clin Microbiol Rev* (2018) 32(1):e00069–18. doi: 10.1128/CMR.00069-18
3. Moreno G, Minocha R, Choy B, Jelfs P, Watts M, Fernandez-Penas P. Cutaneous Non-Tuberculous Mycobacteria in Western Sydney, Australia. Population Study 1996-2013. *Australas J Dermatol* (2018) 59(4):343–5. doi: 10.1111/ajd.12783
4. Mi Z, Liu H, Zhang F. Advances in the Immunology and Genetics of Leprosy. *Front Immunol* (2020) 11:567. doi: 10.3389/fimmu.2020.00567
5. Cadena AM, Flynn JL, Fortune SM. The Importance of First Impressions: Early Events in Mycobacterium Tuberculosis Infection Influence Outcome. *Mbio* (2016) 7(2):e316–42. doi: 10.1128/mBio.00342-16
6. Huang L, Russell DG. Protective Immunity Against Tuberculosis: What Does it Look Like and How do We Find it? *Curr Opin Immunol* (2017) 48:44–50. doi: 10.1016/j.coi.2017.08.001
7. Khan A, Singh VK, Hunter RL, Jagannath C. Macrophage Heterogeneity and Plasticity in Tuberculosis. *J Leukoc Biol* (2019) 106(2):275–82. doi: 10.1002/JLB.MR0318-095RR
8. Cronan MR, Matty MA, Rosenberg AF, Blanc L, Pyle CJ, Espenschied ST, et al. An Explant Technique for High-Resolution Imaging and Manipulation of Mycobacterial Granulomas. *Nat Methods* (2018) 15(12):1098–107. doi: 10.1038/s41592-018-0215-8
9. Cronan MR, Hughes EJ, Brewer WJ, Viswanathan G, Hunt EG, Singh B, et al. A Non-Canonical Type 2 Immune Response Coordinates Tuberculous Granuloma Formation and Epithelialization. *Cell* (2021) 184(7):1757–74. doi: 10.1016/j.cell.2021.02.046
10. Halloum I, Carrere-Kremer S, Blaise M, Viljoen A, Bernut A, Le Moigne V, et al. Deletion of a Dehydratase Important for Intracellular Growth and Cording Renders Rough Mycobacterium Abscessus Avirulent. *Proc Natl Acad Sci USA* (2016) 113(29):E4228–37. doi: 10.1073/pnas.1605477113
11. Mezouar S, Diarra I, Roudier J, Desnues B, Mege JL. Tumor Necrosis Factor-Alpha Antagonist Interferes With the Formation of Granulomatous Multinucleated Giant Cells: New Insights Into Mycobacterium Tuberculosis Infection. *Front Immunol* (2019) 10:1947. doi: 10.3389/fimmu.2019.01947
12. Leal-Calvo T, Martins BL, Bertoluci DF, Rosa PS, de Camargo RM, Germano GV, et al. Large-Scale Gene Expression Signatures Reveal a Microbicidal Pattern of Activation in Mycobacterium Leprae-Infected Monocyte-Derived Macrophages With Low Multiplicity of Infection. *Front Immunol* (2021) 12:647832. doi: 10.3389/fimmu.2021.647832
13. Ma F, Hughes TK, Teles R, Andrade PR, de Andrade SB, Plazyo O, et al. The Cellular Architecture of the Antimicrobial Response Network in Human Leprosy Granulomas. *Nat Immunol* (2021) 22(7):839–50. doi: 10.1038/s41590-021-00956-8
14. Ernst JD, Cornelius A, Desvignes L, Tavs J, Norris BA. Limited Antimycobacterial Efficacy of Epitope Peptide Administration Despite Enhanced Antigen-Specific CD4 T-Cell Activation. *J Infect Dis* (2018) 218 (10):1653–62. doi: 10.1093/infdis/jiy142
15. Pagan AJ, Ramakrishnan L. The Formation and Function of Granulomas. *Annu Rev Immunol* (2018) 36:639–65. doi: 10.1146/annurev-immunol-032712-100022
16. Lawrence T, Natoli G. Transcriptional Regulation of Macrophage Polarization: Enabling Diversity With Identity. *Nat Rev Immunol* (2011) 11 (11):750–61. doi: 10.1038/nri3088
17. Lim YJ, Lee J, Choi JA, Cho SN, Son SH, Kwon SJ, et al. M1 Macrophage Dependent-P53 Regulates the Intracellular Survival of Mycobacteria. *Apoptosis* (2020) 25(1-2):42–55. doi: 10.1007/s10495-019-01578-0
18. Refai A, Gritli S, Barbouche MR, Essafi M. Mycobacterium Tuberculosis Virulent Factor ESAT-6 Drives Macrophage Differentiation Toward the Pro-Inflammatory M1 Phenotype and Subsequently Switches it to the Anti-Inflammatory M2 Phenotype. *Front Cell Infect Microbiol* (2018) 8:327. doi: 10.3389/fcimb.2018.00327
19. Benard A, Sakwa I, Schierloh P, Colom A, Mercier I, Tailleux L, et al. B Cells Producing Type I IFN Modulate Macrophage Polarization in Tuberculosis. *Am J Respir Crit Care Med* (2018) 197(6):801–13. doi: 10.1164/rccm.201707-1475OC
20. Rao MJ, Parasa VR, Lerm M, Svensson M, Brighenti S. Polarization of Human Monocyte-Derived Cells With Vitamin D Promotes Control of Mycobacterium Tuberculosis Infection. *Front Immunol* (2019) 10:3157. doi: 10.3389/fimmu.2019.03157
21. Wang X, Chen S, Ren H, Chen J, Li J, Wang Y, et al. HMGN2 Regulates Non-Tuberculous Mycobacteria Survival *via* Modulation of M1 Macrophage Polarization. *J Cell Mol Med* (2019) 23(12):7985–98. doi: 10.1111/jcmm.14599
22. Abdalla MY, Ahmad IM, Switzer B, Britigan BE. Induction of Heme Oxygenase-1 Contributes to Survival of Mycobacterium Abscessus in Human Macrophages-Like THP-1 Cells. *Redox Biol* (2015) 4:328–39. doi: 10.1016/j.redox.2015.01.012
23. Whang J, Back YW, Lee KI, Fujiwara N, Paik S, Choi CH, et al. Mycobacterium Abscessus Glycopeptidolipids Inhibit Macrophage Apoptosis and Bacterial Spreading by Targeting Mitochondrial Cyclophilin D. *Cell Death Dis* (2017) 8(8):e3012. doi: 10.1038/cddis.2017.420
24. Simoes QJ, de Almeida FA, de Souza AT, de Miranda ASL, Nunes MI, Fuzii HT, et al. Transforming Growth Factor Beta and Apoptosis in Leprosy Skin Lesions: Possible Relationship With the Control of the Tissue Immune Response in the Mycobacterium Leprae Infection. *Microbes Infect* (2012) 14 (9):696–701. doi: 10.1016/j.micinf.2012.02.010
25. de Sousa JR, de Sousa RP, Aarao TL, Dias LJ, Carneiro FR, Fuzii HT, et al. *In Situ* Expression of M2 Macrophage Subpopulation in Leprosy Skin Lesions. *Acta Trop* (2016) 157:108–14. doi: 10.1016/j.actatropica.2016.01.008
26. Shapouri-Moghaddam A, Mohammadian S, Vazini H, Taghadosi M, Esmaeili SA, Mardani F, et al. Macrophage Plasticity, Polarization, and Function in Health and Disease. *J Cell Physiol* (2018) 233(9):6425–40. doi: 10.1002/jcp.26429
27. Yang D, Shui T, Miranda JW, Gilson DJ, Song Z, Chen J, et al. Mycobacterium Leprae-Infected Macrophages Preferentially Primed Regulatory T Cell Responses and was Associated With Lepromatous Leprosy. *PloS Negl Trop Dis* (2016) 10(1):e4335. doi: 10.1371/journal.pntd.0004335

28. Malyshev I, Malyshev Y. Current Concept and Update of the Macrophage Plasticity Concept: Intracellular Mechanisms of Reprogramming and M3 Macrophage "Switch" Phenotype. *BioMed Res Int* (2015) 2015:341308. doi: 10.1155/2015/341308
29. Jackaman C, Yeoh TL, Acuil ML, Gardner JK, Nelson DJ. Murine Mesothelioma Induces Locally-Proliferating IL-10(+) TNF-Alpha (+) CD206 (-) CX3CR1(+) M3 Macrophages That can be Selectively Depleted by Chemotherapy or Immunotherapy. *Oncoimmunology* (2016) 5(6): e1173299. doi: 10.1080/2162402X.2016.1173299
30. Kalish S, Lyamina S, Manukhina E, Malyshev Y, Raetskaya A, Malyshev I. M3 Macrophages Stop Division of Tumor Cells *In Vitro* and Extend Survival of Mice With Ehrlich Ascites Carcinoma. *Med Sci Monit Basic Res* (2017) 23:8–19. doi: 10.12659/msmbr.902285
31. Oksala N, Seppala I, Rahikainen R, Makela KM, Raitoharju E, Illig T, et al. Synergistic Expression of Histone Deacetylase 9 and Matrix Metalloproteinase 12 in M4 Macrophages in Advanced Carotid Plaques. *Eur J Vasc Endovasc Surg* (2017) 53(5):632–40. doi: 10.1016/j.ejvs.2017.02.014
32. Nakai K. Multiple Roles of Macrophage in Skin. *J Dermatol Sci* (2021) S0923-1811(21):00201–2. doi: 10.1016/j.jdermsci.2021.08.008
33. Yang Y, Ma L, Wang C, Song M, Li C, Chen M, et al. Matrix Metalloproteinase-7 in Platelet-Activated Macrophages Accounts for Cardiac Remodeling in Uremic Mice. *Basic Res Cardiol* (2020) 115(3):30. doi: 10.1007/s00395-020-0789-z
34. de Sousa JR, Lucena NF, Sotto MN, Quaresma J. Immunohistochemical Characterization of the M4 Macrophage Population in Leprosy Skin Lesions. *BMC Infect Dis* (2018) 18(1):576. doi: 10.1186/s12879-018-3478-x
35. Gharun K, Senges J, Seidl M, Losslein A, Kolter J, Lohrmann F, et al. Mycobacteria Exploit Nitric Oxide-Induced Transformation of Macrophages Into Permissive Giant Cells. *EMBO Rep* (2017) 18(12):2144–59. doi: 10.15252/embr.201744121
36. Helming L, Gordon S. Molecular Mediators of Macrophage Fusion. *Trends Cell Biol* (2009) 19(10):514–22. doi: 10.1016/j.tcb.2009.07.005
37. Shrivastava P, Bagchi T. IL-10 Modulates *In Vitro* Multinucleate Giant Cell Formation in Human Tuberculosis. *PloS One* (2013) 8(10):e77680. doi: 10.1371/journal.pone.0077680
38. Miyamoto H, Katsuyama E, Miyauchi Y, Hoshi H, Miyamoto K, Sato Y, et al. An Essential Role for STAT6-STAT1 Protein Signaling in Promoting Macrophage Cell-Cell Fusion. *J Biol Chem* (2012) 287(39):32479–84. doi: 10.1074/jbc.M112.358226
39. Herrtwich L, Nanda I, Evangelou K, Nikolova T, Horn V, Sagar, et al. DNA Damage Signaling Instructs Polyploid Macrophage Fate in Granulomas. *Cell* (2016) 167(5):1264–80. doi: 10.1016/j.cell.2016.09.054
40. Wang H, Jiang H, Teles R, Chen Y, Wu A, Lu J, et al. Cellular, Molecular, and Immunological Characteristics of Langhans Multinucleated Giant Cells Programmed by IL-15. *J Invest Dermatol* (2020) 140(9):1824–36. doi: 10.1016/j.jid.2020.01.026
41. Queval CJ, Fearns A, Botella L, Smyth A, Schnettger L, Mitermite M, et al. Macrophage-Specific Responses to Human- and Animal-Adapted Tubercle Bacilli Reveal Pathogen and Host Factors Driving Multinucleated Cell Formation. *PloS Pathog* (2021) 17(3):e1009410. doi: 10.1371/journal.ppat.1009410
42. Abengozar-Muela M, Esparza MV, Garcia-Ros D, Vasquez CE, Echeveste JI, Idoate MA, et al. Diverse Immune Environments in Human Lung Tuberculosis Granulomas Assessed by Quantitative Multiplexed Immunofluorescence. *Mod Pathol* (2020) 33(12):2507–19. doi: 10.1038/s41379-020-0600-6
43. Losslein AK, Lohrmann F, Scheuermann L, Gharun K, Neuber J, Kolter J, et al. Monocyte Progenitors Give Rise to Multinucleated Giant Cells. *Nat Commun* (2021) 12(1):2027. doi: 10.1038/s41467-021-22103-5
44. Cronan MR, Beerman RW, Rosenberg AF, Saelens JW, Johnson MG, Oehlers SH, et al. Macrophage Epithelial Reprogramming Underlies Mycobacterial Granuloma Formation and Promotes Infection. *Immunity* (2016) 45(4):861–76. doi: 10.1016/j.immuni.2016.09.014
45. Lin J, Jiang Y, Liu D, Dai X, Wang M, Dai Y. Early Secreted Antigenic Target of 6-Kda of Mycobacterium Tuberculosis Induces Transition of Macrophages Into Epithelioid Macrophages by Downregulating Inos/NO-Mediated H3K27 Trimethylation in Macrophages. *Mol Immunol* (2020) 117:189–200. doi: 10.1016/j.molimm.2019.11.013
46. Crawford CL. The Epithelioid Cell in Tuberculosis is Secretory and Not a Macrophage. *J Infect Dis* (2015) 212(7):1172–3. doi: 10.1093/infdis/jiv155
47. Nathan C. Macrophages' Choice: Take it in or Keep it Out. *Immunity* (2016) 45(4):710–1. doi: 10.1016/j.immuni.2016.10.002
48. Fachin LR, Soares CT, Belone AF, Trombone AP, Rosa PS, Guidella CC, et al. Immunohistochemical Assessment of Cell Populations in Leprosy-Spectrum Lesions and Reactional Forms. *Histol Histopathol* (2017) 32(4):385–96. doi: 10.14670/HH-11-804
49. Hotamisligil GS. Foundations of Immunometabolism and Implications for Metabolic Health and Disease. *Immunity* (2017) 47(3):406–20. doi: 10.1016/j.immuni.2017.08.009
50. Guerrini V, Gennaro ML. Foam Cells: One Size Doesn't Fit All. *Trends Immunol* (2019) 40(12):1163–79. doi: 10.1016/j.it.2019.10.002
51. Guerrini V, Prideaux B, Blanc L, Bruiners N, Arrigucci R, Singh S, et al. Storage Lipid Studies in Tuberculosis Reveal That Foam Cell Biogenesis is Disease-Specific. *PloS Pathog* (2018) 14(8):e1007223. doi: 10.1371/journal.ppat.1007223
52. Genoula M, Marin FJ, Maio M, Dolotowicz B, Ferreyra M, Milillo MA, et al. Fatty Acid Oxidation of Alternatively Activated Macrophages Prevents Foam Cell Formation, But Mycobacterium Tuberculosis Counteracts This Process *via* HIF-1alpha Activation. *PloS Pathog* (2020) 16(10):e1008929. doi: 10.1371/journal.ppat.1008929
53. Johansen MD, Kasparian JA, Hortle E, Britton WJ, Purdie AC, Oehlers SH. Mycobacterium Marinum Infection Drives Foam Cell Differentiation in Zebrafish Infection Models. *Dev Comp Immunol* (2018) 88:169–72. doi: 10.1016/j.dci.2018.07.022
54. Laval T, Chaumont L, Demangel C. Not Too Fat to Fight: The Emerging Role of Macrophage Fatty Acid Metabolism in Immunity to Mycobacterium Tuberculosis. *Immunol Rev* (2021) 301(1):84–97. doi: 10.1111/imr.12952
55. Luo Y, Tanigawa K, Kawashima A, Ishido Y, Ishii N, Suzuki K. The Function of Peroxisome Proliferator-Activated Receptors PPAR-Gamma and PPAR-Delta in Mycobacterium Leprae-Induced Foam Cell Formation in Host Macrophages. *PloS Negl Trop Dis* (2020) 14(10):e8850. doi: 10.1371/journal.pntd.0008850
56. Arnett E, Weaver AM, Woodyard KC, Montoya MJ, Li M, Hoang KV, et al. Ppargamma Is Critical for Mycobacterium Tuberculosis Induction of Mcl-1 and Limitation of Human Macrophage Apoptosis. *PloS Pathog* (2018) 14(6): e1007100. doi: 10.1371/journal.ppat.1007100
57. Agarwal P, Combes TW, Shojaee-Moradie F, Fielding B, Gordon S, Mizrahi V, et al. Foam Cells Control Mycobacterium Tuberculosis Infection. *Front Microbiol* (2020) 11:1394. doi: 10.3389/fmicb.2020.01394
58. Sarathy JP, Dartois V. Caseum: A Niche for Mycobacterium Tuberculosis Drug-Tolerant Persisters. *Clin Microbiol Rev* (2020) 33(3):e00159–19. doi: 10.1128/CMR.00159-19
59. Genoula M, Marin FJ, Dupont M, Kviatcovsky D, Milillo A, Schierloh P, et al. Formation of Foamy Macrophages by Tuberculous Pleural Effusions Is Triggered by the Interleukin-10/Signal Transducer and Activator of Transcription 3 Axis Through ACAT Upregulation. *Front Immunol* (2018) 9:459. doi: 10.3389/fimmu.2018.00459
60. Palma C, La Rocca C, Gigantino V, Aquino G, Piccaro G, Di Silvestre D, et al. Caloric Restriction Promotes Immunometabolic Reprogramming Leading to Protection From Tuberculosis. *Cell Metab* (2021) 33(2):300–18. doi: 10.1016/j.cmet.2020.12.016
61. Shim D, Kim H, Shin SJ. Mycobacterium Tuberculosis Infection-Driven Foamy Macrophages and Their Implications in Tuberculosis Control as Targets for Host-Directed Therapy. *Front Immunol* (2020) 11:910. doi: 10.3389/fimmu.2020.00910

Conflict of Interest: The authors declare that the research was conducted in the absence of any commercial or financial relationships that could be construed as a potential conflict of interest.

frontiers in Immunology

ORIGINAL RESEARCH
published: 03 December 2021
doi: 10.3389/fimmu.2021.779235

Sirtuin 7 Regulates Nitric Oxide Production and Apoptosis to Promote Mycobacterial Clearance in Macrophages

Su Zhang[1†], Yaya Liu[2†], Xuefeng Zhou[3†], Min Ou[1], Guohui Xiao[1], Fang Li[1], Zhongyuan Wang[1], Zhaoqin Wang[1], Lei Liu[1] and Guoliang Zhang[1]*

[1] National Clinical Research Center for Infectious Diseases, Shenzhen Third People's Hospital, Southern University of Science and Technology, Shenzhen, China, [2] Department of Clinical Oncology, The University of Hong Kong-Shenzhen Hospital, Shenzhen, China, [3] School of Medical Technology, Guangdong Medical University, Dongguan, China

OPEN ACCESS

Edited by:
Rosane MB Teles, University of California, Los Angeles, United States

Reviewed by:
Diego Luis Costa, Universidade de São Paulo, Brazil
Bruno Jorge De Andrade Silva, UCLA David Geffen School of Medicine, United States

***Correspondence:**
Guoliang Zhang
szdsyy@aliyun.com

[†]These authors have contributed equally to this work

Specialty section:
This article was submitted to Microbial Immunology, a section of the journal Frontiers in Immunology

Received: 18 September 2021
Accepted: 18 November 2021
Published: 03 December 2021

Citation:
Zhang S, Liu Y, Zhou X, Ou M, Xiao G, Li F, Wang Z, Wang Z, Liu L and Zhang G (2021) Sirtuin 7 Regulates Nitric Oxide Production and Apoptosis to Promote Mycobacterial Clearance in Macrophages. Front. Immunol. 12:779235. doi: 10.3389/fimmu.2021.779235

The host immune system plays a pivotal role in the containment of *Mycobacterium tuberculosis* (Mtb) infection, and host-directed therapy (HDT) is emerging as an effective strategy to treat tuberculosis (TB), especially drug-resistant TB. Previous studies revealed that expression of sirtuin 7 (SIRT7), a nicotinamide adenine dinucleotide (NAD^+)-dependent deacetylase, was downregulated in macrophages after Mycobacterial infection. Inhibition of SIRT7 with the pan-sirtuin family inhibitor nicotinamide (NAM), or by silencing SIRT7 expression, promoted intracellular growth of Mtb and restricted the generation of nitric oxide (NO). Addition of the exogenous NO donor SNAP abrogated the increased bacterial burden in NAM-treated or SIRT7-silenced macrophages. Furthermore, SIRT7-silenced macrophages displayed a lower frequency of early apoptotic cells after Mycobacterial infection, and this could be reversed by providing exogenous NO. Overall, this study clarified a SIRT7-mediated protective mechanism against Mycobacterial infection through regulation of NO production and apoptosis. SIRT7 therefore has potential to be exploited as a novel effective target for HDT of TB.

Keywords: ***Mycobacterium tuberculosis*, SIRT7, nitric oxide, apoptosis, macrophages**

INTRODUCTION

Tuberculosis (TB) is one of the top 10 causes of death worldwide. Globally in 2019, an estimated 8.9–11.0 million people fell ill with TB. Especially the drug-resistant tuberculosis is the most serious challenges in the clinical treatment of tuberculosis due to lack of effective drugs (1). Consequently, there is an urgent need for new strategies to control TB. Most individuals infected with *Mycobacterium tuberculosis* (Mtb) remain healthy, with less than 10% of individuals with latent TB eventually developing active TB (2). Thus, symptomatic tuberculosis is the result of the host immune system failing against Mtb. While Mtb has evolved diverse strategies to escape the host immune response, host-directed therapies (HDTs) have emerged as a promising area of research to fight TB (3).

Histone acetyltransferases (HATs) and histone deacetylases (HDACs) have central roles in regulating acetylation modification of both histone and non-histone substrates. Acetylation, an important post-translational modification that regulates gene expression, is involved in the regulation of cancer, cell stress, metabolism, aging, and infectious diseases (4). HDACs can be divided into four classes based on their protein structure and sequence homology. Sirtuins belong to the class III HDACs, which are NAD^+-dependent enzymes with protein deacetylase and ADP-ribosylase activities, and comprise the members SIRT1 to SIRT7 (5). SIRT7—the least-studied sirtuin to date—is capable of deacetylation activity (6–8) and has also been shown to exhibit desuccinylation (9), deacylase (10), depropionylation (11), and deglutarylation activities (12).

Nitric oxide (NO) is instrumental in the pathogenesis of TB. NO and O_2^- combine to form highly Reactive Nitrogen Species (RNS) such as NO_3^- and NO_2^- within infected macrophages to drive bacterial death (13). Besides the direct activity against Mtb, NO also mediate apoptosis of activated macrophages to kill intracellular Mtb (14). NO regulating apoptosis appears to be specific to the type of cells, NO activates apoptosis in many cell types including macrophages, pancreatic islets, neurons, and thymocytes (15).

In this study, the role of SIRT7 in the pathogenesis of TB was deciphered using a pan-sirtuin family inhibitor NAM and SIRT7-knockdown macrophages. Mycobacterial infection led to downregulation of SIRT7, and inhibition of SIRT7 activity by nicotinamide (NAM) or knockdown of SIRT7 expression increased the risk of Mycobacterial infection. Concurrently, inhibition of SIRT7 activity by NAM or knockdown of SIRT7 expression also suppressed NO release and apoptosis of macrophages after Mycobacterial infection. Furthermore, this effect of SIRT7 inhibition could be alleviated by addition of the NO donor SNAP, and the level of apoptosis was also enhanced by adding SNAP. In conclusion, this study revealed a novel anti-TB mechanism, with SIRT7 restricting both intracellular Mycobacteria growth by NO release and NO-dependent apoptosis. These findings indicate that SIRT7 could be exploited as a HDT against Mycobacterial infection.

RESULTS

Mycobacterial Infection Downregulates SIRT7 Expression

The sirtuins (SIRTs) family comprises seven members (SIRT1–7) that are dispersed amongst different cellular compartments. The expression level of each member of the SIRT family was detected in Raw264.7 cells by RT-PCR. SIRT2 and SIRT7 exhibited the highest levels of expression (**Figure 1A**), thus further experiments focused on the role of SIRT2 and SIRT7 in Mycobacterial infection. A time-dependent reduction in SIRT7 mRNA expression was observed in Raw264.7 cells infected with the Mtb virulent strain H37Rv, while there were no significant changes in SIRT2 mRNA expression before and after infection (**Figures 1B, C**). Raw264.7 cells were subsequently infected with virulent Mtb H37Rv, avirulent Mtb H37Ra or M. bovis BCG for 24 h, and no significant differences in SIRT2 and SIRT7 expression levels were detected between the Mycobacteria of differing virulence (**Figures 1D, E**). Similar results were detected in human cell lines THP1 (**Supplementary Figures 1A, B**). Furthermore, human monocyte-derived macrophages (hMDMs) obtained from peripheral blood mononuclear cells (PBMCs) of patients with active TB also displayed reduced SIRT7 mRNA expression relative to healthy controls (**Figure 1F**, The information of the patients and healthy controls was shown in **Table 1**). In summary, Mycobacterial infection downregulates SIRT7 expression, indicating an important disease-related effect of SIRT7 on Mtb infection.

SIRT7 Inhibitor NAM Increases the Mycobacteria Burden in Macrophages

To determine whether SIRT7 was essential for controlling Mycobacteria growth, the SIRT7 inhibitor NAM was used to treat Mycobacteria-infected cells. NAM non-selectively inhibits the sirtuin family through competition binding to the NAD+ binding site of the sirtuins (16). The safety of the NAM has been verified and the IC_{50} value was 19.75 mM in Raw264.7 cells (**Figure 2A**). To evaluate whether NAM affected the Mycobacteria burden in macrophages, Raw264.7 cells were pretreated and maintained with 0.01, 1, or 10 mM NAM for 24 h and then infected with a BCG fluorescent reporter strain that expresses GFP (BCG-GFP, MOI 10:1) and analyzed by flow cytometry at 4h, 24h respectively. The results showed that NAM had no significant impact on the phagocytosis rate, but NAM at a concentration of 10 mM increased the Mycobacteria burden in Raw264.7 cells, while lower concentrations of NAM (0.01 and 1 mM) had no effect on the Mycobacteria burden of the cells as indicated by the percentage of GFP-positive cells (**Figures 2B, C**). The number of colony-forming units (CFUs) from lysed Raw264.7 cells infected with H37Rv were also tested at 4h, 48h after infection. The results were consistent with the experiment using BCG-GFP (**Figure 2D**). These findings suggest that SIRT7 restricts intracellular Mycobacteria growth and can be inhibited by the non-selective inhibitor NAM.

SIRT7 Knockdown Increases the Mycobacteria Burden While Overexpression of SIRT7 Protects Cells From Mycobacteria

To further explore whether SIRT7 was essential for controlling mycobacterial growth, SIRT7-deficient Raw264.7 cells were constructed. Lentivirus particles containing SIRT7 shRNA and scrambled control were transduced into Raw264.7 cells, and SIRT7 expression was determined by quantitative RT-PCR and Western blotting after filtering and selecting stably expression cells using puromycin (4 μg/ml) (**Figure 3A**). Flow cytometry analysis of BCG-GFP-infected cells 24h after infection and CFU counts of H37Rv-infected cells 48h after infection revealed that SIRT7 knockdown macrophages had higher bacillary loads compared with those of the control cells (**Figures 3B–D**). But there was no significant differences at 4h

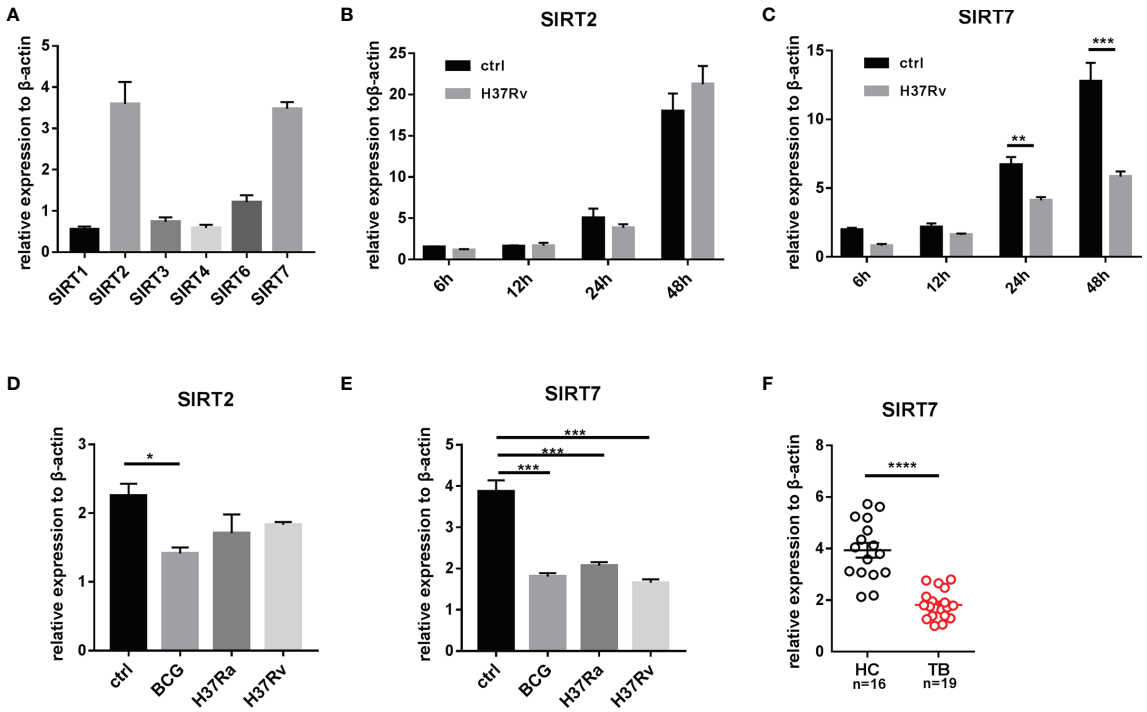

FIGURE 1 | Mycobacteria infection downregulates SIRT7 expression as determined by quantitative RT-PCR analysis. **(A)** Expression levels of sirtuin family members in Raw264.7 cells. **(B, C)** SIRT2 and SIRT7 mRNA expression in Raw264.7 cells at 6, 12, 24, and 48 h after infection with H37Rv (MOI 10:1). **(D, E)** SIRT2 and SIRT7 mRNA expression in Raw264.7 cells infected with Mycobacterial strains with differing virulence. Cells were infected with BCG, H37Ra, and H37Rv, respectively (MOI 10:1) for 4 h, then SIRT2 and SIRT7 expression levels were analyzed 24 h after infection. **(F)** Differences in expression of SIRT7 in hMDMs from healthy individuals and patients with TB. Data are representative of three independent experiments with similar results and are presented as means ± SD. Two way ANOVA was performed in **(B, C)**, One way ANOVA was performed in **(D, E)**, Unpaired Student's t-test was used in **(F)**. *p < 0.05; **p < 0.01; ***p < 0.001; ****p< 0.0001.

after infection between the control and SIRT7 knockdown cells (**Supplementary Figures 2A–C**). In addition, SIRT7 and vector were transduced into Raw264.7 cells by lentivirus (**Figure 3E**). As expected, overexpression of SIRT7 inhibited the growth of intracellular Mycobacteria as indicated by flow cytometry analysis and CFU counts (**Figures 3F–H**) but had no significant impact on the phagocytosis rate (**Supplementary Figures 2D–F**). Together, these data indicate that SIRT7 contributes to the control of Mycobacteria growth in Raw264.7 cells.

SIRT7 Regulates the Generation of NO in Mycobacteria-Infected Macrophages

NO is a key anti-mycobacterial molecule, and production of NO was increased in H37Rv-infected Raw264.7 cells (**Figure 4A**), consistent with reports in the literature (17). To explore whether SIRT7 had a role in NO production, the function of SIRT7 in Raw264.7 cells was inhibited by NAM (10 mM) and then the cells were infected with H37Rv for 24 h and the NO level was measured by Griess reagent method. Addition of NAM downregulated NO production in Raw264.6 cells, similar to the effect of NO synthase inhibitors L-NAME and L-NMMA (**Figure 4B**). The expression level of the NO synthase gene *iNOS* was also downregulated by NAM (**Figure 4C**). Further experiments were conducted to determine whether SIRT7 knockdown could inhibit NO production, and these experiments revealed that NO production after H37Rv infection was significantly decreased by SIRT7 knockdown (**Figure 4D**). The NO production-related gene *iNOS* which metabolize arginine to NO and citrulline was also downregulated by SIRT7

TABLE 1 | Characteristics of patients with active TB and healthy controls.

	Healthy	Active TB	*P*-value
Sample size (no.)	16	19	–
Age (years) (mean ± SD)	44.5 ± 16.22	51.32 ± 19.2	0.2700
Sex (M/F)	10/6	14/5	0.4777

F, Female; M, male. The level of significance was evaluated by unpaired student t-test or Chi-square test. P-value < 0.05 was considered statistically significant.

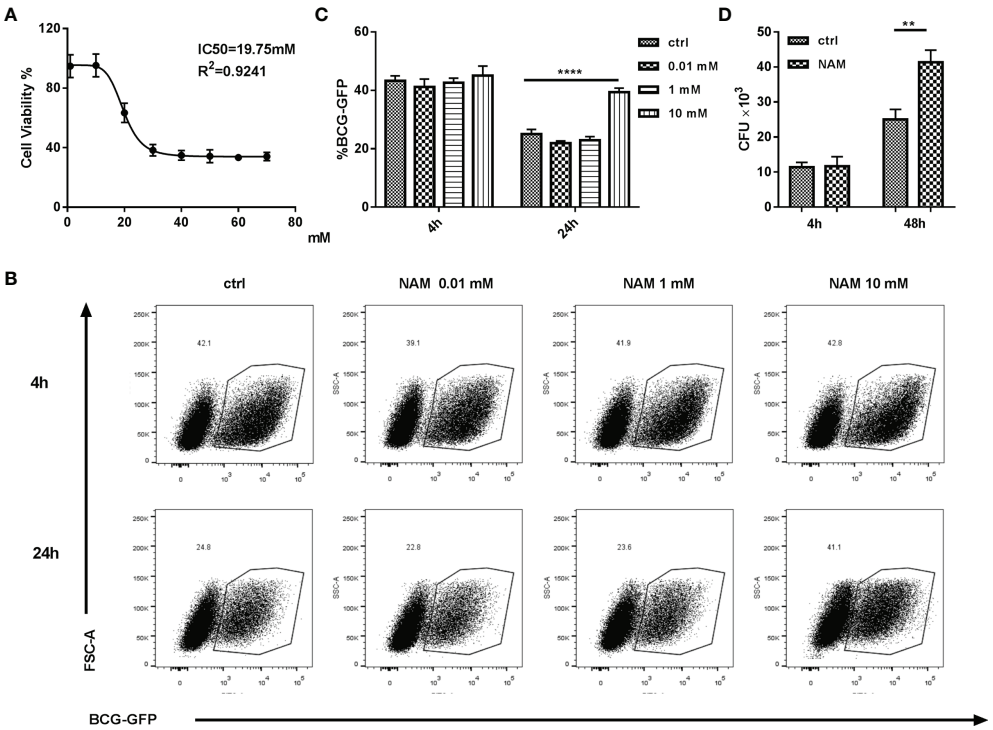

FIGURE 2 | SIRT7 inhibitor NAM increases Mycobacteria burden in Raw264.7 cells. **(A)** Dose-dependent cytotoxicity and IC_{50} values of NAM in Raw264.7 cells. **(B, C)** Raw264.7 cells were pretreated with the indicated doses of NAM 24 h before infection with BCG-GFP (MOI 10:1), and then analyzed by flow cytometry at 4h and 24 h after infection. Representative flow cytometry images of BCG-GFP-positive Raw264.7 cells were captured **(B)** and the percentage of cells positive for GFP were calculated using Flow Jo software **(C)**. **(D)** Colony-forming unit (CFU) counts from Raw264.7 cells treated with or without NAM (10 mM) after 4h and 48h infected with H37Rv. Data represent means ± SD for three independent experiments. Two way ANOVA was performed in **(C, D).** **p < 0.01; ****p< 0.0001.

knockdown (**Figure 4E**). Moreover, overexpression of SIRT7 increased the generation of NO (**Figure 4F**) and the expression of iNOS (**Figure 4G**) in Raw26.47 cells. Furthermore, we detected the *Arg-1* which hydrolyzes arginine to ornithine and urea expression levels. The *Arg-1* expression could also be downregulated by SIRT7 knockdown an upregulated by SIRT7 overexprssion (**Supplementary Figures 3A, B**). However, the enhancement in iNOS levels was around one thousand times higher compared to that of Arg-1 in Mycobacteria-infected Raw264.7 cells (**Supplementary Figure 2C**), so we considered iNOS to play the major role in NO production modulation in Mycobacteria-infected Raw cells. Additionally, it was also reported that high Arg-1 expression preceded the increased induction of iNOS at early time points of infection with mycobacteria (18). These findings confirm that SIRT7-mediated inhibition of Mycobacteria in macrophages is NO dependent.

The NO Donor SNAP Abrogates the NAM or SIRT7 Knockdown-Induced Increase Mycobacteria Burden in Macrophages

To confirm whether SIRT7 controlled Mycobacteria growth *via* NO, the NO donor SNAP (200 μM) was added to suppress the increase in bacterial load caused by NAM (10 mM), which inhibits the function of SIRT7. Compared with the group treated with NAM, flow cytometry analysis of BCG-GFP-infected cells and CFU counts of H37Rv-infected cells both revealed that SNAP alleviated the NAM-induced increase of Mycobacteria burden in Raw264.7 cells (**Figures 5A–C**). Correspondingly, SNAP addition also alleviated the SIRT7 knockdown-induced increase of Mycobacteria burden in Raw264.7 cells (**Figures 6A–C**). Earlier experiments in the current study suggested that SIRT7 regulated NO production in Mycobacteria-infected macrophages, and these findings confirm that SIRT7 restricts intracellular Mycobacteria growth by promoting NO release.

SIRT7 Promoted Elimination of Intracellular Mycobacteria by NO-Dependent Apoptosis

Given that NO was reported to enhance apoptosis in macrophages (19), and apoptosis is usually considered to play a vital role in the host defense against Mtb (20), the ability of SIRT7 to regulate apoptosis in Mycobacteria-infected macrophages was evaluated. Following infection of cells with H37Rv for 24 h, the percentage of apoptotic cells was assessed by Annexin V/propidium iodide (PI) staining assay. Compared with the control group (Raw264.7 cells with scrambled control NC-pLKO.1), SIRT7-knockdown cells had markedly lower

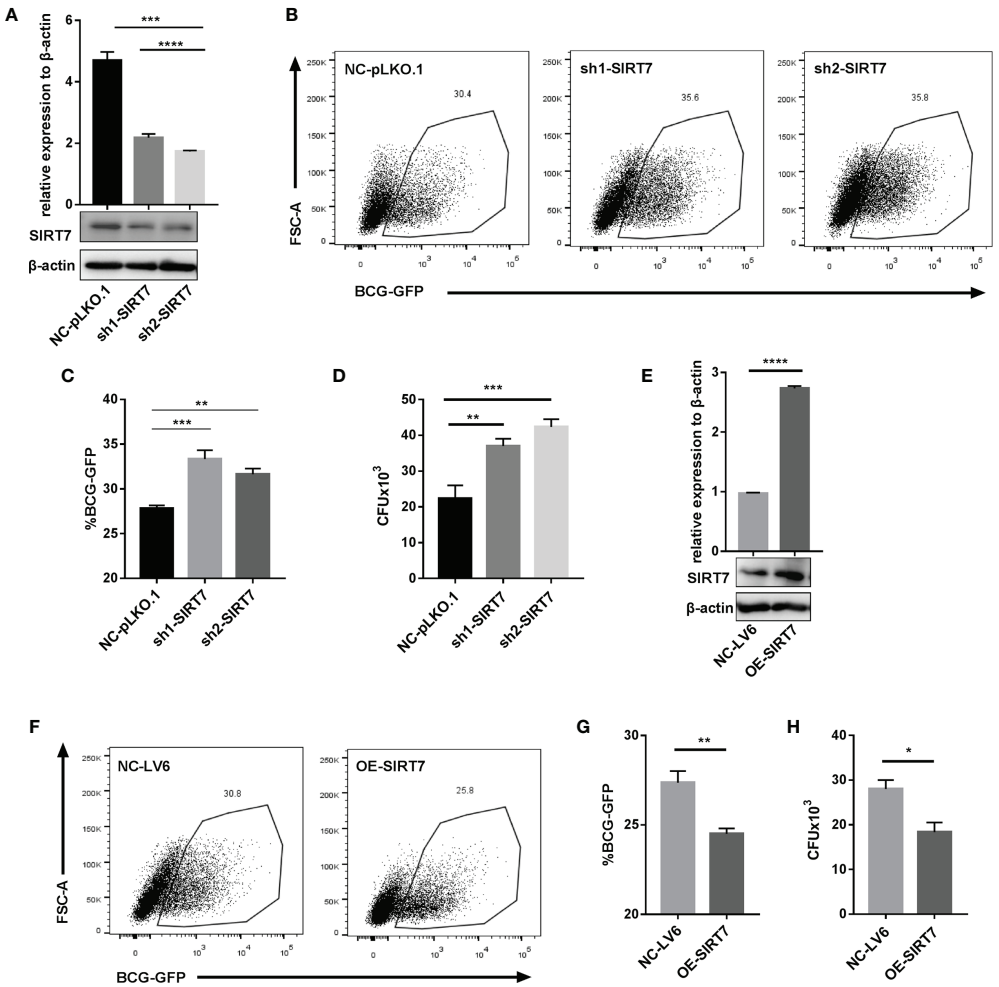

FIGURE 3 | SIRT7 knockdown increases the risk of Mycobacteria infection, while overexpression of SIRT7 protects cells from Mycobacteria. **(A–D)** Raw264.7 cells stably expressing scrambled control (NC-pLKO.1) and two independent SIRT7 shRNAs (sh1-SIRT7 and sh2-SIRT7), respectively, were established. SIRT7 expression levels in these cells were measured by quantitative RT-PCR and Western blot analysis **(A)**. Representative flow cytometry images **(B)** and percentage **(C)** of GFP-positive cells were recorded in the scrambled control and SIRT7-knockdown cells 24 h after infection with BCG-GFP (MOI 10:1). **(D)** Colony-forming unit (CFU) counts in scrambled control and SIRT7-knockdown cells after 48h infection with H37Rv. **(E–H)** Raw264.7 cells stably overexpressing SIRT7 (OE-SIRT7) and vector control (NC-LV6) were established. SIRT7 expression levels in these cells were measured by quantitative RT-PCR and Western blot analysis **(E)**. Representative flow cytometry images **(F)** and percentage **(G)** of GFP-positive cells were recorded in control and SIRT7-overexpressing cells 24 h after infection with BCG-GFP (MOI 10:1). **(H)** CFU counts in vector control and SIRT7-overexpressing cells after 48h infected with H37Rv. Data are representative of three independent experiments with similar results and are presented as means ± SD. One way ANOVA was performed in **(A, C, D)**, Unpaired Student's t-test was used in **(E, G, H)**. *p < 0.05; **p < 0.01; ***p < 0.001; ****p< 0.0001.

percentages of apoptotic cells in total (AnnexinV+) and early (AnnexinV+/PI–) apoptotic ratios, but there were no significant changes in late apoptotic ratios (**Figures 7A–D**). These findings suggested that SIRT7 promotes elimination of intracellular Mycobacteria by inducing apoptosis in macrophages. Earlier experiments in the study showed that SIRT7 promoted NO generation and increased the apoptosis ratio in macrophages, therefore an experiment was conducted to test whether NO played a role in the apoptosis of macrophages induced by SIRT7. SIRT7-knockdown Raw264.7 cells were treated with the NO donor SNAP (200 μM) and then infected with Mtb strain H37Rv. Addition of the NO donor led to significant increases in early apoptotic ratios, but there were no significant changes in late and total apoptotic ratios (**Figures 7E–H**). These findings confirm that SIRT7 promotes elimination of intracellular Mycobacteria by NO-dependent apoptosis.

DISCUSSION

Since Mtb has evolved diverse strategies to escape immune surveillance, HDTs that enhance Mtb-specific immunity are urgently needed. Sirtuins are a conserved family of proteins

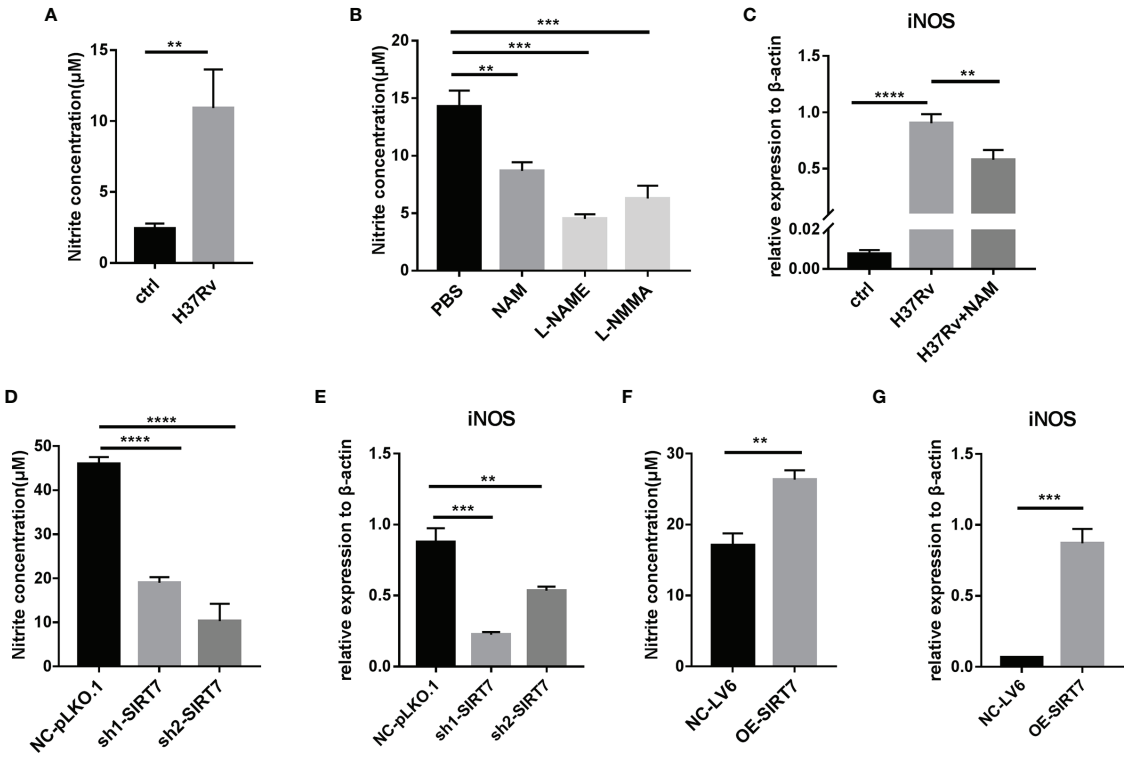

FIGURE 4 | SIRT7 inhibitor NAM or SIRT7-knockdown inhibits nitric oxide (NO) production in Raw264.7 cells. **(A, B)** NO production in Raw264.7 cells was measured by Griess reaction assay 24 h after infection with H37Rv (MOI 10:1) **(A)** or after pretreatment of cells with NAM (10 mM) or NOS inhibitors L-NMME (500 μM) and L-NMMA (500 μM) **(B)**. **(C)** Quantitative RT-PCR analysis of *iNOS* expression levels in infected Raw264.7 cells pretreated with or without NAM. mRNA was collected from the cells 24 h after infection with H37Rv. **(D, E)** NO concentration **(D)** and quantitative RT-PCR analysis of *iNOS* **(E)** expression levels in Raw264.7 cells stably expressing scrambled control (NC-pLKO.1) or two independent SIRT7 shRNAs (sh1-SIRT7 and sh2-SIRT7). **(F, G)** NO concentration **(F)** and quantitative RT-PCR analysis of *iNOS* **(G)** in Raw264.7 cells stably overexpressing SIRT7 (OE-SIRT7) and vector control (NC-LV6). Data are representative of three independent experiments with similar results and are presented as means ± SD. One way ANOVA was performed in **(B–E)**, Unpaired Student's t-test was used in **(A, F, G)**. **p < 0.01; ***p < 0.001; ****p< 0.0001.

(seven recognized members to date) that are NAD+-dependent deacetylases (21). There are previous reports describing anti-Mtb activity of sirtuins. For example, activation of SIRT1 reduced intracellular growth of drug-susceptible and drug-resistant strains of Mtb and induced phagosome-lysosome fusion and autophagy in a SIRT1-dependent manner (22). SIRT1 suppressed TAK1 activation and the subsequent production of inflammatory cytokines *via* the MAPK and NF-κB pathways to fine-tune the excessive inflammatory response to Mtb infection (23). Furthermore, SIRT3 played an anti-Mtb role through coordinating mitochondrial and autophagic cell death functions (24–26), while SIRT2 was reported to play the opposite role in anti-Mtb activities. The SIRT2 inhibitor AGK2 reduced the bacillary load of both drug-sensitive and drug-resistant strains of Mtb (27). However, there remains a different view due to the absence of SIRT2 in myeloid cells not impacting lung cellular responses to Mtb (28). Furthermore, SIRT5 deficiency did not worsen endotoxemia, pneumonia caused by *Klebsiella pneumoniae* or *Streptococcus pneumoniae*, *Escherichia coli*-induced peritonitis, listeriosis, and staphylococcal infection (29). Therefore, different members of the sirtuin family have different roles in fighting Mtb infections. In the current study, the role of SIRT7 in Mtb infection was investigated for the first time. SIRT2 and SIRT7 were the members of the sirtuin family with dominant expression in macrophages. Mtb infection suppressed SIRT7 expression, but there were no significant changes in expression of SIRT2 after Mtb infection, congruent with results reported by Smulan et al. (28). Inhibition of SIRT7 activity by NAM or knockdown of SIRT7 expression increased the risk of Mtb infection. In addition, overexpression of SIRT7 inhibited the growth of intracellular Mtb.

The molecular mechanism of SIRT7 in the host immune response has been explored in recent years. SIRT7 deacetylated and promoted SMAD4 degradation to antagonize TGF-β signaling (30). TGF-β1 exhibited immunosuppressive activity and accelerated the progression of pulmonary TB (31). Loss of SIRT7 decreased expression of TNF, which was essential for protection against Mtb (32, 33). Furthermore, SIRT7 also suppressed the NF-κB signaling pathway to attenuate excessive inflammatory responses (34). In the current study, a new mechanism of SIRT7 anti-Mtb activity was discovered. SIRT7

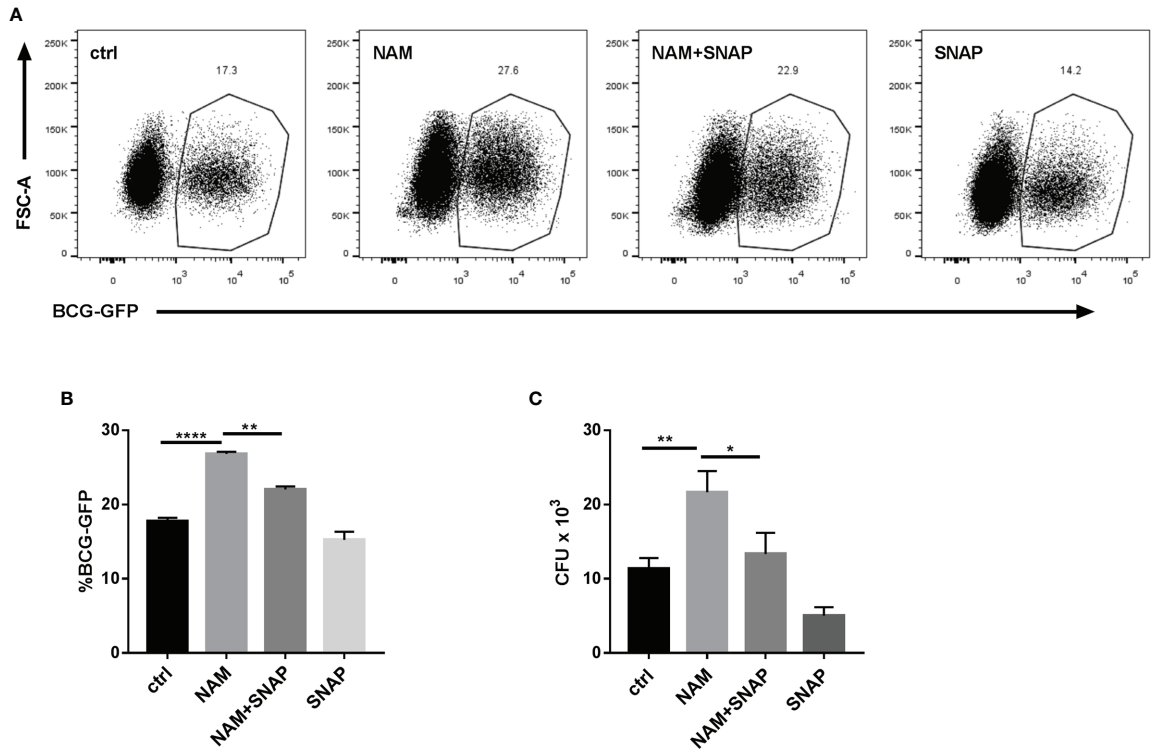

FIGURE 5 | Nitric oxide (NO) donor SNAP abrogates the NAM-induced increase in Mycobacteria burden in Raw264.7 cells. **(A, B)** Raw264.7 cells were pretreated with NAM (10 mM) and/or SNAP (200 μM) 24 h before infection with BCG-GFP (MOI 10:1) and were then analyzed by flow cytometry 24 h after infection. Representative flow cytometry images **(A)** were recorded and the percentage of BCG-GFP-positive Raw264.7 cells **(B)** were calculated by Flow Jo software. **(C)** Colony-forming unit (CFU) counts from Raw264.7 cells treated with NAM (10 mM) and/or SNAP (200 μM) 48h after infection. Data represent means ± SD for three independent experiments. One way ANOVA was performed in **(B, C)**. *p < 0.05; **p < 0.01; ****p< 0.0001.

restricted intracellular Mtb growth by promoting NO release from macrophages. The pan-sirtuin family inhibitor NAM and SIRT7 knockdown both downregulated the NO concentration and the expression level of NO release-related genes in macrophages. In contrast, overexpression of SIRT7 increased the generation of NO in macrophages. Furthermore, the NO donor SNAP abrogated the NAM- or SIRT7-knockdown-induced increase in Mtb burden in macrophages. These data further supported that SIRT7 restricts intracellular Mtb growth by promoting NO release.

In addition to its function as a reactive free radical to execute direct anti-Mtb activities (35), NO is also involved in innate immunity by inducing macrophage apoptosis (36). Thus, the mechanism of apoptosis regulation by SIRT7 was further explored. SIRT7 knockdown in macrophages suppressed early apoptosis of Mtb-infected Raw264.7 cells, while the NO donor SNAP promoted early apoptosis ratios after Mtb infection.

Overall, this study demonstrated for the first time, that SIRT7 has a crucial role in Mtb infection, and aside from regulating NO release to directly kill Mtb, SIRT7 also promoted elimination of intracellular Mtb by NO-dependent apoptosis. However, the molecular mechanism underlying SIRT7 regulation of NO release has yet to be elucidated, and the candidate substrate which SIRT7 directly deacetylates in TB pathogenesis remains unclear. These are the scientific questions that will be addressed in our future work. The findings from the current study suggest there is potential to target SIRT7 in the development of innovative HDTs to improve TB treatment outcomes.

MATERIALS AND METHODS

Cell Culture

Mouse macrophage Raw264.7 cells were purchased from National Collection of Authenticated Cell Cultures, China, and maintained in Dulbecco's modified Eagle's medium (DMEM, Gibco, 11965-092) supplemented with 10% fetal bovine serum (FBS, Gibco, 10091148) and 1% penicillin- streptomycin (Gibco, 15140122). Cells were cultured in a humidified incubator at 37°C and 5% CO_2. In infection experiments, no antibiotic was used.

Bacteria Culture

M. bovis BCG-green fluorescent protein (BCG-GFP) and Mtb standard strains H37Rv, H37Ra, BCG were grown in Middlebrook 7H9 broth (BD Biosciences, 271310) supplemented with 10% Oleic Acid-Dextrose-Catalase (OADC) (BD Biosciences, 212240), 0.5% glycerol, and 0.05% Tween 80 at

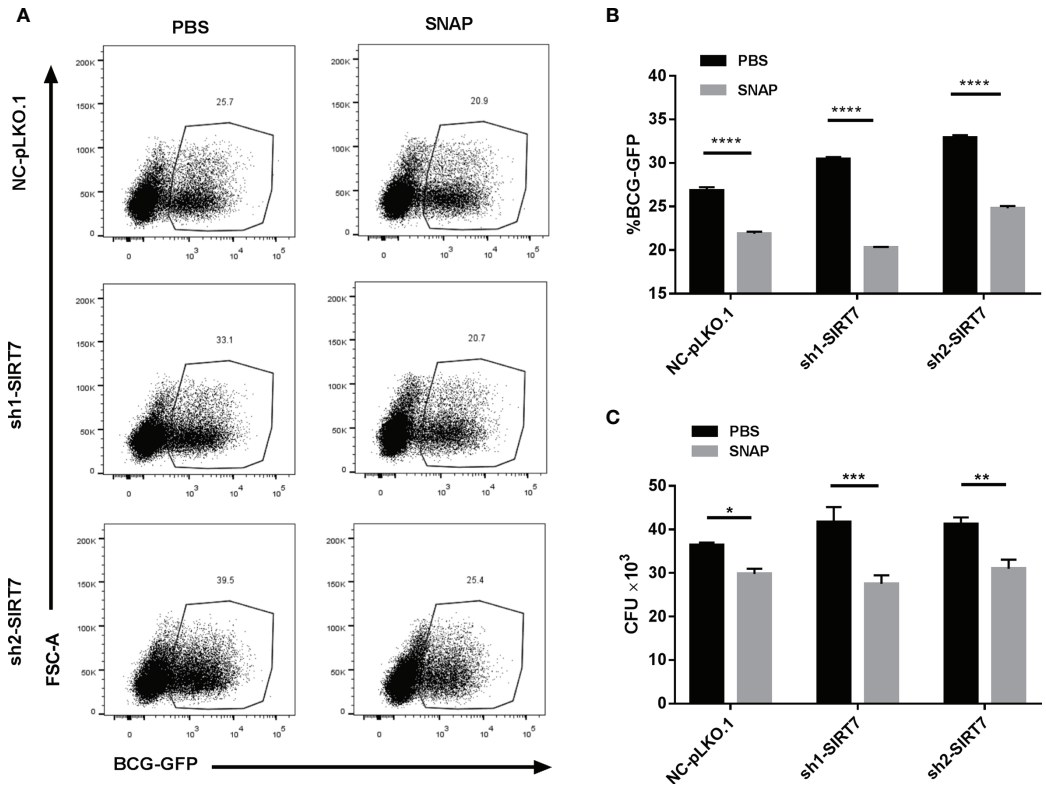

FIGURE 6 | Nitric oxide donor SNAP abrogates the SIRT7-knockdown-induced increase in Mycobacteria burden in Raw264.7 cells. **(A, B)** SIRT7-knockdown Raw264.7 cells were pretreated with SNAP (200 μM) 24 h before infection with BCG-GFP (MOI 10:1) and were then analyzed by flow cytometry 24 h after infection. Representative flow cytometry images **(A)** were recorded and the percentage of BCG-GFP positive Raw264.7 cells **(B)** were calculated by Flow Jo software. **(C)** Colony-forming unit (CFU) counts of SIRT7-knockdown Raw264.7 cells treated with or without SNAP (200 μM) 48h after infection. Data represent means ± SD for three independent experiments. Two way ANOVA was performed in **(B, C)**. *p < 0.05; **p < 0.01; ***p < 0.001; ****p< 0.0001.

37°C for 5 to 7 days to achieve mid-logarithmic phase (optical density at 600 nm [OD_{600}] = 0.3 to 0.8), Cultures were harvested, resuspended in PBS with 0.05% Tween 20, 25% glycerol, and stored at -80°C. One vial of the stock was thawed to calculate CFU per milliliter. On the day of infection, mycobacteria were thawed, washed, and sonicated before use.

Preparation of hMDM

This study was approved by the Ethics Committee of Shenzhen Third People's Hospital (approval number: 2019-038). Informed written consents were obtained from participants prior to venous blood collection. Human peripheral blood mononuclear cells (PBMCs) were isolated by Ficoll density gradient centrifugation (Axis-Shield, AS1114547) and differentiated at $1x10^6$ cells/ml in complete 1640 culture medium supplemented with 30 ng/ml human M-CSF (Gibco, PHC9501) for approximately 7 days.

Drug Administration

Raw264.7 cells were pre-treated with nicotinamide (NAM) (Sigma, 72340) 10mM, or SNAP (MedChemExpress, HY-121526) 200μM, or L-NAME (MedChemExpress, HY-18729A) 500 μM and L-NMMA (MedChemExpress, HY-18732A) 500 μM for 24h before Mtb infection.

Cell Viability Assay

The Raw264.7 cells were seeded at $5x10^4$ cells/well in a 96-well plate in complete DMEM. Different concentration of NAM were added and cultured for an additional 24 h, CCK-8 reagent (Vazyme, A311-02) was added into the well (10 μl/well) and incubated at 37°C for 2 h to measure cell viability. The absorbance was detected at 450nm with a Varioskan LUX Multimode Microplate Reader(Thermo Fisher, Varioskan LUX Multimode Microplate Reader). The cell viability rate (%) of three independent experiments was calculated as the follows:

$$\text{Cell viability rate (\%)} = \frac{\text{OD of treated cells} - \text{OD of background}}{\text{OD of control cells} - \text{OD of background}} \times 100\,\%$$

IC50 values were calculated using a four-parameter logistic curve (GraphPad Prism 7.0).

Lentiviral Vector Construction and Lentivirus Packaging

Targeted sequences - homologous to SIRT7 (GenBank: 209011) and scrambled sequences which had no homology with the

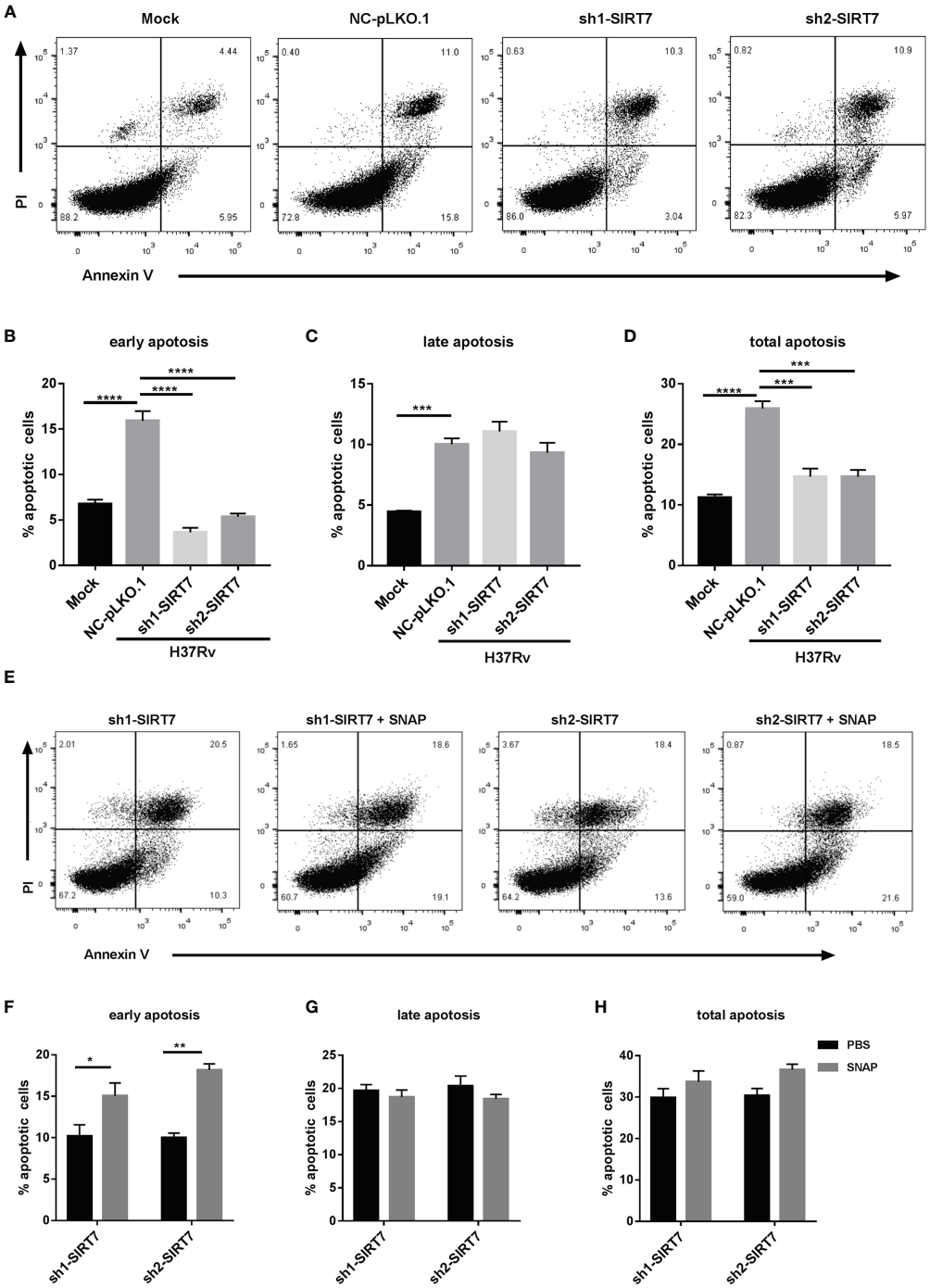

FIGURE 7 | SIRT7 promotes elimination of intracellular Mycobacteria by nitric oxide-dependent apoptosis. Scrambled control (NC-pLKO.1) and SIRT7-knockdown (sh1-SIRT7 and sh2-SIRT7) Raw264.7 cells were infected with H37Rv and apoptosis was detected by Annexin V and propidium iodide (PI) staining. **(A, E)** Representative flow cytometry images of apoptotic cells. **(B–D)** Percentage of apoptotic cells (early, late, and total, respectively) in the scrambled control and SIRT7-knockdown cells. **(F–H)** Percentage of apoptotic cells (early, late, and total, respectively) in the SIRT7-knockdown cells pretreated with or without SNAP (200 μM). The percentages of early, late, and total apoptotic cells were calculated by Flow Jo software. Data are representative of three independent experiments with similar results and are presented as means ± SD. Two way ANOVA was performed in **(B–D)**, One way ANOVA was performed in **(F–H)**. *$p < 0.05$; **$p < 0.01$; ***$p < 0.001$; ****$p< 0.0001$.

mouse gene—were synthesized, annealed, and cloned in the lentiviral expression vector pLKO.1-TRC (Addgene: 10878). SIRT7 whole length CDS was cloned in the lentiviral expression vector pLVML-3×HA-MCS-IRES-Puro using Homologous Recombination strategy (Vazyme, C115), The primers were synthesized in Sangon Biotech (Guangzhou, China) and showed in **Supplementary Table 1**. HEK293T cells were co-transfected with the lentiviral expression vector, packaging vector psPAX2 and envelope vector pMD2.G using Lipofectamine 3000 (Invitrogen, L3000015). Culture supernatants were harvested at 48h, filtered with a 0.45-μm pore size filter.

Raw264.7 Stable Cell Line Construction

Raw264.7 cells were infected with viral supernatants collected from HEK293T cells transfected with lentiviral constructs for 24h, Then washing three times with prewarmed sterile phosphate-buffered saline (PBS) to remove extracellular lentivirus. After 72 h, stable cell lines were sorted by puromycin(2 μg/ml), and the efficiency of knockdown or overexpress was determined by Western blotting.

Mtb Infection and Enumeration of Colony Forming Units (CFU)

Raw264.7 cells were seeded at $2x10^5$ cells/well in a 24-well plate in complete DMEM and infected with Mtb strains H37Rv at a multiplicity of infection (MOI) of 10 for 4h. Then washing three times with prewarmed sterile PBS to remove extracellular bacteria, and cultured with complete DMEM at 37°C and 5% CO_2. After 4h and 48h, Cells were lysed with PBS containing 0.1% SDS, and the lysates were gradient diluted on Middlebrook 7H10 agar (BD Biosciences, 262710) supplemented with 10% OADC, 0.5% glycerol plates and incubated vertically at 37°C for 2-3 weeks. Bacterial colonies were counted and colony-forming unit (CFU) were estimated as per dilution.

BCG-GFP Infected Cells Analysis by Flow Cytometry

Raw264.7 cells were infected with BCG-GFP at a multiplicity of infection (MOI) of 10 for 4h. Then washing three times with prewarmed sterile PBS to remove extracellular bacteria, and cultured with complete DMEM at 37°C and 5% CO_2. Cells were collected in FACS tubes and the percentages of GFP positive cells were measured by flow cytometry (BD Biosciences, Canton II) after 4h and 24h infection and analyzed by FlowJo X 10.0.7 according to the manufacturer's protocol.

Nitric Oxide Assay

The levels of NO were measured by commercial kits (Beyotime, S0021S) according to the manufacturers'protocols. Mtb infection method as was mentioned above, the supernatants were collected for detection after 48h infection. Griess Reagent I 50μl and Griess Reagent II 50μl were added to 50μl supernatants in order. Nitrite concentration was determined by spectrophotometry (540 nm) from a standard curve (0-100 mmol/L) derived from NaNO2.

Apoptosis Assay

The apoptotic cells were measured by FACS using FITC Annexin V Apoptosis Detection Kit (BD Biosciences, 556547). Mtb infection method as was mentioned above, cells were washed twice with cold PBS and stained with the Annexin V- PI reagent. Cellular apotosis levels were detected by flow cytometry (BD Biosciences, Canton II) and analyzed by FlowJo X 10.0.7 according to the manufacturer's protocol.

Quantitative RT-PCR

Total RNA was isolated from cells using Total RNA Kit I (OMEGA, R6834-02) according to the manufacturer's instructions. cDNA was synthesized using ClonExpress Ultra One Step Cloning Kit (Vazyme, C115-02) followed by qRT-PCR using SYBR Green HiScript II Q RT SuperMix for qPCR Kit (Vazyme, R223-01). Real-time quantitative RT-PCR analysis was performed using ABI ViiA7 Real-Time thermal cycler (Thermo Fisher, ABI). The primers used in the study were synthesized in Sangon Biotech (Guangzhou, China) and showed in **Supplementary Table 2**. The mRNA expression levels were normalized to β-actin, and fold induction was calculated by the ΔΔCT method. RT-qPCR was performed in triplicate.

Western Blot

Cells were harvested and lysed in RIPA lysis buffer (Beyotime, P0013B) for 5 min on ice.The protein concentration of the resultant lysates was measured with a bicinchoninic acid (BCA) protein kit (Beyotime, P0010S). Equal amounts of protein from each sample were separated by SDS–PAGE and electro-blotted onto PVDF membranes. The membrane was blocked with 5% skim milk powder solution in PBS with Tween 20 (PBST) for 2h at room temperature and incubated with primary antibodies overnight at 4°C. The membranes were then incubated with relevant secondary antibodies at room temperature for 1 h and visualized by using ECL detection solution (Beyotime, P0018AS). The digital images of the protein bands were acquired using a ChemiDoc MP Imaging System (Bio-rad, ChemiDoc MP). The primary antibodies used in the present study were anti-SIRT7 (*Invitrogen*, PA5-87543), anti-β-actin (CST, 4970L).

Statistical Analysis

All the presented data and results were confirmed in at least three independent experiments. The data were represented as the mean ± SD and analyzed using GraphPad Prism 7.0 software (San Diego, CA). Statistical significance was analysised by One-way ANOVA, Two-way ANOVA or unpaired Student's t-tests. $*$ $p < 0.05$; $**$ $p < 0.01$; $***$ $p < 0.001$; $****$ $p< 0.0001$.

DATA AVAILABILITY STATEMENT

The original contributions presented in the study are included in the article/**Supplementary Material**. Further inquiries can be directed to the corresponding author.

AUTHOR CONTRIBUTIONS

SZ wrote the manuscript. GZ designed experiments. SZ, YL, XZ, MO, GX, and FL performed experiments and analyzed data. ZYW and ZQW provided scientific expertise. LL and GZ supervised the project. All authors contributed to the article and approved the submitted version.

FUNDING

This work was supported by the National Natural Science Foundation of China (No. 82170009, 81873958, 82100013), the National Key Research and Development Plan (No. 2020YFA0907200), the Guangdong Scientific and Technological Foundation (No. 2019B1515120041, 2020B1111170014, 2019A1515110055), the Shenzhen Scientific and Technological Foundation (No. KCXFZ202002011007083, JCYJ20180228162511084, JCYJ20190809104205706), and the Sanming Project of Medicine in Shenzhen (No. SZSM201911009).

SUPPLEMENTARY MATERIAL

The Supplementary Material for this article can be found online at: https://www.frontiersin.org/articles/10.3389/fimmu.2021.779235/full#supplementary-material

REFERENCES

1. *Global Tuberculosis Report 2020*. Geneva: World Health Organization (2020). Licence: CC BY-NC-SA 3.0 IGO.
2. Dye C, Scheele S, Dolin P, Pathania V, Raviglione MC. Consensus Statement. Global Burden of Tuberculosis: Estimated Incidence, Prevalence, and Mortality by Country. WHO Global Surveillance and Monitoring Project. *JAMA* (1999) 282(7):677–86. doi: 10.1001/jama.282.7.677
3. Palucci I, Delogu G. Host Directed Therapies for Tuberculosis: Futures Strategies for an Ancient Disease. *Chemotherapy* (2018) 63(3):172–80. doi: 10.1159/000490478
4. Diallo I, Seve M, Cunin V, Minassian F, Poisson JF, Michelland S, et al. Current Trends in Protein Acetylation Analysis. *Expert Rev Proteomics* (2019) 16(2):139–59. doi: 10.1080/14789450.2019.1559061
5. Arrowsmith CH, Bountra C, Fish PV, Lee K, Schapira M. Epigenetic Protein Families: A New Frontier for Drug Discovery. *Nat Rev Drug Discov* (2012) 11 (5):384–400. doi: 10.1038/nrd3674
6. Barber MF, Michishita-Kioi E, Xi Y, Tasselli L, Kioi M, Moqtaderi Z, et al. SIRT7 Links H3K18 Deacetylation to Maintenance of Oncogenic Transformation. *Nature* (2012) 487(7405):114–8. doi: 10.1038/nature11043
7. Wang WW, Angulo-Ibanez M, Lyu J, Kurra Y, Tong Z, Wu B, et al. A Click Chemistry Approach Reveals the Chromatin-Dependent Histone H3K36 Deacylase Nature of SIRT7. *J Am Chem Soc* (2019) 141(6):2462–73. doi: 10.1021/jacs.8b12083
8. Tanabe K, Liu J, Kato D, Kurumizaka H, Yamatsugu K, Kanai M, et al. LC-MS/MS-Based Quantitative Study of the Acyl Group- and Site-Selectivity of Human Sirtuins to Acylated Nucleosomes. *Sci Rep* (2018) 8(1):2656. doi: 10.1038/s41598-018-21060-2
9. Li L, Shi L, Yang S, Yan R, Zhang D, Yang J, et al. SIRT7 Is a Histone Desuccinylase That Functionally Links to Chromatin Compaction and Genome Stability. *Nat Commun* (2016) 7:12235. doi: 10.1038/ncomms12235
10. Tong Z, Wang M, Wang Y, Kim DD, Grenier JK, Cao J, et al. SIRT7 Is an RNA-Activated Protein Lysine Deacylase. *ACS Chem Biol* (2017) 12(1):300–10. doi: 10.1021/acschembio.6b00954
11. Fukuda M, Yoshizawa T, Karim MF, Sobuz SU, Korogi W, Kobayasi D, et al. SIRT7 has a Critical Role in Bone Formation by Regulating Lysine Acylation of SP7/Osterix. *Nat Commun* (2018) 9(1):2833. doi: 10.1038/s41467-018-05187-4
12. Bao X, Liu Z, Zhang W, Gladysz K, Fung YME, Tian G, et al. Glutarylation of Histone H4 Lysine 91 Regulates Chromatin Dynamics. *Mol Cell* (2019) 76 (4):660–75.e9. doi: 10.1016/j.molcel.2019.08.018
13. Nathan C, Shiloh MU. Reactive Oxygen and Nitrogen Intermediates in the Relationship Between Mammalian Hosts and Microbial Pathogens. *Proc Natl Acad Sci USA* (2000) 97(16):8841–8. doi: 10.1073/pnas.97.16.8841
14. Herbst S, Schaible UE, Schneider BE. Interferon Gamma Activated Macrophages Kill Mycobacteria by Nitric Oxide Induced Apoptosis. *PloS One* (2011) 6(5):e19105. doi: 10.1371/journal.pone.0019105
15. Kim PK, Zamora R, Petrosko P, Billiar TR. The Regulatory Role of Nitric Oxide in Apoptosis. *Int Immunopharmacol* (2001) 1(8):1421–41. doi: 10.1016/s1567-5769(01)00088-1
16. Avalos JL, Bever KM, Wolberger C. Mechanism of Sirtuin Inhibition by Nicotinamide: Altering the NAD(+) Cosubstrate Specificity of a Sir2 Enzyme. *Mol Cell* (2005) 17(6):855–68. doi: 10.1016/j.molcel.2005.02.022
17. Kwon OJ, Kim JH, Kim HC, Suh GY, Park JW, Chung MP, et al. Nitric Oxide Expression in Airway Epithelial Cells in Response to Tubercle Bacilli Stimulation. *Respirology (Carlton Vic)* (1998) 3(2):119–24. doi: 10.1111/j.1440-1843.1998.tb00109.x
18. Schmok E, Abad Dar M, Behrends J, Erdmann H, Ruckerl D, Endermann T, et al. Suppressor of Cytokine Signaling 3 in Macrophages Prevents Exacerbated Interleukin-6-Dependent Arginase-1 Activity and Early Permissiveness to Experimental Tuberculosis. *Front Immunol* (2017) 8:1537. doi: 10.3389/fimmu.2017.01537
19. Zhang X, Jin L, Tian Z, Wang J, Yang Y, Liu J, et al. Nitric Oxide Inhibits Autophagy and Promotes Apoptosis in Hepatocellular Carcinoma. *Cancer Sci* (2019) 110(3):1054–63. doi: 10.1111/cas.13945
20. Lam A, Prabhu R, Gross CM, Riesenberg LA, Singh V, Aggarwal S. Role of Apoptosis and Autophagy in Tuberculosis. *Am J Physiol Lung Cell Mol Physiol* (2017) 313(2):L218–29. doi: 10.1152/ajplung.00162.2017
21. Frye RA. Characterization of Five Human cDNAs With Homology to the Yeast SIR2 Gene: Sir2-Like Proteins (Sirtuins) Metabolize NAD and may Have Protein ADP-Ribosyltransferase Activity. *Biochem Biophys Res Commun* (1999) 260(1):273–9. doi: 10.1006/bbrc.1999.0897
22. Cheng CY, Gutierrez NM, Marzuki MB, Lu X, Foreman TW, Paleja B, et al. Host Sirtuin 1 Regulates Mycobacterial Immunopathogenesis and Represents a Therapeutic Target Against Tuberculosis. *Sci Immunol* (2017) 2(9). doi: 10.1126/sciimmunol.aaj1789
23. Yang H, Hu J, Chen YJ, Ge B. Role of Sirt1 in Innate Immune Mechanisms Against Mycobacterium Tuberculosis *via* the Inhibition of TAK1 Activation. *Arch Biochem biophysics* (2019) 667:49–58. doi: 10.1016/j.abb.2019.04.006
24. Kim TS, Jin YB, Kim YS, Kim S, Kim JK, Lee HM, et al. SIRT3 Promotes Antimycobacterial Defenses by Coordinating Mitochondrial and Autophagic Functions. *Autophagy* (2019) 15(8):1356–75. doi: 10.1080/15548627.2019.1582743
25. Wu T, Jiao L, Bai H, Hu X, Wang M, Zhao Z, et al. The Dominant Model Analysis of Sirt3 Genetic Variants Is Associated With Susceptibility to Tuberculosis in a Chinese Han Population. *Mol Genet Genomics MGG* (2020) 295(5):1155–62. doi: 10.1007/s00438-020-01685-7
26. Smulan LJ, Martinez N, Kiritsy MC, Kativhu C, Cavallo K, Sassetti CM, et al. Sirtuin 3 Downregulation in Mycobacterium Tuberculosis-Infected Macrophages Reprograms Mitochondrial Metabolism and Promotes Cell Death. *mBio* (2021) 12(1). doi: 10.1128/mBio.03140-20
27. Bhaskar A, Kumar S, Khan MZ, Singh A, Dwivedi VP, Nandicoori VK. Host Sirtuin 2 as an Immunotherapeutic Target Against Tuberculosis. *eLife* (2020) 9. doi: 10.7554/eLife.55415
28. Cardoso F, Castro F, Moreira-Teixeira L, Sousa J, Torrado E, Silvestre R, et al. Myeloid Sirtuin 2 Expression Does Not Impact Long-Term Mycobacterium

Tuberculosis Control. *PloS One* (2015) 10(7):e0131904. doi: 10.1371/journal.pone.0131904
29. Heinonen T, Ciarlo E, Théroude C, Pelekanou A, Herderschee J, Le Roy D, et al. Sirtuin 5 Deficiency Does Not Compromise Innate Immune Responses to Bacterial Infections. *Front Immunol* (2018) 9:2675. doi: 10.3389/fimmu.2018.02675
30. Tang X, Shi L, Xie N, Liu Z, Qian M, Meng F, et al. SIRT7 Antagonizes TGF-¦Â Signaling and Inhibits Breast Cancer Metastasis. *Nat Commun* (2017) 8 (1):318. doi: 10.1038/s41467-017-00396-9
31. Dai G, McMurray DN. Effects of Modulating TGF-Beta 1 on Immune Responses to Mycobacterial Infection in Guinea Pigs. *Tubercle Lung Dis Off J Int Union Against Tuberculosis Lung Dis* (1999) 79(4):207–14. doi: 10.1054/tuld.1998.0198
32. Miyasato Y, Yoshizawa T, Sato Y, Nakagawa T, Miyasato Y, Kakizoe Y, et al. Sirtuin 7 Deficiency Ameliorates Cisplatin-Induced Acute Kidney Injury Through Regulation of the Inflammatory Response. *Sci Rep* (2018) 8 (1):5927. doi: 10.1038/s41598-018-24257-7
33. Flynn JL, Goldstein MM, Chan J, Triebold KJ, Pfeffer K, Lowenstein CJ, et al. Tumor Necrosis Factor-Alpha is Required in the Protective Immune Response Against Mycobacterium Tuberculosis in Mice. *Immunity* (1995) 2 (6):561–72. doi: 10.1016/1074-7613(95)90001-2
34. Chen KL, Li L, Li CM, Wang YR, Yang FX, Kuang MQ, et al. SIRT7 Regulates Lipopolysaccharide-Induced Inflammatory Injury by Suppressing the NF-¦ÈB Signaling Pathway. *Oxid Med Cell Longev* (2019) 2019:3187972. doi: 10.1155/2019/3187972
35. Jamaati H, Mortaz E, Pajouhi Z, Folkerts G, Movassaghi M, Moloudizargari M, et al. Nitric Oxide in the Pathogenesis and Treatment of Tuberculosis. *Front Microbiol* (2017) 8:2008. doi: 10.3389/fmicb.2017.02008
36. Ulett GC, Adderson EE. Nitric Oxide is a Key Determinant of Group B Streptococcus-Induced Murine Macrophage Apoptosis. *J Infect Dis* (2005) 191 (10):1761–70. doi: 10.1086/429693

Conflict of Interest: The authors declare that the research was conducted in the absence of any commercial or financial relationships that could be construed as a potential conflict of interest.

Publisher's Note: All claims expressed in this article are solely those of the authors and do not necessarily represent those of their affiliated organizations, or those of the publisher, the editors and the reviewers. Any product that may be evaluated in this article, or claim that may be made by its manufacturer, is not guaranteed or endorsed by the publisher.

frontiers in Immunology

ORIGINAL RESEARCH
published: 12 January 2022
doi: 10.3389/fimmu.2021.752466

GSK-3α/β Activity Negatively Regulates MMP-1/9 Expression to Suppress *Mycobacterium tuberculosis* Infection

Xinying Zhou[†], *Linmiao Lie*[†], *Yao Liang, Hui Xu, Bo Zhu, Yingqi Huang, Lijie Zhang, Zelin Zhang, Qianna Li, Qi Wang, Zhenyu Han, Yulan Huang, Honglin Liu, Shengfeng Hu, Chaoying Zhou, Qian Wen and Li Ma*[*]

Institute of Molecular Immunology, School of Laboratory Medicine and Biotechnology, Southern Medical University, Guangzhou, China

OPEN ACCESS

Edited by:
Veronica Schmitz, Oswaldo Cruz Foundation (Fiocruz), Brazil

Reviewed by:
Catherine W. M. Ong, National University of Singapore, Singapore
Samantha Lynn Bell, Rutgers Biomedical and Health Sciences, United States

***Correspondence:**
Li Ma
mali_61648322@smu.edu.cn

[†]*These authors have contributed equally to this work*

Specialty section:
This article was submitted to Microbial Immunology, a section of the journal Frontiers in Immunology

Received: *03 August 2021*
Accepted: *15 December 2021*
Published: *12 January 2022*

Citation:
Zhou X, Lie L, Liang Y, Xu H, Zhu B, Huang Y, Zhang L, Zhang Z, Li Q, Wang Q, Han Z, Huang Y, Liu H, Hu S, Zhou C, Wen Q and Ma L (2022) GSK-3α/β Activity Negatively Regulates MMP-1/9 Expression to Suppress Mycobacterium tuberculosis Infection. Front. Immunol. 12:752466. doi: 10.3389/fimmu.2021.752466

Tuberculosis (TB) caused by *Mycobacterium tuberculosis* (Mtb) infection is the deadliest infectious disease and a global health problem. Macrophages (Mφs) and neutrophils that can phagocytose Mtb represent the first line of immune response to infection. Glycogen synthase kinase-3α/β (GSK-3α/β) represents a regulatory switch in host immune responses. However, the efficacy and molecular mechanisms of how GSK-3α/β interacts with Mtb infection in Mφs remain undefined. Here, we demonstrated that Mtb infection downregulated GSK-3α/β activity and promoted matrix metalloproteinase-1 (MMP-1) and MMP-9 expressions in Mφs derived from acute monocytic human leukemia THP-1 cells (THP-1-Mφs). We confirmed the upregulation of MMP-9 expression in tissues of TB patients compared with patients of chronic inflammation (CI). In THP-1-Mφs and C57BL/6 mice, GSK-3α/β inhibitor SB216763 significantly increased MMP-1/9 production and facilitated Mtb load, while MMP inhibitors blocked MMP-1/9 expression and Mtb infection. Consistently, GSK-3α/β silencing significantly increased MMP-1/9 expression and Mtb infection, while overexpression of GSK-3α/β and constitutive activated GSK-3α/β mutants significantly reduced MMP-1/9 expression and Mtb infection in THP-1-Mφs. MMP-1/9 silencing reduced Mtb infection, while overexpression of MMP-1/9 promoted Mtb infection in THP-1-Mφs. We further found that GSK-3α/β inhibition increased Mtb infection and MMP-1/9 expression was blocked by ERK1/2 inhibitor. Additionally, we showed that protein kinase C-δ (PKC-δ) and mammalian target of rapamycin (mTOR) reduced GSK-3α/β activity and promoted MMP-1/9 production in Mtb-infected THP-1-Mφs. In conclusion, this study suggests that PKC-δ-mTOR axis suppresses GSK-3α/β activation with acceleration of MMP-1/9 expression through phospho-ERK1/2. These results reveal a novel immune escape mechanism of Mtb and a novel crosstalk between these critical signaling pathways in anti-TB immunity.

Keywords: ***Mycobacteria tuberculosis*, macrophages, GSK-3α/β, MMP-1, MMP-9**

INTRODUCTION

Tuberculosis (TB) caused by *Mycobacterium tuberculosis* (Mtb) infection remains a global health problem (1). TB pathogenesis is driven by a complex interplay between host immune system and survival strategies of the bacterium. Mtb replicates intracellularly, mainly within innate immune cells including macrophages (Mφs) and neutrophils, which act as the early immune responders against Mtb infection. The successful establishment of long-term Mtb infection rests upon its ability to convert Mφs into a permissive cellular niche to circumvent host immune response, which ultimately leads to the development of TB (2). Therefore, understanding of how Mtb infection regulates host factors may facilitate the development of novel targets for TB therapy.

Glycogen synthase kinase-3α/β (GSK-3α/β) is a multifunctional serine/threonine kinase capable of phosphorylating and inactivating glycogen synthase (GS) (3). Under basal cellular conditions, GSK-3α/β is a constitutively active serine/threonine kinase (3). Upon cellular stimuli, GSK-3α and GSK-3β can be phosphorylated on Serine 21 and Serine 9, resulting in loss of kinase activity. GSK-3α/β plays vital roles in host immune responses through regulating different signaling pathways of immune cells (3, 4). Therefore, the dysregulation of GSK-3α/β has been linked to diverse diseases, including infectious disease, cancer, Alzheimer's disease, bipolar disorder, and diabetes (3). In infectious disease, on one hand, GSK-3α/β activation can be detrimental to the host response against *Francisella tularensis* LVS infection by restraining inflammatory cytokine response (5). On the other hand, GSK-3α/β can be beneficial to the host immune response against virus infection through activating IRF3 and NF-κB signaling pathways and IFN-β induction (6). It is reported that Mtb tyrosine phosphatase PtpA led to dephosphorylation of GSK-3α (7). In human primary dendritic cells (DC), Mtb infection modulated pro- and anti-inflammatory cytokine production through mTOR/GSK-3β axis (8). However, the exact efficacy and molecular mechanisms as how GSK-3α/β interacts with Mtb infection in Mφs remain undefined.

Enzymes of matrix metalloproteinases (MMPs) family play key roles in host immune response against TB (9). Among numerous MMPs secreted from monocytes and macrophages infected with Mtb, MMP-1, MMP-2, MMP-3, MMP-8, and MMP-9 are most extensively studied isotypes with critical roles in host defense against Mtb infection (10). In our study, only expression of MMP-1 and MMP-9 was regulated by GSK-3α/β in Mφs. Most of studies pay close attention to collagen breakdown and alveolar destruction mediated by MMP-1 production from Mφs, and initiation of recruitment of new monocytes to develop granuloma mediated by MMP-9 production (11). MMP-1/9 expression can be regulated by multiple signaling pathways. Specifically, extracellular signal-regulated kinase 1/2 (ERK1/2) has been identified in charge of MMP expression, and the phosphorylation status of ERK1/2 is proposed being regulated by GSK-3 in several diseases (12–16). This raised our curiosity as to how GSK-3α/β interacts with MMP-1/9 and ERK1/2 in combating Mtb infection in Mφs.

Evidence indicates that GSK-3α/β represents a point of convergence of different signal transduction pathways of the immune system (3). Inhibition of mammalian target of rapamycin (mTOR) increased GSK-3β activity to regulate pro- and anti-inflammatory cytokine production in LPS-stimulated Mφs (17). Protein kinase C (PKC) has been identified as a key regulatory factor to stimulate mTOR activation (18). PKC activation can also lead to reduction of GSK-3β activity independent of mTOR to control lysosome (19). Thus, it is of an intriguing question whether PKC-mTOR axis plays a crucial role in regulating GSK-3α/β activity and anti-TB immunity. In this study, we show that Mtb infection downregulates GSK-3α/β activity and promotes MMP-1/9 expression in human Mφs. Further investigation identifies that GSK-3α/β combats Mtb infection through MMP-1/9 production, which is regulated by upstream of PKC-mTOR axis and ERK1/2 phosphorylation. These results revealed a novel immune escape mechanism of Mtb in Mφs and a novel crosstalk mechanism between these critical signaling pathways in anti-TB immunity.

MATERIALS AND METHODS

Ethics Approval

This study was approved by the Ethics Committee of Southern Medical University with written informed consent from all subjects. All patients with active pulmonary TB (PTB), lymphatic TB, and chronic inflammation (CI) enrolled in this study have written informed consent. The protocol was approved by the ethics committee of the Southern Medical University. The animal ethical certification and animal handling procedures were approved by the Animal Experimental Center in Southern Medical University. Highly pathogenic microorganism laboratory management commitment letter was approved by Southern Medical University.

Patients

Patients with active PTB, lymphatic TB, and CI were diagnosed in and recruited from the Guangzhou Chest Hospital (Guangzhou, Guangdong, China). We collected six patients with active PTB (4 males and 2 females), six patients with lymphatic TB (2 males and 4 females), and eleven patients with CI (7 nales and 4 females).

Cell Culture

Human acute monocytic leukemia cells (THP-1) were purchased from CELLCOOK (CC1904, Guangzhou, China) and cultured in RPMI-1640 medium (Corning, NY, USA) containing 10% heat-inactivated FBS in 5% CO_2 cell culture incubator at 37°C. THP-1 cells were stimulated with 100 ng/ml phorbol-12-myristate-13-acetate (PMA) (Pepro Tech, NJ, USA) for 48 h to turn into mature Mφs (THP-1-Mφs). THP-1-Mφs were maintained in complete RPMI-1640 medium without PMA treatment for 24 h for further experiments.

Mycobacteria Culture and Infection

Highly pathogenic microorganism laboratory management commitment letter was approved by Southern Medical University. All Mtb infection experiments have been operated

in BSL-3 lab of Southern Medical University. Mtb strain H37Rv (American Type Culture Collection) was cultured in 7H9 broth (Becton Dickinson, New Jersey, USA) with 10% OADC (0.06% (v/v) oleic acid (SIGMA, St. Louis, MO, USA), 5% albumin (SIGMA, St. Louis, MO, USA), 100 mM glucose (GHTECH, Guangzhou, China), 0.003% catalase (SIGMA, St. Louis, MO, USA), and 145 mM NaCl (GHTECH, Guangzhou, China) at 37°C with 5% CO_2. Grinded the clumps of bacteria into bacterium suspension and measured the concentration of bacteria at OD_{600} absorbance. Mtb at multiplicity of infection (MOI) of 5 has been applied to infect THP-1-Mφs for colony-forming assay (CFU), and MOI of 2 has been used to infect THP-1-Mφs for other experiments. Mtb infected mice are kept in biosafety cabinet. The experimental treatment or anatomical operation was carried out on the negative pressure ultra clean table. The infected animals were carried out in the isolation cover and placed on the plate. The experimental area of infected animals is equipped with an electric steam autoclave to disinfect and sterilize various items. Mice excreta, bedding and residual feed can only be discarded after thorough disinfection and sterilization. After the sacrifice, the mice were sent to animal center of Southern medical university and sterilized by high-pressure disinfection and then sealed and packaged for incineration. Cages and experimental equipment were cleaned after high-pressure sterilization.

Treatment of Reagents in Mφs

THP-1-Mφs were pretreated with specific inhibitor of SB216763 for GSK-3α/β (20 μM) (Selleck, Houston, USA), BB94 for MMPs (20 μM) (Selleck, Houston, USA), SB3CT for MMP-9 (Selleck, Houston, USA), GO6983 for PKCs (1 μM) (Selleck, Houston, USA), rapamycin for mTOR (1 μM) (Selleck, Houston, USA), U0126 for ERK (10 μM) (Selleck, Houston, USA), activator of PMA for PKCs (20 μM) (Selleck, Houston, USA), and dimethylsulfoxide (DMSO) as solvent control for 2 h before Mtb infection for 24 or 48 h.

Cell Viability

The Trans Detect Cell Counting Kit-8 (CCK-8) (TransGene Biotech, Beijing, China) was based on the conversion of a water-soluble tetrazolium salt, and 2-(2-methoxy-4-nitrophenyl)-3-(4-nitrophenyl)-5-(2,4-disulfophenyl)-2H-tetrazolium, monosodium salt (WST-8) was used to detect cytotoxicity of THP-1-Mφs. Cells were cultured in 96-well plates at density of 1×10^5 cells/ml for 24 and 48 h. The culture medium was replaced with fresh complete medium containing 10% CCK-8 solution, followed by further incubation for 1–4 h at 37°C. The Varioskan Flash (Thermo Fisher Scientific, Carlsbad, CA, USA) was used to measure absorbance at 450 and 630 nm within 30 min. The relative cell viability was calculated as a percentage of control values (blank).

Small Interfering RNA Transfection and Transfection

Transient small interfering RNA (siRNA) targeting GSK-3α (NM_019884.2), GSK-3β (NM_001146156.2), PKC-α (NM_002737.3), PKC-β (NM_002738.7), PKC-γ (NM_002739.5), PKC-δ (NM_001354680.2), PKC-ϵ (NM_005400.3), MMP-1 (NM_002421.4), MMP-3 (NC_002422.5), MMP-9 (NM_004994.3) and si-NC (negative control) were synthesized by RiboBio according to NCBI gene database. The siRNA target sequences involved in this study were as follows: GSK-3α (1: GAACCCAGCTGCCTAACAA; 2: GATTGGCAATGGCTCATTT; 3: CAAGTTCCCTCAGATTAAA), GSK-3β (1: GGAAGCTTGTGCACATTCA; 2: GGACTATGTTCCGGAAACA; 3: GGACCCAAATGTCAAACTA), MMP-1 (1: GCTTGAAGCTGCTTACGAA; 2: GGACCATGCCATTGAGAAA; 3: GCACATGACTTTCCTGGAA), MMP-3 (1: GAGAAATCCTGATCTTTAA; 2: GCAAGGACCTCGTTTTCAT; 3: GCCAGGGATTAATGGAGAT), MMP-9 (1: GTACCGCTATGGTTACACT; 2: GGTTCCAACTCGGTTTGGA; 3: GCAACGTGAACATCTTCGA), PKC-α (1: GCACAACGTTTCCTATCCA; 2: GAAGGGTTCTCGTATGTCA; 3: GGACTGGGATCGAACAACA), PKC-β (1: GAAGGACGTTGTGATCCAA; 2: GGATGAAACTGACCGATTT; 3: GCTGCTTTGTGGTGCACAA), PKC-δ (1: GCTTCAAGGTTCACAACTA; 2: GCAAGTGCAACATCAACAA), PKC-γ (1: CTCGGAACCTGACGAAACA; 2: CATCGACGATGCCACGAAT; 3: CCCGTAACCTAATTCCTAT), PKC-ϵ (1: GACGTGGACTGCACAATGA; 2: GAGTGTATGTGATCATCGA; 3: GGGCAAAGATGAAGTATAT). Lipofectamine 2000 (Thermo Fisher Scientific, Carlsbad, CA, USA) and optiMEM (Gibco, Life Technologies, NY, USA) as transfection reagent were used to mix with siRNAs at final concentration of 100 nM. The mixed transfection reagents were incubated at room temperature for 20 min and added dropwise into THP-1-Mφs containing RPMI-1640 medium. After incubation for 4–6 h, the culture medium was replaced with fresh complete medium and cells were incubated for another 48 h for further experiments.

Lentiviral-Mediated Overexpression

The X-tremeGENE HP DNA transfection reagent (Roche, Basel, Switzerland) was used and operated according to the manufacturer's instruction. For GSK-3α/β overexpression, pSLenti-SFH-EGFP-P2A-Puro-CMV-MCS-3xFLAG-WPRE vector (OBiO Technology, Shanghai, China) was used as empty lentivirus, pSLenti-SFH-EGFP-P2A-Puro-CMV-GSK3A(S21A)/GSK3B(S9A)-3xFLAG-WPRE were used for GSK-3α/β and GSK-3αS21A/GSK-3βS9A overexpression. For MMP-1, MMP-2, and MMP-9 overexpression, pLVX-Puro vector of MMP-1 (NM_002421.4), MMP-2 (NM_004994.3), and MMP-9 (NM_004994.3) with C-terminal Flag tag were used (OBiO Technology, Shanghai, China). Third-generation lentiviral packaging system with helper plasmids of pLP1, pLP2, and pLP/VSVG were applied. Lentiviral pseudoparticles were generated in HEK293T cells, and virus-containing medium was collected after 72 h posttransfection and concentrated with Lenti-Concentin Virus Precipitation Solution 5× (exCELL EMB810A-1, Beijing, China). Lentiviral pseudoparticles were stored at −80°C for further experiments. THP-1 cell lines were cultured in 6-well plates at a density of 5×10^5 cells per well and transduced with lentiviral pseudoparticles at 37°C for 72 h. After culturing the passaging cells for 7 days, we collected all the cells by flow cytometry (BD Biosciences, San Jose, CA, USA) to select

the green fluorescent protein (GFP)-marked positive ones. GFP-marked THP-1 cells transfected with empty lentivirus has been used as control cells.

RNA Extraction and Quantitative Real-Time PCR

RNA of macrophages lysed with TRIzol (Thermo Fisher Scientific, Carlsbad, CA, USA) was quantified by Nanodrop 2000c (Thermo Fisher Scientific, Carlsbad, CA, USA) and reverse transcribed into the same amount of cDNA by the TransScript One-Step gDNA Removal and cDNA Synthesis SuperMix kit (TransGen Biotech, China). mRNA level of individual gene was quantified by quantitative real-time PCR (qRT-PCR) using a SYBR® Premix Ex TaqTM II (Tli RNaseH Plus) (TaKaRa, Beijing, China) on a LightCycler 480 thermocycler (Roche, Basel, Switzerland). After initial denaturation at 95°C for 2 min, targeted genes were amplified and quantitated (95°C for 15 s, 60°C for 15 s) for 45 cycles, followed by a final extension at 68°C for 20 s. After normalizing all PCR products with respect to GAPDH transcript and using the $2^{-\triangle\triangle CT}$ method to calculate, the expression level of individual genes can be expressed as fold change. The complete primers are GAPDH (F: GTCTCCTCTGAC TTCAACAGCG, R: ACCACCCTGTTGCTGTAGCCAA); TNF-α: (F: CTCTTCTGCCTGCTGCACTTTG, R: ATGGGCTACAGGCTTGTCACTC); IL-1β (F: CCACAGAC CTTCCAGGAGAATG, R: GTGCAGTTCAGTG ATCGTACAGG); IL-6 (F: AGACAGCCACTCACCTCT TCAG, R: TTCTGCCAGTGCCTCTTTGCTG); IL-10 (F: TCTCCGAGATGCCTTCAGCAGA, R: TCAGACAA GGCTTGGCAACCCA); IFN-α (F: TGGGCTGTGATCTG CCTCAAAC, R: CAGCCTTTTGGAACTGGTTGCC); IFN-β (F: CTTGGATTCCTACAAAGAAGCAGC, R: TCCTC CTTCTGGAACTGCTGCA); IFN-γ (F: GAGTGTGGAGA CCATCAAGGAAG, R: TGCTTTGCGTTGGACATTCAA GTC); IRF1 (F: GAGGAGGTGAAAGACCAGAGCA, R: TAGCATCTCGGCTGGACTTCGA); Mx1 (F: GGCTGTT TACCAGACTCCGACA, R: CACAAAGCCTGGCAGC TCTCTA); Rsad2 (F: CCAGTGCAACTACAAATGCGGC, R: CGGTCTTGAAGAAATGGCTCTCC); ISG15 (F: CTCTGAGCATCCTGGTGAGGAA, R: AAGGTCAG CCAGAACAGGTCGT); MMP-1 (F: ATGAAGCAGCCCA GATGTGGAG, R: TGGTCCACATCTGCTCTTGGCA); MMP-2 (F: AGCGAGTGGATGCCGCCTTTAA, R: CATTCCAGGCATCTGCGATGAG); MMP-3 (F: CACTCA CAGACCTGACTCGGTT, R: AAGCAGGATCACAGT TGGCTGG); MMP-8 (F: CAACCTACTGGACCAAGCACAC, R: TGTAGCTGAGGATGCCTTCTCC); MMP-9 (F: GCCAC TACTGTGCCTTTGAGTC, R: CCCTCAGAGAATCG CCAGTACT); GSK-3α (F: GCAGATCATGCGTAAGCTG GAC, R: GGTACACTGTCTCGGGCACATA); GSK-3β (F: CCGACTAACACCACTGGAAGCT, R: AGGATGGTAG CCAGAGGTGGAT); PKC-α (F: GCCTATGGCGTCCTGTTG TATG, R: GAAACAGCCTCCTTGGACAAGG); PKC-β (F: GAGGGACACATCAAGATTGCCG, R: CACCAAT CCACGGACTTCCCAT); PKC-γ (F: CCGCCTGTATTTCG TGATGGAG, R: CGATAGCGATTTCTGCCGCGTA); PKC-δ (F: GCTGACACTTGCCGCAGAGAAT, R: GCCTTTG TCCTGGATGTGGTAC); PKC-ϵ (F: AGCCTCGTTCACGG TTCTATGC, R: GCAGTGACCTTCTGCATCCAGA).

Western Blot Analysis

After washing twice with PBS, cells were lysed with basic lysis buffer (composed of 455 mM Tris HCl (pH 6.8) (Sangon Biotech, Shanghai, China), 41.6 mM SDS (Zhuosheng Biotech, Shanghai, China), 26.9 μM bromophenol blue (Solarbio, Beijing, China), 30% (v/v) glycerol (SIGMA, St. Louis, MO, USA), and 10 μM DL-dithiothreitol (DTT) (SIGMA, St. Louis, MO, USA) to obtain total proteins. The proteins were denatured by heating at 100°C for 5 min, separated by SDS-PAGE and transferred to the PVDF membrane. Then the target protein membranes were cut out according to the precision plus protein TM standards (BIORAD, Hercules, CA, USA). Membranes were blocked with PBS-T (0.1% Tween-20 (GHTECH, Guangzhou, China) containing 5% (w/v) BSA (SIGMA, St. Louis, MO, USA) at room temperature for 1 h and inoculated with primary antibodies at 4°C for 16 h with gentle shaking. After washing for three times with PBS-T, the membranes were incubated with HRP-conjugated goat antirabbit or goat antimouse secondary antibodies (Cell Signaling Technology, Danvers, MA, USA) at room temperature for 1 h and washed for another three times with PBS-T. The separated protein band was visualized using Immobilon Western Chemiluminescence HRP substrate (ECL; Thermo Fisher Scientific, USA). Each measurement was performed in triplicate with similar results, and one representative result was shown. The integrated density of blotting bands was quantitatively analyzed by Image J software (National Institutes of Health, Bethesda, MD, USA) and normalized to 1.0 with GAPDH as a control. The antibodies used in this study are listed in **Supplementary Table S1**.

Enzyme-Linked Immunosorbent Assay

Supernatants were harvested from the infected cells and mouse tissues centrifuged at 12,000 × g for 10 min to remove cell debris after grinding. Samples were assayed using enzyme-linked immunosorbent assay (ELISA) kits for MMP-1 (MultiSciences, Hangzhou, China) and MMP-9 (MultiSciences, Hangzhou, China). All procedures were performed according to the manufacturer's instructions. The ELISA kits were equilibrated to room temperature in advance, and after dissolving and diluting the standard according to the standard curve, the sample supernatant was diluted to appropriate multiple dilutions. Diluted sample supernatant at 100 μl and the standard solution at different concentrations were added to the corresponding wells. Antibody solution (50 μl, 1:100) was then added to each well and all the samples were incubated at room temperature for 2 h. After washing for six times with washing buffer, enzyme solution (100 μl, 1:100) was added to each well and incubated at room temperature for 45 min. After washing repeatedly for six times, chromogenic substrate (100 μl) was added to all wells and incubated for 5–15 min avoiding light. Finally, 100 μl stop solution was added to stop the reaction. We measured the absorbance at 450 and 630 nm within 30 min by a Varioskan Flash (Thermo Fisher Scientific, Carlsbad, CA, USA).

The concentration of the samples was calculated according to the standard curve and the OD value of the samples.

Immunohistochemistry Assay

Archived human lymph node and lung tissues were fixed in 10% formalin, embedded in paraffin wax and deparaffinized in xylene. For immunohistochemical staining, parraffin sections (4 μm) were heated with 0.01 M citric acid of pH 6.0 for 3 min for antigen retrieval. The slices were treated with 3% H_2O_2 for 10 min to react with endogenous peroxidase. Sections were incubated with MMP-9 (1:500, Abcam Cambridge, UK) Ab overnight and secondary biotinylated anti-mouse (1: 50) followed by DAB substrate (UniCureLab). The slices were counterstained by hematoxylin and dehydrated by gradient alcohol. For slices of lungs, because the cells are relatively scattered and few, immunohistochemical staining for MMP-9 was quantified by positive cell rate analysis by using Image Pro Plus 6.0 software (Media Cybernetics, Inc., Rockville, MD, USA). We analyzed the number of positive cells with the same brown-yellow cell nucleus and the total number of cells in each photo, then the percentage of positive cells was calculated. Positive rate (%) is equal to the number of positive cells divided with the total number of cells multiplied with 100. For slices of lymph nodes, because the density and quantity of cells are relatively large, immunohistochemical staining for MMP-9 was quantified by area density analysis by using Image Pro Plus 6.0 software (Media Cybernetics, Inc., Rockville, MD, USA). The accumulated optical density (IOD) and the area of tissue pixels (area) of each photo are obtained. The area density = IOD/area. Higher area density is representative of the higher positive expression level. The antibodies used in this research are listed in **Supplementary Table S1**.

Colony-Forming Unit Assay

THP-1-Mφs were infected with H37Rv of MOI = 5 for 1 h at 37°C (5% CO_2). Cells were then washed with PBS for three times to remove extracellular bacteria, and complete medium was added to culture at different time points. Cells were lysed in ddH_2O containing 0.01% Triton X-100. After serial dilution, 50 μl bacteria solution (1:1,000) was evenly spread on the 7H10 agar plate (Becton Dickinson, New Jersey, USA) and then cultured for 21–28 days at 37°C (5% CO_2). To detect the direct effect of inhibitors on Mtb infection, H37Rv of 1×10^6 was incubated with various inhibitors for 2 h. Mtb suspension was then washed with PBS for three times to remove inhibitors, and complete medium was added to culture at 48 h. A total of 50 μl bacterial solution (1:1,000) was evenly spread on the 7H10 agar plate (Becton Dickinson, New Jersey, USA) and then cultured for 21–28 days at 37°C (5% CO_2).

Animal Treatment

Wild-type female C57BL/6 mice (6 weeks old) were obtained from the Laboratory Animal Center of Southern Medical University. Mice were randomly divided into four groups (n = 4/group) as follows: (1) intraperitoneal saline + DMSO, (2) intraperitoneal saline + SB216763 (20 mg/kg) (Selleck, Houston, TX, USA) dissolved in DMSO, (3) intraperitoneal saline + SB3CT (20 mg/kg) (Selleck, Houston, TX, USA) dissolved in DMSO, and (4) intraperitoneal saline + SB3CT (20 mg/kg) + SB216763 (20 mg/kg) dissolved in DMSO. To establish a pulmonary tuberculosis model, mice were injected H37Rv intraperitoneally with 1×10^6 CFU/mouse on day 0. SB216763-treated mice were administered with saline + SB216763 dissolved in DMSO intravenously at day 0 and then intraperitoneally twice a week until day 28. SB3CT-treated mice were intraperitoneally injected with saline + SB3CT dissolved in DMSO daily until day 28. The control group was injected with saline + DMSO as vehicle control. The mice were sacrificed on days 7 and 28, and lung and spleen tissues were grinded for CFU assay. The supernatant of lung and spleen tissue grinding was used to detect the expression of MMP-9 by ELISA assay.

Statistical Analysis

Statistical analysis was performed with Graphpad Prism 5.0 Software. Results are presented as means ± SD or means ± SEM of at least three independent experiments. Statistical analysis was performed using unpaired Mann-Whitney U test. $^*p \leq 0.05$ and $^{**}p \leq 0.01$ were considered statistically significant.

RESULTS

GSK-3α/β Suppresses Mtb Infection in Mφs and in Mice

To investigate the role of GSK-3α/β activity in TB, we first detected the expression of phosphorylated GSK-3α/β (Ser21/9 and Tyr216/279) and phosphorylated GS in THP-1-Mφs upon Mtb infection by Western blot assay. The results showed that both Ser21/9 and Tyr216/279 phosphorylation of GSK-3α/β were significantly decreased, making it difficult to estimate how GSK-3α/β activity is affected by Mtb infection. We then found that Mtb infection decreased the ratio of phosphorylation level (activated form) to total protein expression of GS, indicating GSK-3α/β activity was inhibited by Mtb infection (**Figure 1A**). Next, GSK-3α/β inhibitor SB216763 was used to evaluate the effect of GSK-3α/β on Mtb infection. SB216763 suppressed GSK-3α/β activity indicated by the decreased ratio of activated GS to total GS upon Mtb infection at different time points (**Figure 1B**). CFU assay showed that SB216763 significantly increased Mtb infection in THP-1-Mφs upon 48 h of infection (**Figure 1C**). These results were found not related to enhancement of cell proliferation with SB216763 treatment by CCK-8 assay (**Supplementary Figure S1A**) or direct increase of Mtb infection (**Supplementary Figure 1B**). Two siRNAs targeting GSK-3α and GSK-3β were used to knock down GSK-3α and GSK-3β. As expected, GSK-3α and GSK-3β silencing decreased mRNA and protein expression without off-target effects between each other, and also decreased GSK-3α/β activity indicated by the ratio of activated GS to total GS upon 48 h of Mtb infection (**Figure 1D**). Correspondingly, GSK-3α and GSK-3β silencing led to a significant increase of Mtb load upon 48 and 72 h Mtb infection (**Figure 1E**). Subsequently, we constructed THP-1-Mφs that stably expressed GSK-3α and GSK-3β, and constitutively

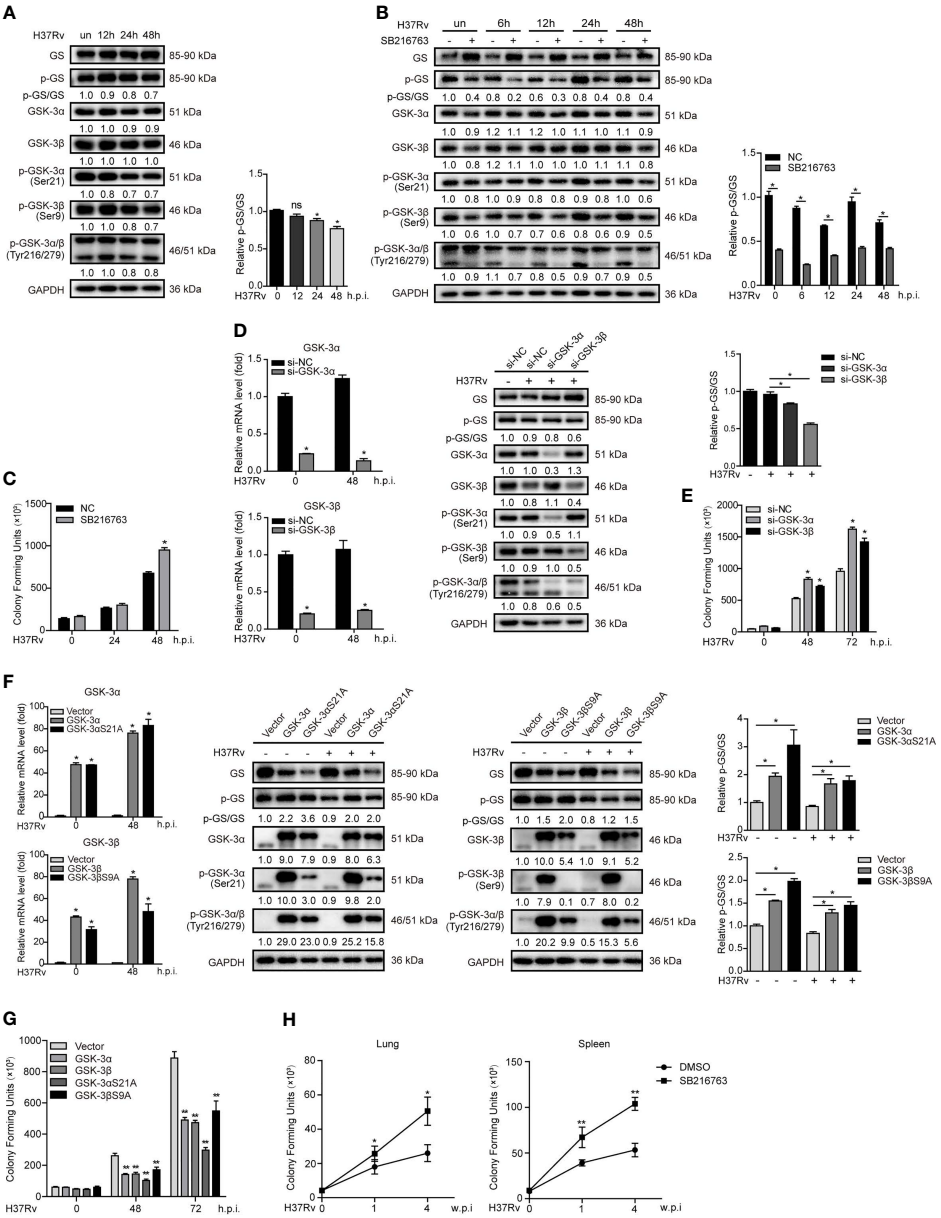

FIGURE 1 | GSK-3α/β suppresses Mtb infection in Mφs and in mice. **(A)** Expressions of GSK-3α/β, phospho-GSK-3α/β, GS, and phospho-GS were detected in THP-1-Mφs upon Mtb infection at indicated time points by Western blot analysis. The ratio of expression of phosphorylated GS to total GS is shown in graph. **(B)** Expressions of GSK-3α/β, phospho-GSK-3α/β, GS, and phospho-GS were detected in THP-1-Mφs with pretreatment of 20 μM SB216763 for 2 h upon Mtb infection at indicated time points by Western blot analysis. The ratio of expression of phosphorylated GS to total GS is shown in graph. **(C)** The intracellular mycobacteria load was detected in THP-1-Mφs with pretreatment of SB216763 at 24 and 48 h.p.i. of Mtb by CFU assay (means ± SD, $n = 3$ independent experiments with each 4 replicates). **(D)** GSK-3α- and GSK-3β-silenced THP-1-Mφs were detected for GSK-3α/β mRNA expression by qRT-PCR, and expressions of GSK-3α/β, phospho-GSK-3α/β, GS, and phospho-GS by Western blot analysis upon 48 h of Mtb infection (means ± SD, $n = 3$ independent experiments with each 4 replicates). The ratio of expression of phosphorylated GS to total GS is shown in graph. **(E)** The intracellular Mtb load was determined by CFU analysis in GSK-3α/β-silenced THP-1-Mφs at 48 and 72 h.p.i. of Mtb (means ± SD, $n = 3$ independent experiments with each 4 replicates). **(F)** THP-1-Mφs overexpressing GSK-3α, GSK-3β, GSK-3αS21A, and GSK-3βS9A were detected for GSK-3α/β mRNA expression by qRT-PCR, and expressions of GSK-3α/β, phospho-GSK-3α/β, GS, and phospho-GS by Western blot analysis upon 48 h of Mtb infection (means ± SD, $n = 3$ independent experiments with each 4 replicates). The ratio of expression of phosphorylated GS to total GS is shown in graph. **(G)** The intracellular bacteria load was detected by CFU analysis in THP-1-Mφs overexpressing GSK-3α, GSK-3β, GSK-3αS21A, and GSK-3βS21A at 48 and 72 h.p.i. of Mtb (means ± SD, $n = 3$ independent experiments with each 4 replicates). **(H)** Mice infected of H37Rv were treated with SB216763 (20 mg/kg, $n = 5$) or DMSO ($n = 5$), and the bacterial load of lungs and spleens were detected by CFU analysis at 1 and 4 weeks postinfection (means ± SD, $n = 3$ independent experiments with each 4 replicates). For Western blot assay, GAPDH served as internal control. Data presented are from one of at least three independent experiments with similar results. The numbers below immunoblot correspond to band-integrated density ration of target protein to GAPDH. $^*p \leq 0.05$ and $^{**}p \leq 0.01$ were considered statistically significant. SB216763: GSK-3α/β inhibitor.

active forms of GSK-3α/β (GSK-3αS21A, GSK-3βS9A) with lentiviral vectors. Overexpressing both wildtype and mutations of GSK-3α/β potently increased levels of mRNA, protein, and the ratio of activated GS to GS (**Figure 1F**) and significantly attenuated intracellular Mtb infection upon 48 and 72 h of infection (**Figure 1G**). These results were not due to the off-target effect of GSK-3α and GSK-3β overexpression because they did not interact with each other by detecting their protein expression respectively (**Supplementary Figure S1C**). Moreover, both wildtype and mutations of GSK-3α/β could inhibit Mtb infection induced by SB216763 treatment for 48 h (**Supplementary Figure S1D**).

We further investigate the effects of GSK-3α/β on Mtb infection in mice. CFU assay showed that SB216763 treatment led to significant increase of bacterial load in lungs and spleens of mice after 1 and 4 weeks of Mtb infection (**Figure 1H**). These data indicated that Mtb infection suppressed in GSK-3α/β plays an important role in Mtb eradication in macrophages and in mice.

GSK-3α/β Inhibits MMP-1/9 Expression in Mtb-Infected Mφs

Autophagy, proinflammatory, and anti-inflammatory cytokines including interferons (IFNs) and IFN-stimulated genes (ISGs) are important host immune responses downstream of GSK-3α/β signaling (2). Upon SB216763 treatment, the conversion of LC3-I to LC3-II indicated by ratio of LC3-II/LC3-I expression was decreased at 8 and 12 hours postinfection (h.p.i.), and modestly increased at 48 h.p.i. Expression of p62 protein increased at 12, 24, and 48 h.p.i. (**Supplementary Figure S2A**). These results indicated that GSK-3α/β activity irregularly regulated autophagy. Expression of IL-6, TNF-α, IL-1β, and IL-10 mRNA was detected in Mtb-infected THP-1-Mφs at 4, 8, 12, 24, and 48 h.p.i. with SB216763 treatment. We found that expression of IL-6 and TNF-α significantly decreased at 48 h.p.i.; however, expression of IL-1β and IL-10 significantly increased at 24 and 48 h.p.i. These cytokines were irregularly regulated by SB216763 treatment (**Supplementary Figure S2B**). We further demonstrated that expression of IFN-α and IFN-γ, as well as Mx1, Rsad2, and ISG15, was not influenced by SB216763 treatment. IFN-β and IRF1 expressions were significantly decreased at 48 h.p.i. (**Supplementary Figure S2C**). Our previous study showed that IRF1 did not affect MMP expression (20). We speculated that GSK-3α/β suppressing Mtb infection might be independent of autophagy, inflammatory cytokine production, and IFN signaling. To further investigate how GSK-3α/β activity affects Mtb infection, MMPs including expression of MMP-1, MMP-2, MMP-3, MMP-8, and MMP-9 were analyzed. We found that Mtb infection significantly increased MMP-1, MMP-3, MMP-8, and MMP-9 but decreased MMP-2 mRNA expression with time (**Supplementary Figure S3A**). Next, we observed that mRNA expression of MMP-1, MMP-3, and MMP-9 was significantly increased by GSK-3α and GSK-3β silencing in THP-1-Mφs upon Mtb infection; however, MMP-3 protein expression was not influenced (**Supplementary Figures S3B, C**). Additionally, MMP-3 silencing did not affect Mtb infection in THP-1-Mφs (**Supplementary Figures S3D, E**). For this reason, we further investigate the molecular mechanism of how GSK-3α/β regulates MMP-1 and MMP-9 upon Mtb infection. We further observed that SB216763 treatment resulted in significant increase of intracellular mRNA and protein expression as well as extracellular supernatant production of MMP-1 and MMP-9 (**Figure 2A**). Inversely, GSK-3α/β overexpression (**Figure 2B**) and its constitutively active forms (GSK-3αS21A, GSK-3βS9A) (**Figure 2C**) significantly decreased intracellular expression and supernatant production of MMP-1 and MMP-9 in Mtb-infected THP-1-Mφs. Subsequently, we demonstrated that SB216763 treatment could decrease the ratio of activated GS to total GS caused by GSK-3α/β and GSK-3αS21A/GSK-3βS9A overexpression, while SB216763 treatment restored intracellular expression and supernatant production of MMP-1 and MMP-9 reduced by GSK-3α/β and GSK-3αS21A/GSK-3βS9A overexpression in THP-1-Mφs (**Figures 2D–F**). These results suggest that GSK-3α/β activation inhibits MMP-1/9 expression in Mtb infection in Mφs.

GSK-3α/β Suppresses Mtb Infection Through Inhibiting MMP-1 and MMP-9 Expressions

Next, we found that Mtb infection significantly increased intracellular and supernatant MMP-1 and MMP-9 expressions in a time-dependent manner in THP-1-Mφs (**Figure 3A**). Increased MMP-9 protein expression has also been observed in lungs of six patients with pulmonary tuberculosis and in lymph nodes of six patients with lymphatic tuberculosis, compared with that in patients of chronic inflammation by immunohistochemistry analysis (**Figure 3B**). These results suggested that MMP-1/9 might play key roles in host response against Mtb infection. We applied BB94, which is a broad spectrum for MMPs including MMP-1/9, to further explore direct effect of MMP-1/9 on tuberculosis. As expected, BB94 reduced Mtb-induced intracellular and supernatant MMP-1 and MMP-9 expressions (**Figure 3C**). CFU assay showed that BB94 treatment significantly decreased intracellular Mtb infection (**Figure 3D**). We exclude the possibility that BB94 inhibited cell growth to suppress Mtb infection because BB94 treatment did not affect cell proliferation detected by CCK-8 assay (**Supplementary Figure S1A**). BB94 did not decrease Mtb infection directly as detected by CFU assay (**Supplementary Figure S1B**). Three siRNAs targeting MMP-1/9 were transfected in THP-1-Mφs, and MMP-1/9 silencing showed potent decrease of MMP-1/9 mRNA and protein expression (**Figure 3E**). CFU assays showed that MMP-1/9 silencing significantly decreased bacterial load in THP-1-Mφs at 48 h postinfection (**Figure 3F**). Correspondingly, overexpression of MMP-1, MMP-2, and MMP-9 in THP-1-Mφs showed a significant increase of MMP-1, MMP-2, and MMP-9 expression (**Figure 3G**), but only MMP-1 and MMP-9 overexpression showed a significant increase of Mtb infection detected by CFU assay (**Figure 3H**). Next, the association of GSK-3α/β with MMP-1/9 in Mtb-infected Mφs and the effect of MMP-1/9 on Mtb infection prompted us to further explore whether GSK-3α/β inhibits Mtb

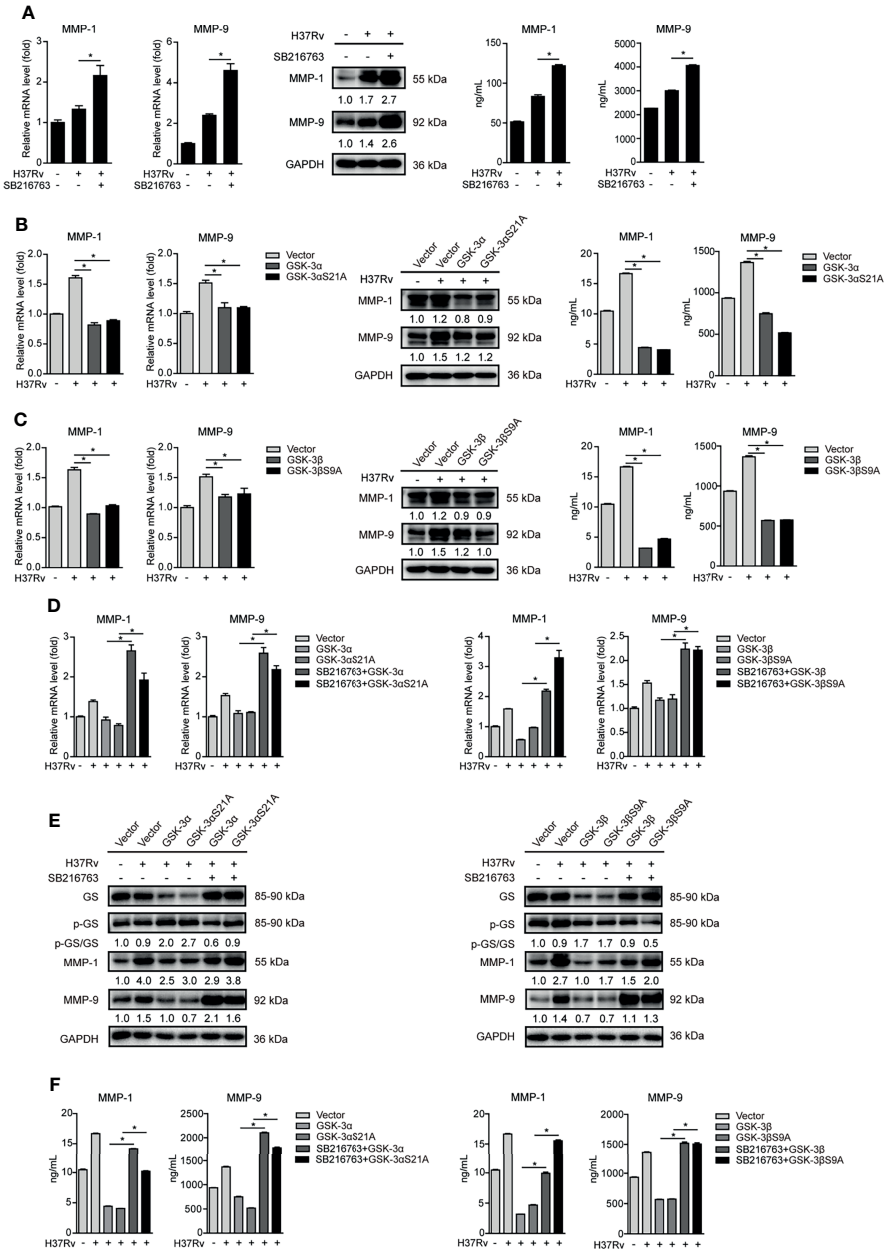

FIGURE 2 | GSK-3α/β inhibits MMP-1/9 expression in Mtb-infected Mφs. **(A)** Intracellular mRNA, protein expression, and secretion of MMP-1/9 were detected in THP-1-Mφs pretreated with SB216763 for 2 h before 48 h of Mtb infection by qRT-PCR, Western blot, and ELISA analyses (means ± SD, $n = 3$ independent experiments with each 4 replicates). **(B, C)** Intracellular mRNA, protein expression, and secretion of MMP-1/9 were detected in THP-1-Mφs overexpressing GSK-3α, GSK-3αS21A, GSK-3β, and GSK-3βS9A with H37Rv infection for 48 h by qRT-PCR, Western blot, and ELISA analyses (means ± SD, $n = 3$ independent experiments with each 4 replicates). **(D–F)** SB216763 was used to treat THP-1-Mφs overexpressing GSK-3α, GSK-3αS21A, GSK-3β, and GSK-3βS9A upon 48 h of Mtb infection, and intracellular mRNA, protein expression, and secretion of MMP-1/9 were detected by qRT-PCR, Western blot, and ELISA analyses (means ± SD, $n = 3$ independent experiments with each 4 replicates). For Western blot assay, GAPDH served as internal control. Data presented are from one of at least three independent experiments with similar results. The numbers below immunoblot correspond to band-integrated density ration of target protein to GAPDH. *$p \leq 0.05$ was considered statistically significant. SB216763: GSK-3α/β inhibitor.

infection through inhibiting MMP-1/9 expression. Our results showed that BB94 obviously diminished MMP-1/9 protein expression promoted by SB216763 treatment (**Figure 3I**). Similarly, BB94 treatment significantly blocked the increased intracellular Mtb infection by SB216763 treatment in THP-1-Mφs upon 48 h of Mtb infection by CFU assay (**Figure 3J**). These results suggest that GSK-3α/β activity negatively regulates MMP-1/9 production to facilitate Mtb infection in Mφs.

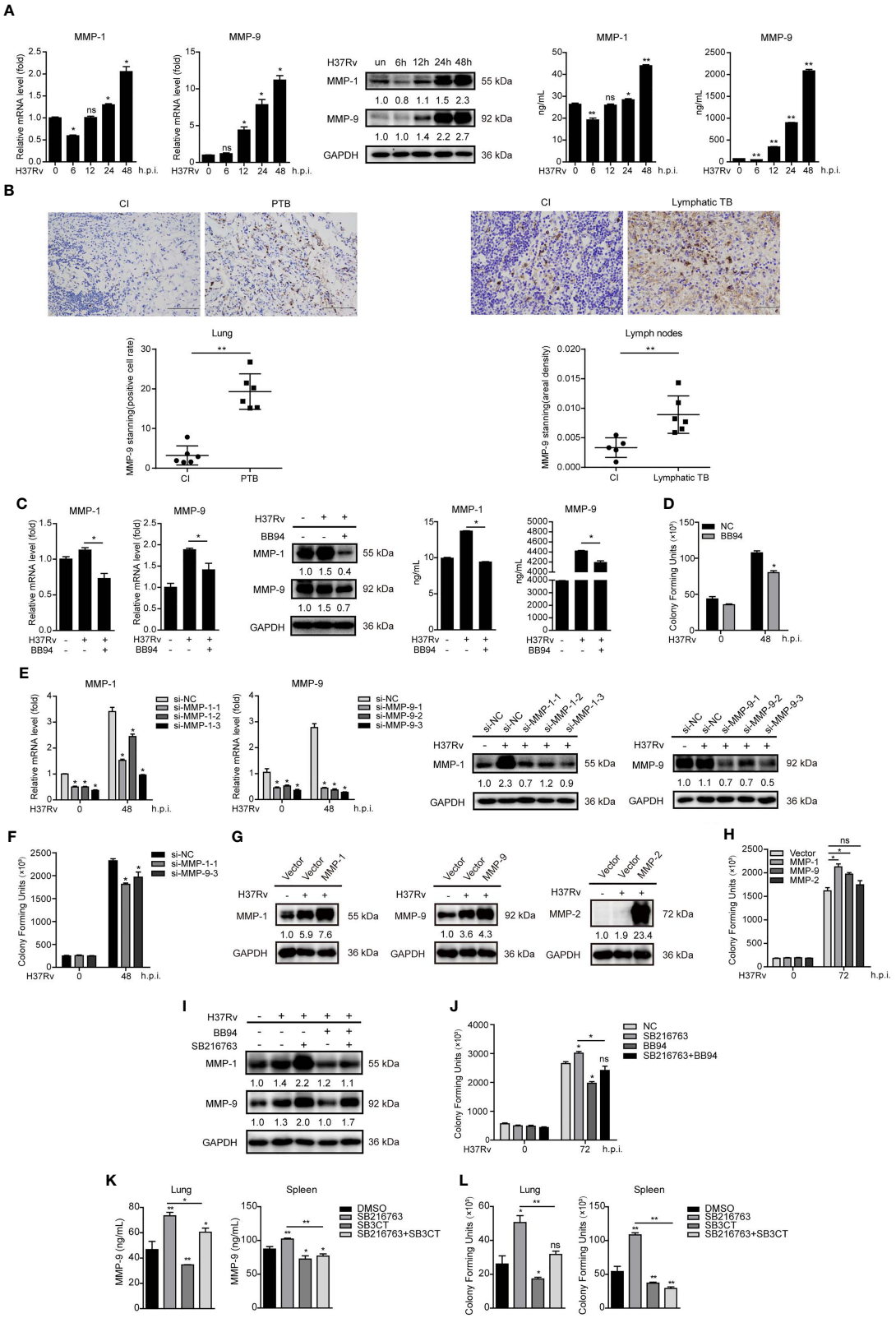

FIGURE 3 | Continued

FIGURE 3 | GSK-3α/β suppresses Mtb infection through inhibiting MMP-1/9 expression. **(A)** Intracellular mRNA, protein expression, and secretion of MMP-1/9 in THP-1-Mφs infected with Mtb at indicated time points were detected by qRT-PCR, Western blot, and ELISA analyses (means ± SD, *n* = 3 independent experiments with each 4 replicates). **(B)** Representative example of immunohistochemical staining for MMP-9 in lung biopsies of six patients with active pulmonary TB (PTB) and six patients with chronic inflammation (CI). Data are quantified by positive cell rate analysis (left). Scale bars, 50 μm. Representative example of immunohistochemical staining for MMP-9 in lymph node biopsies of six patients with lymphatic TB and five patients with chronic inflammation (CI). Data are quantified by area density analysis (right). Scale bars, 20 μm. **(C)** Intracellular mRNA, protein expression, and secretion of MMP-1/9 were analyzed in THP-1-Mφs pretreated with 20 μM BB94 for 2 h at 48 h.p.i. by qRT-PCR, Western blot, and ELISA analysis (means ± SD, *n* = 3 independent experiments with each 4 replicates). **(D)** CFU assay was applied to detect Mtb infection in THP-1-Mφs pretreated with 20 μM BB94 for 2 h at 48 h.p.i. (means ± SD, *n* = 3 independent experiments with each 4 replicates). **(E)** Intracellular mRNA and protein expression of MMP-1/9 were detected in MMP-1- and MMP-9-silenced THP-1-Mφs at 48 h.p.i. by qRT-PCR and Western blot analysis (means ± SD, *n* = 3 independent experiments with each 4 replicates). **(F)** CFU assay was applied to detect intracellular Mtb load in MMP-1 and MMP-9 silencing THP-1-Mφs at 48 h.p.i. (means ± SD, *n* = 3 independent experiments with each 4 replicates). **(G)** MMP-1, MMP-2, and MMP-9 expressions and **(H)** intracellular Mtb infection were detected in THP-1-Mφs with stable overexpression of MMP-1, MMP-2, and MMP-9 by qRT-PCR, Western blot analysis, and CFU assay (means ± SD, *n* = 3 independent experiments with each 4 replicates). **(I)** MMP-1/9 protein expression and **(J)** intracellular Mtb infection were detected in THP-1-Mφs pretreated with SB216763, BB94, or combination for 2 h upon 48 h Mtb infection by Western blot analysis and CFU assay (means ± SD, *n* = 3 independent experiments with each 4 replicates). Mtb-infected mice were treated with DMSO (*n* = 4), SB216763 (20 mg/kg, *n* = 4), SB3CT (20 mg/kg, *n* = 4), and combination of SB216763 with SB3CT (20 mg/kg, *n* = 4) for 4 weeks. **(K)** MMP-9 expression in the supernatant of lungs and spleens were detected by ELISA analysis. **(L)** H37Rv infection of lungs and spleens were detected by CFU assay (means ± SD, *n* = 3 independent experiments with each 4 replicates). For Western blot assay, GAPDH served as an internal control. Data presented are from one of at least three independent experiments with similar results. The numbers below immunoblot correspond to band-integrated density ration of target protein to GAPDH. $^{*}p \leq 0.05$ and $^{**}p \leq 0.01$ were considered statistically significant. BB94, MMP inhibitor; SB3CT, MMP-9 inhibitor; SB216763, GSK-3α/β inhibitor.

As mice do not express MMP-1 orthologue, we further investigated whether the effect of GSK-3α/β on Mtb infection is related to MMP-9 expression in mice (9). Treating with GSK-3α/β inhibitor SB216763 for 4 weeks significantly increased MMP-9 production in the supernatant of lungs and spleens of Mtb-infected mice, whereas MMP-9 inhibitor SB3CT-blocked SB216763 increased MMP-9 expression (**Figure 3K**). Consistently, CFU assay showed that SB3CT significantly decreased bacterial load in the lungs and spleens after 4 weeks of Mtb infection and diminished Mtb infection increased by SB216763 treatment (**Figure 3L**). However, SB3CT did not directly affect Mtb infection as detected by CFU assay (**Supplementary Figure S1B**). These results indicated that GSK-3α/β suppresses Mtb infection through inhibiting MMP-9 expression in mice.

GSK-3α/β Suppresses MMP-1/9 Expression to Inhibit Mtb Infection Through Phospho-ERK1/2

MAPK ERK1/2 is a key regulatory factor in controlling MMP-1/9 expression (21). We found that SB216763 treatment markedly enhanced phosphorylation of ERK1/2 upon Mtb infection at different time points in THP-1-Mφs (**Figure 4A**). To investigate whether GSK-3α/β suppresses MMP-1/9 expression and Mtb infection through ERK1/2 phosphorylation, we used ERK1/2 inhibitor U0126 to treat THP-1-Mφs. The results showed that inhibition of ERK1/2 phosphorylation dramatically suppressed intracellular and supernatant MMP-1/9 expression upon Mtb infection for 48 h (**Figure 4B**). Most importantly, intracellular and supernatant MMP-1/9 expressions induced by SB216763 were totally abolished by U0126 treatment (**Figure 4C**). Consistently, U0126 treatment blocked the increase of Mtb infection mediated by SB216763 treatment at 48 h.p.i. (**Figure 4D**). U0126 or its combination with SB216763 did not affect cell proliferation determined by CCK-8 assay (**Supplementary Figure S1A**). U0126 and SB216763 did not directly influence Mtb infection as detected by CFU assay (**Supplementary Figure S1B**). These results suggest that GSK-3α/β exerts antimicrobial effect through negatively regulating ERK1/2 phosphorylation and subsequent MMP-1/9 expression in Mφs.

MTOR Inhibits GSK-3α/β Activity to Promote Phospho-ERK1/2 Mediated MMP-1/9 Expression During Infection

MTOR has been reported as an important moderating factor of GSK-3α/β activity (22). To investigate whether mTOR participates in regulating GSK-3α/β activity and MMP-1/9 expression, we pretreated THP-1-Mφs with rapamycin of mTOR inhibitor. The results showed that rapamycin suppressed mTOR phosphorylation and intracellular and supernatant MMP-1/9 expressions but promoted GSK-3α/β activity indicated by the increased ratio of activated GS to total GS (**Figure 5A**). Furthermore, we demonstrated that MMP-1/9 expression and ERK1/2 phosphorylation inhibited by rapamycin were restored with SB216763 treatment while rapamycin increased GSK-3α/β activity was reduced with SB216763 treatment (**Figure 5B**). Moreover, the recovery effect of SB216763 treatment on MMP-1/9 expression inhibited by rapamycin was further blocked by U0126 treatment (**Figure 5C**). These results were found not to be related to regulatory cell proliferation with SB216763, rapamycin, or/and U0126 treatment (**Supplementary Figure S1A**). These results suggested that mTOR negatively regulated GSK-3α/β activity to promote ERK1/2 phosphorylation mediated MMP-1/9 expression in Mtb-infected Mφs.

PKC-δ-mTORC Axis Negatively Regulated GSK-3α/β Activity to Promote Phospho-ERK1/2 Mediated MMP-1/9 Expression

It has recently been reported that PKC kinase activity is required for mTOR activation (23), thus we further studied the relationship between PKC and mTOR in regulating GSK-3α/β activity and MMP-1/9 expression. We exploited pan-PKC inhibitor GO6983

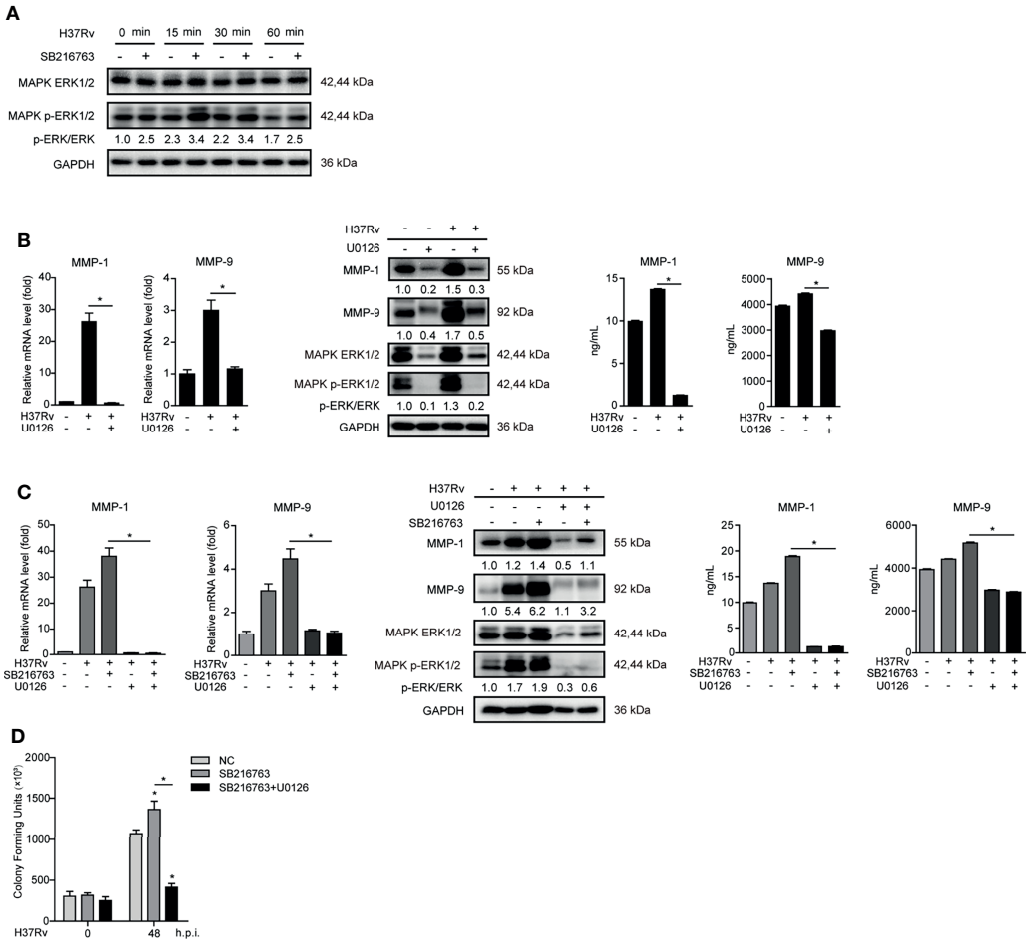

FIGURE 4 | GSK-3α/β suppressed MMP-1/9 expression to inhibit Mtb infection through phospho-ERK1/2. **(A)** Phosphorylation of GSK-3α/β (Ser21/9 and Tyr216/279) and ratio of total GS to phosphorylated GS were detected 2 h pretreated with U0126 in THP-1-Mφs upon Mtb infection at 48 h by Western blot analysis. Intracellular mRNA, protein expression, and secretion of MMP-1/9 were analyzed in THP-1-Mφs **(B)** pretreated with 10 μM U0126 or **(C)** pretreated with 20 μM SB216763, 10 μM U0126, and combination of both for 2 h at 48 h.p.i. by qRT-PCR, Western blot, and ELISA analysis. Expression of ERK1/2 and phospho-ERK1/2 were detected by Western blot analysis (means ± SD, $n = 3$ independent experiments with each 4 replicates). **(D)** Intracellular Mtb load was measured by CFU assays at 48 h.p.i. (means ± SD, $n = 3$ independent experiments with each 4 replicates). For Western blot assay, GAPDH served as an internal control. Data presented are from one of at least three independent experiments with similar results. The numbers below immunoblot correspond to band-integrated density ration of target protein to GAPDH. *$p \leq 0.05$ was considered statistically significant. U0126, ERK1/2 inhibitor; SB216763, GSK-3α/β inhibitor.

to treat THP-1-Mφs. We observed that GO6983 increased the ratio of activated GS to total GS, and it reduced PKC expression, phosphorylation of mTOR and MMP-1/9 expression, indicating that PKCs function upstream of mTOR signaling to regulate GSK-3α/β activity and MMP-1/9 expression (**Figure 6A**). SB216763-abrogated GO6983 enhanced GSK-3α/β activity and restored GO6983-suppressed ERK1/2 phosphorylation and MMP-1/9 expression (**Figure 6B**). Consistently, PKC agonist PMA increased mTOR phosphorylation and MMP-1/9 expression; however, such elevation of MMP-1/9 expression was blocked by rapamycin treatment (**Figure 6C**). These results were also not related to cell proliferation (**Supplementary Figure S1A**).

Such results prompted us to further explore which PKC subtypes affect GSK-3α/β activity and MMP-1/9 expression. We used different siRNAs targeting various PKC subtypes to knock down PKC-α, PKC-β, PKC-γ, PKC-δ, and PKC-ϵ, respectively, and detected mRNA expression of them in THP-1-Mφs upon Mtb infection. All of them were silenced by their own siRNAs according to significant decrease of mRNAs of PKC-α, PKC-β, PKC-γ, PKC-δ, and PKC-ϵ (**Supplementary Figure S4** and **Figure 7A**). Among these PKC subtypes, only silencing of PKC-δ apparently suppressed mRNA expression of MMP-1/9, while silencing of other PKC subtypes showed no or little effect on MMP-1/9 expression (**Supplemental Figure S4**). We further confirmed that PKC-δ silencing decreased intracellular and supernatant MMP-1/9 expression and mTOR phosphorylation and increased GSK-3α/β activity (**Figures 7A, B**). Furthermore, we found that SB216763 treatment restored ERK1/2 phosphorylation and reduced MMP-1/9 expression *via* PKC-δ silencing (**Figure 7C**). Importantly, such recovery effects

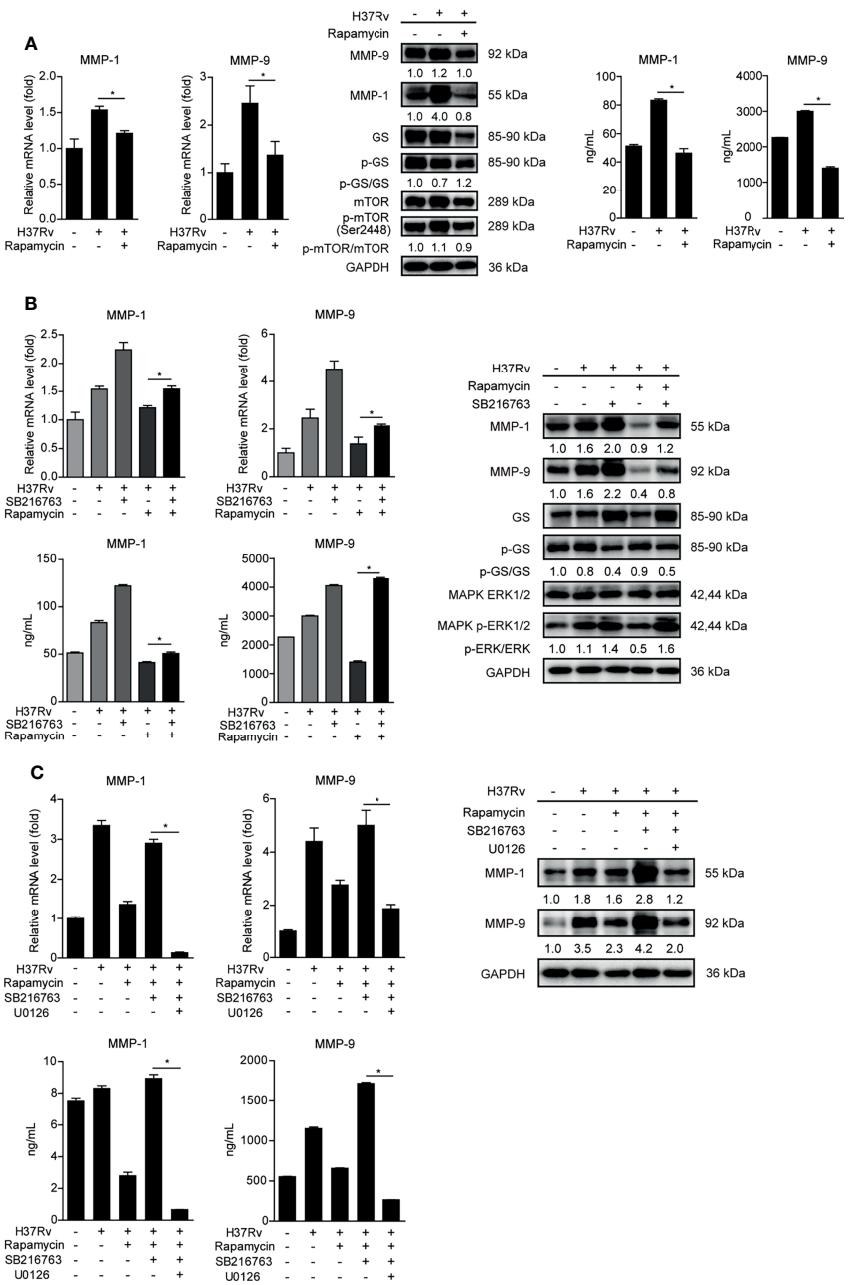

FIGURE 5 | MTOR inhibits GSK-3α/β activity to promote phospho-ERK1/2 mediated MMP-1/9 expression during infection. Intracellular mRNA, protein expression, and secretion of MMP-1/9 were analyzed in THP-1-Mφs with 2 h pretreatment with **(A)** 1 μM rapamycin, **(B)** SB216763, rapamycin, or their combination, **(C)** SB216763, U0126, rapamycin, or their combination by qRT-PCR, Western blot, and ELISA analysis at 48 h postinfection. Expression of GS, ERK1/2, mTOR, and phosphorylation of GS, ERK1/2, and mTOR were detected by Western blot analysis (means ± SD, $n = 3$ independent experiments with each 4 replicates). For Western blot assay, GAPDH served as an internal control. Data presented are from one of at least three independent experiments with similar results. The numbers below immunoblot correspond to band integrated density ration of target protein to GAPDH. *$p \leq 0.05$ was considered statistically significant. U0126, ERK1/2 inhibitor; rapamycin, mTOR inhibitor; SB216763, GSK-3α/β inhibitor.

of SB216763 on MMP-1/9 expression was further blocked by U0126 treatment (**Figure 7D**). Thus, we conclude that PKC-δ-mTOR negatively regulated GSK-3α/β activity to promote phospho-ERK1/2 mediated MMP-1/9 expression during Mtb infection in Mφs.

DISCUSSION

While Mφs and neutrophils represent the first-line responders to Mtb infection, they also provide a major habitat for Mtb to reside in the host. Through a long-term battle with the host, Mtb

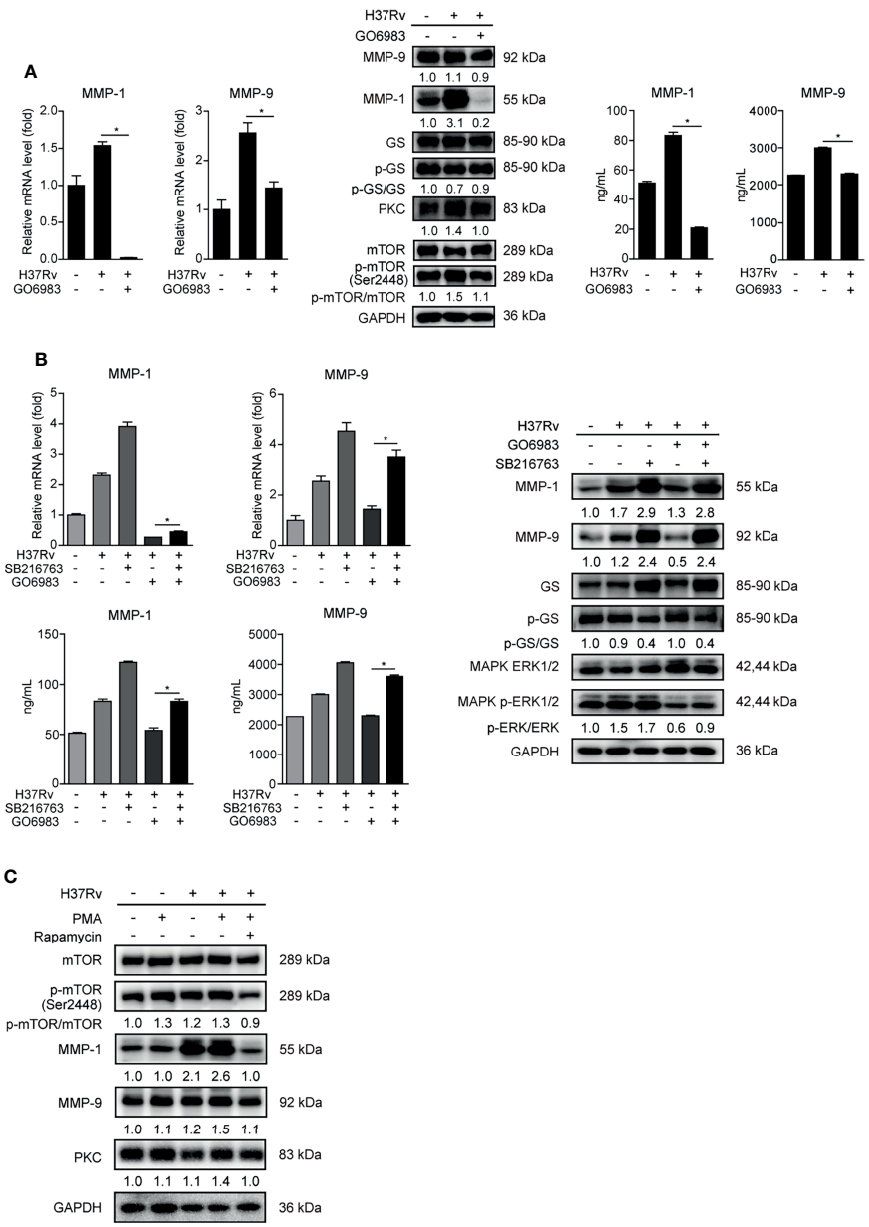

FIGURE 6 | PKCs play a key role in mTOR-regulated GSK-3α/β activity in THP-1-Mφs. Intracellular mRNA, protein expression, and secretion of MMP-1/9 were analyzed in THP-1-Mφs with 2 h pretreatment with **(A)** 1 μM GO6983 and **(B)** SB216763, GO6983, or their combination at 48 h postinfection by qRT-PCR, Western blot, and ELISA analysis. Protein expression of GS, ERK1/2, mTOR, and PKC and phosphorylation of GS, ERK1/2, and mTOR were detected by Western blot analysis (means ± SD, $n = 3$ independent experiments with each 4 replicates). **(C)** Protein expression of MMP-1/9, mTOR, and PKC and phosphorylation of mTOR were detected in THP-1-Mφs pretreated with PMA or the combination of PMA with rapamycin at 48 h.p.i. by Western blot analysis. For Western blot assay, GAPDH served as an internal control. Data presented are from one of at least three independent experiments with similar results. The numbers below immunoblot correspond to band integrated density ration of target protein to GAPDH. *$p \leq 0.05$ was considered statistically significant. GO6983, PKC inhibitor; PMA, PKC activator; SB216763, GSK-3α/β inhibitor.

develops various strategies to regulate host factors and counter the bactericidal activity of the host's immunity, resulting in its survival and proliferation in Mφs (24). In the present study, we find that Mtb infection downregulates GSK-3α/β activity and upregulates MMP-1/9 expression in THP-1-Mφs. MMP-9 expression remarkably increases in both lungs of patients with pulmonary tuberculosis and lymph nodes of patients with lymphatic tuberculosis. However, it cannot be excluded that upregulated MMP-9 was secreted by other host immune cells such as neutrophils in both lung and lymph nodes of TB patients. Macrophage marker can be costained with MMP-9 protein to identify that macrophage-secreted MMP-9 by TB patients for

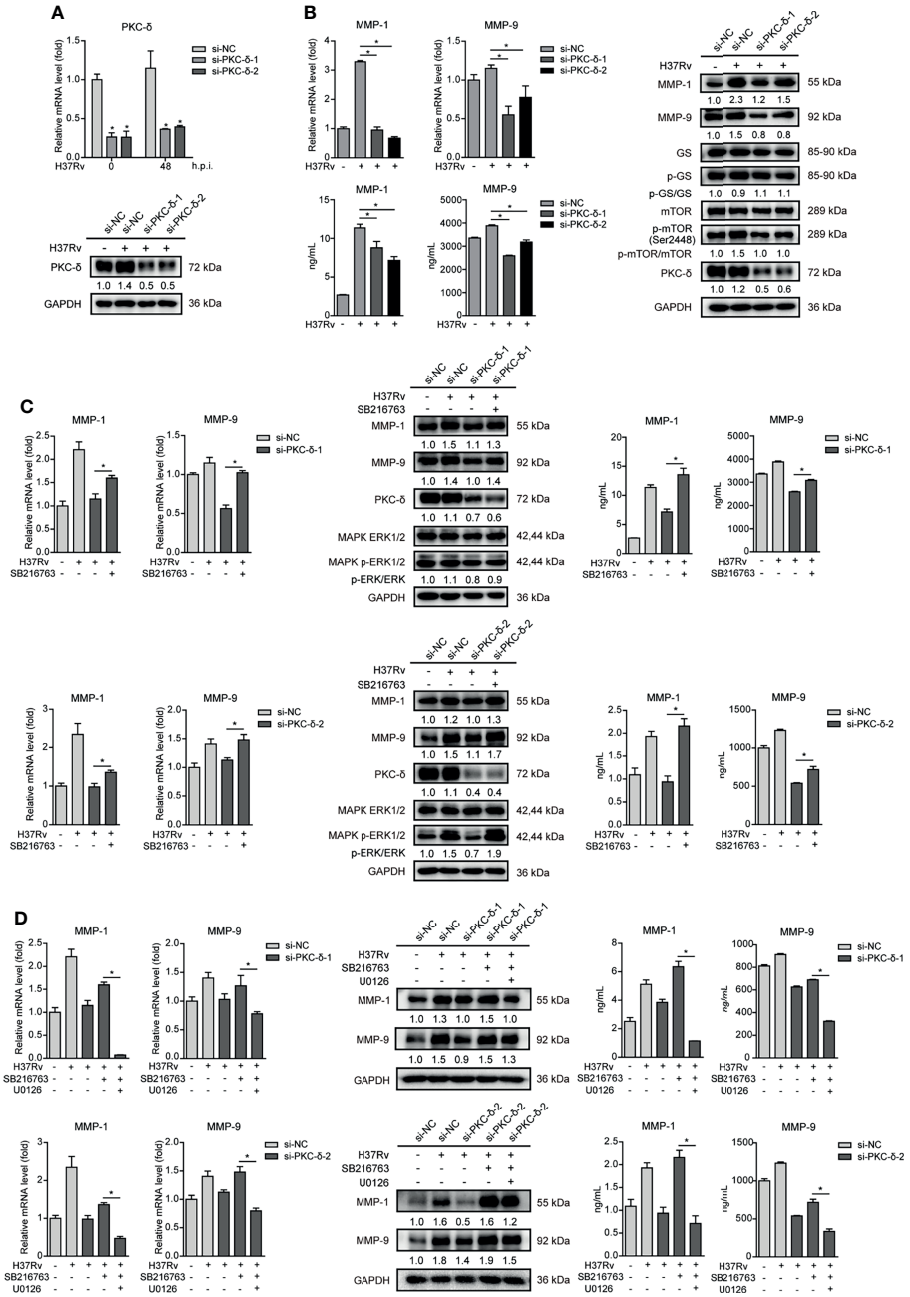

FIGURE 7 | PKC-δ-mTORC axis negatively regulated GSK-3α/β activity to promote phospho-ERK1/2 mediated MMP-1/9 expression. **(A)** PKC-δ expression of mRNA and protein levels were determined in PKC-δ silenced THP-1-Mφs upon 48 h Mtb infection by qRT-PCR and Western blot analysis (means ± SD, $n = 3$ independent experiments with each 4 replicates). Intracellular mRNA, protein expression, and secretion of MMP-1/9 were analyzed in **(B)** silencing PKC-δ, **(C)** silencing PKC-δ, SB216763, or their combination, **(D)** silencing PKC-δ, SB216763, U0126, or their combination in THP-1-Mφs at 48 h postinfection by qRT-PCR, Western blot, and ELISA analysis. Protein expression of GS, mTOR, ERK1/2, and PKC-δ and phosphorylation of GS, mTOR, and ERK1/2 were detected by Western blot analysis (means ± SD, $n = 3$ independent experiments with each 4 replicates). For Western blot assay, GAPDH served as an internal control. Data presented are from one of at least three independent experiments with similar results. The numbers below immunoblot correspond to band-integrated density ration of target protein to GAPDH. $^*p \leq 0.05$ was considered statistically significant. U0126, ERK1/2 inhibitor; SB216763, GSK-3α/β inhibitor.

further study. These results are in agreement with previous observations that Mtb tyrosine phosphatase PtpA dephosphorylated GSK-3α to modulate host Mφs immune responses against Mtb infection (7). Our results also support the findings that MMP-9 expression was strongly upregulated in TB lesions and distal regions of the lung biopsies (25). Additionally, MMP-1 was demonstrated as the principal secreted collagenase and upregulated in the sputum and

bronchoalveolar lavage fluid of TB patients (9). Further investigation identify that Mtb infection promotes MMP-1/9 expression, which further facilitates Mtb infection, while GSK-3α/β suppresses Mtb infection through inhibiting MMP-1/9 expression in Mφs and mice (**Figure 8**). Taken together, these findings have provided a new perspective as how Mtb escapes from host immune responses. However, it is still unknown whether heat-killed Mtb or avirulent mutants including an ESX-1 mutant and an ESX-5 mutant can evade the immune responses as an active strategy. In addition, how Mtb initiates the signaling pathway in Mφs remains unclear in this study. Specific ligands including TLR2, TLR4, TLR9, and cGAS-STING agonists should be applied for further investigation.

As a multifunctional kinase involved in an array of critical cellular processes, GSK-3α/β deserved an important component of host defense system (3). Recent studies, for example, have shown that GSK-3β promotes Mφs inflammatory activation by inhibiting the immune regulatory signaling of AMP-activated protein kinase (AMPK) (26). Human natural killer (NK) cells significantly increased production of TNF and IFN-γ, elevated natural cytotoxicity, and increased antibody-dependent cellular cytotoxicity in the presence of a GSK-3α/β inhibitor *ex vivo* (27). GSK-3β could interact with PD-L1 and play an important role in antitumor T-cell immunity of breast cancer (28). Importantly, autophagy machinery and inflammatory response, representative pivotal host immune strategies in combating Mtb infection, have been identified under the regulation of GSK-3α/β (3, 29–32). In our study, we have detected autophagy and proinflammatory and anti-inflammatory cytokines including IFNs and ISGs upon Mtb infection with treatment of SB216763 in THP-1-Mφs. Autophagy was not regulated by SB216763 treatment in a time-dependent manner. We know that IL-6, TNF-α, and IL-1β are proinflammatory cytokines which can play anti-Mtb infection role and IL-10 is an anti-inflammatory cytokine which can promote Mtb infection. Here, we demonstrated that expression of IL-6 and TNF-α significantly decreased 48 h.p.i.; however, expression of IL-1β and IL-10 significantly increased 24 and 48 h.p.i. with SB216763 treatment. Therefore, whether GSK-3α/β regulates Mtb infection though these cytokines needs to be further investigated. Expression of IFN-α and IFN-γ, as well as Mx1, Rsad2, and ISG15, was not influenced by SB216763 treatment. IFN-β and IRF1 expression was significantly decreased at 48 h.p.i. IFN-β production plays a probacterial role in host-Mtb interactions (33). Our previous study showed that IRF1 did not affect MMP expression upon Mtb infection (20). Thus, we speculate that autophagy, inflammatory cytokine production, and IFN signaling are not the main regulators of GSK-3α/β to suppress Mtb infection in Mφs.

Several MMPs stimulated by Mtb infection have been associated with the initiation and progression of TB. Among them, MMP-1 and MMP-9 are most extensively studied owing to their roles in the creation of the granuloma and destruction of lung tissue (10, 34). It has been reported that MMP-1 plays an important role in the immunopathology of TB. It promotes the collagen breakdown that lead to pulmonary tissue destruction in TB (9). Other studies have shown that MMP-9 enhanced the recruitment of newer Mφs and was associated with nascent granuloma maturation and bacterial growth (35). Previous studies showed that mice treated with MMP inhibitor BB94 exhibited either a delay in granuloma induction (36, 37) or formed smaller granulomas with more collagen (38), suggesting the crucial role of MMPs in regulating cell migration and granuloma formation upon Mtb infection. Furthermore, adjunctive treatment with MMP inhibitors along with front-line anti-TB drugs including isoniazid and rifampin significantly reduced Mtb survival in the lungs by preventing maturation of

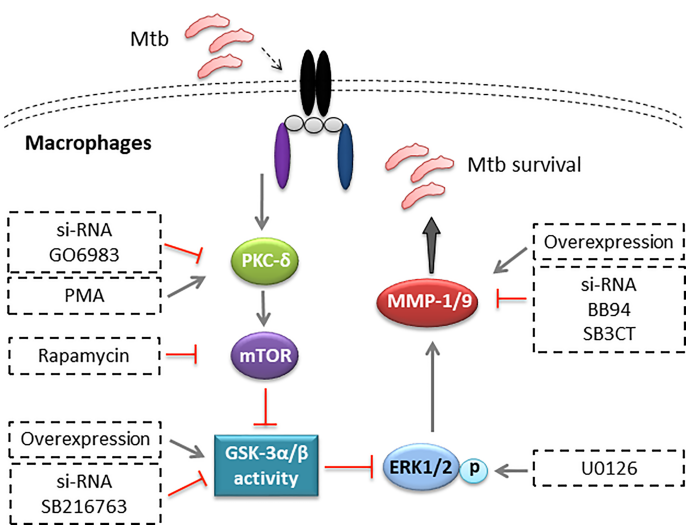

FIGURE 8 | Illustration of model of PKC-δ-mTOR axis negatively regulated GSK-3α/β activity, inhibiting Mtb infection through phospho-ERK1/2 mediated MMP-1/9 expression in Mφs.

granulomas and minimizing the matrix degradation and cavitary lesions (39–41). This new regimen of improved TB treatment by inhibition of MMP activity will help with minimizing the TB-associated morbidity and mortality. Consistently, our current study demonstrates that Mtb infection promoted MMP-1/9 expression and significantly facilitates Mtb survival in Mφs. MMP-9 inhibitor of SB3CT exhibits a significant decrease of Mtb infection in lungs and spleens of mice. Although the potential specific mechanism of MMPs on Mtb infection needs further studies, our study makes a crucial sense in revealing the importance of MMP-1/9 in regulating the immune pathology of Mtb infection.

MMPs have been demonstrated as can be regulated by different signaling pathways especially GSK-3α/β, ERK1/2, JNK, p38 MAPK, or/and NF-κB/AP-1 activation in various diseases (15, 16, 42–44). GSK-3β-regulated MMP expression, for example, was involved in SLFN5-controlled inhibition of cancer cell migration and invasion (45). MMP-9 expression mediated by dysregulation of GSK-3β activity has dramatic consequences on synaptic alterations and dendritic spine morphology (46). In addition, TNF-α and GM-CSF-induced GSK-3α/β inhibition determined the increase of MMP-1 production through a mechanism involving ERK1/2 activation by monocytes (47). Similarly, GSK-3β inhibition mediated ERK1/2 activation followed by the induction of MMP-9 expression in rat primary astrocytes (13). In our study, we find a novel mechanism for GSK-3α/β activity mediated ERK1/2 phosphorylation to exert anti-Mtb effect through suppressing MMP-1/9 expression in Mφs.

Given the fact that GSK-3α/β lies in the crossroads of various signal pathways, we have explored the upstream regulators of GSK-3α/β in Mtb infection. PKC and mTOR pathways represent the most common pathways implicated in the regulation of GSK-3α/β activity. For example, PKC suppressed GSK-3α/β activity, resulting in ERK1/2 phosphorylation, which was essential for MMP-1 production from monocytes (47). Inhibition of mTOR attenuated GSK-3β activity to increase NF-κB p65-associated CREB-binding protein and modulate balance of pro- and anti-inflammatory cytokines (17). In agreement with these findings, this study demonstrated that PKC-δ-mTOR axis promotes ERK phosphorylation-mediated MMP-1/9 expression through suppressing GSK-3α/β activity in Mφs. However, some studies have shown results completely opposite to those of our study regarding how mTOR activity affects MMP expression during Mtb infection (48). These differences might be due to the type of Mφs studied. The exact mechanisms associated with these differences require further investigation. Interestingly, it was reported that GSK-3α/β is involved in the regulation of PKC-δ and mTOR activity. GSK-3α/β decreased PKC-δ activity, attenuating the induction of ERK1/2 phosphorylation by GSK-3α/β inhibition (12). Moreover, GSK-3β regulates mTOR activity as well as in cancer research in hepatocellular carcinoma (HCC) (49). Our study mainly indicated that the PKC-δ-mTOR axis inhibits the activity of GSK-3α/β through ERK1/2 phosphorylation to upregulate the expression of MMP-1/9; the in-depth mechanism whether GSK-3α/β has a negative feedback mechanism for PKC-δ and mTOR requires further research.

In conclusion, we demonstrate that Mtb can escape from host immunity by suppressing GSK-3α/β activation and promoting MMP-1/9 production. Furthermore, GSK-3α/β activity regulated by PKC-δ-mTOR axis inhibits Mtb infection through suppressing phospho-ERK1/2-mediated MMP-1/9 expression in Mφs. This study sheds new light on the molecular insight of host-Mtb interaction and bears significant implications in the development of novel therapeutic approaches for TB.

DATA AVAILABILITY STATEMENT

The raw data supporting the conclusions of this article will be made available by the authors, without undue reservation.

ETHICS STATEMENT

The studies involving human participants were reviewed and approved by the Ethics Committee of the Southern Medical University. The patients/participants provided their written informed consent to participate in this study. The animal study was reviewed and approved by the Ethics Committee of Southern Medical University.

AUTHOR CONTRIBUTIONS

Conceptualization: XZ and LM. Methodology: XZ and LL. Software: XZ and LL. Validation: XZ, LL, and LM. Formal analysis: XZ and LL. Investigation: XZ, LL, YL, HX, BZ, YiH, LZ, ZZ, QL, QWa, ZH, YuH, HL, SH, CZ, and QWe. Resources: XZ, LL, SH, CZ, QWe, and LM. Data curation: XZ and LL. Writing—original draft preparation: XZ, LL, and L. Writing—review and editing: XZ, LL, and LM. Visualization: XZ and LL. Supervision: XZ and LM. Project administration: XZ and LM. Funding acquisition: XZ and LM. All authors read and approved the final manuscript.

FUNDING

This research was funded by the National Natural Science Foundation of China (81772150, 82072242, 82070010, 81801584, 81800013) and Guangdong Basic and Applied Basic Research Foundation (2021A1515010933, 2019A 1515010988, 2018030310486).

SUPPLEMENTARY MATERIAL

The Supplementary Material for this article can be found online at: https://www.frontiersin.org/articles/10.3389/fimmu.2021.752466/full#supplementary-material

REFERENCES

1. Pai M, Behr MA, Dowdy D, Dheda K, Divangahi M, Boehme CC, et al. Tuberculosis. *Nat Rev Dis Primers* (2016) 2:16076. doi: 10.1038/nrdp.2016.76
2. Guirado E, Schlesinger LS, Kaplan G. Macrophages in Tuberculosis: Friend or Foe. *Semin Immunopathol* (2013) 35:563–83. doi: 10.1007/s00281-013-0388-2
3. Wang H, Brown J, Martin M. Glycogen Synthase Kinase 3: A Point of Convergence for the Host Inflammatory Response. *Cytokine* (2011) 53:130–40. doi: 10.1016/j.cyto.2010.10.009
4. Hu X, Paik PK, Chen J, Yarilina A, Kockeritz L, Lu TT, et al. IFN-Gamma Suppresses IL-10 Production and Synergizes With TLR2 by Regulating GSK3 and CREB/AP-1 Proteins. *Immunity* (2006) 24:563–74. doi: 10.1016/j.immuni.2006.02.014
5. Zhang P, Katz J, Michalek SM. Glycogen Synthase Kinase-3beta (GSK3beta) Inhibition Suppresses the Inflammatory Response to Francisella Infection and Protects Against Tularemia in Mice. *Mol Immunol* (2009) 46:677–87. doi: 10.1016/j.molimm.2008.08.281
6. Lei CQ, Zhong B, Zhang Y, Zhang J, Wang S, Shu HB. Glycogen Synthase Kinase 3beta Regulates IRF3 Transcription Factor-Mediated Antiviral Response *via* Activation of the Kinase TBK1. *Immunity* (2010) 33:878–89. doi: 10.1016/j.immuni.2010.11.021
7. Poirier V, Bach H, Av-Gay Y. Mycobacterium Tuberculosis Promotes Anti-Apoptotic Activity of the Macrophage by PtpA Protein-Dependent Dephosphorylation of Host GSK3alpha. *J Biol Chem* (2014) 289:29376–85. doi: 10.1074/jbc.M114.582502
8. Etna MP, Severa M, Licursi V, Pardini M, Cruciani M, Rizzo F, et al. Genome-Wide Gene Expression Analysis of Mtb-Infected DC Highlights the Rapamycin-Driven Modulation of Regulatory Cytokines *via* the mTOR/GSK-3beta Axis. *Front Immunol* (2021) 12:649475. doi: 10.3389/fimmu.2021.649475
9. Elkington P, Shiomi T, Breen R, Nuttall RK, Ugarte-Gil CA, Walker NF, et al. MMP-1 Drives Immunopathology in Human Tuberculosis and Transgenic Mice. *J Clin Invest* (2011) 121:1827–33. doi: 10.1172/JCI45666
10. Friedland JS, Shaw TC, Price NM, Dayer JM. Differential Regulation of MMP-1/9 and TIMP-1 Secretion in Human Monocytic Cells in Response to Mycobacterium Tuberculosis. *Matrix Biol* (2002) 21:103–10. doi: 10.1016/S0945-053X(01)00175-5
11. Salgame P. MMPs in Tuberculosis: Granuloma Creators and Tissue Destroyers. *J Clin Invest* (2011) 121:1686–8. doi: 10.1172/JCI57423
12. Wang Q, Zhou Y, Wang X, Evers BM. Glycogen Synthase Kinase-3 is a Negative Regulator of Extracellular Signal-Regulated Kinase. *Oncogene* (2006) 25:43–50. doi: 10.1038/sj.onc.1209004
13. Kim SD, Yang SI, Kim HC, Shin CY, Ko KH. Inhibition of GSK-3beta Mediates Expression of MMP-9 Through ERK1/2 Activation and Translocation of NF-kappaB in Rat Primary Astrocyte. *Brain Res* (2007) 1186:12–20. doi: 10.1016/j.brainres.2007.10.018
14. Woodard C, Liao G, Goodwin CR, Hu J, Xie Z, Dos Reis TF, et al. A Screen for Extracellular Signal-Regulated Kinase-Primed Glycogen Synthase Kinase 3 Substrates Identifies the P53 Inhibitor iASPP. *J Virol* (2015) 89:9232–41. doi: 10.1128/JVI.01072-15
15. Al-Rashed F, Kochumon S, Usmani S, Sindhu S, Ahmad R. Pam3CSK4 Induces MMP-9 Expression in Human Monocytic THP-1 Cells. *Cell Physiol Biochem* (2017) 41:1993–2003. doi: 10.1159/000475298
16. Ong CW, Pabisiak PJ, Brilha S, Singh P, Roncaroli F, Elkington PT, et al. Complex Regulation of Neutrophil-Derived MMP-9 Secretion in Central Nervous System Tuberculosis. *J Neuroinflamm* (2017) 14:31. doi: 10.1186/s12974-017-0801-1
17. Wang H, Brown J, Gu Z, Garcia CA, Liang R, Alard P, et al. Convergence of the Mammalian Target of Rapamycin Complex 1- and Glycogen Synthase Kinase 3-Beta-Signaling Pathways Regulates the Innate Inflammatory Response. *J Immunol* (2011) 186:5217–26. doi: 10.4049/jimmunol.1002513
18. Zhan J, Chitta RK, Harwood FC, Grosveld GC. Phosphorylation of TSC2 by PKC-Delta Reveals a Novel Signaling Pathway That Couples Protein Synthesis to Mtorc1 Activity. *Mol Cell Biochem* (2019) 456:123–34. doi: 10.1007/s11010-019-03498-8
19. Li Y, Xu M, Ding X, Yan C, Song Z, Chen L, et al. Protein Kinase C Controls Lysosome Biogenesis Independently of Mtorc1. *Nat Cell Biol* (2016) 18:1065–77. doi: 10.1038/ncb3407
20. Zhou X, Yang J, Zhang Z, Zhang L, Lie L, Zhu B, et al. Interferon Regulatory Factor 1 Eliminates Mycobacteria by Suppressing P70 S6 Kinase *via* Mechanistic Target of Rapamycin Signaling. *J Infect* (2019) 79:262–76. doi: 10.1016/j.jinf.2019.06.007
21. Chen WL, Sheu JR, Chen RJ, Hsiao SH, Hsiao CJ, Chou YC, et al. Mycobacterium Tuberculosis Upregulates TNF-Alpha Expression *via* TLR2/ERK Signaling and Induces MMP-1 and MMP-9 Production in Human Pleural Mesothelial Cells. *PLoS One* (2015) 10:e0137979. doi: 10.1371/journal.pone.0137979
22. Koo J, Yue P, Gal AA, Khuri FR, Sun SY. Maintaining Glycogen Synthase Kinase-3 Activity is Critical for mTOR Kinase Inhibitors to Inhibit Cancer Cell Growth. *Cancer Res* (2014) 74:2555–68. doi: 10.1158/0008-5472.CAN-13-2946
23. Elkabets M, Pazarentzos E, Juric D, Sheng Q, Pelossof RA, Brook S, et al. AXL Mediates Resistance to PI3Kalpha Inhibition by Activating the EGFR/PKC/mTOR Axis in Head and Neck and Esophageal Squamous Cell Carcinomas. *Cancer Cell* (2015) 27:533–46. doi: 10.1016/j.ccell.2015.03.010
24. Jayachandran R, BoseDasgupta S, Pieters J. Surviving the Macrophage: Tools and Tricks Employed by Mycobacterium Tuberculosis. *Curr Top Microbiol Immunol* (2013) 374:189–209. doi: 10.1007/82_2012_273
25. Parasa VR, Muvva JR, Rose JF, Braian C, Brighenti S, Lerm M. Inhibition of Tissue Matrix Metalloproteinases Interferes With Mycobacterium Tuberculosis-Induced Granuloma Formation and Reduces Bacterial Load in a Human Lung Tissue Model. *Front Microbiol* (2017) 8:2370. doi: 10.3389/fmicb.2017.02370
26. Zhou H, Wang H, Ni M, Yue S, Xia Y, Busuttil RW, et al. Glycogen Synthase Kinase 3beta Promotes Liver Innate Immune Activation by Restraining AMP-Activated Protein Kinase Activation. *J Hepatol* (2018) 69:99–109. doi: 10.1016/j.jhep.2018.01.036
27. Cichocki F, Valamehr B, Bjordahl R, Zhang B, Rezner B, Rogers P, et al. GSK3 Inhibition Drives Maturation of NK Cells and Enhances Their Antitumor Activity. *Cancer Res* (2017) 77:5664–75. doi: 10.1158/0008-5472.CAN-17-0799
28. Li CW, Lim SO, Xia W, Lee HH, Chan LC, Kuo CW, et al. Glycosylation and Stabilization of Programmed Death Ligand-1 Suppresses T-Cell Activity. *Nat Commun* (2016) 7:12632. doi: 10.1038/ncomms12632
29. Azoulay-Alfaguter I, Elya R, Avrahami L, Katz A, Eldar-Finkelman H. Combined Regulation of Mtorc1 and Lysosomal Acidification by GSK-3 Suppresses Autophagy and Contributes to Cancer Cell Growth. *Oncogene* (2015) 34:4613–23. doi: 10.1038/onc.2014.390
30. Parr C, Carzaniga R, Gentleman SM, Van Leuven F, Walter J, Sastre M. Glycogen Synthase Kinase 3 Inhibition Promotes Lysosomal Biogenesis and Autophagic Degradation of the Amyloid-Beta Precursor Protein. *Mol Cell Biol* (2012) 32:4410–8. doi: 10.1128/MCB.00930-12
31. Liu H, Mi S, Li Z, Hua F, Hu ZW. Interleukin 17A Inhibits Autophagy Through Activation of PIK3CA to Interrupt the GSK3B-Mediated Degradation of BCL2 in Lung Epithelial Cells. *Autophagy* (2013) 9:730–42. doi: 10.4161/auto.24039
32. Martin M, Rehani K, Jope RS, Michalek SM. Toll-Like Receptor-Mediated Cytokine Production Is Differentially Regulated by Glycogen Synthase Kinase 3. *Nat Immunol* (2005) 6:777–84. doi: 10.1038/ni1221
33. Sabir N, Hussain T, Shah SZA, Zhao D, Zhou X. IFN-Beta: A Contentious Player in Host-Pathogen Interaction in Tuberculosis. *Int J Mol Sci* (2017) 18 (12):2725. doi: 10.3390/ijms18122725
34. Price NM, Farrar J, Tran TT, Nguyen TH, Tran TH, Friedland JS. Identification of a Matrix-Degrading Phenotype in Human Tuberculosis *In Vitro* and *In Vivo*. *J Immunol* (2001) 166:4223–30. doi: 10.4049/jimmunol.166.6.4223
35. Volkman HE, Pozos TC, Zheng J, Davis JM, Rawls JF, Ramakrishnan L. Tuberculous Granuloma Induction *via* Interaction of a Bacterial Secreted Protein With Host Epithelium. *Science* (2010) 327:466–9. doi: 10.1126/science.1179663
36. Taylor JL, Hattle JM, Dreitz SA, Troudt JM, Izzo LS, Basaraba RJ, et al. Role for Matrix Metalloproteinase 9 in Granuloma Formation During Pulmonary Mycobacterium Tuberculosis Infection. *Infect Immun* (2006) 74:6135–44. doi: 10.1128/IAI.02048-05
37. Hernandez-Pando R, Orozco H, Arriaga K, Pavon L, Rook G. Treatment With BB-94, a Broad Spectrum Inhibitor of Zinc-Dependent Metalloproteinases,

Causes Deviation of the Cytokine Profile Towards Type-2 in Experimental Pulmonary Tuberculosis in Balb/c Mice. *Int J Exp Pathol* (2000) 81:199–209. doi: 10.1046/j.1365-2613.2000.00152.x
38. Izzo AA, Izzo LS, Kasimos J, Majka S. A Matrix Metalloproteinase Inhibitor Promotes Granuloma Formation During the Early Phase of Mycobacterium Tuberculosis Pulmonary Infection. *Tuberculosis (Edinb)* (2004) 84:387–96. doi: 10.1016/j.tube.2004.07.001
39. Xu Y, Wang L, Zimmerman MD, Chen KY, Huang L, Fu DJ, et al. Matrix Metalloproteinase Inhibitors Enhance the Efficacy of Frontline Drugs Against Mycobacterium Tuberculosis. *PLoS Pathog* (2018) 14:e1006974. doi: 10.1371/journal.ppat.1006974
40. Sabir N, Hussain T, Mangi MH, Zhao D, Zhou X. Matrix Metalloproteinases: Expression, Regulation and Role in the Immunopathology of Tuberculosis. *Cell Prolif* (2019) 52:e12649. doi: 10.1111/cpr.12649
41. Miow QH, Vallejo AF, Wang Y, Hong JM, Bai C, Teo FS, et al. Doxycycline Host-Directed Therapy in Human Pulmonary Tuberculosis. *J Clin Invest* (2021) 131(15):e141895. doi: 10.1172/JCI141895
42. Zeng L, Rong XF, Li RH, Wu XY. Icariin Inhibits MMP1, MMP3 and MMP13 Expression Through MAPK Pathways in IL1betastimulated SW1353 Chondrosarcoma Cells. *Mol Med Rep* (2017) 15:2853–8. doi: 10.3892/mmr.2017.6312
43. Kusumaningrum N, Lee DH, Yoon HS, Kim YK, Park CH, Chung JH. Gasdermin C is Induced by Ultraviolet Light and Contributes to MMP-1 Expression *via* Activation of ERK and JNK Pathways. *J Dermatol Sci* (2018) 90:180–9. doi: 10.1016/j.jdermsci.2018.01.015
44. Huang CF, Teng YH, Lu FJ, Hsu WH, Lin CL, Hung CC, et al. Beta-Mangostin Suppresses Human Hepatocellular Carcinoma Cell Invasion Through Inhibition of MMP-2 and MMP-9 Expression and Activating the ERK and JNK Pathways. *Environ Toxicol* (2017) 32:2360–70. doi: 10.1002/tox.22449
45. Wan G, Liu Y, Zhu J, Guo L, Li C, Yang Y, et al. SLFN5 Suppresses Cancer Cell Migration and Invasion by Inhibiting MT1-MMP Expression *via* AKT/GSK-3beta/Beta-Catenin Pathway. *Cell Signal* (2019) 59:1–12. doi: 10.1016/j.cellsig.2019.03.004
46. Kondratiuk I, Leski S, Urbanska M, Biecek P, Devijver H, Lechat B, et al. GSK-3beta and MMP-9 Cooperate in the Control of Dendritic Spine Morphology. *Mol Neurobiol* (2017) 54:200–11. doi: 10.1007/s12035-015-9625-0
47. Zhang Y, Wahl LM. Cytokine-Induced Monocyte MMP-1 is Negatively Regulated by GSK-3 Through a P38 MAPK-Mediated Decrease in ERK1/2 MAPK Activation. *J Leukoc Biol* (2015) 97:921–7. doi: 10.1189/jlb.3A0413-235R
48. Brace PT, Tezera LB, Bielecka MK, Mellows T, Garay D, Tian S, et al. Mycobacterium Tuberculosis Subverts Negative Regulatory Pathways in Human Macrophages to Drive Immunopathology. *PLoS Pathog* (2017) 13: e1006367. doi: 10.1371/journal.ppat.1006367
49. Fang G, Zhang P, Liu J, Zhang X, Zhu X, Li R, et al. Inhibition of GSK-3beta Activity Suppresses HCC Malignant Phenotype by Inhibiting Glycolysis *via* Activating AMPK/mTOR Signaling. *Cancer Lett* (2019) 463:11–26. doi: 10.1016/j.canlet.2019.08.003

Conflict of Interest: The authors declare that the research was conducted in the absence of any commercial or financial relationships that could be construed as a potential conflict of interest.

Publisher's Note: All claims expressed in this article are solely those of the authors and do not necessarily represent those of their affiliated organizations, or those of the publisher, the editors and the reviewers. Any product that may be evaluated in this article, or claim that may be made by its manufacturer, is not guaranteed or endorsed by the publisher.

Advantages of publishing in Frontiers

OPEN ACCESS
Articles are free to read for greatest visibility and readership

FAST PUBLICATION
Around 90 days from submission to decision

HIGH QUALITY PEER-REVIEW
Rigorous, collaborative, and constructive peer-review

TRANSPARENT PEER-REVIEW
Editors and reviewers acknowledged by name on published articles

Frontiers
Avenue du Tribunal-Fédéral 34
1005 Lausanne | Switzerland

Visit us: www.frontiersin.org
Contact us: frontiersin.org/about/contact

REPRODUCIBILITY OF RESEARCH
Support open data and methods to enhance research reproducibility

DIGITAL PUBLISHING
Articles designed for optimal readership across devices

FOLLOW US
@frontiersin

IMPACT METRICS
Advanced article metrics track visibility across digital media

EXTENSIVE PROMOTION
Marketing and promotion of impactful research

LOOP RESEARCH NETWORK
Our network increases your article's readership